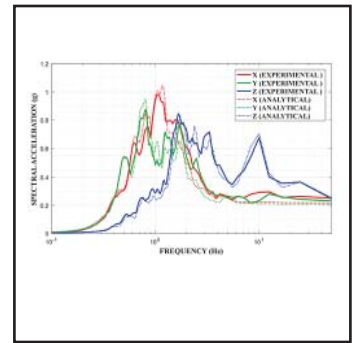
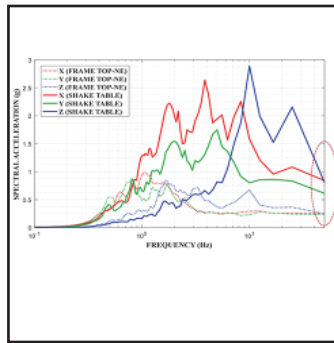


Development and Validation of a Combined Horizontal-Vertical Seismic Isolation System for High-Voltage Power Transformers

by
Donghun Lee and Michael C. Constantinou



Technical Report MCEER-17-0007

November 3, 2017

NOTICE

This report was prepared by the University at Buffalo, State University of New York, as a result of research sponsored by MCEER. Neither MCEER, associates of MCEER, its sponsors, University at Buffalo, State University of New York, nor any person acting on their behalf:

- a. makes any warranty, express or implied, with respect to the use of any information, apparatus, method, or process disclosed in this report or that such use may not infringe upon privately owned rights; or
- b. assumes any liabilities of whatsoever kind with respect to the use of, or the damage resulting from the use of, any information, apparatus, method, or process disclosed in this report.

Any opinions, findings, and conclusions or recommendations expressed in this publication are those of the author(s) and do not necessarily reflect the views of MCEER, the National Science Foundation or other sponsors.

Development and Validation of a Combined Horizontal-Vertical Seismic Isolation System for High-Voltage Power Transformers

by

Donghun Lee¹ and Michael C. Constantinou²

Publication Date: November 3, 2017

Submittal Date: September 8, 2017

Technical Report MCEER-17-0007

- 1 PhD candidate, Department of Civil, Structural and Environmental Engineering, University at Buffalo, State University of New York
- 2 Samuel P. Capen Professor and SUNY Distinguished Professor, Department of Civil, Structural and Environmental Engineering, University at Buffalo, State University of New York

MCEER

University at Buffalo, State University of New York

212 Ketter Hall, Buffalo, NY 14260

E-mail: mceer@buffalo.edu; Website: <http://mceer.buffalo.edu>

Preface

MCEER is a national center of excellence dedicated to the discovery and development of new knowledge, tools and technologies that equip communities to become more disaster resilient in the face of earthquakes and other extreme events. MCEER accomplishes this through a system of multidisciplinary, multi-hazard research, in tandem with complimentary education and outreach initiatives.

Headquartered at the University at Buffalo, The State University of New York, MCEER was originally established by the National Science Foundation in 1986, as the first National Center for Earthquake Engineering Research (NCEER). In 1998, it became known as the Multidisciplinary Center for Earthquake Engineering Research (MCEER), from which the current name, MCEER, evolved.

Comprising a consortium of researchers and industry partners from numerous disciplines and institutions throughout the United States, MCEER's mission has expanded from its original focus on earthquake engineering to one which addresses the technical and socio-economic impacts of a variety of hazards, both natural and man-made, on critical infrastructure, facilities, and society.

The Center derives support from several Federal agencies, including the National Science Foundation, Federal Highway Administration, Department of Energy, Nuclear Regulatory Commission, and the State of New York, foreign governments and private industry.

This report presents the development and validation of a practical three-directional seismic isolation system for use in high-voltage power transformers, although the technology could easily be transferred to building applications. Characteristics of the developed system are: (a) it is a modular extension of a horizontal seismic isolation system consisting of triple Friction Pendulum isolators currently used for power transformers, (b) it consist of two separate systems, one to achieve horizontal seismic isolation and the other to achieve vertical seismic isolation, (c) the horizontal system is highly flexible in order to achieve a high degree of seismic isolation but subject to constraints on displacements for serviceability of the equipment, (d) the vertical system is able to support the weight of the equipment with limited deflection in order to meet serviceability requirements and compactness, (e) all components of the system are readily available from reputable manufacturers, and (f) all components of the system are passive and highly reliable.

ABSTRACT

The electric network of the United States is considered to be critical infrastructure. Electric utility companies and electric power administrators (e.g., Bonneville Power Administration, a federal nonprofit agency) are increasingly interested in strengthening the security and resilience of their networks against earthquakes. Important components of these networks are high voltage electrical transformers. While the equipment or parts of it are tested, there are systematic failures in earthquakes as the equipment is very complex and motion of its internal components is not easily predictable. Utility companies keep in storage a small number of high voltage transformers for use in cases of failures but a widespread failure of equipment in an earthquake would be catastrophic for the communities served by the utility companies as replacement of the failed equipment takes substantial time. Transformers are manufactured by a few companies worldwide and delivery of ordered products typically has a long lead time. Thus, the loss of a transformer has some economic impact but mostly the issue is that of down-time which is unacceptably high. Accordingly, the development of effective and reliable systems for providing seismic protection to electrical equipment is important.

Earlier studies in the use of seismic protective systems for electrical transformers and other equipment produced results that clearly show the benefits of seismic isolation in the horizontal direction. However, vertical ground motions were transmitted through the isolation system unchanged or even slightly magnified. The work described in this report aims at addressing this issue by developing and validating a compact, effective, reasonably priced and highly reliable combined horizontal-vertical seismic isolation system for use on electrical equipment of weight in the range of 300 to 800kip, which is typical of high voltage transformers in the range of 230-500kV. The developed and tested system consists of triple Friction Pendulum bearings for the horizontal isolation system, which are supported by vertically driven spring-damper units. These units form a highly damped vertical damping system.

“This Page Intentionally Left Blank”

ACKNOWLEDGEMENTS

Financial support for this project was provided by the Bonneville Power Administration, Portland, OR with Mr. Leon Kempner, Jr., Ph.D., PE and Mr. Michael J. Riley, PE as the responsible technical officers. The Triple Friction Pendulum isolators were designed and manufactured by Earthquake Protection Systems, Inc., Vallejo, CA. The spring-damper units were designed and manufactured by Taylor Devices, Inc., North Tonawanda, NY. All devices were supplied at no cost to the project. The authors are grateful for the support provided.

“This Page Intentionally Left Blank”

TABLE OF CONTENTS

SECTION	TITLE	PAGE
1	INTRODUCTION	1
2	ANALYTICAL STUDY OF THREE-DIMENSIONAL SEISMIC ISOLATION SYSTEMS FOR HIGH-VOLTAGE POWER TRANSFORMERS	15
2.1	Introduction	15
2.2	Analyzed Combined Horizontal-Vertical Seismic Isolation Systems	19
2.3	Analyzed Transformer Model	23
2.4	Results of Analysis	33
2.5	Study for the Selection of Properties of the Vertical Isolation System	54
3	DESCRIPTION AND PROPERTIES OF MODEL FOR TESTING	63
3.1	Introduction	63
3.2	Description of Transformer Test Model	64
3.3	Description of Seismic Isolation System	70
3.4	Testing and Properties of Spring-Damper Units	78
3.5	Testing and Properties of Triple Friction Pendulum Isolators	81
3.6	Testing and Properties of Spring-Damper Units	91
3.7	Identification of Vertical Frequency and Damping Ratio of Isolated Model	93
4	RESULTS OF SHAKE TABLE TESTING AND ASSESSMENT OF PERFORMANCE	99
4.1	Introduction	99
4.2	Motions Used in Shake Table Testing and Test Matrix	99
4.3	Instrumentation	104
4.4	Results of Shake Table Testing	106
5	ANALYTICAL PREDICTION OF RESPONSE	133
5.1	Introduction	133

TABLE OF CONTENTS (cont'd)

SECTION	TITLE	PAGE
5.2	Analytical Model of Tested Structure	133
5.3	Comparison of Analytical and Experimental Results	140
5.4	Effect of Rocking Motion of the Shake Table on Prediction of Response	187
5.5	Effect of Friction in the Spring-Damper Units	202
5.6	Summary	240
6	EXAMPLES OF ANALYSIS AND DESIGN	241
6.1	Introduction	241
6.2	Seismic Hazard Analysis for the Site and Selection and Scaling of Motions for Dynamic Analysis	242
6.3	Description of Transformer and its Isolation System	246
6.4	Model for Dynamic Analysis	255
6.5	Results of Dynamic Analysis	260
7	SUMMARY AND CONCLUSIONS	275
8	REFERENCES	281
APPENDIX A - EIGENVALUE ANALYSIS OF TRANSFORMER WITH 3D SPRING- DAMPER ISOLATION SYSTEM		285
A-1	Complex Eigenvalue Analysis of Two-Dimensional Representation of Isolated Transformer	285
A-2	Eigenvalue Analysis of Three-Dimensional Representation of Isolated Transformer in Program SAP2000	289
APPENDIX B - PROPERTIES OF TRIPLE FRICTION PENDULUM ISOLATORS USED IN ANALYSIS OF SECTION 2		291
APPENDIX C - EIGENVALUE ANALYSIS FOR TRANSFORMER WITH TRIPLE FP-SPRING-DAMPER SYSTEM		297

TABLE OF CONTENTS (cont'd)

SECTION	TITLE	PAGE
APPENDIX D -	DRAWINGS OF TEST MODEL	301
APPENDIX E -	TEST DATA FOR SPRING-DAMPER UNITS AND TRIPLE FRICTION PENDULUM ISOLATORS	315

LIST OF FIGURES

FIGURE	TITLE	PAGE
1-1	Vertical Response Spectra at Control Point of Non-isolated and Horizontally Isolated Electrical Transformer for Three-Component Excitation	2
1-2	Horizontal Response Spectra (two directions) at Control Point of Non-isolated and Horizontally Isolated Electrical Transformer for Three-Component Excitation	2
1-3	3D Seismic Isolation System Consisting of Air Spring Combined with Flat Rolling (Ball) Bearings and Coil Springs (Tsutsumi et al., 2000)	4
1-4	3D Seismic Isolation System Consisting of Multistage Elastomeric Bearings, Vertical Coil Springs and Horizontal and Vertical Dampers (Tsutsumi et al., 2001)	5
1-5	Rocking Suppression System used in 3D Elastomeric Bearing-Hydraulic Spring System (Kashiwazaki, 2003)	8
1-6	Rocking Prevention Device of Reinforced Air Spring System (Kageyama et al., 2003)	9
1-7	Seismic Isolation System of Chisuikan Building (Tomizawa et al, 2011; Mori et al, 2012)	10
1-8	3D Seismic Isolation System for a House in California (Makris and Constantinou, 1992)	11
1-9	3D Seismic Isolation System developed for a Radar Facility at Shemya Island, Alaska	12
2-1	Seismically Isolated Transformer in Vancouver, WA (courtesy L. Kempner, BPA)	15
2-2	Bushing Parameters (Kitayama et al, 2016)	16
2-3	Examples of 3D Isolation Systems Consisting of Helical Springs and Dampers (top image courtesy of Taylor Devices, Inc.; bottom image courtesy of GERB)	19
2-4	Schematic of Spring-Viscous Damper Device	22
2-5	Behavior of 3D Isolation System Freely Allowed to Rock	23
2-6	Transformer Basic Dimensions (units in inch)	23
2-7	Model of Transformer with 3D Spring-Damper Isolation System	24
2-8	Bushing Representation in Analysis Model	25
2-9	Schematic of Spring-Damper Unit at Each Corner of Transformer	26
2-10	Model of Transformer with 3D Triple FP-Spring-Damper Isolation System	30
2-11	Acceleration Response Spectra at 6Hz Bushing Mount in El Centro 300% Motion	36
2-12	Acceleration Response Spectra at 6Hz Bushing Mount in Pacoima 100% Motion	37
2-13	Acceleration Response Spectra at 6Hz Bushing Mount in Jensen 100% Motion	38

LIST OF FIGURES (cont'd)

FIGURE	TITLE	PAGE
2-14	Acceleration Response Spectra at 6Hz Bushing Mount in Chile 100% Motion	39
2-15	Acceleration Response Spectra 6Hz Bushing Mount Corner in LGPC 100% Motion	40
2-16	Acceleration Response Spectra at 6Hz Bushing Mount in Kobe 100% Motion	41
2-17	Acceleration Response Spectra at 6Hz Bushing Mount in Rio 100% Motion	42
2-18	Acceleration Response Spectra at 6Hz Bushing Mount in Sylmar 100% Motion	43
2-19	Acceleration Response Spectra at 6Hz Bushing Mount for FP-spring-damper System with Vertical Frequency of 2.74Hz and Vertical Damping Ratio of 0.25 (solid line) or 0.50 (dashed line) in Pacoima 100% Motion	44
2-20	Acceleration Response Spectra at 6Hz Bushing Mount of 2D Isolation System (solid line) and 3D Isolation System with Vertical Frequency of 2.0Hz and Damping of 0.50 (dashed line) in Chile 100% Motion	45
2-21	Acceleration Response Spectra at 6Hz Bushing Mount of 2D Isolation System (solid line) and 3D Isolation System with Vertical Frequency of 2.0Hz and Damping of 0.50 (dashed line) in LGPC 100% Motion	46
2-22	Acceleration Response Spectra at 6Hz Bushing Mount of 2D Isolation System (solid line) and 3D Isolation System with Vertical Frequency of 2.0Hz and Damping of 0.50 (dashed line) in Kobe 100% Motion	47
2-23	Acceleration Response Spectra at 6Hz Bushing Mount of 2D Isolation System (solid line) and 3D Isolation System with Vertical Frequency of 2.0Hz and Damping of 0.50 (dashed line) in Rio 100% Motion	48
2-24	Acceleration Response Spectra at 6Hz Bushing Mount of 2D Isolation System (solid line) and 3D Isolation System with Vertical Frequency of 2.0Hz and Damping of 0.50 (dashed line) in Sylmar 100% Motion	49
2-25	Peak Vertical Acceleration at 6Hz Bushing Mount Normalized by Peak Vertical Ground Acceleration	55
2-26	Peak Vertical Acceleration at 6Hz Bushing Top Normalized by Peak Vertical Ground Acceleration	55
2-27	Static and Peak Dynamic Vertical Isolator Displacement Demands	56
2-28	Static and Total Vertical Isolator Displacement Demands	56
3-1	Transformer Model for Shake Table Testing: (a) Braced Frame with Cover Plate and Bushing and (b) Complete Test Model with Added Mass and Seismic Isolation System (configuration allowed to freely rock)	66

LIST OF FIGURES (cont'd)

FIGURE	TITLE	PAGE
3-2	Basic Dimensions of Isolated Transformer Test Model, Free Rocking Configuration	67
3-3	View of Model of Isolated Transformer with Added Base for Limiting Rocking	68
3-4	Schematics of Added Base for Limited Rocking: (a) Front View (b) Plan View (c) Section A-A' and (d) Detail of Connection between Vertical Spring-Damper Unit and Added Plate	69
3-5	Triple FP Isolator Types used in Testing	71
3-6	Spring-Damper Unit	72
3-7	Detail of Spring-Damper Unit for Increasing Shear Spring Stiffness	73
3-8	Details of Connection for System with Base for Limiting Rocking (prior to shimming)	74
3-9	Illustration of Rocking Motion of System Allowing for Free Rocking	74
3-10	Frequencies of Isolated Transformer Test Model (red text and red line) and of Actual Transformer (black text and black line), Free Rocking Configuration	77
3-11	Test Set-up for Spring-Damper Unit	78
3-12	Force-Displacement Loop of Spring-Damper Unit 1 in at Peak Velocity of 0.03in/sec	79
3-13	Force-Displacement Loop of Spring-Damper Unit 1 at Peak Velocity of 6.28in/sec	79
3-14	Peak Damping Force versus Peak Velocity Relationship in Testing at Spring-Damper Units at University at Buffalo and Testing of Dampers at Taylor Devices	81
3-15	Image of Triple FP Isolator Type A of 0.20 Nominal Friction in Test Machine	82
3-16	Recorded Histories of Lateral Motion and Vertical Load in Test with Frequency of 0.3Hz	82
3-17	Experimental and Analytical Normalized Force-Displacement Loops of Triple FP Isolator No. 1 of Type A without Lubrication (nominal friction 0.20)	84
3-18	Experimental and Analytical Normalized Force-Displacement Loops of Triple FP Isolator No. 1 of Type A without Lubrication (nominal friction 0.20) in High Speed Motion and with due Consideration of Stiffness of Inner Rubber Seal	85
3-19	Friction Coefficient-Velocity Relation of Triple FP Isolator of Type A without Lubrication (nominal friction 0.20)	86
3-20	Experimental and Analytical Normalized Force-Displacement Loops of Triple FP Isolator No. 1 of Type A with Lubrication (nominal friction 0.07)	87
3-21	Friction Coefficient-Velocity Relation of Triple FP Isolator of Type A with Lubrication (nominal friction 0.07)	88

LIST OF FIGURES (cont'd)

FIGURE	TITLE	PAGE
3-22	Experimental and Analytical Normalized Force-Displacement Loops of Triple FP Isolator No. 1 of Type B (nominal friction 0.12)	89
3-23	Contact Areas in (a) Un-deformed and (b) Deformed Bearing	90
3-24	Friction Coefficient-Velocity Relation of Triple FP Isolator of Type B (nominal friction 0.12)	90
3-25	Instrumentation Diagram for Accelerometers used in Bushing Identification	91
3-26	Amplitude of Transfer Functions of Top of Bushing Acceleration to Shake Table Extension Acceleration	92
3-27	Instrumentation Diagram Showing Accelerometers and Krypton LED	93
3-28	Instrumentation Diagram Showing Displacement Transducers	94
3-29	Amplitude of Transfer Function and Phase Angle of Isolated Transformer Model in Vertical Direction	98
4-1	5%-Damped Vertical and Horizontal Response Spectra of El Centro Motion Recorded in the Field	101
4-2	5%-Damped Vertical and Horizontal Response Spectra of Pacoima Motion Recorded in the Field	101
4-3	5%-Damped Vertical and Horizontal Response Spectra of Chile Motion Recorded in the Field	102
4-4	5%-Damped Vertical and Horizontal Response Spectra of Taft Motion Recorded in the Field	102
4-5	5%-Damped Vertical and Horizontal Response Spectra of Kobe Motion Recorded in the Field	103
4-6	5%-Damped Vertical and Horizontal Response Spectra of Jensen Motion Recorded in the Field	103
4-7	Additional Krypton LED Transducers Used in Testing of Configuration with Limited Rocking	105
4-8	Additional Displacement Transducers Used in Testing of Configuration with Limited Rocking	105
4-9	5%-Damped Response Spectra at Frame Top at NE Corner and at Shake Table for Configuration with Limited Rocking, FP Isolator Type B with 0.12 Nominal Friction in El Centro 250% Motion	109

LIST OF FIGURES (cont'd)

FIGURE	TITLE	PAGE
4-10	5%-Damped Response Spectra at Frame Top at NE Corner and at Shake Table for Configuration with Limited Rocking, FP Isolator Type B with 0.12 Nominal Friction in Pacoima 75% Motion	109
4-11	5%-Damped Response Spectra at Frame Top at NE Corner and at Shake Table for Configuration with Limited Rocking, FP Isolator Type B with 0.12 Nominal Friction in Chile 100% Motion	110
4-12	5%-Damped Response Spectra at Frame Top at NE Corner and at Shake Table for Configuration with Limited Rocking, FP Isolator Type B with 0.12 Nominal Friction in Taft 400% Motion	110
4-13	5%-Damped Response Spectra at Frame Top at NE Corner and at Shake Table for Configuration with Limited Rocking, FP Isolator Type B with 0.12 Nominal Friction in Kobe 65% Motion	111
4-14	5%-Damped Response Spectra at Frame Top at NE Corner and at Shake Table for Configuration with Limited Rocking, FP Isolator Type B with 0.12 Nominal Friction in Jensen 85% Motion	111
4-15	5%-Damped Response Spectra at Frame Top at NE Corner and at Shake Table for Configuration with Free Rocking, FP Isolator Type B with 0.12 Nominal Friction in El Centro 250% Motion	112
4-16	5%-Damped Response Spectra at Frame Top at NE Corner and at Shake Table for Configuration with Free Rocking, FP Isolator Type B with 0.12 Nominal Friction in Pacoima 60% Motion	112
4-17	5%-Damped Response Spectra at Frame Top at NE Corner and at Shake Table for Configuration with Free Rocking, FP Isolator Type B with 0.12 Nominal Friction in Chile 100% Motion	113
4-18	5%-Damped Response Spectra at Frame Top at NE Corner and at Shake Table for Configuration with Free Rocking, FP Isolator Type B with 0.12 Nominal Friction in Taft 400% Motion	113
4-19	5%-Damped Response Spectra at Frame Top at NE Corner and at Shake Table for Configuration with Free Rocking, FP Isolator Type B with 0.12 Nominal Friction in Kobe 50% Motion	114
4-20	5%-Damped Response Spectra at Frame Top at NE Corner and at Shake Table for Configuration with Free Rocking, FP Isolator Type B with 0.12 Nominal Friction in Jensen 85% Motion	114

LIST OF FIGURES (cont'd)

FIGURE	TITLE	PAGE
4-21	5%-Damped Vertical and Horizontal Response Spectra at Various Frame Top Locations in Horizontal and Vertical Directions for Configuration with Free Rocking, FP Isolator Type B with 0.12 Nominal Friction in Taft 400% Motion	115
4-22	5%-Damped Vertical and Horizontal Response Spectra at Various Frame Top Locations in Horizontal and Vertical Directions for Configuration with Free Rocking, FP Isolator Type B with 0.12 Nominal Friction in Kobe 50% Motion	116
4-23	Comparison of 5%-Damped Response Spectra at Frame Top at NE Corner of Two Tested Configurations with Free Rocking and Limited Rocking, FP Isolator Type B with 0.12 Nominal Friction in El Centro 250% Motion	116
4-24	Comparison of 5%-Damped Response Spectra at Frame Top at NE Corner of Two Tested Configurations with Free Rocking and Limited Rocking, FP Isolator Type B with 0.12 Nominal Friction in Pacoima 50% Motion	117
4-25	Comparison of 5%-Damped Response Spectra at Frame Top at NE Corner of Two Tested Configurations with Free Rocking and Limited Rocking, FP Isolator Type B with 0.12 Nominal Friction in Chile 100% Motion	117
4-26	Comparison of 5%-Damped Response Spectra at Frame Top at NE Corner of Two Tested Configurations with Free Rocking and Limited Rocking, FP Isolator Type B with 0.12 Nominal Friction in Taft 400% Motion	118
4-27	Comparison of 5%-Damped Response Spectra at Frame Top at NE Corner of Two Tested Configurations with Free Rocking and Limited Rocking, FP Isolator Type B with 0.12 Nominal Friction in Kobe 50% Motion	118
4-28	Comparison of 5%-Damped Response Spectra at Frame Top at NE Corner of Two Tested Configurations with Free Rocking and Limited Rocking, FP Isolator Type B with 0.12 Nominal Friction in Jensen 85% Motion	119
4-29	Two Models used in the Representation of the Added Base Connection to the FP Isolator	124
4-30	Comparison of 5%-Damped Experimental and Analytical Response Spectra at Frame Top at NE Corner of Configuration of Limited Rocking, FP Isolator Type B with 0.12 Nominal Friction in El Centro 250% Motion	127
4-31	Comparison of 5%-Damped Experimental and Analytical Response Spectra at Frame Top at NE Corner of Configuration of Limited Rocking, FP Isolator Type B with 0.12 Nominal Friction in Pacoima 75% Motion	128

LIST OF FIGURES (cont'd)

FIGURE	TITLE	PAGE
4-32	Comparison of 5%-Damped Experimental and Analytical Response Spectra at Frame Top at NE Corner of Configuration of Limited Rocking, FP Isolator Type B with 0.12 Nominal Friction in Chile 100% Motion	129
4-33	Comparison of 5%-Damped Experimental and Analytical Response Spectra at Frame Top at NE Corner of Configuration of Limited Rocking, FP Isolator Type B with 0.12 Nominal Friction in Taft 400% Motion	130
4-34	Comparison of 5%-Damped Experimental and Analytical Response Spectra at Frame Top at NE Corner of Configuration of Limited Rocking, FP Isolator Type B with 0.12 Nominal Friction in Kobe 65% Motion	131
4-35	Comparison of 5%-Damped Experimental and Analytical Response Spectra at Frame Top at NE Corner of Configuration of Limited Rocking, FP Isolator Type B with 0.12 Nominal Friction in Jensen 85% Motion	132
5-1	Analytical Model of Tested Model in Configuration of Free Rocking	134
5-2	Bushing Model Details	135
5-3	Schematic of Modeling of Added Base Plate and Plan View of Added Base Plate	136
5-4	Illustration of Ineffectiveness of Shims to Restrain Rotation of the Connection of Added Base Plate to Isolators	137
5-5	Comparison of Experimental and Analytical Results for Configuration of Free Rocking, FP Isolator Type B with 0.12 Nominal Friction in El Centro 250% Motion: (a) 5%-damped Response Spectra at Frame NE Top Corner, (b) Acceleration Histories at Frame NE Top Corner	141
5-6	Comparison of Experimental and Analytical Results for Configuration of Free Rocking, FP Isolator Type B with 0.12 Nominal Friction in El Centro 250% Motion: (a) FP Displacement Histories and Orbit at SW Corner, (b) Vertical Displacement at Spring-damper Unit at NE Corner	142
5-7	Comparison of Experimental and Analytical Results for Configuration of Free Rocking, FP Isolator Type B with 0.12 Nominal Friction in Pacoima 60% Motion: (a) 5%-damped Response Spectra at Frame NE Top Corner, (b) Acceleration Histories at Frame NE Top Corner	143
5-8	Comparison of Experimental and Analytical Results for Configuration of Free Rocking, FP Isolator Type B with 0.12 Nominal Friction in Pacoima 60% Motion: (a) FP Displacement Histories and Orbit at SW Corner, (b) Vertical Displacement at Spring-damper Unit at NE Corner	144

LIST OF FIGURES (cont'd)

FIGURE	TITLE	PAGE
5-9	Comparison of Experimental and Analytical Results for Configuration of Free Rocking, FP Isolator Type B with 0.12 Nominal Friction in Chile 100% Motion: (a) 5%-damped Response Spectra at Frame NE Top Corner, (b) Acceleration Histories at Frame NE Top Corner	145
5-10	Comparison of Experimental and Analytical Results for Configuration of Free Rocking, FP Isolator Type B with 0.12 Nominal Friction in Chile 100% Motion: (a) FP Displacement Histories and Orbit at SW Corner, (b) Vertical Displacement at Spring-damper Unit at NE Corner	146
5-11	Comparison of Experimental and Analytical Results for Configuration of Free Rocking, FP Isolator Type B with 0.12 Nominal Friction in Taft 400% Motion: (a) 5%-damped Response Spectra at Frame NE Top Corner, (b) Acceleration Histories at Frame NE Top Corner	147
5-12	Comparison of Experimental and Analytical Results for Configuration of Free Rocking, FP Isolator Type B with 0.12 Nominal Friction in Taft 400% Motion: (a) FP Displacement Histories and Orbit at SW Corner, (b) Vertical Displacement at Spring-damper Unit at NE Corner	148
5-13	Comparison of Experimental and Analytical Results for Configuration of Free Rocking, FP Isolator Type B with 0.12 Nominal Friction in Kobe 50% Motion: (a) 5%-damped Response Spectra at Frame NE Top Corner, (b) Acceleration Histories at Frame NE Top Corner	149
5-14	Comparison of Experimental and Analytical Results for Configuration of Free Rocking, FP Isolator Type B with 0.12 Nominal Friction in Kobe 50% Motion: (a) FP Displacement Histories and Orbit at SW Corner, (b) Vertical Displacement at Spring-damper Unit at NE Corner	150
5-15	Comparison of Experimental and Analytical Results for Configuration of Free Rocking, FP Isolator Type B with 0.12 Nominal Friction in Jensen 100% Motion: (a) 5%-damped Response Spectra at Frame NE Top Corner, (b) Acceleration Histories at Frame NE Top Corner	151
5-16	Comparison of Experimental and Analytical Results for Configuration of Free Rocking, FP Isolator Type B with 0.12 Nominal Friction in Jensen 100% Motion: (a) FP Displacement Histories and Orbit at SW Corner, (b) Vertical Displacement at Spring-damper Unit at NE Corner	152
5-17	Comparison of Experimental and Analytical Results for Configuration of Limited Rocking, FP Isolator Type A with 0.20 Nominal Friction in El Centro 200% Motion: (a) 5%-damped Response Spectra at Frame NE Top Corner, (b) Acceleration Histories at Frame NE Top Corner	153

LIST OF FIGURES (cont'd)

FIGURE	TITLE	PAGE
5-18	Comparison of Experimental and Analytical Results for Configuration of Limited Rocking, FP Isolator Type A with 0.20 Nominal Friction in El Centro 200% Motion: (a) FP Displacement Histories and Orbit at SW Corner, (b) Vertical Displacement at Spring-damper Unit at NE Corner	154
5-19	Comparison of Experimental and Analytical Results for Configuration of Limited Rocking, FP Isolator Type A with 0.20 Nominal Friction in Pacoima 65% Motion: (a) 5%-damped Response Spectra at Frame NE Top Corner, (b) Acceleration Histories at Frame NE Top Corner	155
5-20	Comparison of Experimental and Analytical Results for Configuration of Limited Rocking, FP Isolator Type A with 0.20 Nominal Friction in Pacoima 65% Motion: (a) FP Displacement Histories and Orbit at SW Corner, (b) Vertical Displacement at Spring-damper Unit at NE Corner	156
5-21	Comparison of Experimental and Analytical Results for Configuration of Limited Rocking, FP Isolator Type A with 0.20 Nominal Friction in Chile 100% Motion: (a) 5%-damped Response Spectra at Frame NE Top Corner, (b) Acceleration Histories at Frame NE Top Corner	157
5-22	Comparison of Experimental and Analytical Results for Configuration of Limited Rocking, FP Isolator Type A with 0.20 Nominal Friction in Chile 100% Motion: (a) FP Displacement Histories and Orbit at SW Corner, (b) Vertical Displacement at Spring-damper Unit at NE Corner	158
5-23	Comparison of Experimental and Analytical Results for Configuration of Limited Rocking, FP Isolator Type A with 0.20 Nominal Friction in Taft 300% Motion: (a) 5%-damped Response Spectra at Frame NE Top Corner, (b) Acceleration Histories at Frame NE Top Corner	159
5-24	Comparison of Experimental and Analytical Results for Configuration of Limited Rocking, FP Isolator Type A with 0.20 Nominal Friction in Taft 300% Motion: (a) FP Displacement Histories and Orbit at SW Corner, (b) Vertical Displacement at Spring-damper Unit at NE Corner	160
5-25	Comparison of Experimental and Analytical Results for Configuration of Limited Rocking, FP Isolator Type A with 0.20 Nominal Friction in Kobe 50% Motion: (a) 5%-damped Response Spectra at Frame NE Top Corner, (b) Acceleration Histories at Frame NE Top Corner	161
5-26	Comparison of Experimental and Analytical Results for Configuration of Limited Rocking, FP Isolator Type A with 0.20 Nominal Friction in Kobe 50% Motion: (a) FP Displacement Histories and Orbit at SW Corner, (b) Vertical Displacement at Spring-damper Unit at NE Corner	162

LIST OF FIGURES (cont'd)

FIGURE	TITLE	PAGE
5-27	Comparison of Experimental and Analytical Results for Configuration of Limited Rocking, FP Isolator Type B with 0.12 Nominal Friction in El Centro 250% Motion: (a) 5%-damped Response Spectra at Frame NE Top Corner, (b) Acceleration Histories at Frame NE Top Corner	163
5-28	Comparison of Experimental and Analytical Results for Configuration of Limited Rocking, FP Isolator Type B with 0.12 Nominal Friction in El Centro 250% Motion: (a) FP Displacement Histories and Orbit at SW Corner, (b) Vertical Displacement at Spring-damper Unit at NE Corner	164
5-29	Comparison of Experimental and Analytical Results for Configuration of Limited Rocking, FP Isolator Type B with 0.12 Nominal Friction in Pacoima 75% Motion: (a) 5%-damped Response Spectra at Frame NE Top Corner, (b) Acceleration Histories at Frame NE Top Corner	165
5-30	Comparison of Experimental and Analytical Results for Configuration of Limited Rocking, FP Isolator Type B with 0.12 Nominal Friction in Pacoima 75% Motion: (a) FP Displacement Histories and Orbit at SW Corner, (b) Vertical Displacement at Spring-damper Unit at NE Corner	166
5-31	Comparison of Experimental and Analytical Results for Configuration of Limited Rocking, FP Isolator Type B with 0.12 Nominal Friction in Chile 100% Motion: (a) 5%-damped Response Spectra at Frame NE Top Corner, (b) Acceleration Histories at Frame NE Top Corner	167
5-32	Comparison of Experimental and Analytical Results for Configuration of Limited Rocking, FP Isolator Type B with 0.12 Nominal Friction in Chile 100% Motion: (a) FP Displacement Histories and Orbit at SW Corner, (b) Vertical Displacement at Spring-damper Unit at NE Corner	168
5-33	Comparison of Experimental and Analytical Results for Configuration of Limited Rocking, FP Isolator Type B with 0.12 Nominal Friction in Taft 400% Motion: (a) 5%-damped Response Spectra at Frame NE Top Corner, (b) Acceleration Histories at Frame NE Top Corner	169
5-34	Comparison of Experimental and Analytical Results for Configuration of Limited Rocking, FP Isolator Type B with 0.12 Nominal Friction in Taft 400% Motion: (a) FP Displacement Histories and Orbit at SW Corner, (b) Vertical Displacement at Spring-damper Unit at NE Corner	170
5-35	Comparison of Experimental and Analytical Results for Configuration of Limited Rocking, FP Isolator Type B with 0.12 Nominal Friction in Kobe 65% Motion: (a) 5%-damped Response Spectra at Frame NE Top Corner, (b) Acceleration Histories at Frame NE Top Corner	171

LIST OF FIGURES (cont'd)

FIGURE	TITLE	PAGE
5-36	Comparison of Experimental and Analytical Results for Configuration of Limited Rocking, FP Isolator Type B with 0.12 Nominal Friction in Kobe 65% Motion: (a) FP Displacement Histories and Orbit at SW Corner, (b) Vertical Displacement at Spring-damper Unit at NE Corner	172
5-37	Comparison of Experimental and Analytical Results for Configuration of Limited Rocking, FP Isolator Type B with 0.12 Nominal Friction in Jensen 85% Motion: (a) 5%-damped Response Spectra at Frame NE Top Corner, (b) Acceleration Histories at Frame NE Top Corner	173
5-38	Comparison of Experimental and Analytical Results for Configuration of Limited Rocking, FP Isolator Type B with 0.12 Nominal Friction in Jensen 85% Motion: (a) FP Displacement Histories and Orbit at SW Corner, (b) Vertical Displacement at Spring-damper Unit at NE Corner	174
5-39	Comparison of Experimental and Analytical Results for Configuration of Limited Rocking, FP Isolator Type A with 0.07 Nominal Friction in El Centro 250% Motion: (a) 5%-damped Response Spectra at Frame NE Top Corner, (b) Acceleration Histories at Frame NE Top Corner	175
5-40	Comparison of Experimental and Analytical Results for Configuration of Limited Rocking, FP Isolator Type A with 0.07 Nominal Friction in El Centro 250% Motion: (a) FP Displacement Histories and Orbit at SW Corner, (b) Vertical Displacement at Spring-damper Unit at NE Corner	176
5-41	Comparison of Experimental and Analytical Results for Configuration of Limited Rocking, FP Isolator Type A with 0.07 Nominal Friction in Pacoima 65% Motion: (a) 5%-damped Response Spectra at Frame NE Top Corner, (b) Acceleration Histories at Frame NE Top Corner	177
5-42	Comparison of Experimental and Analytical Results for Configuration of Limited Rocking, FP Isolator Type A with 0.07 Nominal Friction in Pacoima 65% Motion: (a) FP Displacement Histories and Orbit at SW Corner, (b) Vertical Displacement at Spring-damper Unit at NE Corner	178
5-43	Comparison of Experimental and Analytical Results for Configuration of Limited Rocking, FP Isolator Type A with 0.07 Nominal Friction in Chile 100% Motion: (a) 5%-damped Response Spectra at Frame NE Top Corner, (b) Acceleration Histories at Frame NE Top Corner	179
5-44	Comparison of Experimental and Analytical Results for Configuration of Limited Rocking, FP Isolator Type A with 0.07 Nominal Friction in Chile 100% Motion: (a) FP Displacement Histories and Orbit at SW Corner, (b) Vertical Displacement at Spring-damper Unit at NE Corner	180

LIST OF FIGURES (cont'd)

FIGURE	TITLE	PAGE
5-45	Comparison of Experimental and Analytical Results for Configuration of Limited Rocking, FP Isolator Type A with 0.07 Nominal Friction in Taft 400% Motion: (a) 5%-damped Response Spectra at Frame NE Top Corner, (b) Acceleration Histories at Frame NE Top Corner	181
5-46	Comparison of Experimental and Analytical Results for Configuration of Limited Rocking, FP Isolator Type A with 0.07 Nominal Friction in Taft 400% Motion: (a) FP Displacement Histories and Orbit at SW Corner, (b) Vertical Displacement at Spring-damper Unit at NE Corner	182
5-47	Comparison of Experimental and Analytical Results for Configuration of Limited Rocking, FP Isolator Type A with 0.07 Nominal Friction in Kobe 65% Motion: (a) 5%-damped Response Spectra at Frame NE Top Corner, (b) Acceleration Histories at Frame NE Top Corner	183
5-48	Comparison of Experimental and Analytical Results for Configuration of Limited Rocking, FP Isolator Type A with 0.07 Nominal Friction in Kobe 65% Motion: (a) FP Displacement Histories and Orbit at SW Corner, (b) Vertical Displacement at Spring-damper Unit at NE Corner	184
5-49	Comparison of Experimental and Analytical Results for Configuration of Limited Rocking, FP Isolator Type A with 0.07 Nominal Friction in Jensen 50% Motion: (a) 5%-damped Response Spectra at Frame NE Top Corner, (b) Acceleration Histories at Frame NE Top Corner	185
5-50	Comparison of Experimental and Analytical Results for Configuration of Limited Rocking, FP Isolator Type A with 0.07 Nominal Friction in Jensen 50% Motion: (a) FP Displacement Histories and Orbit at SW Corner, (b) Vertical Displacement at Spring-damper Unit at NE Corner	186
5-51	Experimental Acceleration Histories at Bushing Top and Frame Top NE Corner in Horizontal EW and Vertical Directions for Configuration of Free Rocking, FP Isolator Type B with 0.12 Nominal Friction in El Centro 250% Motion	189
5-52	Comparison of Experimental and Analytical Results of Acceleration Histories at Bushing Top with and without Consideration of Rocking Shake Table Motion in Configuration of Free Rocking, FP Isolator Type B with 0.12 Nominal Friction in El Centro 250% Motion	190
5-53	Comparison of Experimental and Analytical Results of Acceleration Histories at Bushing Top with and without Consideration of Rocking Shake Table Motion in Configuration of Free Rocking, FP Isolator Type B with 0.12 Nominal Friction in Pacoima 60% Motion	191

LIST OF FIGURES (cont'd)

FIGURE	TITLE	PAGE
5-54	Comparison of Experimental and Analytical Results of Acceleration Histories at Bushing Top with and without Consideration of Rocking Shake Table Motion in Configuration of Free Rocking, FP Isolator Type B with 0.12 Nominal Friction in Chile 100% Motion	192
5-55	Comparison of Experimental and Analytical Results of Acceleration Histories at Bushing Top with and without Consideration of Rocking Shake Table Motion in Configuration of Free Rocking, FP Isolator Type B with 0.12 Nominal Friction in Taft 400% Motion	193
5-56	Comparison of Experimental and Analytical Results of Acceleration Histories at Bushing Top with and without Consideration of Rocking Shake Table Motion in Configuration of Free Rocking, FP Isolator Type B with 0.12 Nominal Friction in Kobe 50% Motion	194
5-57	Comparison of Experimental and Analytical Results of Acceleration Histories at Bushing Top with and without Consideration of Rocking Shake Table Motion in Configuration of Free Rocking, FP Isolator Type B with 0.12 Nominal Friction in Jensen 100% Motion	195
5-58	Comparison of Experimental and Analytical Results of Acceleration Histories at Bushing Top with and without Consideration of Rocking Shake Table Motion in Configuration of Limited Rocking, FP Isolator Type B with 0.12 Nominal Friction in El Centro 250% Motion	196
5-59	Comparison of Experimental and Analytical Results of Acceleration Histories at Bushing Top with and without Consideration of Rocking Shake Table Motion in Configuration of Limited Rocking, FP Isolator Type B with 0.12 Nominal Friction in Pacoima 75% Motion	197
5-60	Comparison of Experimental and Analytical Results of Acceleration Histories at Bushing Top with and without Consideration of Rocking Shake Table Motion in Configuration of Limited Rocking, FP Isolator Type B with 0.12 Nominal Friction in Chile 100% Motion	198
5-61	Comparison of Experimental and Analytical Results of Acceleration Histories at Bushing Top with and without Consideration of Rocking Shake Table Motion in Configuration of Limited Rocking, FP Isolator Type B with 0.12 Nominal Friction in Taft 400% Motion	199
5-62	Comparison of Experimental and Analytical Results of Acceleration Histories at Bushing Top with and without Consideration of Rocking Shake Table Motion in Configuration of Limited Rocking, FP Isolator Type B with 0.12 Nominal Friction in Kobe 65% Motion	200

LIST OF FIGURES (cont'd)

FIGURE	TITLE	PAGE
5-63	Comparison of Experimental and Analytical Results of Acceleration Histories at Bushing Top with and without Consideration of Rocking Shake Table Motion in Configuration of Limited Rocking, FP Isolator Type B with 0.12 Nominal Friction in Jensen 85% Motion	201
5-64	Analytical Model of Tested Model in Configuration of Free Rocking with Spring-Damper Unit Friction Included	203
5-65	Comparison of Experimental and Analytical 5%-damped Response Spectra at Frame NE Top Corner With and Without Due Consideration for Friction Forces in Spring-damper Units in Configuration of Free Rocking, FP Isolator Type B with 0.12 Nominal Friction in El Centro 250% Motion	204
5-66	Comparison of Experimental and Analytical Acceleration Histories at Frame NE Top Corner With and Without Due Consideration for Friction Forces in Spring-damper Units in Configuration of Free Rocking, FP Isolator Type B with 0.12 Nominal Friction in El Centro 250% Motion	205
5-67	Comparison of Experimental and Analytical Isolator Displacement Histories With and Without Due Consideration for Friction Forces in Spring-damper Units in Configuration of Free Rocking, FP Isolator Type B with 0.12 Nominal Friction in El Centro 250% Motion	206
5-68	Comparison of Experimental and Analytical 5%-damped Response Spectra at Frame NE Top Corner With and Without Due Consideration for Friction Forces in Spring-damper Units in Configuration of Free Rocking, FP Isolator Type B with 0.12 Nominal Friction in Pacoima 60% Motion	207
5-69	Comparison of Experimental and Analytical Acceleration Histories at Frame NE Top Corner With and Without Due Consideration for Friction Forces in Spring-damper Units in Configuration of Free Rocking, FP Isolator Type B with 0.12 Nominal Friction in Pacoima 60% Motion	208
5-70	Comparison of Experimental and Analytical Isolator Displacement Histories With and Without Due Consideration for Friction Forces in Spring-damper Units in Configuration of Free Rocking, FP Isolator Type B with 0.12 Nominal Friction in Pacoima 60% Motion	209
5-71	Comparison of Experimental and Analytical 5%-damped Response Spectra at Frame NE Top Corner With and Without Due Consideration for Friction Forces in Spring-damper Units in Configuration of Free Rocking, FP Isolator Type B with 0.12 Nominal Friction in Chile 100% Motion	210

LIST OF FIGURES (cont'd)

FIGURE	TITLE	PAGE
5-72	Comparison of Experimental and Analytical Acceleration Histories at Frame NE Top Corner With and Without Due Consideration for Friction Forces in Spring-damper Units in Configuration of Free Rocking, FP Isolator Type B with 0.12 Nominal Friction in Chile 100% Motion	211
5-73	Comparison of Experimental and Analytical Isolator Displacement Histories With and Without Due Consideration for Friction Forces in Spring-damper Units in Configuration of Free Rocking, FP Isolator Type B with 0.12 Nominal Friction in Chile 100% Motion	212
5-74	Comparison of Experimental and Analytical 5%-damped Response Spectra at Frame NE Top Corner With and Without Due Consideration for Friction Forces in Spring-damper Units in Configuration of Free Rocking, FP Isolator Type B with 0.12 Nominal Friction in Taft 400% Motion	213
5-75	Comparison of Experimental and Analytical Acceleration Histories at Frame NE Top Corner With and Without Due Consideration for Friction Forces in Spring-damper Units in Configuration of Free Rocking, FP Isolator Type B with 0.12 Nominal Friction in Taft 400% Motion	214
5-76	Comparison of Experimental and Analytical Isolator Displacement Histories With and Without Due Consideration for Friction Forces in Spring-damper Units in Configuration of Free Rocking, FP Isolator Type B with 0.12 Nominal Friction in Taft 400% Motion	215
5-77	Comparison of Experimental and Analytical 5%-damped Response Spectra at Frame NE Top Corner With and Without Due Consideration for Friction Forces in Spring-damper Units in Configuration of Free Rocking, FP Isolator Type B with 0.12 Nominal Friction in Kobe 50% Motion	216
5-78	Comparison of Experimental and Analytical Acceleration Histories at Frame NE Top Corner With and Without Due Consideration for Friction Forces in Spring-damper Units in Configuration of Free Rocking, FP Isolator Type B with 0.12 Nominal Friction in Kobe 50% Motion	217
5-79	Comparison of Experimental and Analytical Isolator Displacement Histories With and Without Due Consideration for Friction Forces in Spring-damper Units in Configuration of Free Rocking, FP Isolator Type B with 0.12 Nominal Friction in Kobe 50% Motion	218
5-80	Comparison of Experimental and Analytical 5%-damped Response Spectra at Frame NE Top Corner With and Without Due Consideration for Friction Forces in Spring-damper Units in Configuration of Free Rocking, FP Isolator Type B with 0.12 Nominal Friction in Jensen 100% Motion	219

LIST OF FIGURES (cont'd)

FIGURE	TITLE	PAGE
5-81	Comparison of Experimental and Analytical Acceleration Histories at Frame NE Top Corner With and Without Due Consideration for Friction Forces in Spring-damper Units in Configuration of Free Rocking, FP Isolator Type B with 0.12 Nominal Friction in Jensen 100% Motion	220
5-82	Comparison of Experimental and Analytical Isolator Displacement Histories With and Without Due Consideration for Friction Forces in Spring-damper Units in Configuration of Free Rocking, FP Isolator Type B with 0.12 Nominal Friction in Jensen 100% Motion	221
5-83	Comparison of Experimental and Analytical 5%-damped Response Spectra at Frame NE Top Corner With and Without Due Consideration for Friction Forces in Spring-damper Units in Configuration of Limited Rocking, FP Isolator Type B with 0.12 Nominal Friction in El Centro 250% Motion	222
5-84	Comparison of Experimental and Analytical Acceleration Histories at Frame NE Top Corner With and Without Due Consideration for Friction Forces in Spring-damper Units in Configuration of Limited Rocking, FP Isolator Type B with 0.12 Nominal Friction in El Centro 250% Motion	223
5-85	Comparison of Experimental and Analytical Isolator Displacement Histories With and Without Due Consideration for Friction Forces in Spring-damper Units in Configuration of Limited Rocking, FP Isolator Type B with 0.12 Nominal Friction in El Centro 250% Motion	224
5-86	Comparison of Experimental and Analytical 5%-damped Response Spectra at Frame NE Top Corner With and Without Due Consideration for Friction Forces in Spring-damper Units in Configuration of Limited Rocking, FP Isolator Type B with 0.12 Nominal Friction in Pacoima 75% Motion	225
5-87	Comparison of Experimental and Analytical Acceleration Histories at Frame NE Top Corner With and Without Due Consideration for Friction Forces in Spring-damper Units in Configuration of Limited Rocking, FP Isolator Type B with 0.12 Nominal Friction in Pacoima 75% Motion	226
5-88	Comparison of Experimental and Analytical Isolator Displacement Histories With and Without Due Consideration for Friction Forces in Spring-damper Units in Configuration of Limited Rocking, FP Isolator Type B with 0.12 Nominal Friction in Pacoima 75% Motion	227
5-89	Comparison of Experimental and Analytical 5%-damped Response Spectra at Frame NE Top Corner With and Without Due Consideration for Friction Forces in Spring-damper Units in Configuration of Limited Rocking, FP Isolator Type B with 0.12 Nominal Friction in Chile 100% Motion	228

LIST OF FIGURES (cont'd)

FIGURE	TITLE	PAGE
5-90	Comparison of Experimental and Analytical Acceleration Histories at Frame NE Top Corner With and Without Due Consideration for Friction Forces in Spring-damper Units in Configuration of Limited Rocking, FP Isolator Type B with 0.12 Nominal Friction in Chile 100% Motion	229
5-91	Comparison of Experimental and Analytical Isolator Displacement Histories With and Without Due Consideration for Friction Forces in Spring-damper Units in Configuration of Limited Rocking, FP Isolator Type B with 0.12 Nominal Friction in Chile 100% Motion	230
5-92	Comparison of Experimental and Analytical 5%-damped Response Spectra at Frame NE Top Corner With and Without Due Consideration for Friction Forces in Spring-damper Units in Configuration of Limited Rocking, FP Isolator Type B with 0.12 Nominal Friction in Taft 400% Motion	231
5-93	Comparison of Experimental and Analytical Acceleration Histories at Frame NE Top Corner With and Without Due Consideration for Friction Forces in Spring-damper Units in Configuration of Limited Rocking, FP Isolator Type B with 0.12 Nominal Friction in Taft 400% Motion	232
5-94	Comparison of Experimental and Analytical Isolator Displacement Histories With and Without Due Consideration for Friction Forces in Spring-damper Units in Configuration of Limited Rocking, FP Isolator Type B with 0.12 Nominal Friction in Taft 400% Motion	233
5-95	Comparison of Experimental and Analytical 5%-damped Response Spectra at Frame NE Top Corner With and Without Due Consideration for Friction Forces in Spring-damper Units in Configuration of Limited Rocking, FP Isolator Type B with 0.12 Nominal Friction in Kobe 65% Motion	234
5-96	Comparison of Experimental and Analytical Acceleration Histories at Frame NE Top Corner With and Without Due Consideration for Friction Forces in Spring-damper Units in Configuration of Limited Rocking, FP Isolator Type B with 0.12 Nominal Friction in Kobe 65% Motion	235
5-97	Comparison of Experimental and Analytical Isolator Displacement Histories With and Without Due Consideration for Friction Forces in Spring-damper Units in Configuration of Limited Rocking, FP Isolator Type B with 0.12 Nominal Friction in Kobe 65% Motion	236
5-98	Comparison of Experimental and Analytical 5%-damped Response Spectra at Frame NE Top Corner With and Without Due Consideration for Friction Forces in Spring-damper Units in Configuration of Limited Rocking, FP Isolator Type B with 0.12 Nominal Friction in Jensen 85% Motion	237

LIST OF FIGURES (cont'd)

FIGURE	TITLE	PAGE
5-99	Comparison of Experimental and Analytical Acceleration Histories at Frame NE Top Corner With and Without Due Consideration for Friction Forces in Spring-damper Units in Configuration of Limited Rocking, FP Isolator Type B with 0.12 Nominal Friction in Jensen 85% Motion	238
5-100	Comparison of Experimental and Analytical Isolator Displacement Histories With and Without Due Consideration for Friction Forces in Spring-damper Units in Configuration of Limited Rocking, FP Isolator Type B with 0.12 Nominal Friction in Jensen 85% Motion	239
6-1	Target UHS Spectrum (2475 year return period) and MCE_R Spectra for Site	243
6-2	5%-damped Horizontal Resultant Spectra (RotD50) of 11 Scaled Motions and Average and Target Spectra	246
6-3	5%-damped Vertical Spectra of 11 Scaled Motions and Average Spectrum	246
6-4	Longitudinal and Transverse Sections of Example Transformer	247
6-5	Longitudinal and Transverse Direction Sections of Seismically Isolated Transformer with Free Rocking	248
6-6	Three-dimensional Schematic of Foundation	249
6-7	Foundation and Isolation System Sections of System with Free Rocking	250
6-8	Foundation and Isolation System Sections of System with Restrained Rocking	251
6-9	Section of Triple Friction Pendulum Isolator	252
6-10	Force-displacement Relations of Triple FP isolators	253
6-11	Schematic of Vertical Spring-Damper Unit	254
6-12	Model of Isolated Transformer (Free to Rock) Used in Response History Analysis	257
6-13	Two-dimensional Representations of Isolated Transformer (Free to Rock) in (a) Longitudinal/vertical Plane and (b) Transverse/vertical Plane	258
6-14	Distribution of Mass in Simplified Model of Isolated Transformer (Free to Rock)	259
6-15	5%-Damped Response Spectra of Acceleration at CM of Transformer for Lower Bound Friction in 100% Intensity Motion	269
6-16	5%-Damped Response Spectra of Acceleration at CM of Transformer for Lower Bound Friction in 150% Intensity Motion	270
6-17	5%-Damped Response Spectra of Acceleration at CM of Transformer for Upper Bound Friction in 100% Intensity Motion	271
6-18	5%-Damped Response Spectra of Acceleration at CM of Transformer for Upper Bound Friction in 150% Intensity Motion	272

LIST OF FIGURES (cont'd)

FIGURE	TITLE	PAGE
6-19	Peak Acceleration at CM of Bushing in 3D Isolation System with Restrained Rocking in Motion Valparaiso (100%) as Function of Base Moment of Inertia	273
A-1	Two-dimensional Representation of Spring-Damper Isolated Transformer in (a) Longitudinal (1-2)-Vertical Plane and (b) Transverse (3-4)-Vertical Plane	286
A-2	Damper Installation Angles	287
B-1	Section of Triple FP Isolator	292
B-2	Force-Displacement Loops of Triple FP Isolator for Lower and Upper Friction Conditions	293
C-1	Two-dimensional Representation of Triple FP and Spring-Damper Isolated Transformer in (a) Longitudinal (1-2) and (b) Transverse (3-4) Directions	298
E-1	(a) Displacement History and (b) Force-Displacement Loops of Spring-Damper Units in Test at Peak Velocity of 0.03in/sec (frequency of 0.005Hz)	316
E-2	(a) Displacement History and (b) Force-Displacement Loops of Spring-Damper Units in Test at Peak Velocity of 3.14in/sec (frequency of 0.5Hz)	317
E-3	(a) Displacement History and (b) Force-Displacement Loops of Spring-Damper Units in Test at Peak Velocity of 6.28in/sec (frequency of 1.0Hz)	318
E-4	Experimental and Analytical Normalized Force-Displacement Loops of Triple FP Isolator No.1 of Type A without Lubrication (nominal friction 0.20)	319
E-5	Experimental and Analytical Normalized Force-Displacement Loops of Triple FP Isolator No.2 of Type A without Lubrication (nominal friction 0.20)	320
E-6	Experimental and Analytical Normalized Force-Displacement Loops of Triple FP Isolator No.3 of Type A without Lubrication (nominal friction 0.20)	321
E-7	Experimental and Analytical Normalized Force-Displacement Loops of Triple FP Isolator No.4 of Type A without Lubrication (nominal friction 0.20)	322
E-8	Experimental and Analytical Normalized Force-Displacement Loops of Triple FP Isolator No. 2 of Type B (nominal friction 0.12)	323
E-9	Experimental and Analytical Normalized Force-Displacement Loops of Triple FP Isolator No. 2 of Type A with Lubrication (nominal friction 0.07)	324

LIST OF TABLES

TABLE	TITLE	PAGE
1-1	Proposed 3D Seismic Isolation Systems for FBR Nuclear Power Plants (Inoue K. et al., 2004)	7
2-1	Characteristics of Bushings (Kitayama et al, 2016)	17
2-2	Lumped Mass Distribution Cases Considered in Study	27
2-3	Frequencies, Damping Ratio and Mode Shapes of Transformer with 3D Spring-Damper Isolation System (vertical and longitudinal direction model)	28
2-4	Frequencies, Damping Ratio and Mode Shapes of Transformer with 3D Spring-Damper Isolation System (vertical and transverse direction model)	28
2-5	Properties of Triple FP Isolator Used in Analytical Study	30
2-6	Frequencies, Damping Ratio and Mode Shapes of Transformer with 3D Triple FP and Spring-Damper Isolation System (Case 1 Mass Distribution)	31
2-7	Frequencies, Damping Ratio and Mode Shapes of Transformer with 3D Triple FP and Spring-Damper Isolation System (Case 2 Mass Distribution)	32
2-8	Motions used in Response History Analysis and Characteristics as Recorded	33
2-9	Peak Acceleration Values for 3D Isolated and Non-isolated Transformer (in g)	51
2-10	Effect of Vertical Damping on Peak Acceleration Values for 3D FP-Spring-Damper System in Pacoima Motion	52
2-11	Peak Dynamic Displacement Values for 3D Isolated and Non-isolated Transformer (in inch)	53
2-12	Peak Vertical Acceleration Values (in g) Non-isolated 418kip Transformer, 2D Isolated Transformer with Triple FP System and 3D Isolated Transformer with Triple FP and Spring-Damper System of $f_v=2.0\text{Hz}$ and $\beta_v=0.50$	57
2-13	Properties of Analyzed Transformers with 3D FP-spring-damper Isolation System	58
2-14	Displacement Demands at Bushing Top, FP Isolators, and Spring-Damper Units for System with $K=44\text{ kip/in}$ and $C=3.4\text{kip-s/in}$ (HRES: resultant horizontal displacement)	60
2-15	Peak Displacements and Forces in Spring-Damper Units for System with $K=44\text{ kip/in}$ and $C=3.4\text{kip-s/in}$ in Upper Bound Friction Case	61
2-16	Design Parameters for Vertical Isolation System Unit	62

LIST OF TABLES (cont'd)

TABLE	TITLE	PAGE
3-1	Design Parameters for Spring-Damper Unit for Shake Table Testing	73
3-2	List of Instruments used in Identification and Seismic Tests of Model on Shake Table	94
4-1	Characteristics of Earthquake Motions Used in Shake Table Testing at 100% Level	100
4-2	Test Matrix	104
4-3	List of Additional Instruments Used in Testing of Configuration with Limited Rocking	106
4-4	Recorded Values of Peak Acceleration of Tested Systems	121
4-5	Recorded Values of Peak Isolator Displacement of Tested Systems	122
4-6	Recorded Values of Peak Model Angle of Rotation of Tested Systems	123
4-7	Calculated Frequencies of Model of Configurations with Free Rocking and Limited Rocking in Program SAP2000	125
5-1	Triple FP Isolator Parallel Model Parameters in Program SAP2000	138
5-2	Calculated Frequencies of Model and Assigned Damping Ratio	139
5-3	Tests for which Experimental Results are Compared to Analytical Results	140
6-1	Spectral Parameters for Site	243
6-2	Characteristics of Selected Motions and Scale Factors	245
6-3	Properties of Triple FP Isolator Assumed in Analysis	252
6-4	Response and Design Parameters for Spring-Damper Units (two values apply for earthquake motions scaled by factors of 100% and 150%)	255
6-5	Frequencies, Damping Ratio and Mode Shapes of the Example Transformer with Isolation System that is Free to Rock	259
6-6	FP Isolator Peak Resultant Horizontal Displacement (in inch)	263
6-7	Transformer Peak Accelerations at CM of Transformer (in g)	264
6-8	Bushing Peak Accelerations at CM of Bushing (in g)	265
6-9	Spring-damper System Peak Vertical Displacement, Velocity and Force for Lower Bound Friction	266
6-10	Spring-damper System Peak Vertical Displacement, Velocity and Force for Upper Bound Friction	267

LIST OF TABLES (cont'd)

TABLE	TITLE	PAGE
6-11	Bushing Top Peak Displacements (in inch)	268
A-1	Results of Eigenvalue Analysis of Isolated Transformer with Spring-Damper System in Mass Distribution Case 1	288
A-2	Frequencies and Images of Mode Shapes Obtained in Program SAP2000 for 3D Uniform Mass Model of Transformer with Spring-Damper Isolation System	289
B-1	Properties of Triple FP Isolator	292
B-2	Parameters of Parallel Model of Triple FP Isolator in Program SAP2000	294
C-1	Results of Eigenvalue Analysis of Isolated Transformer with Triple FP and Spring-Damper System in Mass Distribution Case 1	299

“This Page Intentionally Left Blank”

SECTION 1

INTRODUCTION

Seismic isolation systems developed and widely implemented provide only protection against the horizontal components of earthquake motion. The vertical ground motion is transmitted unchanged through or even magnified by the isolation system. Furthermore, the vertical ground motion may affect and cause reduction of the effectiveness of the isolation system in the horizontal direction. This behavior is illustrated in the figures below where spectra of recorded motion at the control point (connection of bushing to steel plate) are presented for the recent tests of a transformer model with full size Triple Friction Pendulum isolators and without isolation at the University at Buffalo (Oikonomou et al, 2016). Figure 1-1 compares vertical response spectra at a point on the transformer above the horizontal-only isolators when identical three component earthquake excitations were applied to the isolated and the non-isolated model (the spectra were obtained from the recorded acceleration histories). The spectra also show the design spectrum (IEEE, 2005) for the vertical direction. It is clear that there is no vertical isolation effect as the response spectra are about the same (or a little larger or a little smaller) for the isolated and the non-isolated models, with both being much higher than the design spectrum.

Figure 1-2 shows the horizontal response spectra at the control point for three-component seismic excitation. Evidently, the horizontal-only isolation system is very effective as the spectral accelerations of the isolated model are much less than those of the non-isolated model and fall well below the IEEE design spectrum.

The utility of a practical seismic isolation system that is effective in all three directions is evident in these results. Efforts to develop three-dimensional seismic isolation systems were hampered by the requirement to carry the weight of the isolated structure, to shift the vertical frequency to sufficiently low values and to have a compact system. Many of these efforts targeted floor systems in buildings where the Japanese construction industry developed and implemented a number of similar systems based on sliding isolators and vertical spring-damper systems carrying light loads and being of unclear performance. Yet a number of systems have been developed and are presented and critiqued in this document. All are implementable but they are characterized by either inefficiency or extreme complexity.

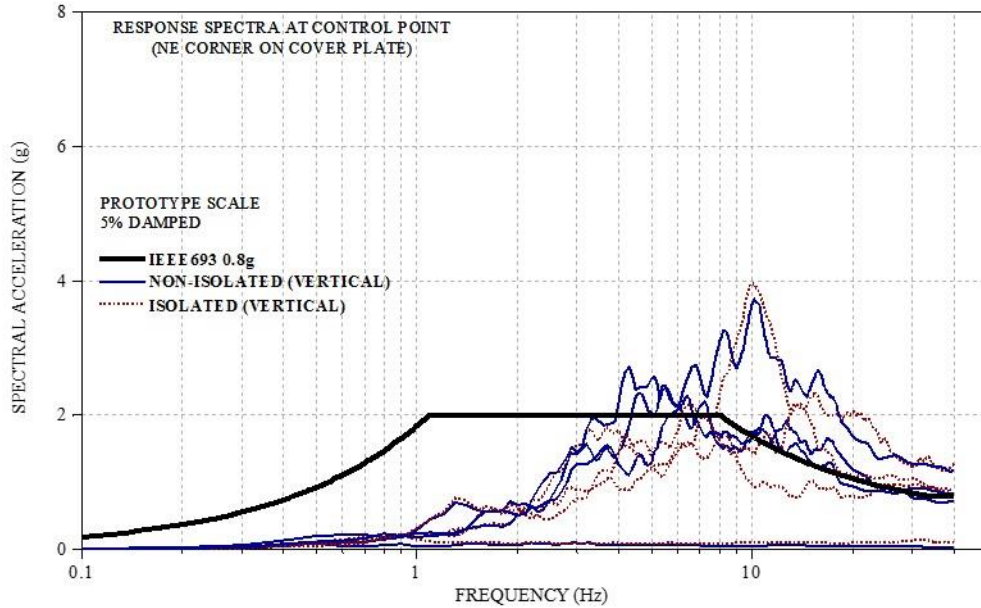


Figure 1-1 Vertical Response Spectra at Control Point of Non-isolated and Horizontally Isolated Electrical Transformer for Three-Component Excitation

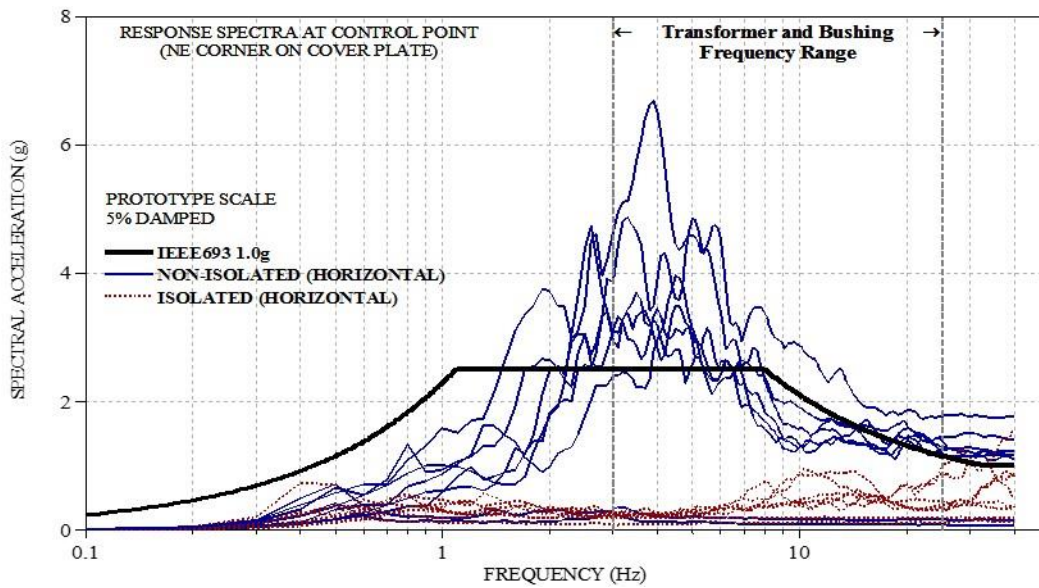


Figure 1-2 Horizontal Response Spectra (two directions) at Control Point of Non-isolated and Horizontally Isolated Electrical Transformer for Three-Component Excitation

Helical coil springs capable of deforming in all three directions, and when needed enhanced by viscous or viscoelastic devices, have been used as effective shock and vibration isolation systems for decades. In such applications where the dynamic excitation is of high frequency, the

isolation system is relatively stiff and static and dynamic displacements are very small, so that the system is easily implemented. The same type of system has been proposed and actually used in a small number of applications for the seismic protection of equipment and small residential buildings (houses). Makris and Constantinou (1992) experimentally and analytically investigated one such system consisting of helical springs and visco-elastic fluid dampers. The system operated primarily as a three dimensional damping system owing to the fact that the frequencies of the isolated structure could not be sufficiently low for effective seismic isolation. Specifically for the case of two residential buildings constructed in the Los Angeles at that time, the least frequency was 1.6Hz in the rocking mode and the corresponding damping ratio was 0.23. Analysis showed that there was some benefit provided by the system but the high frequencies and the resulting rocking response tended to magnify accelerations to values larger than the peak ground accelerations. This was later confirmed in recordings of the response of the buildings in the 1994 Northridge Earthquake (Makris and Deoskar, 1996). A study is presented later in this report that better exposes the limitations of such a system when used in the seismic isolation of electrical transformers.

The Japanese industry investigated three-dimensional seismic isolation systems for nearly 20 years. At around 2000, the Japan Energy Atomic Research Institute (JEARI) proposed two types of three-dimensional (3D) isolation systems for use in nuclear power structures. Both included a horizontal seismic isolation system consisting of either (a) flat rolling (ball) bearings with stiffness provided by springs and damping provided by fluid dampers or (b) elastomeric bearings. The vertical isolation system consisted of either coil or air springs together with viscous dampers (Tsutsumi et al., 2000 and 2001). Important characteristics of the systems are the separation of the vertical and horizontal isolation systems by the use of a very stiff base and the prevention of rocking by a variety of mechanisms. Figure 1-3 shows a model tested in Japan consisting of four air springs serving as the vertical isolation system and coil springs with rolling (ball) bearings serving as the horizontal isolation system. The coil springs were designed to provide a 1Hz horizontal frequency. In testing, the frequencies were determined to be 0.37Hz in a combined rocking/horizontal mode and 1.06Hz in the vertical direction. The system lacked any restraint against rotation although it included a complicated hydraulic leveling system for the rolling bearings. The vertical frequency f_v and the vertical static deflection δ_v are related through

$\delta_v = g / (4\pi^2 f_v^2)$ so that a frequency of 1.06Hz corresponds to a static deflection of 220mm, which is large. The complexity of the system, the use of unreliable components in the rolling bearings, air springs and hydraulic leveling systems, and the large static deflection makes this system unacceptable for the seismic isolation of electrical equipment.

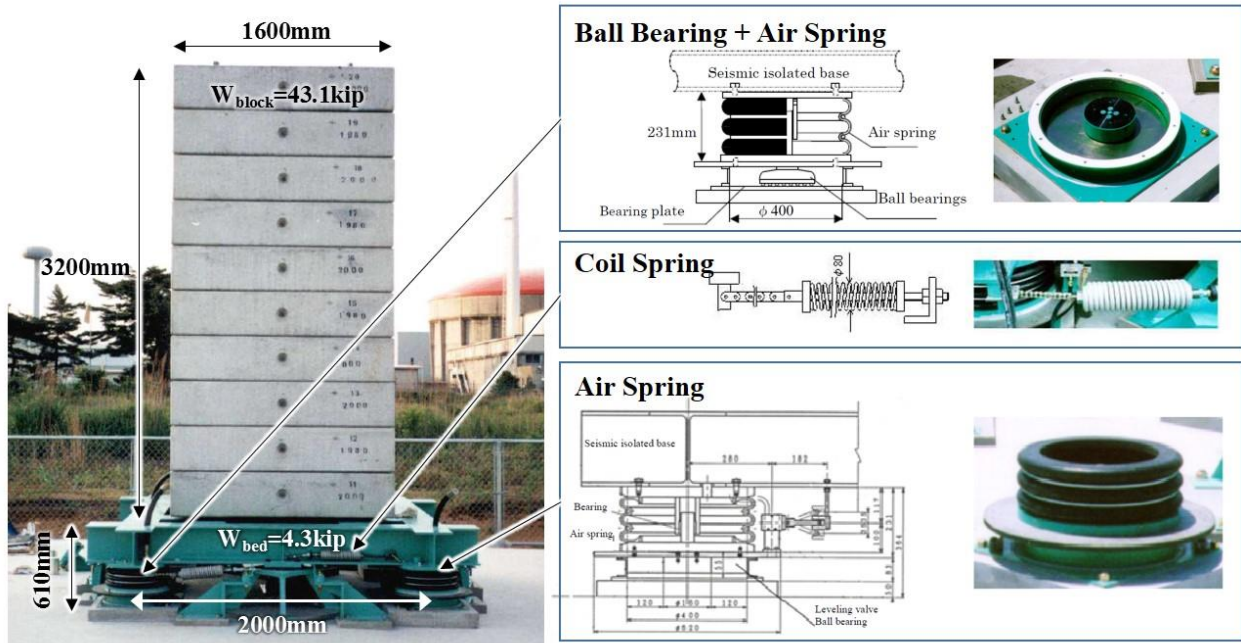


Figure 1-3 3D Seismic Isolation System Consisting of Air Spring Combined with Flat Rolling (Ball) Bearings and Coil Springs (Tsutsumi et al., 2000)

The second 3D isolation system is illustrated in Figure 1-4. This system consists of elastomeric isolators and fluid dampers for the horizontal isolation system and coil springs and dampers for the vertical isolation system. The two systems are separated by a stiff base and the vertical springs are guided so that rocking is minimized. In the model used in testing (Figure 1-4) multi-staged elastomeric bearings were used due to the light weight of the model. This is also the only option for use of elastomeric bearings in the isolation of equipment due to the light supported weight. For a nuclear structure application, single elastomeric bearings are to be used. Note the bent base frame separating the two systems which appears to be an attempt to reduce the height of the system and to lower the center of gravity. Testing of the model revealed the following

frequencies: (a) 0.45Hz in the horizontal direction, (b) 1.45Hz in a combined rocking/horizontal mode and (c) 2.0Hz in the vertical direction. This is a useful design that is similar in characteristics with the tested transformer isolation systems in this report. Nevertheless, the complexity and cost in the use of the combined multi-stage elastomeric bearings and dampers for horizontal isolation, use of a double base, and its height make the use of this system problematic in an electrical transformer application.

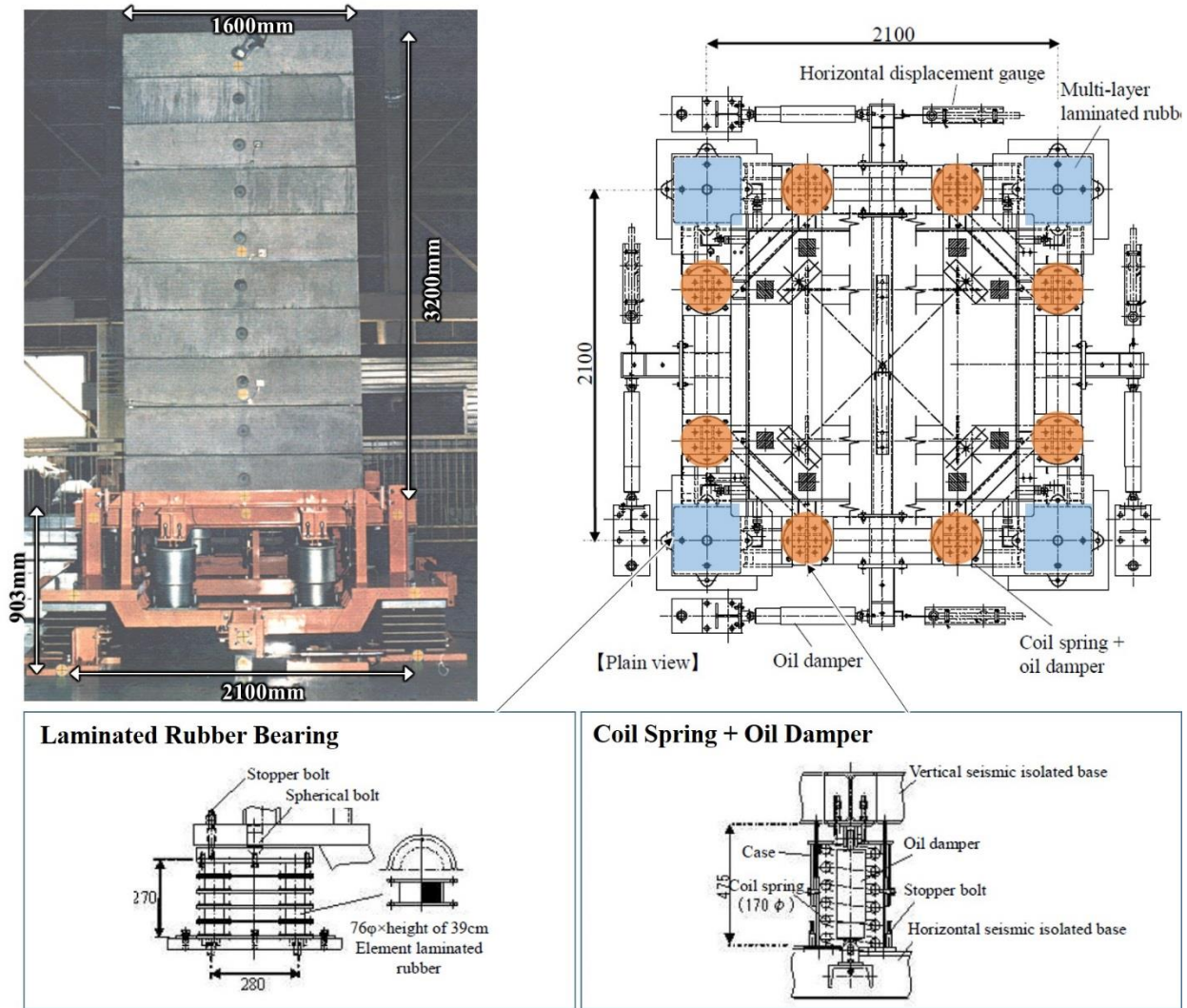


Figure 1-4 3D Seismic Isolation System Consisting of Multistage Elastomeric Bearings, Vertical Coil Springs and Horizontal and Vertical Dampers (Tsutsumi et al., 2001)

During a five year period starting in 2000, the Japanese industry concentrated on the development of 3D seismic isolation systems for use in the protection of Fast Breeder Nuclear

Reactors (FBR). The FBR design requires thin walls to reduce large thermal stresses in components, which contradicts the requirement for thick walls to resist large seismic loads (Inoue et al., 2004), so that seismic isolation was a necessity. The Ministry of Economy, Trade and Industry of Japan funded a research and development effort by the Japanese construction industry. Nine different 3D seismic isolation system concepts were proposed, six were selected for further evaluation and finally three were built and tested (Inoue et al., 2004). These systems are (a) Elastomeric Bearing-Air Spring System (Suhara et al., 2003, 2005), (b) Elastomeric Bearing-Hydraulic Spring System (Kashiwazaki et al., 2003), and (c) Reinforced Air Spring System (Kageyama et al., 2004). They are described in Table 1-1 and in the narrative below.

(a) Elastomeric Bearing-Air Spring System

The system consists of rolling (vertically) air springs as the vertical isolators and elastomeric bearings as the horizontal isolators, placed as shown in Table 1-1 with the elastomeric bearing on top of the rolling air spring. The vertical air spring device comprises of an air compartment to which the air pressure is maintained by a system of air tanks, piping and controls. The design vertical load per unit is 9.8MN and the vertical frequency is 0.5Hz with a corresponding damping ratio of 0.40. The static deflection for a system with a 0.5Hz frequency is about 1m, which is excessive. However, the height of the air spring is only 1.4m due to the fact that load will first be developed during construction while the system is unpressurized and then the system will be pressurized so that the static deflection will not materialize. To restrain rocking motion, a rocking suppression system was developed utilizing vertical oil dampers, accumulators and other hydraulic hardware. The oil dampers also provide viscous damping in the vertical direction. Note that the air springs are guided vertically by a rolling system which introduces friction. Testing of the system (Suhara et al., 2003) identified friction to be about 0.03 of the supported weight.

The type of elastomeric bearing used in this system is not clear. However, based on Japanese practice it could be (a) a high damping rubber bearing, (b) a low or high damping elastomeric bearing in combination with oil or steel dampers or (c) a lead-rubber bearing.

Table 1-1 Proposed 3D Seismic Isolation Systems for FBR Nuclear Power Plants (Inoue K. et al., 2004)

System	Developer	Configuration	Horizontal Isolation System	Vertical Isolation System	Rocking Suppression System	Vertical Frequency (Hz)/Damping Ratio	Horiz. Frequency (Hz)/Damping
Elastomeric Bearing-Air Spring System	Shimizu Corporation		Elastomeric bearings	Air springs and oil dampers	Hydraulic system with accumulators to control motion of oil dampers	0.50/40%	0.36/NA
Elastomeric Bearing-Hydraulic Spring System	Ishikawajima Harima Heavy Industries		Elastomeric high damping bearings	Oil spring/dampers with accumulators (with external orificing)	Hydraulic system to control motion of vertical spring damper	0.50/20%	0.54/16% (high damping rubber)
Reinforced Air Spring System	Obayashi Corporation		Horizontal/vertical air spring system and horizontal dampers	Horizontal/vertical air spring system and vertical dampers	Vertical oil dampers with wire cable control system	0.35/20%	0.27/20%

(b) Elastomeric Bearing-Hydraulic Spring System

The system consists of elastomeric high damping bearings for horizontal isolation, each of which is placed below a vertical oil spring and damper unit to provide the vertical flexibility and damping. The vertical units are guided to only move vertically. The vertical units utilize external accumulators to control the vertical stiffness together with external orificing to provide the damping. A separate hydraulic system is used to control rocking. The complexity of the rocking suppression system is evident in drawings of the system in Figure 1-5 (Kashiwazaki et al, 2003).

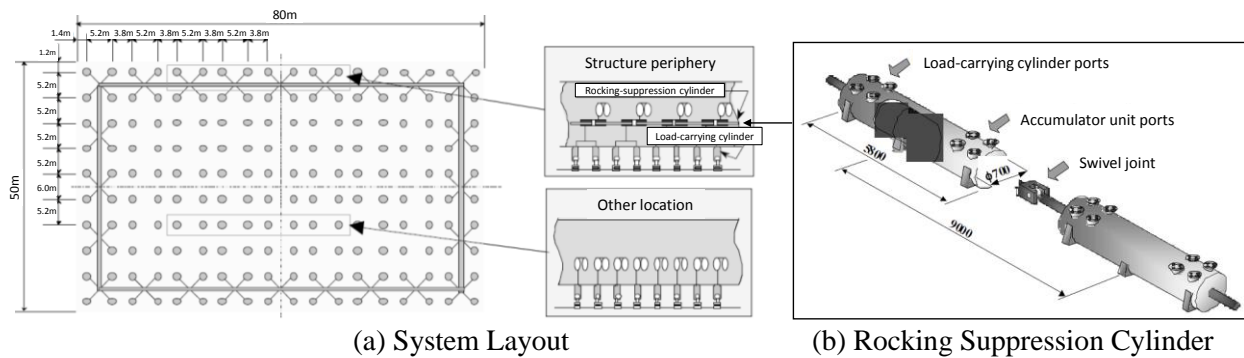


Figure 1-5 Rocking Suppression System used in 3D Elastomeric Bearing-Hydraulic Spring System (Kashiwazaki, 2003)

(c) Reinforced Air Spring System

The system consists of a three dimensional air spring capable of motion in all directions. The air is maintained in the system by a rubber/polyester sheet reinforced with cables. Damping is provided by vertical and horizontal oil dampers. The vertical oil dampers are provided with a cable control system to prevent rocking. The rocking prevention system is illustrated in Figure 1-6. An additional rocking prevention system was also proposed (Kageyama et al, 2003 and 2004).

The air spring unit is massive in size with about 10m diameter and 4m height to support a weight of up to 70MN and provide a vertical frequency of 0.35Hz and a horizontal frequency of 0.27Hz with damping ratio of 20% in both directions.

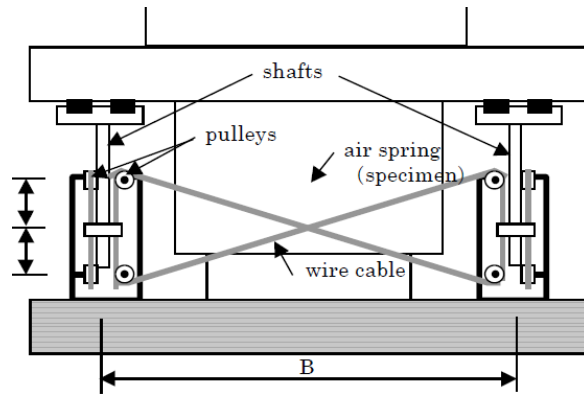


Figure 1-6 Rocking Prevention Device of Reinforced Air Spring System (Kageyama et al., 2003)

More recently, Shimizu Corporation in collaboration with Kozo Keikaku Engineering refined the Elastomeric Bearing-Air Spring System of Table 1-1 resulting in the horizontal-vertical isolation system illustrated in Figure 1-7 (Tomizawa et al, 2011; Mori et al., 2012). The system makes use of elastomeric bearings supported by a stiff base with vertical air springs below. A guiding system is used to transfer shear force and prevent the air springs from being subjected to lateral deformation. Vertical dampers that are hydraulically connected, per Figure 1-7, provide vertical damping and restrain rocking. Horizontal dampers are used to provide damping in the horizontal direction. The images in Figure 1-7 are of a small 3-story apartment building (total floor area about 550m²), called “Chisuikan” that was built with this system in 2011. Measurements of response of the building during the March 2011 Tohoku Earthquake showed that the vertical frequency was 0.77Hz and the horizontal frequency was 0.43Hz. The excitation was not strong (PGA of about 0.1g) and the recorded roof horizontal accelerations were essentially the same as those of the ground. The recorded vertical accelerations in the building were 0.034g for a ground vertical acceleration of 0.046g.

The complexities and potential costs of these systems are apparent. Moreover, the use of air or fluid to support the weight, the use of accumulators, hydraulic piping and valves makes the entire system unreliable and in need of continued maintenance. They are certainly unacceptable for use in electrical transformers where simplicity, reliability, lack of or minimum maintenance requirements and cost are the most important considerations.

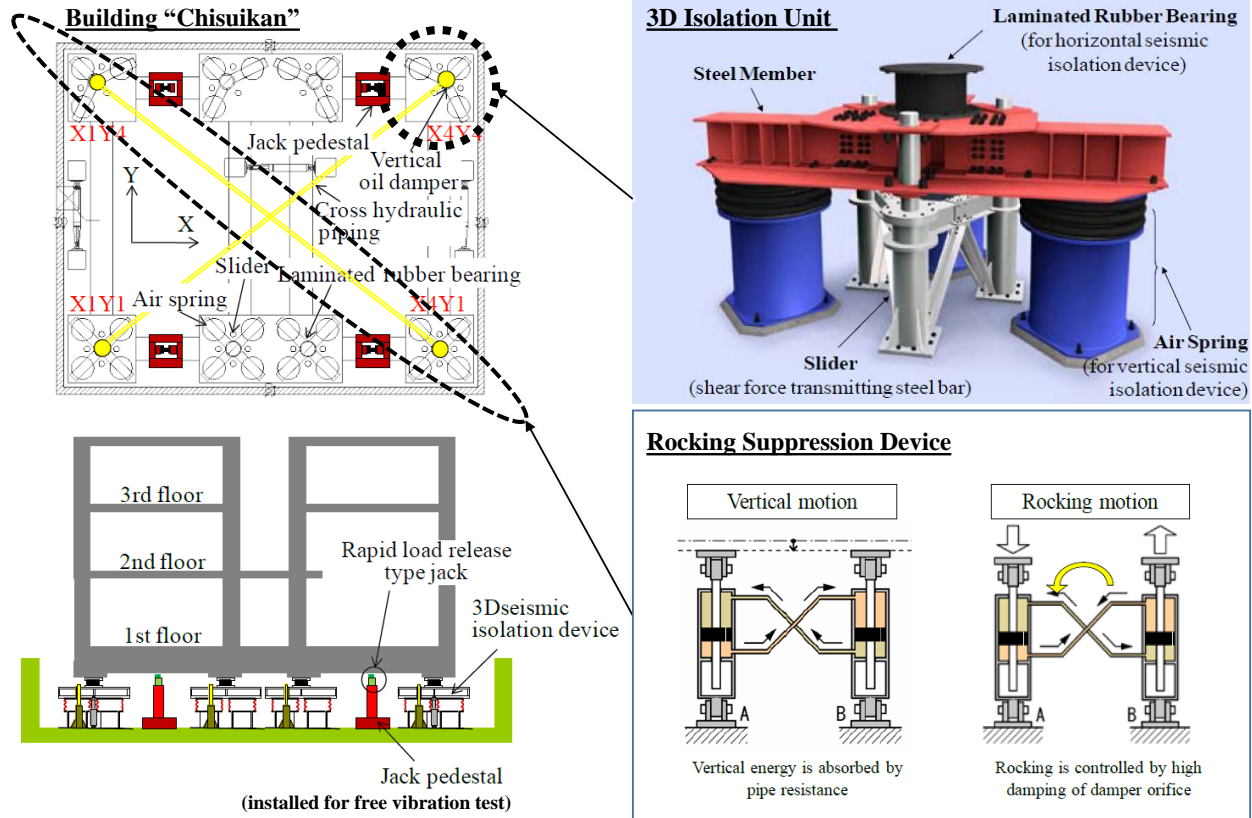


Figure 1-7 Seismic Isolation System of Chisuikan Building (Tomizawa et al, 2011; Mori et al, 2012)

A practical, but limited in effectiveness, 3D seismic isolation system has been proposed by GERB of Germany and actually studied at UB in the late 1980s, including shake table testing (Makris and Constantinou, 1992). The entire structure is mounted on helical (coil) springs which provide flexibility in all directions. Due to the fact that the springs need to be stiff enough to carry the weight of the structure, the lateral flexibility is also limited. The lowest frequency is

achieved in the rocking mode. For the example building presented in Makris and Constantinou (1992), the lowest frequency was 1.6Hz, which is large for effective isolation. Figure 1-8 shows a view of the analyzed small residential building. The system required complex analysis due to type of damper used. Nevertheless, the system could provide limited isolation in all three directions. Rocking would be an issue as it would amplify the response of sensitive vertical elements like bushings in transformers. Other than two applications of residential structures in the Los Angeles area and a number of 230kV capacitor banks in Xian, China installed in 1999, the idea did not materialize into wide-spread applications. The reason may have been the fact that for the benefit of some reduction of response in the vertical direction there was limited isolation in the horizontal direction. Also, the system makes use of what is now considered obsolete damping devices that add to the stiffness of the springs and are highly dependent on temperature and frequency, and the system properties were not optimized.



Figure 1-8 3D Seismic Isolation System for a House in California (Makris and Constantinou, 1992)

Around 1999 a 3D seismic isolation system was developed and its parts tested for a radar facility of the US Missile Defense System on the Shemya Island in Alaska. The system was complex and required near absolute rigidity under service loads and capability for quick and precise

repositioning after an earthquake. The system was semi-active to achieve the requirements for rigidity and re-positioning. However, the main components, excluding the semi-active part, were readily available (springs, dampers and single Friction Pendulum bearings). Following the events of September 11, 2001, the priority for the missile defense system was changed and the radar facility was not built. Figure 1-9 illustrates the main components of this isolation system. The vertical fuse positioners in this figure provided the required rigidity and repositioning following an earthquake. The devices were activated (quickly released by either hydraulic or explosive means) on the basis of ground acceleration information provided by sensors. Note that the horizontal truss members were used to prevent horizontal movement of the springs.

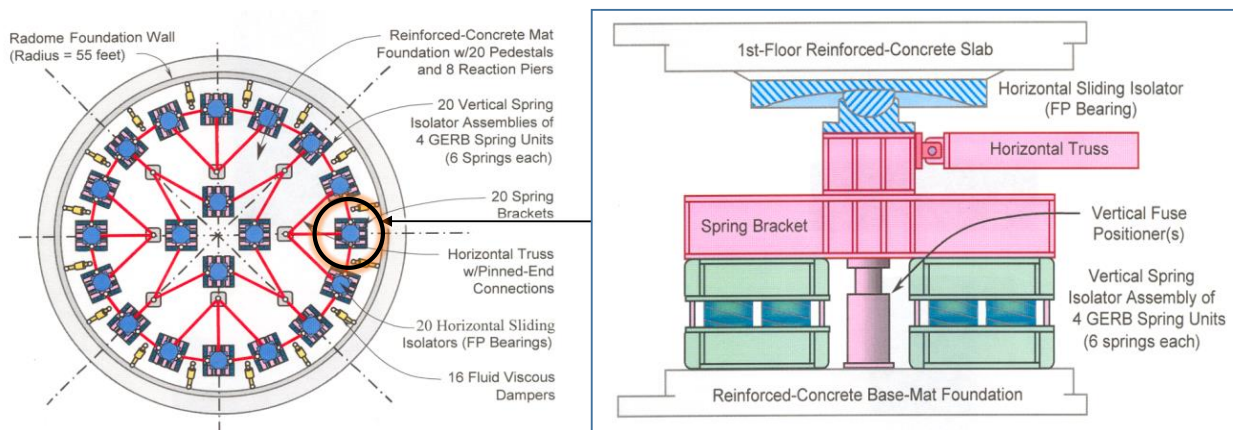


Figure 1-9 3D Seismic Isolation System developed for a Radar Facility at Shemya Island, Alaska

Elastomeric bearings with low shape factor were considered in an attempt to provide some vertical flexibility. In 1969, a three-story elementary school building was built in Yugoslavia utilizing cubes of rubber in a crude attempt to provide a 3D seismic isolation system (Staudacher et al., 1970). The unreinforced rubber bearings did not have sufficient capacity to sustain the gravity loads, had obvious signs of significant bulging and they experienced creep. The building was eventually demolished.

Kajima Corporation of Japan built, in the mid-1980s, one structure on their research campus in Tokyo with low shape factor (4) elastomeric bearings (Kelly, 1988). The attempt was to provide some vertical flexibility for vibration isolation in the vertical direction, but not vertical seismic

isolation. Nevertheless, significant creep in the low shape factor bearings required periodic adjustment of the height of the bearings, which were eventually removed and replaced.

Aiken et al. (1989) and Tajirian et al. (1990) tested several types of elastomeric bearings with a shape factor of 2.5, which is aimed at achieving a horizontal frequency of 0.5Hz and a vertical frequency of 5Hz. The purpose of the testing was to investigate the application of such bearings in the 3D seismic isolation of nuclear structures. More recently, Okamura et al. (2011) tested scaled bearings of various shape factors in a range of 8 to 14, and concluded that elastomeric isolation systems with a horizontal frequency of 0.29Hz and a vertical frequency of 8Hz can reduce the seismic response of nuclear reactor structures. The high vertical frequency of 5Hz or larger and the associated low damping (less than 15%) are insufficient to provide for seismic isolation in the vertical direction. This will be demonstrated in Section 2 of this report when analytical studies are presented. Also, low shape factors severely limit the capacity of the bearings to carry vertical load and deform laterally. Moreover, the aforementioned issues with creep should persist although not evaluated in these studies.

The preceding review of 3D seismic isolation system development demonstrated that (a) purely elastomeric isolation systems cannot provide effective vertical isolation due to their high frequency and other problems of creep and low capacity to carry vertical load and deform laterally, (b) helical spring and damper systems generally have all frequencies larger than about 1.5Hz to be able to provide effective isolation in all directions, (c) effective 3D isolation systems developed in Japan are exceptionally complex utilizing air springs, accumulators, piping, valves and leveling systems that require continued maintenance, are likely unreliable and are costly. They are certainly unacceptable for use in the seismic isolation of electrical transformers where reliability, minimum maintenance, compactness and reasonable costs are required.

The objective of the work described in this report was to develop and validate a practical three-directional seismic isolation system for high-voltage power transformers. Requirements of the system were as follows. The system should be a modular extension of a horizontal seismic isolation system currently used for power transformers. The system should consist of two

separate systems, one to achieve horizontal seismic isolation and the other to achieve vertical seismic isolation. The horizontal system should be highly flexible in order to achieve a high degree of seismic isolation within the constraints of displacements for serviceability of the equipment. The vertical system should be able to support the weight of the equipment with limited deflection in order to meet serviceability requirements and compactness. If needed, a rocking restraint system should be developed. All components of the system should be readily available from reputable manufacturers. All components of the system should be passive and highly reliable. A large scale model of an electrical transformer should be built and tested on the shake table in real time scale. The acquired test data should be used to demonstrate the effectiveness of the system and to validate analytical models for the prediction of the dynamic response.

The report describes the development and experimental validation of a three-dimensional seismic isolation system that fulfils the requirements stated above. It consists of highly flexible triple Friction Pendulum bearings for the horizontal isolation system, which are supported by vertically driven spring-damper units. The units provide limited flexibility in the vertical direction in order to control deflections and meet serviceability requirements. They also provide high damping so that the system in the vertical direction acts like a highly damped damping system rather than as a flexible seismic isolation system.

SECTION 2

ANALYTICAL STUDY OF THREE-DIMENSIONAL SEISMIC ISOLATION SYSTEMS FOR HIGH-VOLTAGE POWER TRANSFORMERS

2.1 Introduction

This section presents an analytical study of the response of a sample electrical transformer with 3D seismic isolation systems. The purpose of the study is to (a) investigate the effectiveness of systems based on helical springs and dampers, (b) investigate the effectiveness of a combined system consisting of triple Friction Pendulum bearings for the horizontal isolation system and spring and viscous dampers for the vertical isolation system, and (c) determine practical parameters for the isolation systems that have promise for application.

In the study, a transformer of a weight of 418 kip, including a concrete basemat supported by isolators, is considered. The dimensions, weight and distribution of weight are those of a recently isolated transformer in Vancouver, WA (Oikonomou et al, 2016). Figure 2-1 shows the isolated transformer. The isolation system consists of triple Friction Pendulum bearings providing only horizontal isolation. The transformer is assumed to have three inclined bushings of as-installed frequencies of 3, 6 and 10Hz, which represent a wide range.



Figure 2-1 Seismically Isolated Transformer in Vancouver, WA (courtesy L. Kempner, BPA)

Bushings are considered critical for assessing failure of a transformer (Kitayama et al, 2016). Accordingly, a range of frequencies for the bushings has been considered as it is important in the calculation of the response of the bushings. The total weight, distribution of weight, size and connection details for the three bushings considered in this study are identical to those of the bushing used in the model for shake table testing. The dimensional and weight distribution characteristics of various bushings are listed in Table 2-1 (Kitayama et al, 2016) with reference to Figure 2-2. Of these, bushing No. 6 is essentially the same as the one used in the testing reported in this report but for the as-installed frequency which varied to cover a range of values representative of typical cases per Table 2-1 (3 to 10Hz). Note that per Figure 2-2 a bushing is divided into upper and lower parts that are separated by a connection housing (termed plate in this report) to which the bushing is connected. This plate is shown in Figure 2-2 to have a thickness $2H_F$. Other geometric parameters are: H_{UB} is the length of the bushing's upper part, H_{LB} is the length of the bushing's lower part, H_{CM_UB} is the distance of the flange to the center of mass of the bushing's upper part, H_{CM_LB} is the distance of the flange to the center of mass of the bushing's lower part, m_{UB} is the mass of the bushing's upper part, m_{LB} is the mass of the bushing's lower part and m_{CH} is the mass of the connection housing.

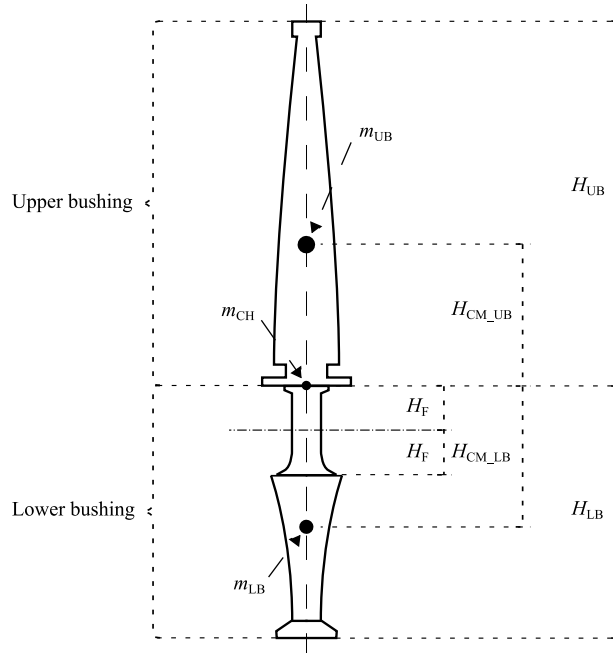


Figure 2-2 Bushing Parameters (Kitayama et al, 2016)

Table 2-1 Characteristics of Bushings (Kitayama et al, 2016)

Property	Unit	Bushing 1	Bushing 2	Bushing 3	Bushing 4a	Bushing 4b	Bushing 5	Bushing 6	Bushing 7	Bushing 8
Manufacturer		G.E.	G.E.	G.E.	HSP	HSP	Trench	ABB	ABB	ABB
Material of insulator		Porcelain	Porcelain	Porcelain	Composite	Composite	Composite	Porcelain	Porcelain	Porcelain
Voltage capacity	kV	500	550	550	230	230	500	196/230	550	550
Designation		GE-500 - TypeU	GE-500 - TypeU	GE-500 - TypeU	HSP-230-1200	HSP-230-1200	500D004 C_3	196w0800 bz	T550W 2000UD	T550Z 3000SE
Total height	in	290.0	244.8	244.8	150.7	150.7	257.2	151.4	295.0	255.2
Length over mounting flange: H_{UB}	in	204.0	194.8	194.8	91.2	91.2	192.2	91.4	208.3	190.2
Length below mounting flange: H_{LB}	in	86.0	50.0	50.0	59.5	59.5	65.0	60.0	86.7	65.0
Max dia. Over mounting flange	in	20.0	25.0	25.0	11.6	11.6	19.8	11.8	23.0	18.7
Max. dia. Below mounting flange	in	20.0	18.8	18.8	8.3	8.3	12.4	10.0	23.0	16.8
Diameter of mounting flange	in	35.0	33.0	33.0	24.0	24.0	28.5	24.0	34.2	27.0
Total weight	lbs	4000	2800	2810	510	385	1850	840	4330	2180
Location of CG. (above flange)	in	57.5	57.5	57.5	17.0	17.0	65.5	14.0	47.0	54.8
Upper bushing weight: $m_{UB,g}$	lbs	2744	2148	2156	248	172	1307	447	3012	1570
Location of upper bushing CG: H_{CM_UB}	in	96.0*	87.6*	87.6*	45.0	45.0	96.0	34.0	90.0	85.2
Lower bushing weight: $m_{LB,g}$	lbs	1156	552	554	162	113	443	293	1218	510
Location of lower bushing CG: H_{CM_LB}	in	38.9*	59.2*	59.2*	27.0	27.0	24.5	28.0	59.0	39.0

Property	Unit	Bushing 1	Bushing 2	Bushing 3	Bushing 4a	Bushing 4b	Bushing 5	Bushing 6	Bushing 7	Bushing 8
Connection housing weight: $m_{CH} * g$	lbs	100	100	100	100	100	100	100	100	100
Weight per unit length	lb/in	13.45	11.03	11.07	2.72	1.89	6.80	4.89	14.34	8.15
Distance to the flange (half of center pocket): H_F	in	13.6*	11.5*	11.5*	8.25	8.25	11.5	13.4	13.6	11.5
Fixed base frequency: f_{Fix}	Hz	5.15*	9.36*	9.36*	8.32	8.04	5.15	21.00	9.37	9.35
As-installed frequency: f_{AI}	Hz	3.30-3.90	4.20	4.25	7.75	6.79	3.25	11.25	2.57	7.70
*Estimated value										

A review of the performance of transformers in earthquakes (Kitayama et al, 2016) considering empirical data over at least 20 years has shown that failure of transformers may be predicted by the peak value of acceleration of the bushing at its upper part center of mass. This single parameter is capable of predicting the behavior of the bushing provided it is modelled as a rigid element connected to the body of the transformer by flexible elements to properly represent the vertical and horizontal (or rocking) frequencies (the latter is the as-installed frequency in Table 2-1). Kitayama et al (2016) determined that values of acceleration at the center of mass of the upper part of porcelain bushings in the range of 1g to 2g represented well empirical data for which there was a 50% probability of failure. The lower limit applied to failure of bushings by oil leakage while the upper limit applied to failures by breakage of bushings or failures at other components of the transformer. Most commonly observed bushing failures are fracture of porcelain bushings, slippage at the bottom of porcelain bushing and subsequent oil leakage, and fracture at the bushing flange (Gilani et al, 2001).

2.2 Analyzed Combined Horizontal-Vertical Seismic Isolation Systems

Two three-dimensional seismic isolation systems are considered:

- 1) A system consisting of vertical helical (coil) springs and linear viscous dampers. Figure 2-3 shows images of how the system looks. The image at the top is a vibration isolation system used to suppress vibrations of equipment in the launching platform of the space shuttle (courtesy of Taylor Devices, Inc.). The image at the bottom is one of the aforementioned isolated capacitor banks in China (GERB system, circa 1999 or 2000).

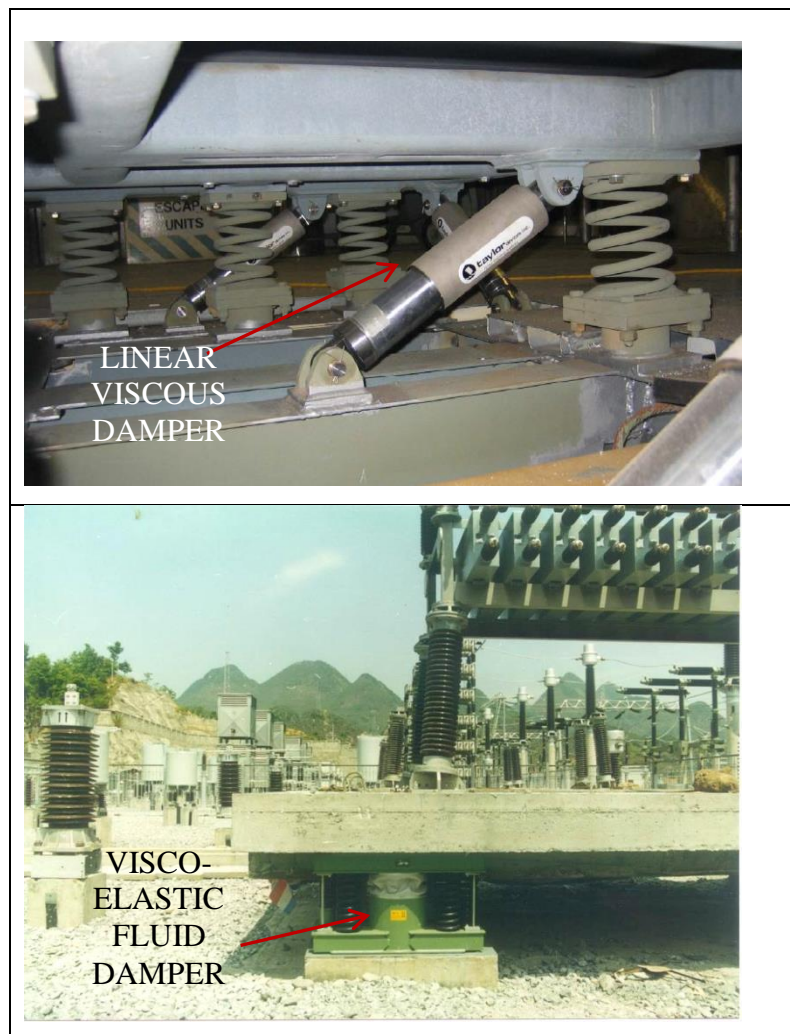


Figure 2-3 Examples of 3D Isolation Systems Consisting of Helical Springs and Dampers (top image courtesy of Taylor Devices, Inc.; bottom image courtesy of GERB)

The two systems shown in Figure 2-3 employ helical (coil) springs to provide the vertical and lateral flexibility. The coil spring consists of material (steel) of modulus of elasticity E and shear modulus G , and has wire diameter d , mean winding diameter D , free (unloaded) height L_o and n windings. When subjected to a vertical load P , the vertical stiffness is given by (Wahl, 1949):

$$K_V = \frac{Gd^4}{8nD^3} \quad (2-1)$$

Equation (2-1) is in the simplest possible form and does not account for changes in the slope of the mean diameter of the coils under deformation, which are of importance in precision springs. The horizontal stiffness of coil springs depends on the boundary conditions and the vertical load so that testing is typically needed to obtain the stiffness value. Herein, use is made of the equations provided in the German Standard DIN 2089 (1984) which is now superseded by the European Standards:

$$K_H = K_V \left(\frac{\xi}{\xi - 1 + \frac{1}{\lambda \left(0.5 + \frac{G}{E}\right)} \cdot \varepsilon \cdot \tan(\lambda \xi \varepsilon)} \right) \quad (2-2)$$

$$\varepsilon = \sqrt{\left(0.5 + \frac{G}{E}\right) \left(\frac{G}{E} + \frac{1 - \xi}{\xi}\right)} \quad (2-3)$$

In these equations, ξ is the spring compression normalized by the initial length L_o and λ is the slenderness ratio:

$$\xi = \frac{P}{K_V L_o} \quad \lambda = \frac{L_o}{D} \quad (2-4)$$

The horizontal stiffness is dependent on the vertical load and increases with increasing vertical load, although it is possible to effectively eliminate the dependency on load by proper selection of the spring dimensions. For example, consider a spring of steel ($E=29000\text{ksi}$, $G=11155\text{ksi}$) with $d=1.75\text{inch}$, $D=5.5\text{inch}$, $L_o=10\text{inch}$ and $n=4$. Then $K_V=19.7\text{kip/in}$ and $K_H=14.6\text{kip/inch}$ for load $P=26\text{kip}$ ($K_H=14.5\text{kip/inch}$ for $P=13\text{kip}$). A

coil spring is stable for $0.1 < \xi < 2/3$ and $\lambda < 2.6$ (DIN 2089, 1984). When checking the stability of the spring, it is stable as $\xi = 0.13$ and $\lambda = 1$. The spring has a compression displacement capacity of less than 3inch.

The damper shown in the top image of Figure 2-3 is a linear viscous damper for which the damper axial force F_D is related to the velocity V in the direction of the damper axis by the following equation:

$$F_D = CV \quad (2-5)$$

The damper shown in the bottom image of the figure is a visco-elastic fluid damper of which the behavior is complex and described in Makris and Constantinou (1991 and 1992). In the simplest possible representation, the device may be represented by a linear spring and linear viscous damper.

The results presented in this report apply for the particular configuration of the 3D spring and damper system shown in the top image of Figure 2-3, which allows for most flexibility in selecting the vertical and horizontal damping parameters based on the damper constant and inclination. The results approximately apply for the second system shown in Figure 2-3.

- 2) A system consisting of triple Friction Pendulum (FP) isolators placed on top of a vertically driven spring-damper system. The FP isolators serve as the horizontal isolator and the spring-damper system as the vertical isolator. This is the system tested in two different configurations, one as analyzed in this section with allowance for rocking of the supported equipment and one featuring a stiffening diaphragm to limit rocking.

The spring-damper device is shown in Figure 2-4. It features a telescopic sleeve system to act as a shear pin and to also prevent (limit) rotation (rocking of the top plate with respect to the bottom). Realistically, some small angle of rotation is possible, specified to be 0.1 degrees in the constructed device but assumed zero in the analysis reported in this section. Also, the coil springs of the device have internal pins that limit the spring length available for shear deformation so that the shear and torsional stiffness are increased. This is needed as torsional ground motion and random transfer of torque from the FP isolator above will cause

twisting of the springs and magnification of the angle of twist due to the large compressive forces in the springs (the device without restraint at individual springs has negative torsional stiffness and is unstable).

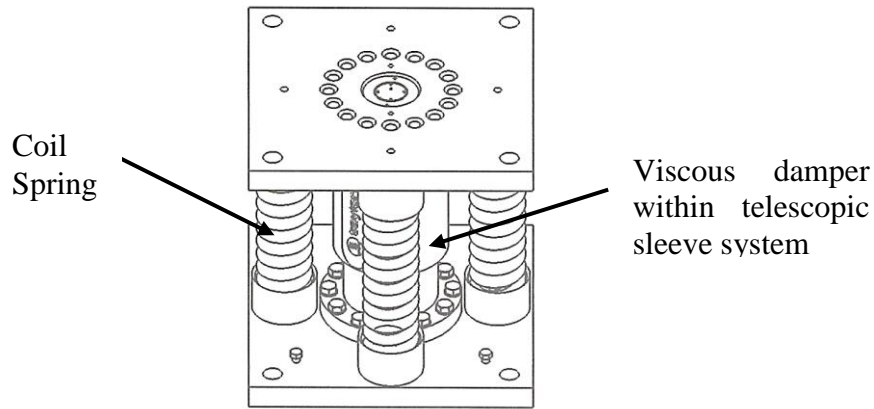


Figure 2-4 Schematic of Spring-Viscous Damper Device

Figure 2-5 illustrates the behavior of the considered system that allows free rocking of the isolated structure. In Figure 2-5 the isolated structure is supported by four triple FP isolators, which in turn are supported by four vertical spring-damper devices. The bottom concave plate of the triple FP isolators is allowed to rotate by an angle of rotation β that is limited by the telescopic sleeve system of the spring-damper unit. In general, angle β is small and limited to 0.1 degrees. The top plate of the triple FP isolators is free to rotate as the FP isolators have no resistance to rocking. This is possible because the spring-damper system allows for relative vertical motion at each support. The rocking angle α is limited by the ability of the spring-damper system to move vertically. The study conducted in this section intends to also establish the limit for this angle. In general, angle α is much larger than angle β . Based on the actual system developed and tested, this angle is of the order of 1 degree.

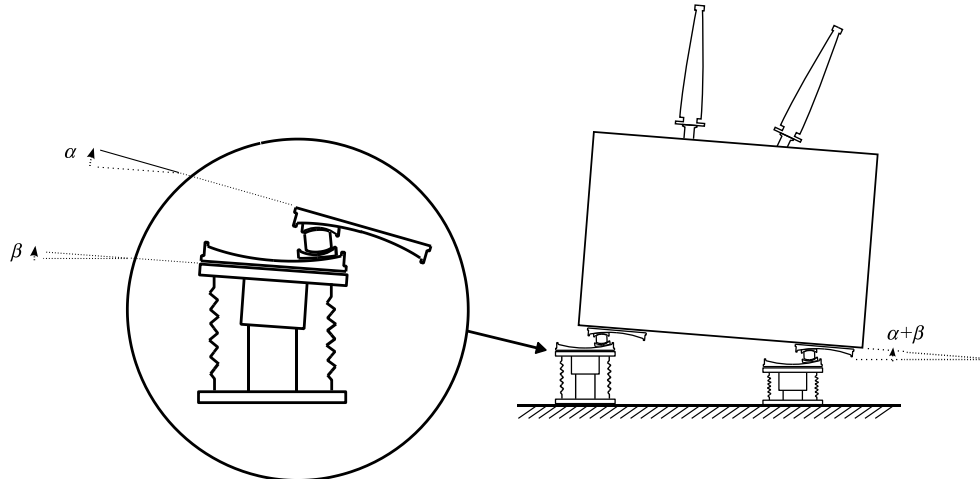


Figure 2-5 Behavior of 3D Isolation System Allowed to Freely Rock

2.3 Analyzed Transformer Model

The transformer of Figure 2-1 was modelled and analyzed. The transformer has a weight of 380kip. The basic dimensions are shown in Figure 2-6. Its center of mass (CM in Figure 2-6) is located at a height of 81 inches. The center of mass is essentially located at the geometric center so that the reactions at four symmetrically located supports are essentially the same. The plan dimensions of the base are 227inch by 110inch. We assume that the isolators will be centered at the corners of the footprint of the transformer. The distance of 110inch in the transverse direction controls the rocking frequency of the isolated equipment, which will be low.

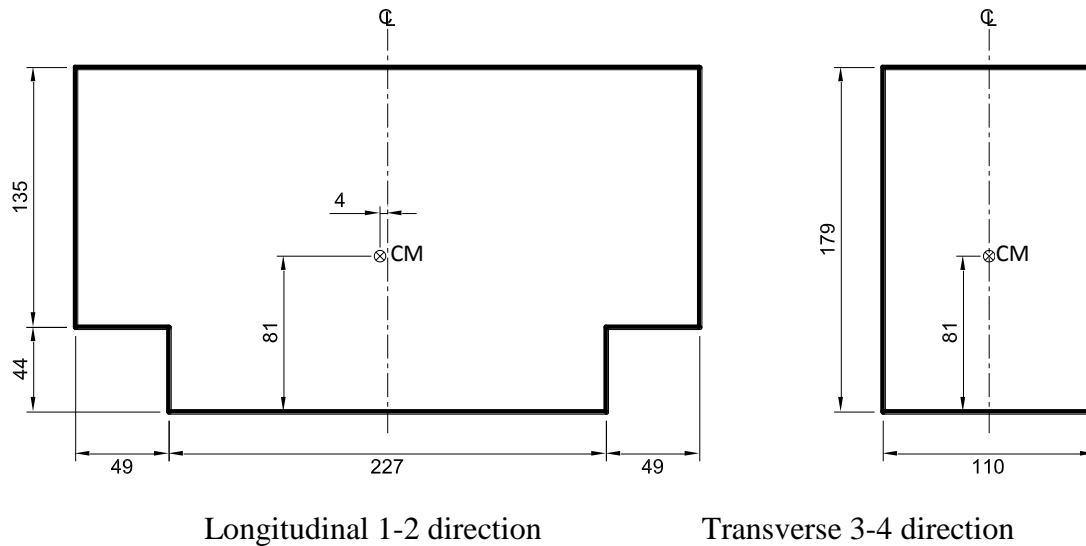


Figure 2-6 Transformer Basic Dimensions (units in inch)

Figure 2-7 shows the model for dynamic analysis as implemented in the SAP2000 program (Computer and Structures, 2015) for the case of the 3D spring-damper system. The model basically consisted of a very stiff frame with a rigid plate at the top having the plan dimensions of 227inch by 110inch and a height of 86inch, which represents the height to the center of mass plus an additional 5inch for the base. The base supporting the equipment on top of the isolators is assumed to have a weight of 38kip, for a total isolated weight of 418kip. This represents a typical weight, although the interest is to develop a system that can be used for loads in the range of 300 to 500kip (plus weight of basemat) without any redesign or modification of the isolation hardware. For equipment of larger weights, each component of the isolation system will have to be modified.

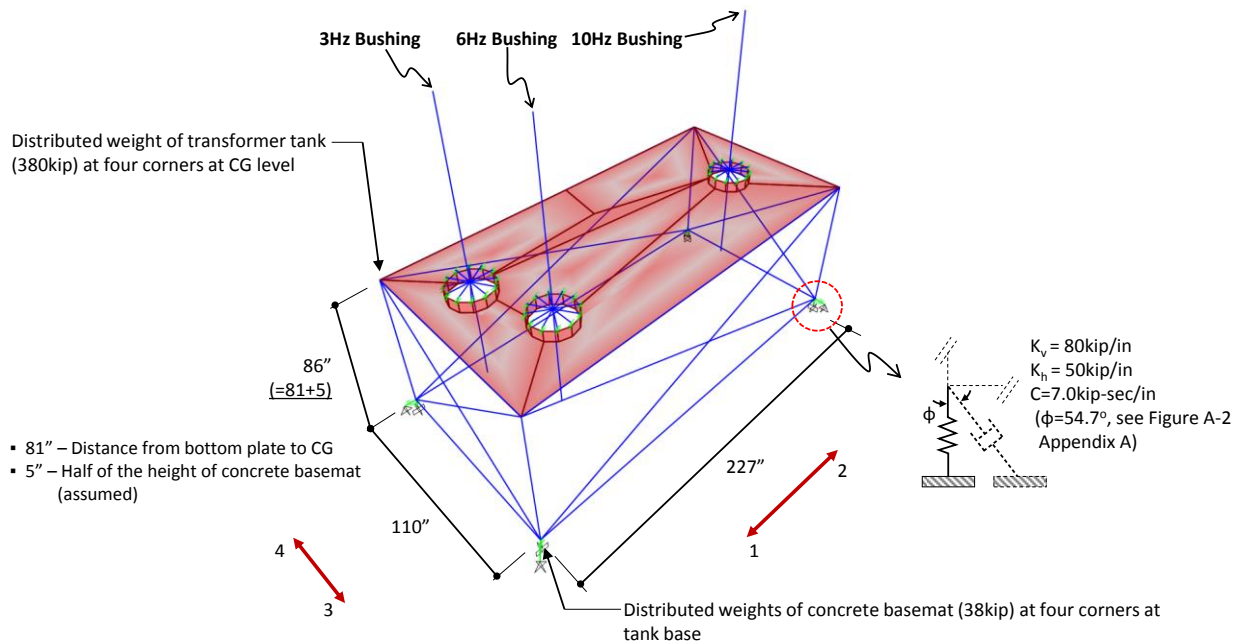


Figure 2-7 Model of Transformer with 3D Spring-Damper Isolation System

The weight of the transformer (380kip) was lumped at the height of 86inch and at the four corners as shown in Figure 2-7. Also, the weight of the base (38kip) was lumped at the four corners directly above the isolators. The effect of the distribution of weight was investigated as it affects the rocking frequency of the system and will be presented later in this report. Three bushings were assumed installed as shown in Figure 2-7 with each adding a weight of 0.84kip to the model. Each bushing was modeled as a rigid bar with weights of 0.447kip and 0.293kip

lumped at the location of the centers of mass for the upper and lower parts, and 0.1kip at the location where the bushing connects to the plate (per Table 2-1). Details of the bushing model are shown in Figure 2-8. The weight distribution and length are those of bushing No. 6 in Table 2-1. Beam elements around the bushing base as shown in Figure 2-8 were assigned properties so that the rocking (as-installed) frequencies of the three bushings were 3, 6, and 10Hz. The corresponding vertical frequencies were 7.6Hz, 15.4Hz, and 25.7Hz, respectively. Note that the beam elements shown in Figure 2-8 are rigid and that the vertical and rocking flexibilities of the bushing are obtained from the stiffness assigned to each vertical spring shown in Figure 2-8. Inherent damping in the transformer model was specified as 5% of critical damping in each mode of vibration.

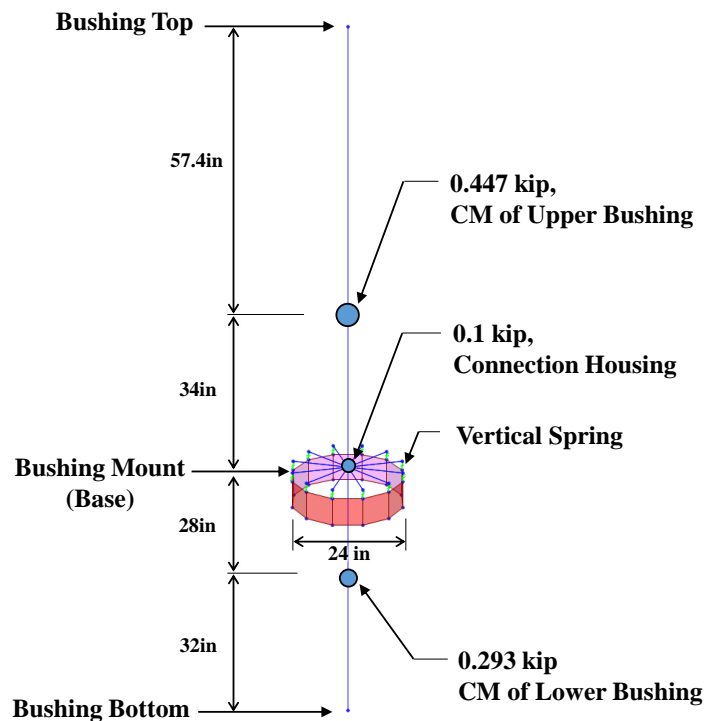


Figure 2-8 Bushing Representation in Analysis Model

The parameters used for the 3D spring-damper isolation system are presented in Figure 2-7. It is assumed that coil springs placed at each of the four corners of the model have a vertical stiffness of 80kip/in and a horizontal stiffness of 50kip/in. Note that these values are rounded stiffness values for group of four springs of the properties previously discussed ($d=1.75$ inch, $D=5.5$ inch, $L_0=10$ inch and $n=4$). Also, four dampers (configured as shown in the top image of Figure 2-3 and in the illustration of Figure 2-9) are used with a damping constant $C=7.0$ kip-sec/in (per

Equation 2-5) and placed one at each corner inclined with respect to the three axes by an angle $\phi=54.7$ degrees (see Figure A-2 in Appendix A for damper installation angles). The effective damping constant in each of the three orthogonal directions at each support is $C\cos^2\phi=2.33$ kip-sec/in. For the supported weight of 418kip (the additional 2.5kip weight of bushings was not considered), the vertical frequency is 2.74Hz and the vertical damping ratio is 0.25. For comparison, the building shown in Figure 1-8 and described in Makris and Constantinou (1992) had a weight of 138kip and a vertical frequency based only on the stiffness of the supporting springs equal to 2.67Hz. However, the visco-elastic dampers used in that building contributed to the stiffness so that the vertical frequency was instead nearly 3.5Hz and the corresponding damping ratio was 0.27. While it is desirable to further reduce the vertical frequency, this requires reduction of the vertical stiffness, which results in reduction of the horizontal stiffness and significantly affects the fundamental frequency, which becomes too low. The fundamental mode is one that combines rocking and lateral displacement, so that a low fundamental frequency results in significant rocking and magnification of response. This was predicted by analysis and observed in recordings during an earthquake (Makris and Deoskar, 1996). For the building in Makris and Constantinou (1992) the fundamental frequency was 1.6Hz and for the isolated transformer of Figure 2-7 is about 1.3Hz (see Table 2-3 and Table 2-4 for eigenvalue analysis results for three mass distribution cases discussed in below). The value of a frequency, other than the vertical frequency, depends on the assumed distribution of mass as the related modes contain an important rocking component (related to the mass moment of inertia). Appendix A presents details of the results of analysis for the frequencies, mode shapes and damping ratios of the analyzed system. Below we present summary results for the case of the 3D spring-damper system of Figure 2-7.

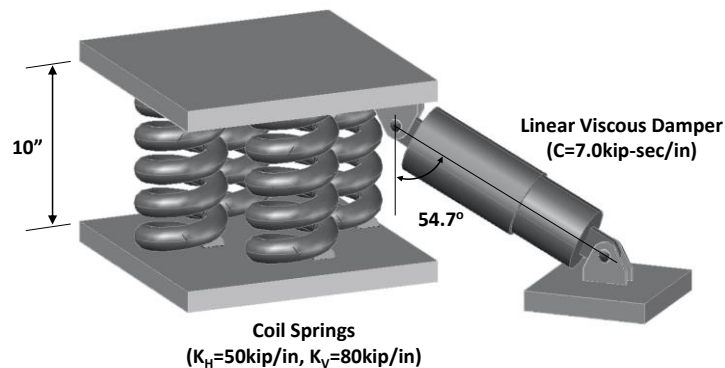


Figure 2-9 Schematic of Spring-Damper Unit at Each Corner of Transformer

Consider three cases of lumped mass distribution as shown in Table 2-2. Tables 2-3 and 2-4 present values of the frequencies and damping ratio (based on complex eigenvalue analysis) and mode shapes (based on the undamped equations of motion) for the three cases of mass distribution for the 3D spring-damper system of Figure 2-7. The analysis was two-dimensional (see Appendix A) in the transverse (3-4) and vertical directions, and in the longitudinal (1-2) and vertical directions. The mode shapes are normalized so that the larger of the displacements of the center of mass in the horizontal direction, u , or the vertical direction, v , is equal to unity. The rotational displacement is denoted as θh , where θ is the rotation of the center of mass and h is the distance of the isolator top to the center of mass ($=86\text{in}$). Thus, θh denotes the horizontal displacement at some point away of the center of mass due to rotation.

Table 2-2 Lumped Mass Distribution Cases Considered in Study

	Case 1	Case 2	Case 3
Transformer Mass Top View			
Basemat Mass Top View			
Side View 1-2 Direction			
Side View 3-4 Direction			

Table 2-3 Frequencies, Damping Ratio and Mode Shapes of Transformer with 3D Spring-Damper Isolation System (vertical and longitudinal direction model)

Mass Distribution		Case 1			Case 2			Case 3		
Parameter		Mode 1	Mode 2	Mode 3	Mode 1	Mode 2	Mode 3	Mode 1	Mode 2	Mode 3
Frequency (Hz)		1.76	2.74	3.29	1.83	2.74	4.36	1.90	2.74	14.27
Damping Ratio		0.21	0.25	0.39	0.23	0.25	0.48	0.25	0.25	1.51
Mode Shape	u	1	0	1	1	0	1	1	0	1
	v	0	1	0	0	1	0	0	1	0
	θh	0.38	0	-1.45	0.31	0	-3.38	0.29	0	-47.28

Table 2-4 Frequencies, Damping Ratio and Mode Shapes of Transformer with 3D Spring-Damper Isolation System (vertical and transverse direction model)

Mass Distribution		Case 1			Case 2			Case 3		
Parameter		Mode 1	Mode 2	Mode 3	Mode 1	Mode 2	Mode 3	Mode 1	Mode 2	Mode 3
Frequency (Hz)		1.31	2.74	4.13	1.36	2.74	5.19	1.38	2.74	5.88
Damping Ratio		0.14	0.25	0.54	0.15	0.25	0.66	0.16	0.25	1.15
Mode Shape	u	1	0	1	1	0	1	1	0	1
	v	0	1	0	0	1	0	0	1	0
	θh	0.70	0	-2.91	0.66	0	-5.22	0.63	0	-19.23

The results in Tables 2-3 and 2-4 demonstrate that the mass distribution only affects the third mode of vibration that is dominated by rocking and some out-of-phase horizontal displacement, and is highly damped. The first mode (horizontal motion with a significant in-phase rocking contribution) and the second mode (vertical motion) are practically unaffected by the assumption of mass distribution. Note that the vertical static deflection δ_V is related to the vertical frequency f_v by Equation (2-6) so for a vertical frequency of 2.74Hz the static deflection is 1.3inch, which is appropriate given the size of the considered springs.

$$\delta_V = \frac{g}{4\pi^2 f_v^2} \quad (2-6)$$

The lowest frequency of the system is about 1.3Hz (Table 2-4) associated with a mode of combined horizontal and rocking motion. Further reduction of the frequency to values

comparable to those of a horizontal-only seismic isolation system (less than 0.5Hz) would require substantial reduction of the vertical frequency too, which would have rendered the system impractical due to large static deflections.

Results of dynamic analysis are presented for the case 1 mass distribution having in mind that in reality the mass distribution when lumped should be somewhere in-between cases 1 and 2. Case 3 is unrealistic.

The second 3D seismic isolation system considered in the study consisted of four triple FP isolators identical to those installed at the Vancouver, WA transformer (see Figure 2-1 and Oikonomou, 2016). Each of these isolators was supported by a spring-viscous damper unit configured as shown in Figure 2-4. Figure 2-10 shows a schematic of the model in program SAP2000 used for the dynamic analysis. Note that a mass weighing 0.5kip is placed in-between the each triple FP isolator model and the vertical spring-damper unit to represent the combined weight of the bottom part of the FP isolator and of top half of the spring-damper unit. The spring-damper unit is restrained to only move vertically so that per the description of the system in Figure 2-5, angle β is zero. Nevertheless, the Triple FP isolator model in the analysis allows for free rotation of the bearing in all directions which leads to unrestrained rocking of the isolated transformer.

The properties of the Triple FP isolators were those determined in the production testing of the isolators of the Vancouver, WA transformer and then adjusted to obtain upper and lower bound friction coefficient values for the analysis. The procedures followed for the determination of the properties and the adjustment are those described in McVitty and Constantinou (2015). Details of the properties and the configuration of the Triple FP isolator are provided in Appendix B. Table 2-5 presents a summary of the properties.

Inherent damping in the model was specified as 5% of critical in each mode of vibration but for the first three modes (translation in the two horizontal directions and torsion). For the construction of the damping matrix in SAP2000, the post-elastic stiffness of the triple FP isolators was used in order to avoid “leakage of damping” per directions in Sarlis and Constantinou (2010).

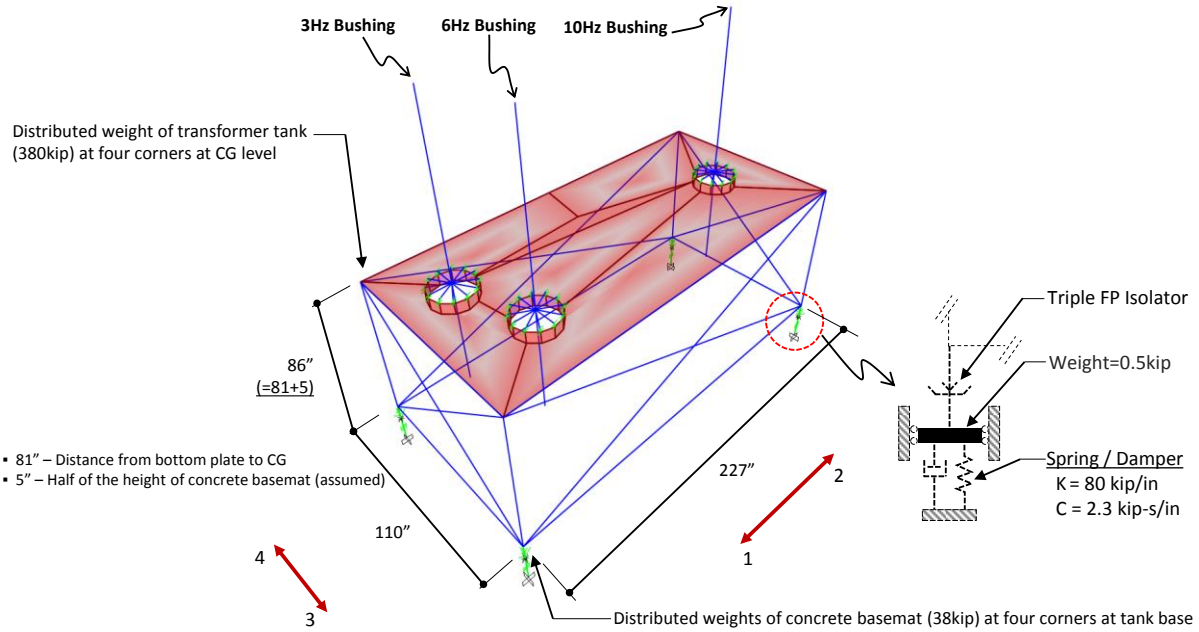


Figure 2-10 Model of Transformer with 3D Triple FP-Spring-Damper Isolation System

Table 2-5 Properties of Triple FP Isolator Used in Analytical Study

Property	Description	Value
$\mu_1=\mu_4$ (lower/upper bound)	Coefficient of friction of surfaces 1 and 4 at high speed (f_{max})	0.11/0.15
$\mu_2=\mu_3$ (lower/upper bound)	Coefficient of friction of surfaces 2 and 3 at high speed (f_{max})	0.08/0.09
$R_{1eff}=R_{4eff}$	Effective radii of surfaces 1 and 4	36.0inch
$R_{2eff}=R_{3eff}$	Effective radii of surfaces 2 and 3	6.0inch
$d_1^*=d_4^*$	Actual displacement capacity on surfaces 1 and 4	6.46inch
$d_2^*=d_3^*$	Actual displacement capacity on surfaces 2 and 3	0.75inch
$f_{min}=f_{max}/2$, rate parameter=1.27sec/in for all surfaces		

The vertical spring stiffness at each support spring-damper unit is $K=80\text{kip/in}$ and the damping constant of the linear viscous damper is $C=2.3\text{kip-sec/in}$, which result in a vertical frequency of 2.74Hz and a vertical damping ratio equal to 0.25. Some studies were also conducted for a damping ratio in the vertical direction equal to 0.50.

Tables 2-6 and 2-7 present values of the frequencies and damping ratio (based on complex eigenvalue analysis) and mode shapes (based on the undamped equations of motion) for the 3D triple FP and spring-damper system when the FP isolators are represented in the horizontal direction as springs with stiffness equal to their shear stiffness when friction is neglected ($W/2R_{\text{leff}}=104.5\text{kip}/(2 \times 36\text{in})=1.45\text{kip/in}$). The results in Table 2-6 are for the case 1 of lumped mass distribution which was the one utilized in the dynamic analysis (as described in Figure 2-10 and Table 2-2). The results in Table 2-7 are for case 2 of mass distribution as described in Table 2-2. More detailed results are presented in Appendix C. The analysis was two-dimensional (see Appendix C) in the transverse (3-4) and vertical directions, and in the longitudinal (1-2) and vertical directions. The mode shapes are normalized so that the largest displacement of the center of mass in the horizontal direction, u , or the vertical direction, v , is equal to unity. The rotational displacement is denoted as θh , where θ is the rotation of the center of mass and h is the distance of the isolator top to the center of mass (86in). Note that there was no effective damping assigned for the effect of friction so that the calculated damping ratio in the mode associated with horizontal motion is zero.

Table 2-6 Frequencies, Damping Ratio and Mode Shapes of Transformer with 3D Triple FP and Spring-Damper Isolation System (Case 1 Mass Distribution)

Direction		Longitudinal (1-2)-Vertical			Transverse (3-4)-Vertical		
Parameter		Mode 1	Mode 2	Mode 3	Mode 1	Mode 2	Mode 3
Frequency (Hz)		0.37	2.68	2.74	0.36	2.54	2.74
Damping Ratio		0	0.24	0.25	0	0.22	0.25
Mode Shape	u	1	1	0	1	1	0
	v	0	0	1	0	0	1
	θh	0.009	-57.46	0	0.043	-51.37	0

Table 2-7 Frequencies, Damping Ratio and Mode Shapes of Transformer with 3D Triple FP and Spring-Damper Isolation System (Case 2 Mass Distribution)

Direction		Longitudinal (1-2)-Vertical			Transverse (3-4)-Vertical		
Parameter		Mode 1	Mode 2	Mode 3	Mode 1	Mode 2	Mode 3
Frequency (Hz)		0.37	2.74	3.71	0.36	2.74	3.32
Damping Ratio		0	0.25	0.33	0	0.25	0.29
Mode Shape	u	1	0	1	1	0	1
	v	0	1	0	0	1	0
	θh	0.009	0	-110.96	0.043	0	-88.72

The results in Tables 2-6 and 2-7 reveal a behavior that is very different than that of the 3D spring-damper system (Tables 2-3 and 2-4). Specifically:

- 1) The fundamental mode is characterized by nearly a pure horizontal motion (rotation contributes less than one twentieth of the motion at the center of mass) with a low frequency of 0.37Hz. By comparison the 3D spring-damper system has a fundamental frequency of 1.3Hz. Accordingly, it is expected that the triple FP and spring-damper system will be much more effective in isolating in the horizontal direction.
- 2) The second mode of vibration (or the third mode in case 2, Table 2-7) is one of purely rocking motion (with a minute horizontal motion component). By comparison, the 3D spring-damper system has its third mode associated with rocking but the mode is one of combined rocking and horizontal displacement motion.
- 3) The third mode of vibration (or the second mode in case 2, Table 2-7) is one of purely vertical motion which for the assumed distribution of mass is closely spaced to the second mode of vibration. The two modes separate when the distribution of mass is changed to that of case 2 in Table 2-2. Nevertheless, the use of the mass distribution per case 1 with closely spaced modes should result in some worsening of the response and it is thus appropriate to conduct the study using this distribution.

2.4 Results of Dynamic Response History Analysis

Dynamic response history analysis was conducted with the historic earthquake motions listed in Table 2-8 together with their characteristics. The selected motions include far-field and near-field motions at a range of distances from the fault and with strong ground motion. Particularly, the Pacoima motion is of near-fault with pulse-like characteristics and also a dominant vertical frequency of about 3Hz, which is very close to the vertical frequency of the isolation system. The motions were used in the analysis exactly as recorded with the exception of the El Centro record that was scaled up by a factor of 3. All three components of motion were used in the analysis with the stronger of the two horizontal components applied in the transverse (3-4) direction of the model.

Table 2-8 Motions used in Response History Analysis and Characteristics as Recorded

	Designation	Earthquake	Recording Station	Moment Magnitude	rRup (km)	Component	Peak Ground Acceleration (g)
1	El Centro	1940 Imperial Valley, CA	El Centro	6.9	6.09	S00E	0.35
						N90W	0.21
						Vertical	0.21
2	Pacoima	1971 San Fernando, CA	Pacoima Dam	6.6	1.8	164	1.22
						254	1.24
						Vertical	0.69
3	Jensen	1994 Northridge, CA	Jensen Filter Plant	6.7	5.4	022	0.57
						292	0.99
						Vertical	0.76
4	Chile	2010 Chile	Concepcion	8.8	105.0	97	0.61
						07	0.65
						Vertical	0.58
5	LGPC	1989 Loma Prieta, CA	LGPC	6.9	3.9	00	0.57
						90	0.61
						Vertical	0.90
6	Kobe	1995 Kobe, Japan	Kobe University	6.9	0.9	00	0.28
						90	0.31
						Vertical	0.45
7	Rio	1992 Cape Mendocino, CA	Rio Dell	7.0	28.0	270	0.39
						360	0.55
						Vertical	0.20
8	Sylmar	1994 Northridge, CA	Sylmar, County Hospital	6.7	9.9	000	0.60
						360	0.84
						Vertical	0.54

Results are presented in terms of the following quantities.

1) Response Spectra Above Isolators

Acceleration response spectra for 5%-damping are presented for the motion calculated at mount (base) of the 6Hz bushing (see Figures 2-7 and 2-8 for location). Note that the model above the isolators is essentially rigid so the calculated spectra are practically the same as the spectra at the mount of the 3Hz and the 10Hz bushings but for some differences caused by rocking and the effect of the distance of the three bushings from the center of rotation. Spectra are presented for the three directions: longitudinal (1-2), transverse (3-4) and vertical (V). For the case of the triple FP isolator-spring-damper system, the spectra are presented only for the case of upper bound friction, which resulted in the highest acceleration response.

Figures 2-11 to 2-18 compare the calculated spectra for the two analyzed 3D isolation systems for the eight motions of Table 2-8. The graphs include the ground motion spectra for revealing the effect of isolation and also include the IEEE 693(2005) Required Response Spectrum (RRS, 5%-damped) for a peak horizontal ground acceleration of 0.5g (high), the corresponding IEEE vertical spectrum defined as 80% of the horizontal spectrum, and the IEEE 693 spectra magnified by a factor of 2 to denote the spectra typically used for the qualification of high voltage bushings mounted on a transformer.

Note that in the figures, solid colored lines represent the ground motion spectra and the dashed colored lines represent the response spectra at the mount of the 6Hz bushing. It is clear in these spectra that the 3D Triple FP-spring-damper system has a substantially better performance than the 3D spring-damper system. This is particularly pronounced in the horizontal response spectra where in the 3D triple FP-spring-damper system the spectra above the isolators are substantially reduced by comparison to the ground spectra, whereas in the 3D spring-damper system the spectra are either slightly reduced or in some cases are even increased.

In the vertical direction the FP-spring-damper system shows a better performance than the spring-damper system as typified in the results for the El Centro and Jensen motions in Figures 2-11 and 2-13. In the case of the Pacoima motion in Figure 2-12 (and to a lesser extent in Figure 2-15 for the LGPC motion), there is a magnification of the spectral acceleration in the 2-5Hz frequency range, due to the fact that this motion has a dominant vertical frequency in that range which coincides the fundamental vertical frequency of the system (2.74Hz). This is a motion with near fault, pulse-like characteristics and a strong vertical component. An additional analysis of the 3D FP-spring-damper system was conducted in the Pacoima motion with the damping in the vertical direction increased from 0.25 to 0.50. The vertical frequency was kept at 2.74Hz. Spectra of the motion at the 6Hz bushing mount are presented in Figure 2-19 where they are compared to the spectra for the system with damping ratio of 0.25. Evidently, there is reduction of the vertical response with increasing damping without any effect on the horizontal response.

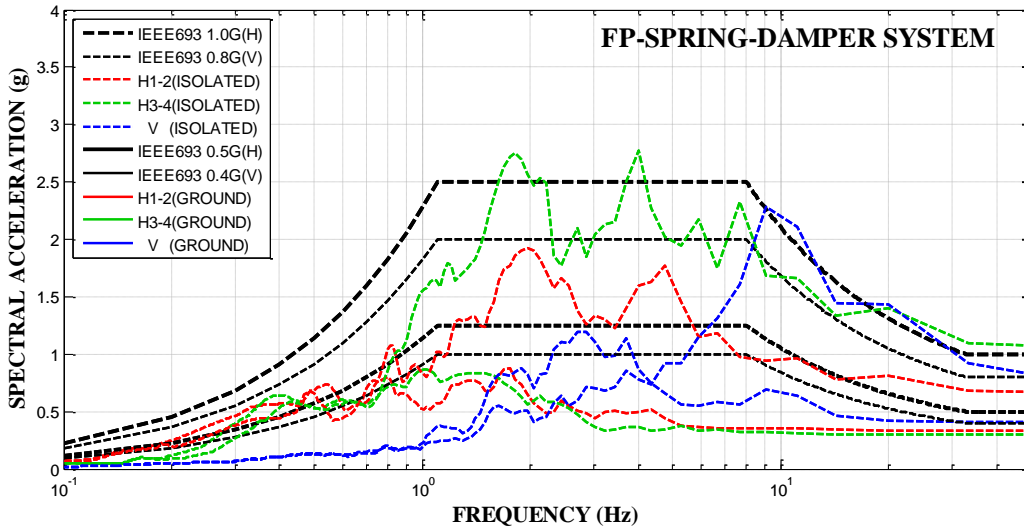
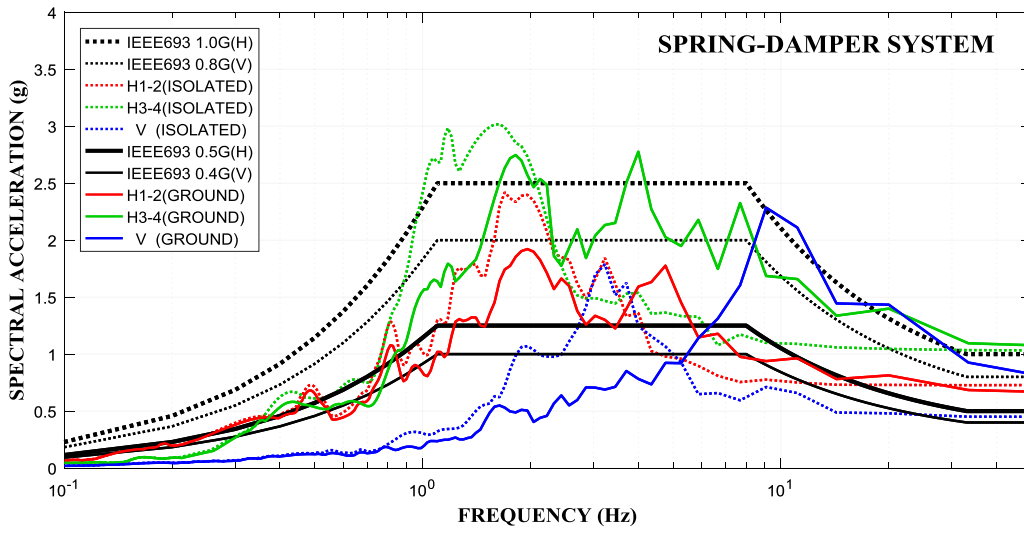


Figure 2-11 Acceleration Response Spectra at 6Hz Bushing Mount in El Centro 300% Motion

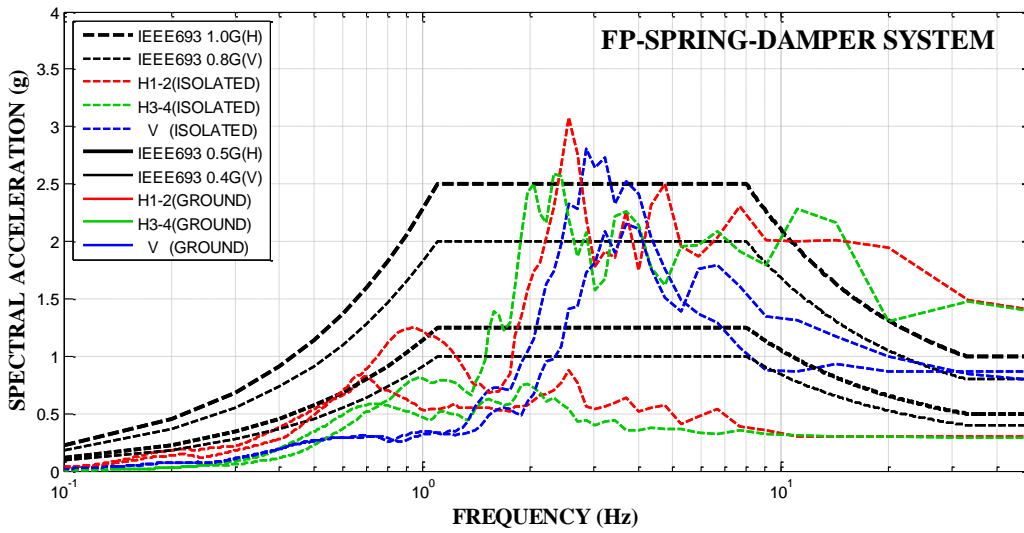
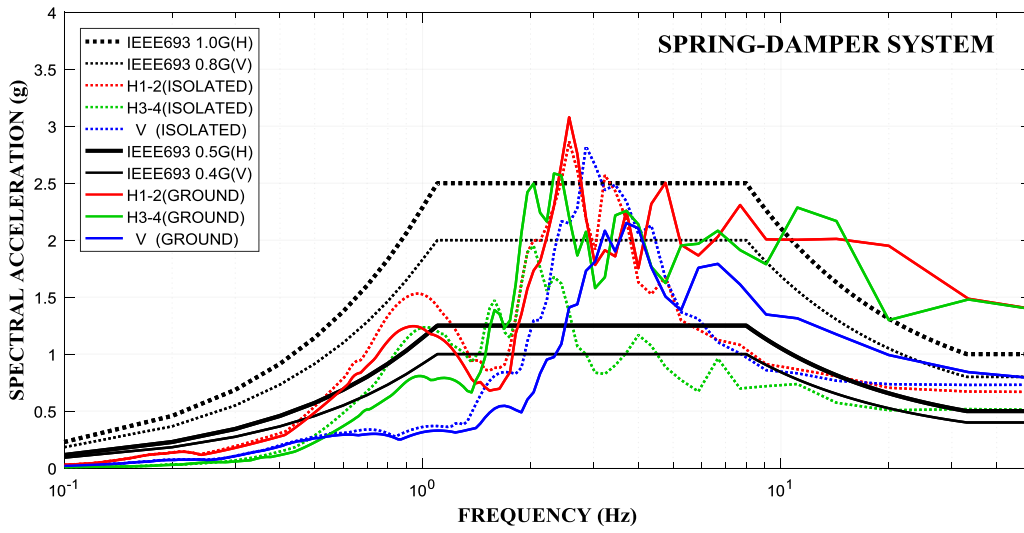


Figure 2-12 Acceleration Response Spectra at 6Hz Bushing Mount in Pacoima 100% Motion

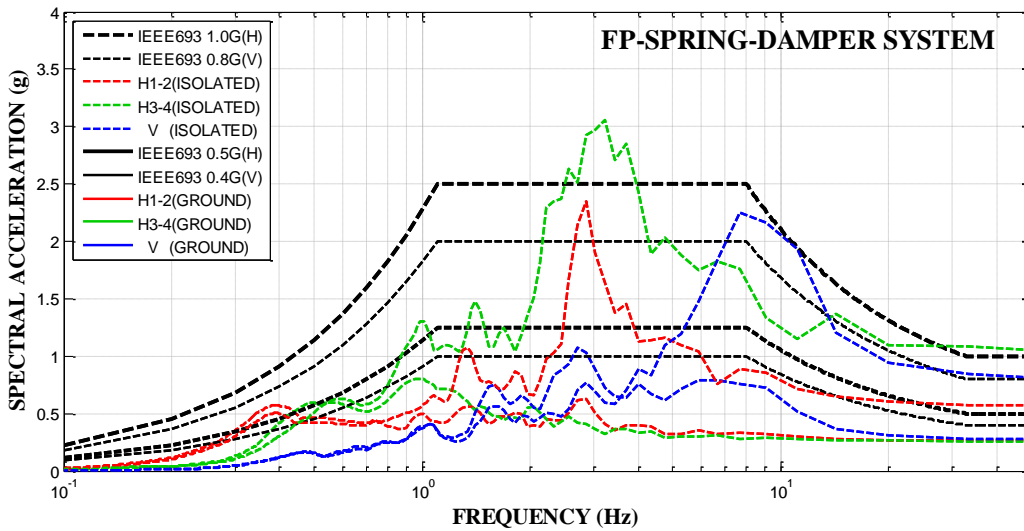
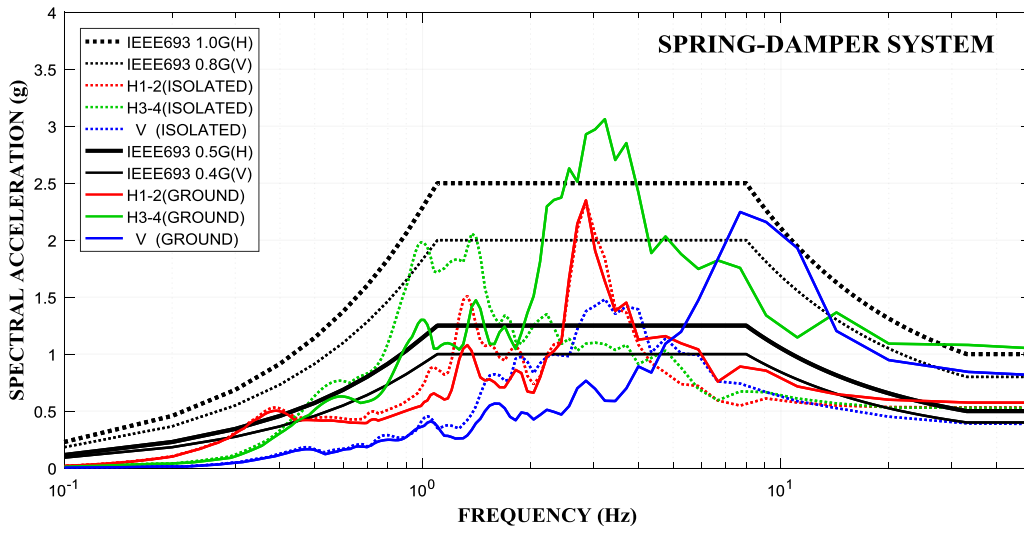


Figure 2-13 Acceleration Response Spectra at 6Hz Bushing Mount in Jensen 100% Motion

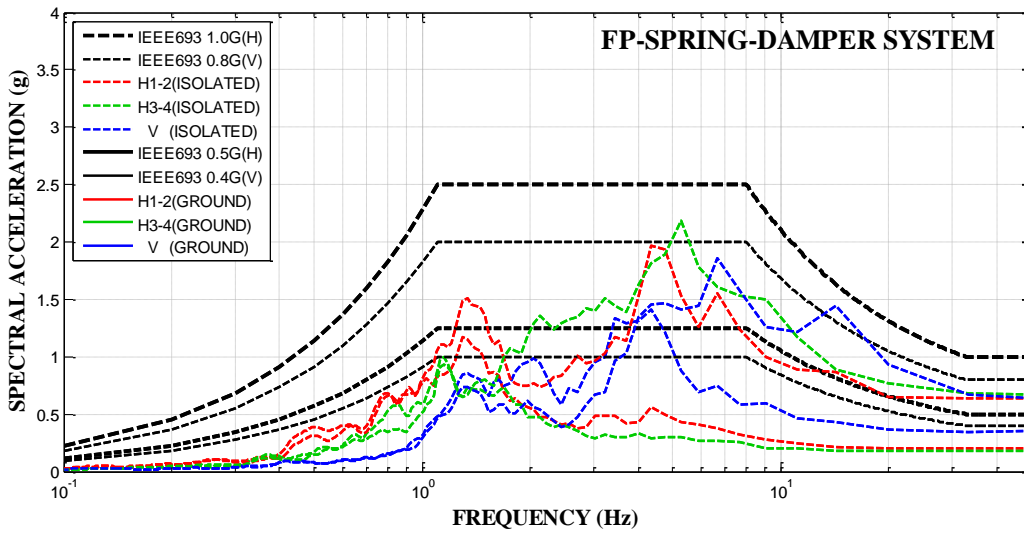
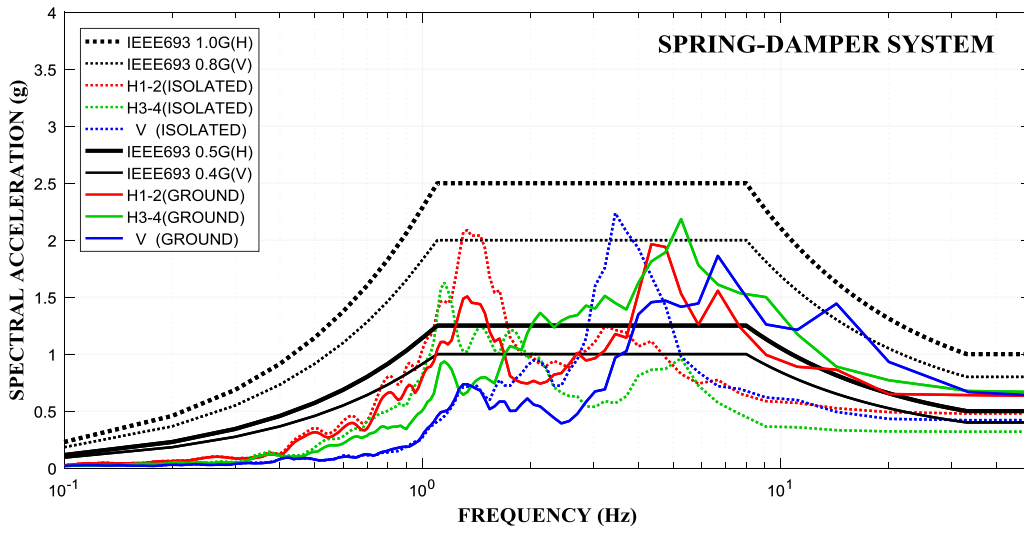


Figure 2-14 Acceleration Response Spectra at 6Hz Bushing Mount in Chile 100% Motion

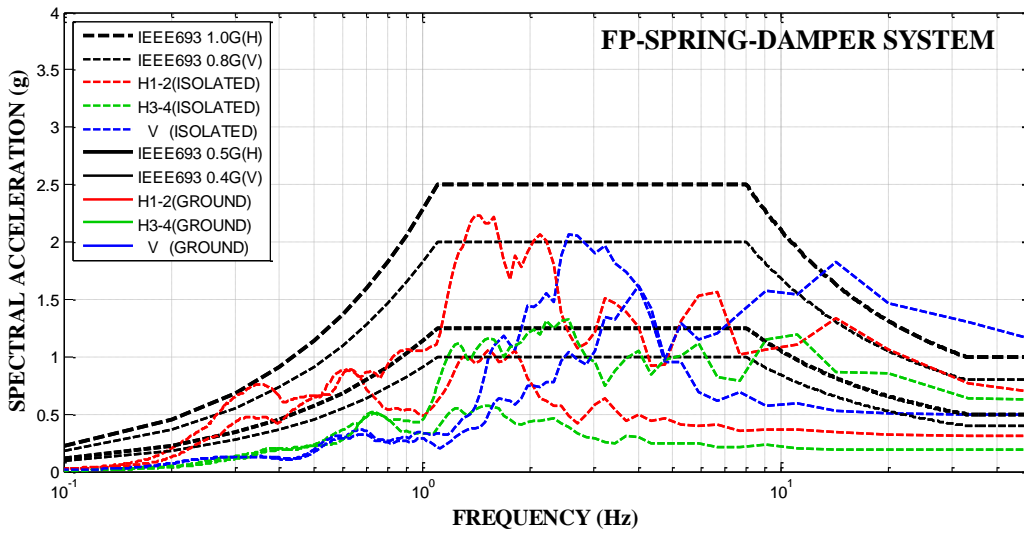
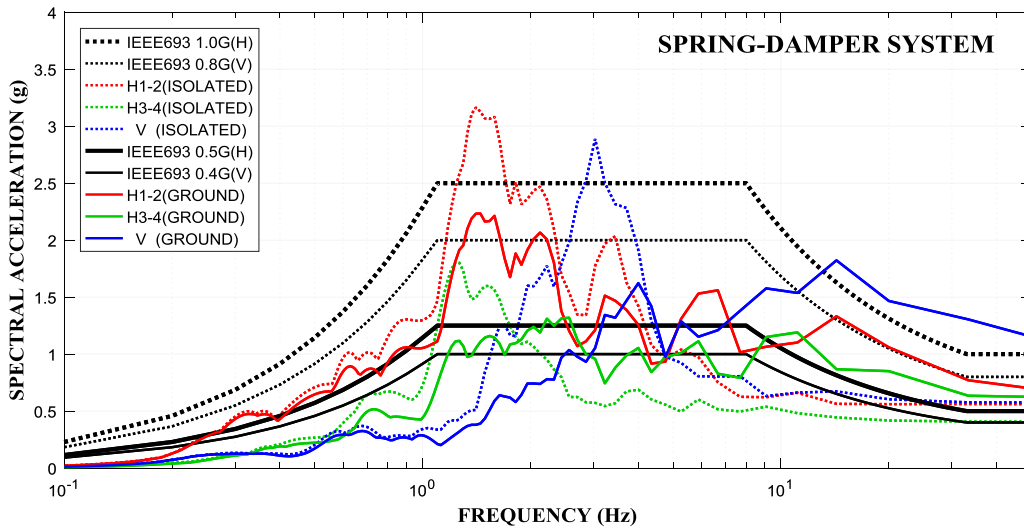


Figure 2-15 Acceleration Response Spectra 6Hz Bushing Mount Corner in LGPC 100% Motion

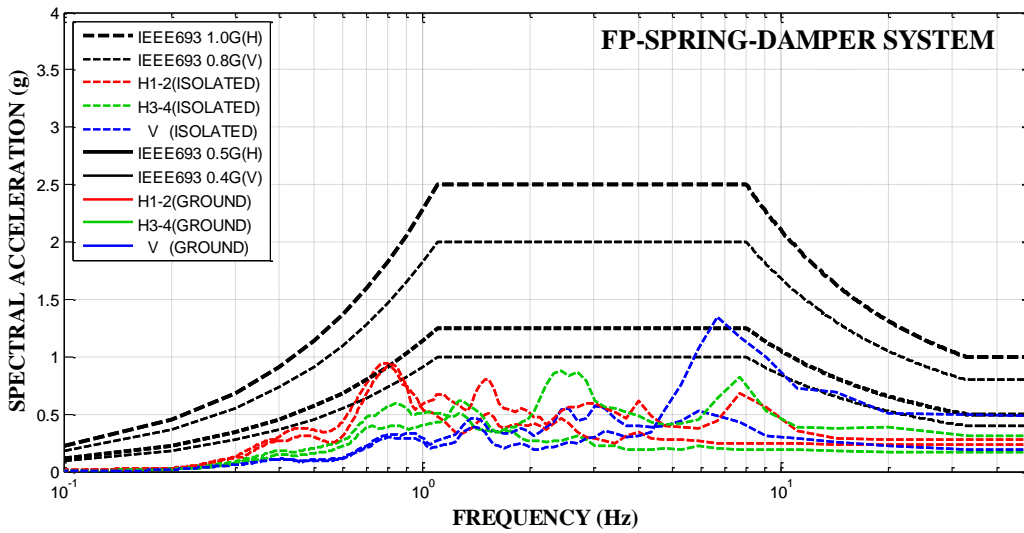
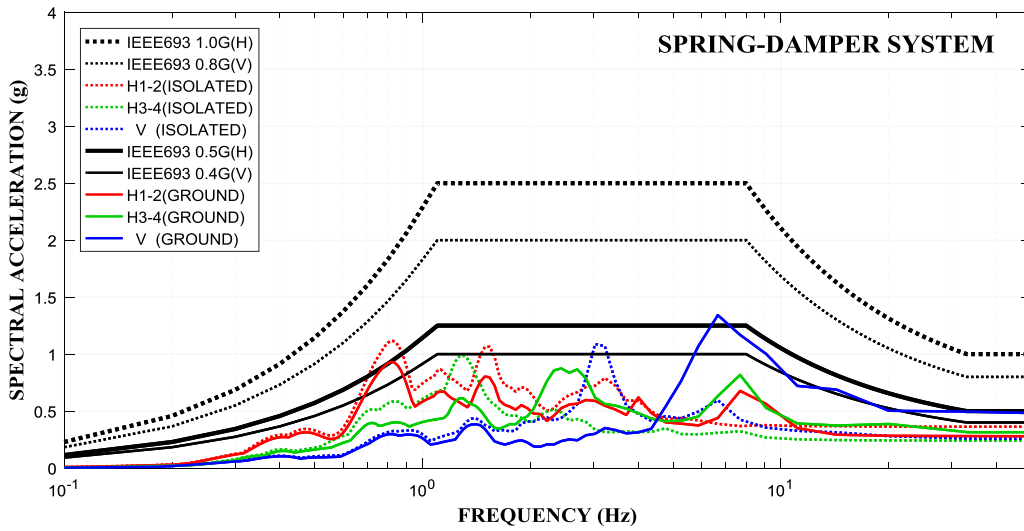


Figure 2-16 Acceleration Response Spectra at 6Hz Bushing Mount in Kobe 100% Motion

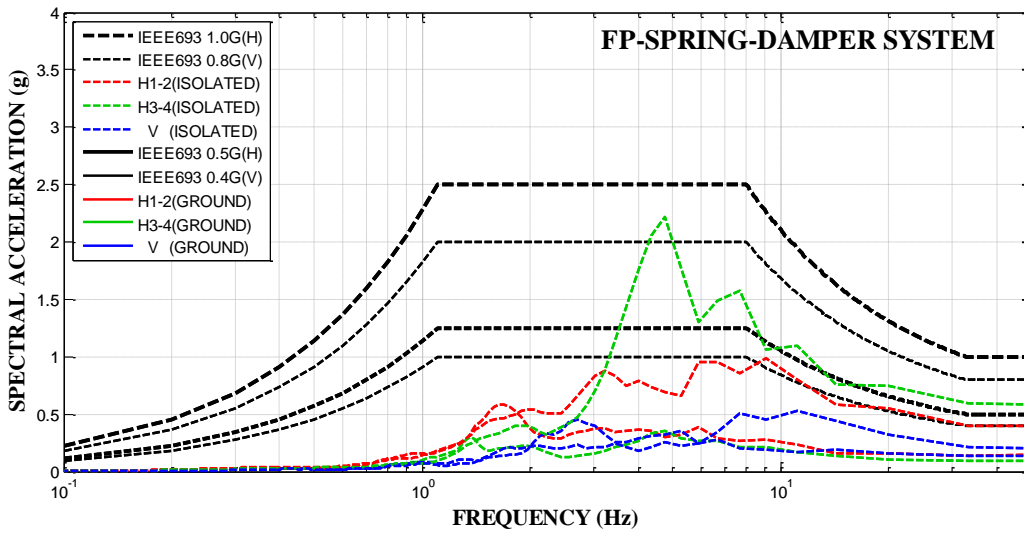
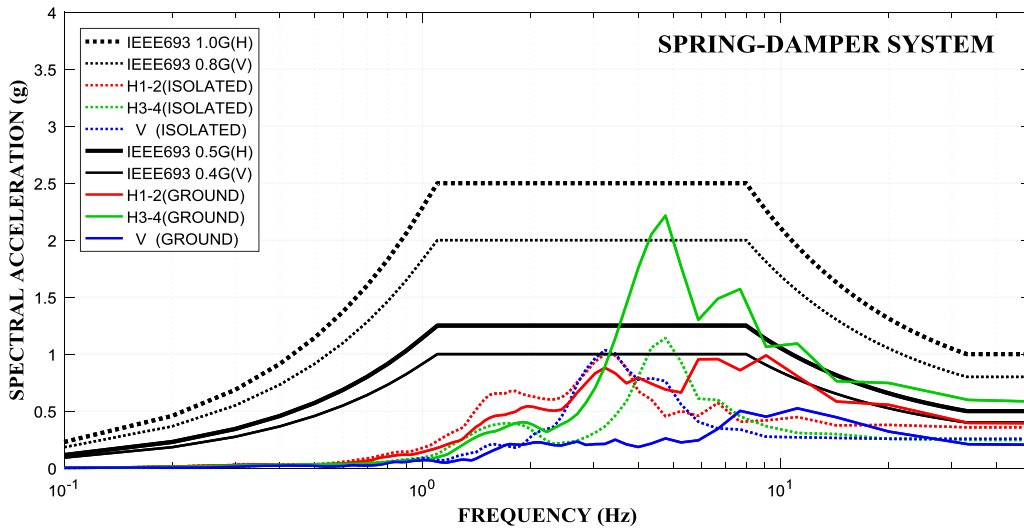


Figure 2-17 Acceleration Response Spectra at 6Hz Bushing Mount in Rio 100% Motion

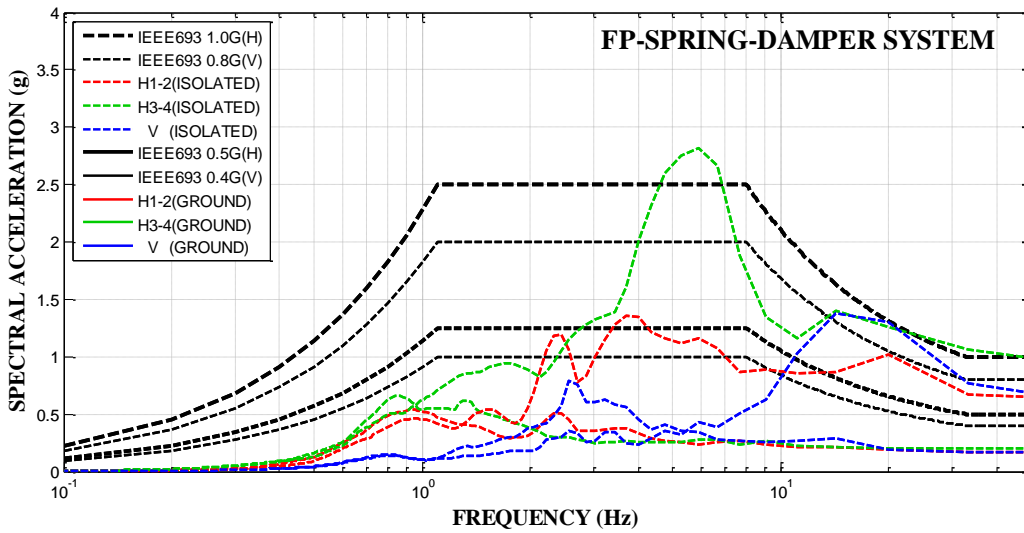
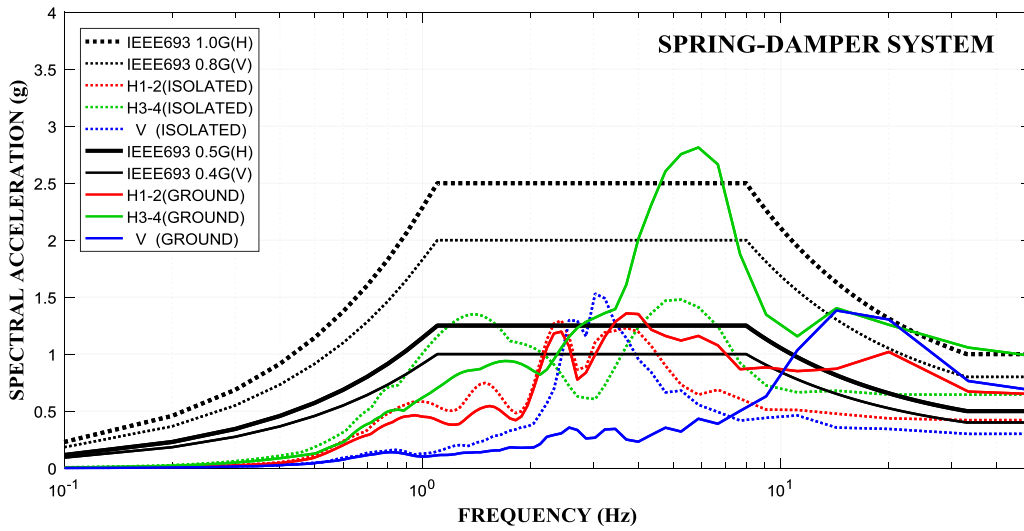


Figure 2-18 Acceleration Response Spectra at 6Hz Bushing Mount in Sylmar 100% Motion

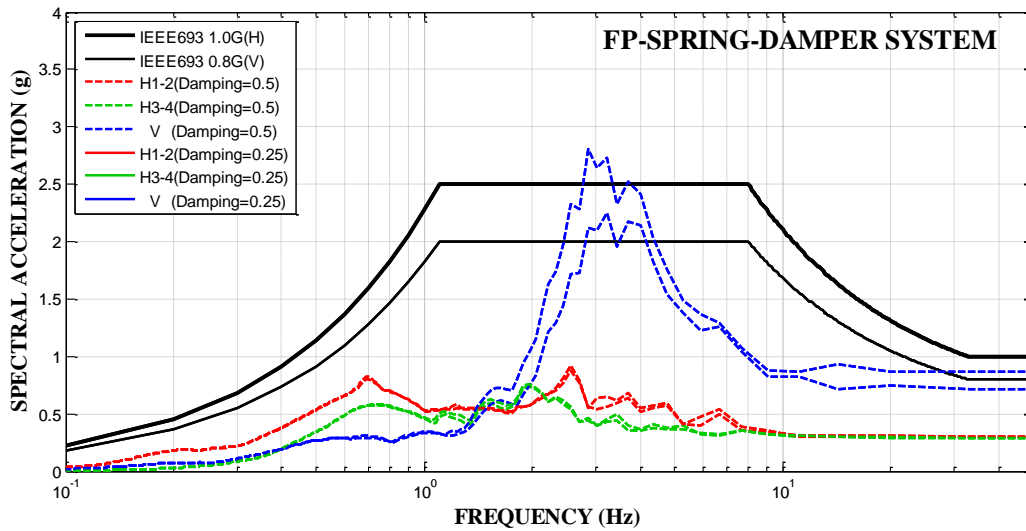


Figure 2-19 Acceleration Response Spectra at 6Hz Bushing Mount for FP-spring-damper System with Vertical Frequency of 2.74Hz and Vertical Damping Ratio of 0.25 (solid line) or 0.50 (dashed line) in Pacoima 100% Motion

Having concluded that the 3D FP-spring-damper system provides for superior isolation performance, additional studies were conducted in which (a) the 2D version of the system (just the triple FP isolators) was compared to the 3D version for the same FP isolators supported by the vertical spring-damper system, and (b) the parameters of the vertical isolation system were changed to a vertical frequency of 2.0Hz and to a damping ratio of 0.50. The frequency of 2.0Hz is presumed to be the lowest practical value that results in a manageable static deflection (2.45inch per Equation 2-6). The higher damping ratio reduces the vertical acceleration as observed in the results of Figure 2-19. Calculated 5%-damped response spectra at the 6Hz bushing mount for the 2D and 3D systems are compared in Figures 2-20 to 2-24 for five of the motions in Table 2-8. Again, solid colored lines represent the ground motion spectra and the dashed colored lines represent the response spectra at the 6Hz bushing. It is evident that the 2D and the 3D isolation systems have nearly identical response spectra in the horizontal directions. In the vertical direction, the response spectra of the 2D isolated transformer are identical or a little higher than the ground spectra, whereas the response spectra of the 3D isolated transformer show substantial reduction.

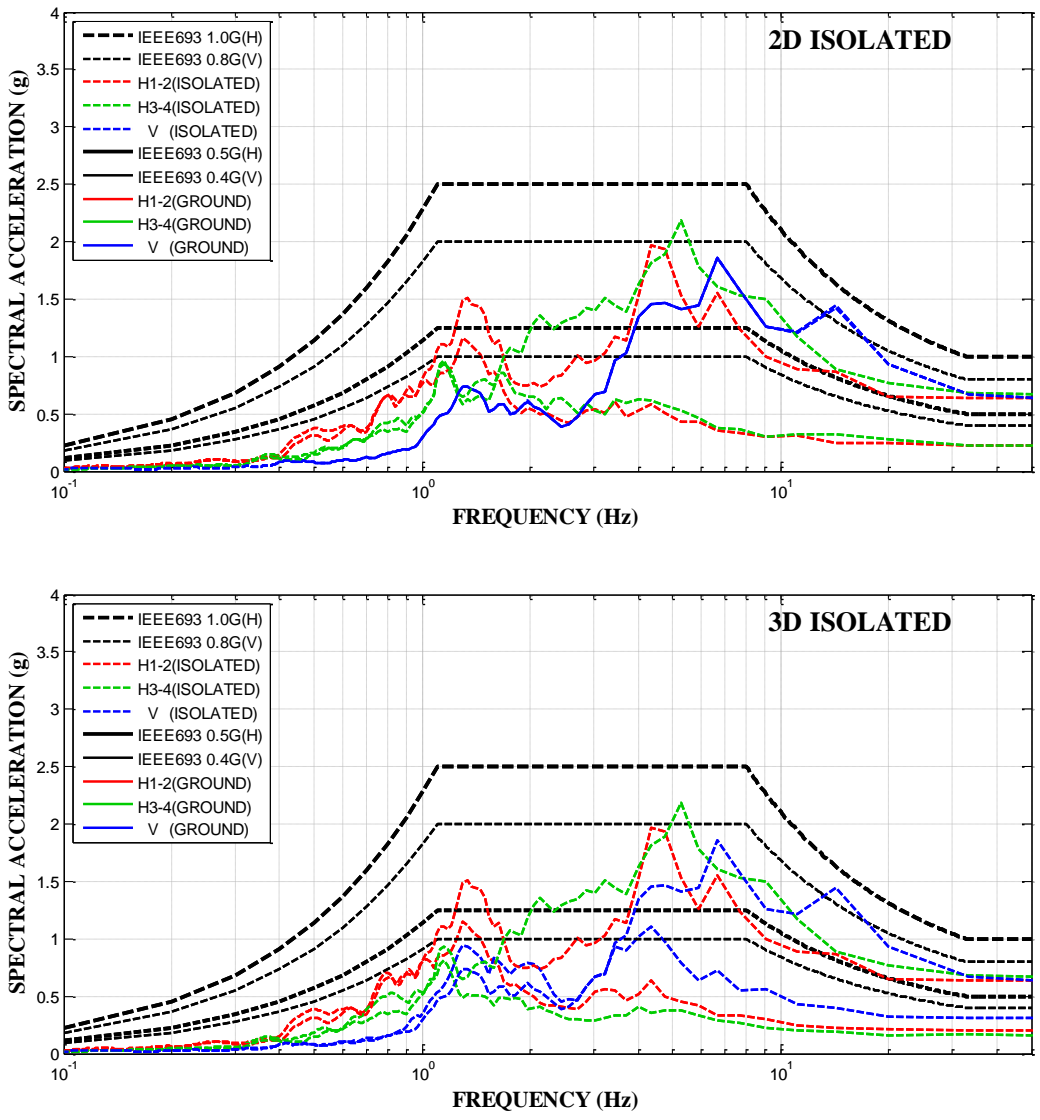


Figure 2-20 Acceleration Response Spectra at 6Hz Bushing Mount of 2D Isolation System (solid line) and 3D Isolation System with Vertical Frequency of 2.0Hz and Damping of 0.50 (dashed line) in Chile 100% Motion

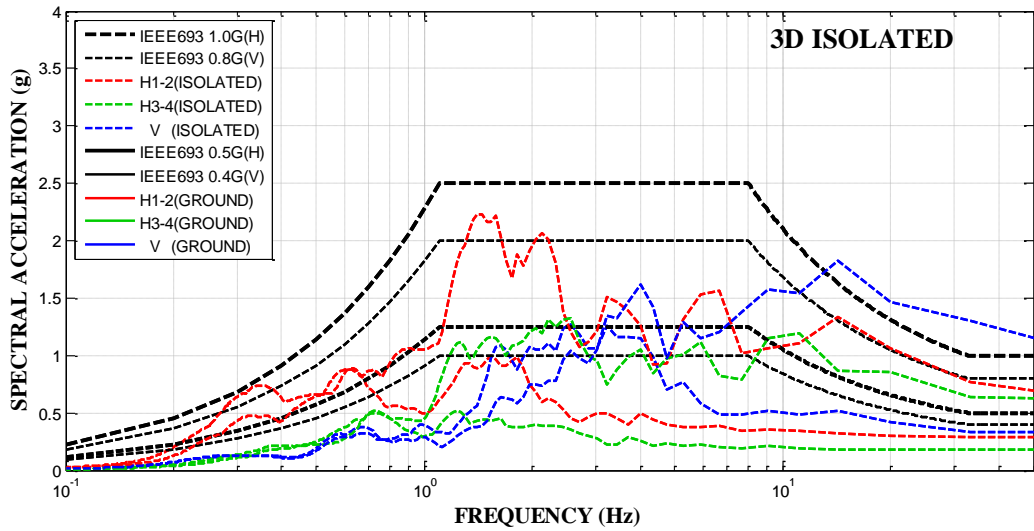
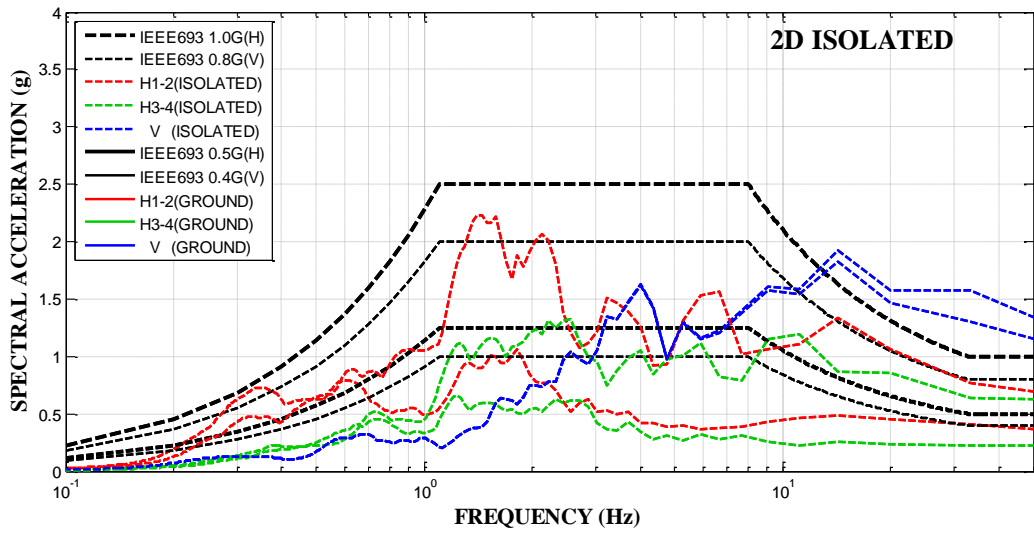


Figure 2-21 Acceleration Response Spectra at 6Hz Bushing Mount of 2D Isolation System (solid line) and 3D Isolation System with Vertical Frequency of 2.0Hz and Damping of 0.50 (dashed line) in LGPC 100% Motion

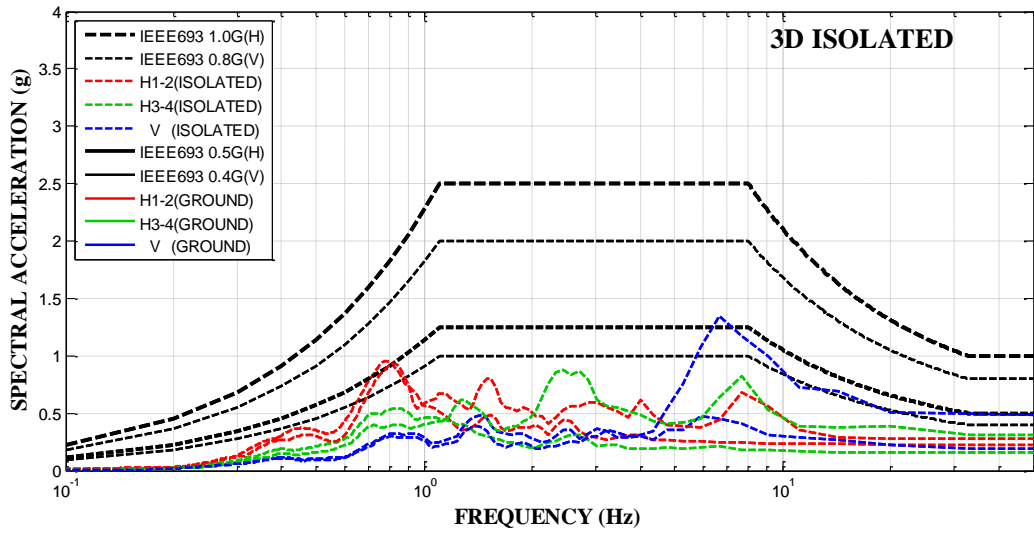
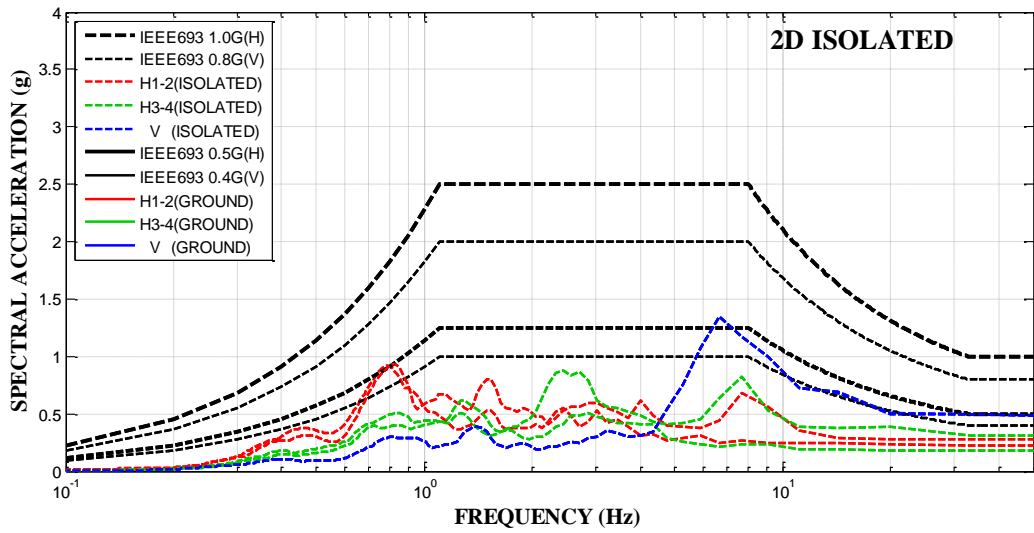


Figure 2-22 Acceleration Response Spectra at 6Hz Bushing Mount of 2D Isolation System (solid line) and 3D Isolation System with Vertical Frequency of 2.0Hz and Damping of 0.50 (dashed line) in Kobe 100% Motion

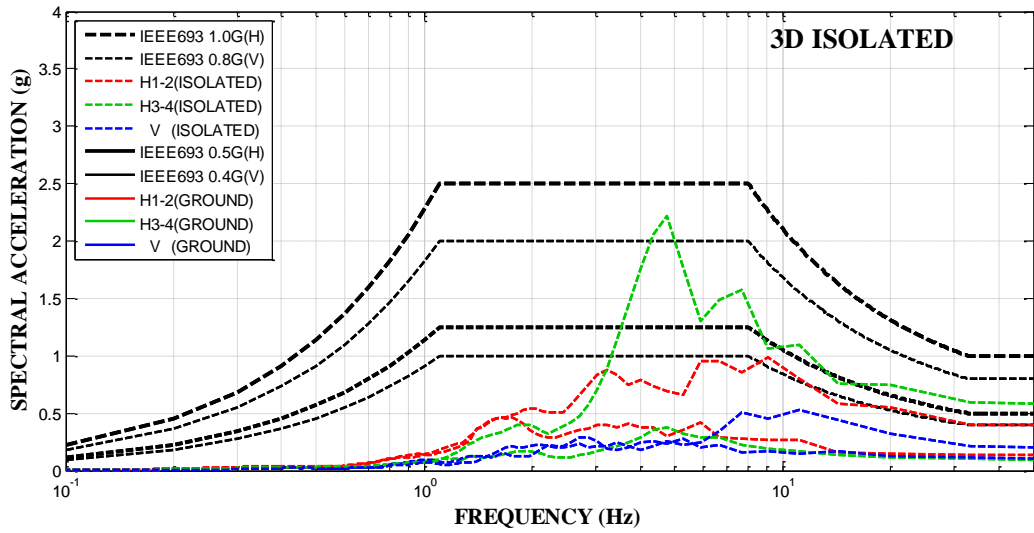
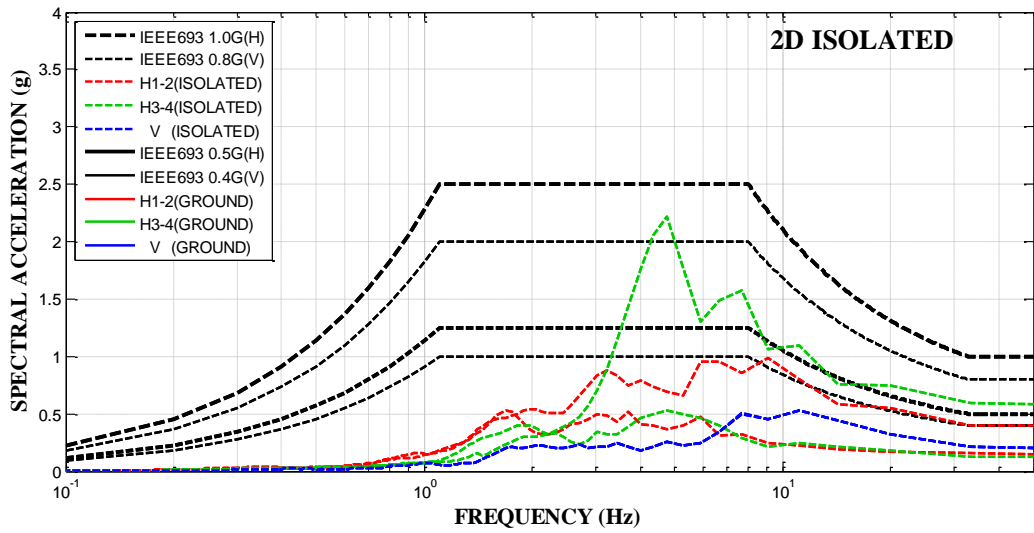


Figure 2-23 Acceleration Response Spectra at 6Hz Bushing Mount of 2D Isolation System (solid line) and 3D Isolation System with Vertical Frequency of 2.0Hz and Damping of 0.50 (dashed line) in Rio 100% Motion

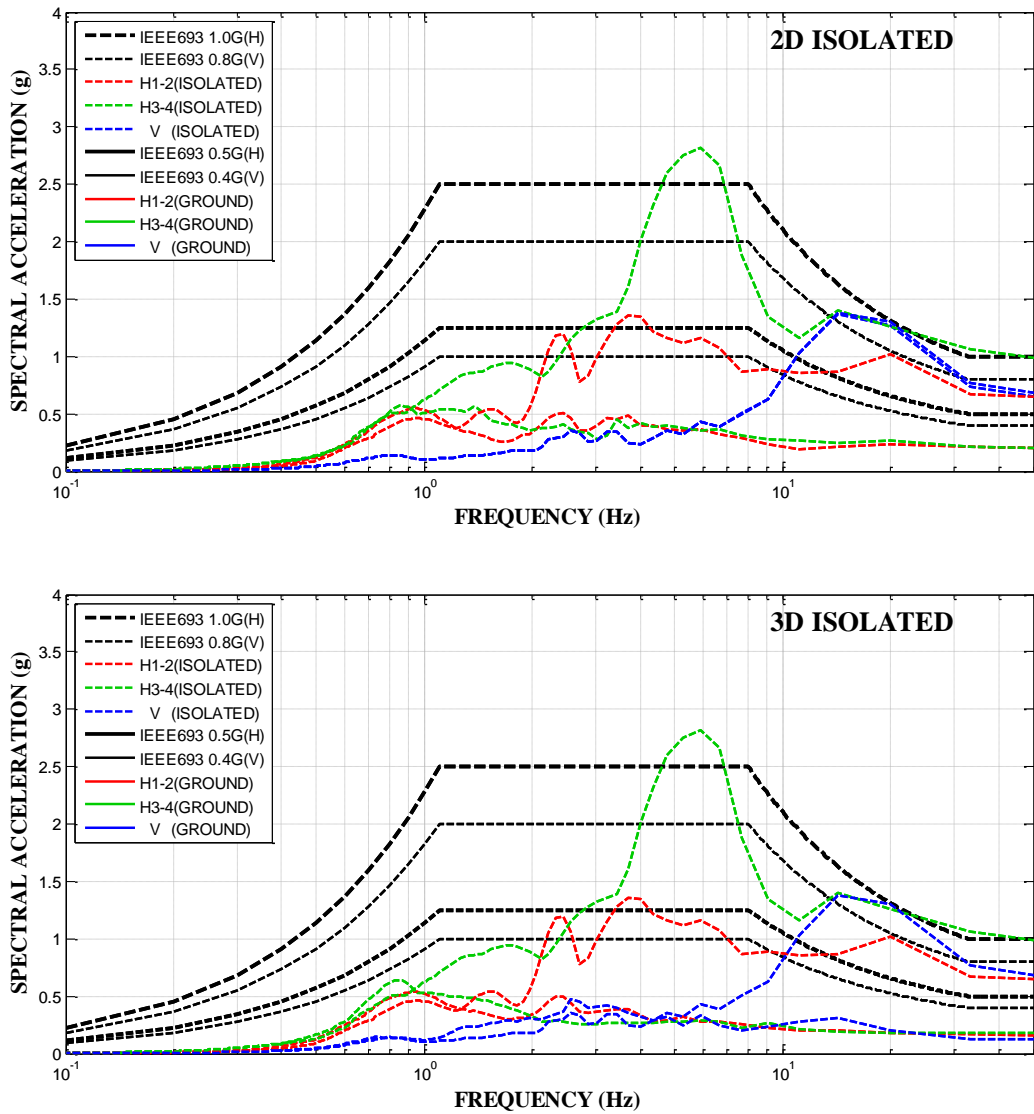


Figure 2-24 Acceleration Response Spectra at 6Hz Bushing Mount of 2D Isolation System (solid line) and 3D Isolation System with Vertical Frequency of 2.0Hz and Damping of 0.50 (dashed line) in Sylmar 100% Motion

2) Peak Acceleration Values

Peak values of acceleration were calculated for each motion at each of the three bushing tops and at a location just above the isolators (see Figure 2-8 for locations), and compared in Table 2-9 for the two 3D isolation systems and for the non-isolated transformer assuming that the transformer base is pinned to the foundation at the four corners. The systems compared in Table 2-9 are:

- a) 3D-FP-spring-damper system ($f_v=2.74\text{Hz}$ and $\beta_v=0.25$) in the upper bound friction conditions, denoted as FP-S-D (UB),
- b) 3D-FP-spring-damper system ($f_v=2.74\text{Hz}$ and $\beta_v=0.25$) in the lower bound friction conditions, denoted as FP-S-D (LB),
- c) 3D-Spring-damper system, denoted as S-D ($f_v=2.74\text{Hz}$ and $\beta_v=0.25$), and
- d) Non-isolated transformer.

The results in Table 2-9 demonstrate the following:

- a) The 3D FP-spring-damper system has substantially lower accelerations than the non-isolated transformer in all directions at all locations. Exception is the special case of the Pacoima motion in the vertical direction and for the acceleration of the rigid frame and of the 10Hz frequency bushing. This case is further investigated later in this report.
- b) The 3D spring-damper system has mixed performance when compared to the non-isolated transformer. For some response quantities and for some motions there is reduction of response and for some other response quantities and for other motions there is increase of response.

Additional analyses were conducted by increasing the vertical damping (value of constant C increased from 2.3kip-sec/in to 4.6kip-sec/in-see Figure 2-19) so that the damping ratio increased from 0.25 to 0.50. Table 2-10 presents results for the peak acceleration of the 6 Hz bushing of the 3D FP-spring-damper isolated transformer where it is demonstrated that the increased damping has a beneficial effect in reducing the acceleration in the vertical direction but also in the horizontal direction as a result of reduced rocking. Note that the increase in vertical damper constant resulted in an increase of the vertical mode damping ratio from 0.25 to 0.50 and also caused an increase in the damping ratio in the rocking mode by a factor of 2 too. These results indicate that a damping ratio of 0.50 in the vertical direction may be desirable in reducing rocking and in reducing the vertical acceleration response.

Table 2-9 Peak Acceleration Values for 3D Isolated and Non-isolated Transformer (in g)

Earthquake	Model	3Hz Bushing Top			6Hz Bushing Top			10Hz Bushing Top			Above Isolator		
		1-2	3-4	V	1-2	3-4	V	1-2	3-4	V	1-2	3-4	V
El Centro 300%	FP-S-D(LB)	0.69	0.77	0.55	0.53	1.06	0.47	0.55	0.79	0.42	0.40	0.32	0.39
	FP-S-D(UB)	0.95	1.01	0.55	0.78	1.27	0.47	0.59	1.03	0.42	0.34	0.30	0.40
	S-D	2.29	3.61	0.70	0.96	2.97	0.48	0.88	2.14	0.53	0.73	1.02	0.45
	Non-isolated	2.10	3.00	1.50	1.39	2.36	1.39	0.81	1.21	0.79	0.64	1.05	0.63
Pacoima 100%	FP-S-D(LB)	0.94	0.91	1.08	0.77	0.91	0.90	0.68	0.82	0.91	0.30	0.24	0.84
	FP-S-D(UB)	1.15	1.21	1.06	0.87	1.22	0.92	0.81	1.33	0.91	0.29	0.29	0.86
	S-D	3.37	2.35	1.16	0.88	2.00	0.93	0.72	1.20	0.97	0.66	0.50	0.92
	Non-isolated	6.61	7.26	1.74	6.40	7.36	1.10	5.80	6.63	0.77	1.22	1.24	0.69
Jensen 100%	FP-S-D(LB)	0.77	0.79	0.62	0.71	0.76	0.34	0.72	0.45	0.34	0.24	0.21	0.29
	FP-S-D(UB)	0.85	1.14	0.60	0.74	1.05	0.33	0.70	0.74	0.35	0.26	0.26	0.27
	S-D	2.79	4.21	0.74	0.77	2.23	0.45	0.70	1.72	0.51	0.53	0.52	0.39
	Non-isolated	1.48	3.51	1.80	0.98	2.62	1.13	0.89	2.62	0.89	0.57	0.99	0.76
Chile 100%	FP-S-D(LB)	1.00	0.96	0.68	0.77	0.85	0.40	0.60	0.82	0.34	0.17	0.13	0.34
	FP-S-D(UB)	1.14	1.14	0.69	0.82	1.06	0.49	0.69	1.01	0.36	0.20	0.18	0.37
	S-D	1.71	2.21	0.68	0.58	1.84	0.44	0.49	0.91	0.34	0.48	0.32	0.39
	Non-isolated	1.99	2.92	1.78	1.91	2.28	1.27	1.62	2.45	0.74	0.61	0.65	0.58
LGPC 100%	FP-S-D(LB)	0.96	0.86	0.69	0.56	0.82	0.50	0.85	0.59	0.47	0.32	0.19	0.47
	FP-S-D(UB)	1.03	0.90	0.63	0.91	0.78	0.52	0.89	0.64	0.44	0.31	0.19	0.50
	S-D	2.59	1.59	0.88	0.97	1.22	0.53	0.73	0.75	0.53	0.56	0.41	0.47
	Non-isolated	4.48	4.08	1.44	4.53	4.20	1.65	4.12	3.67	1.64	0.57	0.61	0.90
Kobe 100%	FP-S-D(LB)	0.47	0.57	0.44	0.47	0.56	0.26	0.46	0.44	0.27	0.19	0.14	0.26
	FP-S-D(UB)	0.59	0.65	0.41	0.59	0.52	0.25	0.55	0.39	0.27	0.23	0.17	0.19
	S-D	1.13	0.87	0.54	0.37	0.49	0.26	0.34	0.43	0.22	0.36	0.24	0.25
	Non-isolated	0.58	0.74	1.27	0.51	0.79	0.65	0.46	0.61	0.54	0.28	0.31	0.45
Rio 100%	FP-S-D(LB)	0.66	0.63	0.24	0.49	0.93	0.24	0.42	0.67	0.14	0.12	0.08	0.13
	FP-S-D(UB)	0.77	0.69	0.27	0.73	1.14	0.25	0.57	0.80	0.15	0.14	0.09	0.13
	S-D	1.43	1.39	0.37	0.45	1.66	0.42	0.33	0.78	0.24	0.35	0.24	0.37
	Non-isolated	1.76	2.53	0.37	1.78	2.52	0.41	1.79	2.15	0.25	0.39	0.55	0.20
Sylmar 100%	FP-S-D(LB)	0.54	0.50	0.30	0.43	0.72	0.24	0.36	0.56	0.18	0.13	0.15	0.18
	FP-S-D(UB)	0.80	0.67	0.30	0.71	0.92	0.28	0.63	0.63	0.19	0.17	0.20	0.17
	S-D	1.96	2.45	0.49	0.61	3.08	0.48	0.42	1.17	0.32	0.41	0.64	0.41
	Non-isolated	2.66	6.47	0.39	2.18	5.82	1.17	1.98	5.15	0.77	0.60	0.84	0.54

Table 2-10 Effect of Vertical Damping on Peak Acceleration Values for 3D FP-Spring-Damper System in Pacoima Motion

Earthquake	Location	Model	Peak Acceleration of 6Hz Bushing (g)		
			1-2	3-4	V
Pacoima 100%	Bushing Top	FP-S-D (C=2.3kip-s/in)	0.87	1.22	0.92
		FP-S-D (C=4.6kip-s/in)	0.81	1.07	0.71
	Bushing Mount	FP-S-D (C=2.3kip-s/in)	0.29	0.29	0.86
		FP-S-D (C=4.6kip-s/in)	0.30	0.29	0.71

3) Peak Displacements with Respect to Ground

Peak values of displacement with respect to the ground were calculated for each motion at each bushing top (see Figure 2-8 for location) and at the isolator level and are presented in Table 2-11 for the two 3D isolated and the non-isolated transformer. The displacement values presented is the peak resultant horizontal displacement and the peak vertical displacement, all with respect to the ground. The reported values do not include the static component of displacement in the vertical direction, which equals 1.3inch (for frequency of 2.74Hz). For the 3D FP-spring-damper system, the results are for the case of vertical damping ratio equal to 0.25.

The results show that the vertical dynamic spring displacement of the FP-spring-damper system is about 1inch which is small enough to result in a compact vertical system.

Table 2-11 Peak Dynamic Displacement Values for 3D Isolated and Non-isolated Transformer (in inch)

Earthquake	Model	3Hz Bushing		6Hz Bushing		10Hz Bushing		Isolator	
		H _{RESULTANT}	V						
El Centro 300%	FP-S-D(LB)	18.58	0.88	19.06	0.79	19.11	0.49	17.90	2.17
	FP-S-D(UB)	14.16	0.77	14.22	0.85	14.10	0.50	13.65	2.31
	S-D	7.95	1.10	8.01	0.95	7.55	0.64	1.42	2.35
	Non-isolated	1.13	0.30	0.24	0.08	0.18	0.01	NA	NA
Pacoima 100%	FP-S-D(LB)	16.01	1.07	16.10	1.01	16.13	1.02	14.93	2.53
	FP-S-D(UB)	14.47	1.06	14.51	1.03	14.49	1.02	13.42	2.56
	S-D	5.95	1.11	4.26	1.54	4.20	1.01	1.20	2.18
	Non-isolated	1.10	0.35	0.29	0.06	0.28	0.01	NA	NA
Jensen 100%	FP-S-D(LB)	10.92	0.63	11.06	0.40	11.14	0.44	10.83	1.80
	FP-S-D(UB)	9.97	0.59	9.90	0.41	10.02	0.45	8.52	1.94
	S-D	6.34	0.78	4.46	0.79	4.06	0.50	1.02	1.77
	Non-isolated	1.87	0.37	0.16	0.06	0.20	0.02	NA	NA
Chile 100%	FP-S-D(LB)	4.38	0.49	4.63	0.42	4.63	0.38	4.42	1.88
	FP-S-D(UB)	3.69	0.49	3.79	0.44	3.87	0.38	3.58	1.97
	S-D	3.65	0.51	2.73	0.49	2.51	0.47	0.79	0.99
	Non-isolated	0.89	0.37	0.21	0.07	0.12	0.01	NA	NA
LGPC 100%	FP-S-D(LB)	14.50	0.83	14.92	0.62	14.96	0.56	14.09	0.77
	FP-S-D(UB)	11.40	0.87	11.54	0.71	11.58	0.58	10.98	0.73
	S-D	4.60	1.01	3.37	0.93	3.17	0.63	1.20	1.36
	Non-isolated	0.76	0.29	0.21	0.08	0.15	0.03	NA	NA
Kobe 100%	FP-S-D(LB)	6.32	0.34	6.26	0.22	6.28	0.29	5.70	1.67
	FP-S-D(UB)	5.65	0.36	5.76	0.24	5.85	0.28	5.37	1.73
	S-D	2.46	0.47	1.97	0.33	1.90	0.33	0.65	0.71
	Non-isolated	0.43	0.26	0.14	0.03	0.09	0.01	NA	NA
Rio 100%	FP-S-D(LB)	2.49	0.18	2.43	0.16	2.44	0.19	2.30	0.30
	FP-S-D(UB)	2.50	0.19	2.60	0.16	2.61	0.19	2.33	0.30
	S-D	2.46	0.43	1.53	0.27	1.52	0.30	0.63	0.63
	Non-isolated	0.53	0.07	0.18	0.02	0.11	0.00	NA	NA
Sylmar 100%	FP-S-D(LB)	4.29	0.24	4.09	0.28	4.10	0.26	3.41	0.40
	FP-S-D(UB)	4.41	0.26	4.39	0.31	4.50	0.28	3.56	0.51
	S-D	3.83	0.51	4.66	0.78	3.96	0.39	1.01	1.46
	Non-isolated	1.02	0.09	0.30	0.06	0.19	0.01	NA	NA

2.5 Study for the Selection of Properties of the Vertical Isolation System

The studied 3D FP-spring-damper system has been determined to be an effective three-dimensional seismic isolation system. However, the analyzed system was relatively stiff in the vertical direction ($f_v=2.74\text{Hz}$) and lightly damped ($\beta_v=0.25$) so its isolation effectiveness in the vertical direction may be improved. Note that the vertical stiffness of the FP-spring-damper system was selected to be comparable to that of the 3D spring-damper isolation system, but it can be lower without affecting the fundamental frequency of the isolated equipment.

A parametric study of the isolated transformer with the characteristics of Figure 2-10 was conducted in which the following three parameters were varied, whereas all other parameters remained the same:

- 1) The weight of the equipment was 320, 418 and 520kip,
- 2) The vertical isolator stiffness was varied so that the vertical frequency varied in the range of 1.5 to 2.75Hz, and
- 3) The vertical isolator damping constant was varied so that the vertical damping ratio varied in the range of 0.2 to 0.7.

Figures 2-25 and 2-26 present the calculated peak vertical accelerations at the 6Hz bushing mount and at the top, respectively, as function of the vertical frequency and damping ratio for the eight three-component ground motions of Table 2-8. The peak acceleration values are normalized by the peak ground acceleration of each motion (PGA per Table 2-8, for the case of the El Centro earthquake, the PGA in Table 2-8 was scaled up by factor of 3). The results are for the case of the 418kip transformer model and for the triple FP isolators having the upper bound friction properties per Table 2-5 as these conditions resulted in the largest acceleration response. The results demonstrate that (a) reducing the vertical frequency has benefits in reducing the vertical acceleration and (b) increasing the vertical damping to about 0.50 has further benefits in reducing sensitivity to the value of the vertical frequency. On the basis of these results it is desirable to select the properties of the vertical isolation system so that the vertical frequency is 2.0Hz and damping ratio is 0.50, depending however on the demands for vertical displacement,

which is investigated in Figures 2-27 and 2-28 where the vertical displacement demands are presented.

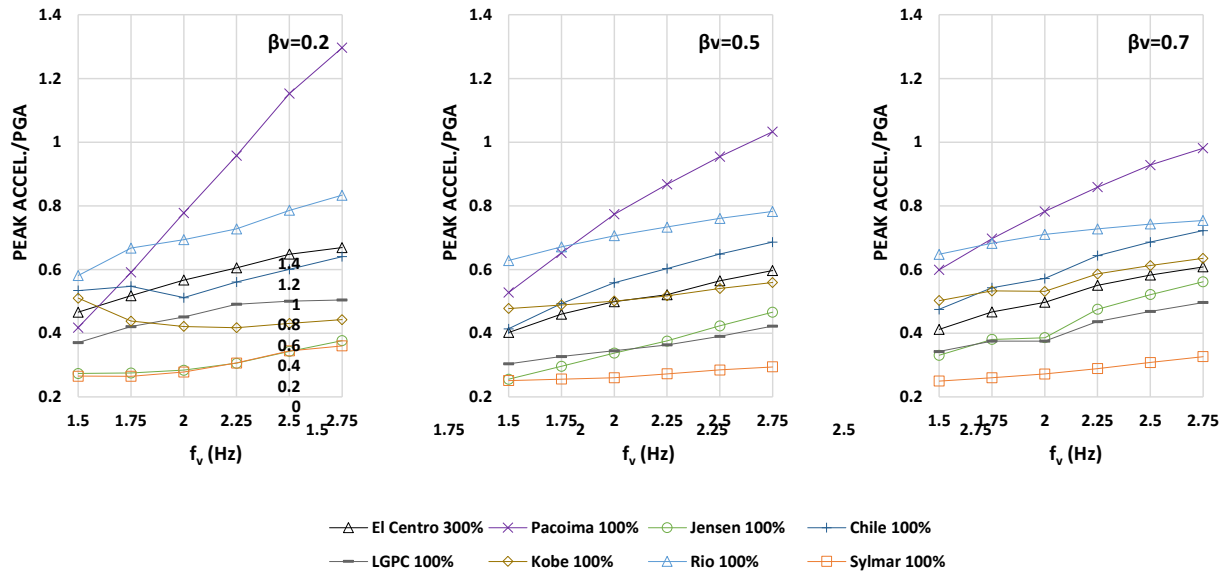


Figure 2-25 Peak Vertical Acceleration at 6Hz Bushing Mount Normalized by Peak Vertical Ground Acceleration

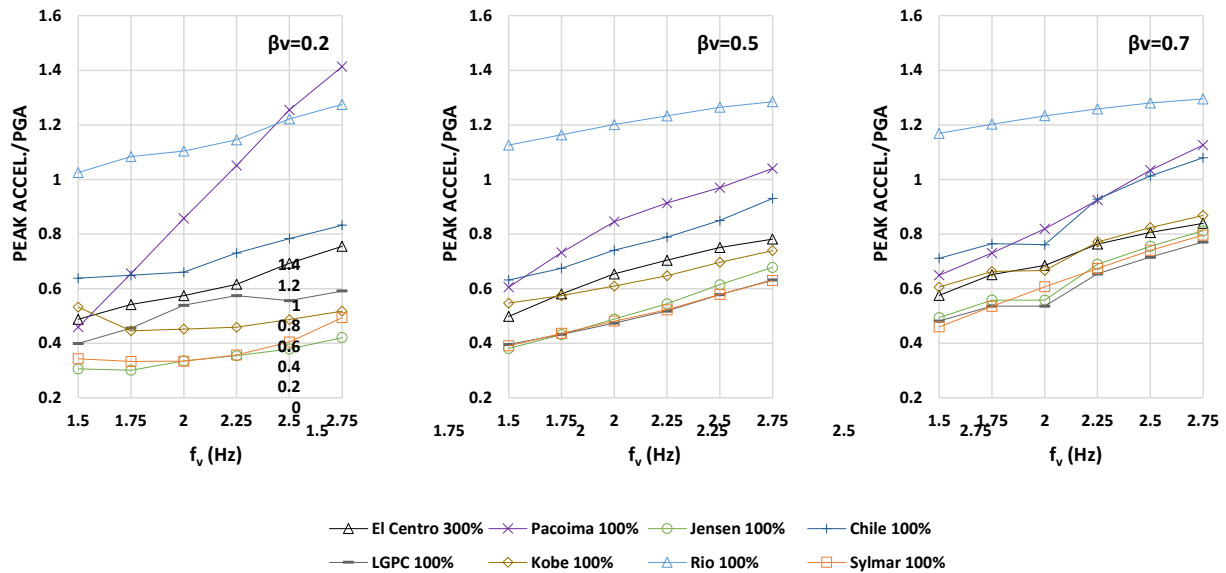


Figure 2-26 Peak Vertical Acceleration at 6Hz Bushing Top Normalized by Peak Vertical Ground Acceleration

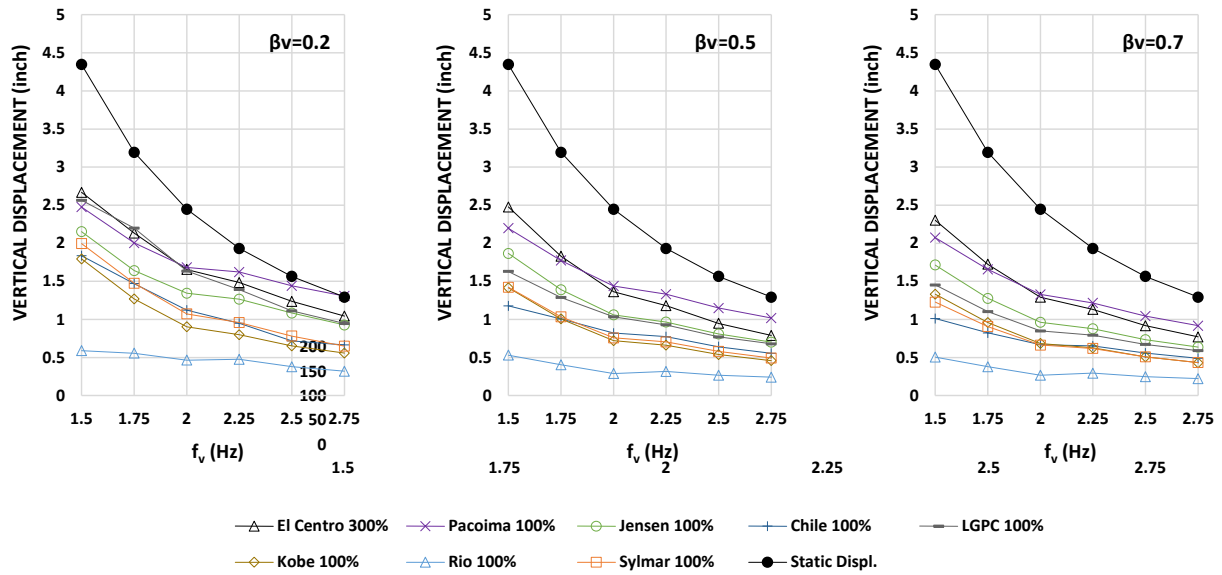


Figure 2-27 Static and Peak Dynamic Vertical Isolator Displacement Demands

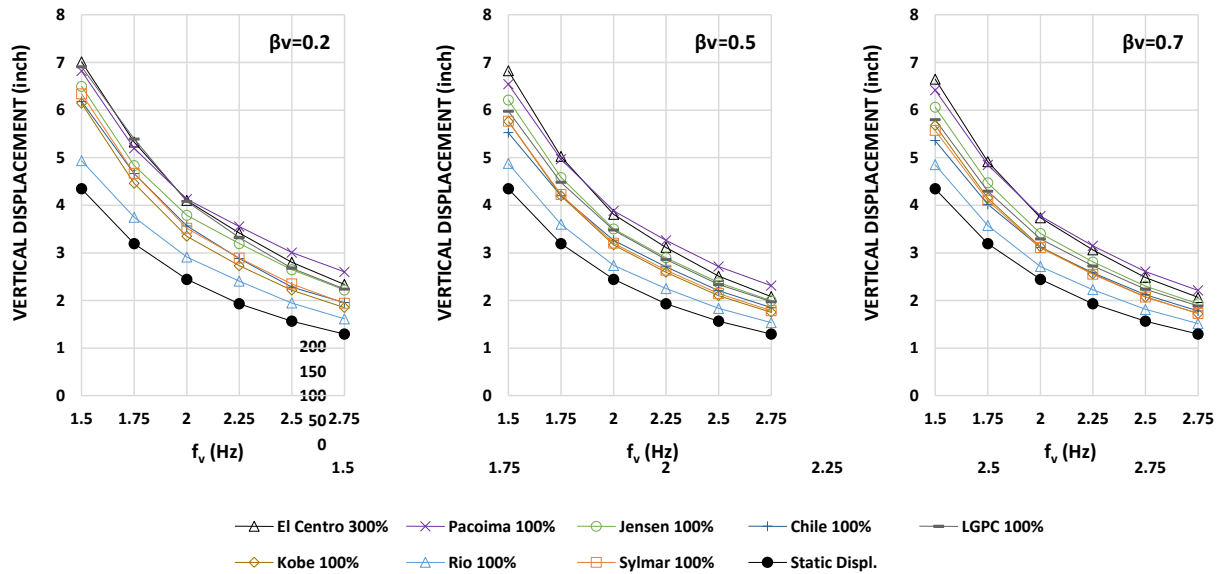


Figure 2-28 Static and Total Vertical Isolator Displacement Demands

Note that the results in Figures 2-27 and 2-28 are for the vertical isolator with the maximum dynamic demand which differs depending on the motion used and the characteristics of the vertical isolation system due to effects these have on the rocking response. Based on the results of these figures, a system with vertical frequency of 2.0Hz and a damping ratio of 0.50 will have

a static vertical displacement of 2.4inch and a dynamic displacement of 1.6inch for a total of 4.0inch, which is entire practical.

The 2.0Hz frequency and 0.50 damping ratio vertical isolation system was further investigated and results are presented in Table 2-12 where the peak vertical acceleration at the 6Hz bushing mount and top are compared for the 418kip transformer when non-isolated, when isolated by the 2D triple FP system (2D-isolated) and when isolated by the 3D triple FP and spring-damper system with $f_v=2.0\text{hz}$ and $\beta_v=0.50$ (3D-isolated). The upper bound friction values were used as they resulted in the largest accelerations. The comparison in Table 2-12 together with the acceleration response spectra presented in Figures 2-20 to 2-24 demonstrate the benefits offered by the 3D isolation system with the selected parameters of 2.0Hz vertical frequency and 0.50 vertical damping ratio.

Table 2-12 Peak Vertical Acceleration Values (in g) for Non-isolated 418kip Transformer, 2D Isolated 418kip Transformer with Triple FP System and 3D Isolated 418kip Transformer with Triple FP and Spring-Damper System with $f_v=2.0\text{Hz}$ and $\beta_v=0.50$

Model	Response Location	El Centro 300%	Pacoima 100%	Jensen 100%	Chile 100%	LGPC 100%	Kobe 100%	Rio 100%	Sylmar 100%
Non-isolated	6Hz Bushing Mount	0.63	0.69	0.76	0.58	0.90	0.45	0.20	0.54
	6 Hz Bushing Top	1.39	1.10	1.13	1.27	1.65	0.65	0.41	1.17
2D-isolated	6Hz Bushing Mount	0.60	0.69	0.80	0.57	0.91	0.45	0.19	0.47
	6 Hz Bushing Top	1.55	1.16	1.27	1.55	1.83	0.68	0.48	1.28
3D-isolated	6Hz Bushing Mount	0.31	0.53	0.26	0.32	0.31	0.23	0.14	0.14
	6 Hz Bushing Top	0.41	0.58	0.37	0.43	0.43	0.27	0.24	0.26

The effect of the weight of the transformer is investigated next. It is presumed that the properties of the vertical isolation system are fixed so that at each of the four supports the stiffness is $K=44\text{kip/in}$ and the damping constant is $C=3.4\text{kip-sec/in}$ which result in a frequency of 2.0Hz and damping ratio of 0.50 for the transformer of 418kip weight. The weight is now considered to be 320kip, 418kip and 520kip, while the transformer dimensions are assumed un-changed, and analyses are performed to obtain information on the effect on the isolator displacement demands.

This enables the selection of the design parameters for the vertical isolation system to be used in applications of transformer weights of 300 to 500kip (plus additional weight for the isolation system installation).

Table 2-13 presents the properties of the isolation system in the three cases of transformer weight. Note that the weight affects friction in addition to the vertical frequency and damping. The frictional properties of the triple FP isolators were determined based on test data of isolators at a load of 105kip (thus representative of the 418kip transformer) and then adjusted to reflect the effect of larger or lesser vertical loads following the paradigm in the examples in McVitty and Constantinou (2015).

Table 2-13 Properties of Analyzed Transformers with 3D FP-spring-damper Isolation System

Transformer Weight (kip)	Vertical Stiffness (K) and Vertical Damping Constant (C) Per Support	Vertical Frequency (f_v) and Vertical Damping Ratio (β_v)	Friction Coefficient in Triple FP Isolators (Lower Bound/Upper Bound)	
			$\mu_1 = \mu_4$	$\mu_2 = \mu_3$
320	K=44 kip/in and C=3.4kip-s/in	$f_v=2.3\text{Hz}$ and $\beta_v=0.56$	0.120/0.160	0.100/0.115
418	K=44 kip/in and C=3.4kip-s/in	$f_v=2.0\text{Hz}$ and $\beta_v=0.50$	0.110/0.150	0.080/0.090
520	K=44 kip/in and C=3.4kip-s/in	$f_v=1.8\text{Hz}$ and $\beta_v=0.44$	0.100/0.140	0.070/0.085

Results of the analysis are presented in Table 2-14 where the peak displacements of the top of the 6Hz bushing and of the isolators are presented. The isolator displacement demands are the resultant horizontal displacement of the FP isolators and the vertical displacement of the spring-damper units (static component and total components are reported). These values are useful in the isolation system design. The value of displacement (peak resultant in the horizontal direction and the peak vertical displacement of the bushing top) are useful in the design of electric cables connected to the bushings. Two values of the vertical displacement of the spring-damper unit are reported. They are the static displacement due to the transformer weight and the total value (static plus dynamic displacement). For example, the values 1.91/2.37 mean that the static displacement is 1.91inch and a total displacement (static plus dynamic) is 2.37inch. The

dynamic component is $2.37-1.91=0.46$ inch. Note that for the El Centro 300% and Pacoima 100% motions the isolator displacement demands exceed the capacity of the bearings which is about 13inch so that the results would apply for bearings with larger concave plate diameter.

Additional results on the peak displacement and peak forces for spring-damper units are presented in Table 2-15. The values are those calculated in the upper bound friction case, which resulted in the largest values. On the basis of these results Table 2-16 has been prepared to present the parameters for the vertical spring-damper isolation system. Note that four units are used each with vertical stiffness of $K=44$ kip/inch and linear viscous damping constant $C=3.4$ kip-sec/inch to support transformers of total weight of 320 to 520kip. The static displacement demand is 3inch and an additional dynamic displacement capacity required of ± 2.0 inch (total is 5.0inch) is required. The peak total vertical force per spring-damper unit is 235kip and the lateral force that the unit needs to resist is about 0.3 times the supported weight or about 40kip. The overturning moment in this table is the overturning moment (including $P\Delta$ effects) of the FP isolator at its displacement capacity.

The table also includes information on the parameters of an alternative vertical isolation system with a vertical frequency of 2.5Hz at the nominal weight of 418kip. The parameters of the system were obtained in Figures 2-27 and 2-28 that are limited to displacement demands so that there is no information on the required force demands.

Table 2-14 Displacement Demands at Bushing Top, FP Isolators, and Spring-Damper Units for System with K=44 kip/in and C=3.4kip-s/in (H_{RES}: resultant horizontal displacement)

Earthquake	Triple FP Friction	W=320kip				W=418kip				W=520kip			
		6Hz Bushing Top		Isolator	Spring-Damper	6Hz Bushing Top		Isolator	Spring-Damper	6Hz Bushing Top		Isolator	Spring-Damper
		H _{RES}	V	H _{RES}	V ¹	H _{RES}	V	H _{RES}	V ¹	H _{RES}	V	H _{RES}	V ¹
El Centro 100%	Lower Bound	2.78	2.23	1.77	1.91 /2.37	3.22	2.88	1.97	2.49 /3.06	3.47	3.02	2.05	3.09 /3.76
	Upper Bound	2.16	2.38	1.36	1.91 /2.43	2.82	2.97	1.70	2.49 /3.14	3.01	3.07	1.69	3.09 /3.86
El Centro 200%	Lower Bound	9.81	6.47	7.17	1.91 /2.59	11.06	7.90	8.04	2.49 /3.32	12.35	9.36	8.85	3.09 /4.14
	Upper Bound	6.86	5.44	5.11	1.91 /2.73	7.20	6.56	6.02	2.49 /3.50	7.72	6.95	6.09	3.09 /4.28
El Centro 300%	Lower Bound	22.71	16.03	16.62	1.91 /2.99	24.45	18.13	17.75	2.49 /3.95	26.52	20.09	19.11	3.09 /4.94
	Upper Bound	17.08	11.86	12.54	1.91 /2.88	18.43	13.95	13.44	2.49 /3.81	19.80	15.58	14.25	3.09 /4.78
Pacoima 100%	Lower Bound	18.18	8.26	13.95	1.91 /3.03	19.32	8.64	14.58	2.49 /3.84	20.11	8.90	14.98	3.09 /4.64
	Upper Bound	15.32	7.66	11.83	1.91 /3.05	16.84	8.30	12.75	2.49 /3.88	17.50	8.68	13.07	3.09 /4.70
Jensen 100%	Lower Bound	11.38	9.61	8.63	1.91 /2.74	12.59	10.48	10.50	2.49 /3.57	15.15	10.91	12.49	3.09 /4.46
	Upper Bound	9.05	8.70	6.72	1.91 /2.71	10.30	10.52	7.92	2.49 /3.50	10.98	11.18	8.05	3.09 /4.34
Chile 100%	Lower Bound	5.48	3.24	3.67	1.91 /2.44	6.42	3.15	4.28	2.49 /3.16	7.06	3.42	4.67	3.09 /3.88
	Upper Bound	4.26	3.21	2.76	1.91 /2.53	5.36	3.50	3.46	2.49 /3.27	5.71	3.83	3.62	3.09 /3.99
LGPC 100%	Lower Bound	16.72	7.04	12.45	1.91 /2.68	18.46	7.40	13.50	2.49 /3.45	19.80	7.71	14.29	3.09 /4.26
	Upper Bound	12.36	5.86	9.01	1.91 /2.78	14.69	6.45	10.47	2.49 /3.48	15.80	6.95	11.17	3.09 /4.20
Kobe 100%	Lower Bound	7.38	3.15	5.24	1.91 /2.41	8.01	3.63	5.64	2.49 /3.12	8.15	3.95	5.66	3.09 /3.83
	Upper Bound	5.88	2.86	4.10	1.91 /2.46	7.66	3.45	5.32	2.49 /3.17	8.00	3.76	5.48	3.09 /3.92
Rio 100%	Lower Bound	3.39	0.96	2.28	1.91 /2.14	3.33	1.07	2.26	2.49 /3.12	3.18	1.16	2.16	3.09 /3.83
	Upper Bound	3.35	0.93	2.25	1.91 /2.16	3.26	1.07	2.17	2.49 /2.74	3.30	1.18	2.14	3.09 /3.37
Sylmar 100%	Lower Bound	3.39	3.94	2.92	1.91 /2.36	3.33	4.35	3.05	2.49 /3.07	3.18	4.76	3.16	3.09 /3.75
	Upper Bound	3.88	3.87	2.92	1.91 /2.51	3.78	4.34	2.84	2.49 /3.20	3.48	4.52	2.47	3.09 /3.94

¹ Static displacement/total displacement of spring-damper units

Table 2-15 Peak Displacements and Forces in Spring-Damper Units for System with K=44 kip/in and C=3.4kip-s/in in Upper Bound Friction Case

Earthquake	Total Weight (kip)	Peak Displacement (in)	Peak Spring Force (kip)	Peak Damper Force (kip)	Peak Total Force (kip)
Static	320	1.91	84.2	-	84.2
	418	2.49	109.5	-	109.5
	520	3.09	135.8	-	135.8
El Centro 100%	320	2.43	107.1	16.8	109.7
	418	3.14	138.0	18.1	140.7
	520	3.86	170.0	21.4	172.4
El Centro 200%	320	2.73	119.9	25.9	127.3
	418	3.50	153.9	28.3	163.4
	520	4.28	188.5	32.6	199.2
El Centro 300%	320	2.88	126.9	30.6	138.4
	418	3.81	167.5	34.3	175.7
	520	4.78	210.5	40.0	217.6
Pacoima 100%	320	3.05	134.0	51.6	151.5
	418	3.88	170.9	58.4	190.3
	520	4.70	206.8	60.2	227.4
Jensen 100%	320	2.71	119.1	42.2	128.8
	418	3.50	154.2	42.3	164.6
	520	4.34	191.1	41.7	201.1
Chile 100%	320	2.53	111.3	33.0	124.4
	418	3.27	143.7	33.9	154.8
	520	3.99	175.5	37.4	188.5
LGPC 100%	320	2.78	122.4	30.7	131.4
	418	3.48	153.1	36.2	163.8
	520	4.20	184.7	40.9	199.1
Kobe 100%	320	2.46	108.3	24.5	115.2
	418	3.17	139.3	23.0	147.5
	520	3.92	172.4	23.7	179.5
Rio 100%	320	2.16	94.9	14.4	102.5
	418	2.74	120.4	15.6	126.8
	520	3.37	148.2	17.9	155.2
Sylmar 100%	320	2.51	110.6	21.4	118.5
	418	3.20	140.9	25.4	151.9
	520	3.94	173.2	28.4	184.8

Table 2-16 Design Parameters for Vertical Isolation System Unit

System Characteristics for 418kip Transformer	$f_v=2.0\text{Hz}$, $\beta_v=0.50$	$f_v=2.5\text{Hz}$, $\beta_v=0.50$
Static load (maximum value)	130kip	130kip
Static deflection (for maximum load)	3.0inch	1.5inch
Stiffness per unit	44kip/inch	65kip/inch
Damping constant per unit (linear viscous damping)	3.4kip-sec/inch	4.2kip-sec/inch
Dynamic deflection	$\pm 2.0\text{inch}$	$\pm 1.5\text{inch}$
Total deflection	5.0inch	3.0inch
Peak axial force per unit	235kip	-
Peak damping force per unit	85kip	-
Peak lateral force per unit (to be resisted by unit)	65kip	-
Peak overturning moment per unit (to be resisted by unit)	1800kip-inch	-

SECTION 3

DESCRIPTION AND PROPERTIES OF MODEL FOR TESTING

3.1 Introduction

The combined triple FP isolators and vertical spring-damper system studied in Section 2 is selected as the system to develop its components and to test. It is noted that the extensive research efforts in Japan, described in Section 1, have resulted in the development of a number of systems with similar configurations as the one envisioned in this work. However, none of those systems was found to be acceptable for application in the seismic protection of electrical transformers due to their complexity, use of active components, lack of reliability and obviously prohibitive cost. Rather, the components of the system should be passive, highly reliable and readily available from reputable manufacturers. The analytical study in Section 2 established the desired characteristics of the system.

A decision was made to test a large model in real time scale and at the largest possible weight that could be safely supported on the shake table at the University at Buffalo. This led to a model of weight of 68.1kip and 72.4kip in two tested configurations. This weight is the one supported by the spring-damper units. The weight supported by the FP isolators is less by the weight of the top part of the spring damper units (each 0.3kip), the bottom part of the FP isolators (each 0.5kip) and the additional base (4.35kip) in one of the two tested configurations. The gravity load on the FP isolators was 64.9kip or 16.2kip per isolator.

Four triple FP isolators identical to those used in the Washington, WA were obtained from Earthquake Protection Systems, Inc. Tests of the isolators at the University at Buffalo showed that friction in these bearings was larger than in the actual application due to the reduced load on each bearing of the tested model (16.2kip vs 105kip in the actual application) leading to a nominal friction value of 0.20 instead of 0.12. In some tests the bearings were lubricated in the laboratory in a rudimentary effort to reduce friction and a nominal friction of about 0.07 was achieved but in somehow unstable conditions. Then a second set of isolators was acquired from Earthquake Protection Systems, Inc. in which the contact surfaces were altered so that the contact pressure

increased and a nominal friction of 0.12 was achieved, as desired for the actual application. Thus tests were conducted with three different FP isolator friction values. The three sets of FP isolators also had some other small differences that will be described later in this section.

The vertical spring-damper units were designed and manufactured at Taylor Devices, Inc. on the basis of specifications described in this report. The main characteristics of the spring-damper units were to provide a vertical frequency of 2.0Hz and a corresponding damping ratio of 0.50 for the initially estimated model weight of 67kip. The actual model weight varied from 68.1 to 72.4kip so that the vertical frequency and damping were slightly different. The units were then tested at the University at Buffalo and their properties verified.

Two configurations of the isolation system were tested on the shake table. One was as studied in Section 2 and schematically depicted in Figure 2-5. In this configuration, the transformer is allowed to freely rock on the supporting springs. Rocking can be limited by a combination of increased rocking frequency (by placement of the bearings at larger distance from each other) and high vertical damping (hence the use of damping ratio of 0.50). The system with allowance for free rocking is very desirable because of its simplicity and ease in construction. However, there are special cases where rocking needs to be restricted (Kitayama et al, 2016). For such cases, a second configuration was developed and tested in which a stiff base was placed between the vertical spring-damper units and the triple FP isolators above.

The experimental program included (a) testing of the triple FP isolators, (b) testing of the spring-damper devices, (c) identification of as-installed properties of the bushing on top of the frame representing the transformer, (d) identification of the properties of the isolated test model, and (e) shake table testing of the isolated test model. There was no testing performed without the isolation system or with only the horizontal isolation system.

3.2 Description of Transformer Test Model

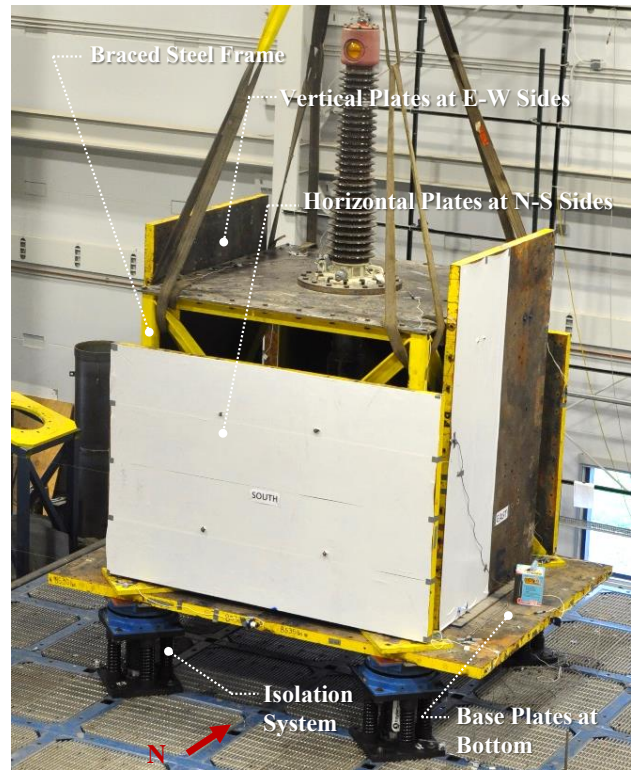
Figure 3-1 presents the transformer model. Figure 3-1 (a) shows the model prior to adding steel plates to represent the weight of the transformer and prior to adding the isolation system. As shown it was used in the identification of the as-installed properties of the bushing. The frame is 8ft x 8ft

x 8ft braced frame of which details are presented in Appendix D. A 0.75inch thick steel cover plate supported a bushing at the center. Figure 3-1 (b) shows the completed transformer model. The frame of Figure 3-1(a) was bolted on top of a base consisting of two inter-connected plates and then four additional plates were placed on the frame sides for added mass. Each of these plates had a weight of 8.6kip. The total weight of the model including the top concave plates of the triple FP isolators (that is the horizontally seismically isolated weight) was 64.9kip. The total weight supported by the spring-damper units (64.9kip plus weight of bottom part of FP isolators and top part of spring-damper units) was 68.1kip. In this configuration, the vertical frequency of the isolated model is 1.92Hz and the corresponding damping ratio is 0.50. These values are based on the actual stiffness and damping constant of the spring-damper units as measured in tests (6.4kip/in vs the specified 6.8kip/in and 0.53kip-sec/in vs the specified 0.54kip-sec/in). The frequency and damping ratio would have been 1.98Hz and 0.49, respectively, if the stiffness and damping constant were 6.8kip/in and 0.54kip-sec/in, respectively. Figure 3-2 shows schematics of the isolated transformer model with information on the basic dimensions and the location of the center of mass. The mass moment of inertia about the center of mass of the test model was calculated to be $I_{CM}=621\text{kip-in-s}^2$. In the calculation only the mass above the center of the FP isolators was considered (corresponding weight is 64.9kip).

The bushing used in the testing was measured and found to have the dimensional properties of bushing No. 6 of Table 2-1 but its weight was measured at 890lb instead of 840lb. It was assumed that the locations of the centers of mass of the upper and lower bushing parts were the same as those of bushing No. 6 of Table 2-1 and that the weight was distributed as 490lb at the upper part, 100lb at the connection to the plate and 300lb at the lower part.



(a)



(b)

Figure 3-1 Transformer Model for Shake Table Testing: (a) Braced Frame with Cover Plate and Bushing and (b) Complete Test Model with Added Mass and Seismic Isolation System (configuration allowed to freely rock)

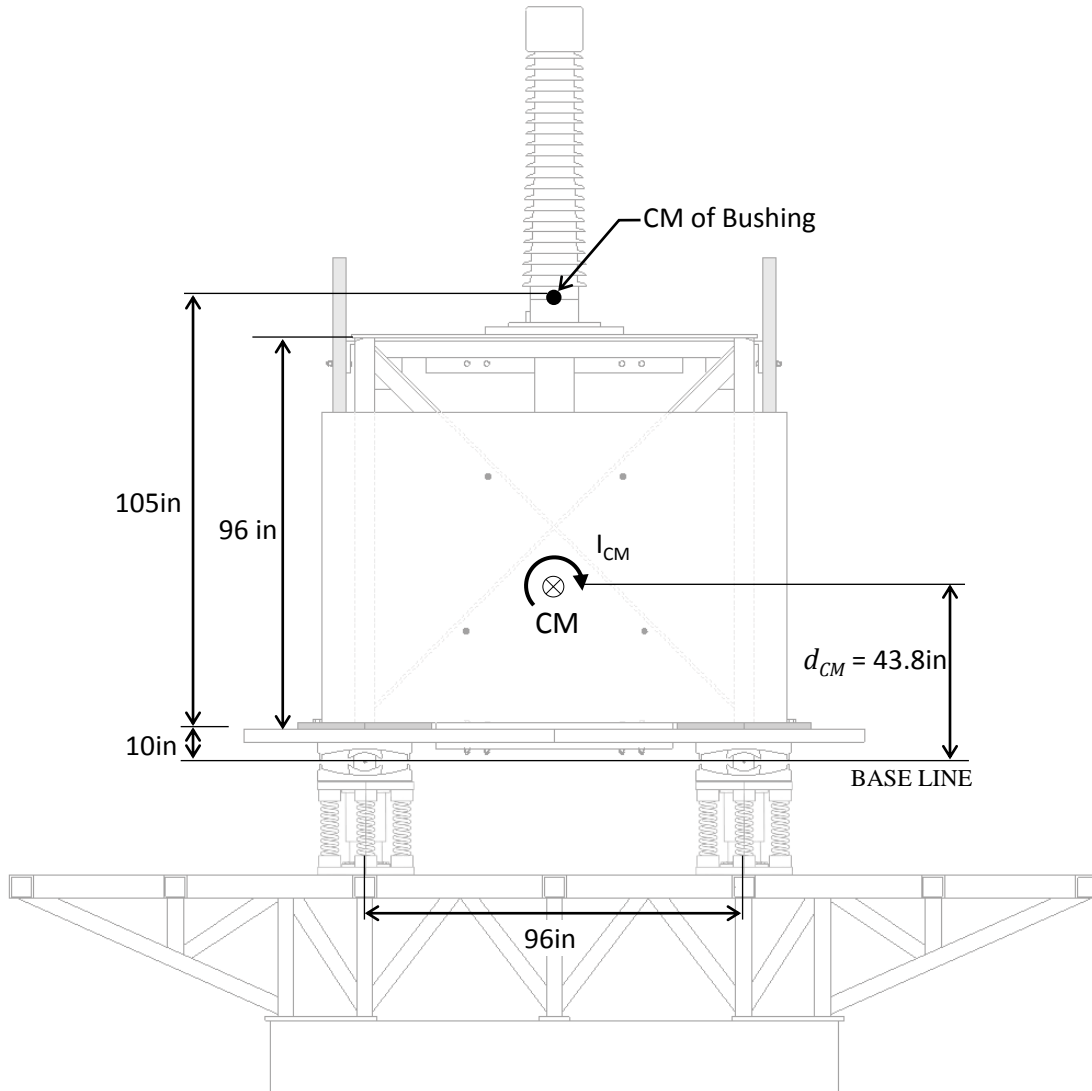


Figure 3-2 Basic Dimensions of Isolated Transformer Test Model, Free Rocking Configuration

A second isolation system configuration was also tested in which a stiff steel base was installed between the vertical spring-damper units and the triple FP isolators as shown in the photograph of Figure 3-3 and the schematic of Figure 3-4.

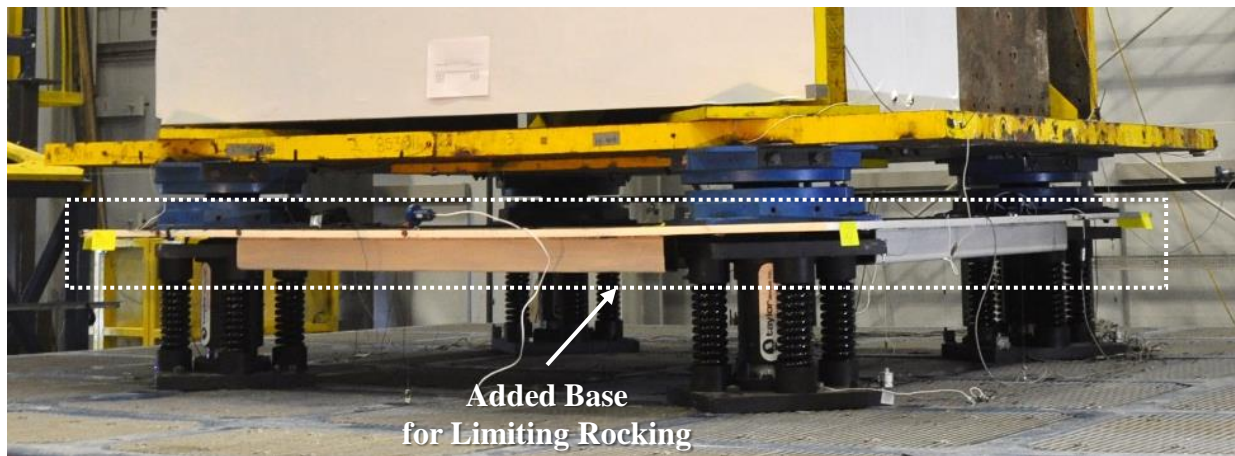


Figure 3-3 View of Model of Isolated Transformer with Added Base for Limiting Rocking

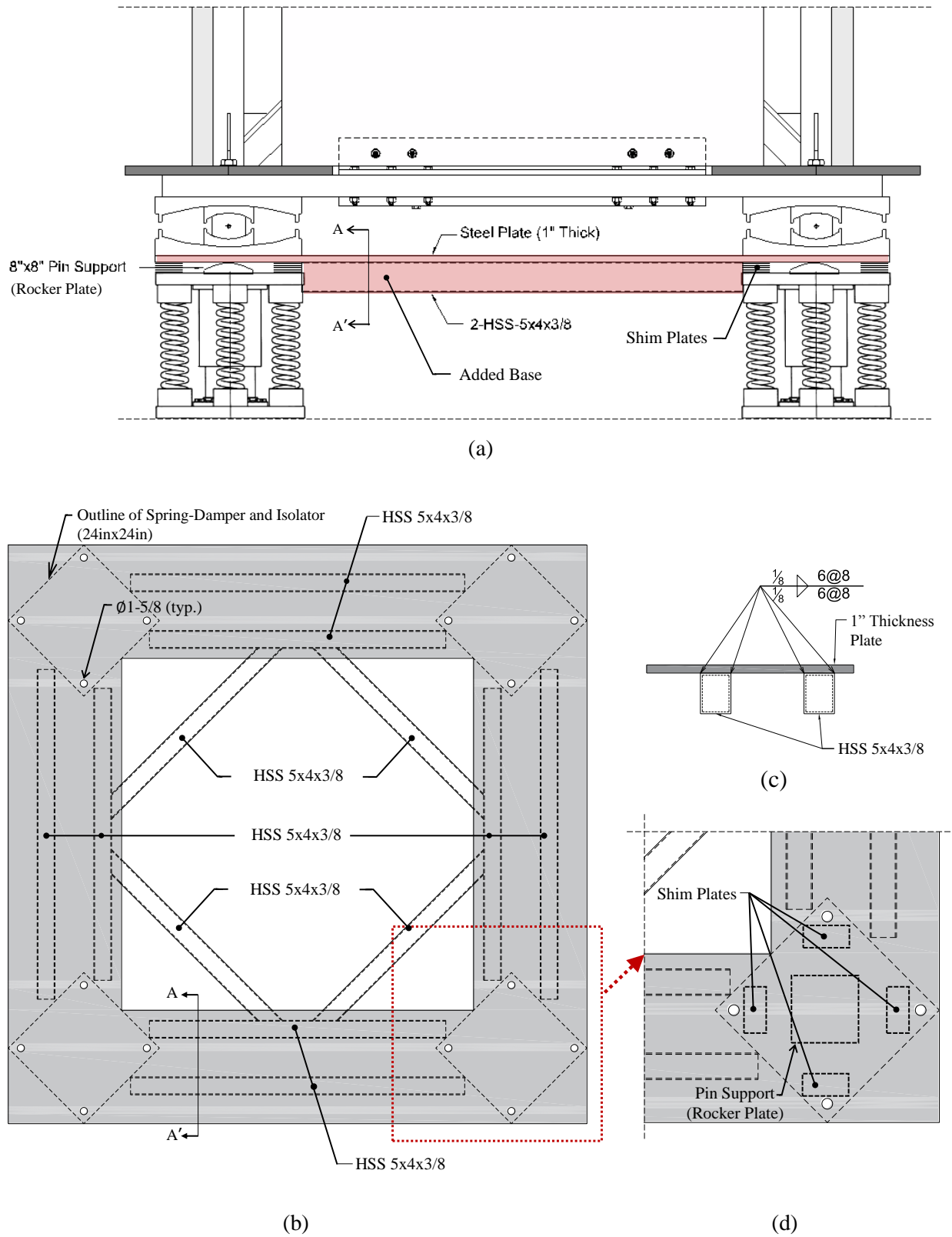


Figure 3-4 Schematics of Added Base for Limited Rocking: (a) Front View (b) Plan View (c) Section A-A' and (d) Detail of Connection between Vertical Spring-Damper Unit and Added Plate

The addition of the base was only partially effective in restraining rocking as an extremely stiff base was required to do so. This is evident in the Japanese systems reviewed in Section 1 where the size of the bases used for restraining rocking is substantial. It is also demonstrated in the design examples presented in Section 6. Moreover, there is an added complexity in adding the base. When placed on top of the spring-damper units, load is not concentrically transferred to the unit due to imperfections in the base. Load is transferred somewhere on top of the 24inch by 24inch top plate of each unit towards the interior of the model. As a result of this unavoidable event, the spring-damper units are subject to large eccentric load that results in lateral load on the vertical telescopic system used to drive the unit in vertical motion. The result is added friction in the vertical direction which may be substantial and is unknown. To prevent this from occurring, a rocker plate was placed at the center of each spring-damper device as shown in Figure 3-4 so that load is transferred concentrically. To provide the required stiffness, the space between the rocker plate, the base above and the plate below was shimmed with thin steel plates. In the field the operation will have to include careful shimming and grouting in similarity to what is often done in the installation of Friction Pendulum bearings for the seismic retrofit of existing structures. In the model only shims were used without grouting so that additional flexibilities were introduced and the added base did not have an important effect in restraining rocking. This issue is discussed in more detail in Section 4.

The addition of the rocking restraining base added a weight of 4.35kip on top of the spring-damper units for a total of 72.44kip on top of the spring-damper units so that the vertical frequency was 1.86Hz and the damping ratio was 0.48 when calculated based on the measured values of spring stiffness and viscous damping constant.

3.3 Description of Seismic Isolation System

The seismic isolation system consisted of four triple FP isolators and four vertical spring-damper units. Figure 3-5 shows sections of the two different types of triple FP isolators used in the testing. Note that the two types have only small differences in geometry with the most important difference being that one has an interior restrainer ring and the other does not. Three different sets of frictional properties of the isolators were tested. They are designated by the “nominal friction” values of

0.20, 0.12 and 0.07. The nominal friction is defined as the lateral force at zero displacement normalized by the vertical load. The actual frictional properties require description of friction for each sliding surface per Appendix B. Nominal friction of 0.20 was achieved with the isolator type A of Figure 3-5. This high friction value, which is undesirable, was the result of the low load (16.2kip) carried by this full size isolator in the shake table testing (designed to have a nominal friction of about 0.12 at load of about 105kip). Isolator type A was then partially lubricated in the laboratory at the University at Buffalo using liquid lubricants to result in a nominal friction of 0.07 but with somehow unstable conditions. Isolator type B, shown in Figure 3-5, was obtained from Earthquake Protection Systems, Inc. and was designed to provide the desired nominal friction of 0.12. The friction value of 0.12 is the lower bound value of nominal friction for the full size bearing per Appendix B. This corresponds to the friction values on each sliding surface as presented in Appendix B for the lower bound conditions.

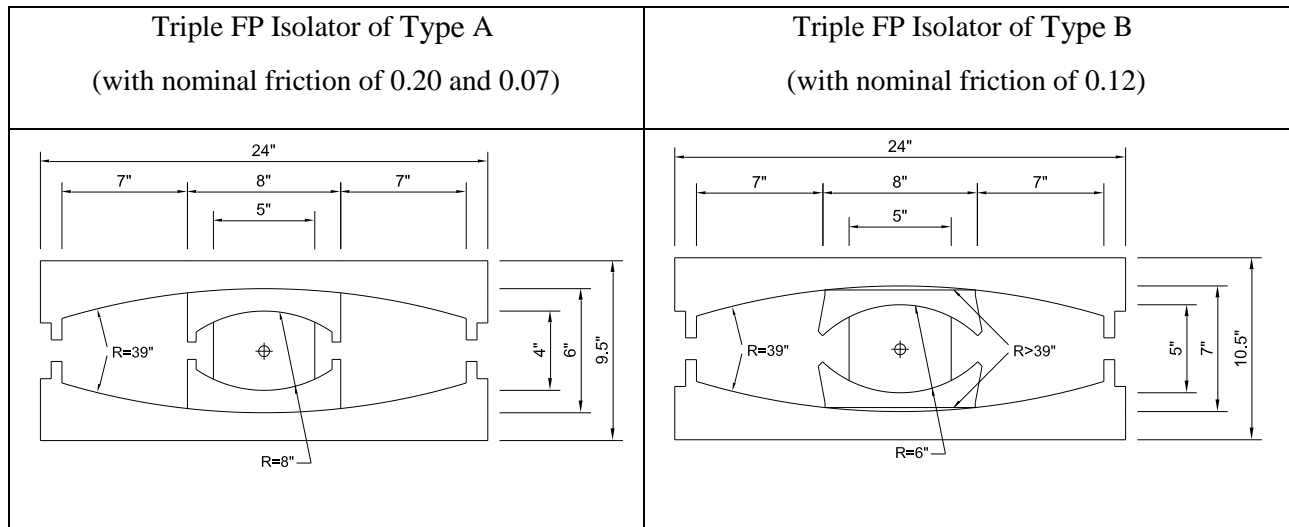


Figure 3-5 Triple FP Isolator Types used in Testing

A spring-damper unit is shown in Figure 3-6 in a three-dimensional rendering and a section with basic dimensions. The spring-damper supports a load of 17.0kip in the configuration without the added base used limiting rocking. With the added base, it carried a load of 18.1kip. Its design parameters and properties are listed in Table 3-1.

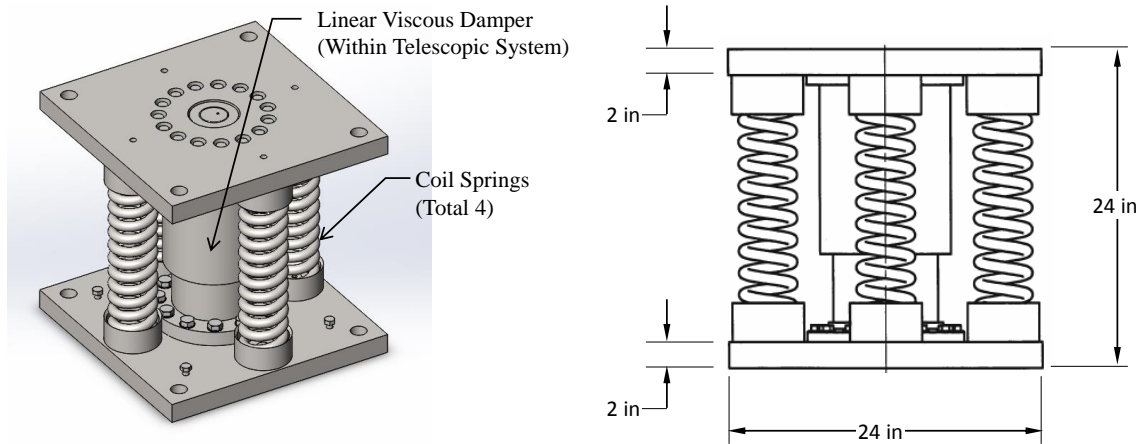


Figure 3-6 Spring-Damper Unit

Figure 3-7 shows details of the spring-damper unit. Each spring was fitted with an interior pin used to limit the length available for shear deformation while maintaining the full length for axial deformation. This was needed in order to increase the shear stiffness and prevent torsional instability of individual units. This is of importance only in the configuration without the rocking-restraining base. Torsional instability is caused by the random transfer of torque from the FP isolator above and the fact that when the vertical springs are compressed they develop negative shear stiffness. That is, when the springs are compressed by a large vertical force, upon small lateral deformation (due to torque) they apply force in the direction of motion, which is thus amplified. This force when combined with the shear stiffness of the springs may result in negative stiffness (Sarlis et al, 2013). Figure 3-7 demonstrates the ease of installation of the system. The triple FP isolators are simply placed on top of the spring units without the need to have load-transfer rocker plates and shimming as discussed earlier. By comparison, Figure 3-8 shows a detail of the connection of the triple FP isolator to the spring-damper unit when the stiffening base is used (in this case the pins for increasing the spring shear stiffness are not needed as the added base provides for stability of the system).

Table 3-1 Design Parameters for Spring-Damper Unit for Shake Table Testing

Static load (kip)	17.0
Static deflection (inch)	2.5
Stiffness (kip/inch)	6.8
Damping constant (linear viscous damping) (kip-sec/in)	0.54
Dynamic deflection (inch)	±1.25
Total deflection (inch)	3.75
Peak axial force (kip)	27.0
Peak damping force (kip)	11.0
Peak lateral force to be resisted by unit (kip)	6.5
Peak overturning moment to be resisted by unit (kip-inch)	200.0



Figure 3-7 Detail of Spring-Damper Unit for Increasing Shear Spring Stiffness

When the triple FP isolators are placed directly on top of the spring-damper units, the resulting 3D seismic isolation system is free to rotate (rock) due to the lack of any bending resistance in the FP isolators (in the absence of friction, the isolators behave as rollers). Rocking occurs while the spring-damper units only move vertically. Therefore, the spring-damper units experience differential vertical motion. This is illustrated in Figure 3-9.

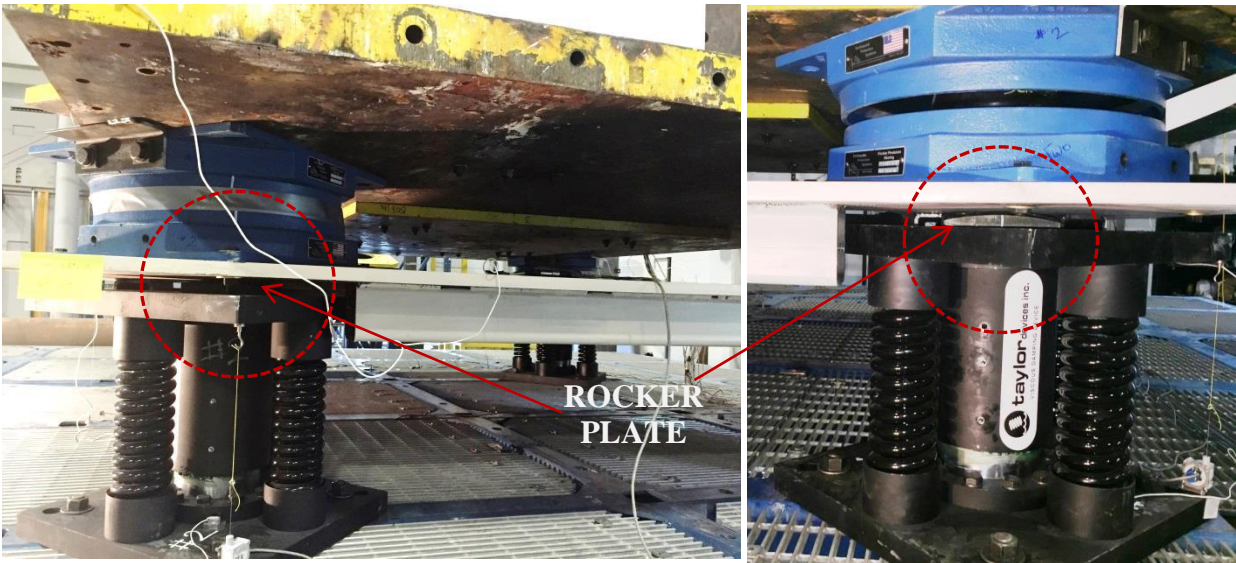


Figure 3-8 Details of Connection for System with Base for Limiting Rocking (prior to shimming)

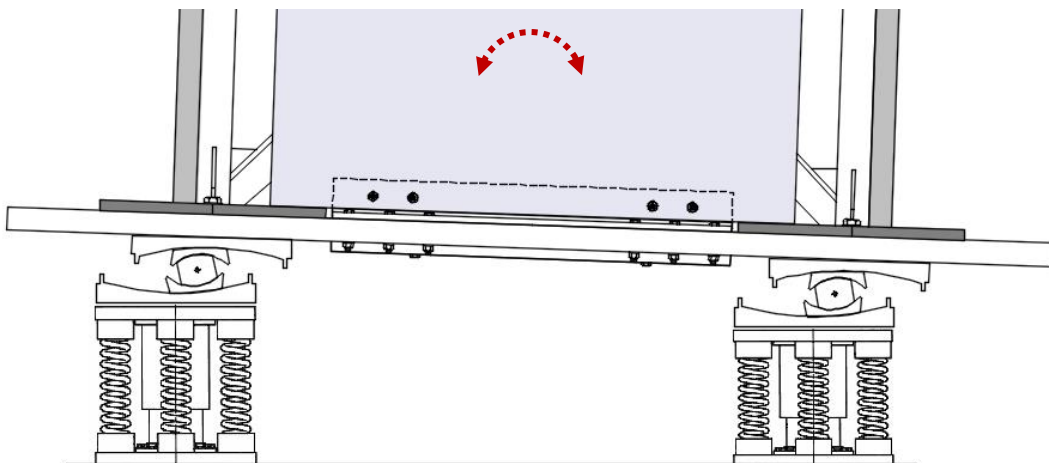


Figure 3-9 Illustration of Rocking Motion of System Allowing for Free Rocking

The modal properties of the isolated transformer test model in the configuration that is free to rock (as shown in Figure 3-9) has been investigated and compared to the modal properties of the sample transformer studied in Section 2 and Appendices A and C. Note that the properties of the studied transformer are those of the transformer isolated in Vancouver, WA, and shown in Figure 2-1. For the modal analysis of the transformer test model, the undamped version of Equations (A-3) was used but reduced to the form below since the vertical degree-of-freedom is uncoupled from the others.

$$\begin{bmatrix} m & 0 \\ 0 & I_{CM} \end{bmatrix} \begin{pmatrix} \ddot{u} \\ \ddot{\theta} \end{pmatrix} + \begin{bmatrix} 4K_h & -4K_h d_{CM} \\ -4K_h d_{CM} & 4K_h d_{CM}^2 + K_v l^2 \end{bmatrix} \begin{pmatrix} u \\ \theta \end{pmatrix} = \begin{pmatrix} 0 \\ 0 \end{pmatrix} \quad (3-1)$$

In Equation (3-1), d_{CM} is the vertical distance between the center of mass of the test model and the pivot point of the FP isolators (=43.8inch), l is the distance between the spring-damper units (=96inch) and I_{CM} is the mass moment of inertia (=621kip-in-s²) (see Figure 3-2). The mass corresponds to the tested weight of 64.9kip (the weight supported by the spring-damper units is 68.1kip but the weight supported by the FP isolators is 64.9kip). Solution of the eigenvalue problem resulted in the following expressions for the two frequencies:

$$f_{1,2} = \frac{1}{2\pi} \sqrt{\left(\frac{2K_h}{m} + \frac{4K_h d_{CM}^2 + K_v l^2}{2I_{CM}}\right) \pm \sqrt{\left(\frac{2K_h}{m} + \frac{4K_h d_{CM}^2 + K_v l^2}{2I_{CM}}\right)^2 - \frac{4K_h K_v l^2}{m I_{CM}}} \quad (3-2)$$

In Equations (3-1) and (3-2), K_v is the vertical stiffness of an individual spring-damper unit (=6.4kip/in as determined in the testing of the devices) and K_h is the horizontal stiffness of an individual triple FP isolator. During motion of the triple FP isolator, its actual horizontal stiffness varies from $W/2R_{eff1}$ to $W/2R_{eff2}$ where R_{eff1} is equal to 36inch for the isolator of type A in Figure 3-5 and 35.5in for the isolator of type B in the same figure. The radius R_{eff2} is equal to 6inch for the isolator of type A in Figure 3-5 and 3.5in for the isolator of type B in the same figure (Fenz and Constantinou, 2008). The third frequency of the model is the vertical frequency which is 1.92Hz. The three frequencies of the model were calculated and plotted in Figure 3-10 as function of the ratio of stiffness K_h/K_v . Note that actual values of this ratio are between 0.037 and 0.38. The figure also includes values of the three frequencies of the isolated transformer models studied in Section 2 for total weight of 320, 418 and 520kip distributed per mass distribution cases 1 and 2 in Table 2-2, and with the vertical spring-damper unit stiffness being such that the vertical frequency is 2.0Hz. Note that the exact distribution of mass in the actual transformer is not known and is assumed to be somewhere between cases 1 and 2 in Table 2-2.

The results in Figure 3-10 show that the test model has its fundamental frequency within the bounds of the fundamental frequency of the actual transformer. However, the second frequency

(one with a dominant rocking component) is lower in the test model than in the actual transformer. The reason is the smaller distance between supports in the test model (96inch versus 110inch to 227inch in the actual transformer) and the distribution of mass in the test model. The second frequency could be increased in the test model by lowering the center of mass of the model and by increasing the distance between supports. The latter could not be done given the large weight of the model and the requirement to support it at specific locations. The distribution of mass could not be changed without reducing the weight (removal of two vertical plates at the East and West sides as shown in Figure 3-1 and replacing with two smaller plates) and then adding weight directly on the base plate of the model. Both actions required additional costs in the acquisition of steel plates and were not considered. As a result the tested transformer model exhibited a lower rocking frequency than in a real application which resulted in some magnification of the rocking response. This was thought to be acceptable and desirable as (a) it provided for a more challenging interrogation of the isolation system, and (b) the acquired response data included a strong rocking component and thus were more challenging to predict analytically and validate the analytical models. The prediction of the response in the presence of rocking motion was further complicated when it was observed that the shake table exhibited some undesirable rocking motion due to inability to fully control the shake table at the tested large model weight.

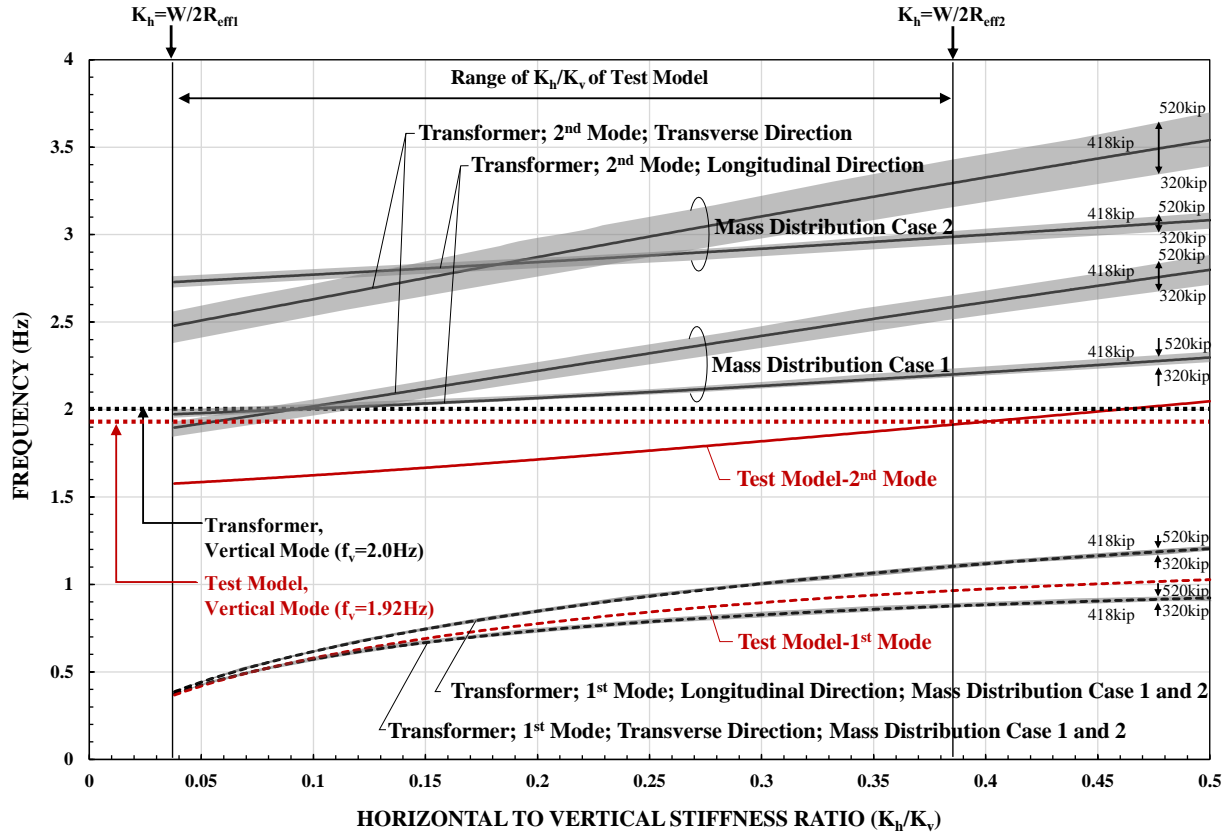


Figure 3-10 Frequencies of Isolated Transformer Test Model (red text and red line) and of Actual Transformer (black text and black line), Free Rocking Configuration

3.4 Testing and Properties of Spring-Damper Units

The four Spring-damper units were tested at the University at Buffalo. Each device was installed in the bearing testing machine as shown in Figure 3-11. The loading beam of the machine weighted 4.18kip so that it could induce a vertical displacement of 0.6inch to the device. Accordingly, the vertical machine actuators were first activated to lift the beam weight and eliminate the displacement and then vertical motion was imposed as follows: (a) a slow motion to a static deflection of 2.3inch over a period of 200second, (b) four and half cycles of harmonic motion of 1inch amplitude and frequency of 0.005Hz or 0.5Hz or 1Hz, and (c) a slow return to the origin. Note that the static deflection and dynamic displacement amplitude were reduced by comparison to the design parameters of the units due to limitations in the displacement capacity of the vertical actuators.

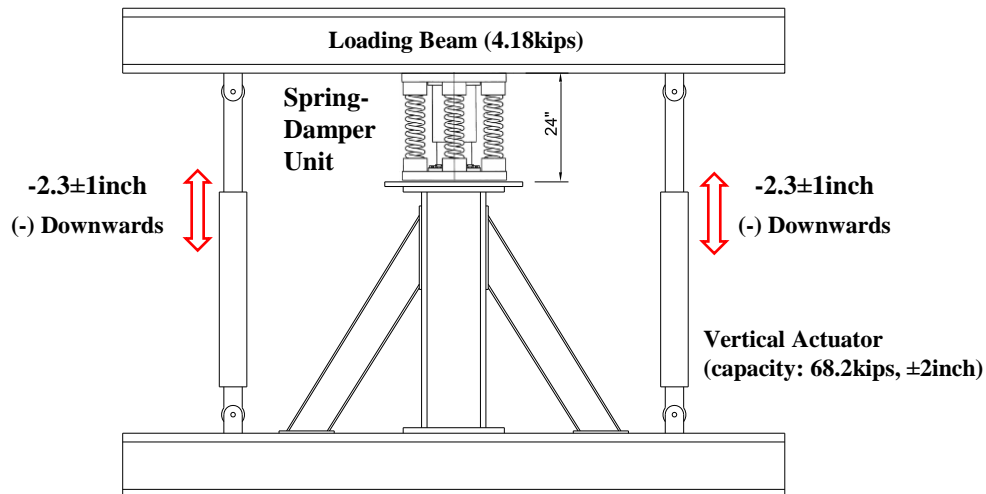


Figure 3-11 Test Set-up for Spring-Damper Unit

Figure 3-12 presents the recorded force-displacement loops in a test at frequency of 0.005Hz and Figure 3-13 the loops in a test at frequency of 1Hz. In the first test the peak velocity of motion was 0.03 in/s so that there no measureable viscous damping force. The force-displacement loops at this frequency can be used to obtain the device stiffness and friction. Note that friction is caused by the telescopic system used to drive the spring-damper unit in the vertical direction, where tight tolerances result in some friction force and from friction in the seals of the dampers. The friction

force measured in the results of Figures 3-12 and 3-13 per device is about 0.7kip. The loops in the test at frequency of 1Hz (peak velocity is 6.28in/sec) clearly show the effect of the viscous force.

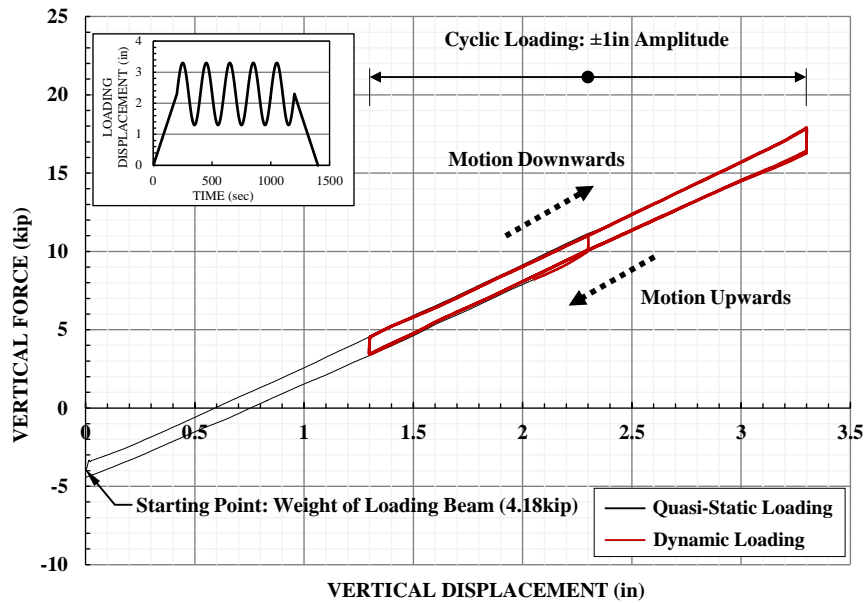


Figure 3-12 Force-Displacement Loop of Spring-Damper Unit 1 in at Peak Velocity of 0.03in/sec

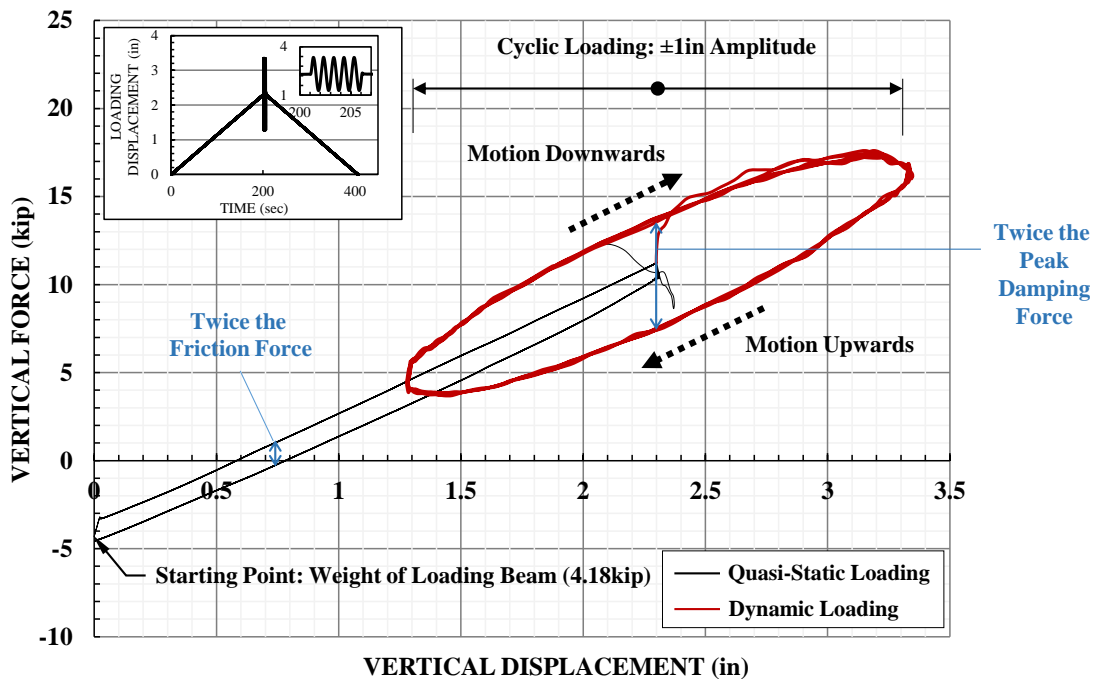


Figure 3-13 Force-Displacement Loop of Spring-Damper Unit 1 at Peak Velocity of 6.28in/sec

A complete set of test data (loops as those of Figure 3-13) for each test and unit are presented in Appendix E. Figure 3-14 presents results on the measured peak damping force as function of the

peak velocity from the tests conducted at the University at Buffalo and from the tests of only the dampers (prior to assembly) conducted at Taylor Devices, Inc. (tested at velocities of approximately 10.5 and 21.0in/sec). The data shown in Figure 3-14 include 6 points at each of the two velocities for each of the dampers tested at Taylor Devices (these were data for tension and compression for each of three cycles). Note that the force in the graph of Figure 3-14 includes a friction force, which was obtained in the testing of the complete spring-damper-telescopic tube units at the University at Buffalo (see Figure 3-13 for definition of damping and friction forces). The data in Figure 3-14 reveal the friction force in each device (as the damping force at zero velocity) and the damping constant (as the slope of the force-velocity curve). Indeed, the relation may be represented as linear. The test data in Figures 3-12 to 3-14 and those of Appendix E reveal:

- 1) The friction force varies between about 0.5 and 0.9kip (average 0.65kip). The total friction force is 2.6kip, which amounts to 0.038 of the supported model weight.
- 2) The damping constant per unit is 0.53kip-sec/in (best fit of curves in Figure 3-14). The specified value (Table 3-1) is 0.54kip-sec/in.
- 3) The spring stiffness per unit is 6.4kip/in. The specified value (Table 3-1) is 6.8kip/in.

The friction force measured in the spring-damper units originates in the seal of the dampers and in the telescopic system used to drive the system in the vertical direction. While tested on the shake table for identification of the properties in the vertical direction (see later in this section), there was no evidence of friction in the devices as the transfer functions obtained could be very accurately predicted by a linear elastic and linear viscous representation (see Figure 3-29). Also, in the analytical prediction of the experimental response presented in Section 5 use of friction in the spring-damper units resulted in a worse prediction of the response than a model in which friction was neglected (results to be provided in Section 5). This led to the assumption that the friction measured in the tests (Figure 3-14) was the result of some significant lateral force applied at the spring units in the test machine due to the high horizontal stiffness of the units and rotation of the loading beam of the test machine. Accordingly, it should not be included in the analytical prediction of the response.

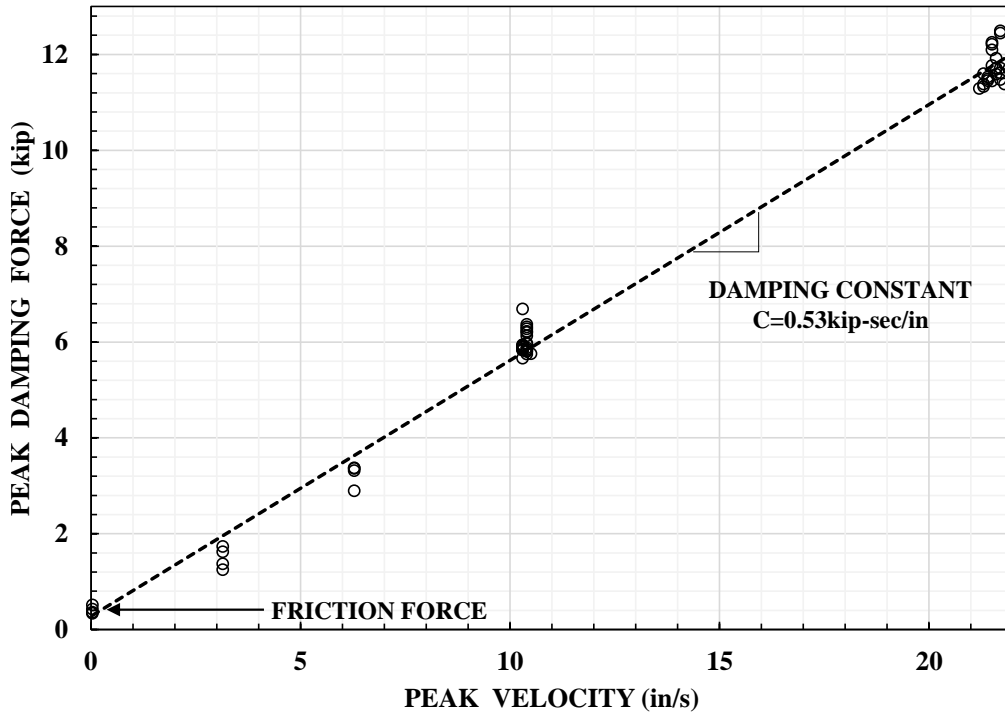


Figure 3-14 Peak Damping Force versus Peak Velocity Relationship in Testing at Spring-Damper Units at University at Buffalo and Testing of Dampers at Taylor Devices

3.5 Testing and Properties of Triple Friction Pendulum Isolators

Three sets of four Triple FP isolators (per Figure 3-5) were tested in the isolator test machine at University at Buffalo. All tests were conducted with the outer seal removed in order to expose the internal components as shown in the photograph of Figure 3-15. Each test consisted of the following protocol: (a) the bearing was loaded to a vertical force of about 16.2kip (actual load on bearings was 16.2kip), (b) slow lateral motion was imposed to a displacement of 5.5inch (capacity of system is 6.0inch) over a period of 60 seconds, see Figure 3-16, (c) a pause for 5 seconds was imposed, and (d) a return to the origin at amplitude of 5.5inch plus two fully reversed cycles were imposed at frequencies of 0.005, 0.01, 0.2 and 0.3Hz (total of four tests). The peak velocities achieved in the tests at each of the frequencies were 0.2, 3.5, 6.9, and 10.4 in/s. Figure 3-16 presents the recorded histories of the imposed lateral motion and of the axial load on a bearing in the 0.3Hz test. There is some fluctuation of the vertical force in the test, which diminished as the frequency of testing was reduced.

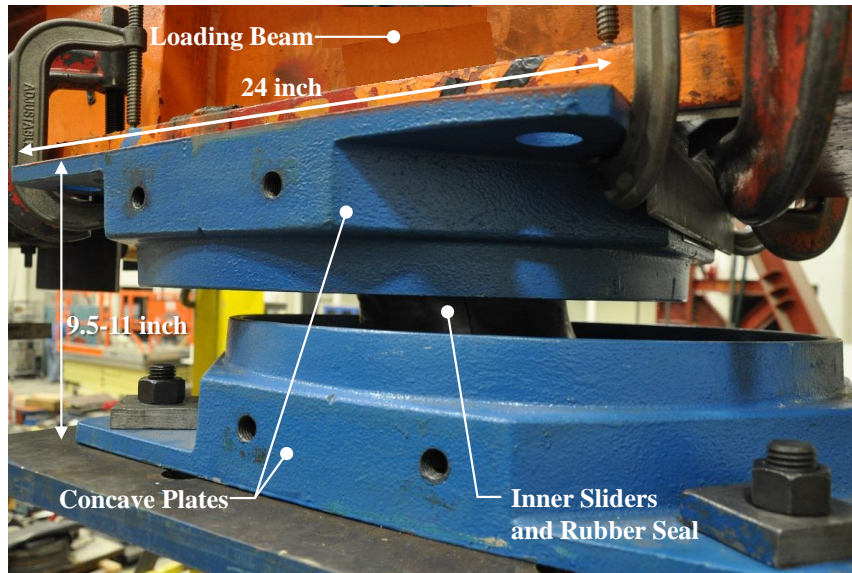


Figure 3-15 Image of Triple FP Isolator Type A of 0.20 Nominal Friction in Test Machine

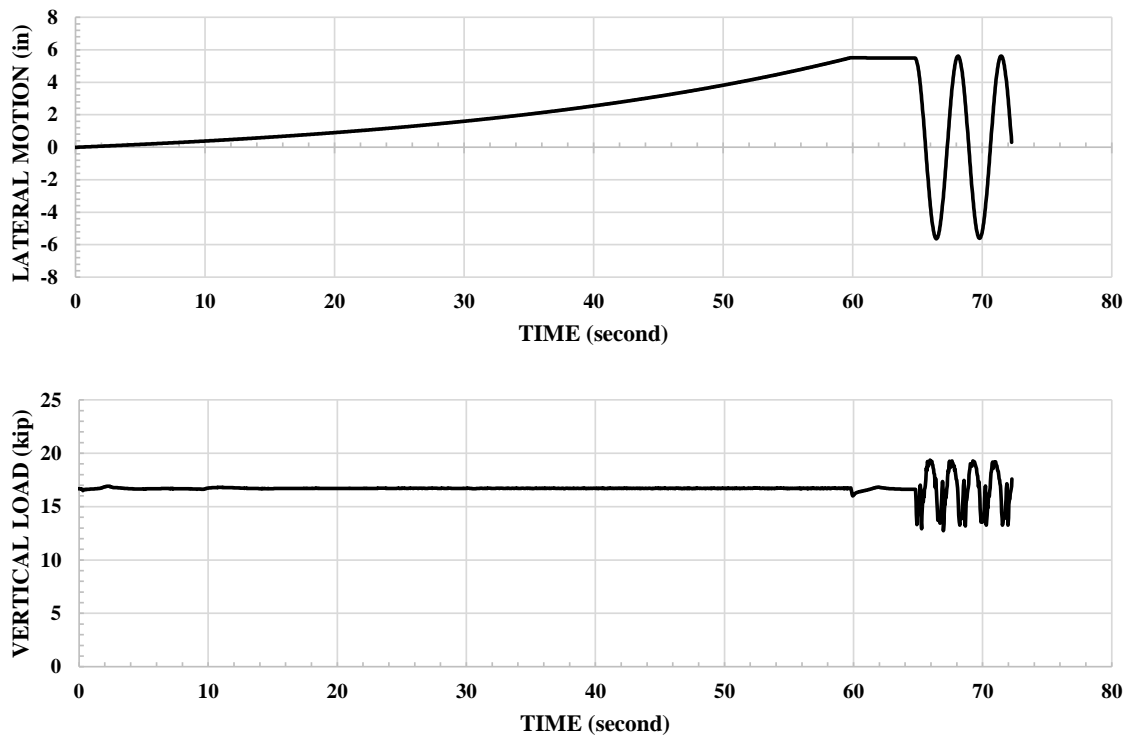


Figure 3-16 Recorded Histories of Lateral Motion and Vertical Load in Test with Frequency of 0.3Hz

Figure 3-17 presents loops of recorded lateral force (normalized by the instantaneous vertical load) versus displacement of one isolator of type A (per Figure 3-5) with high friction. These isolators

were identical to the isolators used in the Vancouver, WA transformer (Figure 2-1; also Oikonomou et al, 2016). They were intended for use under load of 105kip for which the expected nominal friction (force at zero displacement divided by vertical force) is 0.12. The tests showed that at the tested load of 16.7kip the nominal friction is about 0.20. The isolators were tested with the inner seal intact as shown in Figure 3-16.

Analytically derived force-displacement loops based on the theory of Fenz and Constantinou (2008) are also shown in Figure 3-17 where the values of friction used for each sliding surface are listed in each graph. Note that friction changes as the velocity of motion increases, hence friction is velocity dependent. (The friction coefficient μ_i , $i = 1$ to 4 is numbered from the lower to upper sliding surface). The data in Figure 3-17 provide the information needed to calibrate the model of friction for this bearing. A complete set of test data (loops as those of Figure 3-17) for each test and isolator are presented in Appendix E.

It is noted that the analytical model under-estimates the stiffness of the unloading branch of the force-displacement loops. This was due to the fact that the analytical model did not consider the effect on stiffness of the inner seal (see Figure 3-15). The significance of the inner seal stiffness diminishes at large vertical load (as the bearing stiffness is proportional to the vertical load) but is of some influence at lighter loads. The effect of the rubber seal becomes important under uplift conditions for which the newly develop theory of Sarlis and Constantinou (2013) can be used. Figure 3-18 compares the experimental force-displacement loop of isolator No.1 in the highest speed test with an analytical loop predicted by the theory of Sarlis and Constantinou (2013) with due account of the seal contribution. In the analytical model, the seal stiffness was calculated as a function of seal deformation u_s , given by:

$$K_s = \frac{\pi E b x}{2(x+u_s)^2} t \quad (3-3)$$

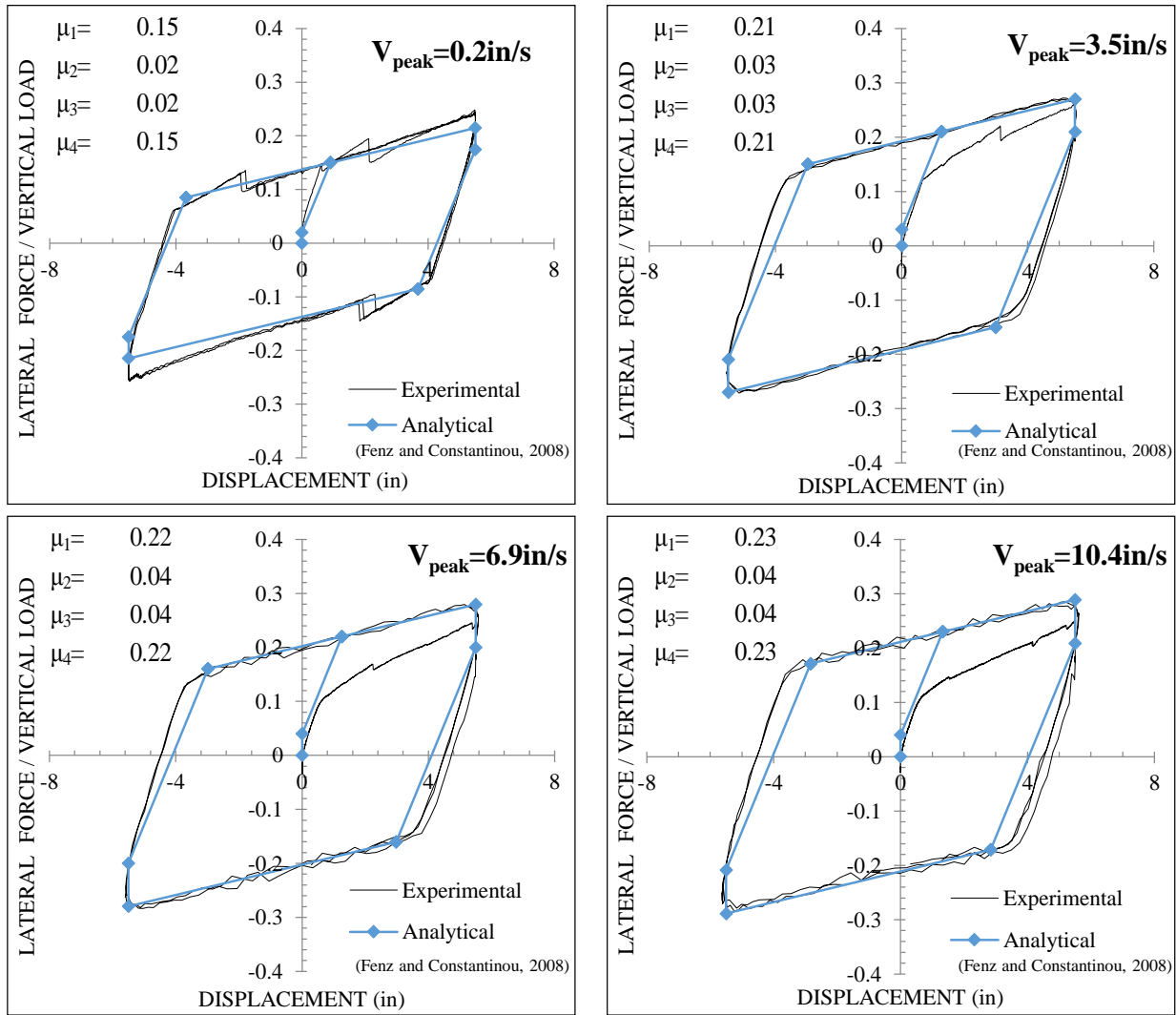


Figure 3-17 Experimental and Analytical Normalized Force-Displacement Loops of Triple FP Isolator No. 1 of Type A without Lubrication (nominal friction 0.20)

In (3-3), E is the elastic modulus of the rubber (1400psi), b is the diameter of the inner slider (8inch), x (1inch) is the vertical clearance distance between inner sliders, and t (0.125inch) is the thickness of the rubber seal. The analytical prediction is now excellent but of little significance as analysis of dynamic response without the effect of the seal does not result in any important difference in the response.

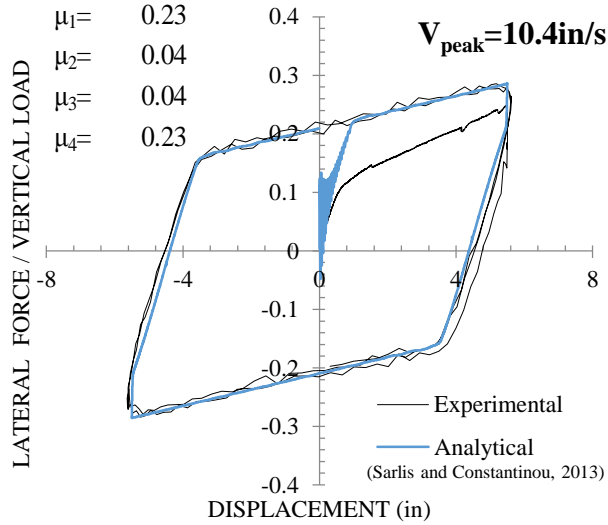


Figure 3-18 Experimental and Analytical Normalized Force-Displacement Loops of Triple FP Isolator No. 1 of Type A without Lubrication (nominal friction 0.20) in High Speed Motion and with due Consideration of Stiffness of Inner Rubber Seal

The velocity dependence of the coefficient of friction is typically described by the following equation (Constantinou et al, 1990):

$$f = f_{\max} - (f_{\max} - f_{\min})e^{-aV} \quad (3-4)$$

where f_{\max} and f_{\min} are values of the coefficient of sliding friction valid for large velocity and for quasi-static conditions, respectively, V is the velocity of sliding and “ a ” is the rate parameter used to describe the velocity-dependence of friction. In obtaining the parameters of the model from the test data, the sliding velocity on surfaces 1 and 4 was assumed to be half of the total velocity (test velocity). The value of the friction coefficient was taken as the average of the values of the four isolators tested. Figure 3-19 presents the experimental values of the coefficient of friction on the two large surfaces ($\mu_1=\mu_4$) as function of velocity and analytically predicted values using Equation (3-4). The model parameters that best fit the data for surfaces 1 and 4 are $f_{\max}=0.24$, $f_{\min}=0.14$ and $a = 0.7\text{sec/in}$. For the inner surfaces 2 and 3 the test data in Figure 3-17 support a model with parameters $f_{\max}=0.04$, $f_{\min}=0.02$ and $a = 0.7\text{sec/in}$ (parameter a was arbitrarily selected to be the same as that of surfaces 1 and 4).

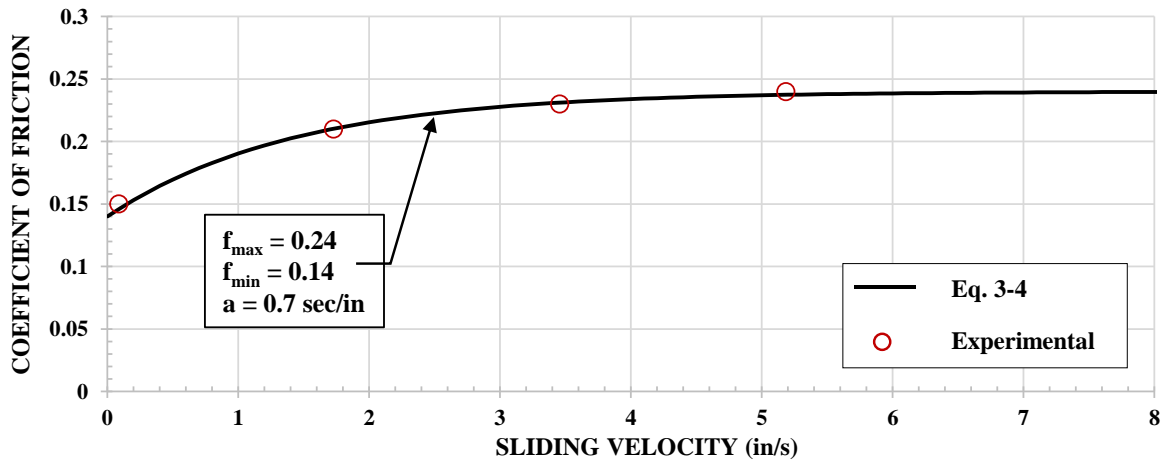


Figure 3-19 Friction Coefficient-Velocity Relation of Triple FP Isolator of Type A without Lubrication (nominal friction 0.20)

The triple FP isolators of type A without lubrication were used in the shake table testing and then they were removed from the model, the internal seals were removed and the inner and outer sliding surfaces were lubricated using liquid lubricants in a rudimentary method to reduce friction to the desired level of a nominal friction of 0.12. The inner sliding surfaces were completely lubricated whereas the outer sliding surfaces were lubricated over portion of the contact area. For both surfaces, the lubricant was applied to the soft material that is in contact with stainless steel and was rubbed-in in an effort to infuse the material with the lubricant. Testing was then conducted without the inner seal, which were cut for reaching the interior of the bearing.

Figure 3-20 presents experimental and analytical loops (Fenz and Constantinou, 2008) at the four velocities for isolator No. 1 of the tested bearings. The loops show some irregularity in behavior due likely to the rudimentary lubrication applied in the laboratory. Nevertheless, the general behavior is predictable by theory and the results have been used to calibrate the model of friction as shown in the results of Figure 3-21. Nominal friction is 0.07, which is low. The model parameters that best fit the data for surfaces 1 and 4 are $f_{\max}=0.08$, $f_{\min}=0.055$ and $a = 0.5\text{sec/in}$. For the inner surfaces 2 and 3 the test data in Figure 3-20 support a model with parameters $f_{\max}=0.02$, $f_{\min}=0.015$ and $a = 0.5\text{sec/in}$ (parameter a was arbitrarily selected to be the same as that of surfaces 1 and 4).

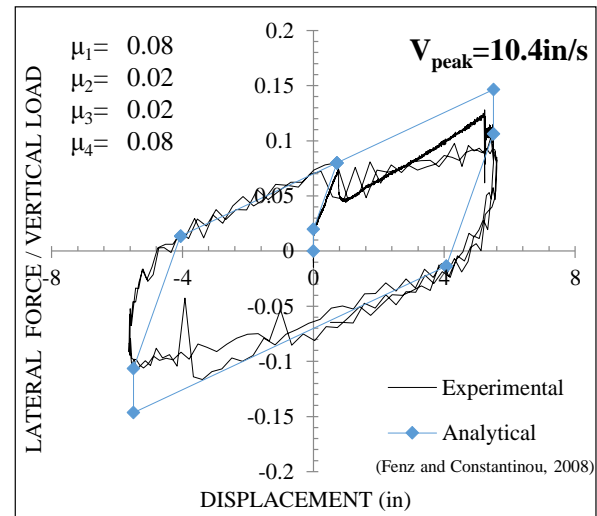
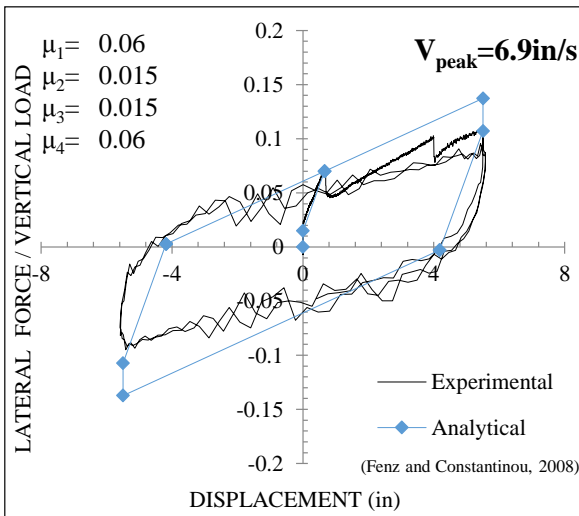
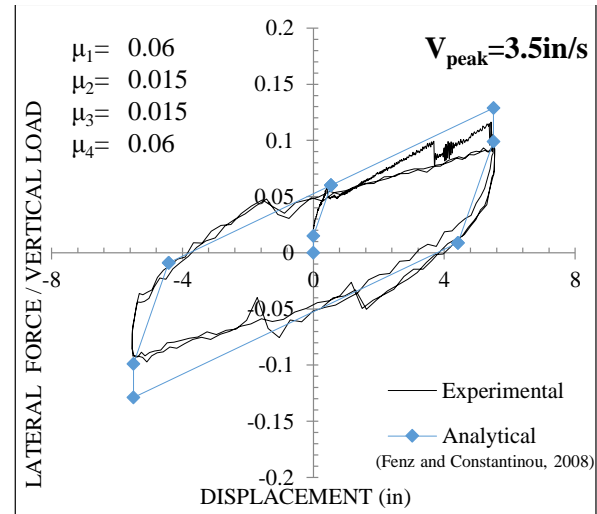
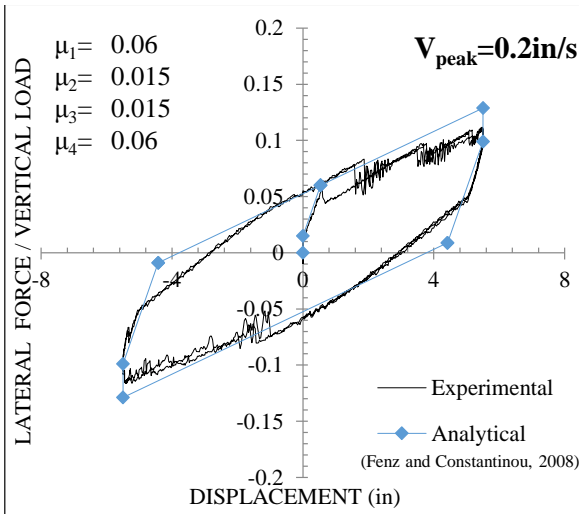


Figure 3-20 Experimental and Analytical Normalized Force-Displacement Loops of Triple FP Isolator No. 1 of Type A with Lubrication (nominal friction 0.07)

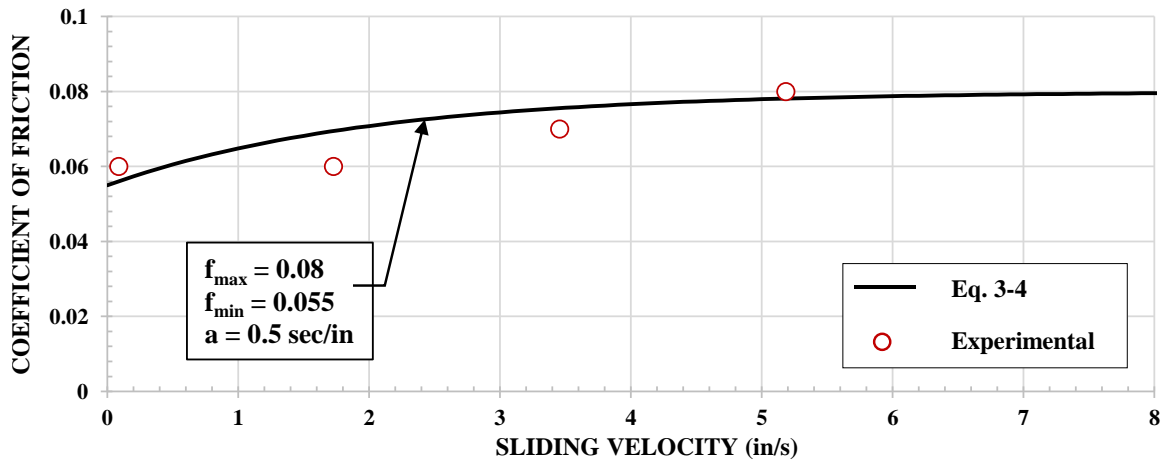


Figure 3-21 Friction Coefficient-Velocity Relation of Triple FP Isolator of Type A with Lubrication (nominal friction 0.07)

Figure 3-22 presents experimental loops of lateral force (normalized by instantaneous vertical load) versus displacement of one isolator of type B (per Figure 3-5) with modified contact surfaces to achieve the desired friction. This set of isolators is slightly different in geometry than the isolators of type A. The isolators were tested with the inner seal removed. Analytically derived force-displacement loops (Fenz and Constantinou, 2008) are also shown in Figure 3-22 where the values of friction used for each sliding surface are listed in each graph. The nominal friction is 0.12, as desired, but the experimental loops show stiffness that is less than what the theory predicts. Efforts were made to check the fidelity of the measurements and it was concluded that the recorded behavior is real. We theorize that this behavior is the result of the changes in the contact area in order to achieve higher pressure at the load of 16.2kip (bearings are intended for load of over 100kip) and thus achieve lower friction. The inner sliders were machined to have an outer radius of curvature larger than 39inch (see Figure 3-5) so that contact was on an annular disk at the perimeter of the surface. This is illustrated in Figure 3-23. Upon lateral deformation, the distribution of force drastically changes so that load is transferred through contact areas at opposing edges of the top and bottom surfaces. This certainly affects moment equilibrium which is known to affect behavior per the theory of Sarlis and Constantinou (2013) (which, however, is based on the assumption that the contact area is circular and not annular as in this case). There is

no theory to account for this case. Nevertheless, analyses using the model of Fenz and Constantinou (2008) with the actual radii of curvature values of the bearings and then again using artificial values of the radii so that the test data are matched, resulted in insignificant differences in the calculated response of the isolated model. Accordingly, analytical results will be presented using models with the actual radii of the bearings.

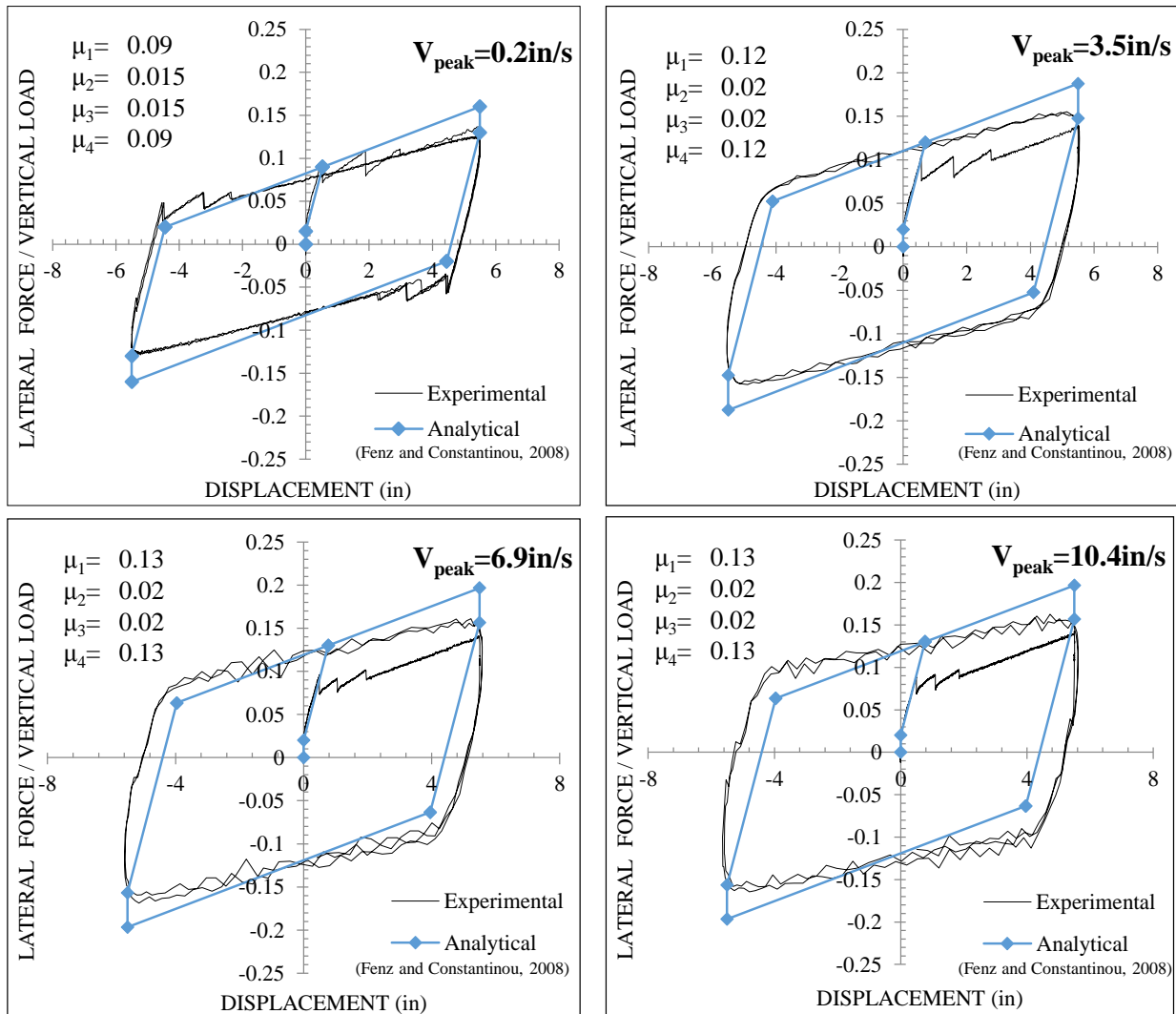


Figure 3-22 Experimental and Analytical Normalized Force-Displacement Loops of Triple FP Isolator No. 1 of Type B (nominal friction 0.12)

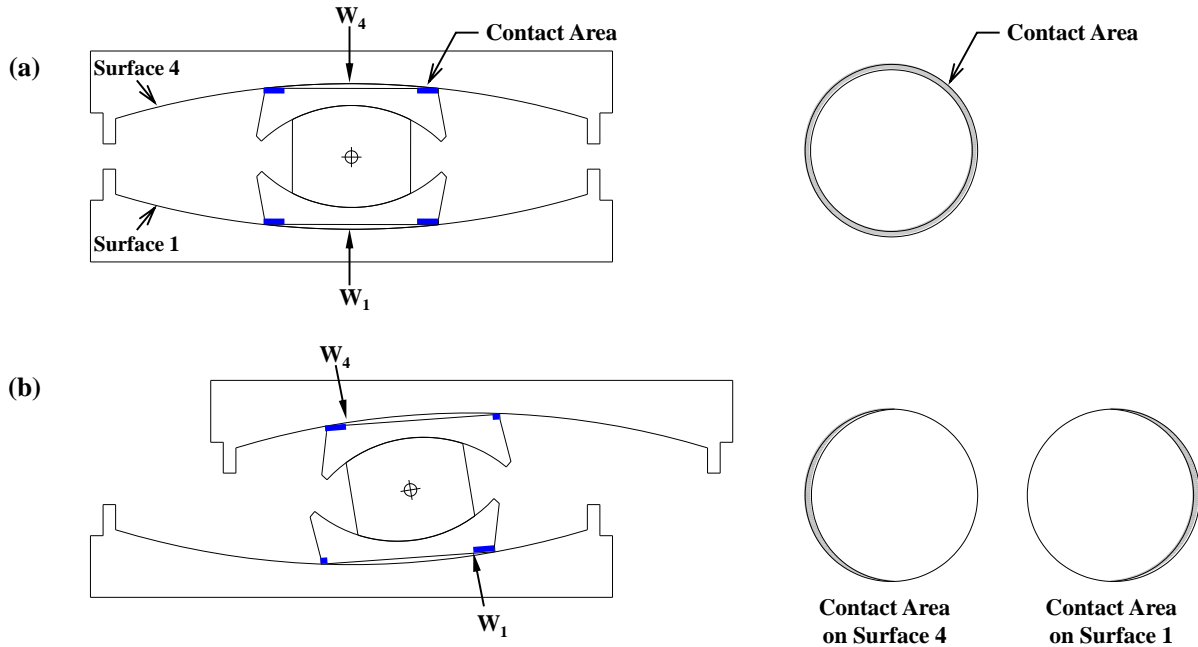


Figure 3-23 Contact Areas in (a) Un-deformed and (b) Deformed Bearing

Figure 3-24 presents the experimental values of the coefficient of friction for the bearing of type B on the two large surfaces ($\mu_1=\mu_4$) as function of velocity and analytically predicted values using Equation (3-4). The model parameters that best fit the data for surfaces 1 and 4 are $f_{\max}=0.13$, $f_{\min}=0.09$ and $a = 0.7\text{sec/in}$. For the inner surfaces 2 and 3 the test data in Figure 3-22 support a model with parameters $f_{\max}=0.02$, $f_{\min}=0.015$ and $a = 0.7\text{sec/in}$ (parameter a was arbitrarily selected to be the same as that of surfaces 1 and 4).

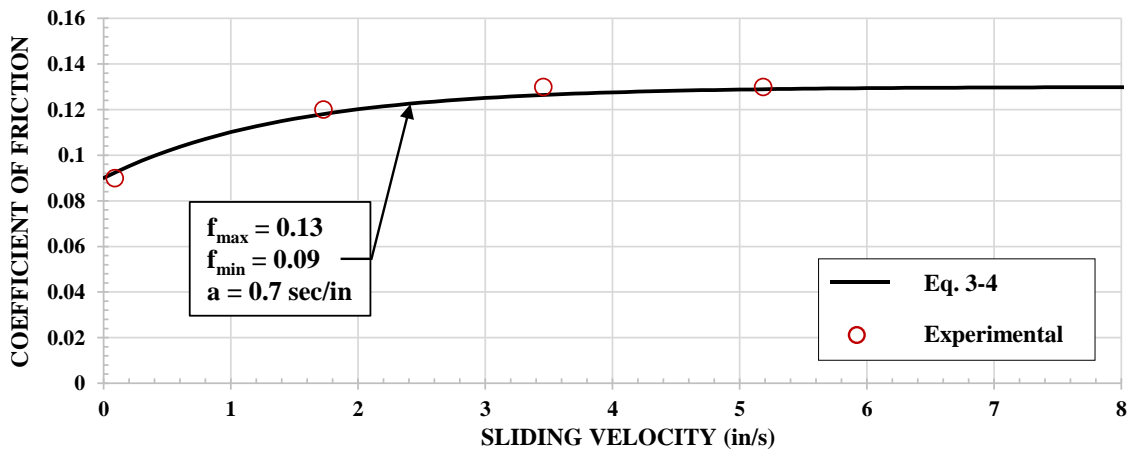


Figure 3-24 Friction Coefficient-Velocity Relation of Triple FP Isolator of Type B (nominal friction 0.12)

3.6 Identification of As-Installed Properties of Bushing

The as-installed frequency and the corresponding damping ratio of the bushing were identified in testing of the model shown in Figure 3-1(a). Testing consisted of white noise excitation in the two horizontal directions and the vertical direction. The white noise excitation was banded in the range of 0.05 to 50Hz and its amplitude was 0.1g. Instruments used were accelerometers at the bushing top, the bushing connection to the supporting plate, at the shake table extension and at the shake table as shown in Figure 3-25. Note that accelerometers are denoted as “abtx”, etc. (“abtx” is the name for the accelerometer at the bushing top in the x direction). Also, the motion of the shake table extension was monitored with string potentiometers (named “spextxn” etc.)

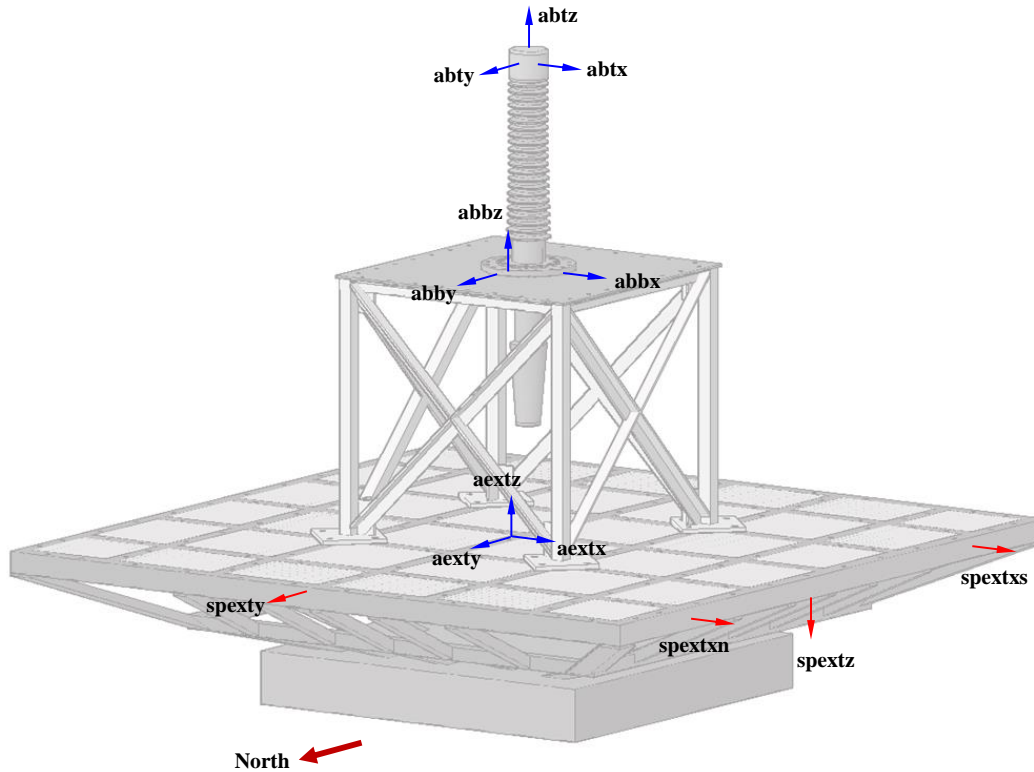


Figure 3-25 Instrumentation Diagram used in Bushing Identification

Figure 3-26 presents graphs of the amplitude of the transfer functions obtained as the amplitude of the Fourier Transform of the acceleration history recorded at the bushing top divided by the Fourier Transform of the acceleration history recorded at the shake table extension. Transfer functions for the two horizontal and the vertical directions are presented.

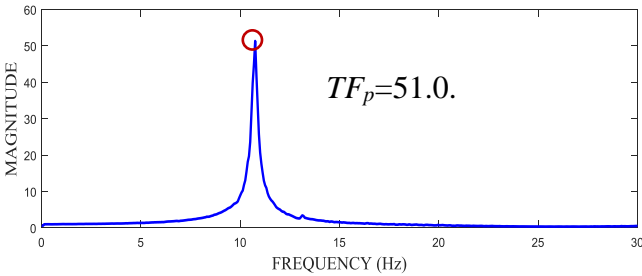
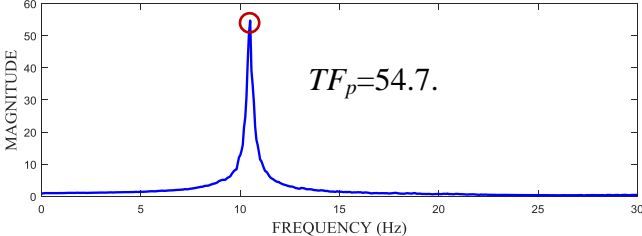
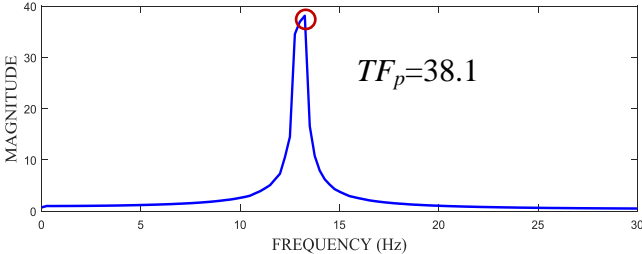
Direction	Transfer Function Amplitude	Extracted Parameters
North-South		$f=10.8\text{Hz}$ $\xi=0.010$
East-West		$f=10.5\text{Hz}$ $\xi=0.009$
Vertical		$f=13.3\text{Hz}$ $\xi=0.013$

Figure 3-26 Amplitude of Transfer Functions of Top of Bushing Acceleration to Shake Table Extension Acceleration

The transfer functions contain only one peak, thus indicating a single mode of vibration within the range of zero to 30Hz. The system is lightly damped so the location of the single peak reveals the frequency and the peak of the amplitude of the transfer function TR_p is related to the damping ratio ξ by:

$$TR_p = \frac{1}{2\xi} \quad (3-5)$$

The results in Figure 3-26 reveal that as-installed frequencies of the bushing in the two horizontal directions are essentially the same and close to the as-installed frequency for bushing No. 6 in Table 2-1. The vertical frequency is larger than the horizontal frequencies in consistency with

other studies reported in Kitayama et al (2016). The identification testing also revealed that the bushing is very lightly damped with damping ratio of about 0.01.

3.7 Identification of Vertical Frequency and Damping Ratio of Isolated Model

The model was assembled on the shake table as shown in Figure 3-1(b) in the configurations allowing for free rocking. In this condition, the triple FP isolators were locked to prevent lateral deformation by installing side plates. The model was fully instrumented as shown in Figures 3-27 and 3-28. A list of the instruments is presented in Table 3-2. Figures 3-27 and 3-28 show the location and names of accelerometers, displacement transducers and light emitting diodes (LED) used with a Krypton video-based motion recording system (capable of acquiring data on position, velocity and acceleration).

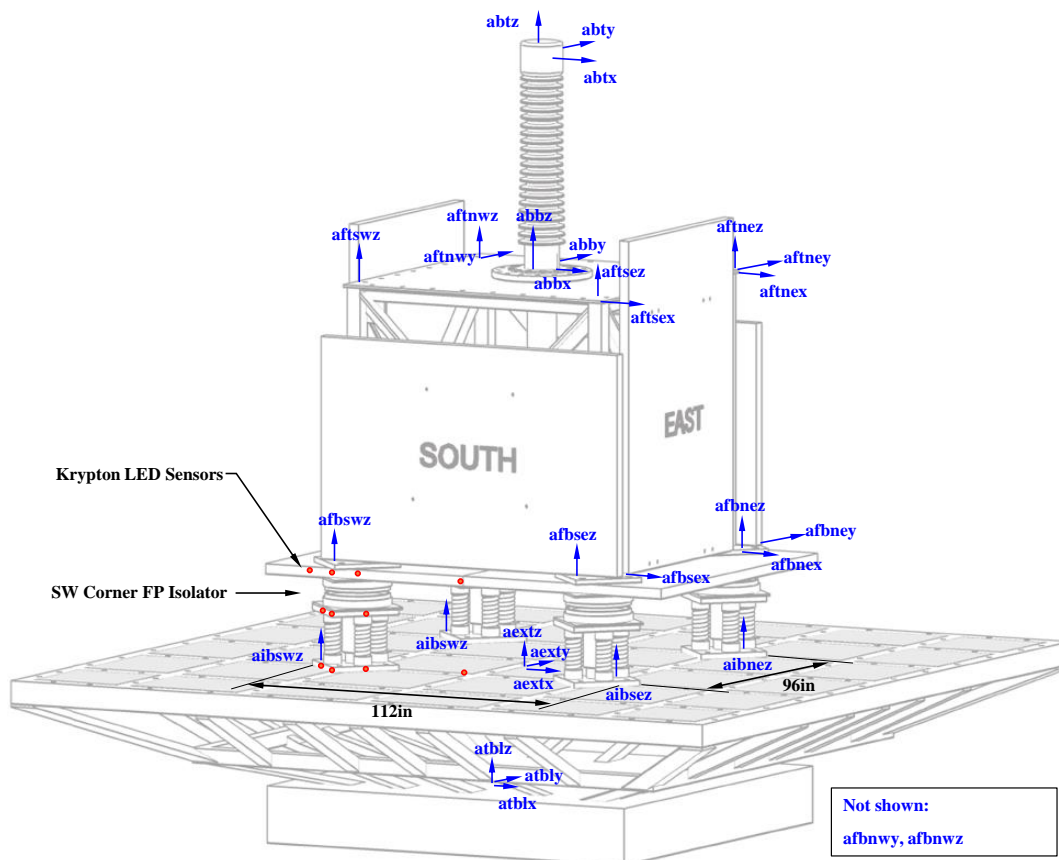


Figure 3-27 Instrumentation Diagram Showing Accelerometers and Krypton LED

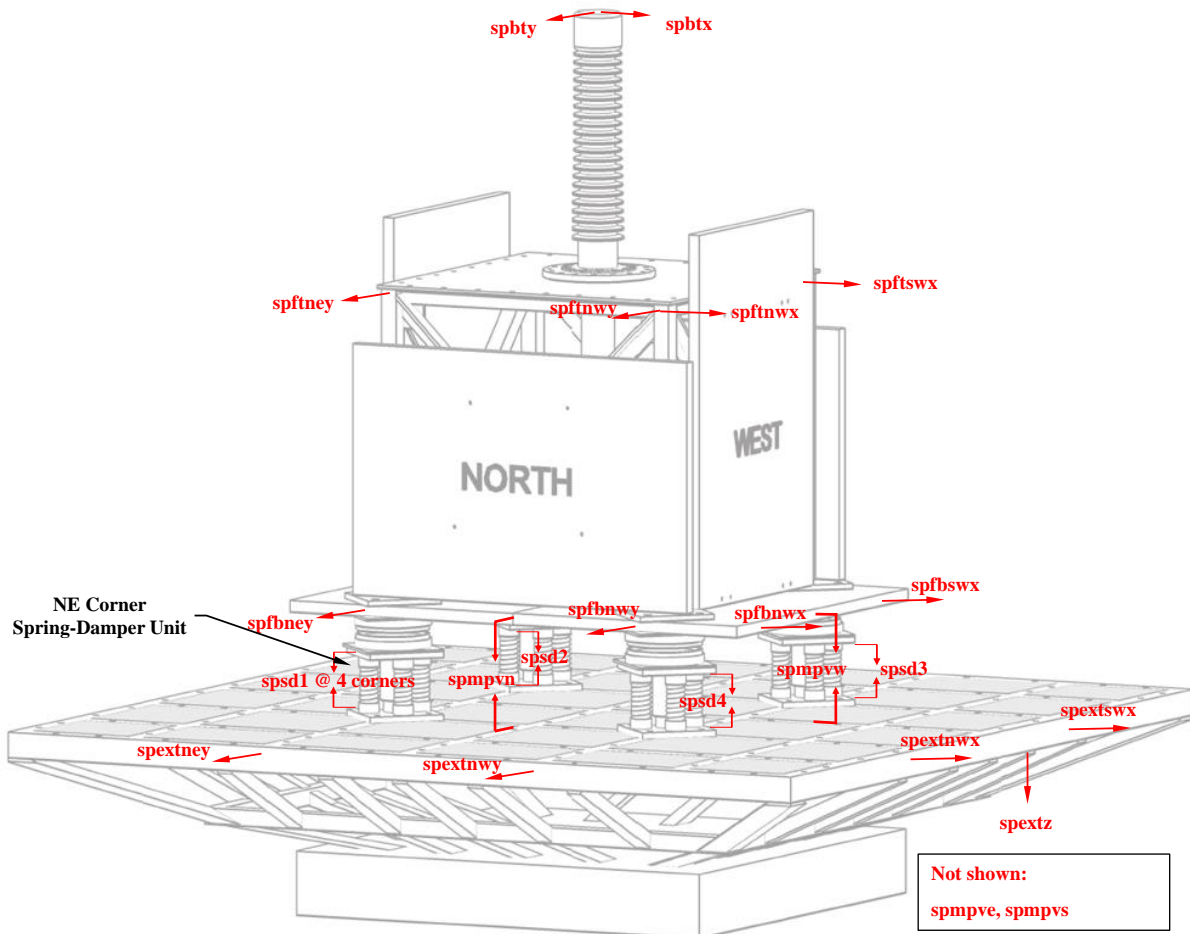


Figure 3-28 Instrumentation Diagram Showing Displacement Transducers

Table 3-2 List of Instruments used in Identification and Seismic Tests of Model on Shake Table

Notation	Instrument	Measured Quantity	Location	Direction
astx	Accelerometer	Table acceleration	Center of shake table	E-W
asty	Accelerometer	Table acceleration	Center of shake table	N-S
astz	Accelerometer	Table acceleration	Center of shake table	Vertical
aextx	Accelerometer	Table extension acceleration	Center of table extension	E-W
aexty	Accelerometer	Table extension acceleration	Center of table extension	N-S
aextz	Accelerometer	Table extension acceleration	Center of table extension	Vertical
abtx	Accelerometer	Bushing top acceleration	Top of bushing	E-W
abty	Accelerometer	Bushing top acceleration	Top of bushing	N-S
abtz	Accelerometer	Bushing top acceleration	Top of bushing	Vertical

Table 3-2 (continued)

Notation	Instrument	Measured Quantity	Location	Direction
abbx	Accelerometer	Bushing base acceleration	Base plate of bushing	E-W
abby	Accelerometer	Bushing base acceleration	Base plate of bushing	N-S
abbz	Accelerometer	Bushing base acceleration	Base plate of bushing	Vertical
aftnex	Accelerometer	Frame top acceleration	NE corner of frame top	E-W
aftsex	Accelerometer	Frame top acceleration	SE corner of frame top	E-W
aftney	Accelerometer	Frame top acceleration	NE corner of frame top	N-S
aftnwy	Accelerometer	Frame top acceleration	NW corner of frame top	N-S
aftnez	Accelerometer	Frame top acceleration	NE corner of frame top	Vertical
aftsez	Accelerometer	Frame top acceleration	SE corner of frame top	Vertical
aftswz	Accelerometer	Frame top acceleration	SW corner of frame top	Vertical
aftnwz	Accelerometer	Frame top acceleration	NW corner of frame top	Vertical
afbnex	Accelerometer	Frame bottom acceleration	NE corner of frame base	E-W
afbsex	Accelerometer	Frame bottom acceleration	SE corner of frame base	E-W
afbney	Accelerometer	Frame bottom acceleration	NE corner of frame base	N-S
afbny	Accelerometer	Frame bottom acceleration	NW corner of frame base	N-S
afbnez	Accelerometer	Frame bottom acceleration	NE corner of frame base	Vertical
afbsez	Accelerometer	Frame bottom acceleration	SE corner of frame base	Vertical
afbswz	Accelerometer	Frame bottom acceleration	SW corner of frame base	Vertical
afbwnz	Accelerometer	Frame bottom acceleration	NW corner of frame base	Vertical
aibnez	Accelerometer	Table extension acceleration	Base of Spring-damper at NE corner	Vertical
aibsez	Accelerometer	Table extension acceleration	Base of Spring-damper at SE corner	Vertical
aibswz	Accelerometer	Table extension acceleration	Base of Spring-damper at SW corner	Vertical
aibwnz	Accelerometer	Table extension acceleration	Base of Spring-damper at NW corner	Vertical
spextnw	String-pot	Table extension displacement	West side of table extension at north	E-W
spextsw	String-pot	Table extension displacement	West side of table extension at south	E-W
spextney	String-pot	Table extension displacement	North side of table extension at east	N-S
spextnwy	String-pot	Table extension displacement	North side of table extension at west	N-S
spextz	String-pot	Table extension displacement	West side of table extension	Vertical
spbtx	String-pot	Bushing displacement	Top of bushing	E-W

Table 3-2 (continued)

Notation	Instrument	Measured Quantity	Location	Direction
spbty	String-pot	Bushing displacement	Top of bushing	N-S
spftnwx	String-pot	Frame displacement	NW corner of frame top	E-W
spftswx	String-pot	Frame displacement	SW corner of frame top	E-W
spftney	String-pot	Frame displacement	NE corner of frame top	N-S
spftnwy	String-pot	Frame displacement	NW corner of frame top	N-S
spfbnwx	String-pot	Frame displacement	NW corner of frame base	E-W
spfbswx	String-pot	Frame displacement	SW corner of frame base	E-W
spfbney	String-pot	Frame displacement	NE corner of frame base	N-S
spfbnwy	String-pot	Frame displacement	NW corner of frame base	N-S
spsd1e	String-pot	Relative displacement of Spring-damper	East corner of Spring-damper at NE side	Vertical
spsd1w	String-pot	Relative displacement of Spring-damper	West corner of Spring-damper at NE side	Vertical
spsd1n	String-pot	Relative displacement of Spring-damper	North corner of Spring-damper at NE side	Vertical
spsd1s	String-pot	Relative displacement of Spring-damper	South corner of Spring-damper at NE side	Vertical
spsd2	String-pot	Relative displacement of Spring-damper	East corner of Spring-damper at SE side	Vertical
spsd3	String-pot	Relative displacement of Spring-damper	West corner of Spring-damper at SW side	Vertical
spsd4	String-pot	Relative displacement of Spring-damper	West corner of Spring-damper at NW side	Vertical
spmpve	String-pot	Relative displacement of base mass plate	East middle of base plate	Vertical
spmpvw	String-pot	Relative displacement of base mass plate	West middle of base plate	Vertical
spmpvs	String-pot	Relative displacement of base mass plate	South middle of base plate	Vertical
spmpvn	String-pot	Relative displacement of base mass plate	North middle of base plate	Vertical
dbw	Krypton LED	Table extension displacement	Bottom west of Spring-damper at SW side	E-W, N-S, V
dbm	Krypton LED	Table extension displacement	Bottom middle of Spring-damper at SW side	E-W, N-S, V
dbe	Krypton LED	Table extension displacement	Bottom east of Spring-damper at SW side	E-W, N-S, V
table	Krypton LED	Table extension displacement	Center of shake table	E-W, N-S, V
dtw	Krypton LED	Spring-damper displacement	Top west of Spring-damper at SW side	E-W, N-S, V
dtm	Krypton LED	Spring-damper displacement	Top middle of Spring-damper at SW side	E-W, N-S, V
dte	Krypton LED	Spring-damper displacement	Top east of Spring-damper at SW side	E-W, N-S, V
btw	Krypton LED	Triple FP isolator displacement	Top west of Triple FP isolator	E-W, N-S, V

Table 3-2 (continued)

Notation	Instrument	Measured Quantity	Location	Direction
Btm	Krypton LED	Triple FP isolator displacement	Top middle of Triple FP isolator	E-W, N-S, V
bte	Krypton LED	Triple FP isolator displacement	Top east of Triple FP isolator	E-W, N-S, V
massplt	Krypton LED	Triple FP isolator displacement	Middle of base plate	E-W, N-S, V

Identification of the properties of the model in the vertical direction was performed by exciting the model in the vertical direction using a 0.05 to 50Hz banded white noise of 0.1g amplitude. Amplitudes of transfer functions and phase angles were obtained from the Fourier Transform of the recorded vertical acceleration above and below the spring-damper units and are shown in Figure 3-29. Specifically the data used was as follows: (a) the average value of the four vertical acceleration values recorded at each time step at the four bases of vertical spring-damper units was the input, and (b) the average value of the four vertical acceleration values recorded at each time step at the four bases of the frame was the output. Figure 3-29 also shows the analytically derived amplitude of the transfer function (TR) and the phase angle given by the following equations for a single-degree-of-freedom linear elastic and linear viscous system (Harris and Piersol, 2002):

$$TR = \left\{ \frac{1 + [2\xi(f/f_n)^2]}{[1 - (f/f_n)^2]^2 + [2\xi(f/f_n)]^2} \right\}^{1/2} \quad (3-6)$$

$$\text{Phase Angle} = \tan^{-1} \frac{2\xi(f/f_n)^3}{1 - (f/f_n)^2 + (2\xi f/f_n)^2} \quad (3-7)$$

In these equations, f_n and ξ are the undamped frequency and damping ratio of the single-degree-of-freedom system, respectively. The figure shows that the experimental data are in very good agreement with predictions of the single-degree-of-freedom representation for a frequency of 1.92Hz and a damping ratio of 0.50. These represent the experimental values of the frequency and damping ratio in the vertical direction. They are identical to the analytically calculated values.

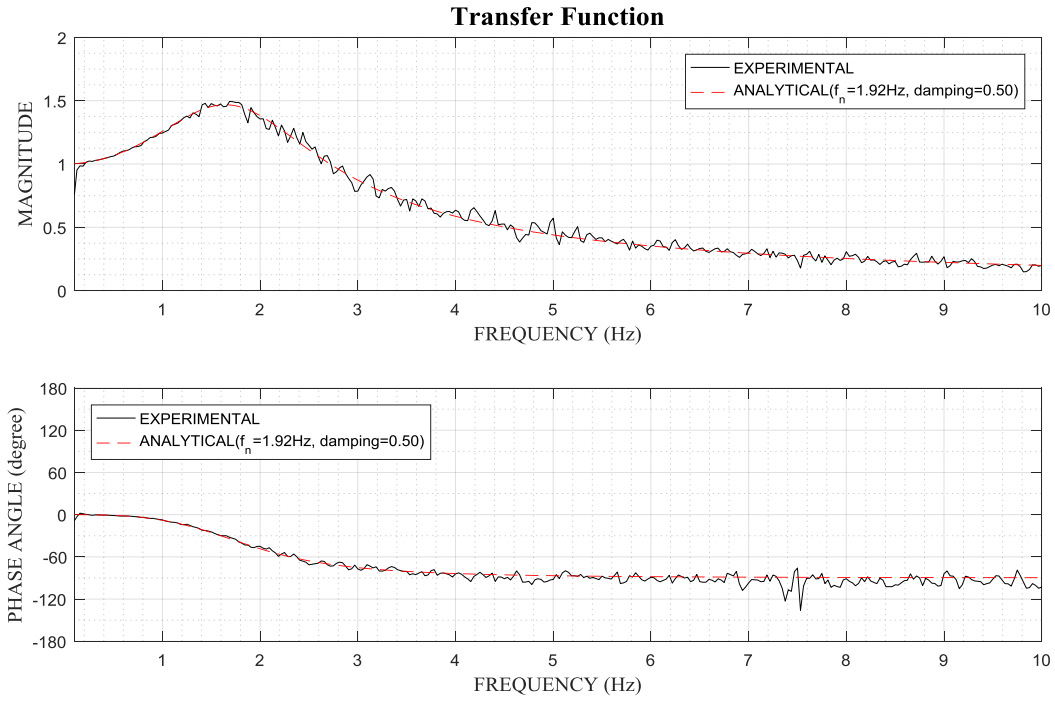


Figure 3-29 Amplitude of Transfer Function and Phase Angle of Isolated Transformer Model in Vertical Direction

SECTION 4

RESULTS OF SHAKE TABLE TESTING AND ASSESSMENT OF PERFORMANCE

4.1 Introduction

This section presents experimental results obtained in the shake table testing of the test model described in Section 3. Two configurations were tested, one allowing for free rocking of the isolated transformer model (see Figures 3-1, 3-2 and 3-7) and one with an added base to limit rocking of the isolated model (see Figures 3-3, 3-4 and 3-8). Additional experimental data are presented in Appendix F.

4.2 Motions Used in Shake Table Testing and Test Matrix

Table 4-1 presents the motions used in the shake table testing and their main characteristics. The table lists the characteristics of the motions as recorded, whereas in the shake table testing the motions were scaled either up or down in amplitude only without any scaling in time. That is, all tests were conducted in real time. The test results are identified by the “designation” of the earthquake record per Table 4-1 and a percentage value. The value denotes the scale factor applied to the acceleration histories of the original record. For example, El Centro 300% denotes a motion with three components as recorded at the station mentioned in Table 4-1 but scaled up by a factor of 3.

The 5%-damper spectra of the components of these six motions used in the testing are presented in Figures 4-1 to 4-6. The spectra are of the motions as recorded in the field.

Table 4-1 Characteristics of Earthquake Motions Used in Shake Table Testing at 100% Level

Designation	Earthquake	Recording Station	Moment Magnitude	rRup (km)	Component	Peak Ground Motion		
						Accel. (g)	Vel. (in/sec)	Displ. (in)
El Centro	1940 Imperial Valley	El Centro	6.9	6.09	S00E	0.35	13.2	4.3
					N90W	0.21	14.5	7.8
					V	0.21	4.3	2.2
Pacoima	1971 San Fernando	Pacoima Dam	6.6	1.8	164	1.22	45.0	15.4
					254	1.24	22.5	5.0
					V	0.69	23.3	11.5
Chile	2010 Chile	Concepcion	8.8	105.0	97	0.61	17.0	5.1
					07	0.65	14.6	3.6
					V	0.58	8.6	2.5
Taft	1952 Kern County	Taft Lincoln School	7.4	38.9	N21E	0.16	6.2	2.6
					S69E	0.18	7.0	3.6
					V	0.11	2.6	2.0
Kobe	1995 Kobe, Japan	Takarazuka	6.9	3.0	90	0.65	28.6	8.2
					00	0.70	32.7	10.5
					V	0.43	13.7	4.9
Jensen	1994 Northridge	Jensen Filter Plant	6.7	5.4	022	0.57	30.0	16.5
					292	1.00	26.5	9.6
					V	0.76	11.0	3.0

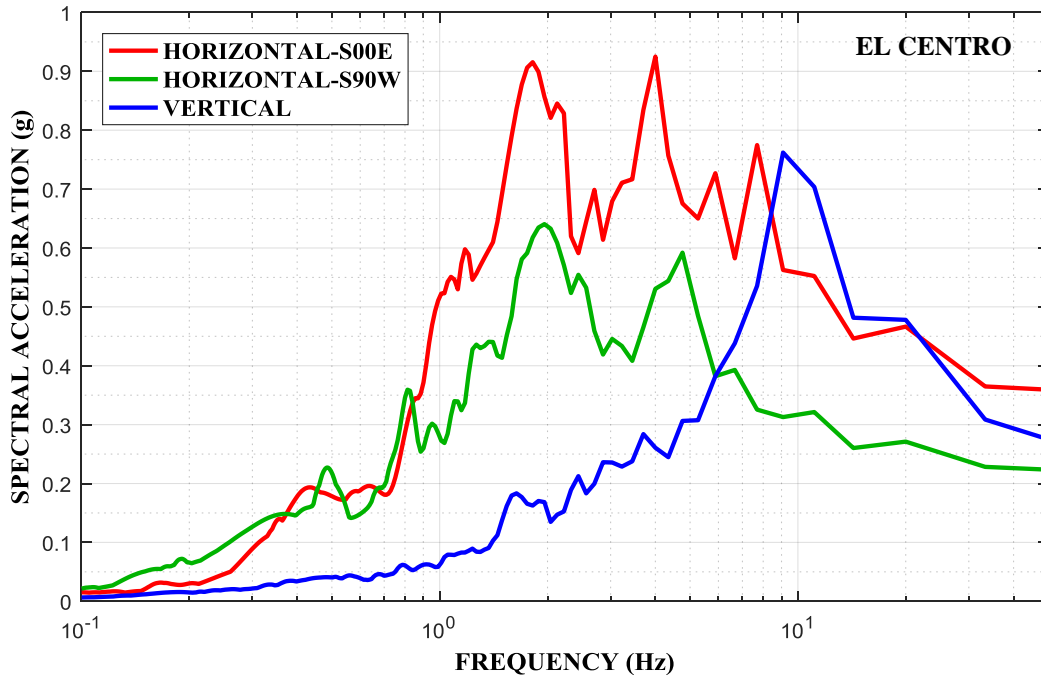


Figure 4-1 5%-Damped Vertical and Horizontal Response Spectra of El Centro Motion Recorded in the Field

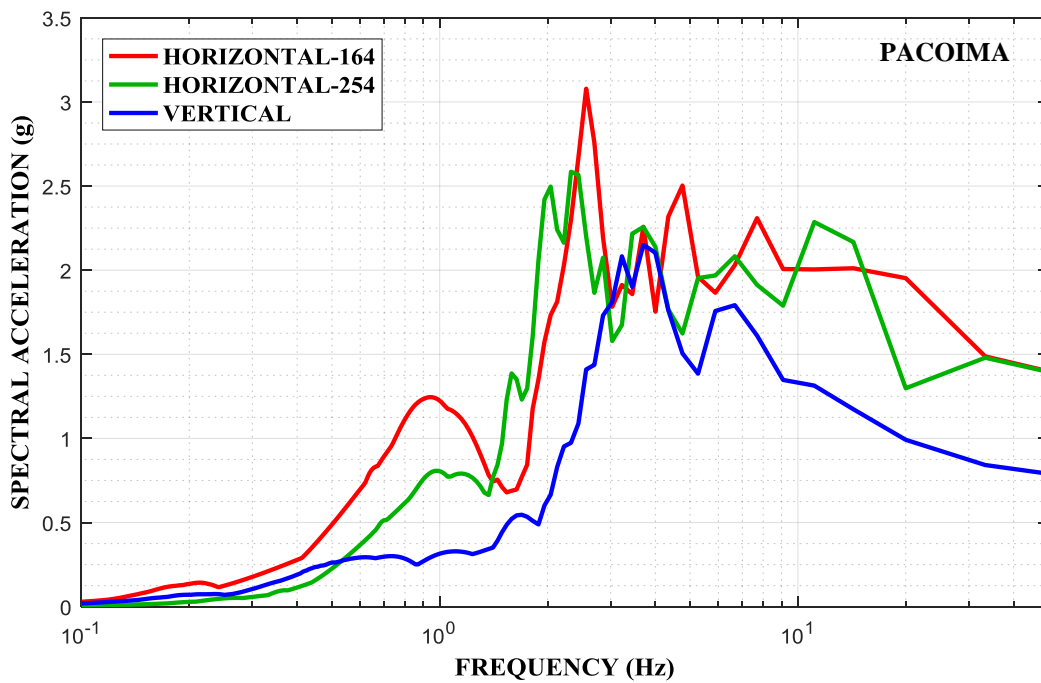


Figure 4-2 5%-Damped Vertical and Horizontal Response Spectra of Pacoima Motion Recorded in the Field

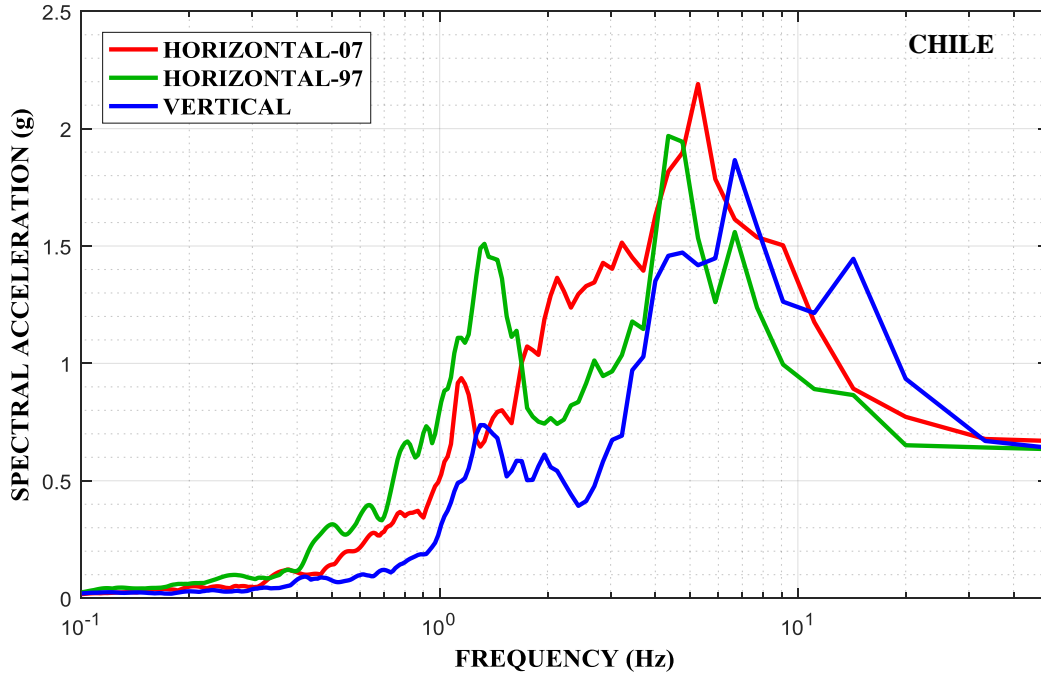


Figure 4-3 5%-Damped Vertical and Horizontal Response Spectra of Chile Motion Recorded in the Field

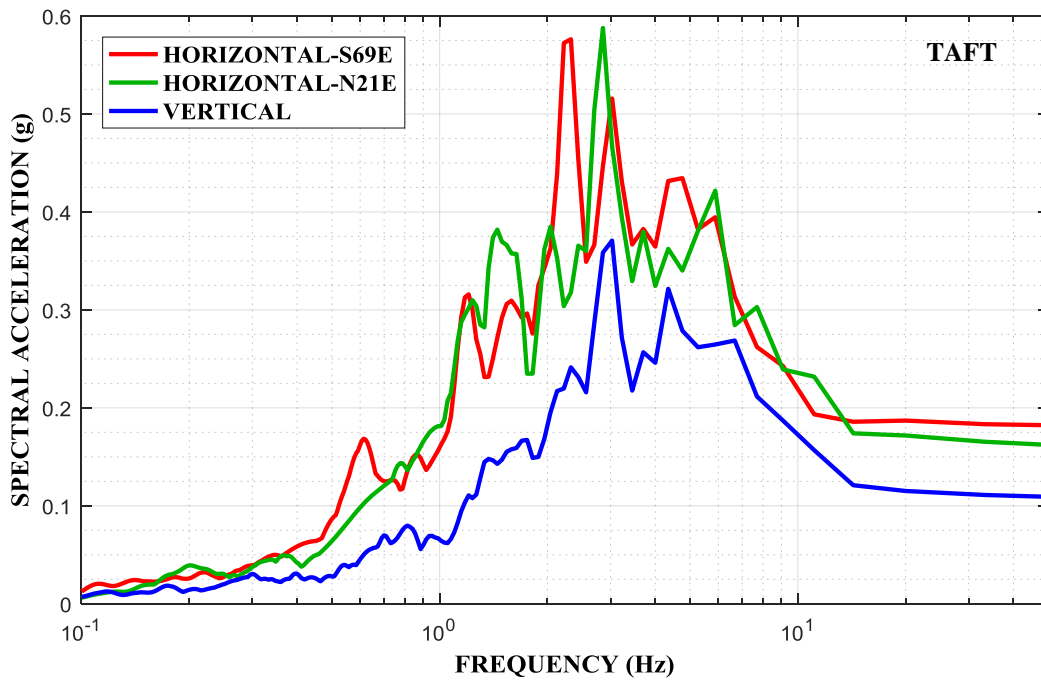


Figure 4-4 5%-Damped Vertical and Horizontal Response Spectra of Taft Motion Recorded in the Field

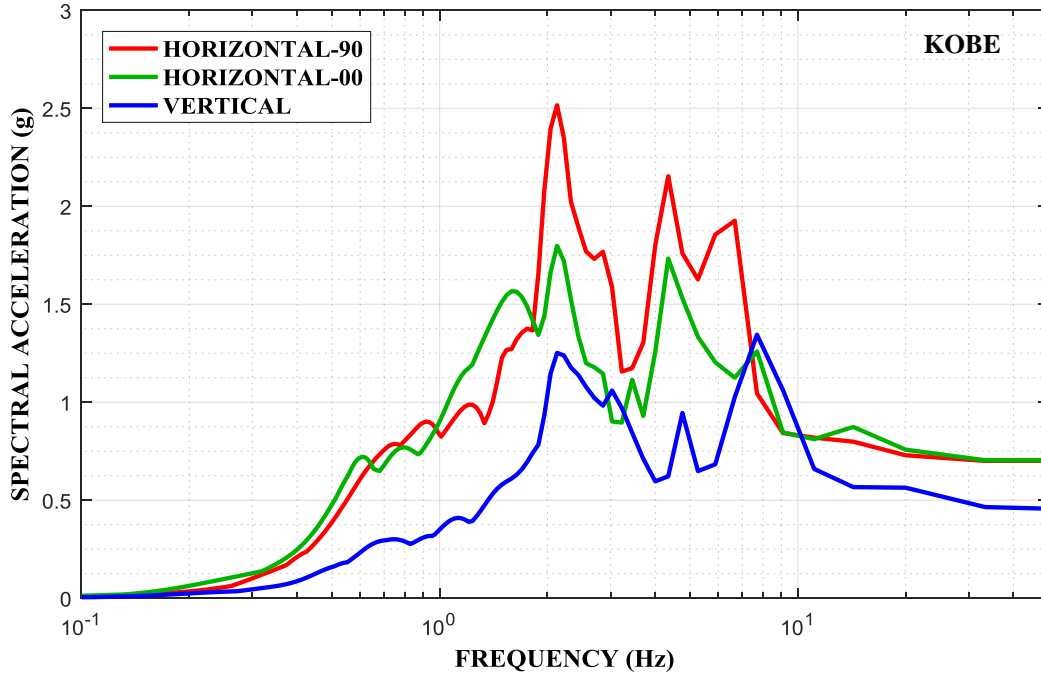


Figure 4-5 5%-Damped Vertical and Horizontal Response Spectra of Kobe Motion Recorded in the Field

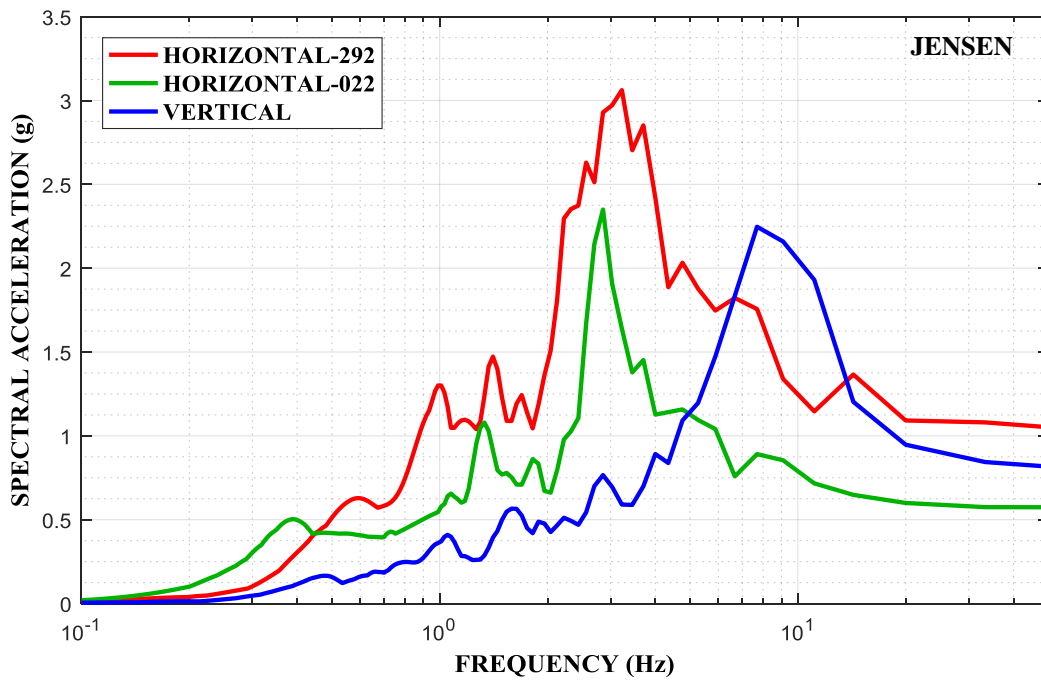


Figure 4-6 5%-Damped Vertical and Horizontal Response Spectra of Jensen Motion Recorded in the Field

Two configurations of the test model were tested (a configuration allowing for free rocking and a configuration limiting rocking) with three different value of nominal friction. Table 4-2 presents the test matrix. The tests in Table 4-2 are those of the largest seismic intensity for each of the systems tested. Other tests have also been conducted at lower intensities, results of which will be presented in selected cases where responses of different systems are compared for the same earthquake intensity.

Table 4-2 Test Matrix

Isolation System	Model Configuration			
	Allowing Free Rocking	Limiting Rocking		
FP Isolator Nominal Friction	0.12	0.20	0.12	0.07
Earthquake Motion	El Centro 250%	El Centro 200%	El Centro 250%	El Centro 250%
	Pacoima 60%	Pacoima 65%	Pacoima 75%	Pacoima 65%
	Chile 100%	Chile 100%	Chile 100%	Chile 100%
	Taft 400%	Taft 300%	Taft 400%	Taft 400%
	Kobe 50%	Kobe 50%	Kobe 65%	Kobe 65%
	Jensen 100%	-	Jensen 85%	Jensen 50%

4.3 Instrumentation

The instruments used in the testing of the configuration with free rocking were presented in Figures 3-25, 3-27 and 3-28 and were listed in Table 3-2. When the additional base was installed for limiting rocking, additional instruments were used as shown in Figures 4-7 and 4-8. Table 4-3 lists these additional instruments.

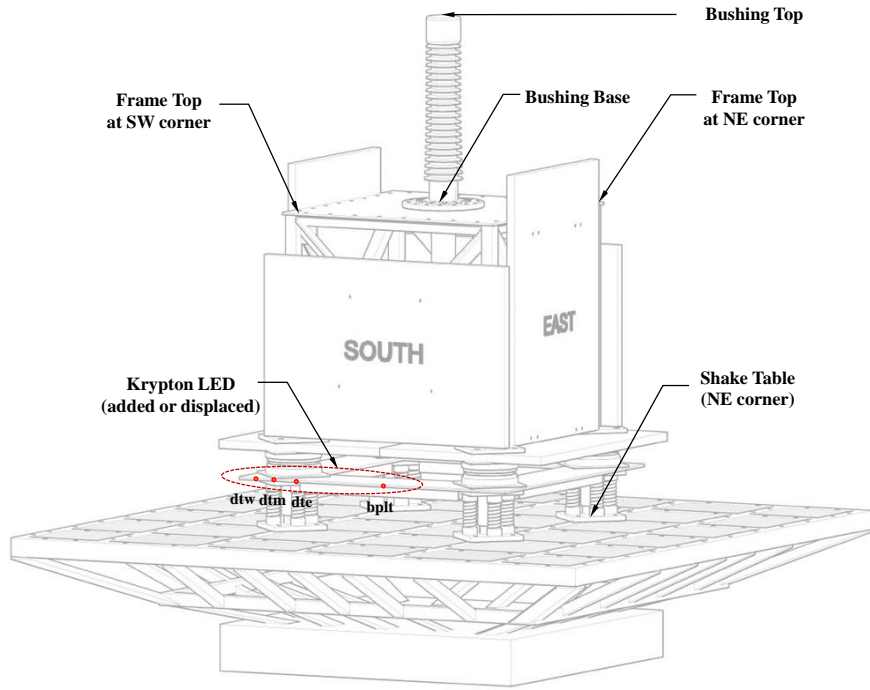


Figure 4-7 Additional Krypton LED Transducers Used in Testing of Configuration with Limited Rocking

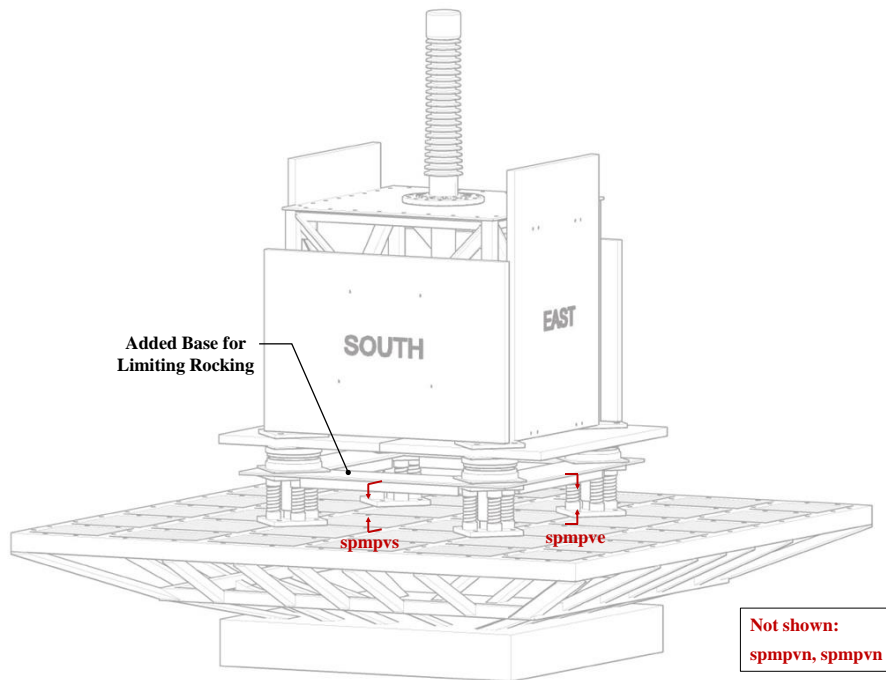


Figure 4-8 Additional Displacement Transducers Used in Testing of Configuration with Limited Rocking

Table 4-3 List of Additional Instruments Used in Testing of Configuration with Limited Rocking

Notation	Instrument	Measured Quantity	Location	Direction
spmpve	String-pot	Relative displacement of added base w.r.t. shake table	East middle of added base	Vertical
spmpvw	String-pot	Relative displacement of added base w.r.t. shake table	West middle of added base	Vertical
spmpvs	String-pot	Relative displacement of added base w.r.t. shake table	South middle of added base	Vertical
spmpvn	String-pot	Relative displacement of added base w.r.t. shake table	North middle of added base	Vertical
dtw	Krypton LED	Spring-damper displacement	Added base at the same horizontal position as used in rocking free configuration	E-W, N-S, V
dtm	Krypton LED	Spring-damper displacement	Added base at the same horizontal position as used in rocking free configuration	E-W, N-S, V
dte	Krypton LED	Spring-damper displacement	Added base at the same horizontal position as used in rocking free configuration	E-W, N-S, V
bplt	Krypton LED	Table extension displacement	South middle of added base	E-W, N-S, V

4.4 Results of Shake Table Testing

Results of the shake table testing are presented in tables where peak response quantities are presented and in response spectra of the acceleration histories recorded at various locations of the tested model. The response quantities presented are:

- 1) Response spectra for 5% damping calculated using the recorded acceleration histories at the NE corner of the model frame top and at the shake table below the isolator at the NE corner as shown in Figure 4-7. In selected cases spectra for other locations at the top corners of the frame are presented in order to demonstrate differences caused by rocking of the model.
- 2) Peak acceleration values recorded at the accelerometers installed at the bushing top, bushing base and frame top at the NE corner, and the shake table at the NE corner as shown in Figure 4-7.
- 3) Peak FP isolator horizontal resultant displacement at the SW corner of the model.
- 4) Peak spring-damper unit vertical displacement at the NE corner.

5) Peak angle of rotation of test model obtained as described below.

While the horizontal displacement of the isolation system was measured at a single isolator, there was no torsion of the isolated structure so that all isolators experienced the same displacements. This result was verified by the measurement of horizontal displacement by the string-pots installed at each corner of the test model (for example, instruments “spftswx” and “spftnwx” in Figure 3-28). For the configuration with limited rocking, the horizontal displacement of the isolator was calculated as the difference of the displacement at the lower part of the isolator (recorded at the added base between the FP isolators and the spring-damper unit below) and the displacement at the upper part of the isolator (recorded at the base plate). The Krypton system was used in the measurement of displacements. For the configuration that allowed for free rocking (the additional base between FP isolators and spring-dampers units was removed), the measurement of the displacement for the lower part of the isolator was based on the Krypton LED installed at the top of the spring-damper unit (see Figure 3-27 and Figure 4-7).

The vertical displacement of the spring-damper units is reported only for the NE corner unit where four string-pots were installed at the four sides of the unit. The reported value is the average of the four values recorded so that the reported value is the vertical displacement of the center of the unit. Note that there was some small rotation of the spring-damper units, the maximum value of which was recorded in the test with motion Jensen 100% to be 0.01rad (0.57degrees).

The angle of rotation of the model in the configuration allowing for free rocking was obtained by dividing the difference in vertical displacements at the opposite sides of the base plate above the FP isolators by the distance between those instruments. The vertical displacements were measured by string-pots installed between the shake table extension and the mid-point of each side on the base plate above the FP isolators at EW and NS locations. In the configuration with limited rocking, the same string-pots were used but they were attached between the shake table extension and the added base plate in-between the FP isolators and the spring-damper units (see Figure 3-28 and Figure 4-8).

The isolation system with isolator type B of nominal friction equal to 0.12 was tested in both configurations with limited rocking and with free rocking (see Figure 3-5 for the configuration of type B isolator). This level of nominal friction is the one desired and achievable with the tested isolator type for the full size transformer. This case is selected to present results of the response spectra and to compare the two configurations.

Figures 4-9 to 4-14 present 5%-damped response spectra of the acceleration histories recorded at the shake table below the isolators and at the frame NE corner top above the isolators in the configuration with limited rocking and with isolator type B with nominal friction of 0.12 in the six tests of Table 4-2. The substantial reduction in the peak values of acceleration is evident (highlighted in the spectra at the frequency of 50Hz) but in a couple of cases discussed later. Moreover, there is substantial reduction in all horizontal spectra over a wide range of frequencies and in the vertical spectra over a smaller frequency range. The latter is apparently the result of the higher frequency of the vertical isolation system (1.86Hz) by comparison to that of the horizontal isolation system (0.37Hz, see first mode frequency curve at $K_h=W/2R_{eff1}$ in Figure 3-10, although the figure applies for the configuration of free rocking).

Figures 4-15 to 4-20 present 5%-damped response spectra of the accelerations histories recorded at the shake table below the isolators and at the frame NE corner top above the isolators in the configuration with free rocking and with isolator type B with nominal friction of 0.12 in the six tests of Table 4-2. Again, the benefits of isolation are seen in the reduction of the peak values of acceleration (highlighted in the spectra at the frequency of 50Hz) and the reduction in the horizontal spectra over a wide range of frequencies and in the vertical spectra over a smaller frequency range.

The results demonstrate that in two tests (Taft and Kobe) there was small reduction in the peak vertical acceleration on the frame above the isolators. Also, in the configuration with free rocking there was even a small increase in the vertical peak value of acceleration in the Kobe motion (Figure 4-19). The reason is that both these motions have strong spectral components in the horizontal and vertical directions in the range of 2 to 3Hz, which relate to the rocking and vertical frequencies of the model.

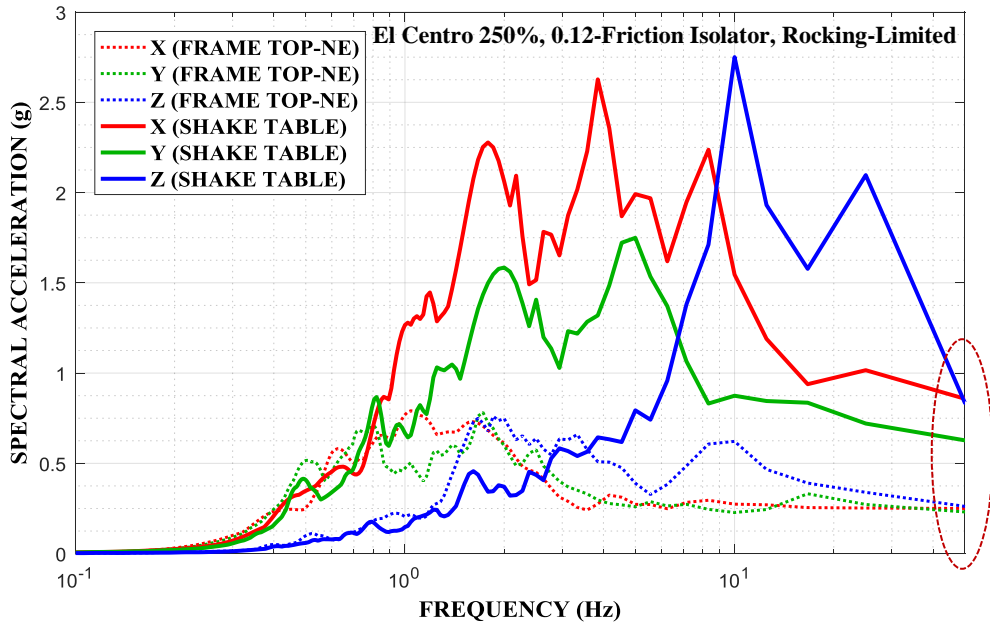


Figure 4-9 5%-Damped Response Spectra at Frame Top at NE Corner and at Shake Table for Configuration with Limited Rocking, FP Isolator Type B with 0.12 Nominal Friction in El Centro 250% Motion

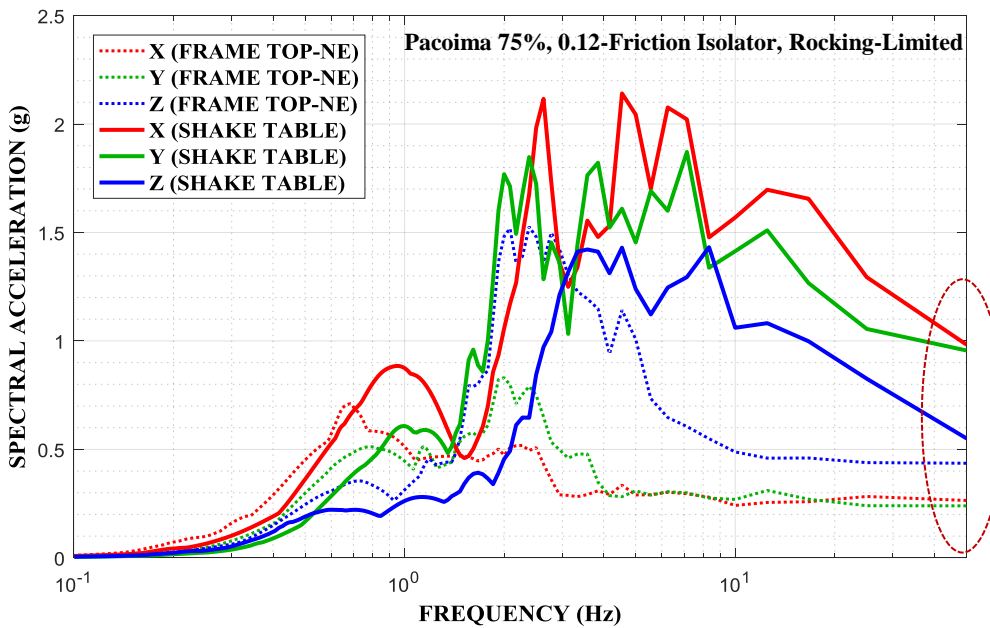


Figure 4-10 5%-Damped Response Spectra at Frame Top at NE Corner and at Shake Table for Configuration with Limited Rocking, FP Isolator Type B with 0.12 Nominal Friction in Pacoima 75% Motion

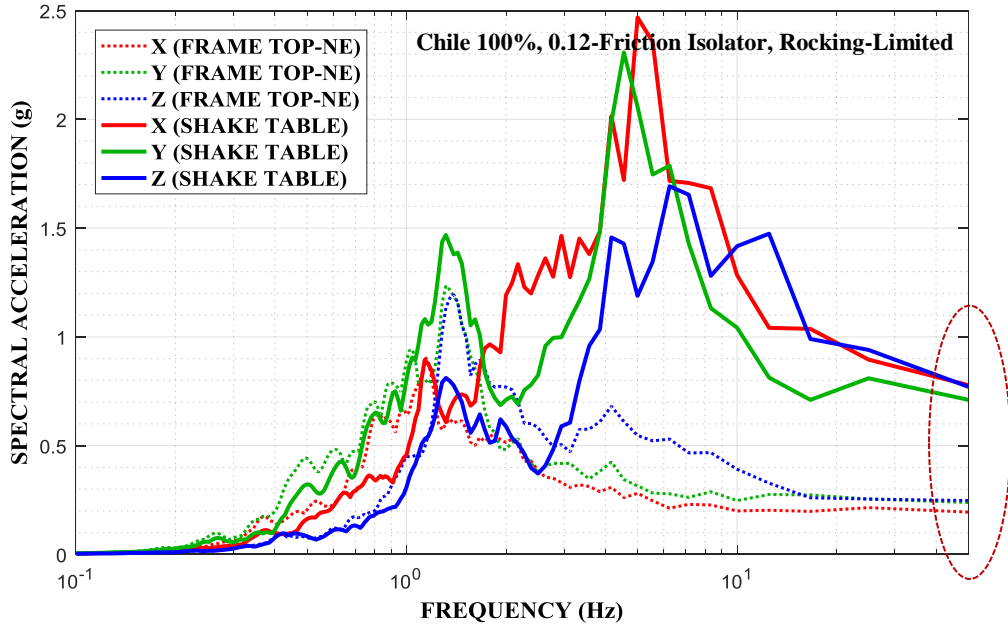


Figure 4-11 5%-Damped Response Spectra at Frame Top at NE Corner and at Shake Table for Configuration with Limited Rocking, FP Isolator Type B with 0.12 Nominal Friction in Chile 100% Motion

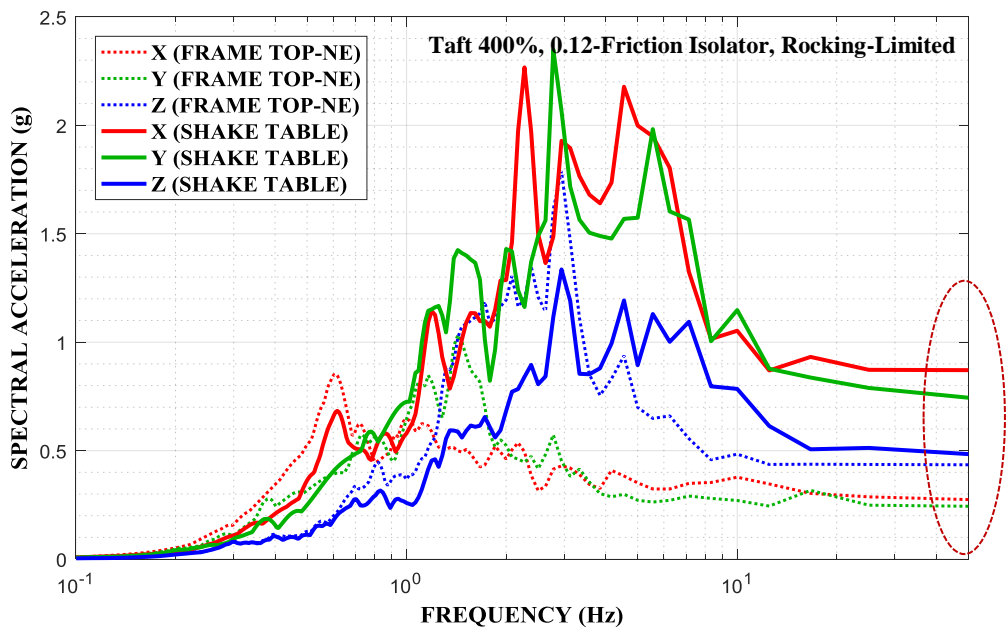


Figure 4-12 5%-Damped Response Spectra at Frame Top at NE Corner and at Shake Table for Configuration with Limited Rocking, FP Isolator Type B with 0.12 Nominal Friction in Taft 400% Motion

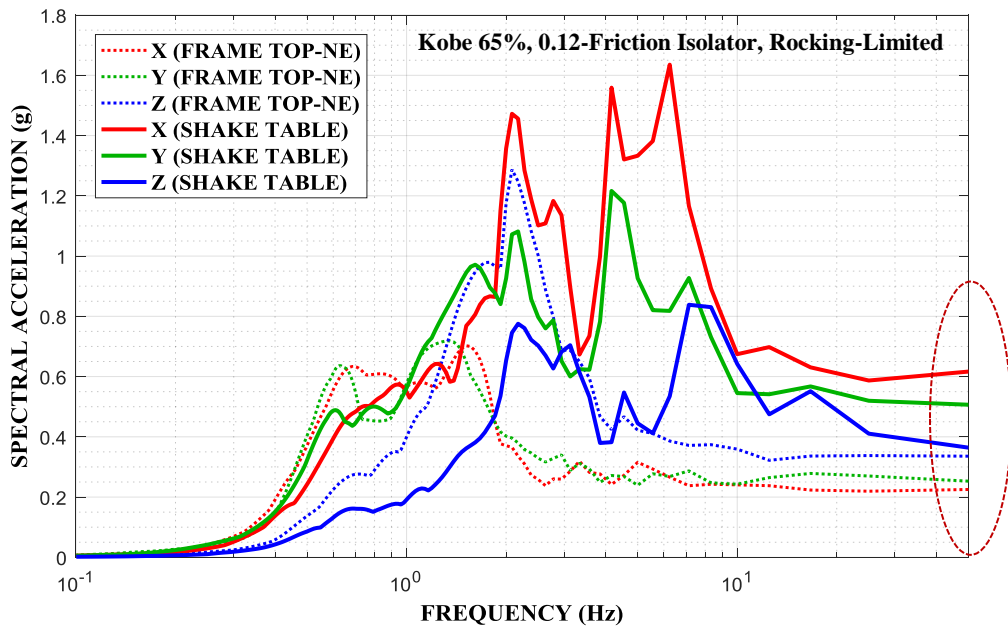


Figure 4-13 5%-Damped Response Spectra at Frame Top at NE Corner and at Shake Table for Configuration with Limited Rocking, FP Isolator Type B with 0.12 Nominal Friction in Kobe 65% Motion

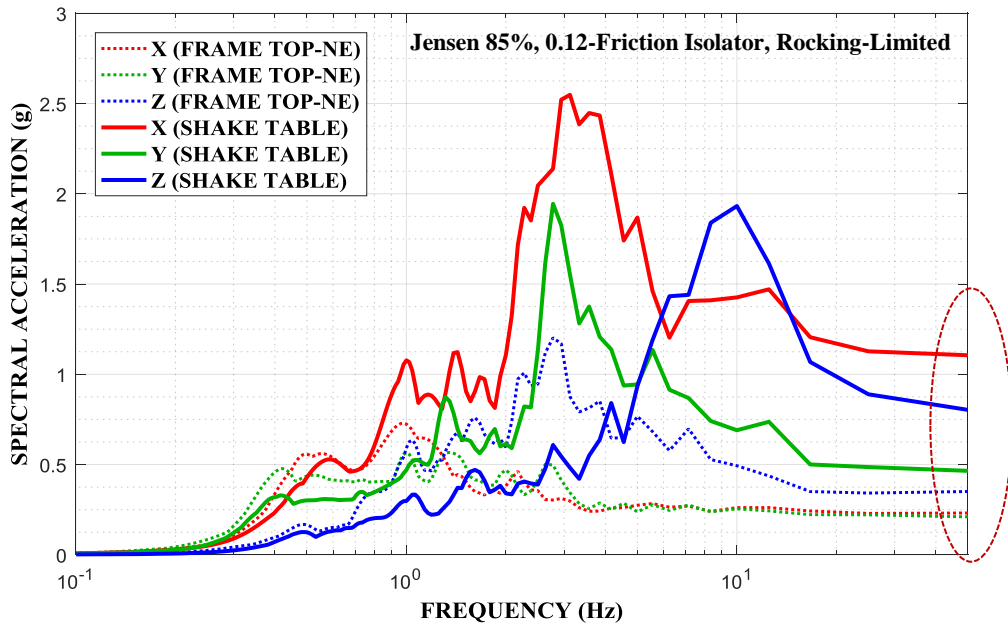


Figure 4-14 5%-Damped Response Spectra at Frame Top at NE Corner and at Shake Table for Configuration with Limited Rocking, FP Isolator Type B with 0.12 Nominal Friction in Jensen 85% Motion

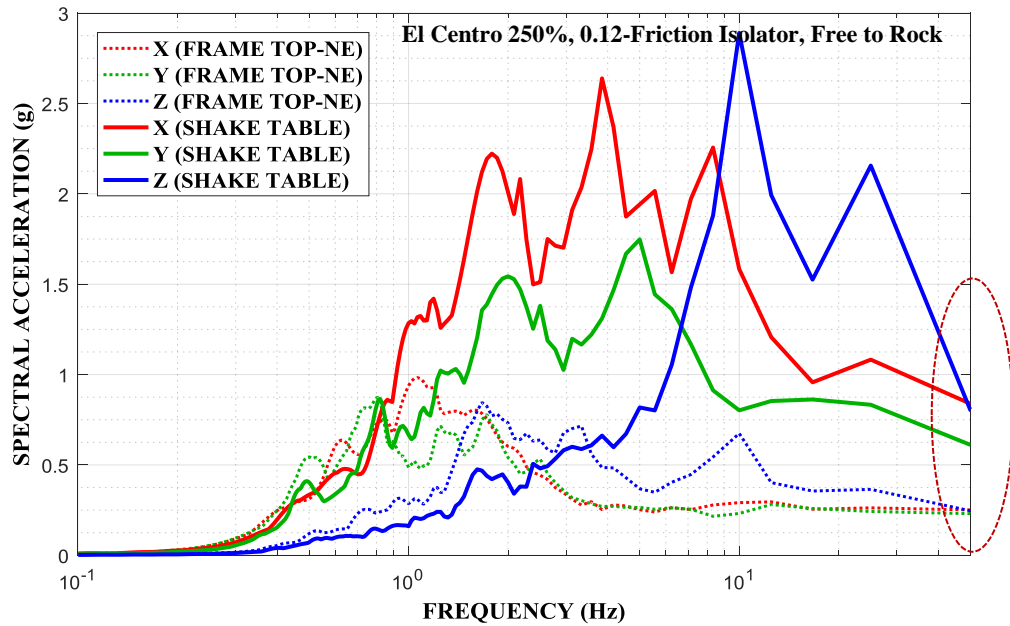


Figure 4-15 5%-Damped Response Spectra at Frame Top at NE Corner and at Shake Table for Configuration with Free Rocking, FP Isolator Type B with 0.12 Nominal Friction in El Centro 250% Motion

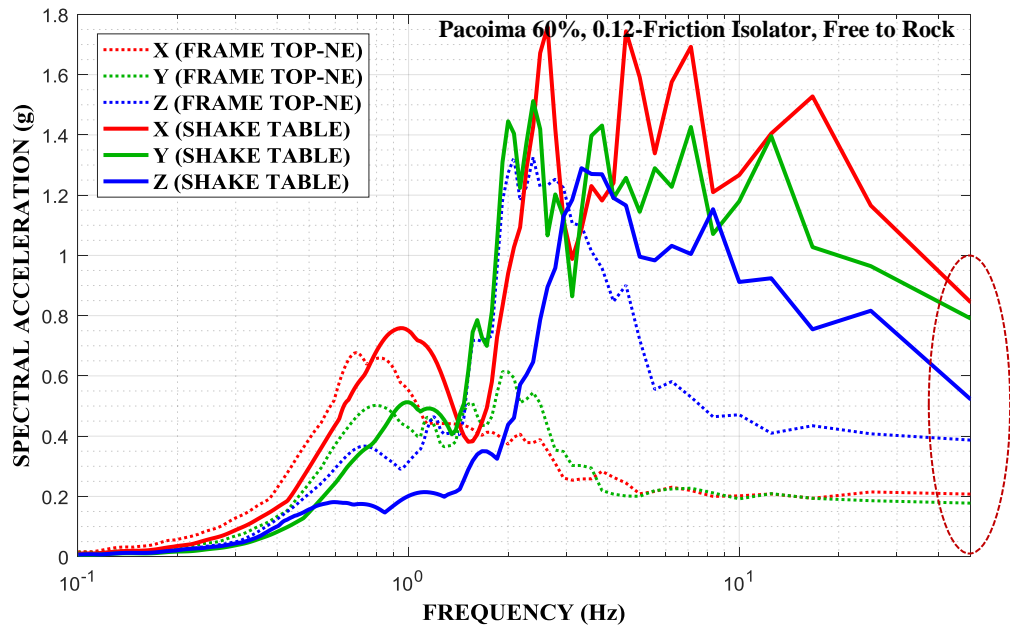


Figure 4-16 5%-Damped Response Spectra at Frame Top at NE Corner and at Shake Table for Configuration with Free Rocking, FP Isolator Type B with 0.12 Nominal Friction in Pacoima 60% Motion

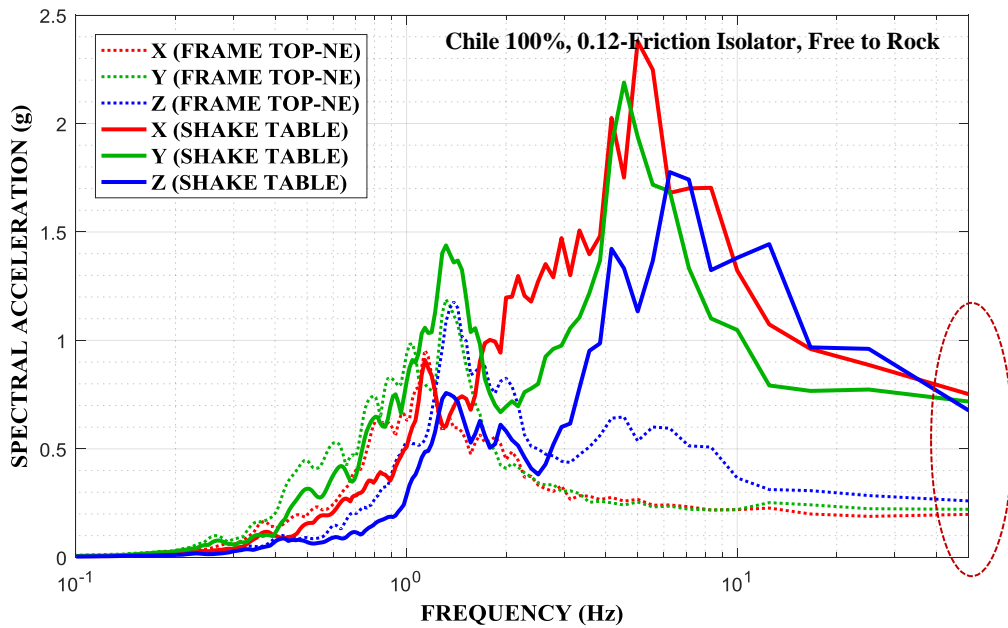


Figure 4-17 5%-Damped Response Spectra at Frame Top at NE Corner and at Shake Table for Configuration with Free Rocking, FP Isolator Type B with 0.12 Nominal Friction in Chile 100% Motion

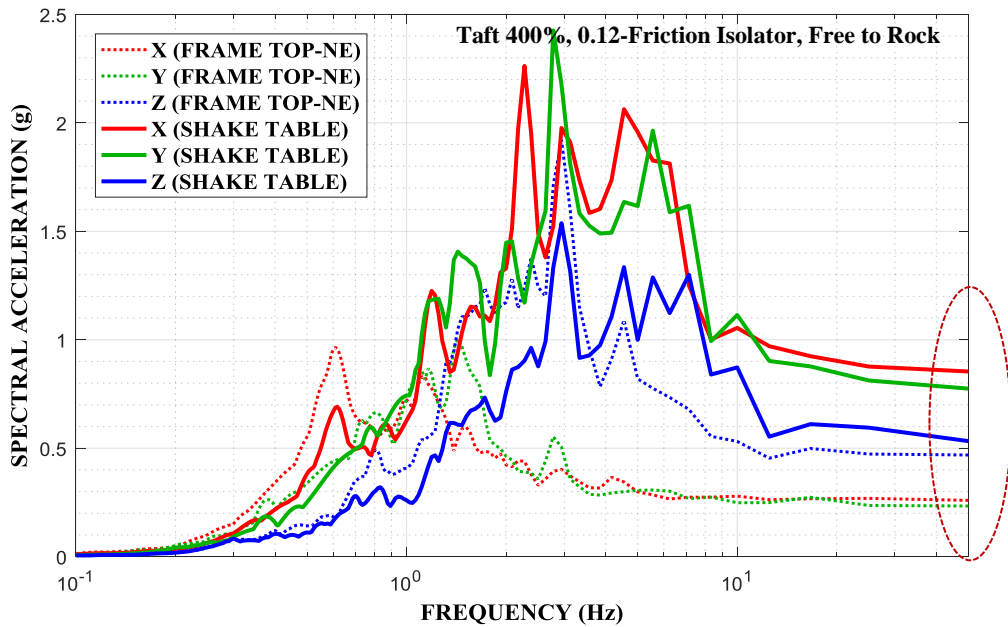


Figure 4-18 5%-Damped Response Spectra at Frame Top at NE Corner and at Shake Table for Configuration with Free Rocking, FP Isolator Type B with 0.12 Nominal Friction in Taft 400% Motion

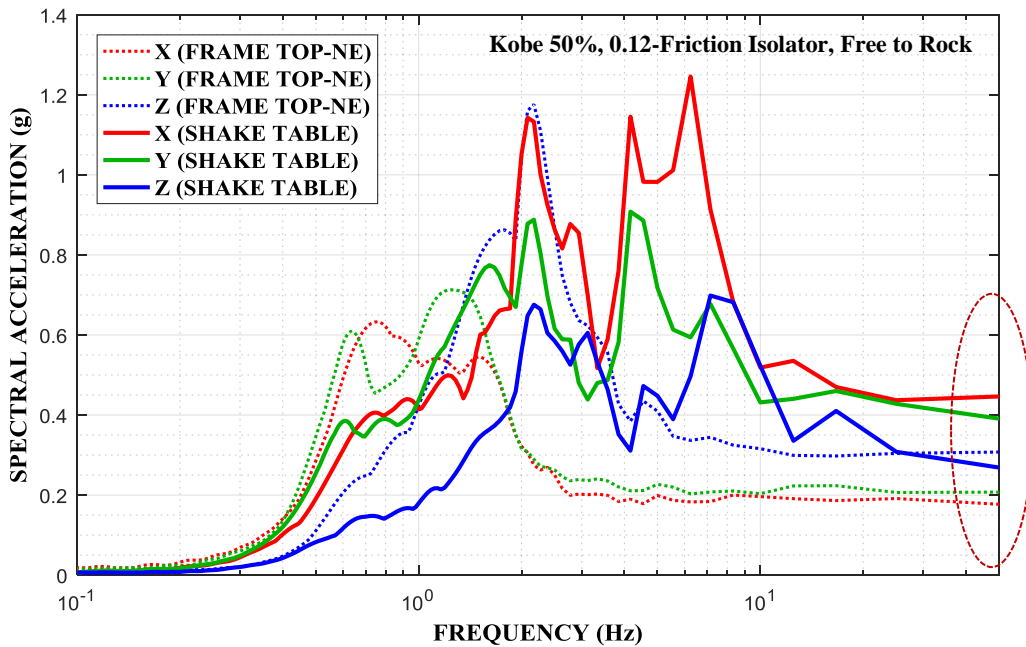


Figure 4-19 5%-Damped Response Spectra at Frame Top at NE Corner and at Shake Table for Configuration with Free Rocking, FP Isolator Type B with 0.12 Nominal Friction in Kobe 50% Motion

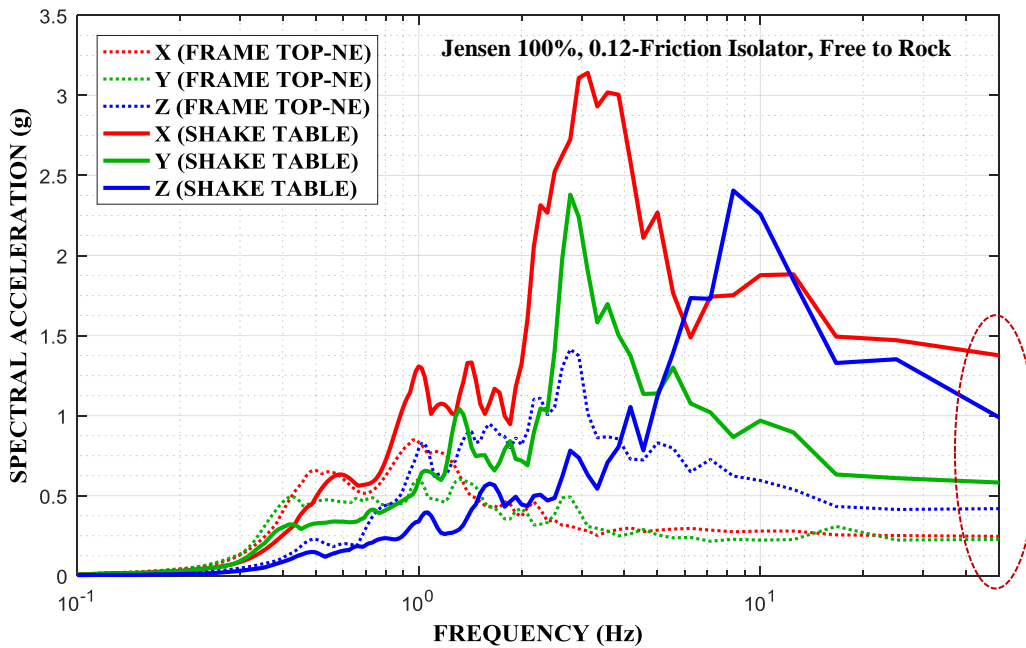


Figure 4-20 5%-Damped Response Spectra at Frame Top at NE Corner and at Shake Table for Configuration with Free Rocking, FP Isolator Type B with 0.12 Nominal Friction in Jensen 85% Motion

It should be noted that the tested model exhibited rocking, including the case of the configuration with limited rocking. To show the effect of rocking on the response spectra, Figures 4-21 and 4-22 compare the response spectra of the vertical and horizontal accelerations measured at the frame at various corner top locations for two selected motions in the system with free rocking. There are small differences in the horizontal response spectra at opposing corners of the model but there are substantial differences in the vertical spectra. The results in Figures 4-21 and 4-22 indicate significant rocking about an axis perpendicular to the diagonal NE-SW direction.

The two tested configurations, with free rocking and with limited rocking, did not have significant differences in response. Figures 4-23 to 4-28 compare the 5%-damped spectra of the acceleration histories recorded at the frame top at the NE corner in the six motions of the test matrix in Table 4-2 and for the two tested configurations. Note that in some tests the highest intensity motion used in the testing was not the same for the two configurations. The comparisons are presented for tests of the same seismic intensity.

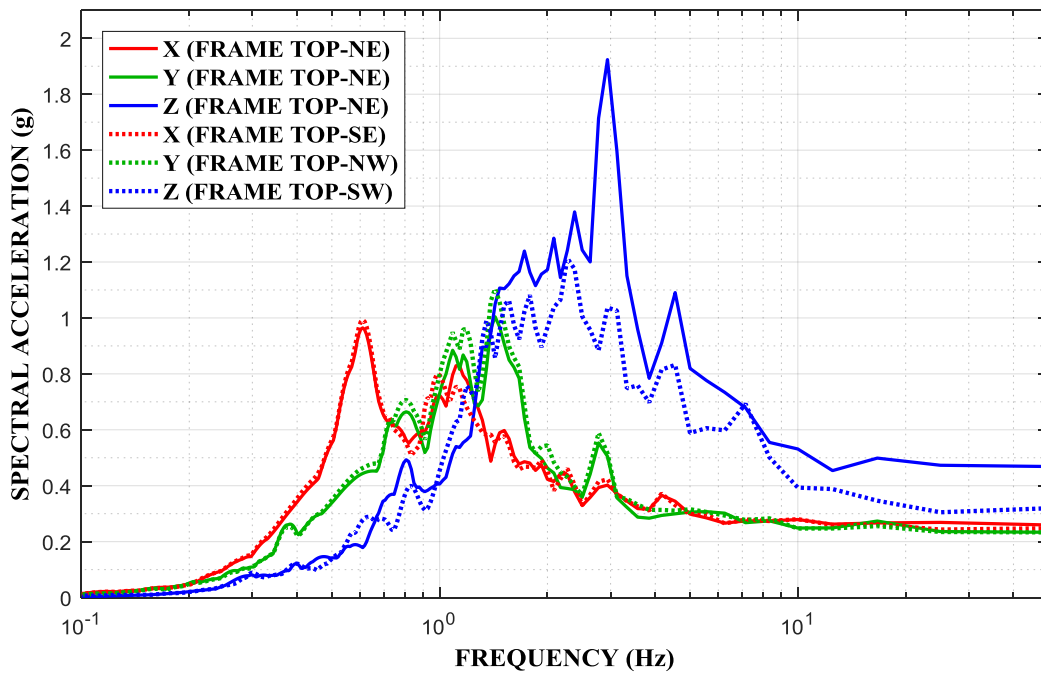


Figure 4-21 5%-Damped Vertical and Horizontal Response Spectra at Various Frame Top Locations in Horizontal and Vertical Directions for Configuration with Free Rocking, FP Isolator Type B with 0.12 Nominal Friction in Taft 400% Motion

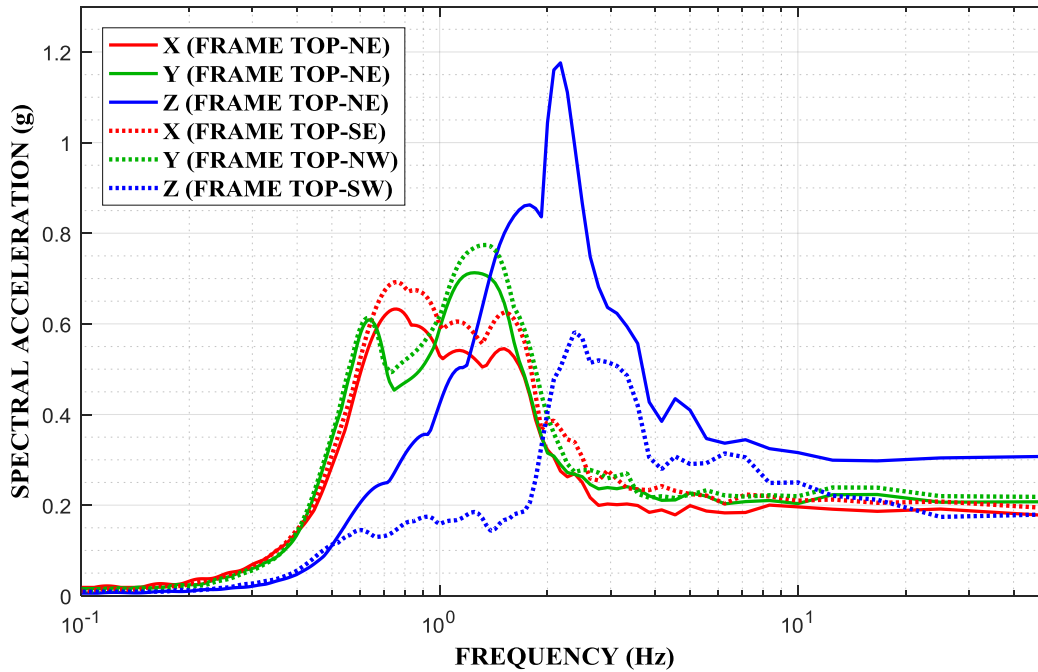


Figure 4-22 5%-Damped Vertical and Horizontal Response Spectra at Various Frame Top Locations in Horizontal and Vertical Directions for Configuration with Free Rocking, FP Isolator Type B with 0.12 Nominal Friction in Kobe 50% Motion

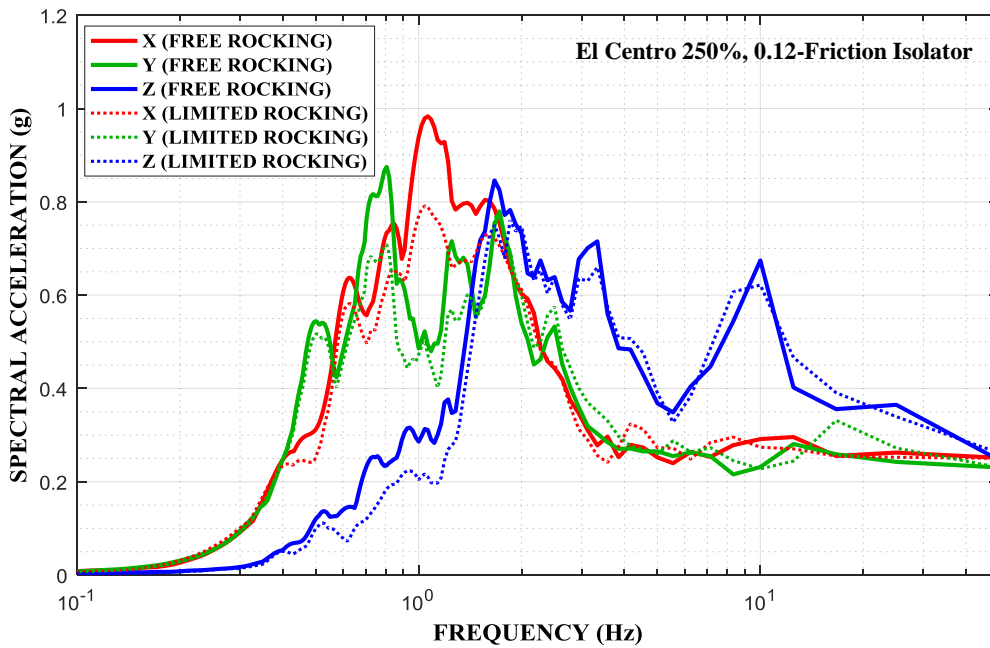


Figure 4-23 Comparison of 5%-Damped Response Spectra at Frame Top at NE Corner of Two Tested Configurations with Free Rocking and Limited Rocking, FP Isolator Type B with 0.12 Nominal Friction in El Centro 250% Motion

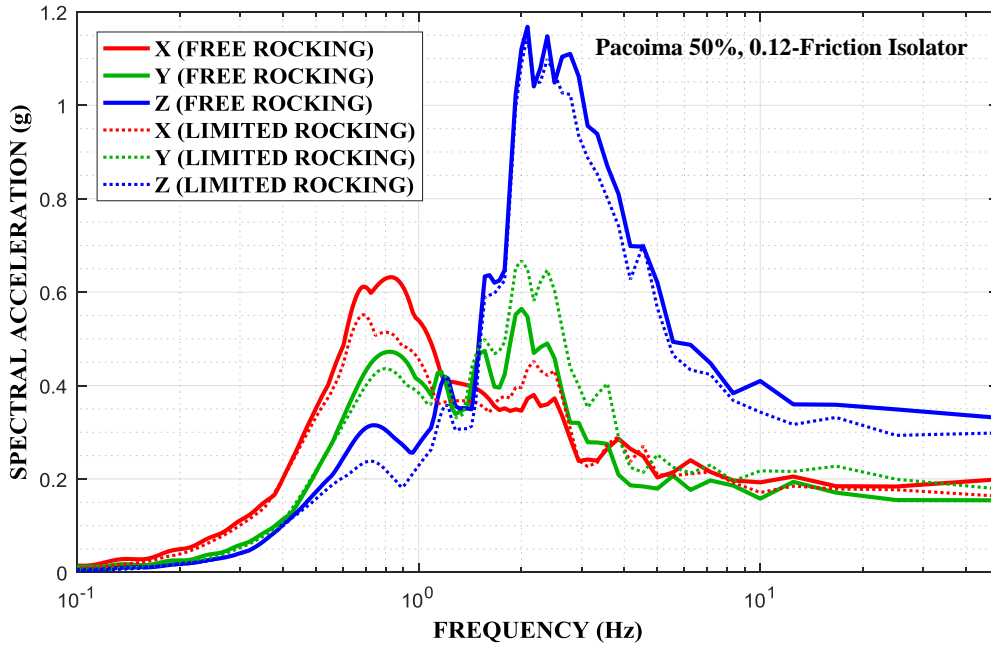


Figure 4-24 Comparison of 5%-Damped Response Spectra at Frame Top at NE Corner of Two Tested Configurations with Free Rocking and Limited Rocking, FP Isolator Type B with 0.12 Nominal Friction in Pacoima 50% Motion

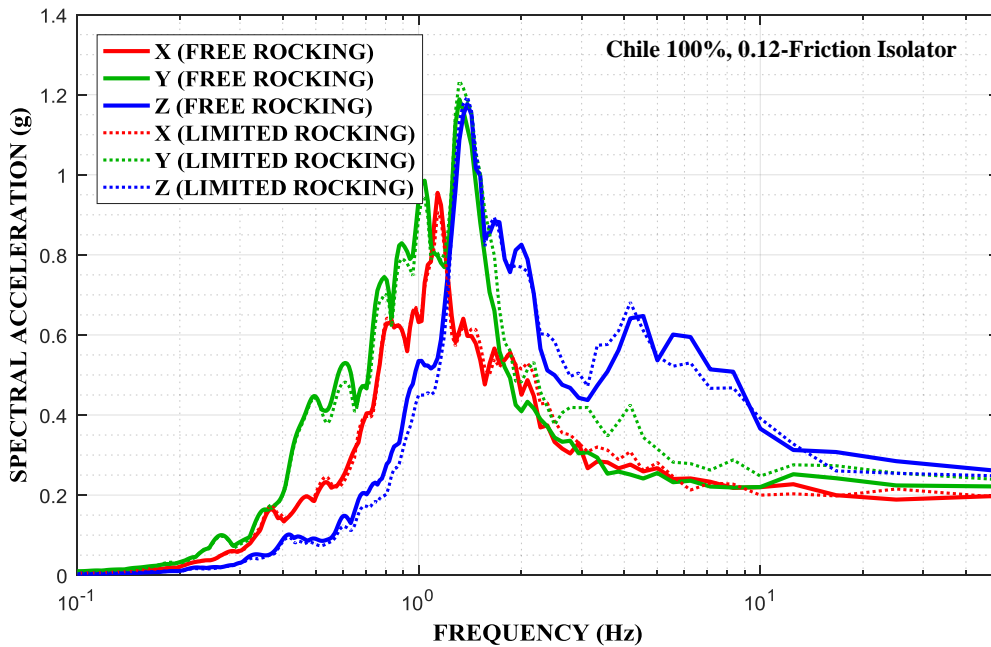


Figure 4-25 Comparison of 5%-Damped Response Spectra at Frame Top at NE Corner of Two Tested Configurations with Free Rocking and Limited Rocking, FP Isolator Type B with 0.12 Nominal Friction in Chile 100% Motion

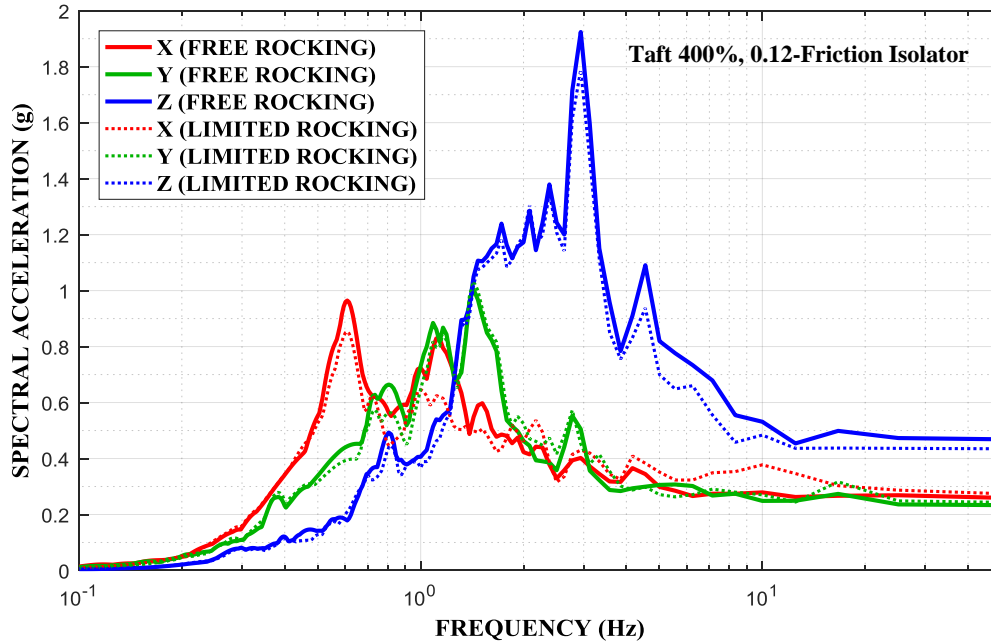


Figure 4-26 Comparison of 5%-Damped Response Spectra at Frame Top at NE Corner of Two Tested Configurations with Free Rocking and Limited Rocking, FP Isolator Type B with 0.12 Nominal Friction in Taft 400% Motion

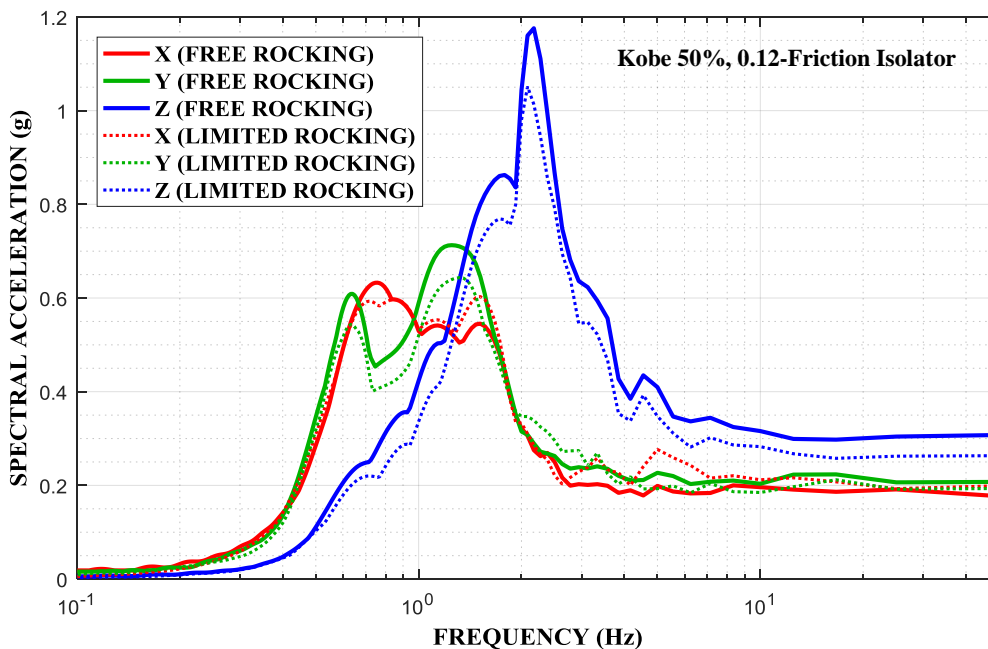


Figure 4-27 Comparison of 5%-Damped Response Spectra at Frame Top at NE Corner of Two Tested Configurations with Free Rocking and Limited Rocking, FP Isolator Type B with 0.12 Nominal Friction in Kobe 50% Motion

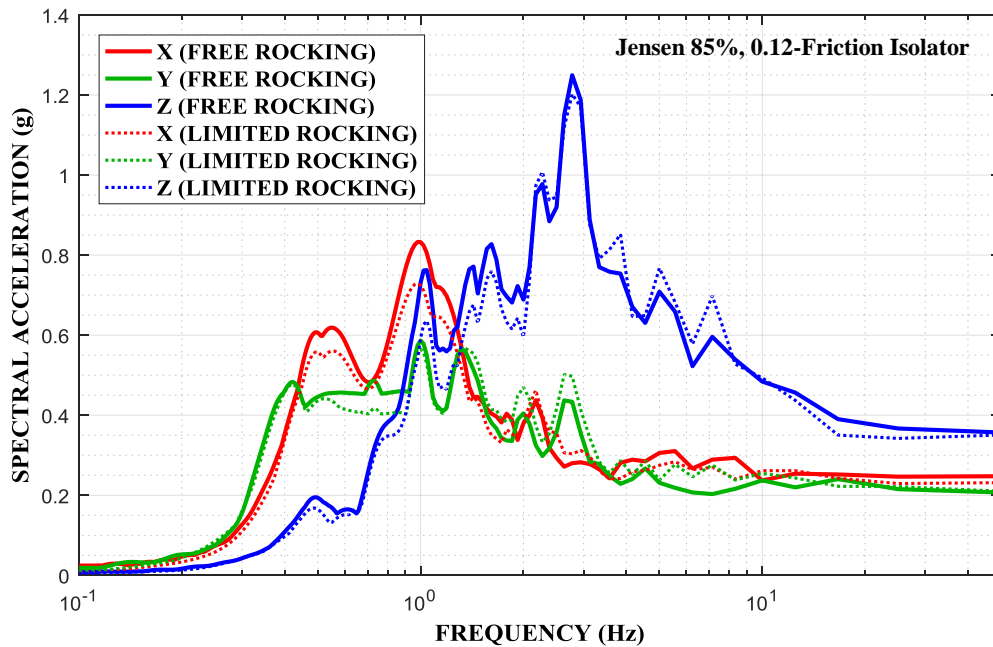


Figure 4-28 Comparison of 5%-Damped Response Spectra at Frame Top at NE Corner of Two Tested Configurations with Free Rocking and Limited Rocking, FP Isolator Type B with 0.12 Nominal Friction in Jensen 85% Motion

The results in Figures 4-23 to 4-28 reveal small differences in the spectra of the recorded acceleration response. It appears that the system with limited rocking has a little lower peak vertical acceleration response (value of spectral acceleration at large frequency) but the difference may actually be due to small differences in the shake table motion given the difficulties to control the table and the large model weight (to be discussed in Section 5). More information on the response of the two configurations is revealed by inspecting the results of Tables 4-4 to 4-6 which present (a) the recorded peak values of acceleration at the shake table, frame top, bushing base and bushing top, (b) the FP isolator resultant horizontal displacement, (c) the spring-damper unit vertical displacement, and (d) the peak value of the model angle of rotation about the two horizontal axes.

The results for the two configurations of the same isolation system properties (isolator type B, nominal friction 0.12) reveal that (a) there are differences in the peak vertical shake table acceleration that may explain the small differences in the vertical response spectra, (b) the bushing top peak accelerations and the FP isolator peak resultant horizontal displacements are

less in the configuration with free rocking than in the configuration with limited rocking, and (c) the spring-damper unit peak vertical displacement and the peak angle of rotation of the model are less in the configuration with limited rocking than in the configuration with free rocking, although the differences are small.

The results of Tables 4-4 to 4-6 also reveal the effect of friction on the response of the isolated model of the configuration with limited rocking. In general, increases in friction result in the expected reduction in FP isolator displacements and increase in horizontal accelerations at the frame top, bushing base and bushing top.

Table 4-4 Recorded Values of Peak Acceleration of Tested Systems

Peak Acceleration (g)													
Configuration		Free to Rock			Limited Rocking								
FP Isolator		Type B 0.12 Friction			Type A 0.20 Friction			Type B 0.12 Friction			Type A 0.07 Friction		
Motion	Location	EW	NS	V									
El Centro 200%	Bushing Top	0.54	0.45	0.36	0.78	0.72	0.39	0.67	0.63	0.42	0.74	0.52	0.41
	Bushing Base	0.22	0.21	0.37	0.38	0.37	0.39	0.23	0.20	0.41	0.26	0.19	0.42
	Frame Top ¹	0.21	0.20	0.19	0.36	0.36	0.24	0.22	0.20	0.19	0.28	0.20	0.19
	Shake Table ²	0.63	0.43	0.53	0.64	0.44	0.63	0.66	0.46	0.62	0.65	0.46	0.61
Pacoima 50%	Bushing Top	0.46	0.41	0.42	0.73	0.62	0.50	0.63	0.63	0.48	0.47	0.52	0.50
	Bushing Base	0.19	0.15	0.44	0.34	0.25	0.49	0.18	0.17	0.49	0.16	0.13	0.50
	Frame Top ¹	0.18	0.15	0.33	0.32	0.24	0.33	0.16	0.18	0.29	0.17	0.13	0.31
	Shake Table ²	0.70	0.60	0.38	0.64	0.57	0.34	0.64	0.57	0.32	0.63	0.58	0.34
Chile 100%	Bushing Top	0.57	0.48	0.83	0.78	0.75	0.77	0.70	0.69	0.79	0.57	0.61	0.66
	Bushing Base	0.22	0.23	0.81	0.30	0.35	0.77	0.20	0.23	0.75	0.18	0.22	0.67
	Frame Top ¹	0.19	0.21	0.25	0.29	0.33	0.31	0.19	0.24	0.24	0.17	0.21	0.21
	Shake Table ²	0.74	0.68	0.63	0.75	0.65	0.69	0.76	0.67	0.70	0.78	0.67	0.69
Taft 300%	Bushing Top	0.41	0.50	0.31	0.73	0.74	0.37	0.64	0.64	0.31	0.69	0.56	0.31
	Bushing Base	0.21	0.21	0.30	0.29	0.37	0.35	0.23	0.20	0.33	0.22	0.18	0.31
	Frame Top ¹	0.21	0.20	0.36	0.27	0.35	0.39	0.22	0.19	0.33	0.21	0.19	0.32
	Shake Table ²	0.60	0.56	0.37	0.58	0.56	0.36	0.57	0.54	0.32	0.58	0.53	0.34
Kobe 50%	Bushing Top	0.35	0.36	0.25	0.67	0.57	0.25	0.47	0.45	0.24	0.43	0.58	0.27
	Bushing Base	0.19	0.21	0.22	0.30	0.29	0.25	0.21	0.18	0.25	0.19	0.20	0.26
	Frame Top ¹	0.18	0.20	0.30	0.28	0.30	0.31	0.19	0.19	0.26	0.16	0.20	0.27
	Shake Table ²	0.44	0.38	0.26	0.45	0.36	0.28	0.42	0.36	0.25	0.44	0.37	0.25
Jensen 50%	Bushing Top	0.57	0.52	0.32	-	-	-	0.62	0.61	0.33	0.58	0.66	0.34
	Bushing Base	0.19	0.17	0.33	-	-	-	0.19	0.14	0.36	0.18	0.15	0.34
	Frame Top ¹	0.19	0.17	0.24	-	-	-	0.19	0.16	0.24	0.16	0.14	0.19
	Shake Table ²	0.58	0.27	0.36	-	-	-	0.56	0.26	0.42	0.61	0.25	0.42

1. Frame top: Peak acceleration recorded at NE corner of top of frame
2. Shake table: Peak acceleration recorded at NE corner of shake table extension

Table 4-5 Recorded Values of Peak Isolator Displacement of Tested Systems

Peak Isolator Displacement (inch)								
Configuration	Free to Rock		Limited Rocking					
FP Isolator	Type B 0.12 Friction		Type A 0.20 Friction		Type B 0.12 Friction		Type A 0.07 Friction	
Motion	Resultant H ¹	V ²	Resultant H ¹	V ²	Resultant H ₁	V ²	Resultant H ¹	V ²
El Centro 200%	4.73	+0.65 -0.68	4.44	+0.81 -0.74	5.38	+0.65 -0.50	6.84	+0.60 -0.44
Pacoima 50%	5.17	+0.78 -0.91	4.86	+0.89 -0.86	5.21	+0.79 -0.66	6.18	+0.90 -0.54
Chile 100%	4.11	+0.75 -0.85	4.07	+1.06 -0.96	4.89	+0.82 -0.79	7.03	+0.66 -0.72
Taft 300%	4.25	+0.87 -0.85	5.14	+1.09 -1.08	4.39	+0.79 -0.71	5.29	+0.72 -0.62
Kobe 50%	2.95	+0.83 -1.17	3.30	+0.92 -1.10	3.22	+0.78 -1.05	4.93	+0.67 -0.86
Jensen 50%	3.09	+0.56 -0.64	-	-	3.24	+0.64 -0.57	4.23	+0.51 -0.35

1: Peak resultant horizontal displacement measured by Krypton LED sensors installed at Triple FP isolator at the SW corner.
2: Peak dynamic component of vertical displacement is the average value of four string-pots installed at the NE spring-damper unit. (+) sign is upwards and (-) sign is downwards.

Table 4-6 Recorded Values of Peak Model Angle of Rotation of Tested Systems

Peak Angle of Rotation (degrees)								
Configuration	Free to Rock		Limited Rocking					
FP Isolator	Type B 0.12 Friction		Type A 0.20 Friction		Type B 0.12 Friction		Type A 0.07 Friction	
Motion	EW Axis	NS Axis						
El Centro 200%	0.66	0.57	0.74	0.76	0.56	0.55	0.55	0.48
Pacoima 50%	0.66	0.38	0.61	0.46	0.50	0.39	0.44	0.36
Chile 100%	0.54	0.61	0.70	0.71	0.55	0.57	0.40	0.50
Taft 300%	0.68	0.55	0.61	0.73	0.54	0.48	0.44	0.46
Kobe 50%	0.49	0.54	0.58	0.62	0.51	0.52	0.45	0.45
Jensen 50%	0.49	0.39	-	-	0.51	0.38	0.48	0.32

In an attempt to explain the small differences in the recorded response of the two configurations of free rocking and of limited rocking for the same isolator properties, results on the frequencies of the two configurations are presented. The model used in the calculation of the frequencies was developed in program SAP2000 and was also used in the dynamic response history analysis of the model. Details of the model are presented in Section 5. Herein we only describe important aspects of the model. The model included the flexibilities of the frame above the isolators and a realistic representation of the flexibilities of the steel cover plate that supported the bushing. The mass of the model was mostly lumped at the eight corners of the frame with additional mass distributed per length of each skeletal member and in plane for the cover plate (details are provided in Section 5). The bushing was modeled as rigid with the mass lumped at the centers of mass of the upper and lower parts (see Figure 2-2). This model differs in the distribution of mass than the model used in the analytical calculation of frequencies which are presented in the graph of Figure 3-10. This has a small effect on the calculation of the rocking frequency of the model.

Figure 4-29 illustrates details of two models developed for the isolated transformer model with the added base for limiting rocking. The first model assumes that the added base is rigidly connected to the top of each spring-damper unit. The added base was represented by a beam of moment of inertia calculated for the cross section of the added plate and two square tube sections (see Figure 3-4). The second model assumes that there is some rotational flexibility at the connection of the added base to the top of the spring-damper unit. Also, the distribution of stiffness of the added base is more refined to better represent the actual details shown in Figure 3-4.

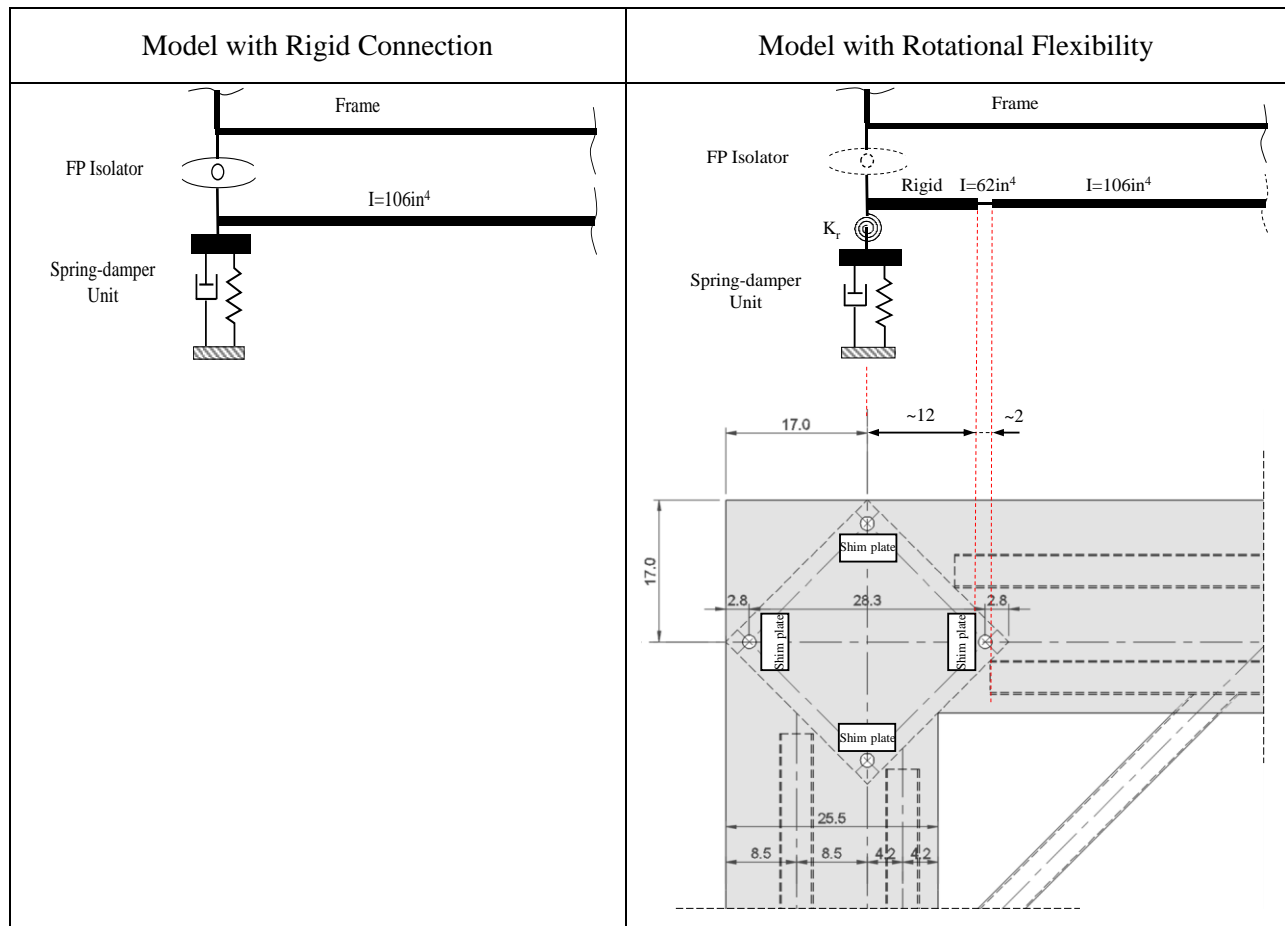


Figure 4-29 Two Models used in the Representation of the Added Base Connection to the FP Isolator

The value of the rotational spring constant K_r shown in Figure 4-29 was determined by trial and error procedures to be 1050kip-in/rad so that the calculated response of the tested model in seismic excitation was the closest (subjectively) to the measured response in most but not all

tests. Results of eigenvalue analysis with this model and the model without the added base (free to rock) are presented in Table 4-7. In the eigenvalue analysis, each FP isolator was represented by its post-elastic stiffness $W/2R_{eff1}$. Modes 1 and 2 (also 4 and 5) are identical as the model is symmetric. The torsional mode has the same frequency as the translational modes as a result of using a lumped mass representation with most of the mass placed directly above the isolators. Note that the model with limited rocking is heavier by the 4.35kip weight of the added base. This explains the difference in the vertical frequency. Also it should be noted that the rocking frequency of the free to rock model is lower than the one in Figure 3-10 (1.44Hz vs 1.57Hz). This is due differences in the distribution of mass used in the two analysis models.

The results of the eigenvalue analysis demonstrate insignificant differences between the configuration that is free to rock and the configuration with limited rocking in which the added plate connection to the FP isolator is flexible. The case of the rigid connection would be representative when the gap between the added plate and the spring-damper unit (the two were separated by a rocker plate-see Figure 3-8 and Section 5) is grouted with high stiffness material. However, in the test model the gap was filled with steel shims over small plan areas that certainly allowed for some small rotation. The situation is better represented with the model with rotational flexibility but with uncertainty on the value of the rotational stiffness.

Table 4-7 Calculated Frequencies of Model of Configurations with Free Rocking and Limited Rocking in Program SAP2000

Mode		Configuration		
		Free to Rock	Limited Rocking Rigid Connection	Limited Rocking Flexible Connection
1,2 and 3	Horizontal X and Y, Torsion	0.37Hz	0.37Hz	0.37Hz
4 and 5	Rocking about X and about Y axis	1.44Hz	5.24Hz	1.47Hz
6	Vertical	1.92Hz	1.86Hz	1.86Hz

Figures 4-30 to 4-35 present comparisons of experimental and analytical response spectra at the NE top corner of the tested frame in six tests of the configuration with limited rocking, FP

isolators of type B with nominal friction of 0.12. The seismic input for the analysis was the one recorded at the base of the model during testing and included only the three translational components. As discussed in Section 5, the shake table exhibited some rocking motion as a result of the large weight of the model and inability to fully control the shake table. The rocking shake table motion did not have a significant effect on the isolator motion or the response spectra at the frame of the model so that the rocking shake table motion was not included in the analysis of which results are presented in Figures 4-30 to 4-35. However, the shake table rocking motion had an important effect on the horizontal acceleration of the top of the bushing. Details are provided in Section 5.

It is evident in the results of Figures 4-30 to 4-35 that in some tests the rigid connection model provides for a better prediction whereas in others the flexible connection model provides for a better prediction. It is likely that the shims used in securing the connection between the added base and the spring-damper unit (a) provided for some rotational flexibility that may have been different in the two principal directions (due to different number of shims used as the gap varied and due to differences in the applied preload) and (b) the rotational flexibility may have changed from test to test due to loosening and re-application of the preload on the shims (tightening of bolts). Particularly, the results in Figure 4-30 for the El Centro motion were acquired first in the testing of the model and the connection was likely closest to the rigid condition than the flexible condition. The results in Figure 4-30 show a better prediction by the rigid connection model than the flexible connection model for the horizontal response. However, based on the majority of results and particularly when comparing the vertical response, it is very likely that the connection of the added plate to the spring-damper unit was flexible as determined in the model calibration and reported in more detail in Section 5. The authors believe that the configuration of limited rocking had a flexible connection in most tests so that it had small differences with the configuration of free rocking. Accordingly, analytical results are presented only for the case of flexible connection.

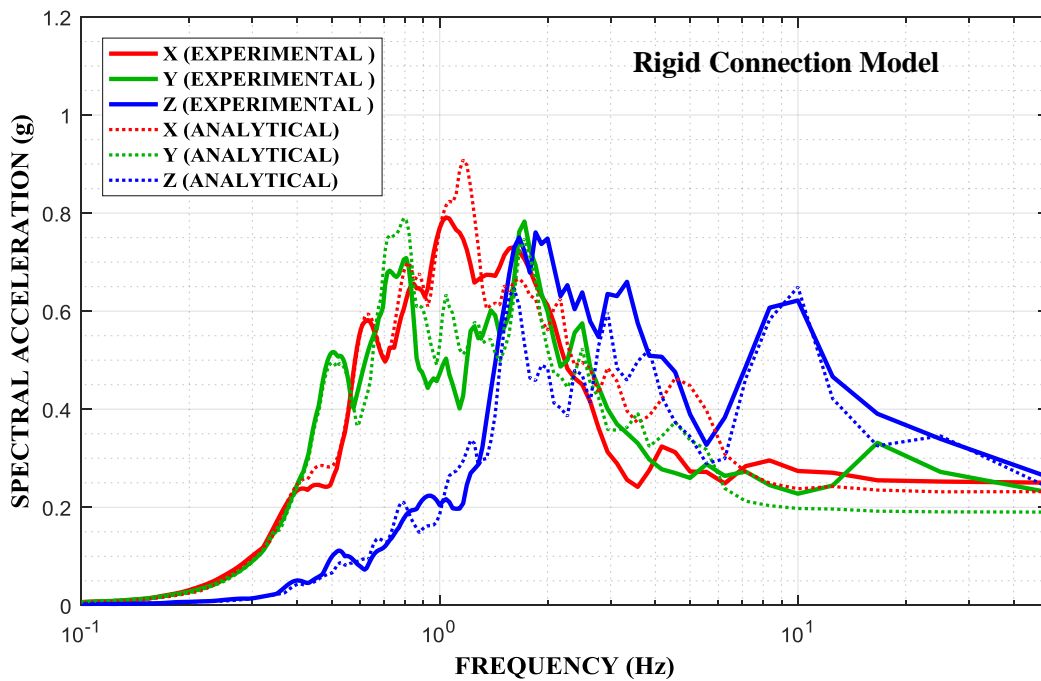
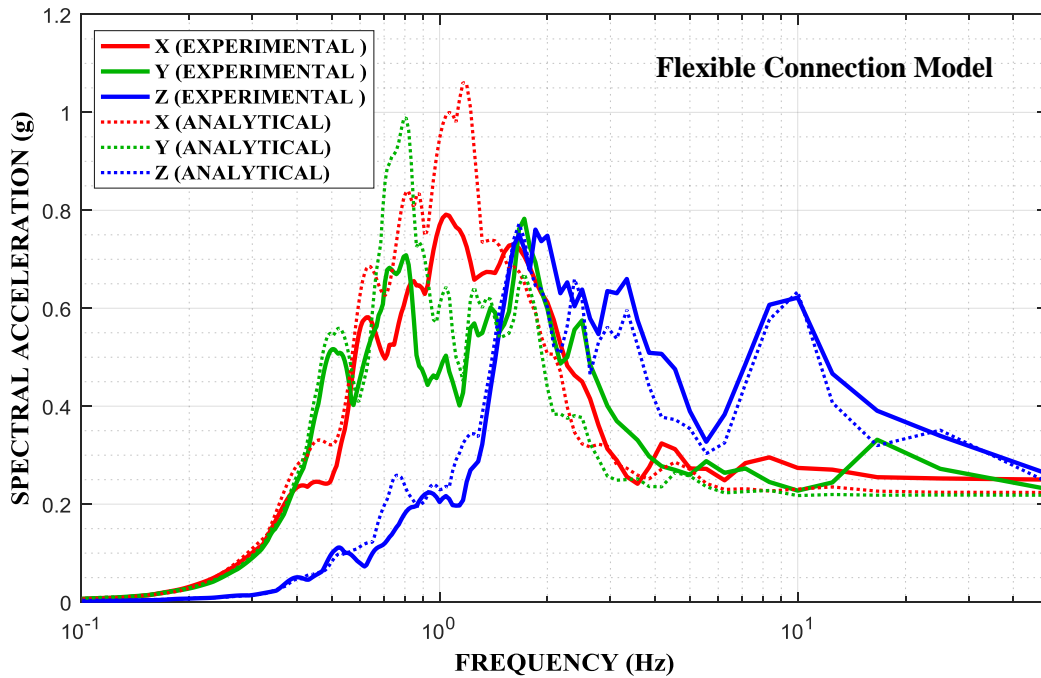


Figure 4-30 Comparison of 5%-Damped Experimental and Analytical Response Spectra at Frame Top at NE Corner of Configuration of Limited Rocking, FP Isolator Type B with 0.12 Nominal Friction in El Centro 250% Motion

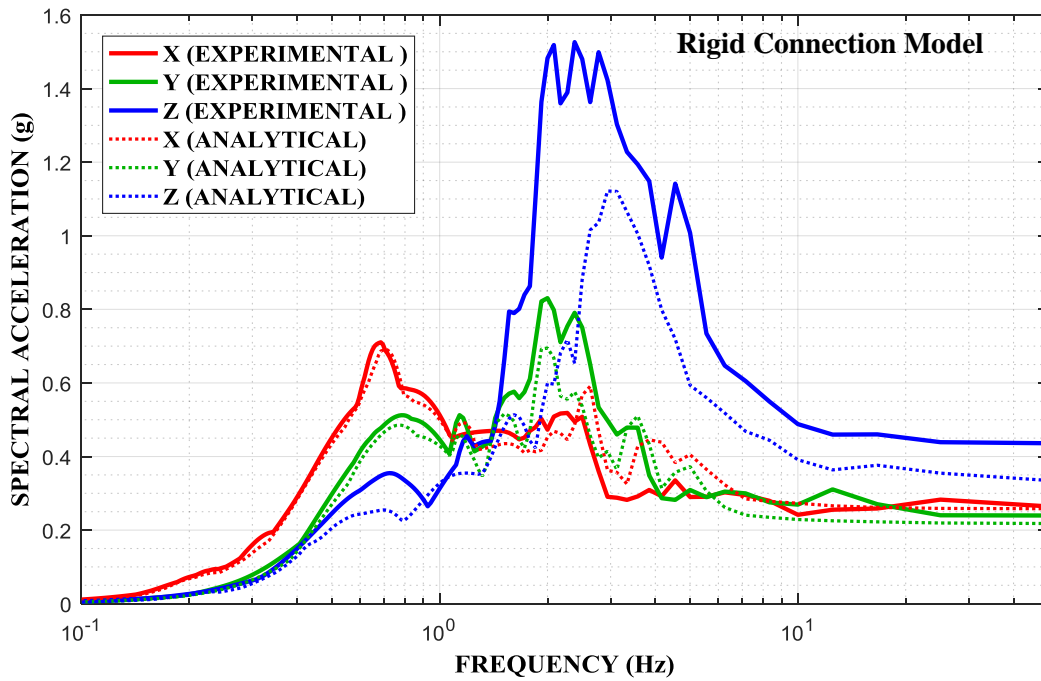
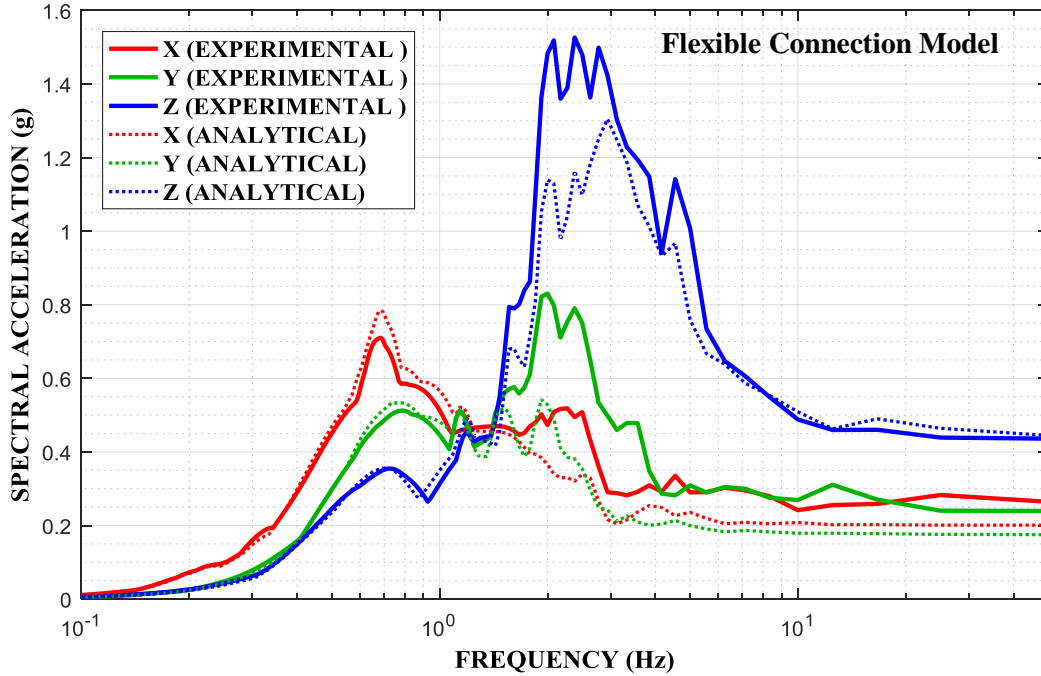


Figure 4-31 Comparison of 5%-Damped Experimental and Analytical Response Spectra at Frame Top at NE Corner of Configuration of Limited Rocking, FP Isolator Type B with 0.12 Nominal Friction in Pacoima 75% Motion

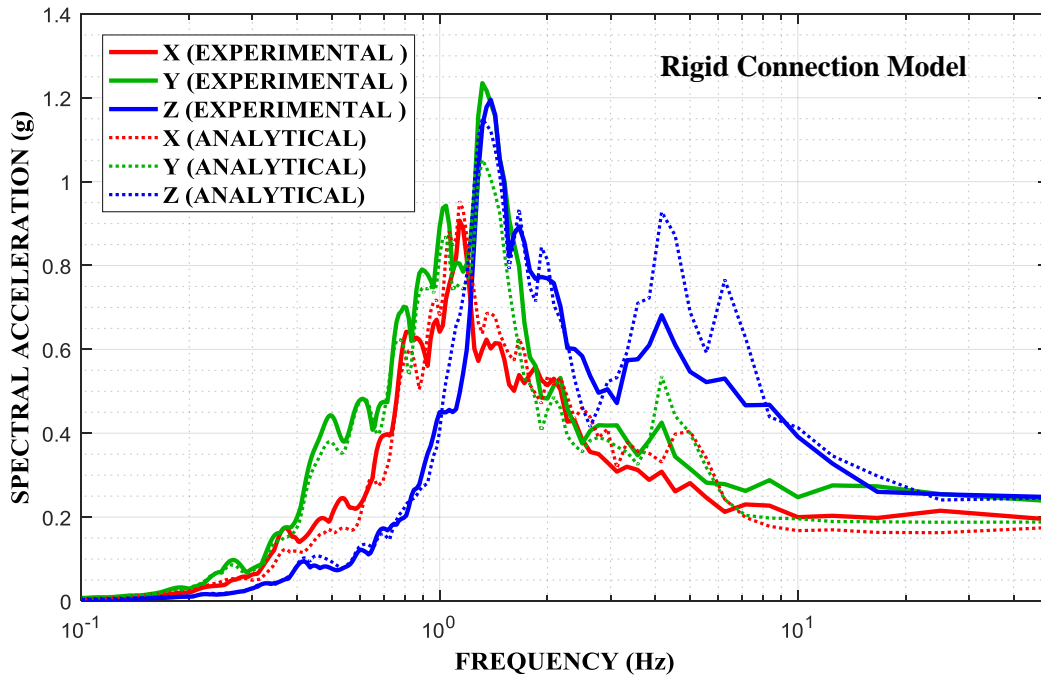
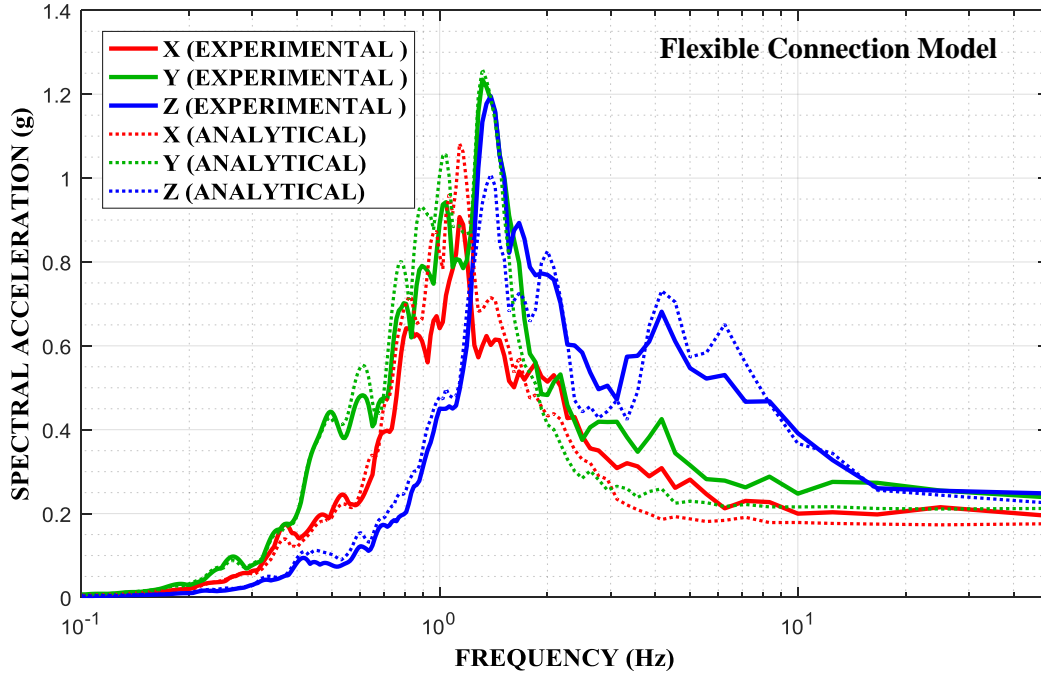


Figure 4-32 Comparison of 5%-Damped Experimental and Analytical Response Spectra at Frame Top at NE Corner of Configuration of Limited Rocking, FP Isolator Type B with 0.12 Nominal Friction in Chile 100% Motion

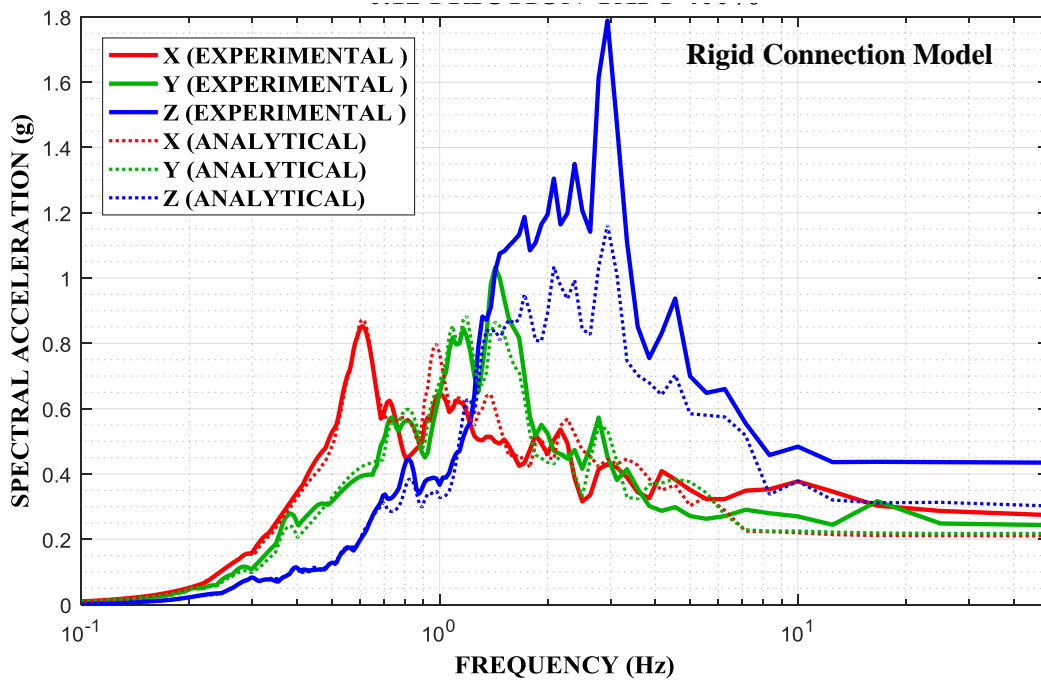
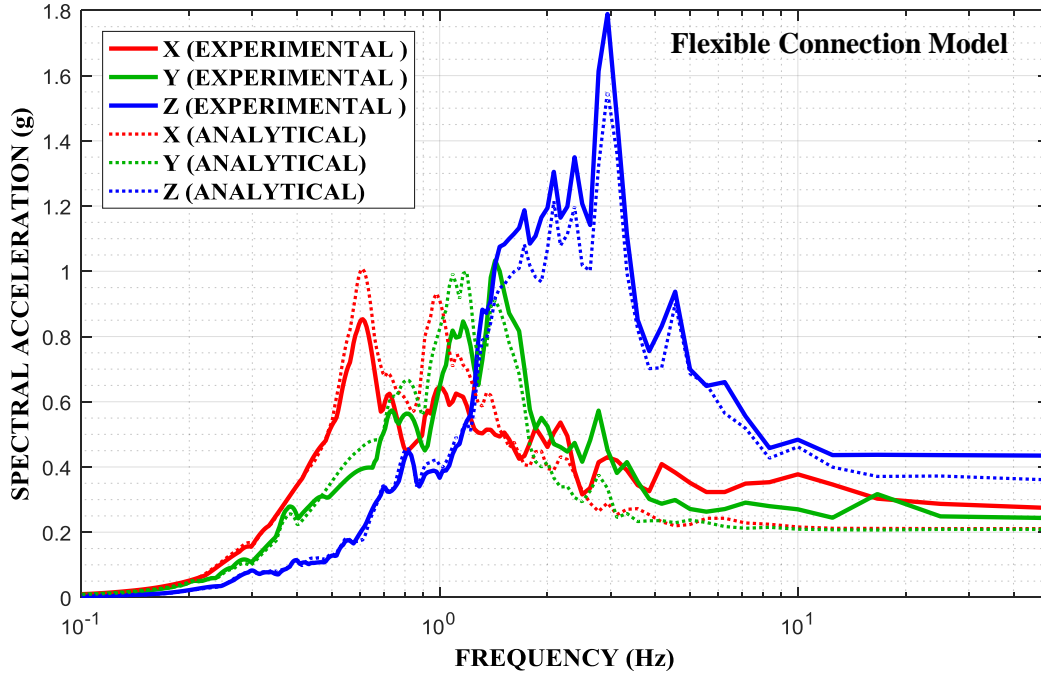


Figure 4-33 Comparison of 5%-Damped Experimental and Analytical Response Spectra at Frame Top at NE Corner of Configuration of Limited Rocking, FP Isolator Type B with 0.12 Nominal Friction in Taft 400% Motion

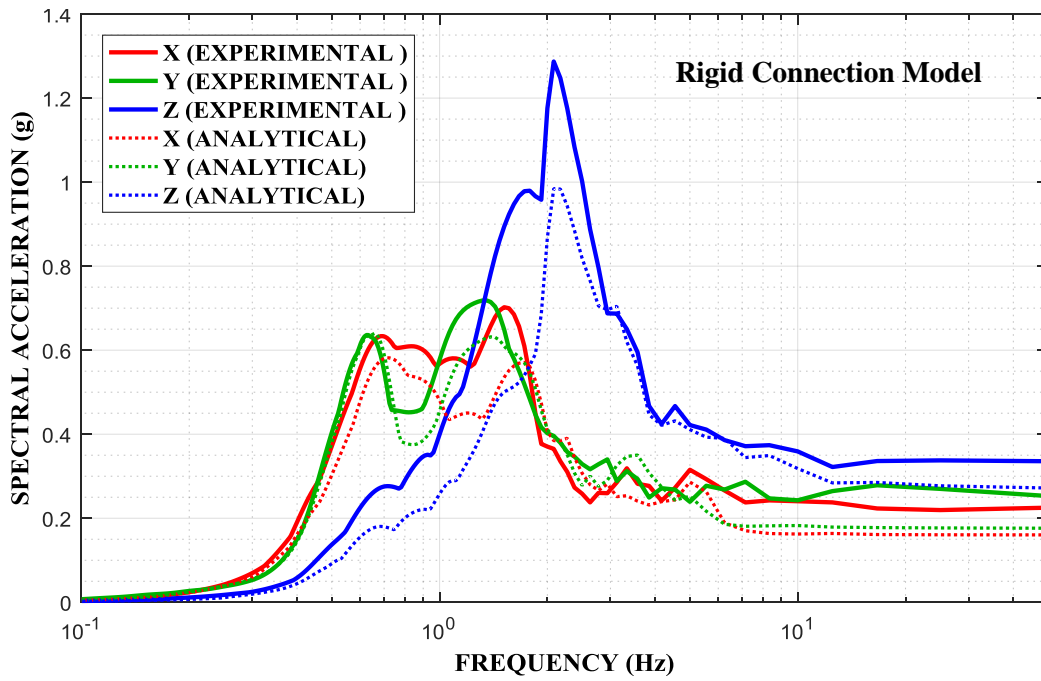
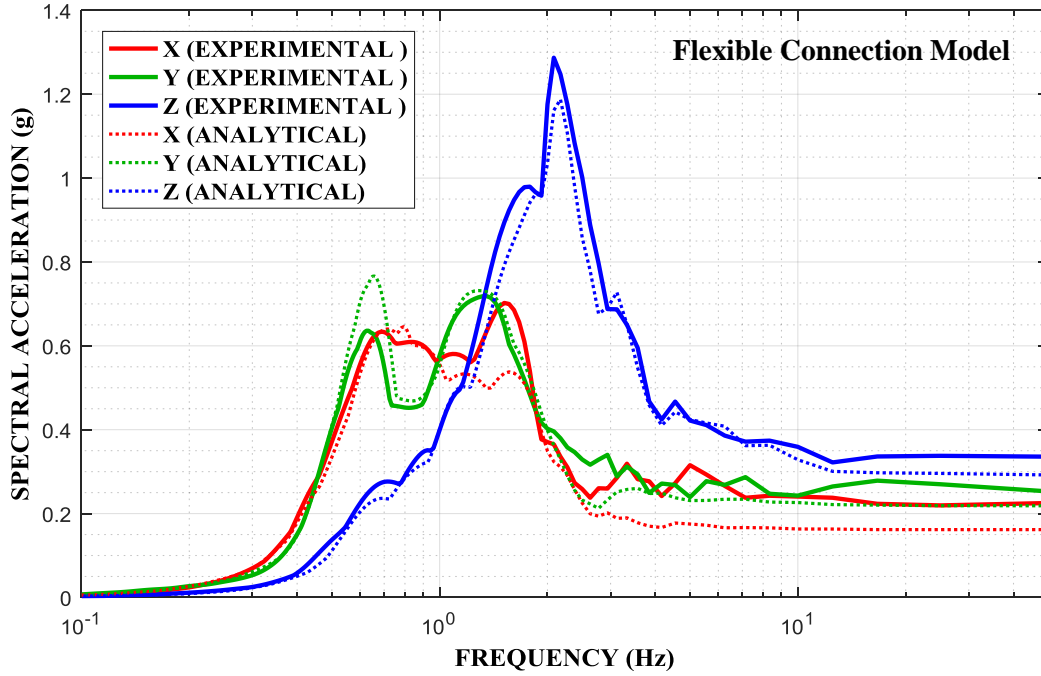


Figure 4-34 Comparison of 5%-Damped Experimental and Analytical Response Spectra at Frame Top at NE Corner of Configuration of Limited Rocking, FP Isolator Type B with 0.12 Nominal Friction in Kobe 65% Motion

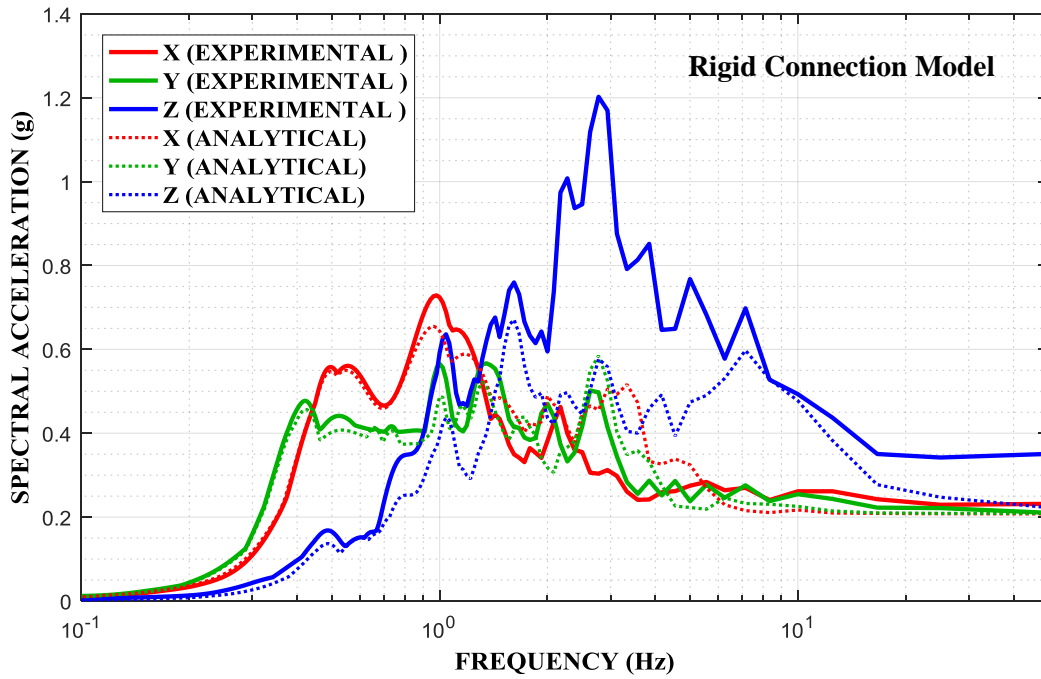
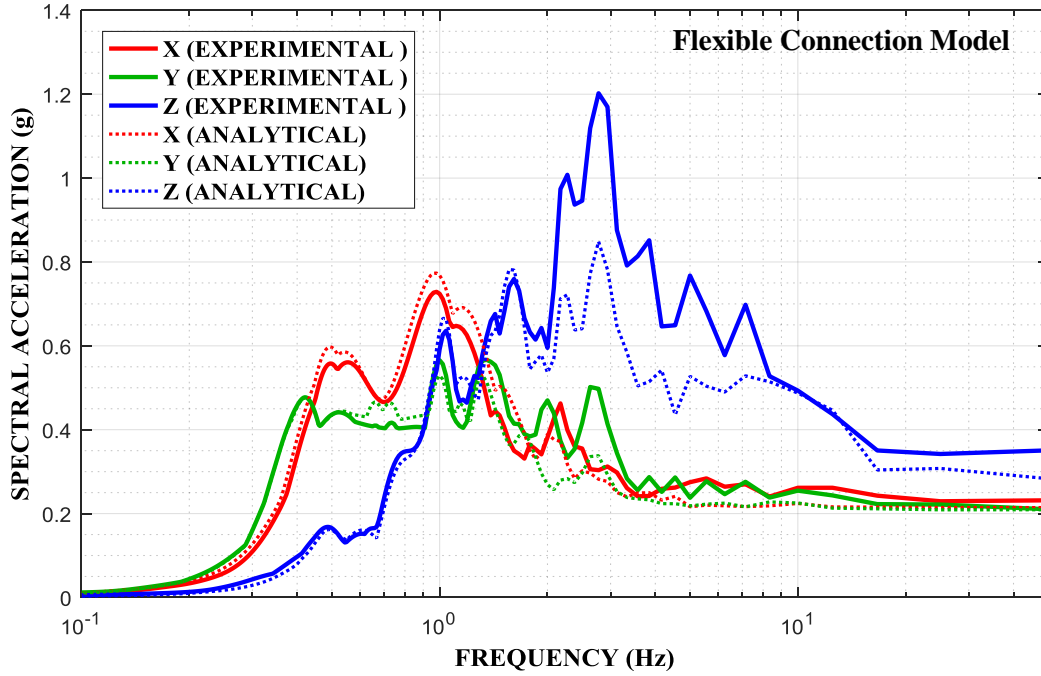


Figure 4-35 Comparison of 5%-Damped Experimental and Analytical Response Spectra at Frame Top at NE Corner of Configuration of Limited Rocking, FP Isolator Type B with 0.12 Nominal Friction in Jensen 85% Motion

SECTION 5

ANALYTICAL PREDICTION OF RESPONSE

5.1 Introduction

This section describes the analytical model developed to predict the response of the test model and compares the analytically predicted response to the experimental response. The analytical model was developed in the commercial analysis program SAP2000 (Computer and Structures, 2016).

5.2 Analytical Model of Tested Structure

Figure 5-1 illustrates a three-dimensional image of the analytical model in the configuration that allowed for free rocking. Detailed drawings of the test model are presented in Appendix D. The analytical model consists of a space frame with a top plate that supports the bushing, the bushing connection to the top plate, lumped masses at the frame top and bottom corners and the isolation system representation below. The model of the space frame with the cover plate and bushing on top differed from the model developed by Kong and Reinhorn (2010) and also used in the studies of Fahad and Reinhorn (2012), Koliou et al (2012) and Oikonomou et al (2016) in the study of the seismic response of fixed and horizontally isolated transformers, in the way the top plate and the bushing connection to the top plate were modeled.

Beam elements were used to model the frame using the actual geometry and material properties. The cover plate was modeled by plate elements that were rigid in plane and in bending. The connection of the bushing to the cover plate through an adapter plate was modeled by rigid beam elements and springs in similarity to the modeling in Section 2 and as described below in detail. The plates used to form a base and to provide the needed mass also provided significant in-plane and out-of-plane stiffness at the supports of the frame so that their effect was accounted for by using the rigid body constraints of SAP2000 at the bottom joints of the columns of the analytical model. Each spring-damper unit was modeled by vertically driven spring and linear viscous damper of constants $K=6.44\text{kip/in}$ and $C=0.53\text{kip-sec/in}$. Friction was not included in the spring-damper unit model. The effect of friction will be investigated later in this section.

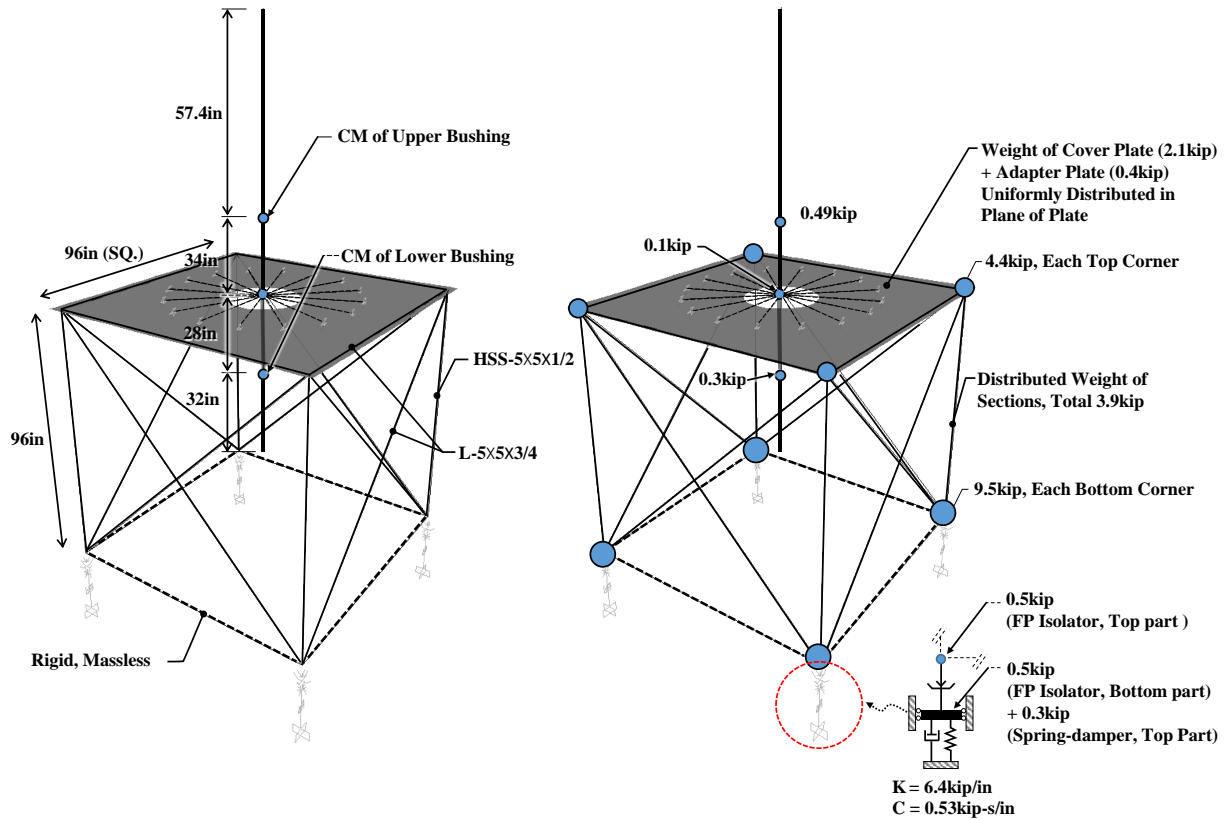


Figure 5-1 Analytical Model of Tested Model in Configuration of Free Rocking

Figure 5-2 presents a close-up view of the bushing model and its connection to the adapter plate. The connection was modeled using beam elements with properties selected such that the vertical and horizontal frequencies of the as-installed bushing were those determined in the identification tests described in Section 3. Specifically, 16 rigid beam elements of 35.5inch length were symmetrically placed as shown in Figure 5-2 and connected to the rigidly modelled plate below by vertical springs (the lateral degrees of freedom are restrained), each of which had a stiffness of 1kip/in. The bushing was modeled as rigid with its mass lumped at the point of connection to the adapter plate (0.1kip) and at the centers of mass of the upper part (0.49kip) and the lower part (0.3kip) as shown in Figures 5-1 and 5-2. In this configuration, the bushing model has a vertical frequency of 13.3Hz and a horizontal (rocking) frequency was 10.7Hz (actual frequencies as determined in identification tests were 13.3Hz in the vertical, 10.5Hz in E-W direction and 10.8Hz in N-S direction-see Figure 3-26).

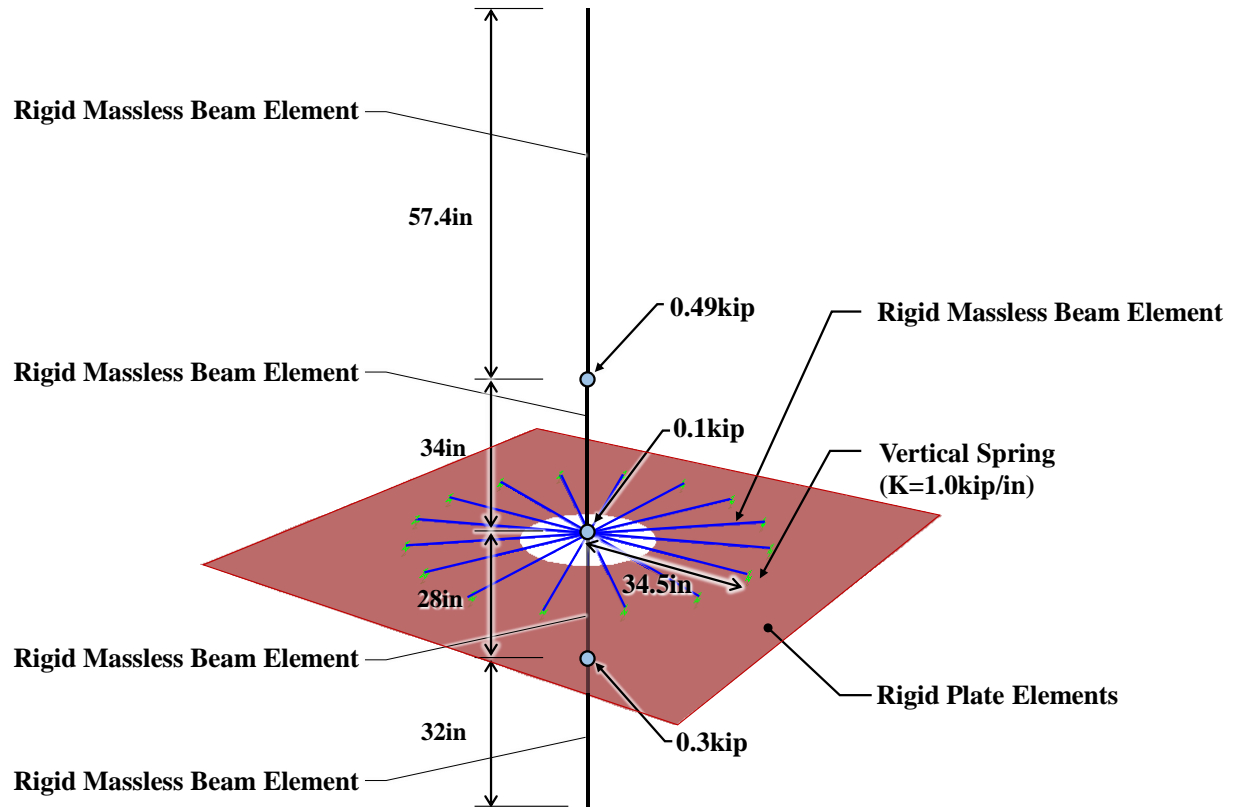


Figure 5-2 Bushing Model Details

When an added base plate was installed to limit rocking, the model used for the analysis was identical to the one of Figures 5-1 and 5-2 but for added beam elements and masses between the FP isolator model and the mass (0.8kip) representing the bottom of the FP isolator and the top of the spring-damper unit, as shown in Figure 5-3. The added base was represented by a beam of moment of inertia calculated for the cross section of the added plate and two square tube sections (see Figure 3-4). The model includes some rotational flexibility at the connection of the added base to the top of the spring-damper unit. The value of the rotational stiffness $K_r=1050\text{kip-in/rad}$ was determined by trial and error procedures so that the results of the analytical model in response history analysis were closest to the experimental results. Note that the source of the rotational flexibility at the connection of the added base plate to spring-damper unit top is the use of the four piles of the shims without grouting as shown in Figures 5-3 and 5-4. The shims allowed for some limited rotation, so the result was that the two tested configurations of free rocking (without the added base) and of limited rocking had very close response. As discussed

in Section 4, it is likely that the situation evolved from a condition closer to the rigid connection at the start of testing to one of the flexible connection as testing progressed and the connection loosened. Ideally, the space between the base plate and the top plate of the spring-damper unit (separated by the rocker plate) should be grouted but this was avoided in the laboratory for simplicity and due to the long time needed for the grout to achieve the required strength.

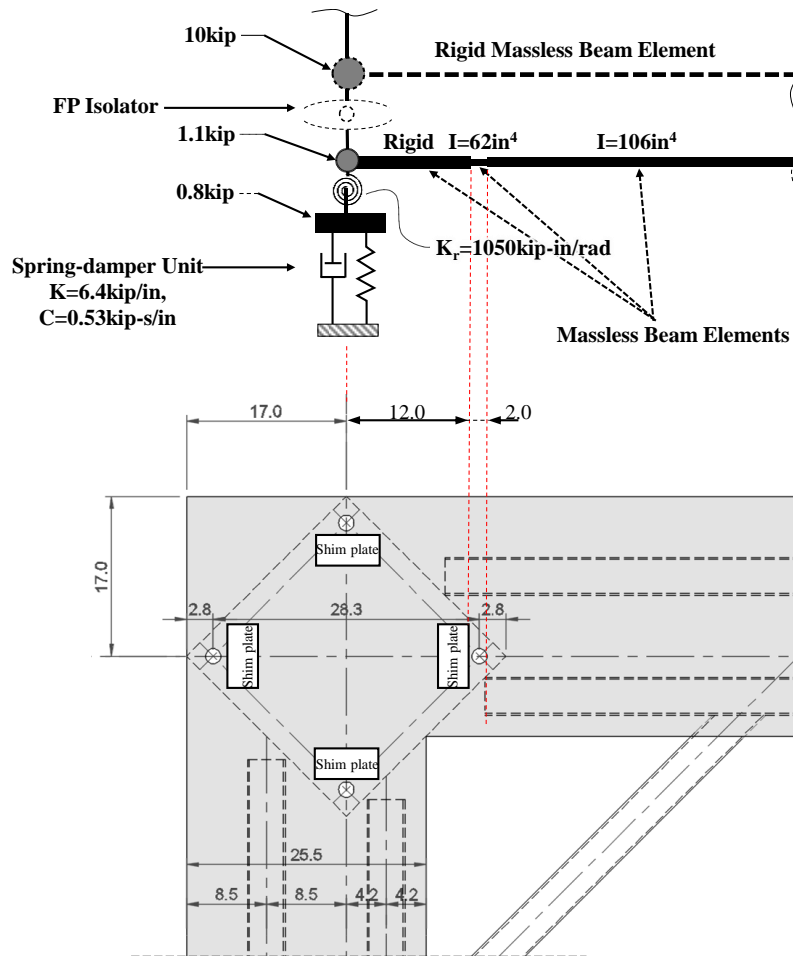


Figure 5-3 Schematic of Modeling of Added Base Plate and Plan View of Added Base Plate (dimensions in inch)

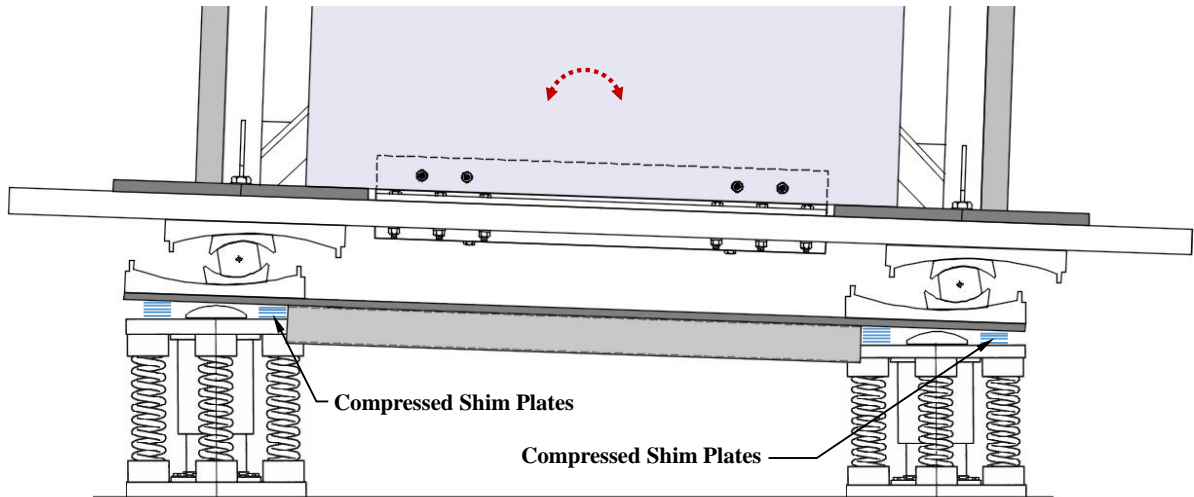


Figure 5-4 Illustration of Ineffectiveness of Shims to Restrain Rotation of the Connection of Added Base Plate to Isolators

The triple FP isolators were modeled using the parallel model (Sarlis and Constantinou, 2010) and with the frictional properties identified in the isolator tests presented in Section 3.5. Table 5-1 presents the model parameters for the three isolator types used in the testing. The parameters in the table were calculated based on the supported weight by each isolator (including half of the isolator weight), which was 16.2kip for each FP isolator for both tested configurations. Note that the parallel model is valid for displacements prior to initiation of stiffening of the isolator, which was the case for all tests.

Table 5-1 Triple FP Isolator Parallel Model Parameters in Program SAP2000 (see Figure 3-5 for dimensions of the isolators)

Isolation System		Model Configuration							
		Free to Rock		Limited Rocking					
FP Isolator Type and Nominal Friction		Type B 0.12 Friction		Type A 0.20 Friction		Type B 0.12 Friction		Type A 0.07 Friction	
Single FP Element of Parallel Model		FP1	FP2	FP1	FP2	FP1	FP2	FP1	FP2
Supported Weight	kip	8.1	8.1	8.1	8.1	8.1	8.1	8.1	8.1
Element Height	inch	10.5	10.5	9.5	9.5	10.5	10.5	9.5	9.5
Shear Deformation Location	inch	5.25	5.25	4.25	4.25	5.25	5.25	4.25	4.25
Vertical Stiffness	kip/in	13558	13558	14985	14985	13558	13558	14985	14985
Elastic Stiffness	kip/in	10.1	2.1	12.6	1.1	10.1	2.1	9.5	1.1
Effective Stiffness	kip/in	0	0.229	0	0.225	0	0.229	0	0.225
Radius	inch	0	35.5	0	36.0	0	35.5	0	36.0
Friction Coefficient SLOW	-	0.03	0.14	0.03	0.23	0.03	0.14	0.03	0.07
Friction Coefficient FAST	-	0.04	0.20	0.04	0.40	0.04	0.20	0.04	0.10
Rate Parameter	sec/in	0.35	0.35	0.35	0.35	0.35	0.35	0.25	0.25
Rotational Inertia	kip-in-sec ²	5.72 x10 ⁻³							
Rotational/Torsional Stiffness (R1,R2,R3)	kip-in/rad	0	0	0	0	0	0	0	0

Each spring-damper unit was modeled using a linear spring element with spring constant equal to 0.64kip/inch and a linear viscous damper element with damper constant equal to 0.53kip-sec/inch as shown in Figure 5-3. The spring and damper elements were constrained to only move in the vertical direction.

Eigenvalue analysis of the model in which the horizontal stiffness of the triple FP isolators was specified to be the post-elastic stiffness ($\text{weight}/2R_{\text{eff1}}$) resulted in the frequencies and modes presented in Table 5-2. Inherent damping in the model was specified as 0.01 only for the modes associated with dominant bushing motion as presented in Table 5-2. All other modes were specified zero damping but were actually damped either by the vertical dampers in the isolation system or effectively by friction in the FP isolators.

Table 5-2 Calculated Frequencies of Model and Assigned Damping Ratio

Mode	Mode Description	Configuration		Assigned Damping Ratio
		Free to Rock	Limited Rocking	
1,2 and 3	Entire model in two horizontal directions and torsion	0.37Hz	0.37Hz	0.0
4 and 5	Entire model in rocking about two horizontal axes	1.44Hz	1.47Hz	0.0
6	Entire model vertical	1.92Hz	1.86Hz	0.0
7 and 8	Bushing rocking motion about two horizontal axes	11.0Hz	11.2Hz	0.01
9	Bushing vertical motion	13.4Hz	13.4Hz	0.01

Nonlinear response history analysis was conducted using the Fast Nonlinear Analysis (FNA) option in the program SAP2000 in which 200 Ritz vectors were used. To develop the vertical load of the transformer, a vertical acceleration of 1g was applied, developed gradually over a period of 10 second, then followed by 10 second of idle time and then followed by dynamic tri-axial seismic motion. For each analyzed case the isolators were assumed to be in the initial centered position without accounting for the non-centered position that the FP isolators may have been as a result of random permanent offsets. The observed permanent FP isolator displacements were small to have any important effect on the prediction of the behavior of the analyzed model. In the experimental data presented in the figures that follow the histories of isolator displacement were adjusted to start at zero so they are directly comparable to the analytical histories.

5.3 Comparison of Analytical and Experimental Results

Comparisons of experimental and analytical results are presented for the selected cases of tests presented in Table 5-3. These cases represent the tests of the highest seismic intensity for each of the isolation systems and model configurations tested. For each case in Table 5-3 graphs are presented that compare the following responses:

- 1) Response spectra (5%-damped) and histories of the horizontal (in two principal model directions) and vertical acceleration at the NE top corner of the model (see Figure 4-7).
- 2) Histories of the FP isolator at the SW corner (see Figure 3-27) displacements in the two principal directions and orbit.
- 3) Vertical spring-damper unit displacement history at the NE corner (see Figure 3-28). The experimental value is the average of the values recorded at the four corners of the NE spring-damper unit as shown in Figure 3-28.

Figures 5-5 to 5-50 present the comparisons of experimental and analytical results for all cases in Table 5-3.

Table 5-3 Tests for which Experimental Results are Compared to Analytical Results

Model Configuration	Free to Rock	Limited Rocking		
FP Isolator Type and Nominal Friction	Type B 0.12 Friction	Type A 0.20 Friction	Type B 0.12 Friction	Type A 0.07 Friction
Earthquake Motion	El Centro 250%	El Centro 200%	El Centro 250%	El Centro 250%
	Pacoima 60%	Pacoima 65%	Pacoima 75%	Pacoima 65%
	Chile 100%	Chile 100%	Chile 100%	Chile 100%
	Taft 400%	Taft 300%	Taft 400%	Taft 400%
	Kobe 50%	Kobe 50%	Kobe 65%	Kobe 65%
	Jensen 100%		Jensen 85%	Jensen 50%

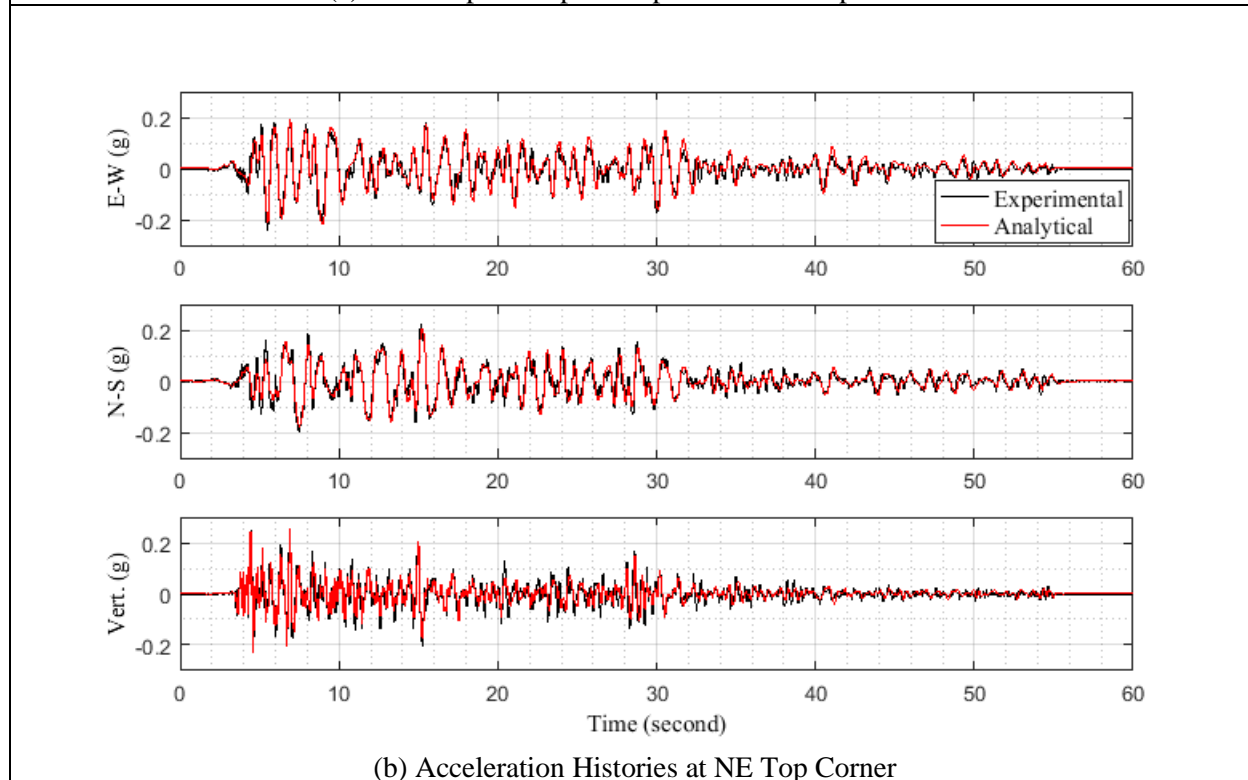
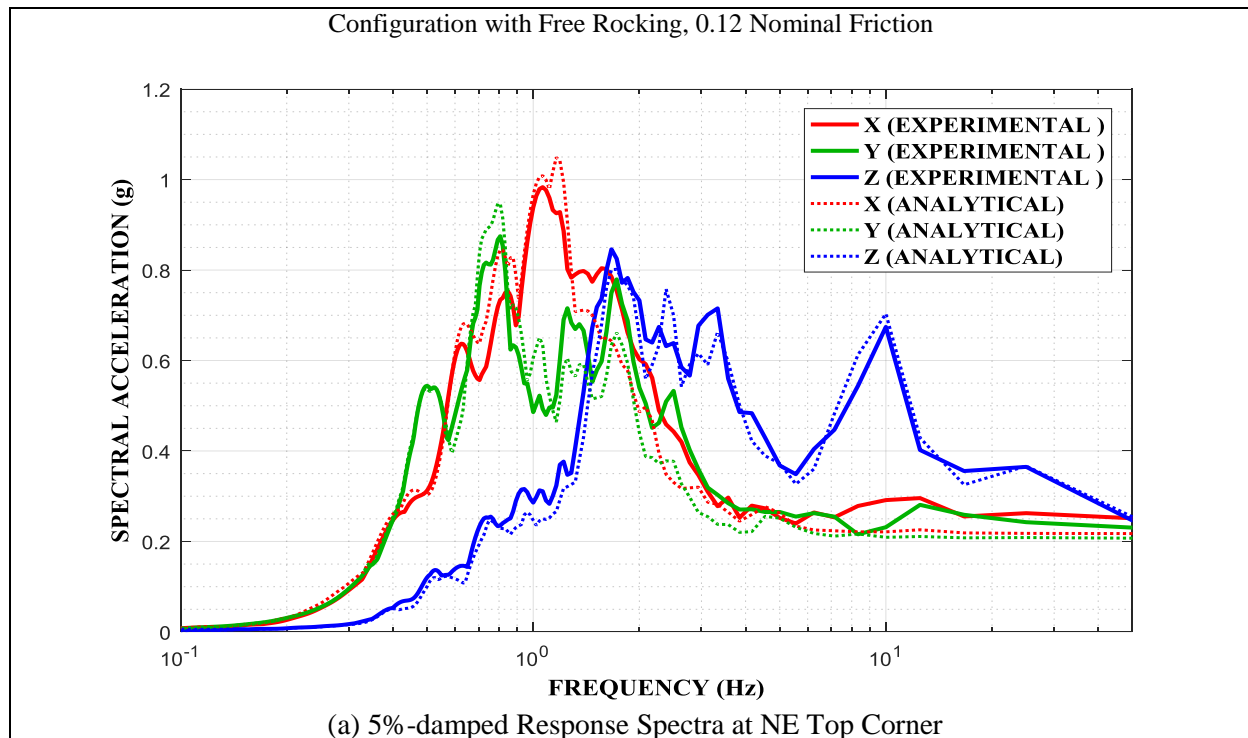


Figure 5-5 Comparison of Experimental and Analytical Results for Configuration of Free Rocking, FP Isolator Type B with 0.12 Nominal Friction in El Centro 250% Motion: (a) 5%-damped Response Spectra at Frame NE Top Corner, (b) Acceleration Histories at Frame NE Top Corner

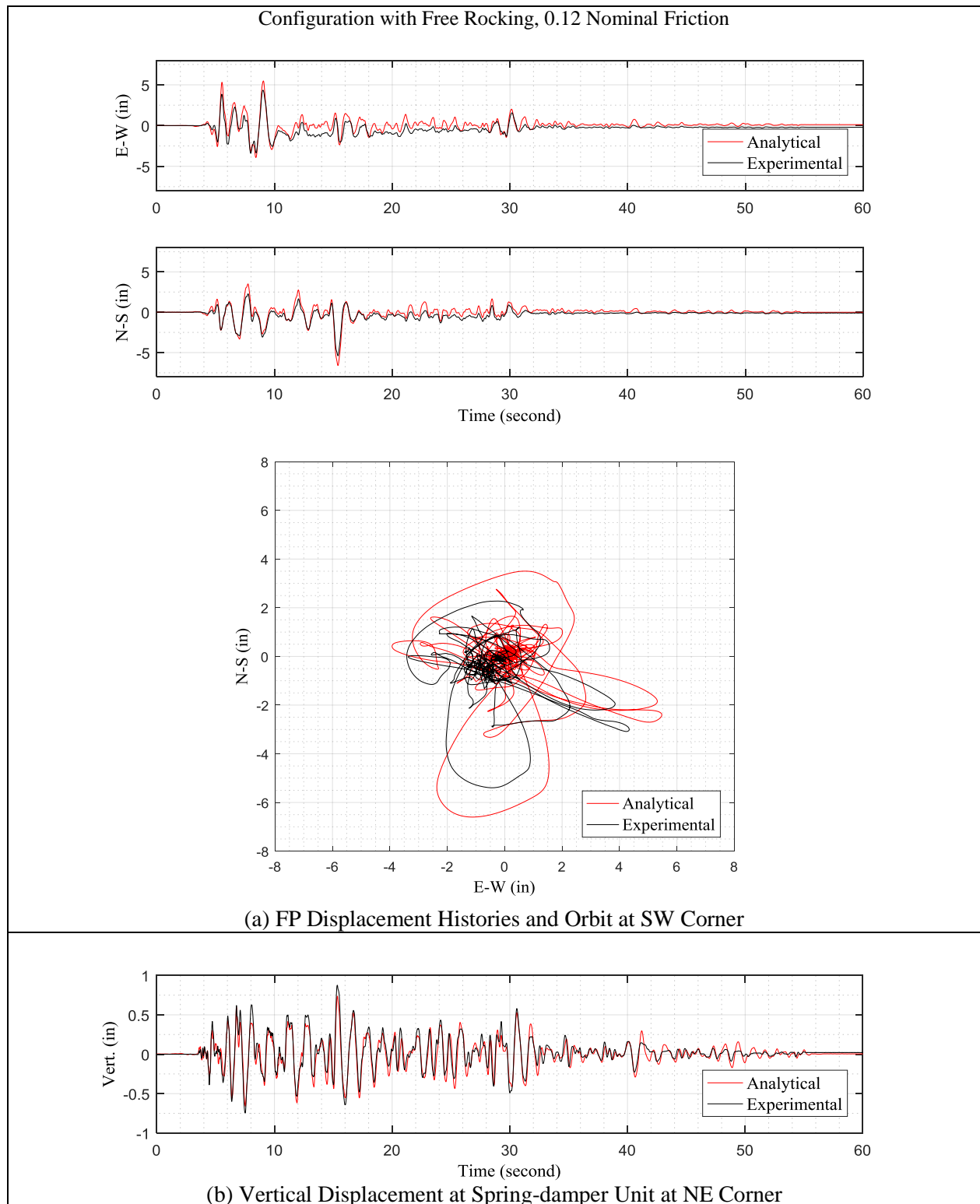


Figure 5-6 Comparison of Experimental and Analytical Results for Configuration of Free Rocking, FP Isolator Type B with 0.12 Nominal Friction in El Centro 250% Motion: (a) FP Displacement Histories and Orbit at SW Corner, (b) Vertical Displacement at Spring-damper Unit at NE Corner

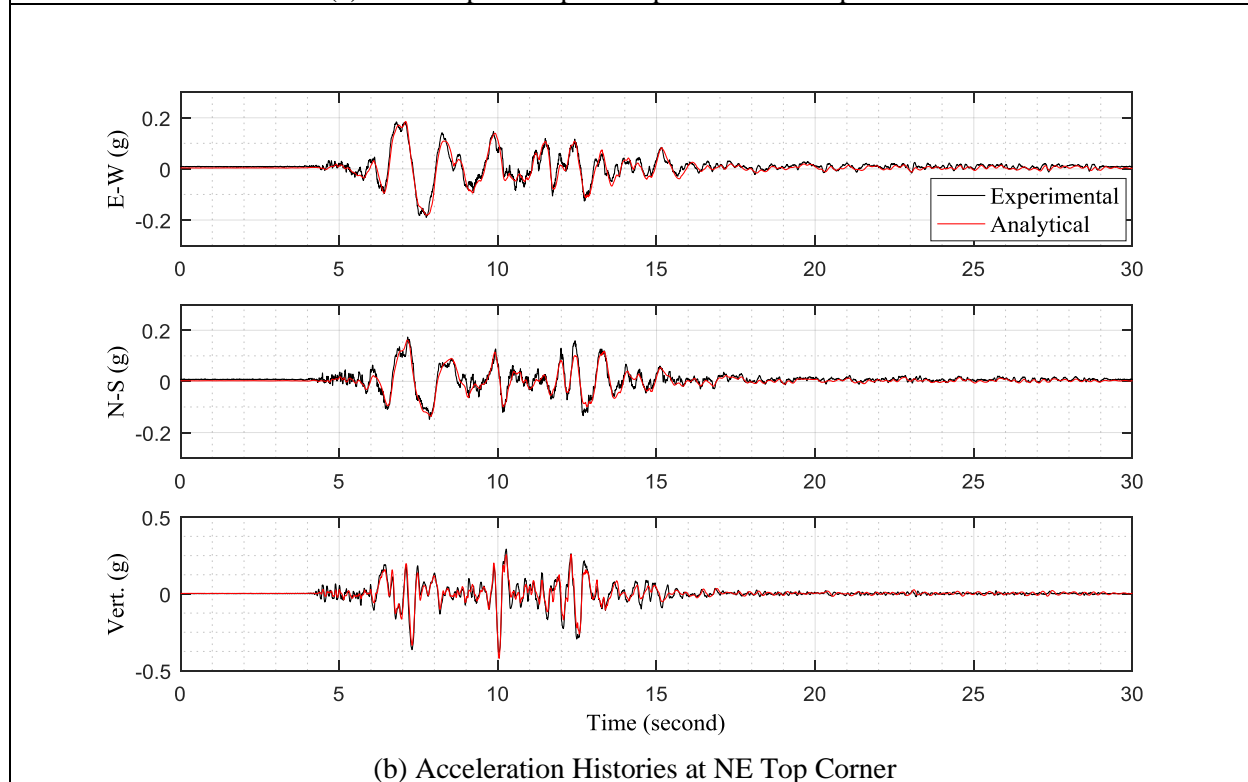
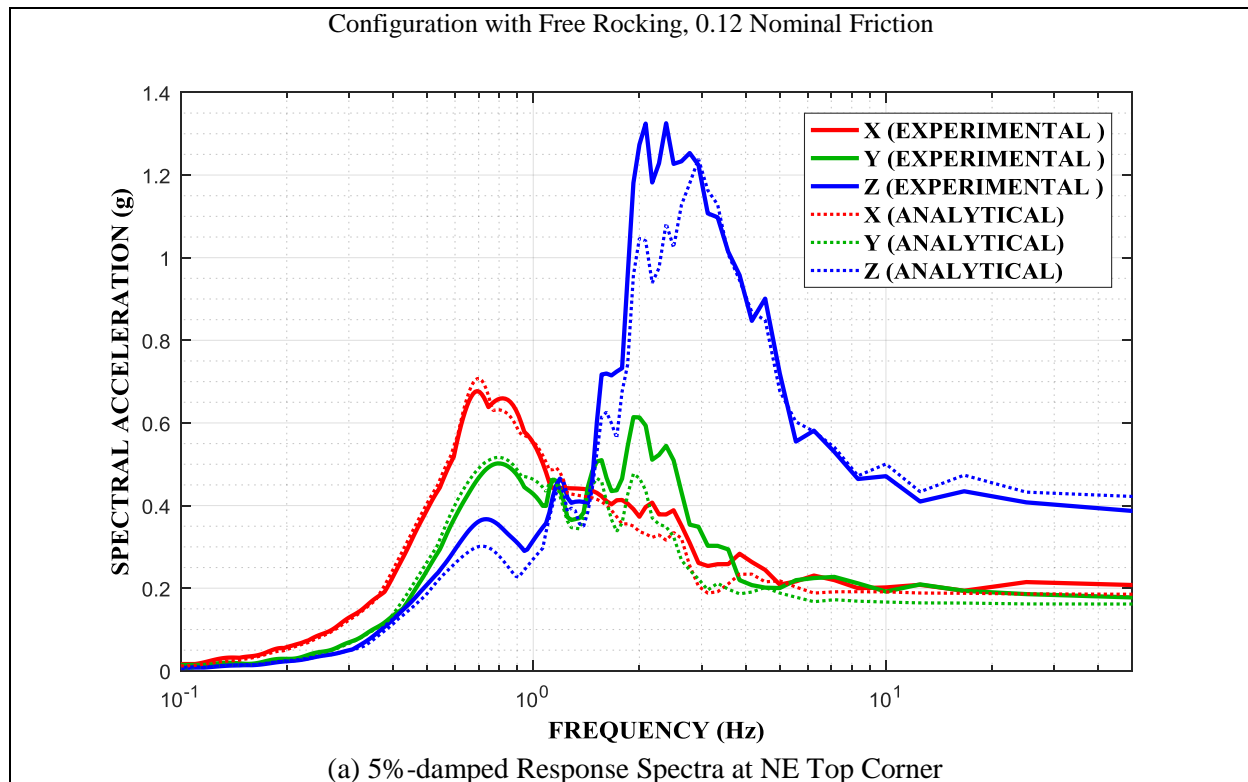


Figure 5-7 Comparison of Experimental and Analytical Results for Configuration of Free Rocking, FP Isolator Type B with 0.12 Nominal Friction in Pacoima 60% Motion: (a) 5%-damped Response Spectra at Frame NE Top Corner, (b) Acceleration Histories at Frame NE Top Corner

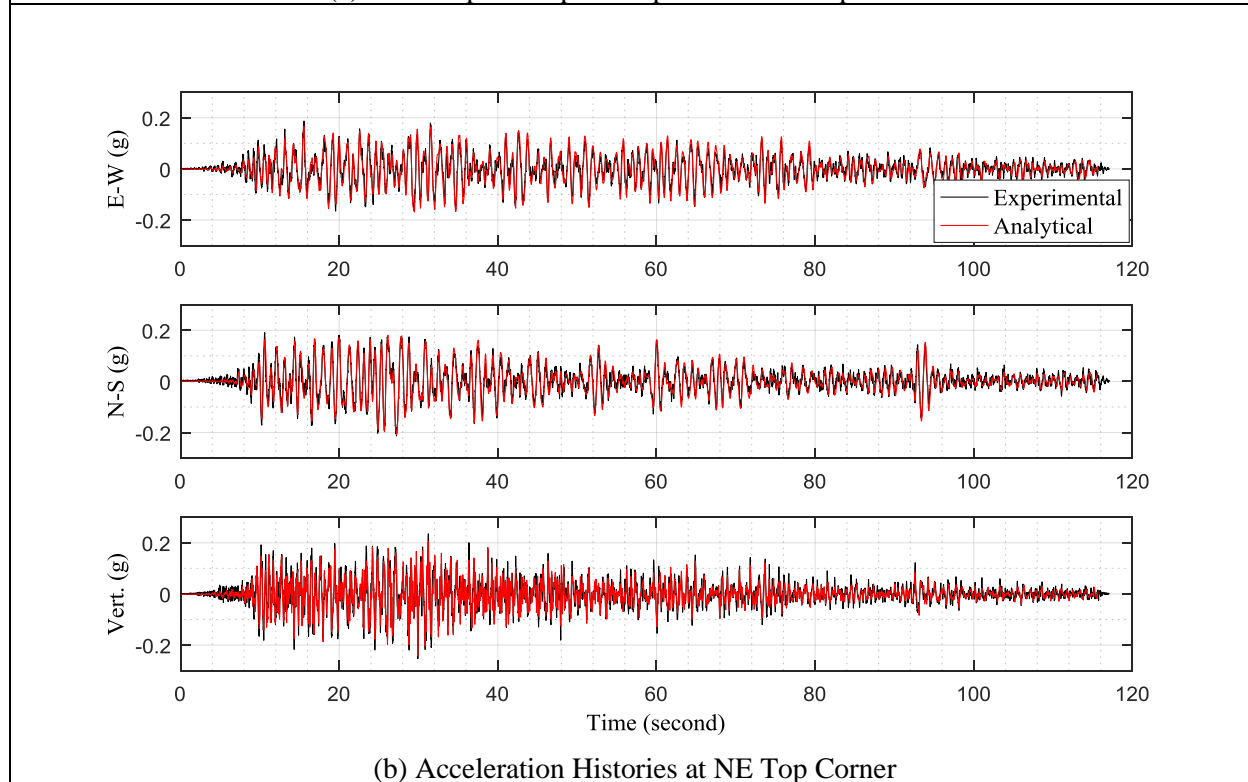
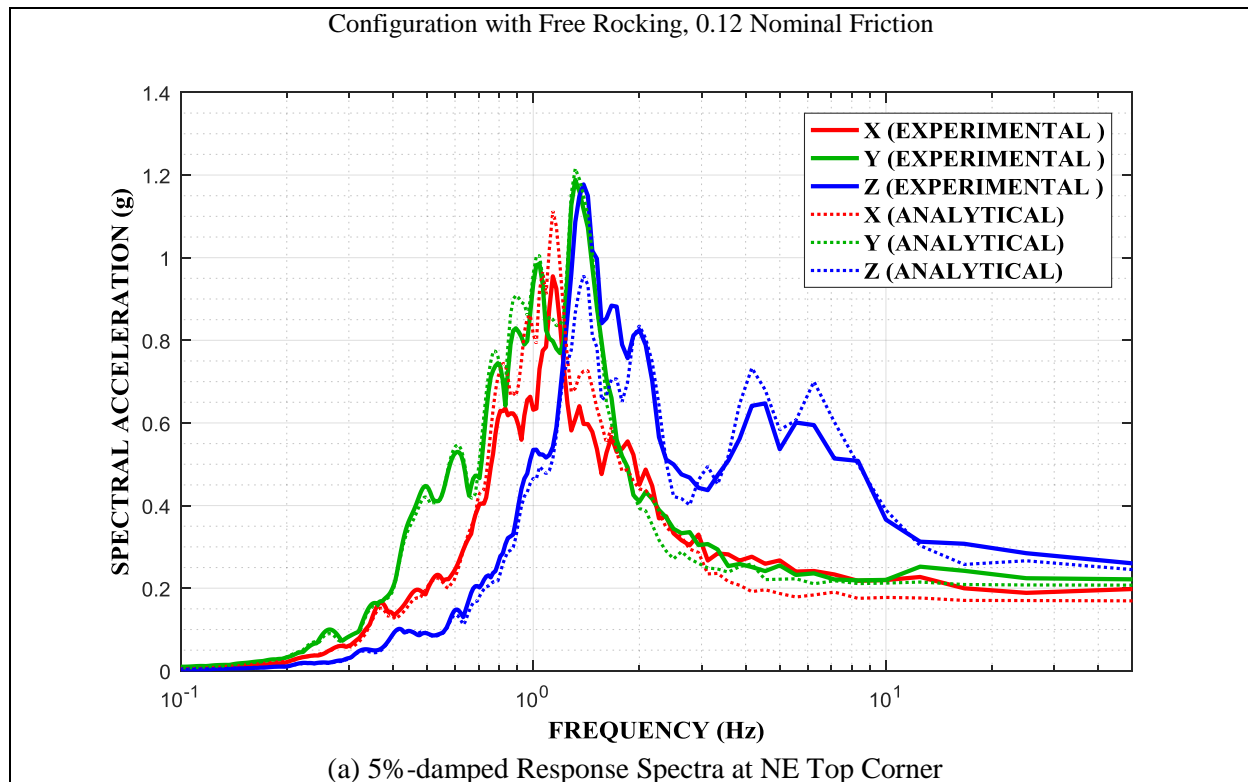


Figure 5-9 Comparison of Experimental and Analytical Results for Configuration of Free Rocking, FP Isolator Type B with 0.12 Nominal Friction in Chile 100% Motion: (a) 5%-damped Response Spectra at Frame NE Top Corner, (b) Acceleration Histories at Frame NE Top Corner

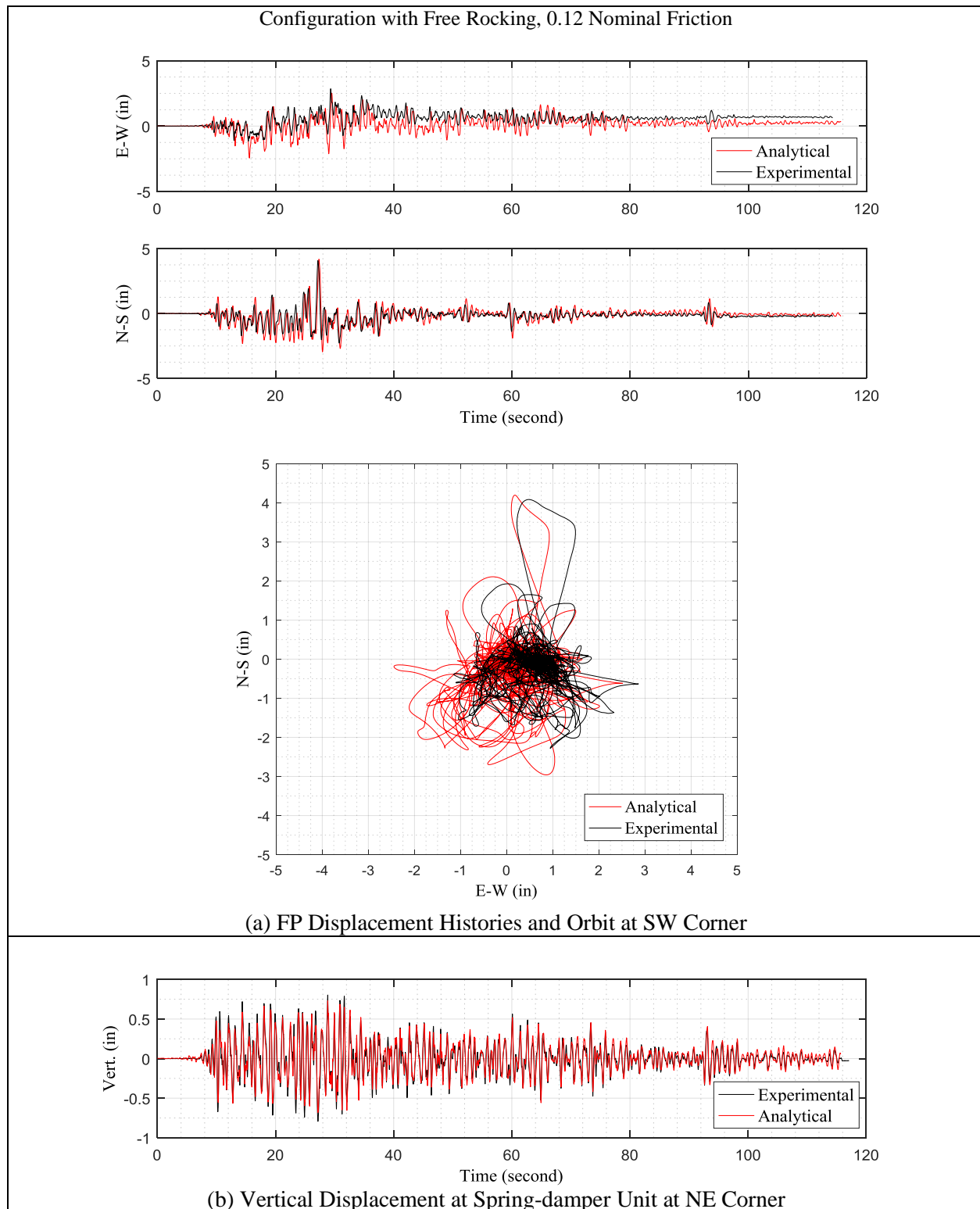


Figure 5-10 Comparison of Experimental and Analytical Results for Configuration of Free Rocking, FP Isolator Type B with 0.12 Nominal Friction in Chile 100% Motion: (a) FP Displacement Histories and Orbit at SW Corner, (b) Vertical Displacement at Spring-damper Unit at NE Corner

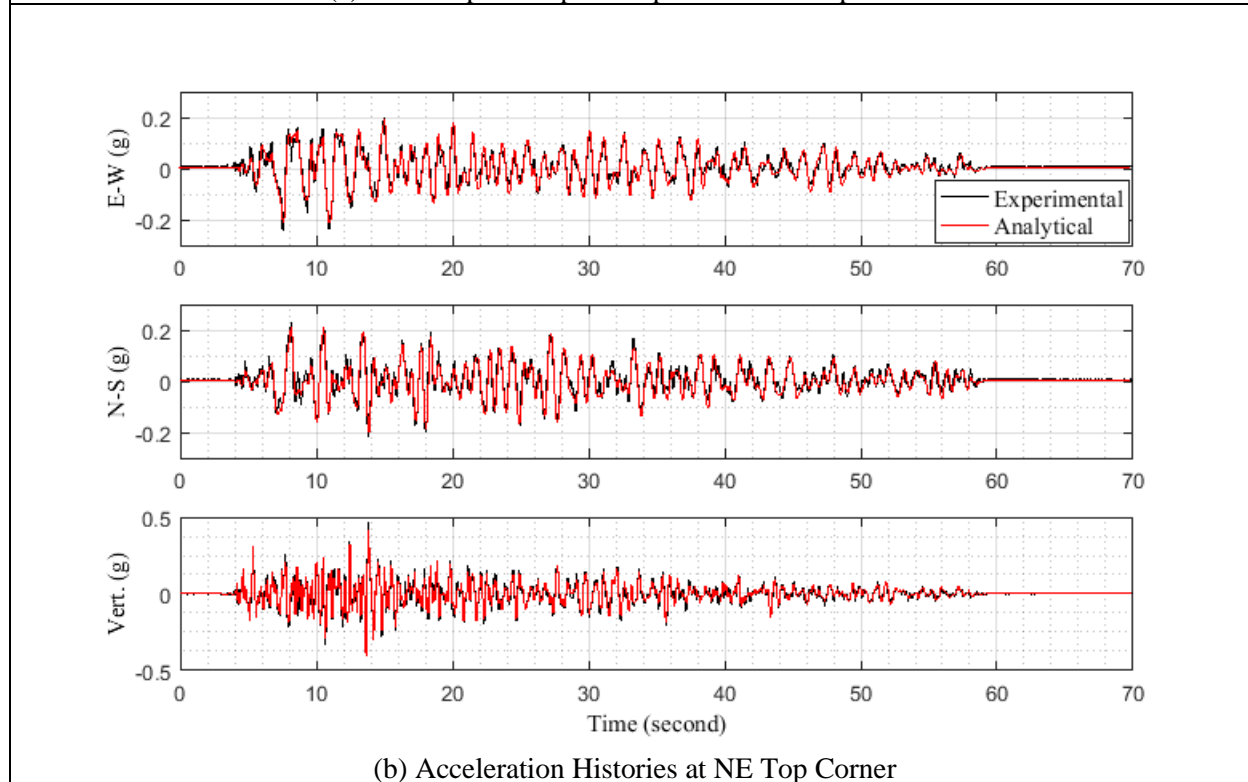
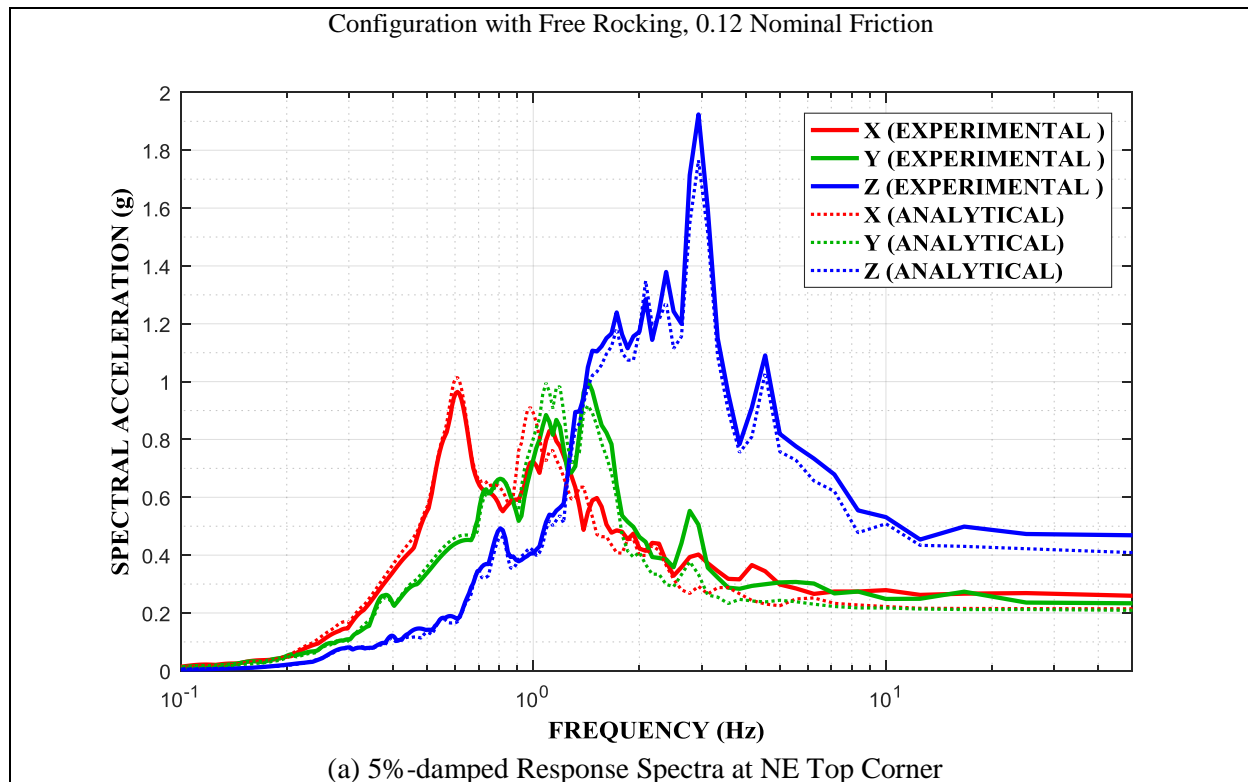


Figure 5-11 Comparison of Experimental and Analytical Results for Configuration of Free Rocking, FP Isolator Type B with 0.12 Nominal Friction in Taft 400% Motion: (a) 5%-damped Response Spectra at Frame NE Top Corner, (b) Acceleration Histories at Frame NE Top Corner

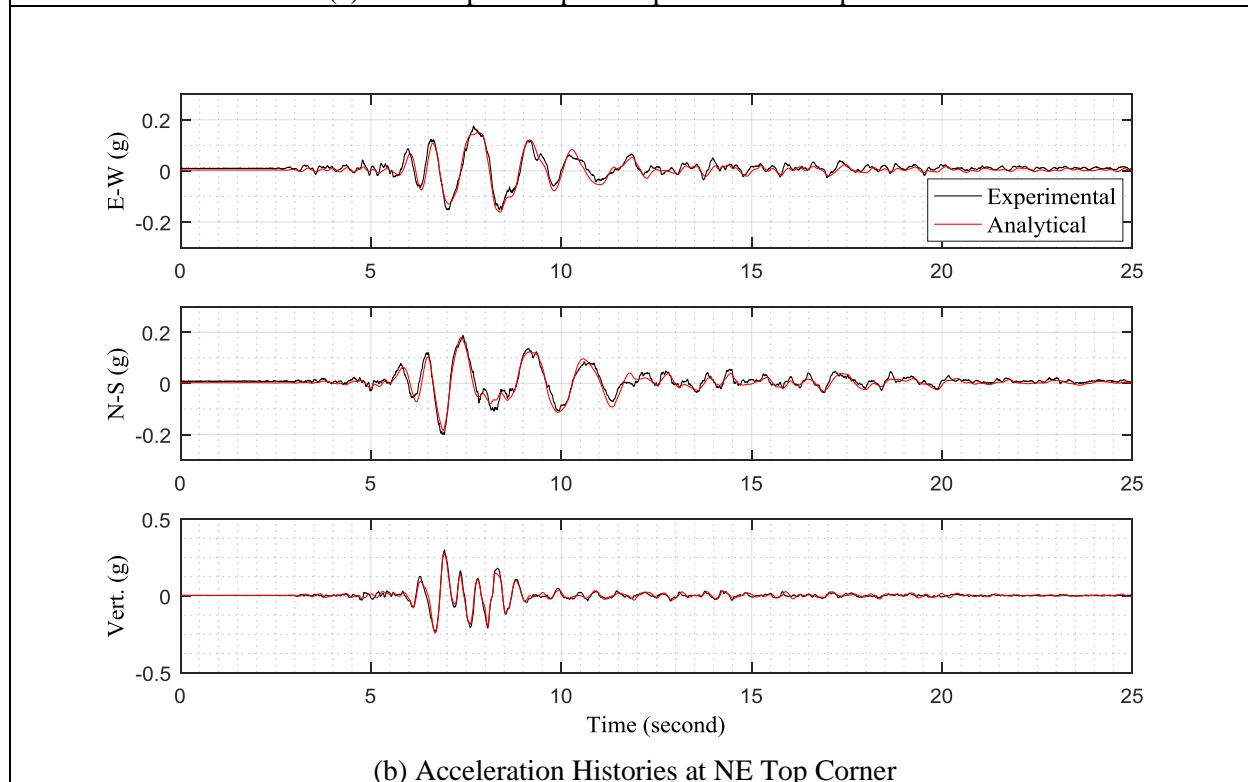
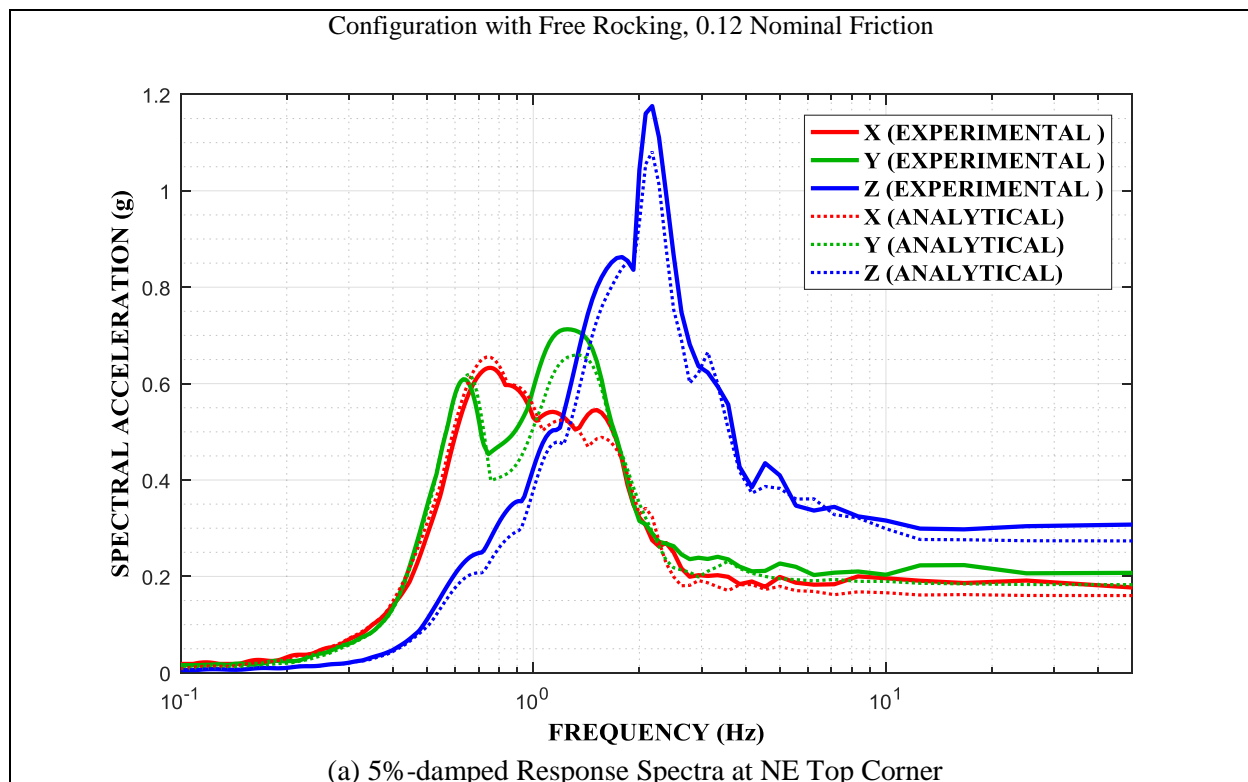


Figure 5-13 Comparison of Experimental and Analytical Results for Configuration of Free Rocking, FP Isolator Type B with 0.12 Nominal Friction in Kobe 50% Motion: (a) 5%-damped Response Spectra at Frame NE Top Corner, (b) Acceleration Histories at Frame NE Top Corner

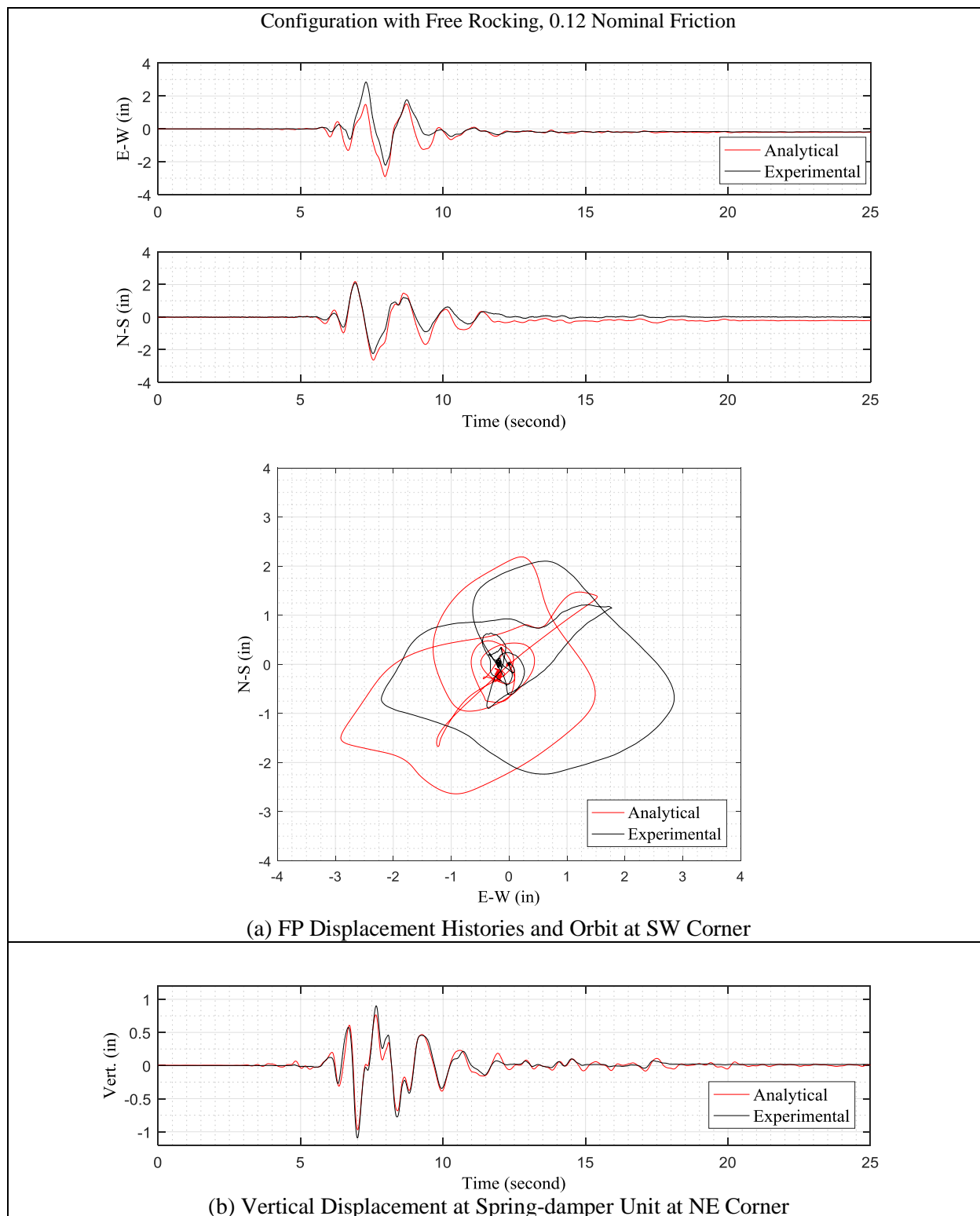


Figure 5-14 Comparison of Experimental and Analytical Results for Configuration of Free Rocking, FP Isolator Type B with 0.12 Nominal Friction in Kobe 50% Motion: (a) FP Displacement Histories and Orbit at SW Corner, (b) Vertical Displacement at Spring-damper Unit at NE Corner

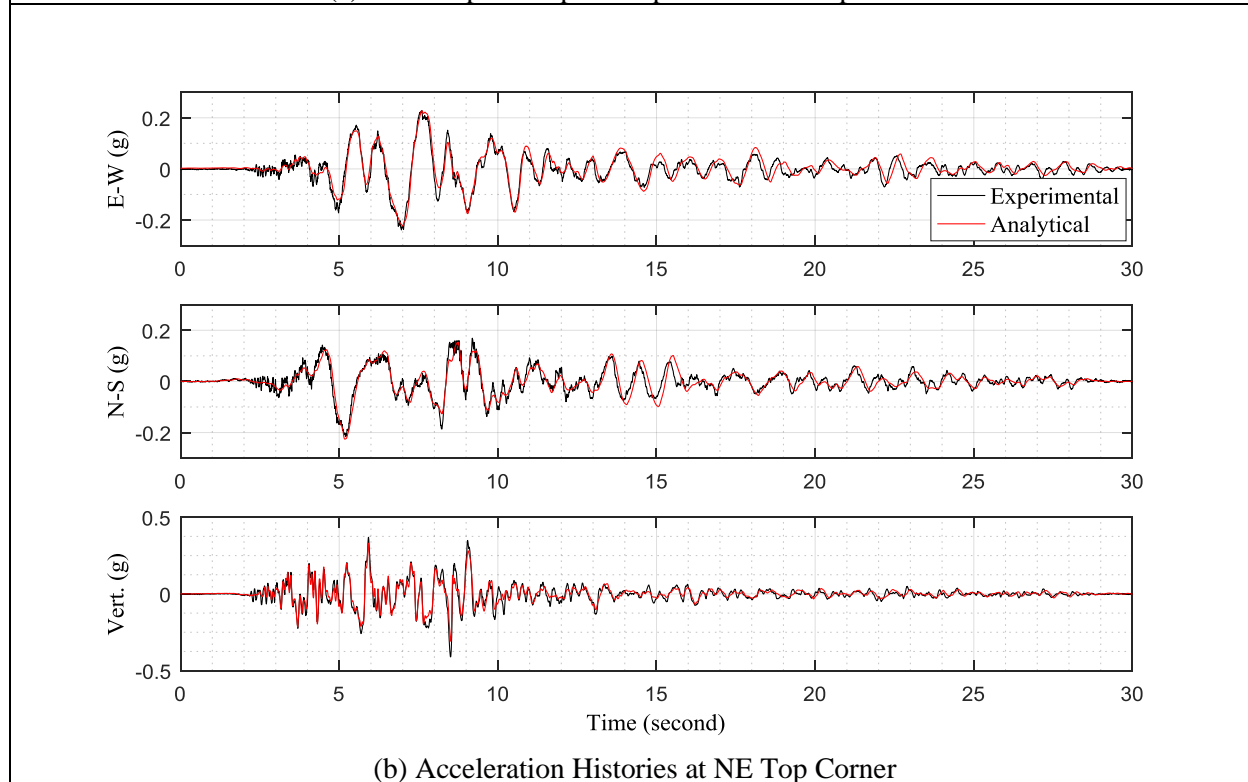
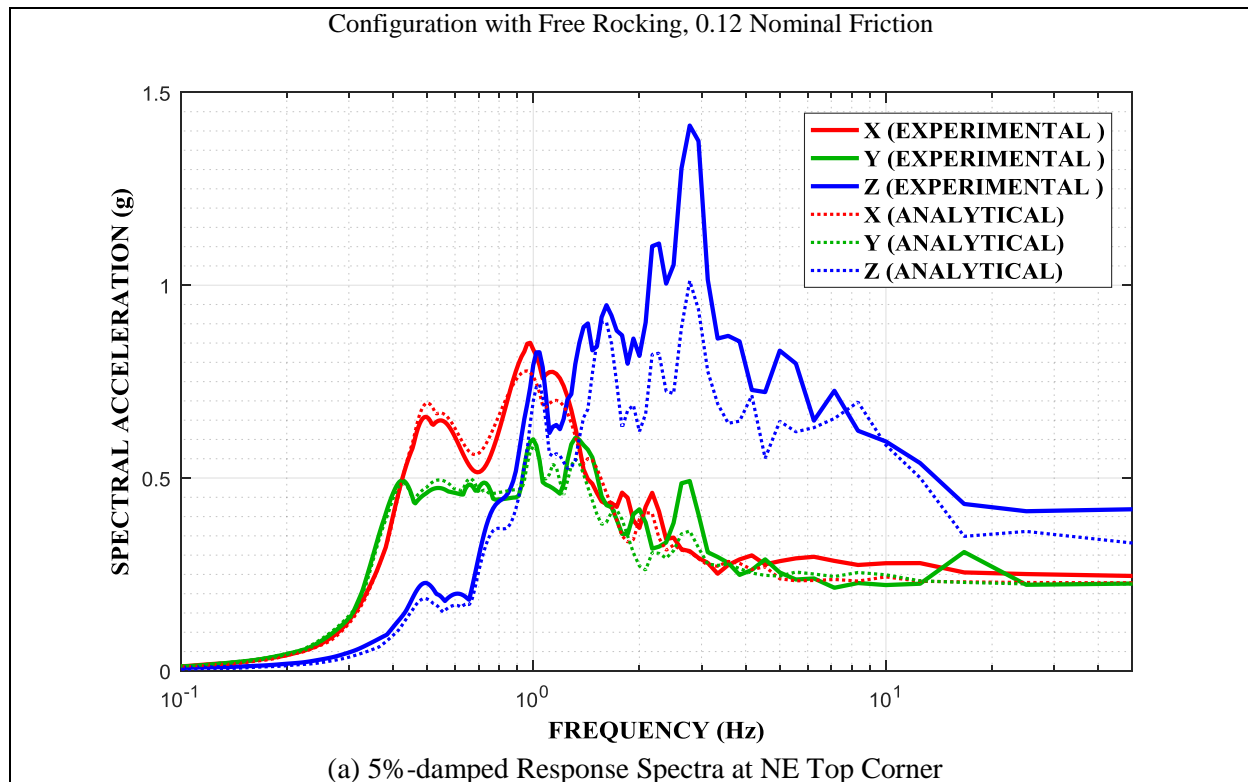


Figure 5-15 Comparison of Experimental and Analytical Results for Configuration of Free Rocking, FP Isolator Type B with 0.12 Nominal Friction in Jensen 100% Motion: (a) 5%-damped Response Spectra at Frame NE Top Corner, (b) Acceleration Histories at Frame NE Top Corner

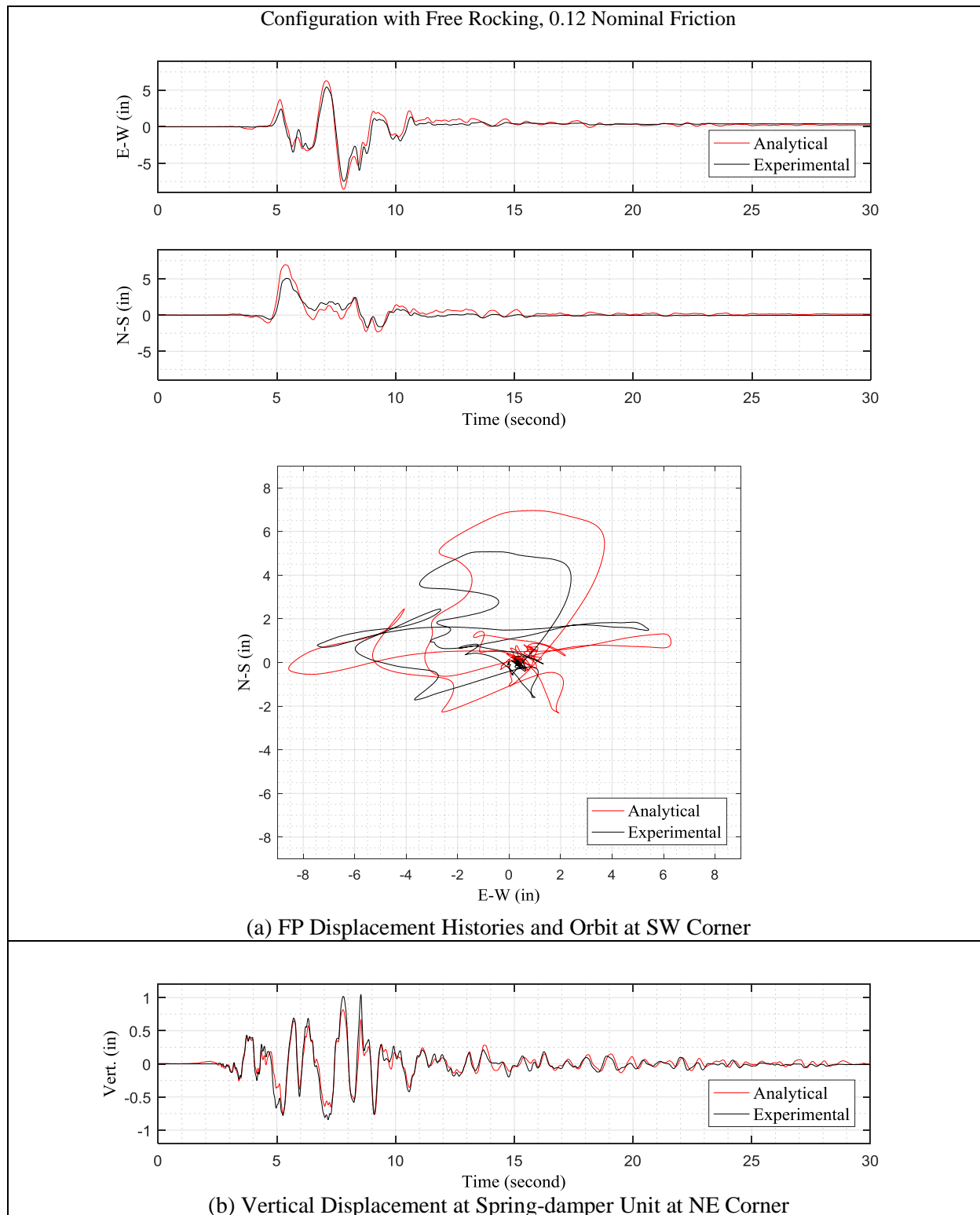


Figure 5-16 Comparison of Experimental and Analytical Results for Configuration of Free Rocking, FP Isolator Type B with 0.12 Nominal Friction in Jensen 100% Motion: (a) FP Displacement Histories and Orbit at SW Corner, (b) Vertical Displacement at Spring-damper Unit at NE Corner

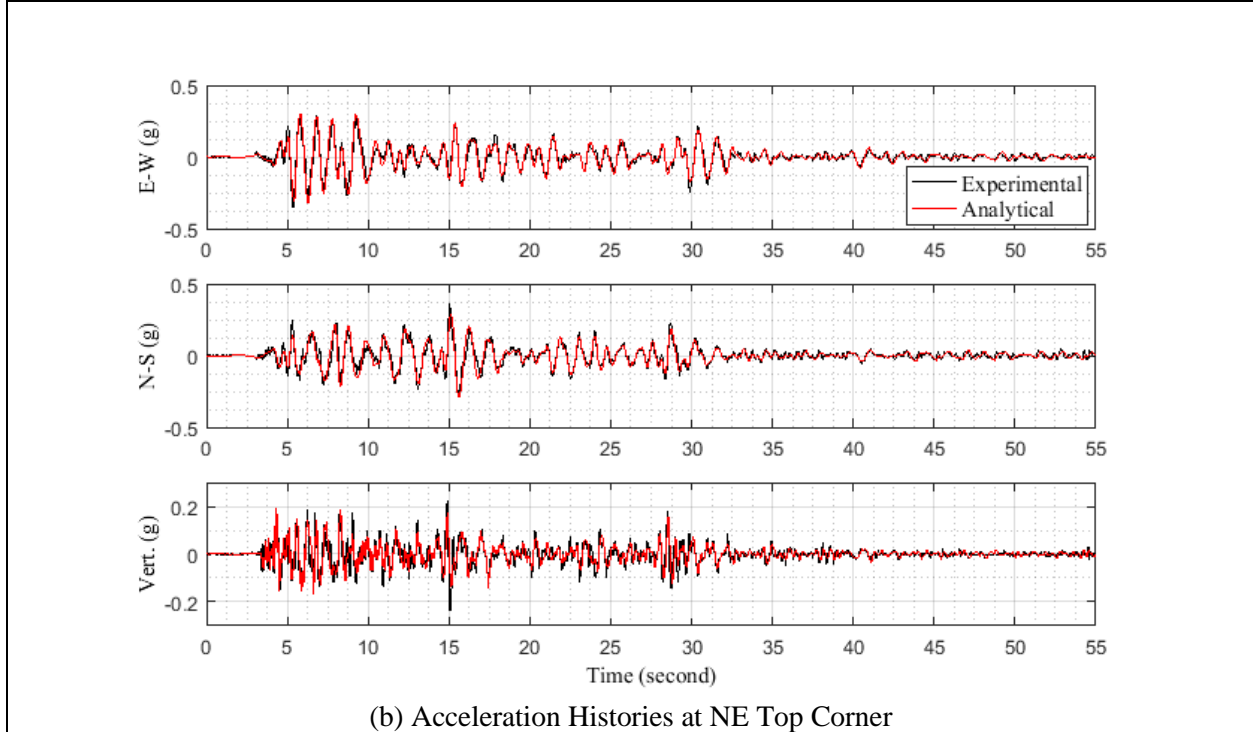
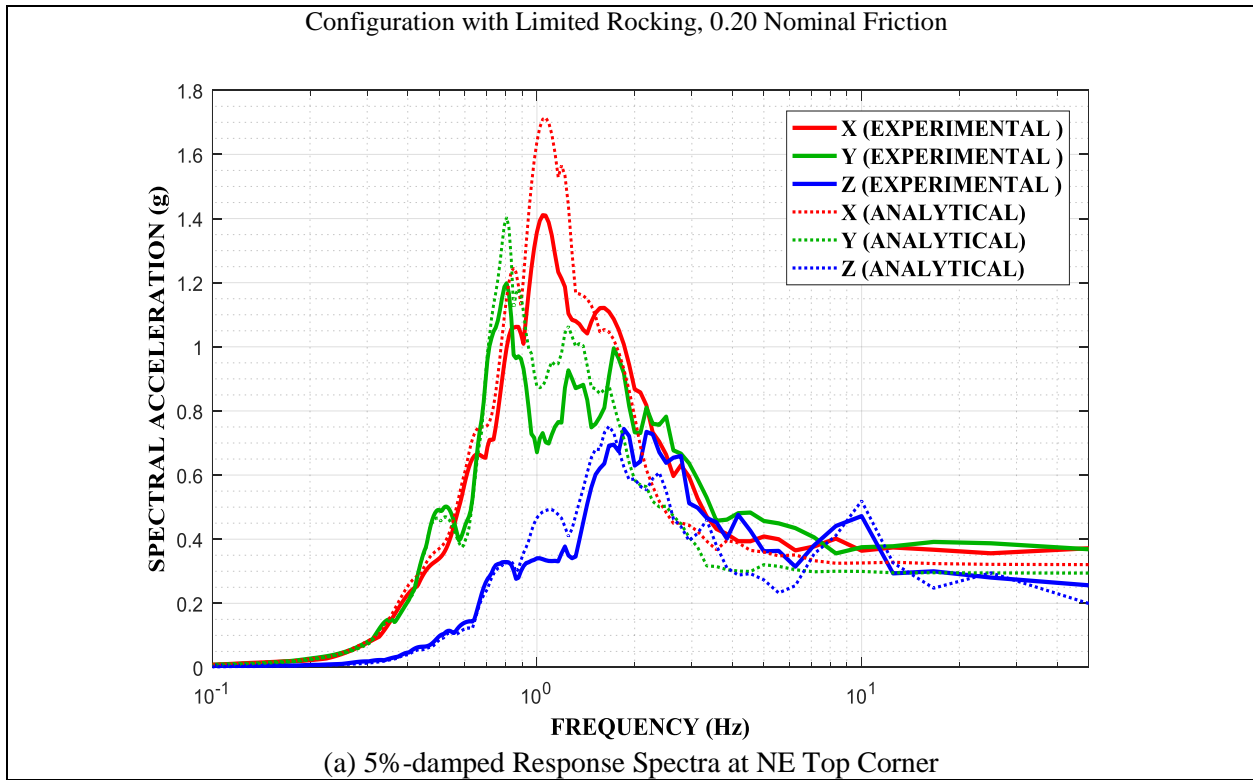


Figure 5-17 Comparison of Experimental and Analytical Results for Configuration of Limited Rocking, FP Isolator Type A with 0.20 Nominal Friction in El Centro 200% Motion: (a) 5%-damped Response Spectra at Frame NE Top Corner, (b) Acceleration Histories at Frame NE Top Corner

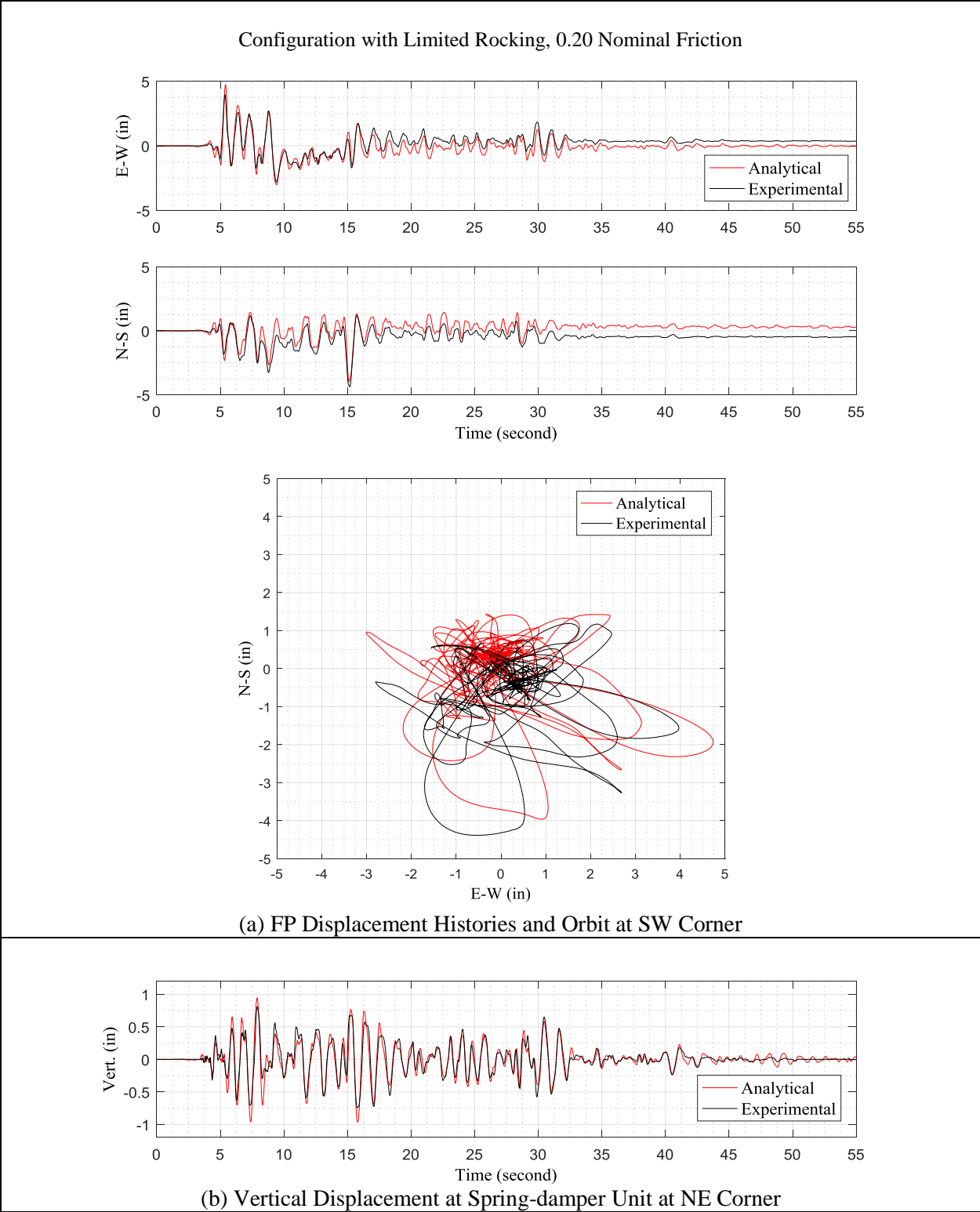


Figure 5-18 Comparison of Experimental and Analytical Results for Configuration of Limited Rocking, FP Isolator Type A with 0.20 Nominal Friction in El Centro 200% Motion: (a) FP Displacement Histories and Orbit at SW Corner, (b) Vertical Displacement at Spring-damper Unit at NE Corner

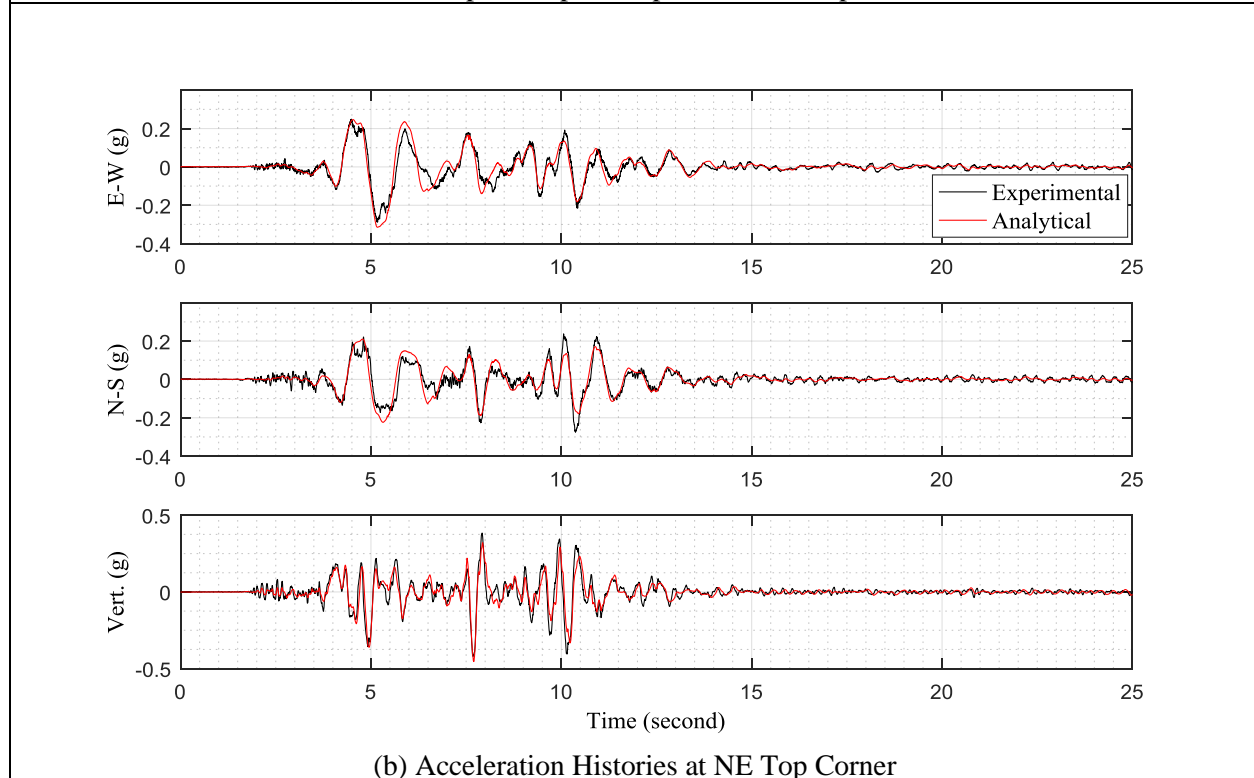
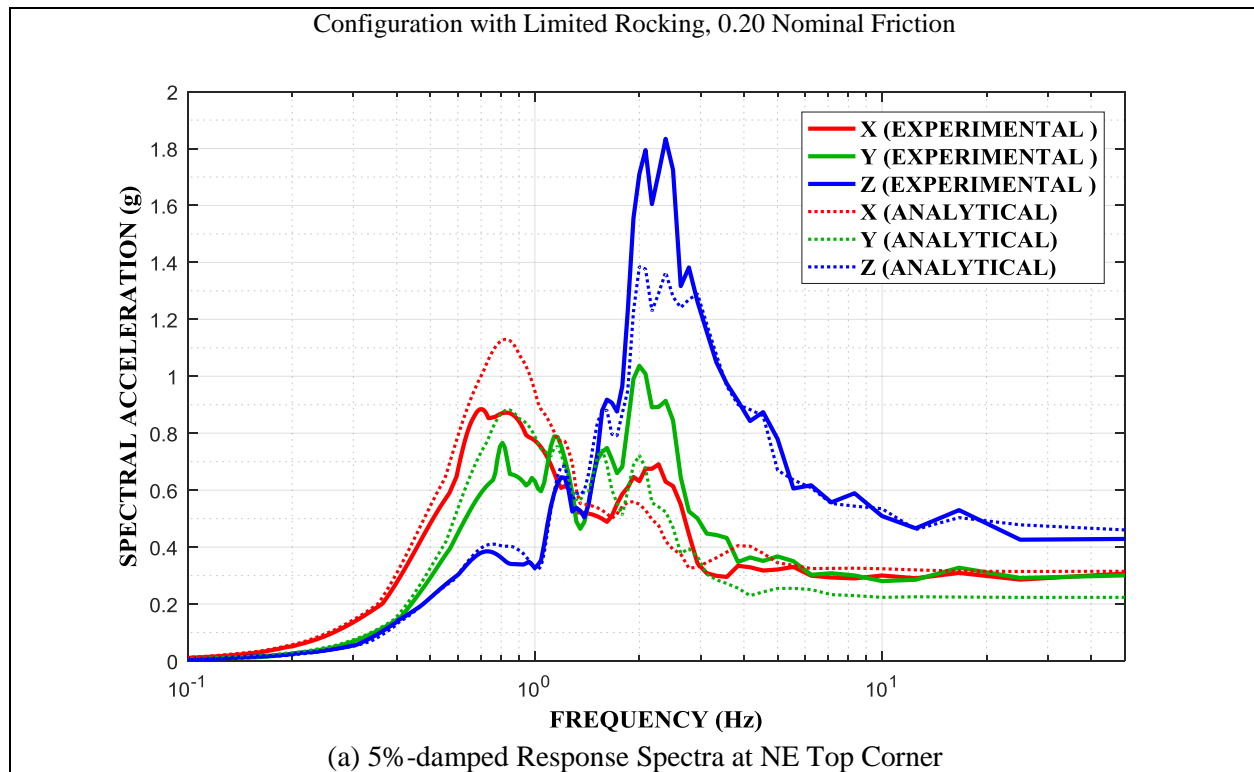


Figure 5-19 Comparison of Experimental and Analytical Results for Configuration of Limited Rocking, FP Isolator Type A with 0.20 Nominal Friction in Pacoima 65% Motion: (a) 5%-damped Response Spectra at Frame NE Top Corner, (b) Acceleration Histories at Frame NE Top Corner

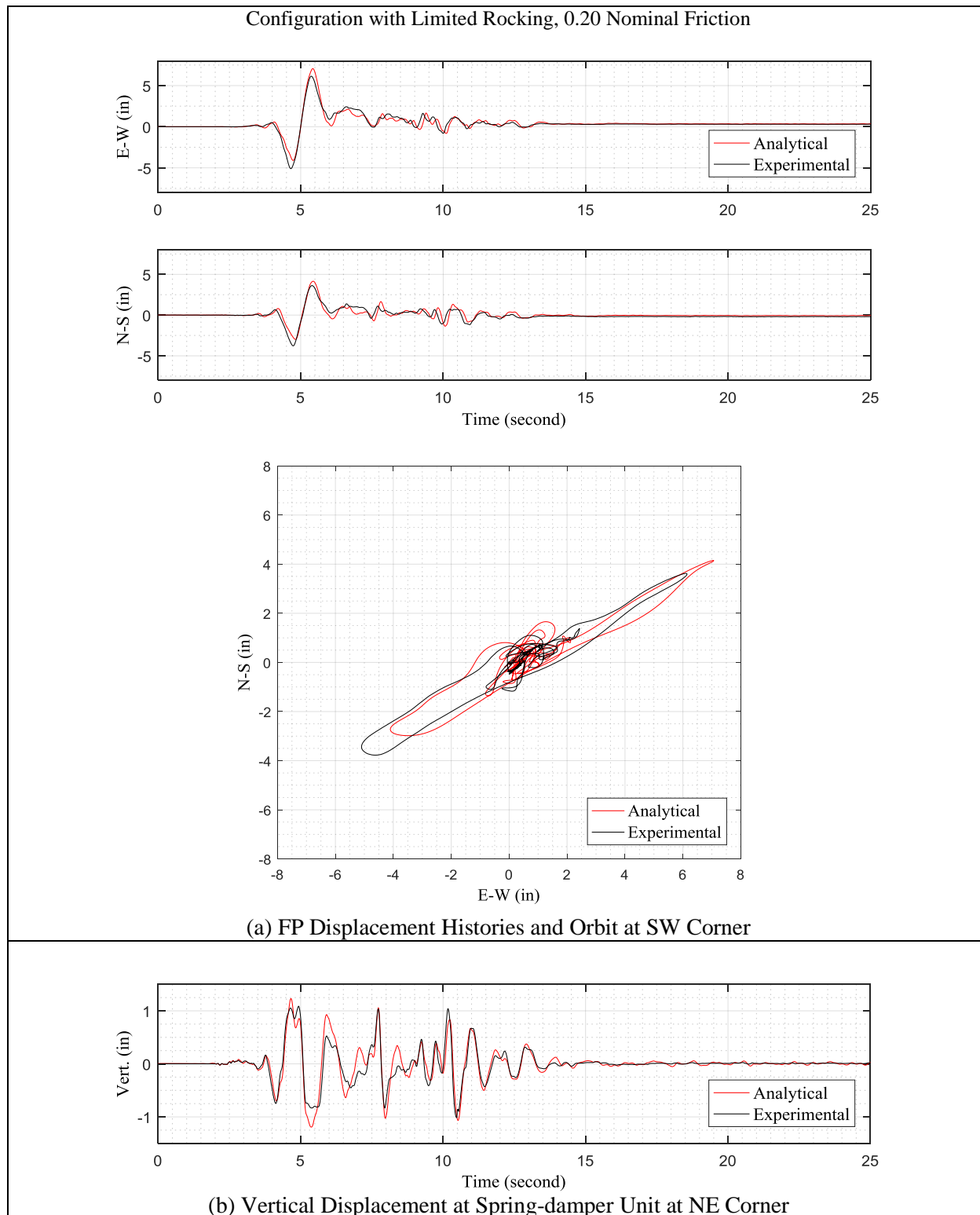


Figure 5-20 Comparison of Experimental and Analytical Results for Configuration of Limited Rocking, FP Isolator Type A with 0.20 Nominal Friction in Pacoima 65% Motion: (a) FP Displacement Histories and Orbit at SW Corner, (b) Vertical Displacement at Spring-damper Unit at NE Corner

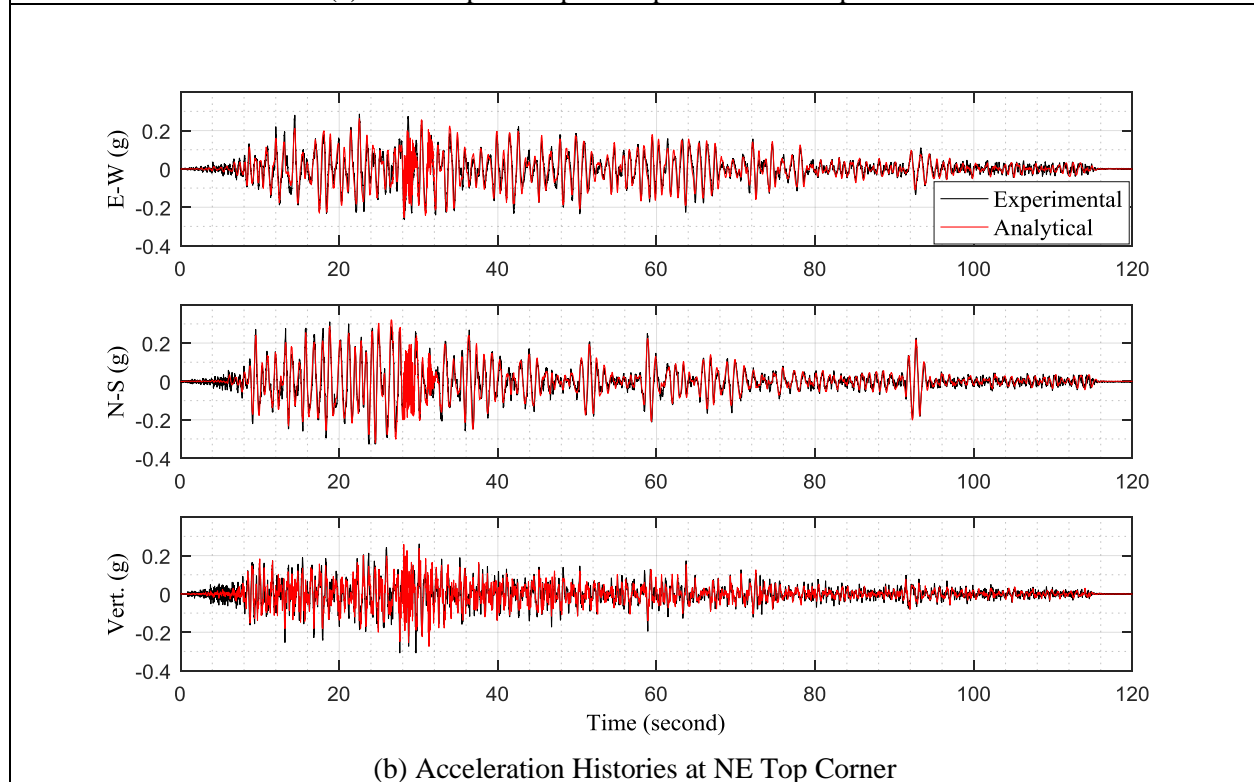
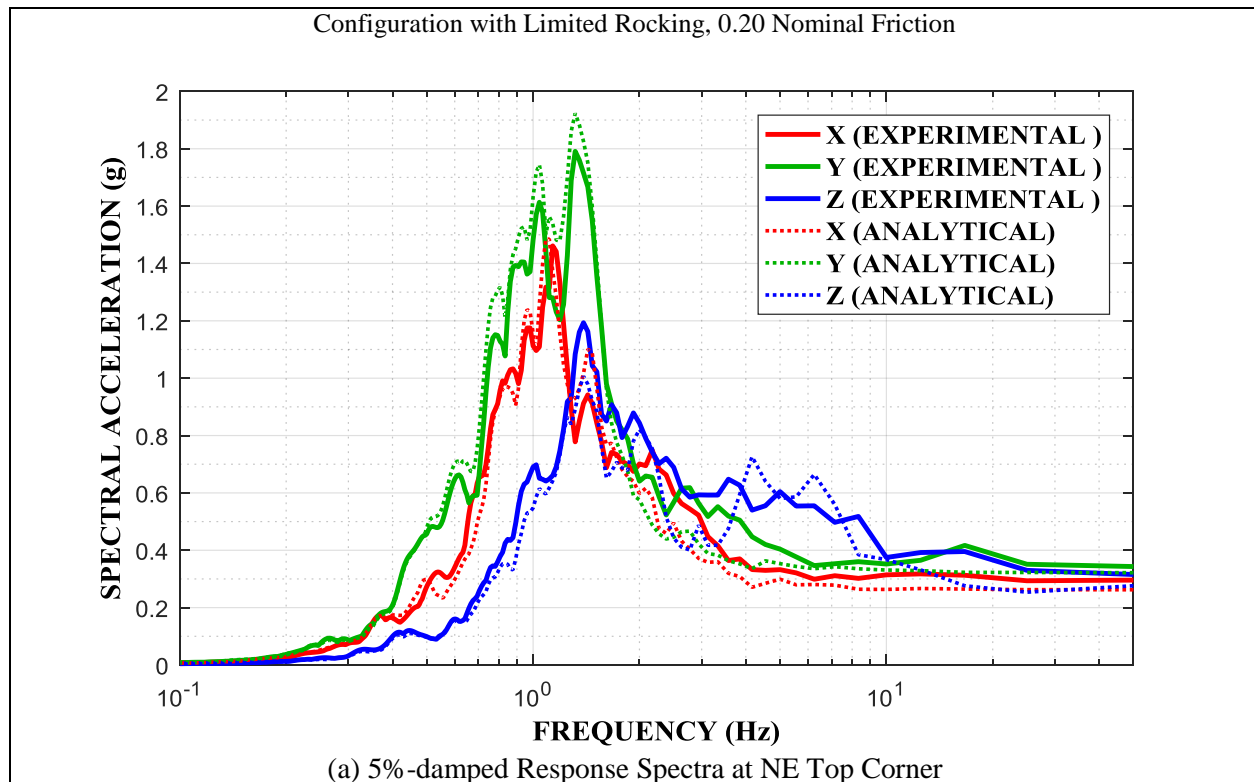


Figure 5-21 Comparison of Experimental and Analytical Results for Configuration of Limited Rocking, FP Isolator Type A with 0.20 Nominal Friction in Chile 100% Motion: (a) 5%-damped Response Spectra at Frame NE Top Corner, (b) Acceleration Histories at Frame NE Top Corner

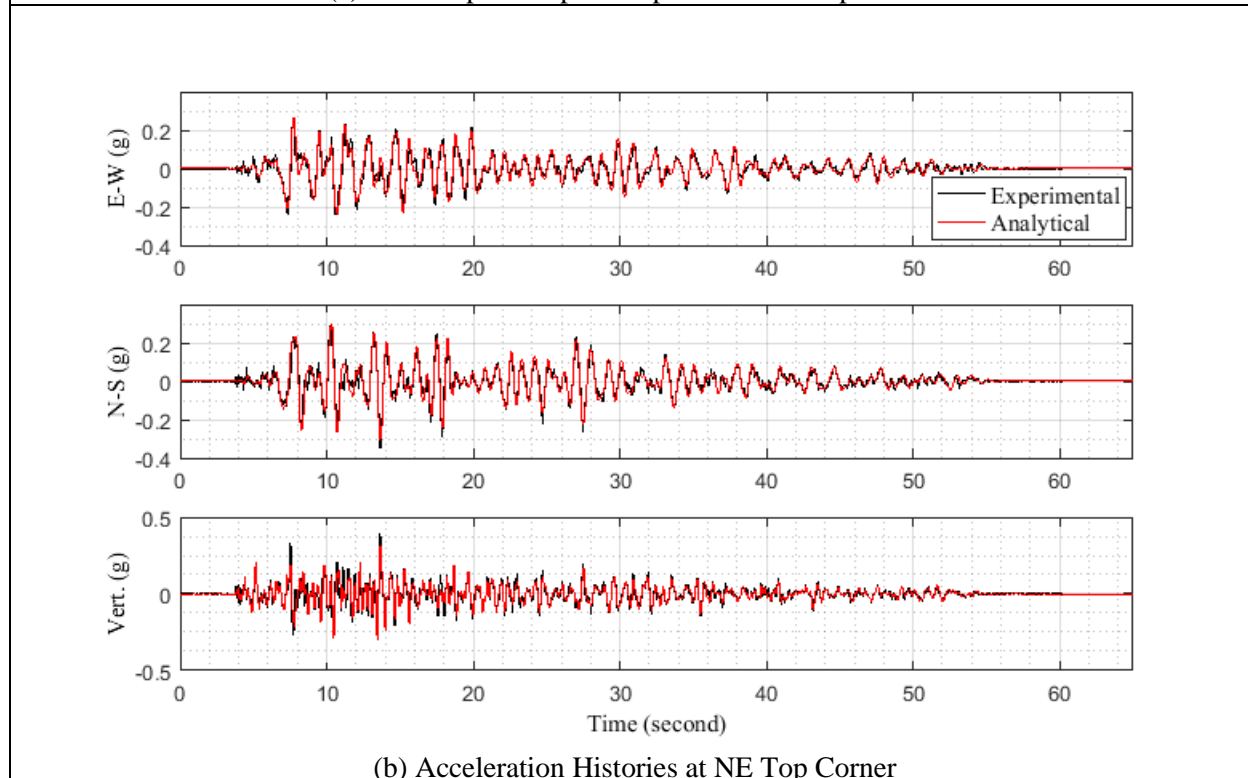
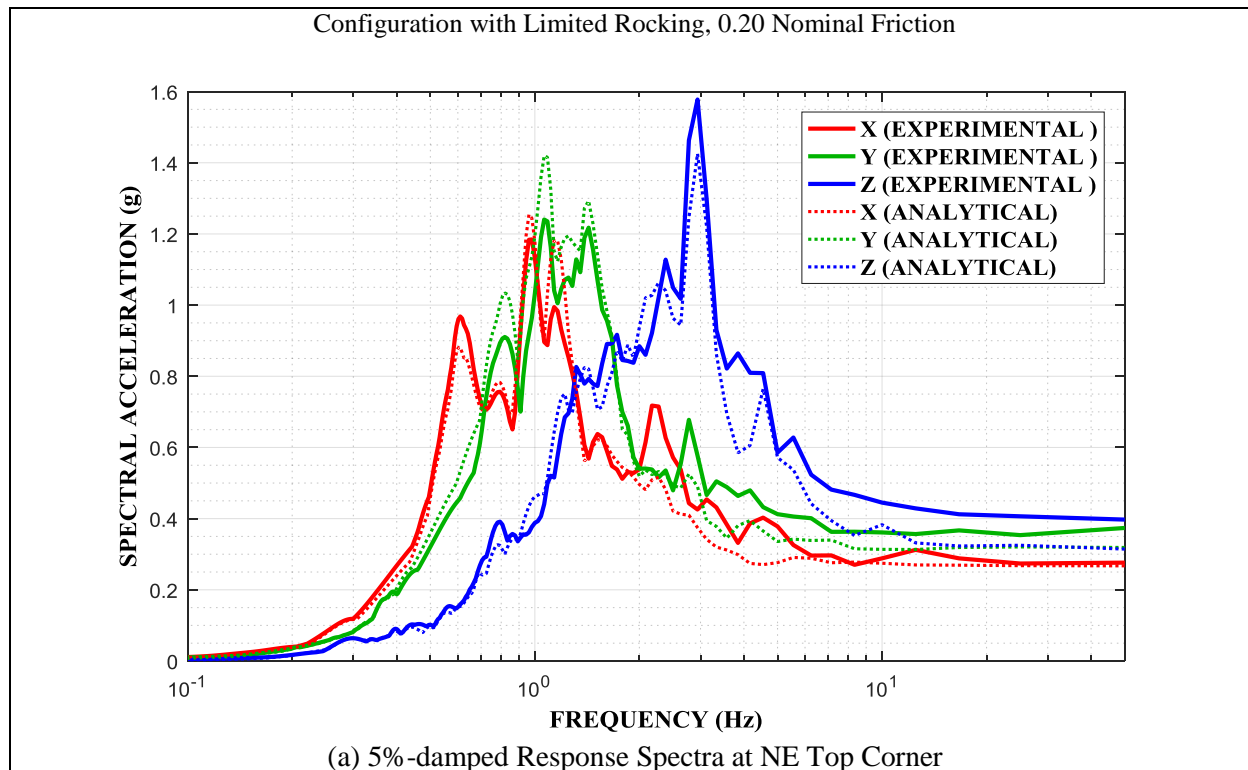


Figure 5-23 Comparison of Experimental and Analytical Results for Configuration of Limited Rocking, FP Isolator Type A with 0.20 Nominal Friction in Taft 300% Motion: (a) 5%-damped Response Spectra at Frame NE Top Corner, (b) Acceleration Histories at Frame NE Top Corner

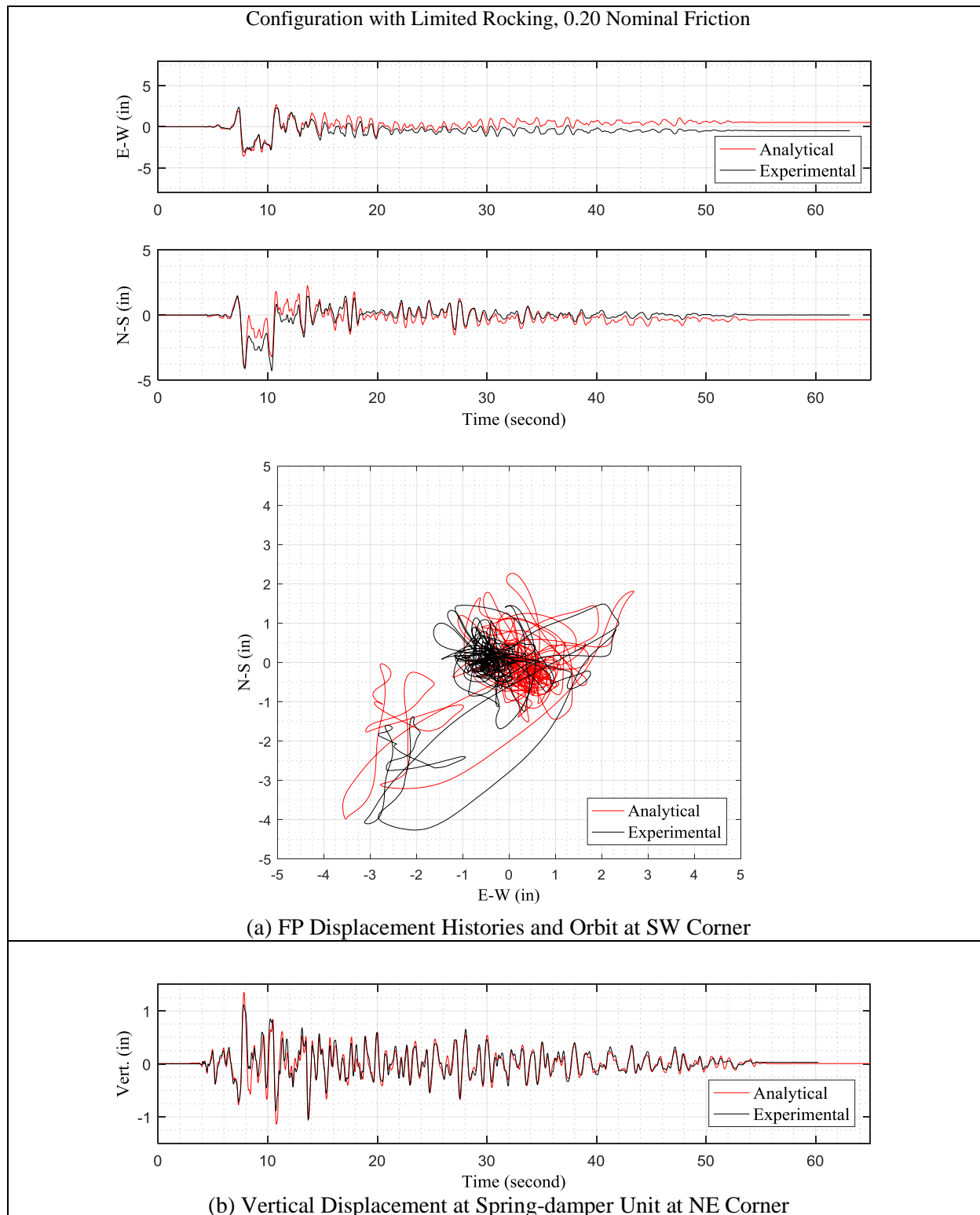


Figure 5-24 Comparison of Experimental and Analytical Results for Configuration of Limited Rocking, FP Isolator Type A with 0.20 Nominal Friction in Taft 300% Motion: (a) FP Displacement Histories and Orbit at SW Corner, (b) Vertical Displacement at Spring-damper Unit at NE Corner

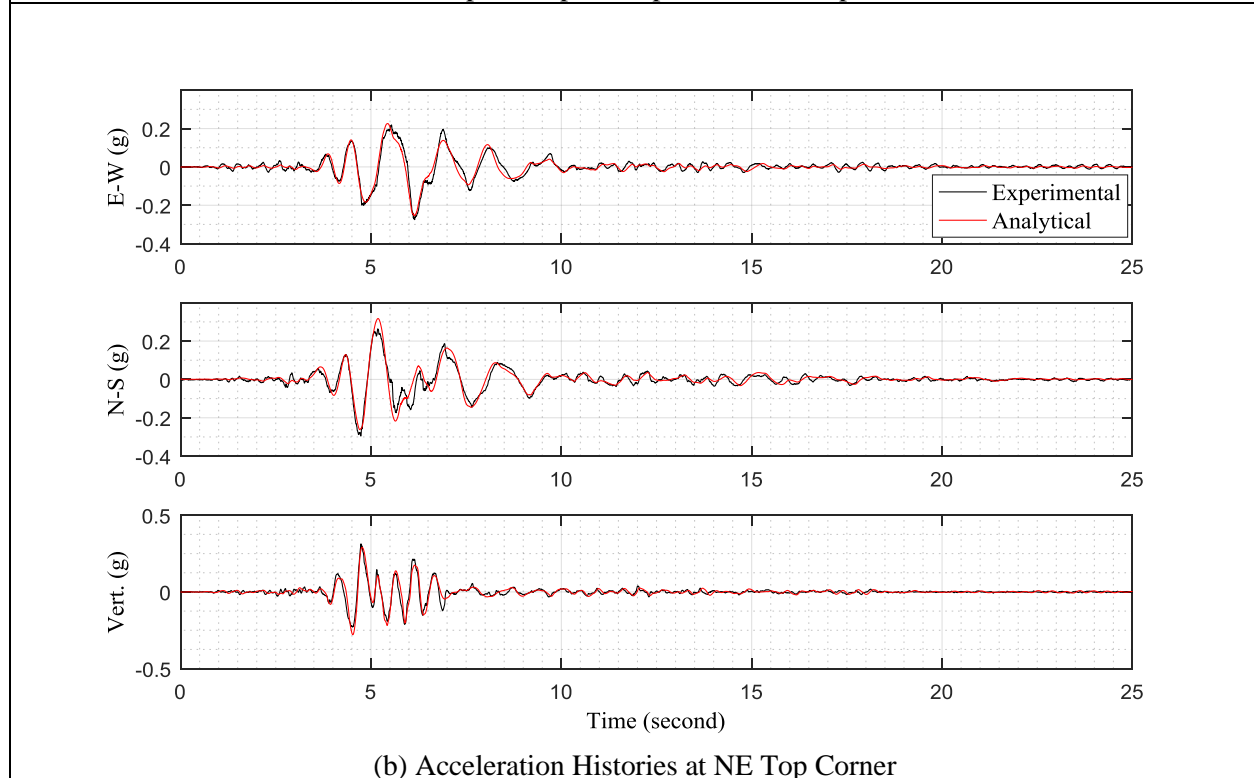
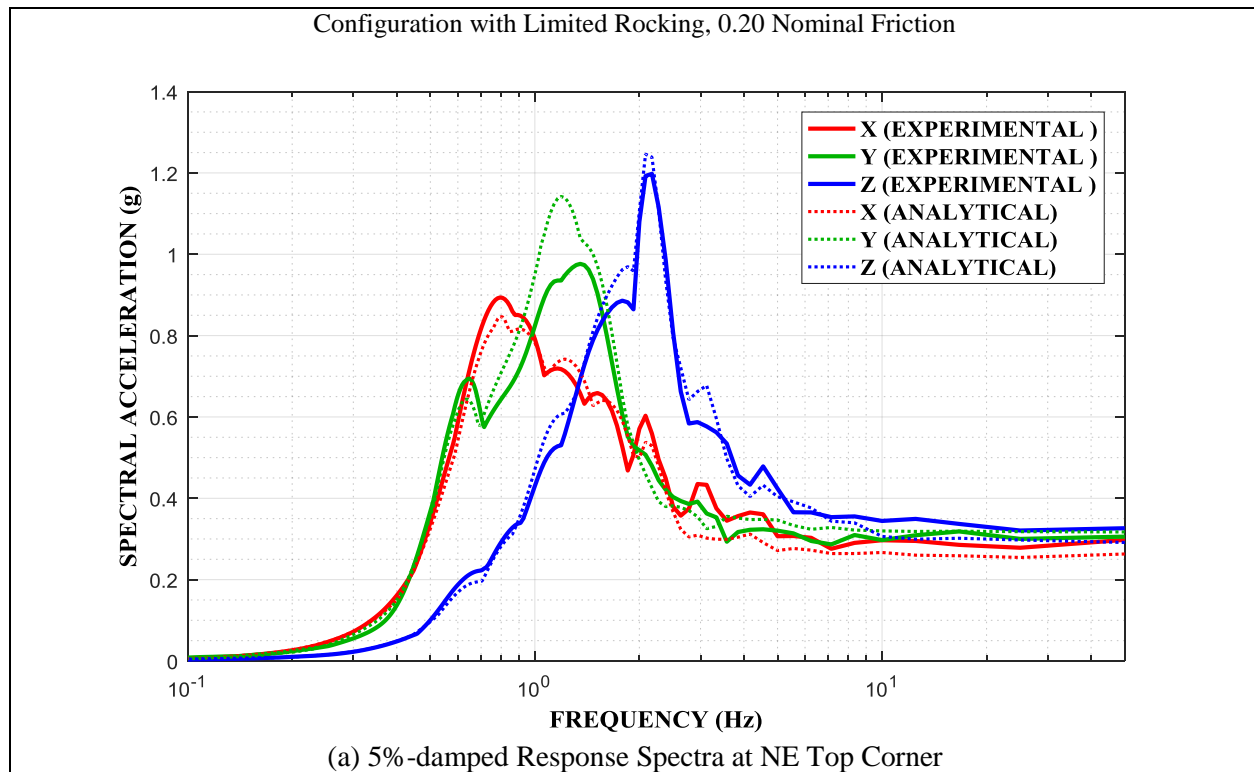


Figure 5-25 Comparison of Experimental and Analytical Results for Configuration of Limited Rocking, FP Isolator Type A with 0.20 Nominal Friction in Kobe 50% Motion: (a) 5%-damped Response Spectra at Frame NE Top Corner, (b) Acceleration Histories at Frame NE Top Corner

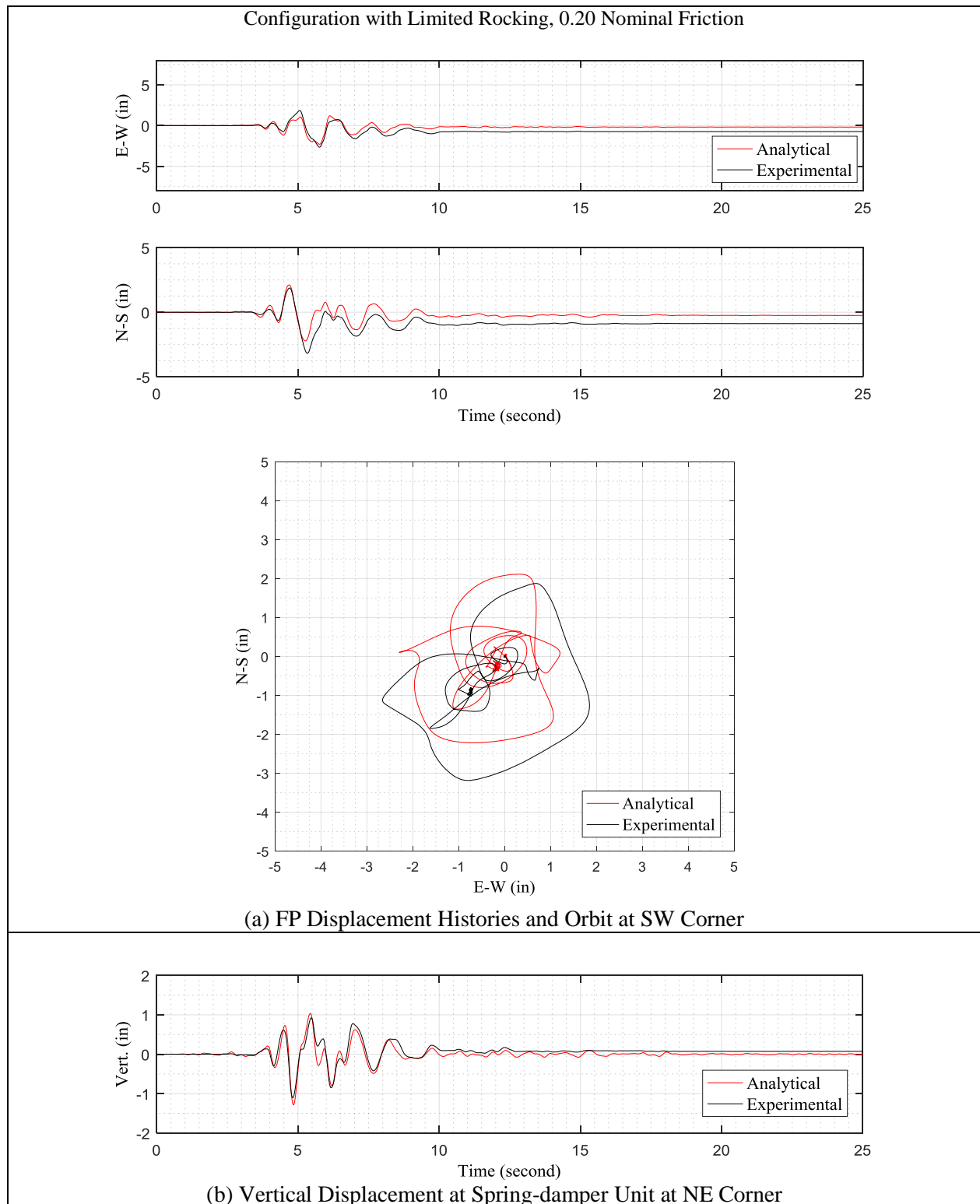


Figure 5-26 Comparison of Experimental and Analytical Results for Configuration of Limited Rocking, FP Isolator Type A with 0.20 Nominal Friction in Kobe 50% Motion: (a) FP Displacement Histories and Orbit at SW Corner, (b) Vertical Displacement at Spring-damper Unit at NE Corner

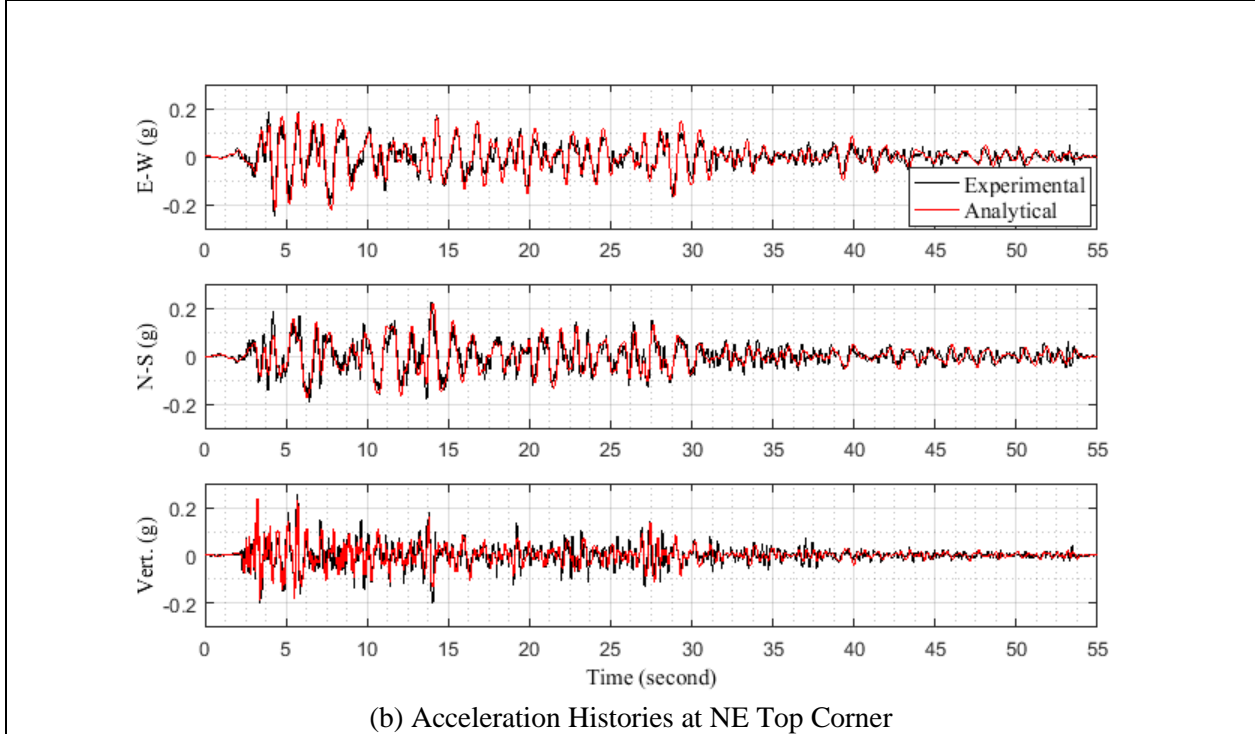
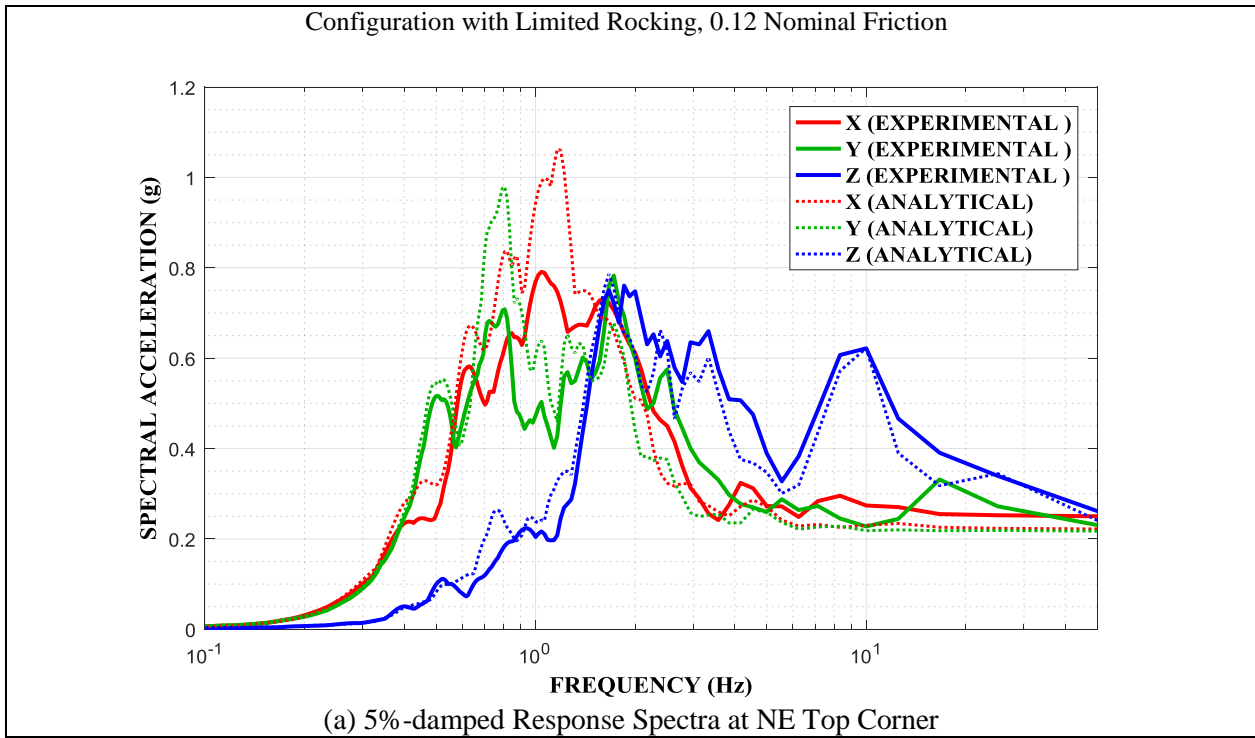


Figure 5-27 Comparison of Experimental and Analytical Results for Configuration of Limited Rocking, FP Isolator Type B with 0.12 Nominal Friction in El Centro 250% Motion: (a) 5%-damped Response Spectra at Frame NE Top Corner, (b) Acceleration Histories at Frame NE Top Corner

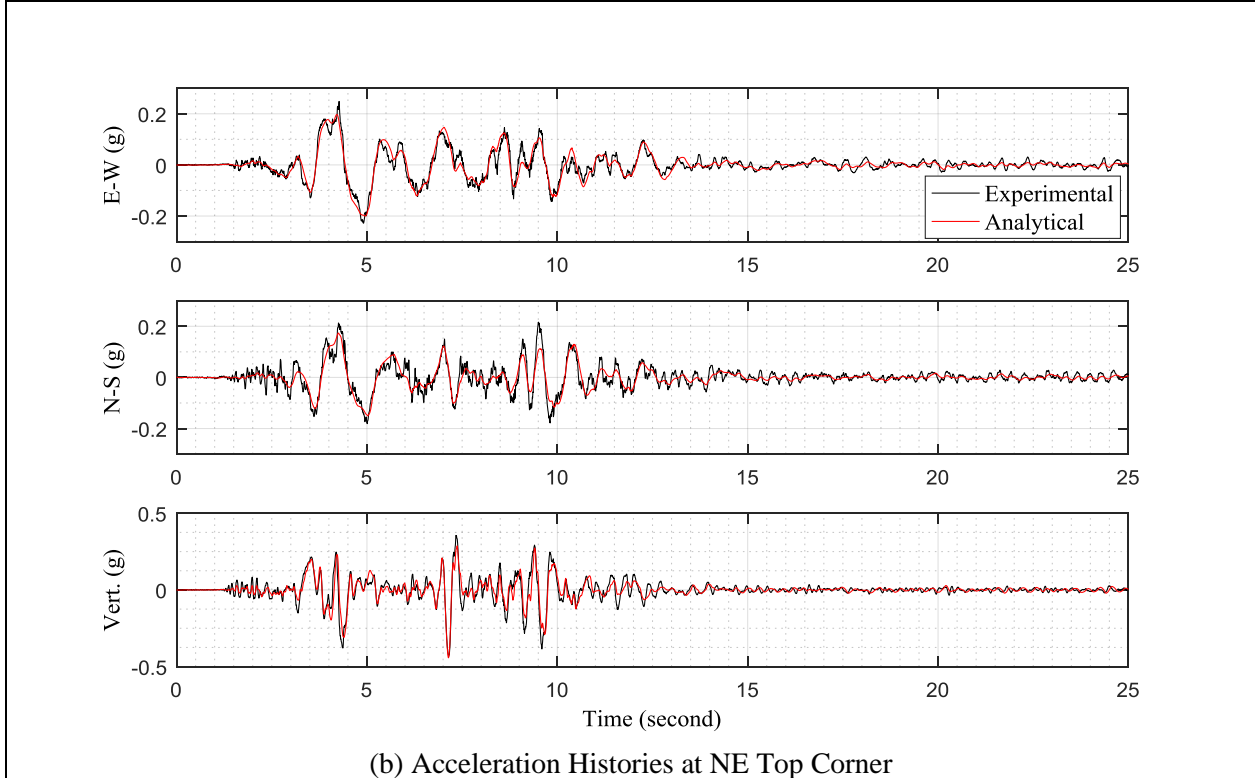
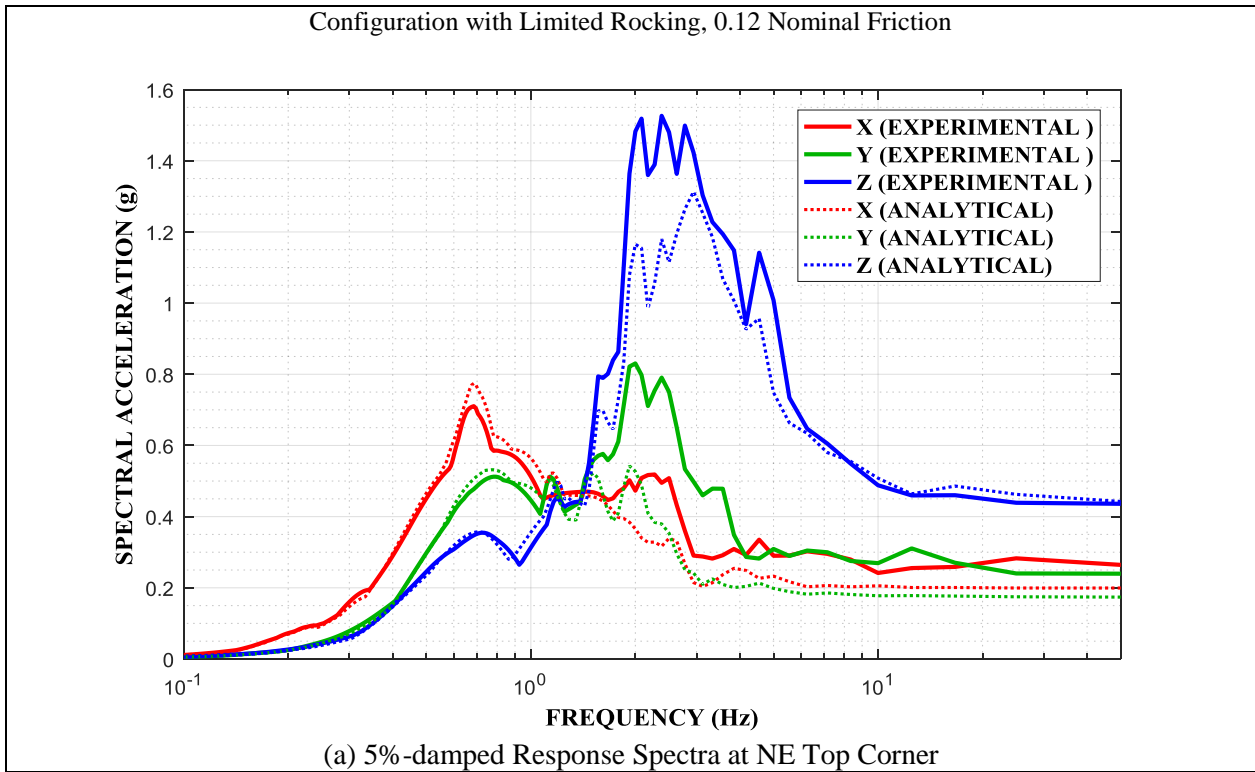


Figure 5-29 Comparison of Experimental and Analytical Results for Configuration of Limited Rocking, FP Isolator Type B with 0.12 Nominal Friction in Pacoima 75% Motion: (a) 5%-damped Response Spectra at Frame NE Top Corner, (b) Acceleration Histories at Frame NE Top Corner

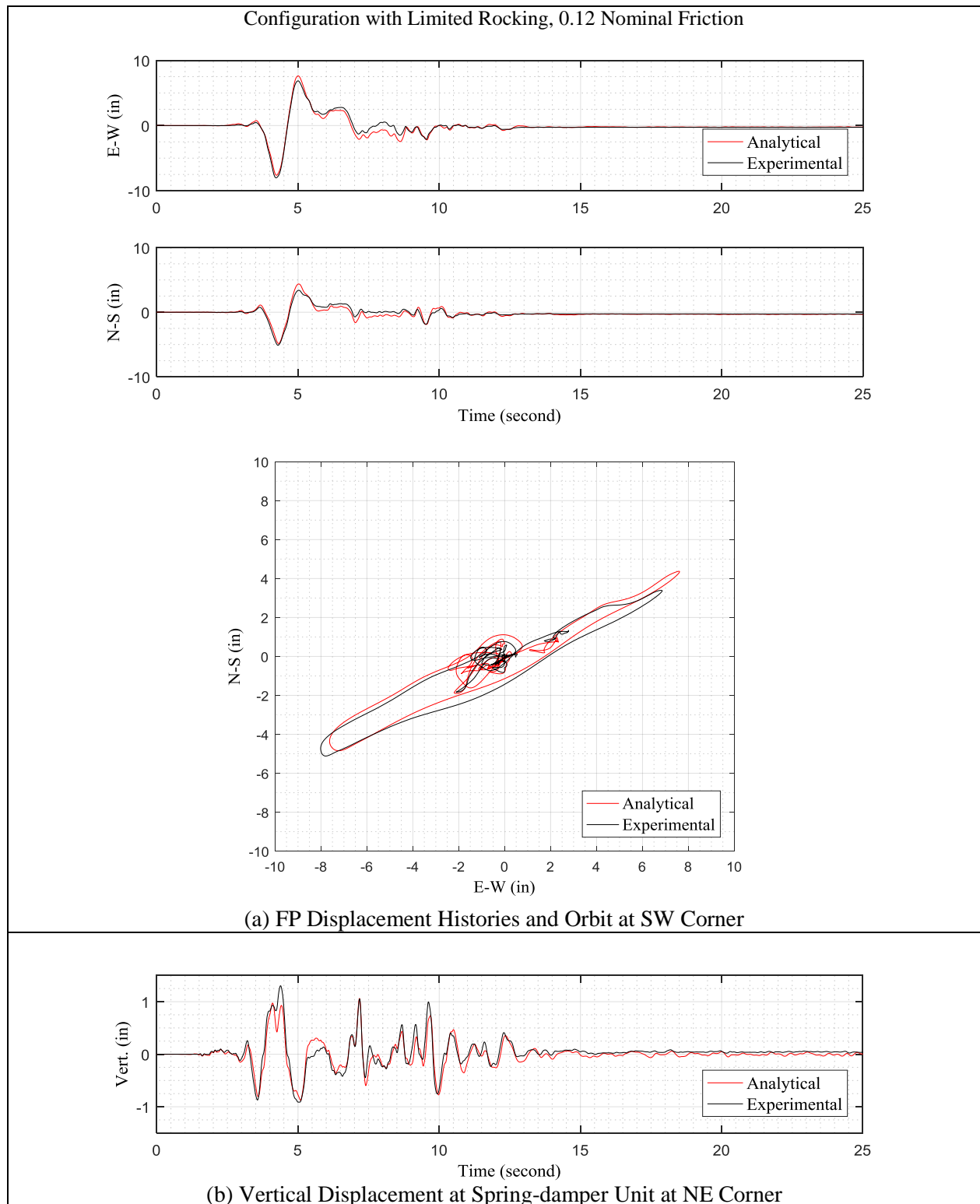


Figure 5-30 Comparison of Experimental and Analytical Results for Configuration of Limited Rocking, FP Isolator Type B with 0.12 Nominal Friction in Pacoima 75% Motion: (a) FP Displacement Histories and Orbit at SW Corner, (b) Vertical Displacement at Spring-damper Unit at NE Corner

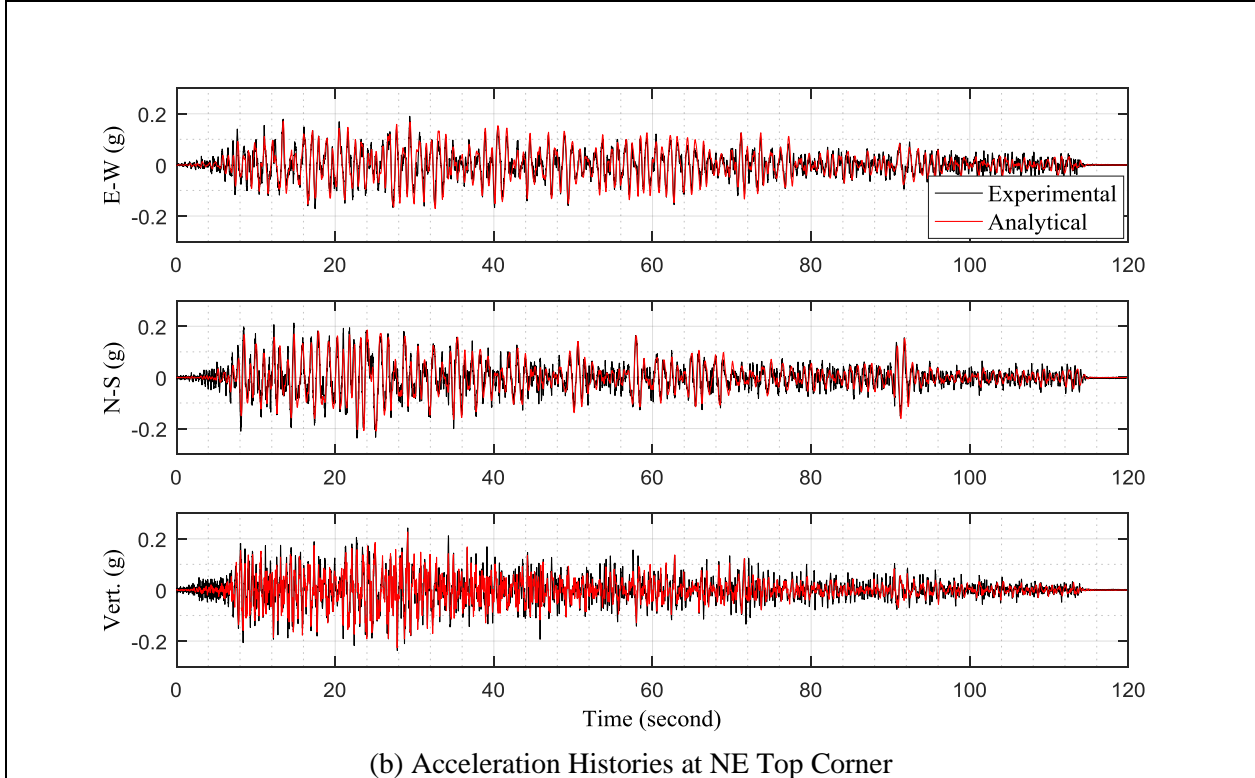
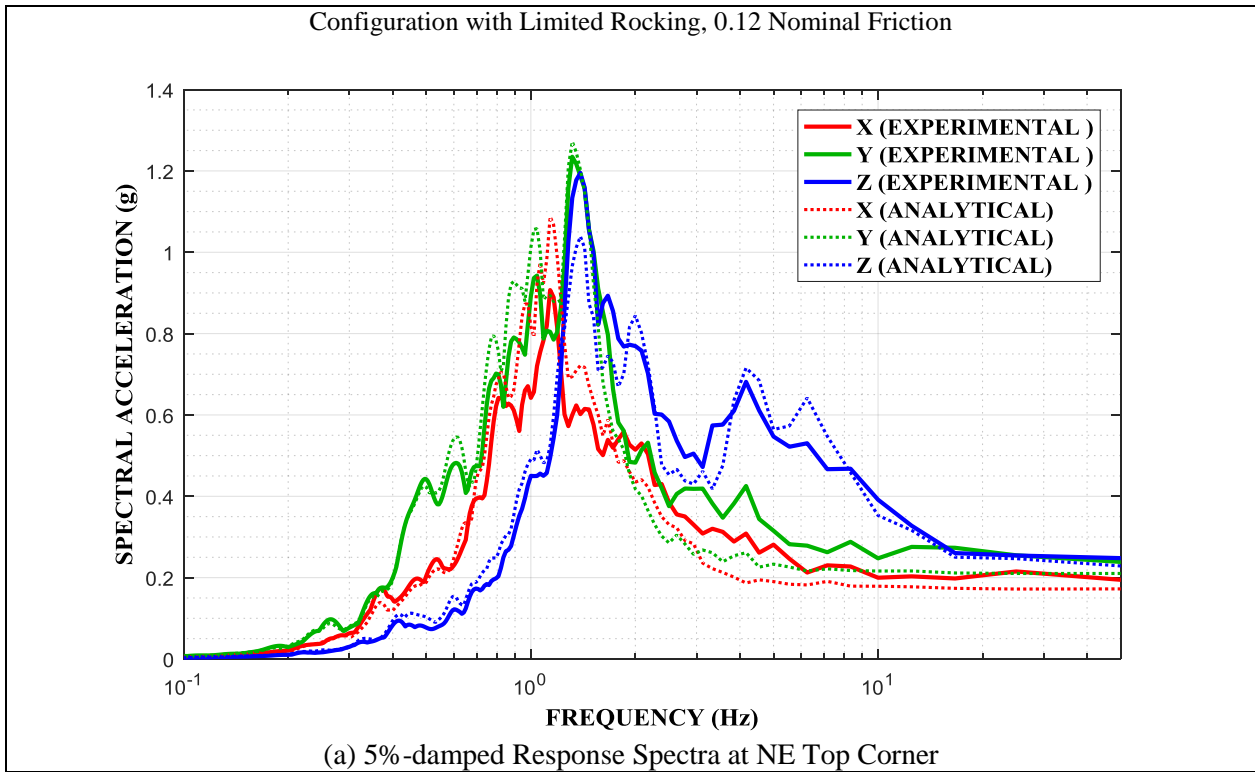


Figure 5-31 Comparison of Experimental and Analytical Results for Configuration of Limited Rocking, FP Isolator Type B with 0.12 Nominal Friction in Chile 100% Motion: (a) 5%-damped Response Spectra at Frame NE Top Corner, (b) Acceleration Histories at Frame NE Top Corner

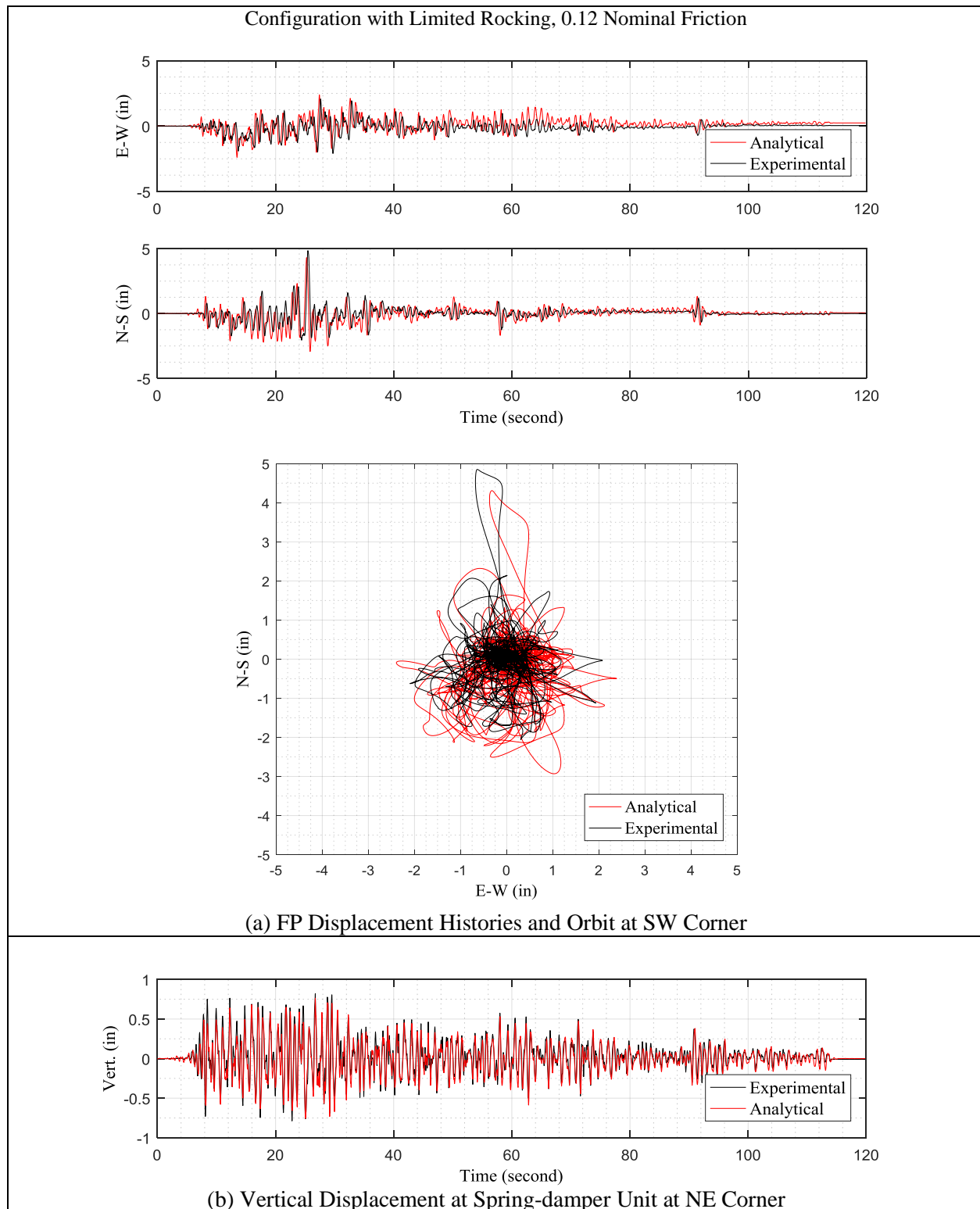


Figure 5-32 Comparison of Experimental and Analytical Results for Configuration of Limited Rocking, FP Isolator Type B with 0.12 Nominal Friction in Chile 100% Motion: (a) FP Displacement Histories and Orbit at SW Corner, (b) Vertical Displacement at Spring-damper Unit at NE Corner

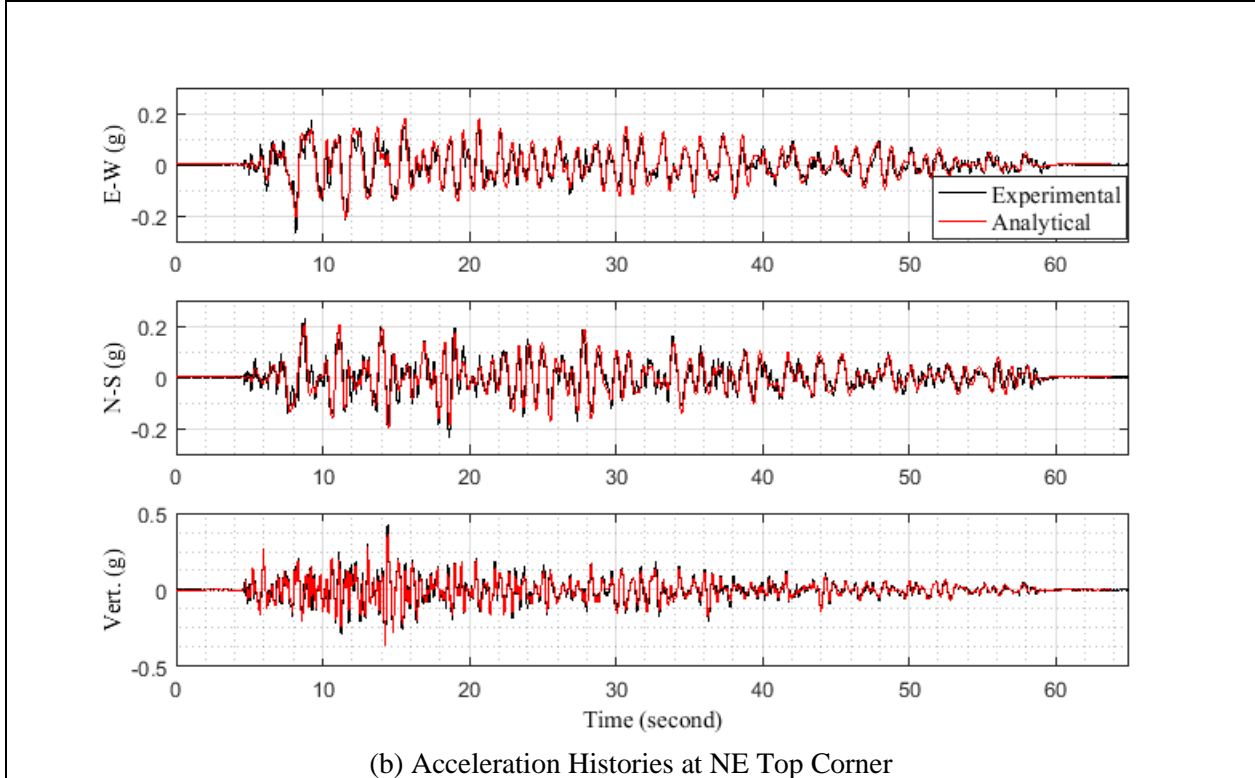
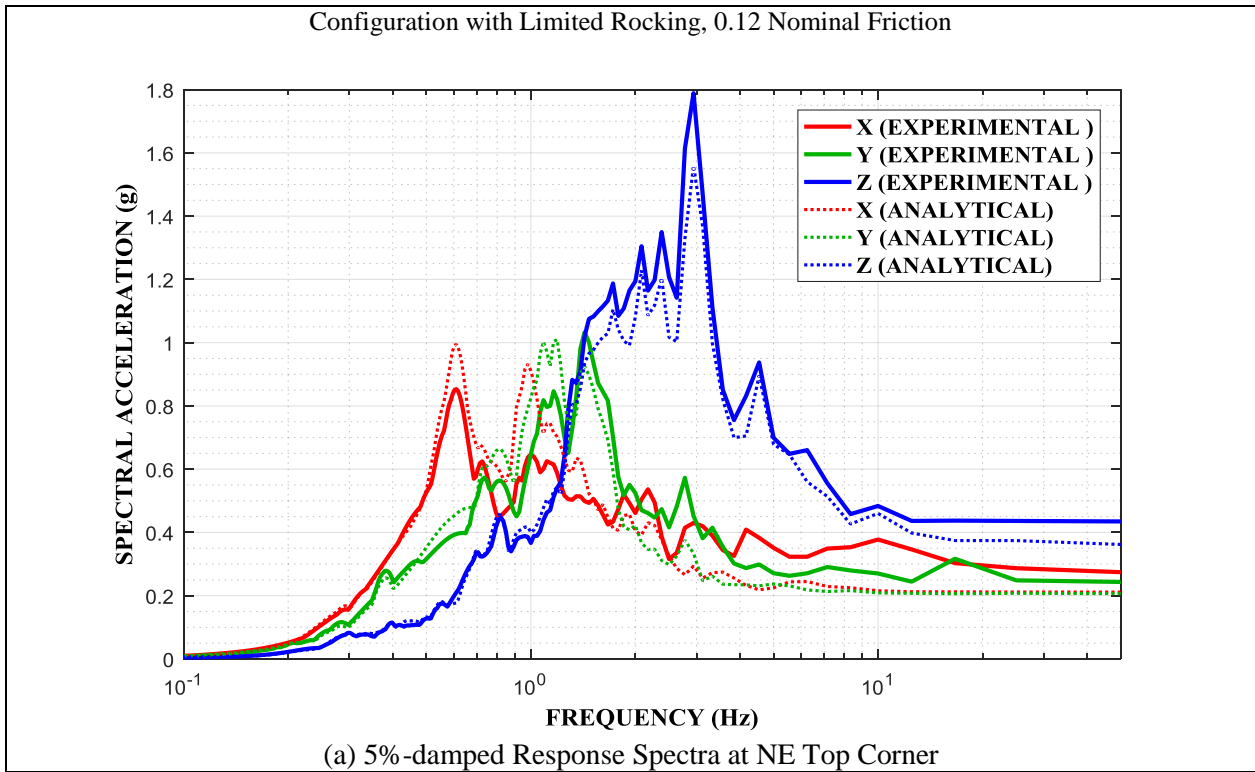


Figure 5-33 Comparison of Experimental and Analytical Results for Configuration of Limited Rocking, FP Isolator Type B with 0.12 Nominal Friction in Taft 400% Motion: (a) 5%-damped Response Spectra at Frame NE Top Corner, (b) Acceleration Histories at Frame NE Top Corner

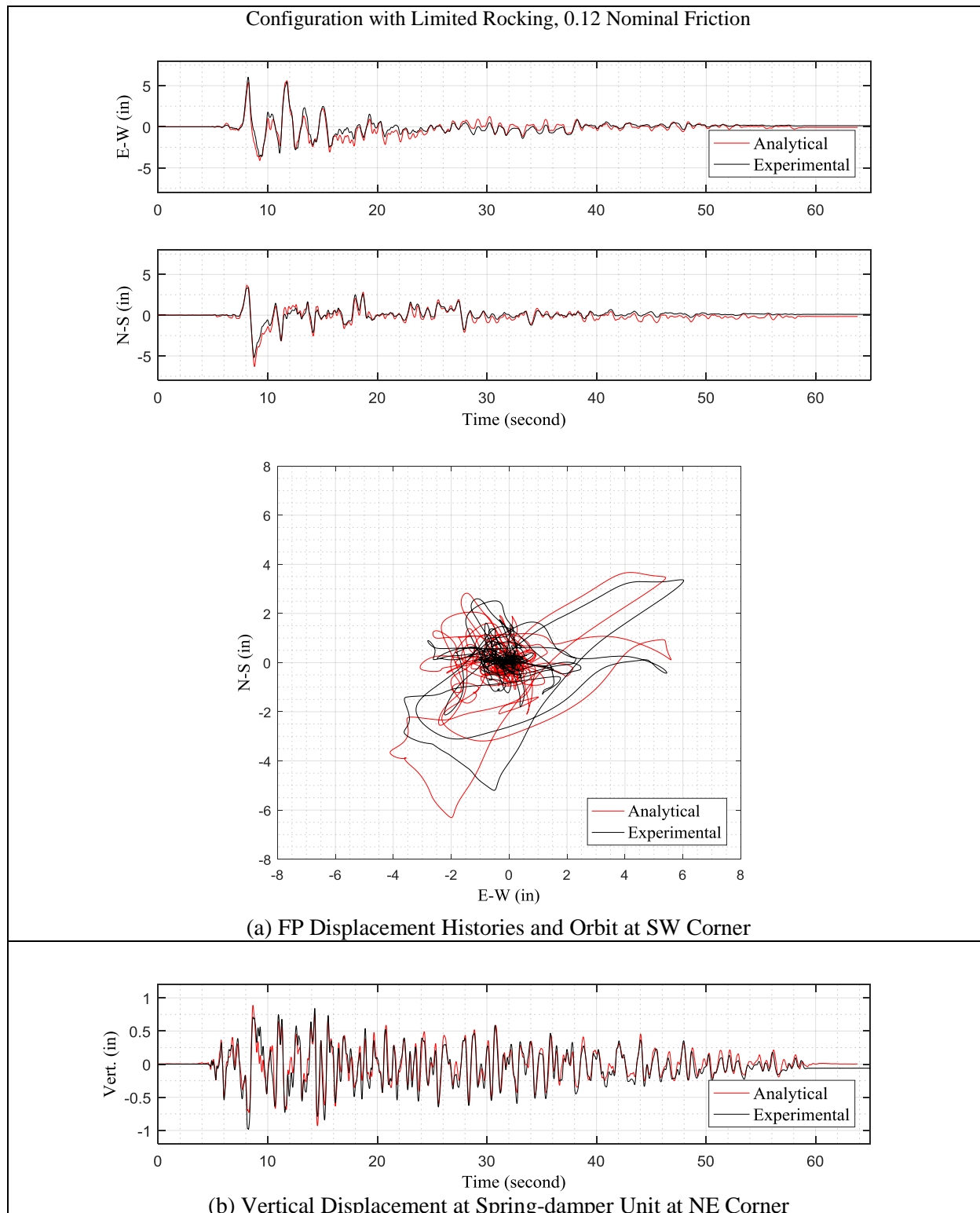


Figure 5-34 Comparison of Experimental and Analytical Results for Configuration of Limited Rocking, FP Isolator Type B with 0.12 Nominal Friction in Taft 400% Motion: (a) FP Displacement Histories and Orbit at SW Corner, (b) Vertical Displacement at Spring-damper Unit at NE Corner

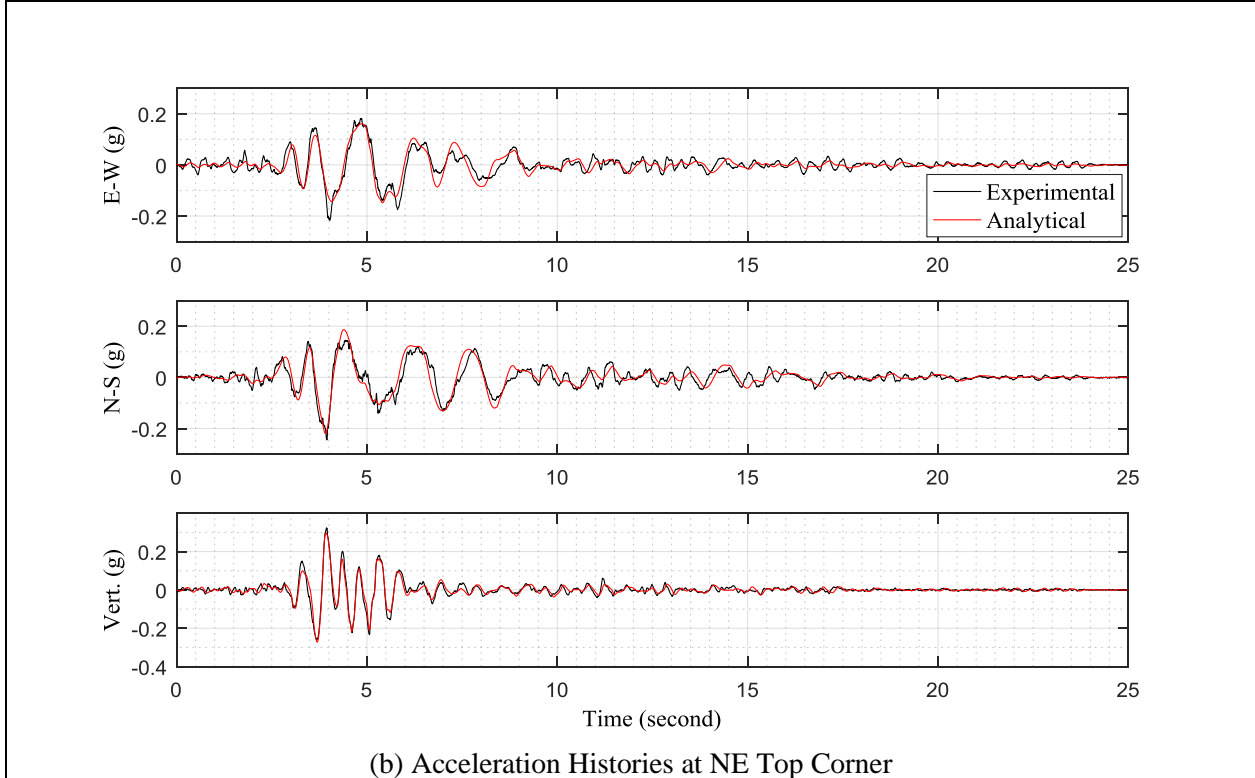
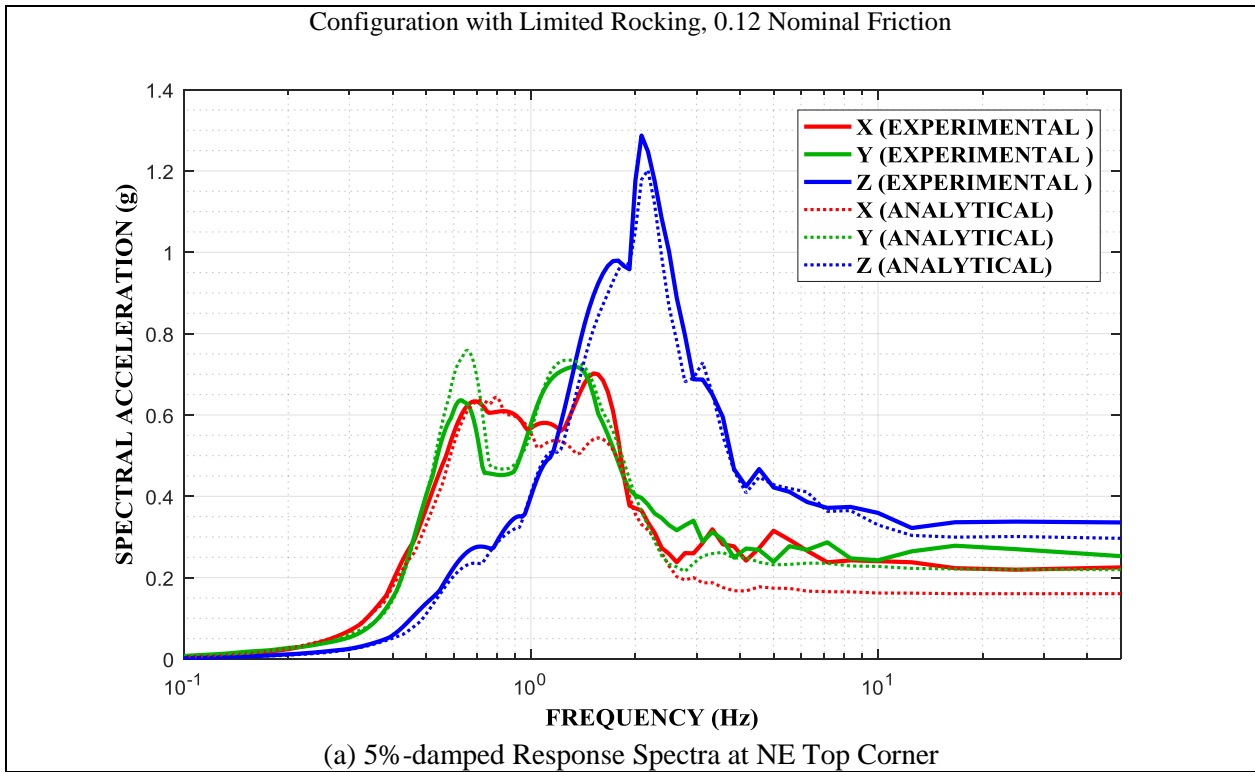


Figure 5-35 Comparison of Experimental and Analytical Results for Configuration of Limited Rocking, FP Isolator Type B with 0.12 Nominal Friction in Kobe 65% Motion: (a) 5%-damped Response Spectra at Frame NE Top Corner, (b) Acceleration Histories at Frame NE Top Corner

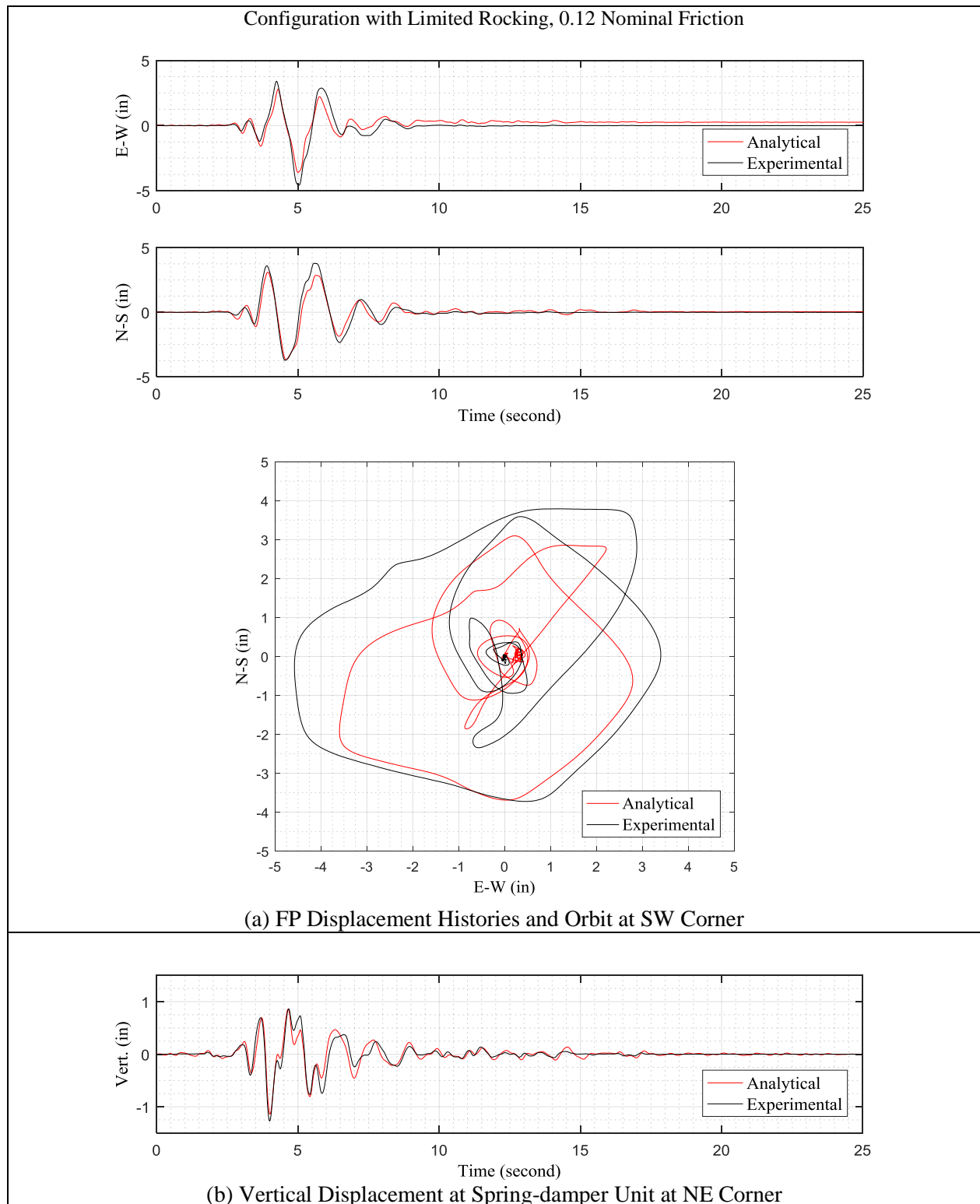


Figure 5-36 Comparison of Experimental and Analytical Results for Configuration of Limited Rocking, FP Isolator Type B with 0.12 Nominal Friction in Kobe 65% Motion: (a) FP Displacement Histories and Orbit at SW Corner, (b) Vertical Displacement at Spring-damper Unit at NE Corner

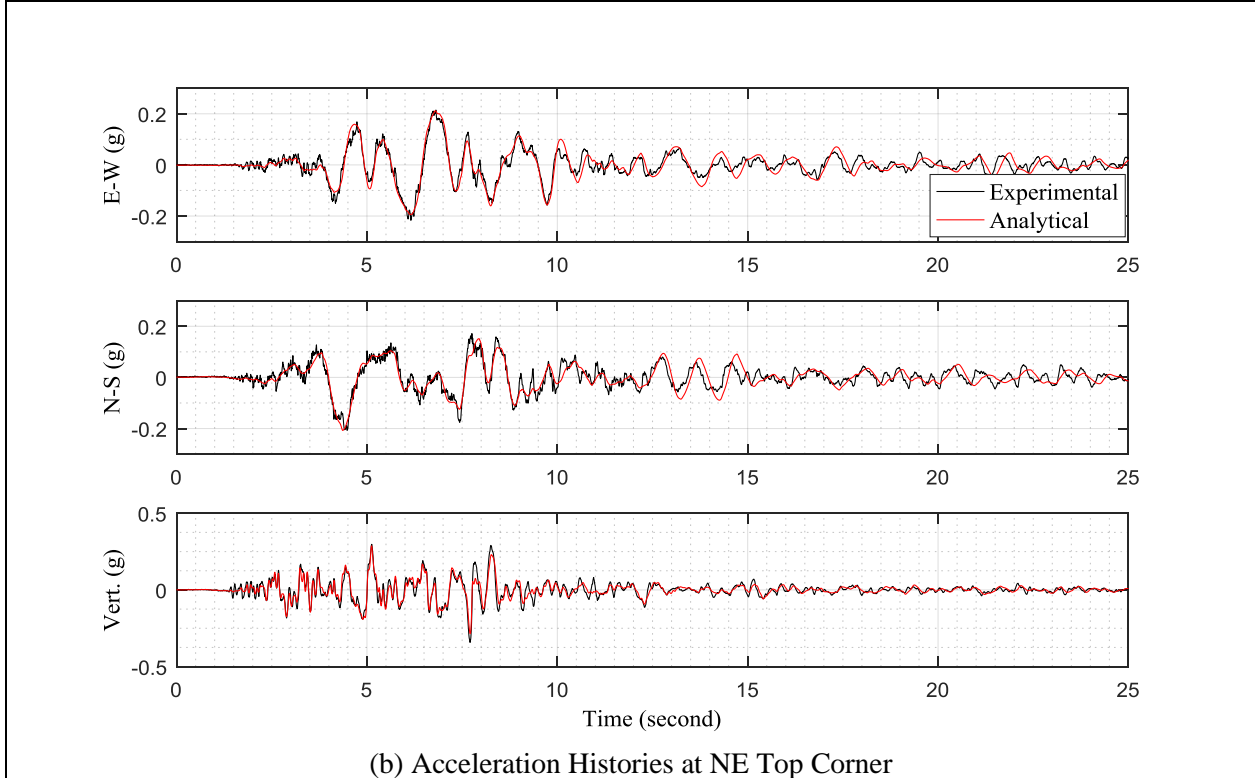
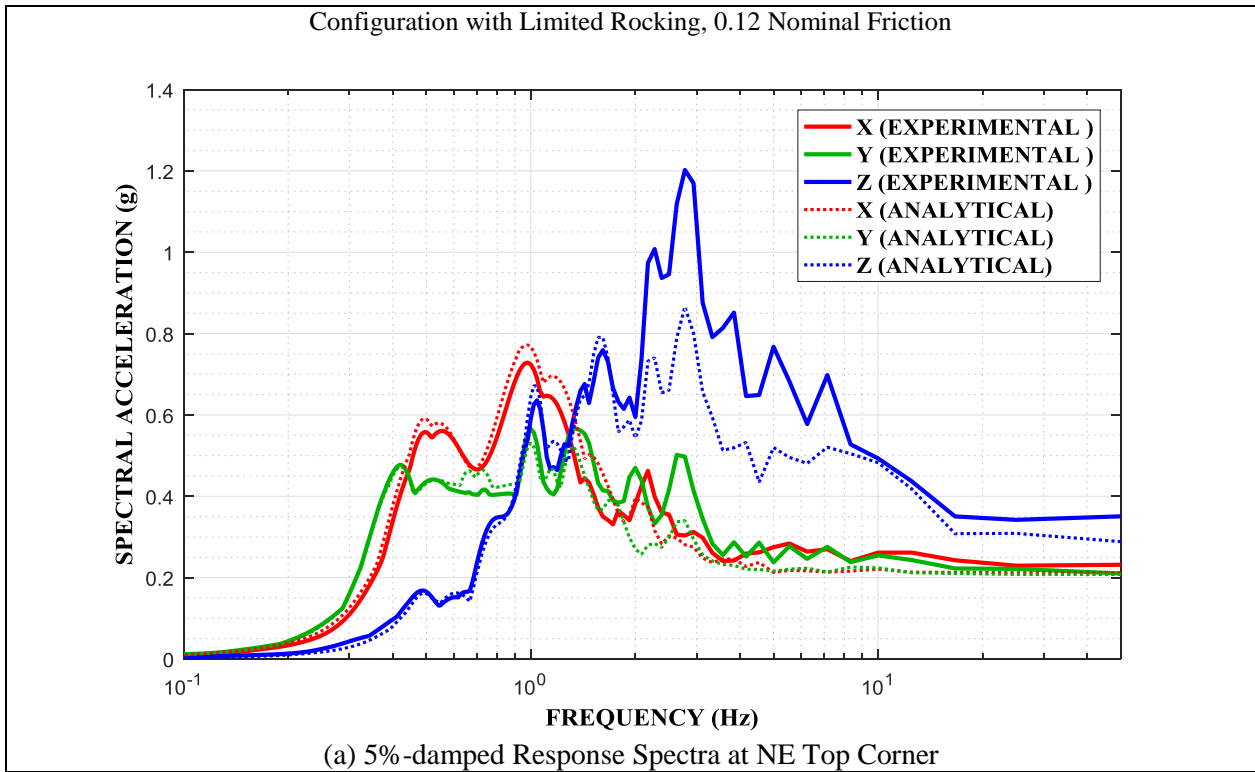


Figure 5-37 Comparison of Experimental and Analytical Results for Configuration of Limited Rocking, FP Isolator Type B with 0.12 Nominal Friction in Jensen 85% Motion: (a) 5%-damped Response Spectra at Frame NE Top Corner, (b) Acceleration Histories at Frame NE Top Corner

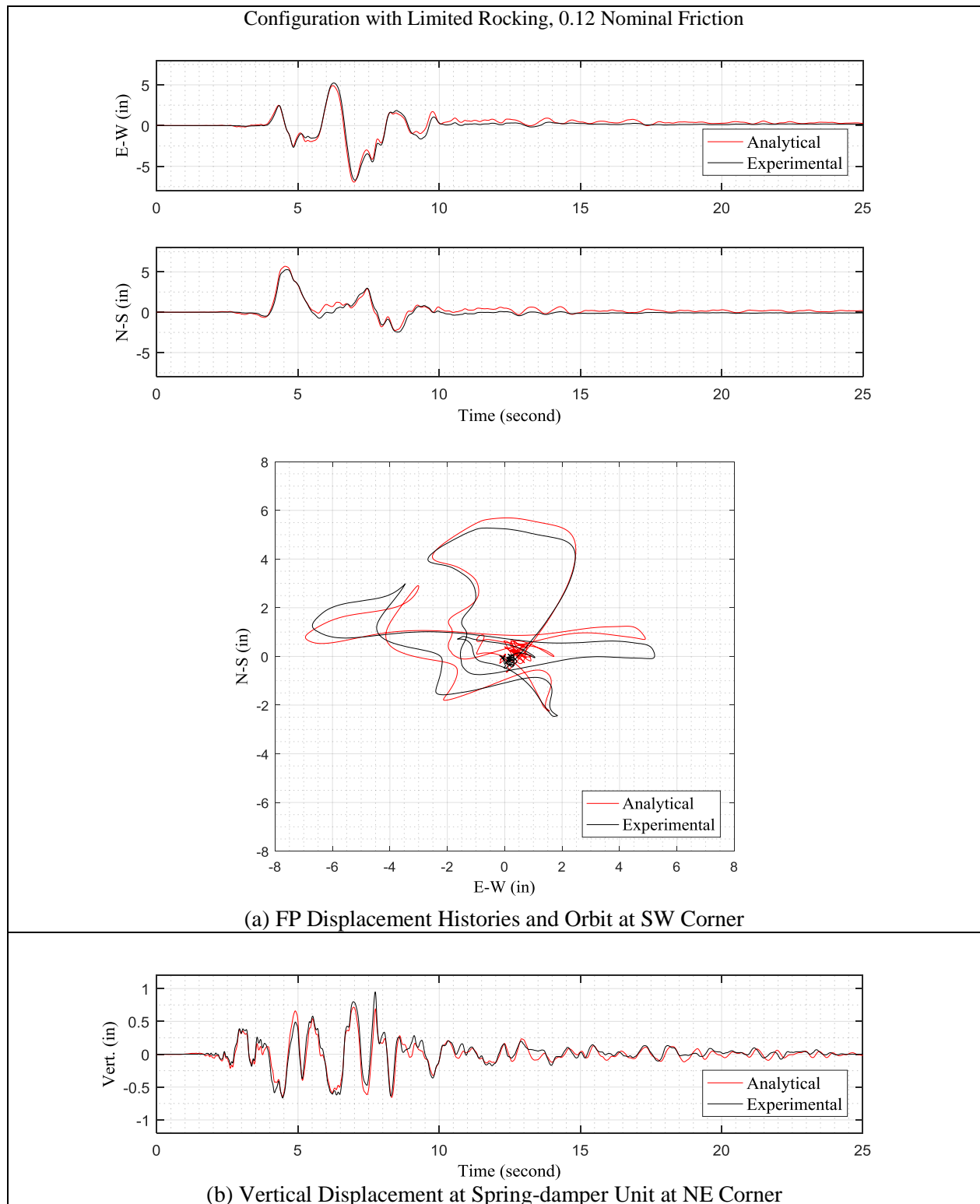


Figure 5-38 Comparison of Experimental and Analytical Results for Configuration of Limited Rocking, FP Isolator Type B with 0.12 Nominal Friction in Jensen 85% Motion: (a) FP Displacement Histories and Orbit at SW Corner, (b) Vertical Displacement at Spring-damper Unit at NE Corner

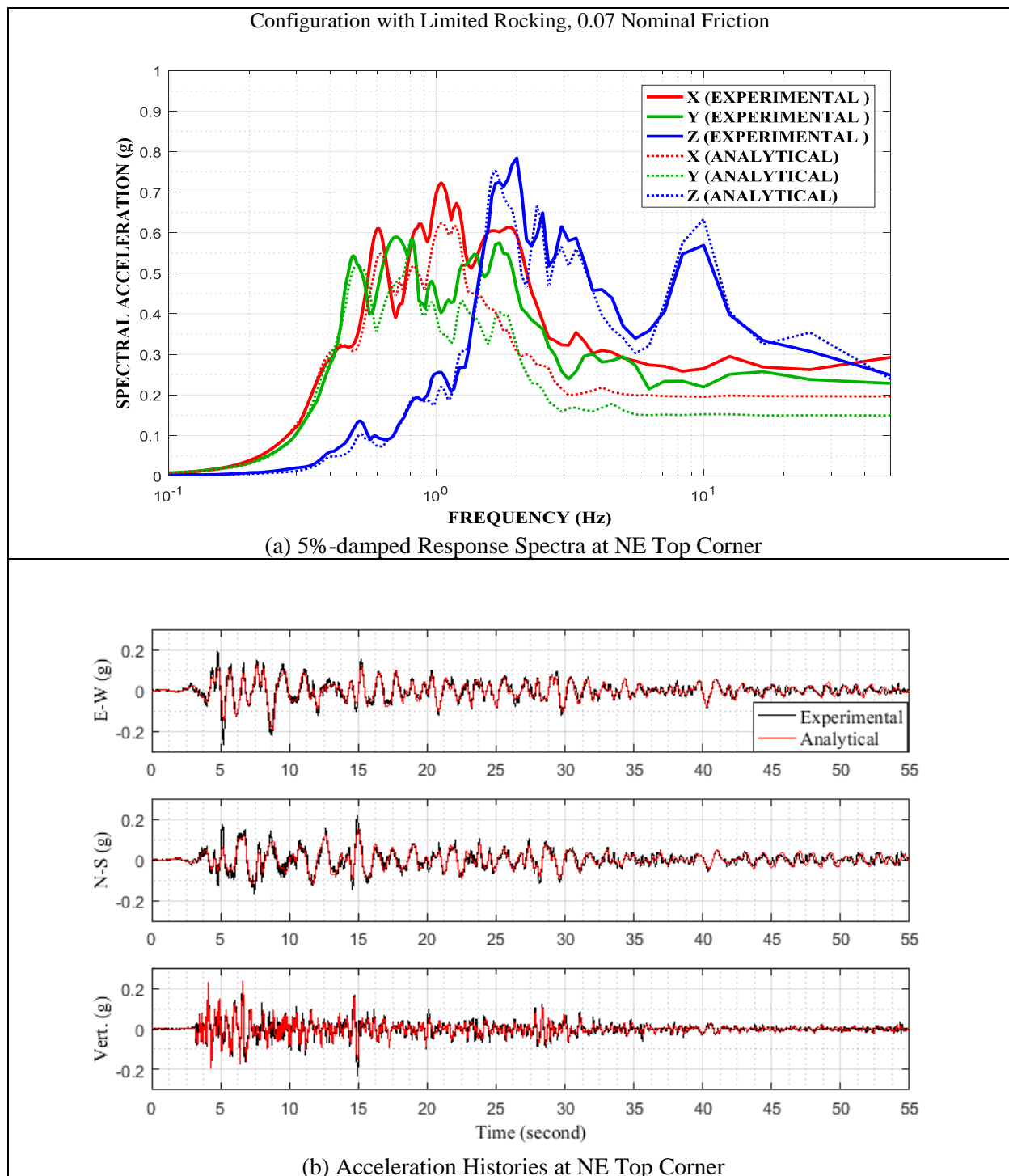


Figure 5-39 Comparison of Experimental and Analytical Results for Configuration of Limited Rocking, FP Isolator Type A with 0.07 Nominal Friction in El Centro 250% Motion: (a) 5%-damped Response Spectra at Frame NE Top Corner, (b) Acceleration Histories at Frame NE Top Corner

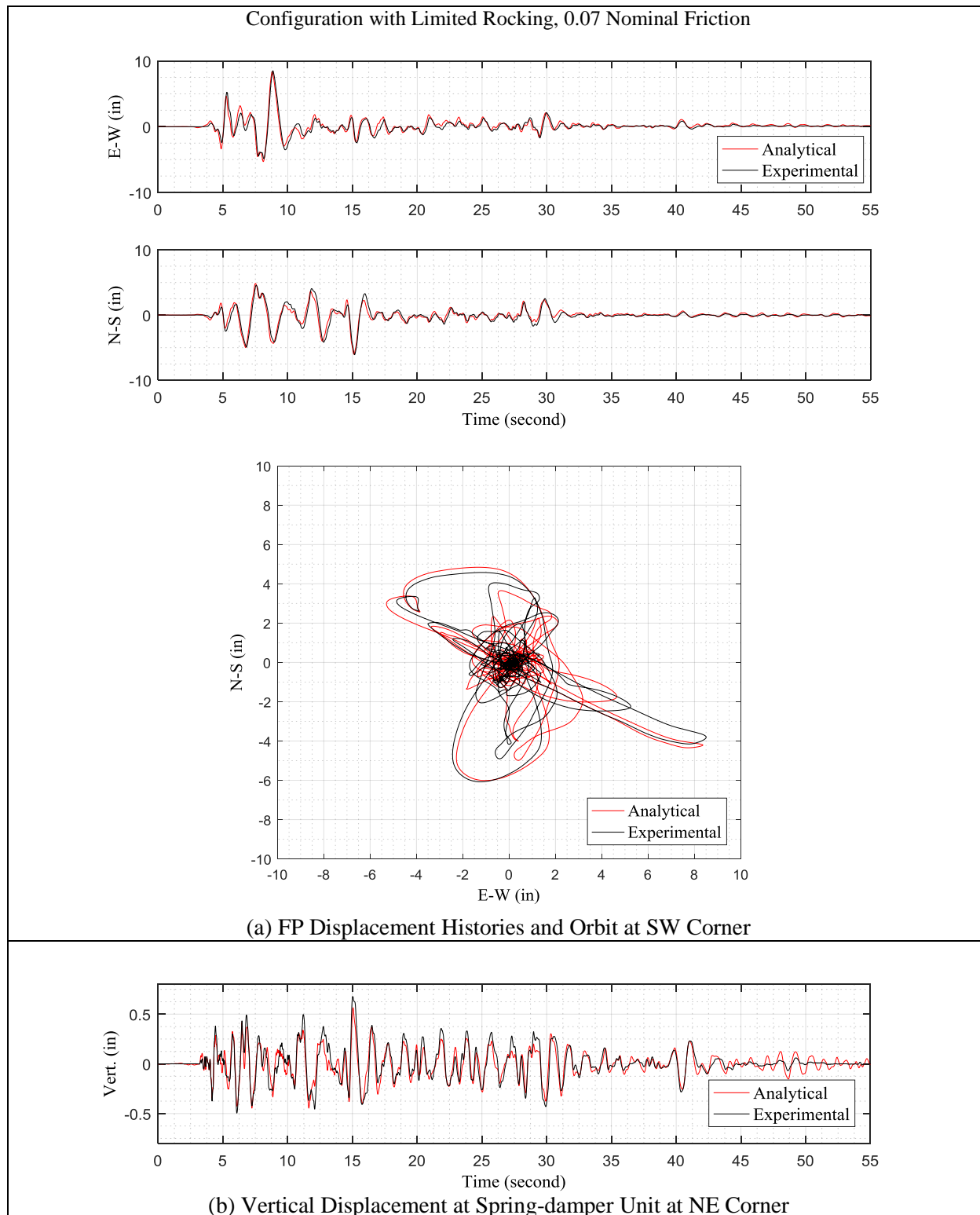


Figure 5-40 Comparison of Experimental and Analytical Results for Configuration of Limited Rocking, FP Isolator Type A with 0.07 Nominal Friction in El Centro 250% Motion: (a) FP Displacement Histories and Orbit at SW Corner, (b) Vertical Displacement at Spring-damper Unit at NE Corner

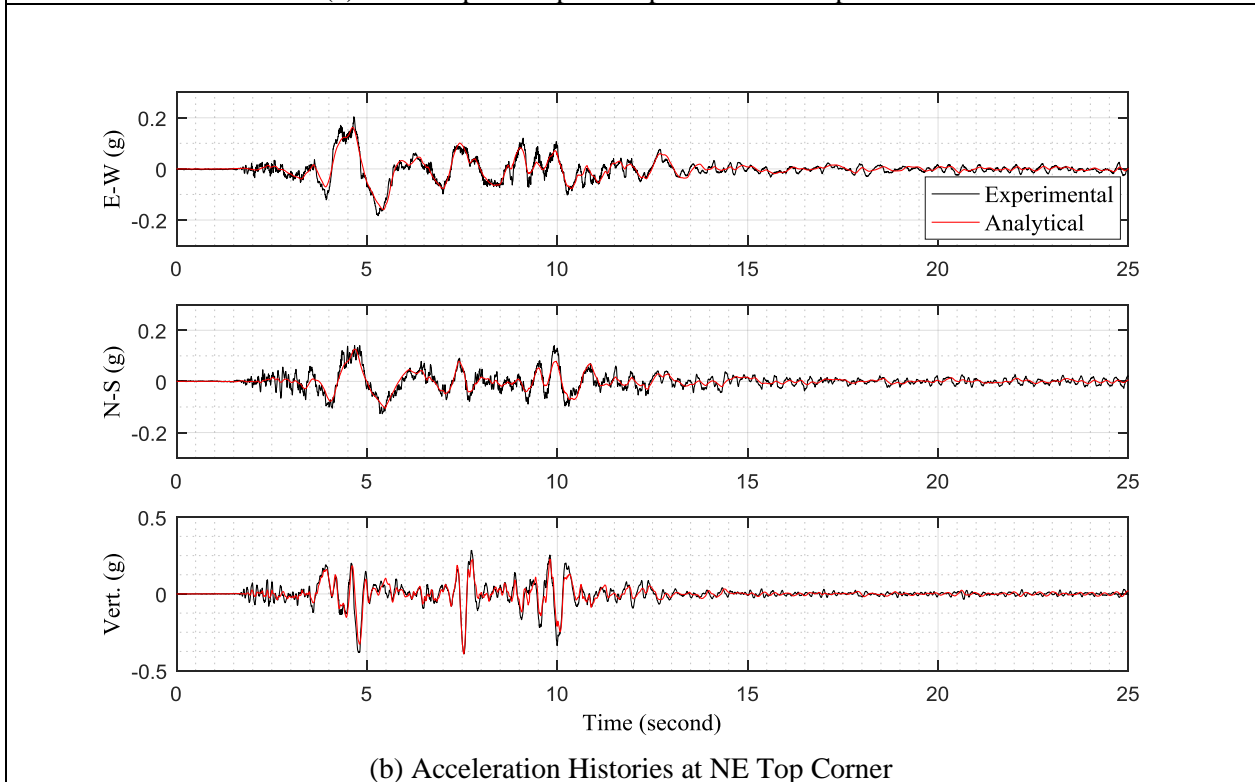
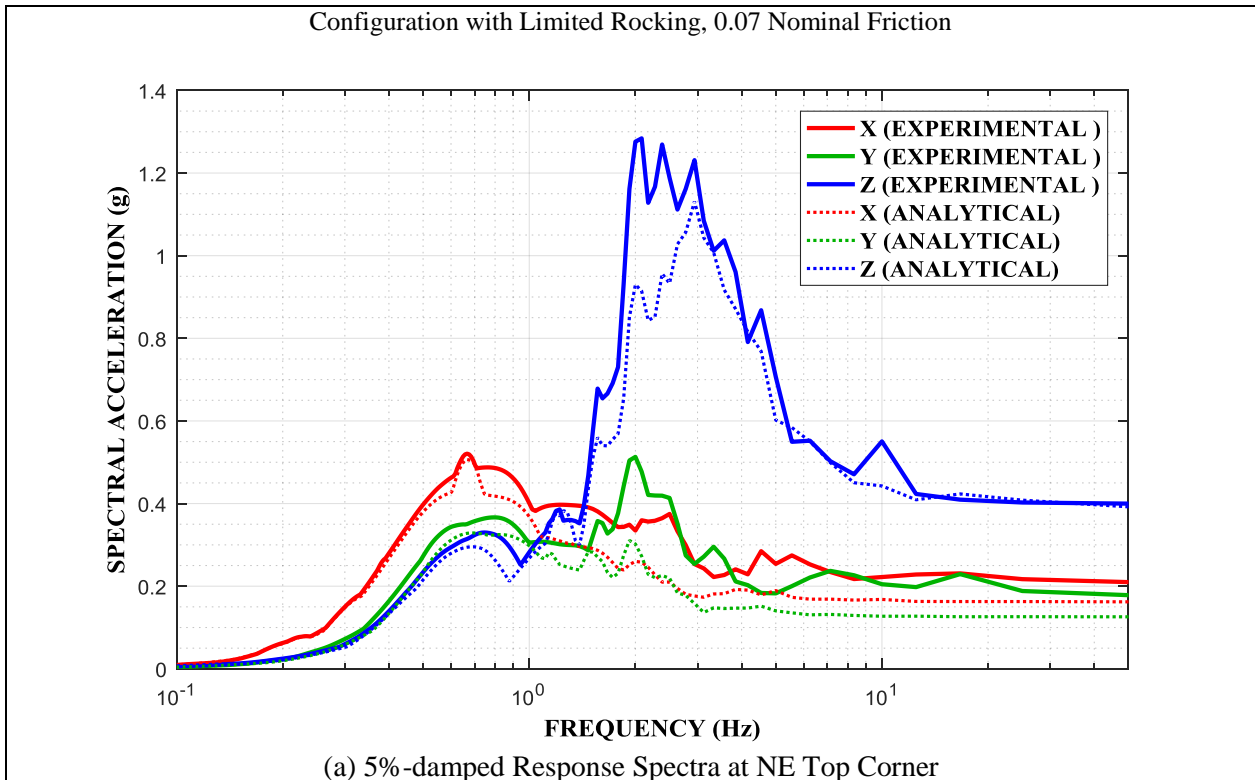


Figure 5-41 Comparison of Experimental and Analytical Results for Configuration of Limited Rocking, FP Isolator Type A with 0.07 Nominal Friction in Pacoima 65% Motion: (a) 5%-damped Response Spectra at Frame NE Top Corner, (b) Acceleration Histories at Frame NE Top Corner

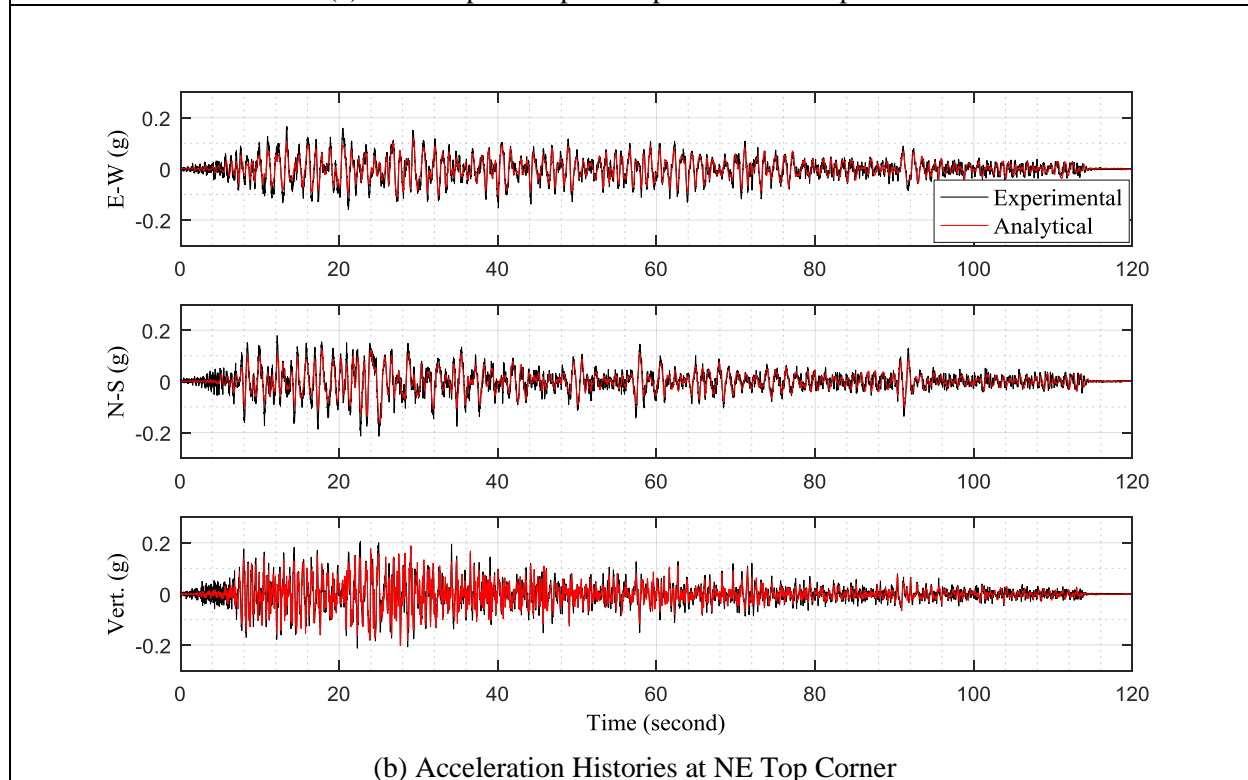
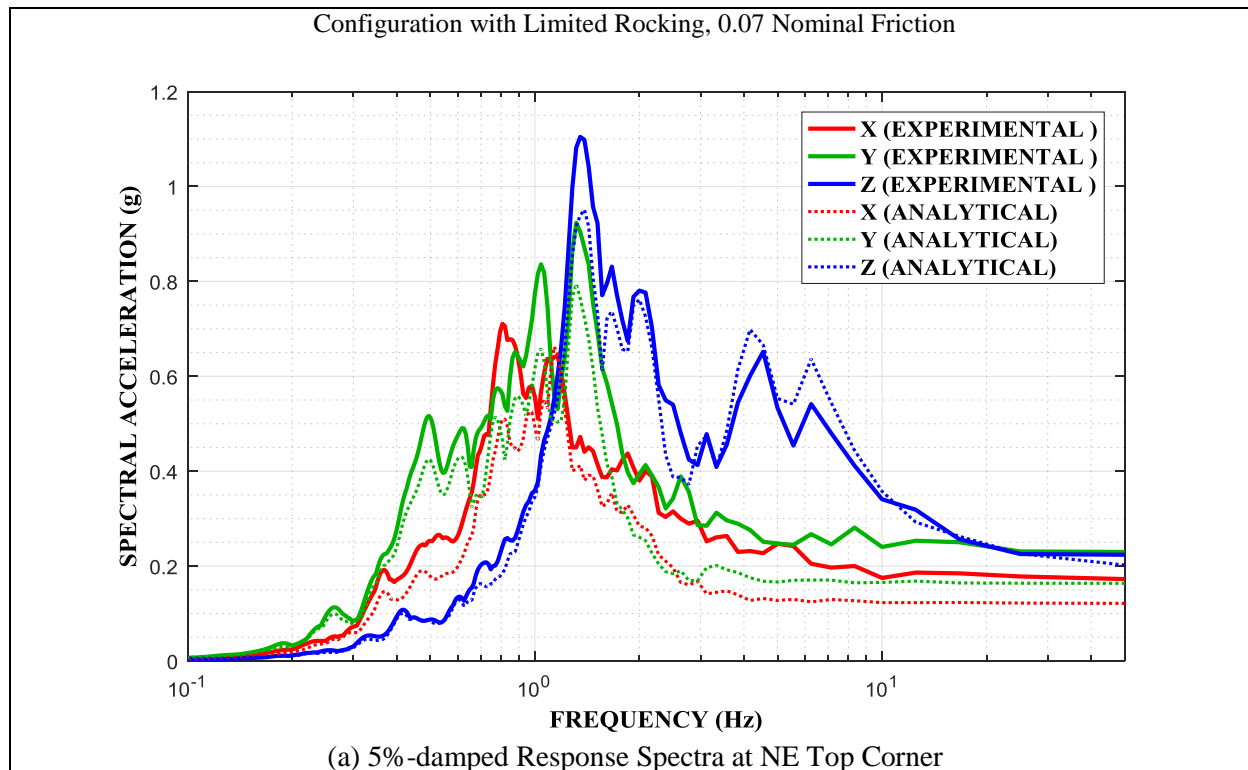


Figure 5-43 Comparison of Experimental and Analytical Results for Configuration of Limited Rocking, FP Isolator Type A with 0.07 Nominal Friction in Chile 100% Motion: (a) 5%-damped Response Spectra at Frame NE Top Corner, (b) Acceleration Histories at Frame NE Top Corner

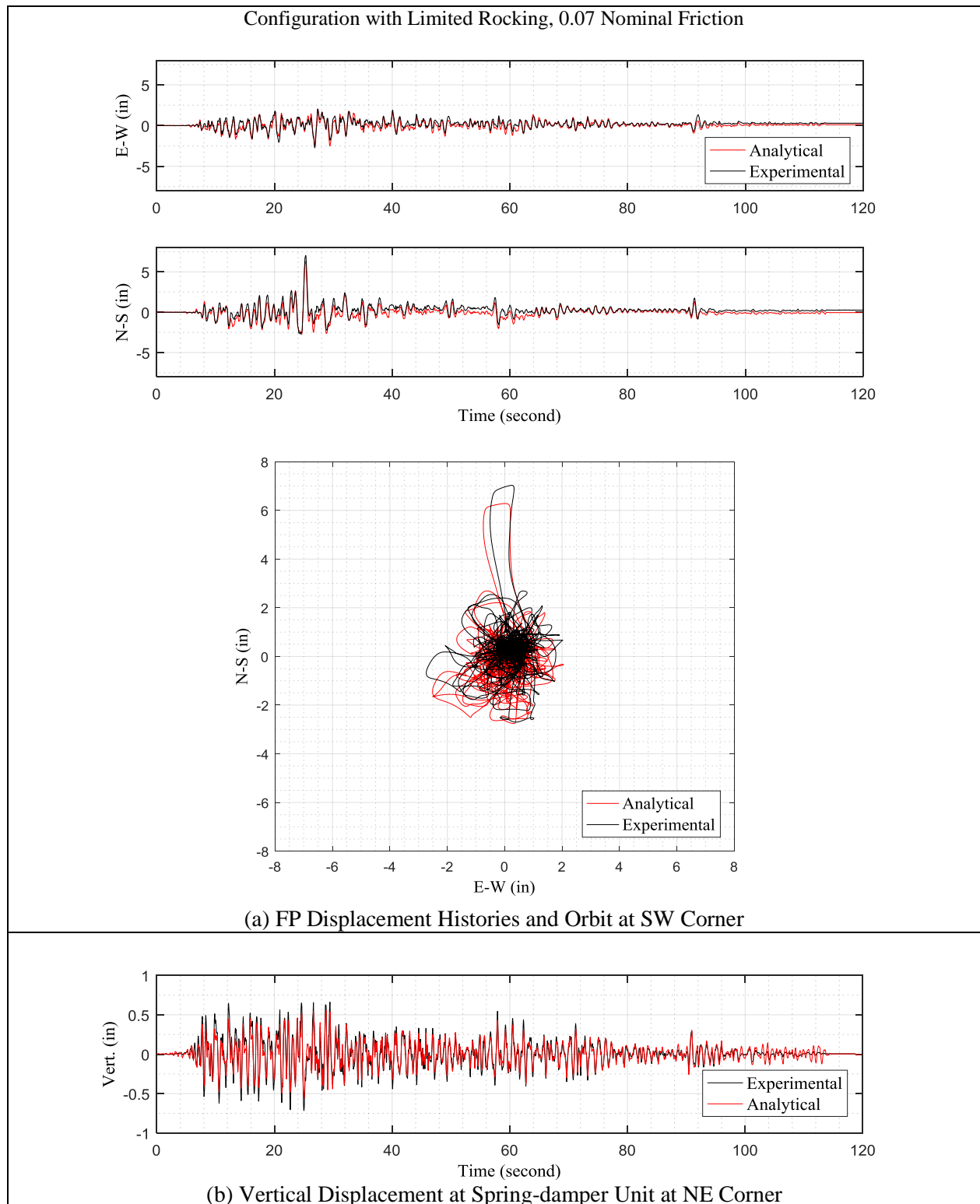


Figure 5-44 Comparison of Experimental and Analytical Results for Configuration of Limited Rocking, FP Isolator Type A with 0.07 Nominal Friction in Chile 100% Motion: (a) FP Displacement Histories and Orbit at SW Corner, (b) Vertical Displacement at Spring-damper Unit at NE Corner

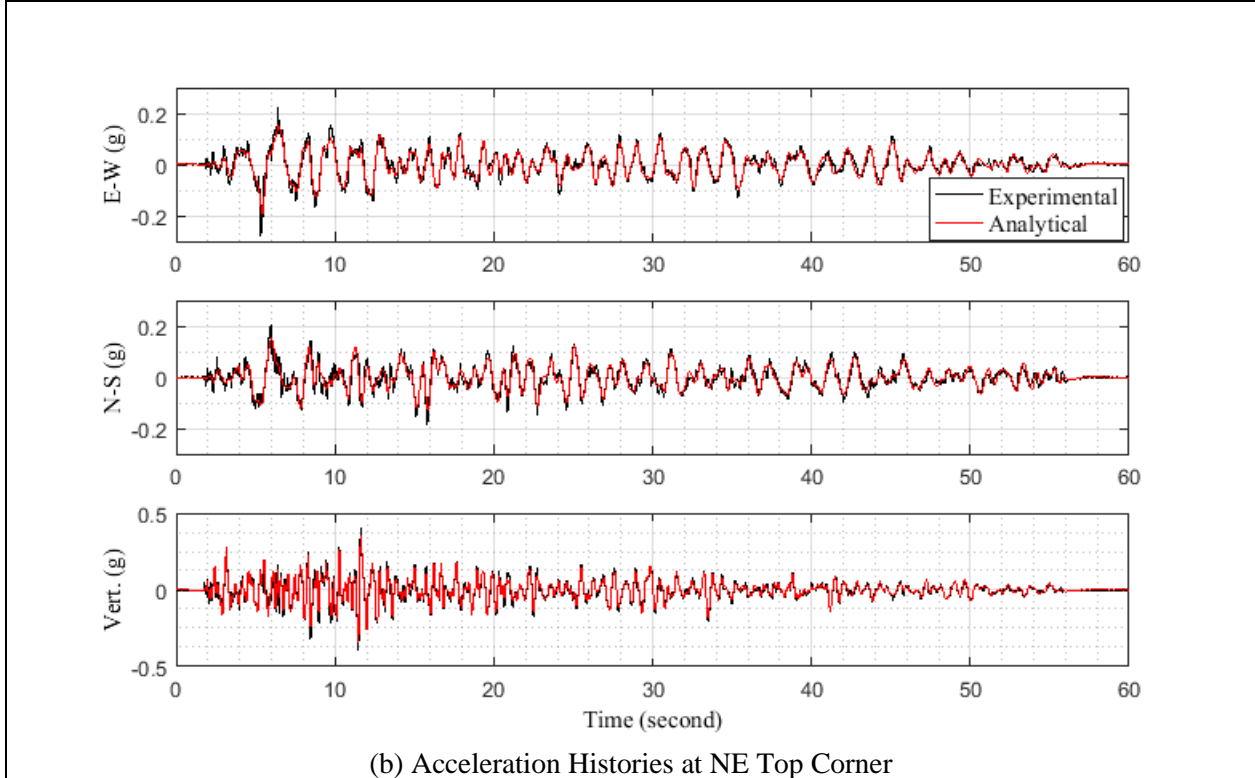
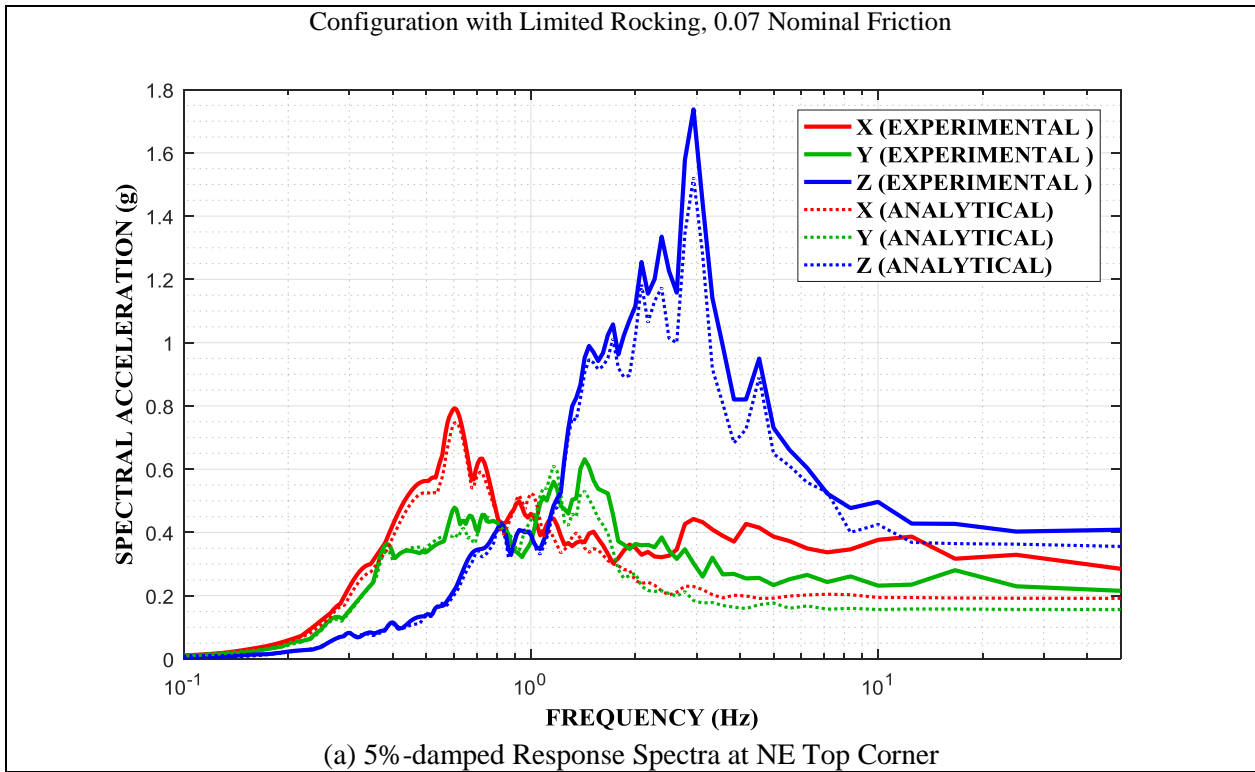


Figure 5-45 Comparison of Experimental and Analytical Results for Configuration of Limited Rocking, FP Isolator Type A with 0.07 Nominal Friction in Taft 400% Motion: (a) 5%-damped Response Spectra at Frame NE Top Corner, (b) Acceleration Histories at Frame NE Top Corner

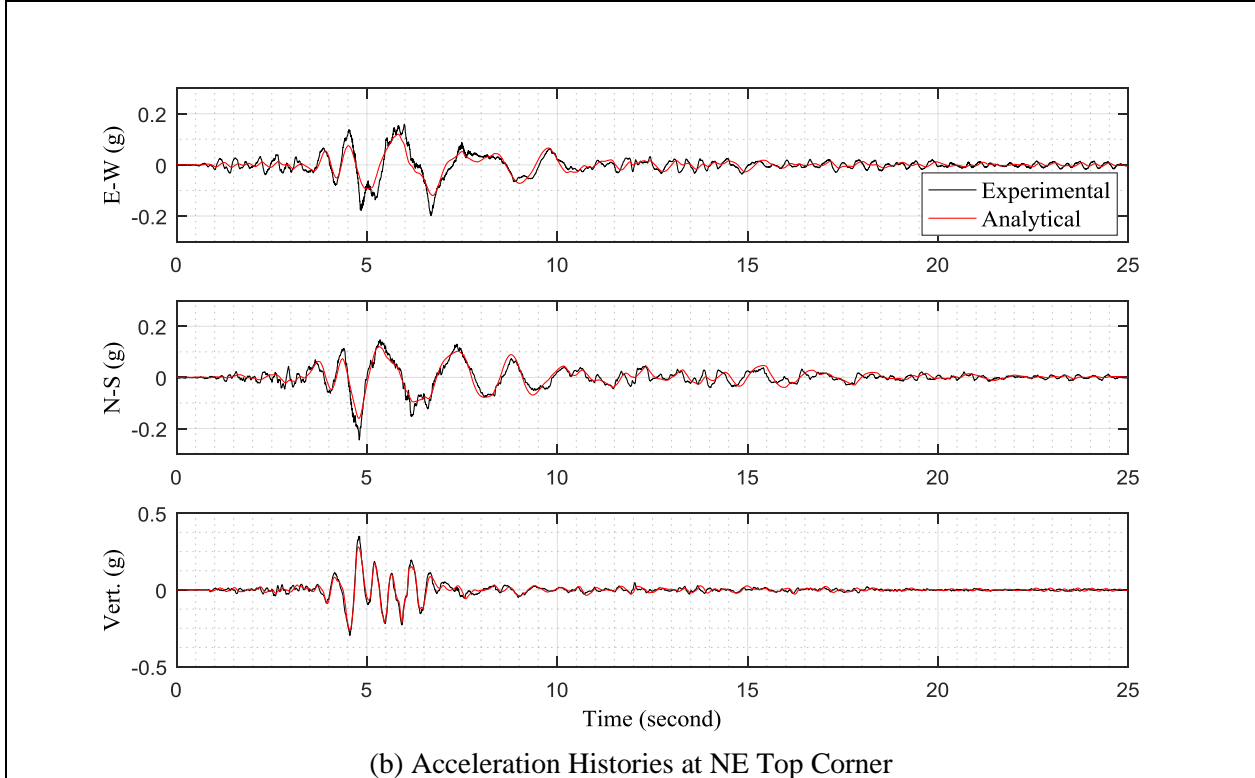
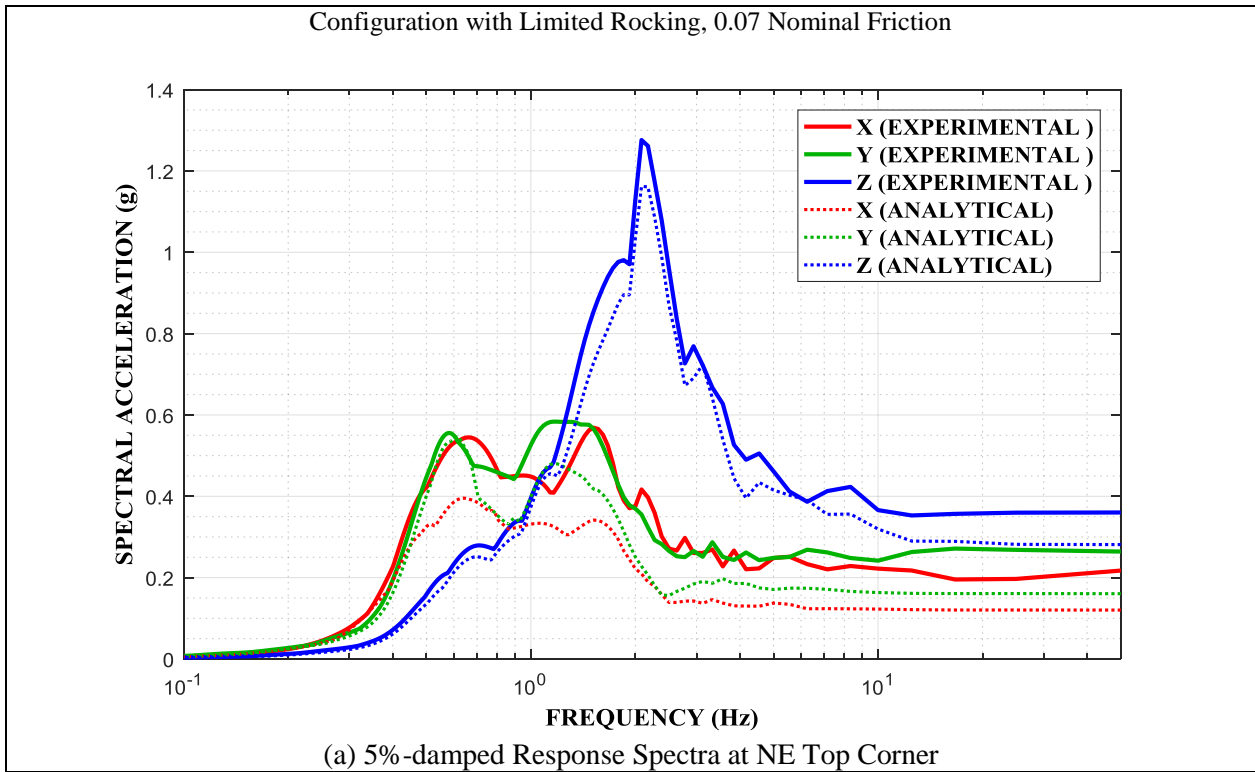


Figure 5-47 Comparison of Experimental and Analytical Results for Configuration of Limited Rocking, FP Isolator Type A with 0.07 Nominal Friction in Kobe 65% Motion: (a) 5%-damped Response Spectra at Frame NE Top Corner, (b) Acceleration Histories at Frame NE Top Corner

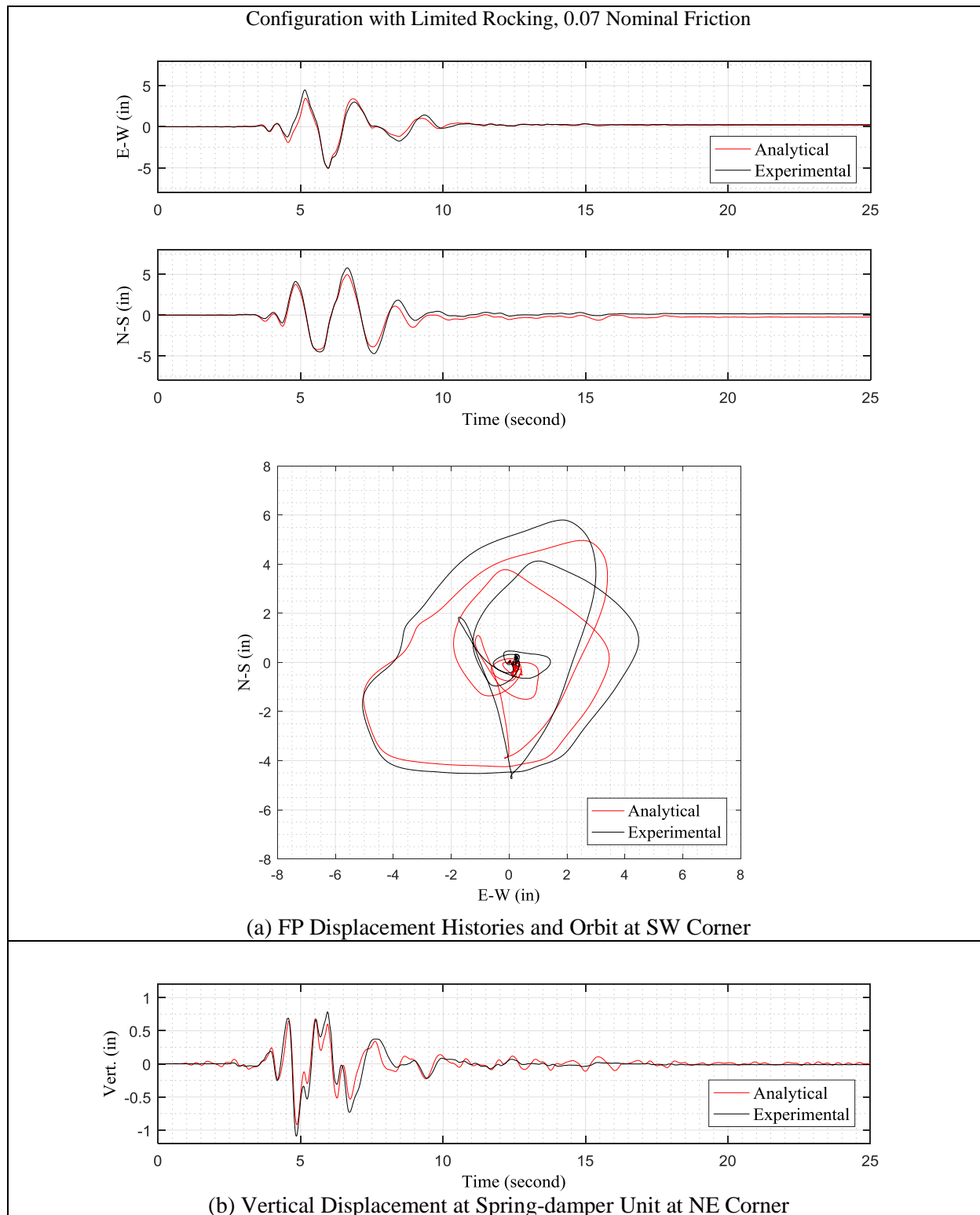


Figure 5-48 Comparison of Experimental and Analytical Results for Configuration of Limited Rocking, FP Isolator Type A with 0.07 Nominal Friction in Kobe 65% Motion: (a) FP Displacement Histories and Orbit at SW Corner, (b) Vertical Displacement at Spring-damper Unit at NE Corner

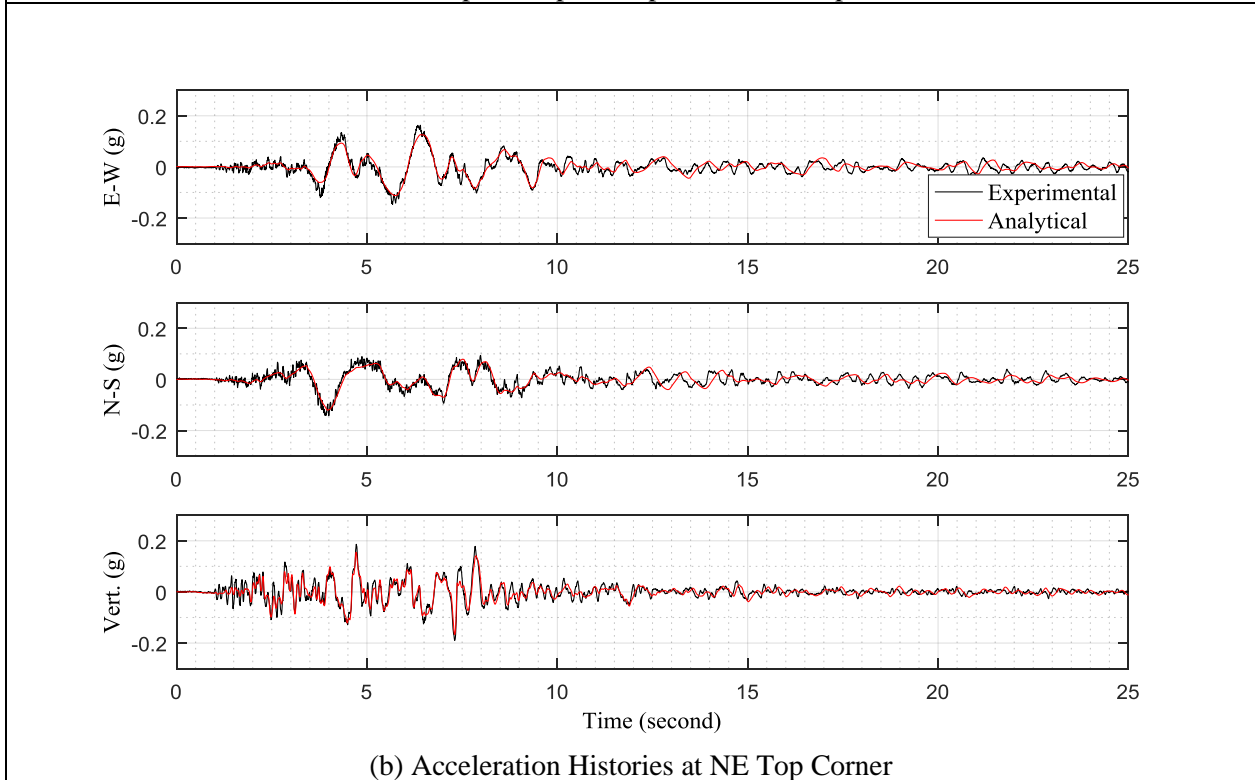
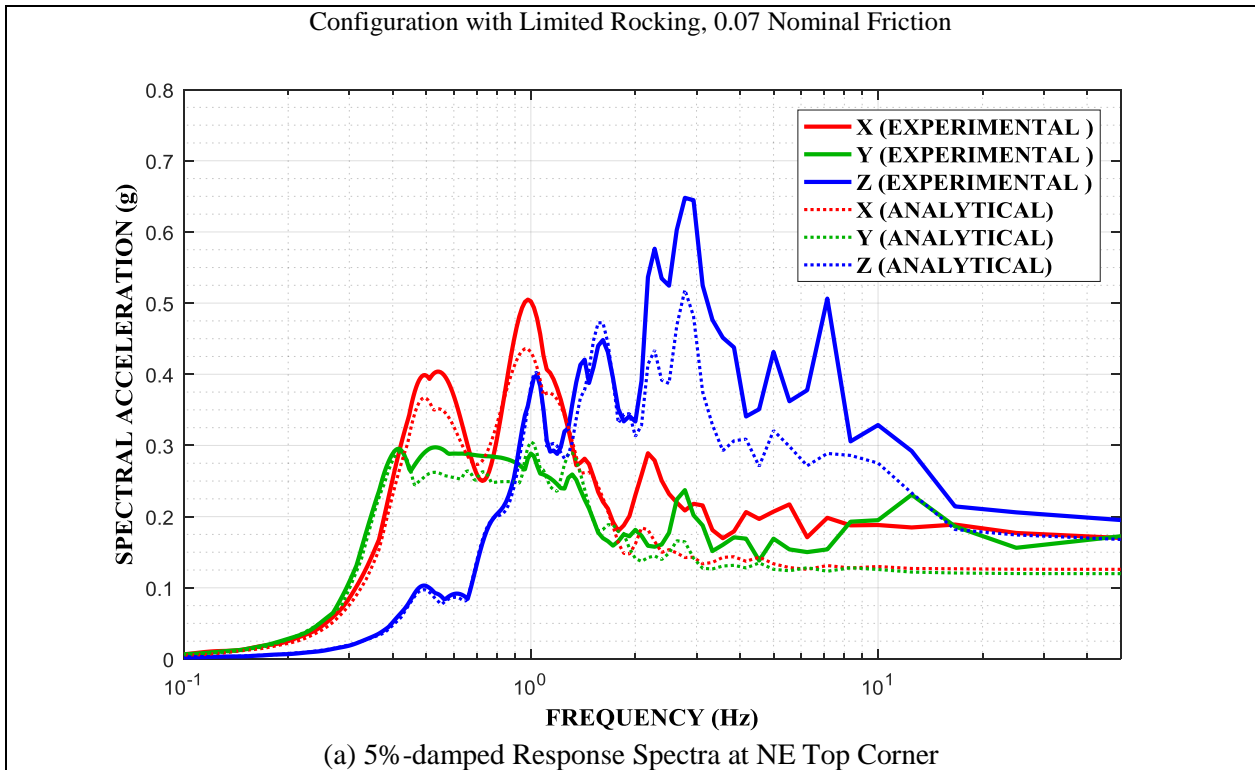


Figure 5-49 Comparison of Experimental and Analytical Results for Configuration of Limited Rocking, FP Isolator Type A with 0.07 Nominal Friction in Jensen 50% Motion: (a) 5%-damped Response Spectra at Frame NE Top Corner, (b) Acceleration Histories at Frame NE Top Corner

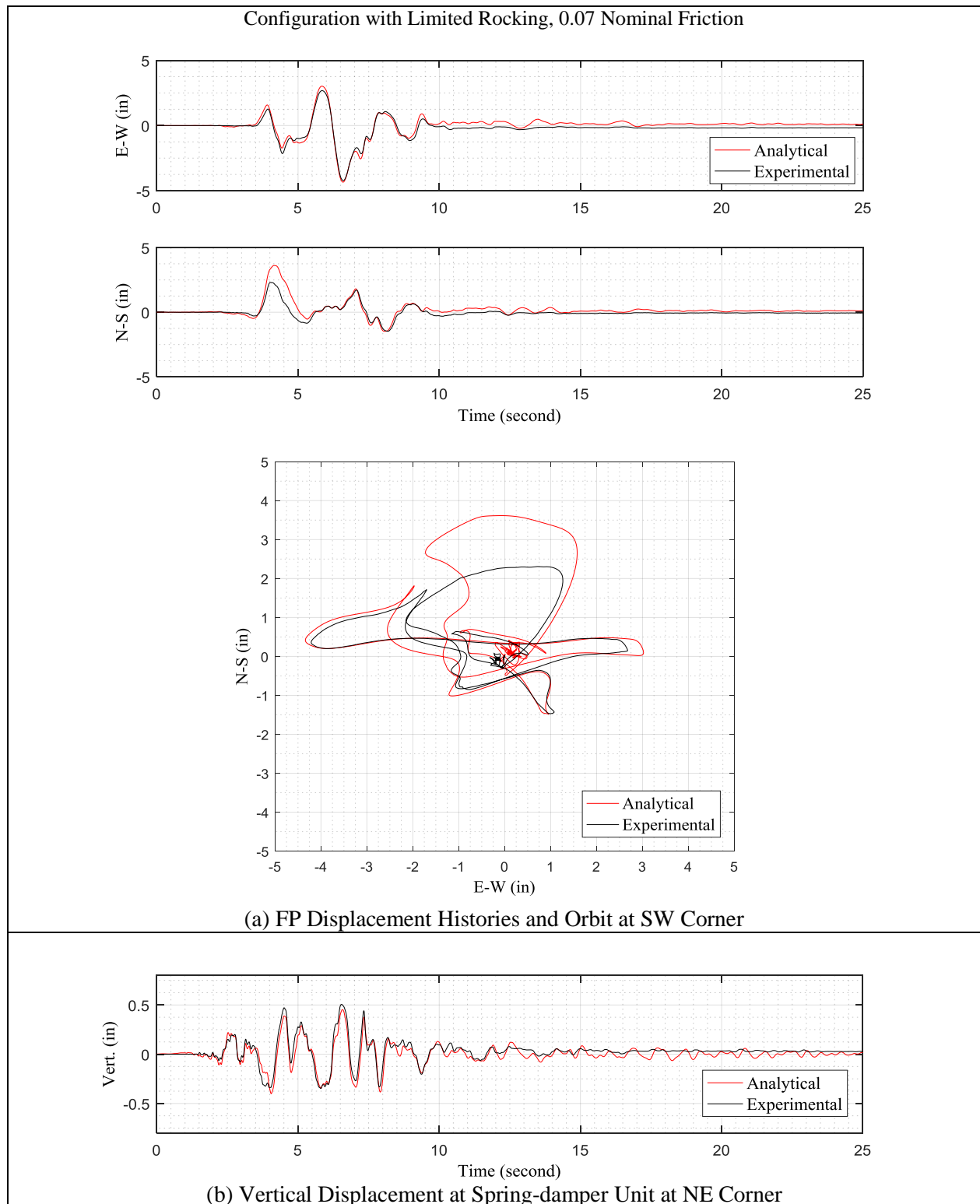


Figure 5-50 Comparison of Experimental and Analytical Results for Configuration of Limited Rocking, FP Isolator Type A with 0.07 Nominal Friction in Jensen 50% Motion: (a) FP Displacement Histories and Orbit at SW Corner, (b) Vertical Displacement at Spring-damper Unit at NE Corner

The comparisons of analytical and experimental responses in Figures 5-5 to 5-50 demonstrate a good capability to predict the experimental response in a relatively complex system exhibiting three-dimensional motion with significant rotations and highly nonlinear behavior. Specifically, it appears that the prediction is better in the case of the systems with friction of 0.12 and 0.07 in both tested configurations despite uncertainties in the behavior of the bearings (see Section 3 on behavior of bearing of type B, nominal friction of 0.12 and on bearing type A of nominal friction of 0.07).

5.4 Effect of Rocking Motion of the Shake Table on Prediction of Response

The results in Figure 5-5 to 5-50 do not include the acceleration response of the bushing top of which the response was amplified by comparison to the acceleration of the frame top corner for which comparisons of responses were presented. Figure 5-51 compares the experimental acceleration histories at the bushing top and at the frame NE top corner in the horizontal EW and the vertical direction in the test with El Centro 250% motion for the configuration of free rocking and FP isolator type B with 0.12 nominal friction. The recorded accelerations at the bushing top are significantly larger than the accelerations recorded at the frame top. The magnification is apparently caused by the flexibility of the bushing supporting plate given that the motion at the bushing top contains dominant frequencies of about 10Hz in the horizontal direction and 13Hz in the vertical direction, which are the as-installed frequencies of the bushing in the horizontal and vertical directions, respectively (see Figure 3-26).

Moreover, the response of the bushing was affected by the shake table rocking motion which also contained high frequencies of the order of the as-installed frequencies of the bushing. The effect of rocking shake table motion is revealed in comparisons of experimental and analytical results of the bushing top acceleration history in analyses in which the shake table input is neglected and then considered. Figures 5-52 to 5-63 present these comparisons for several cases of configurations with free rocking and limited rocking and FP isolators type B with 0.12 nominal friction. The shake table rocking motion was determined by using the difference in vertical acceleration records of accelerometers of “aibsez” and “aibswz” in the E-W axis and

“aibnez” and “aibsez” in the N-S axis, and then dividing by the distance between the instruments (see Figure 3-27). It should be noted that the rocking table motion was calculated from measurements that included some errors (due to lack of rigidity of the shake table extension). These errors introduced parasitic high frequency components at frequencies of 20Hz and larger. Nevertheless, the effect of the table rocking motion on the response of the tested model presented in Figures 5-5 to 5-50 was minor and was not included in the analytical calculation. The results in Figures 5-52 to 5-63 clearly demonstrate that the rocking shake table motion affected the bushing top accelerations and particularly the horizontal acceleration. Regardless, the analytical model with or without the rocking shake table input still under-predicted the bushing top acceleration in some cases and it appears that this is the result of the amount of damping assumed in the analytical model. Based on the identification results of Figure 3-26, the damping ratio in modes associated with the bushing motion was assigned the value of 0.01 (see Table 5-2). The value may have been lower as analyses with lower value of damping produced results closer to the experimental results than those obtained with damping ratio of 0.01.

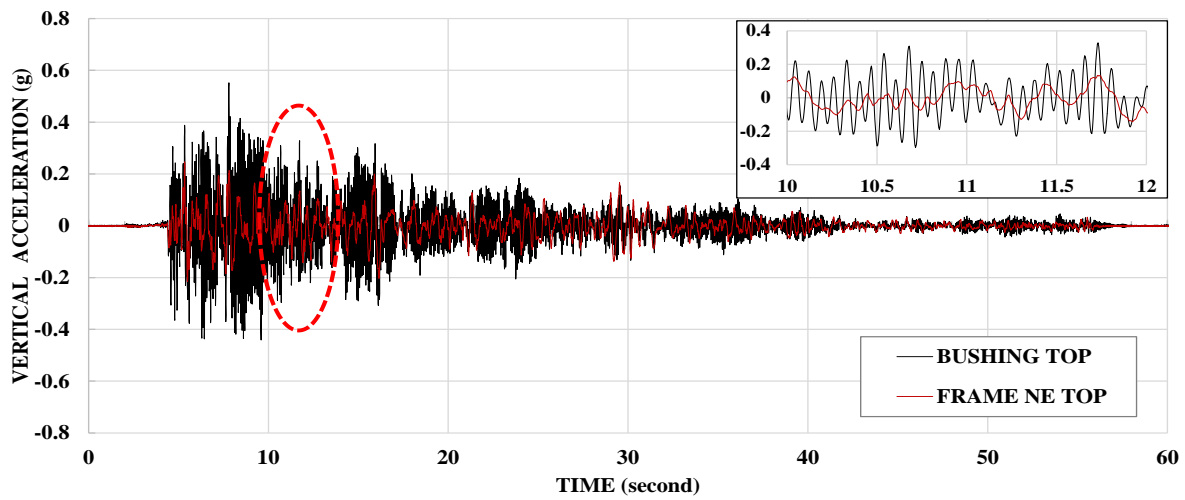
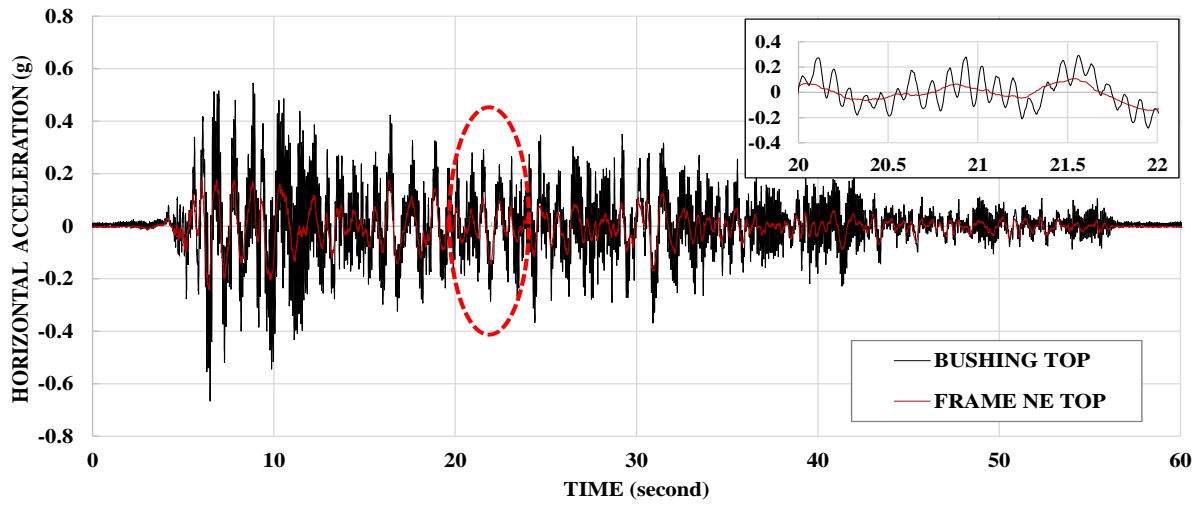


Figure 5-51 Experimental Acceleration Histories at Bushing Top and Frame Top NE Corner in Horizontal EW and Vertical Directions for Configuration of Free Rocking, FP Isolator Type B with 0.12 Nominal Friction in El Centro 250% Motion

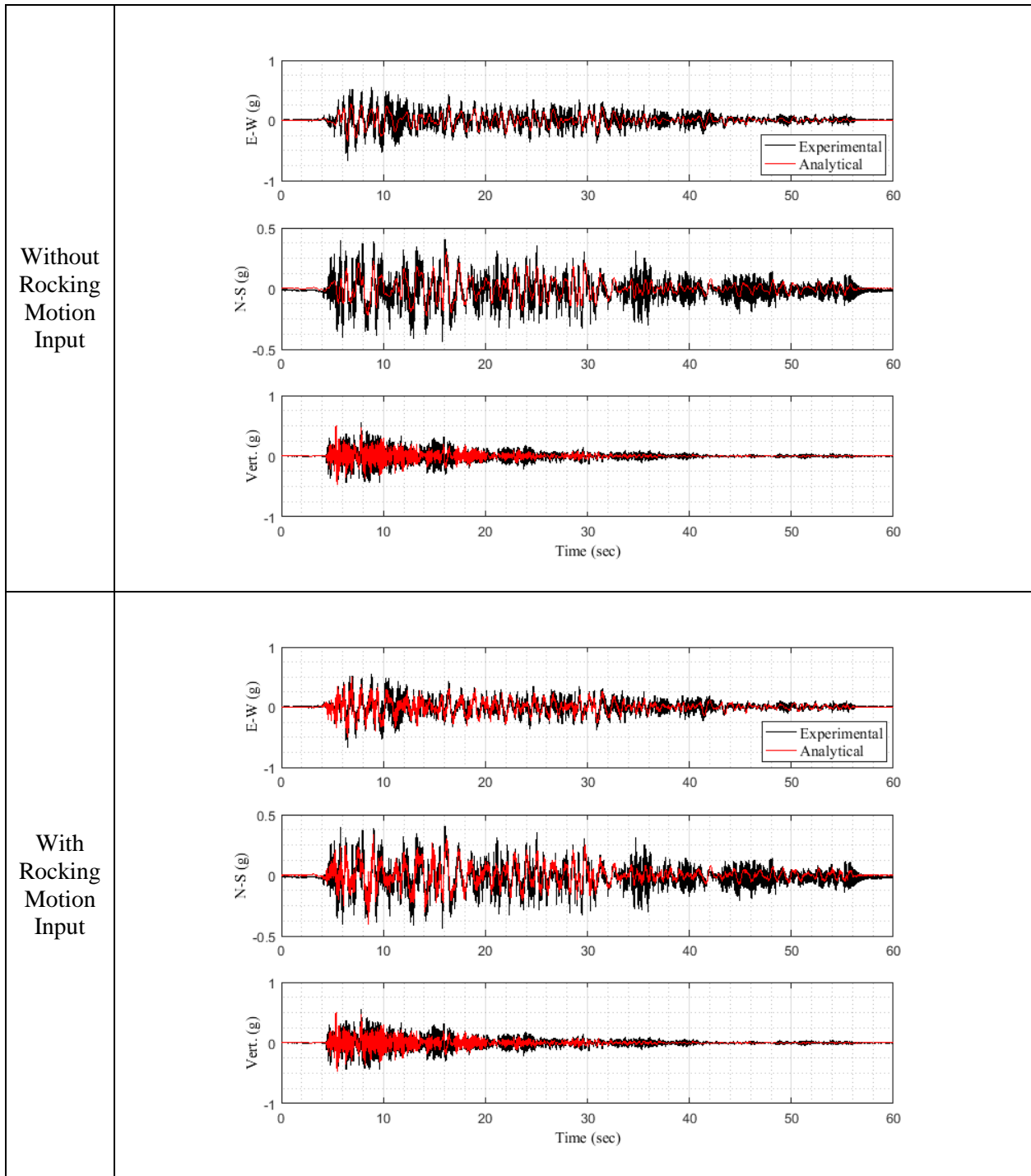


Figure 5-52 Comparison of Experimental and Analytical Results of Acceleration Histories at Bushing Top with and without Consideration of Rocking Shake Table Motion in Configuration of Free Rocking, FP Isolator Type B with 0.12 Nominal Friction in El Centro 250% Motion

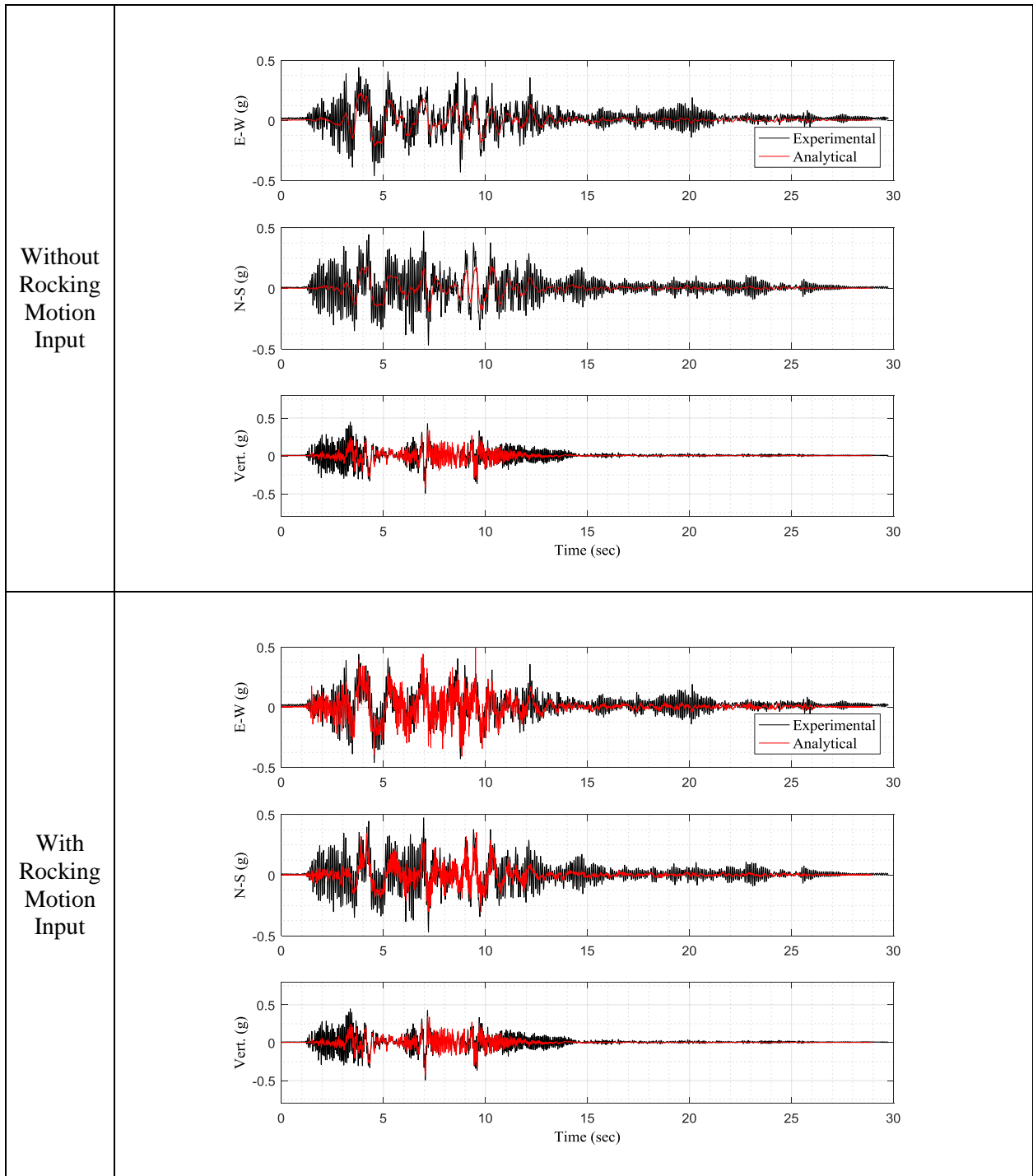


Figure 5-53 Comparison of Experimental and Analytical Results of Acceleration Histories at Bushing Top with and without Consideration of Rocking Shake Table Motion in Configuration of Free Rocking, FP Isolator Type B with 0.12 Nominal Friction in Pacoima 60% Motion

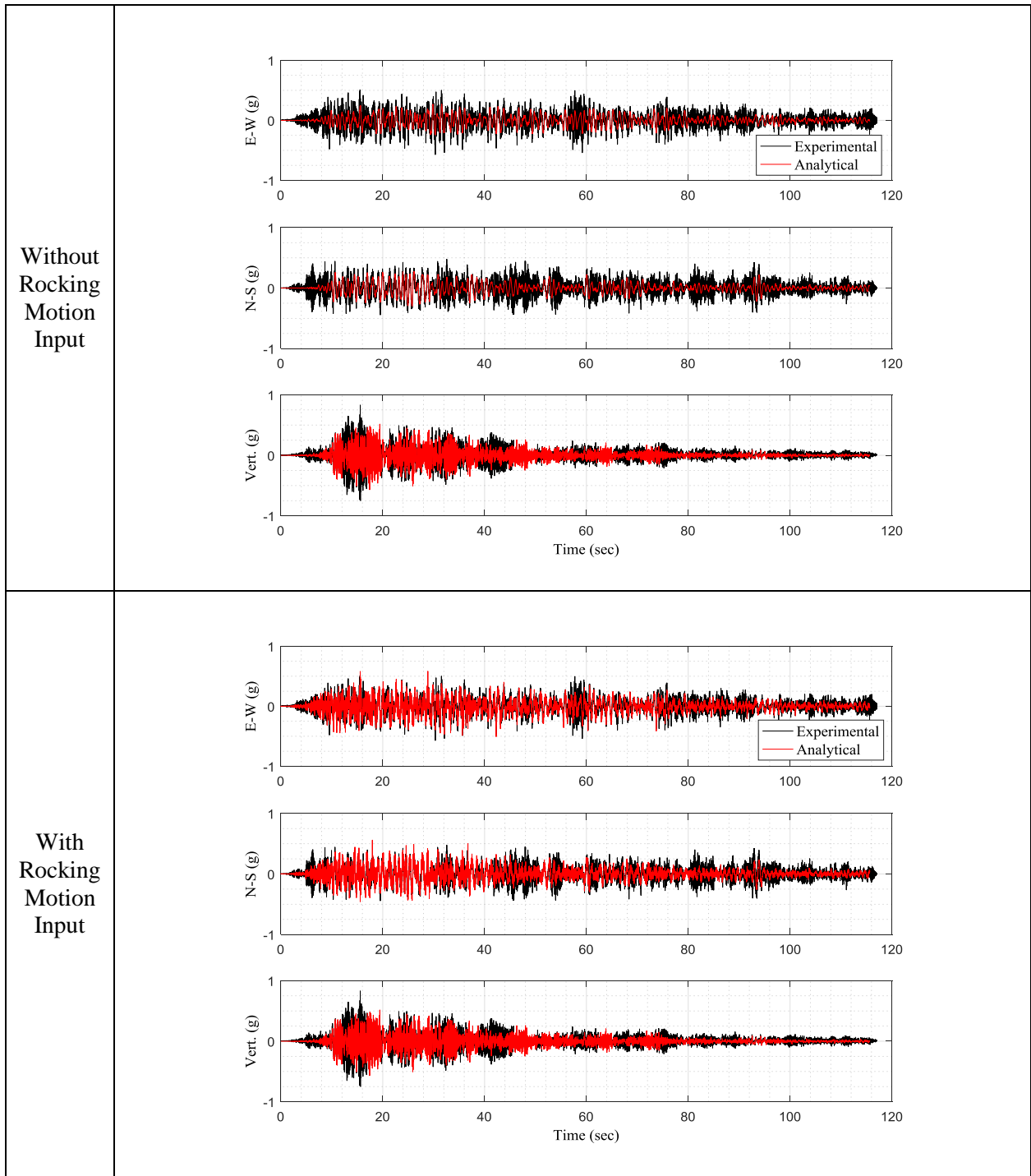


Figure 5-54 Comparison of Experimental and Analytical Results of Acceleration Histories at Bushing Top with and without Consideration of Rocking Shake Table Motion in Configuration of Free Rocking, FP Isolator Type B with 0.12 Nominal Friction in Chile 100% Motion

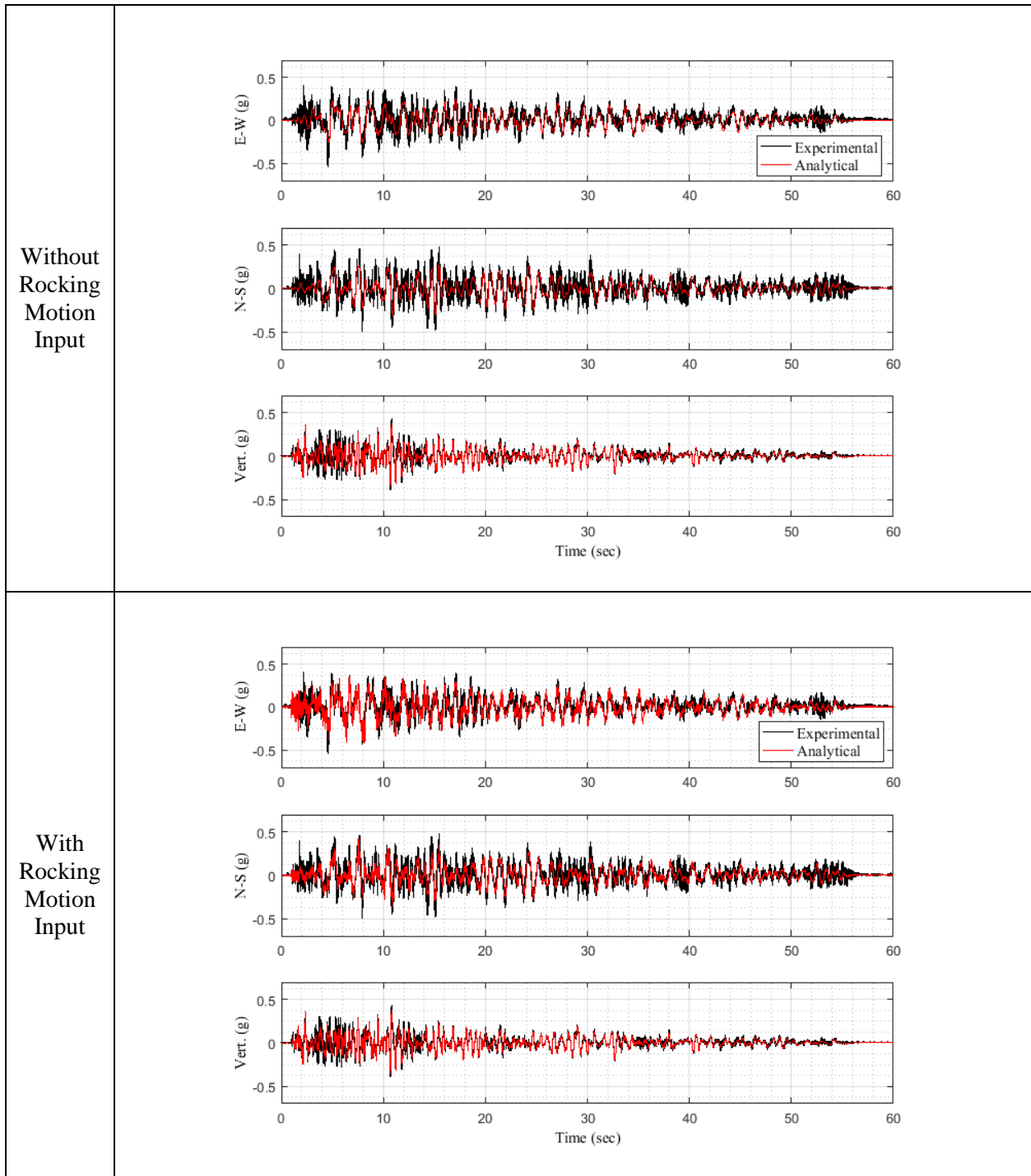


Figure 5-55 Comparison of Experimental and Analytical Results of Acceleration Histories at Bushing Top with and without Consideration of Rocking Shake Table Motion in Configuration of Free Rocking, FP Isolator Type B with 0.12 Nominal Friction in Taft 400% Motion

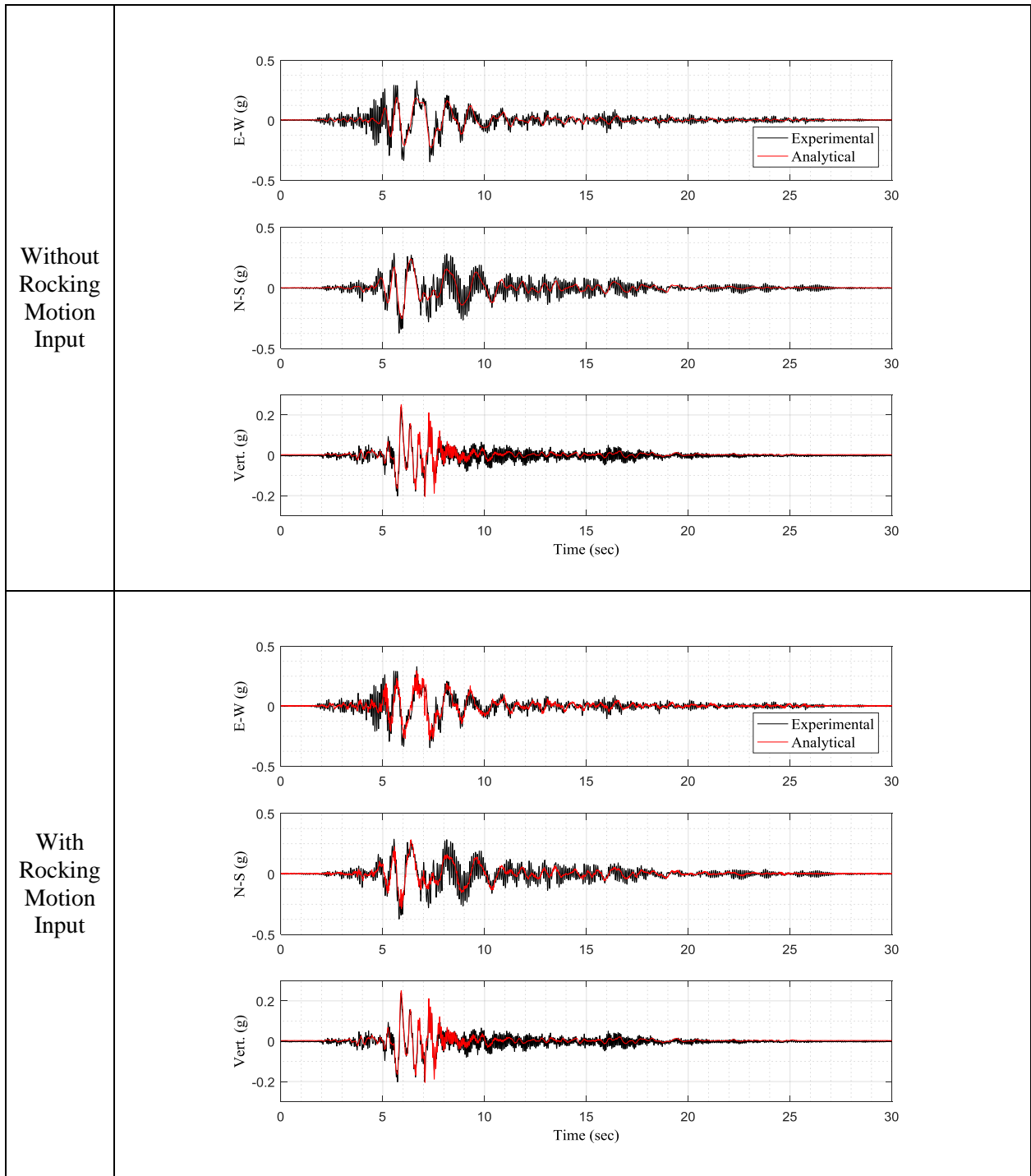


Figure 5-56 Comparison of Experimental and Analytical Results of Acceleration Histories at Bushing Top with and without Consideration of Rocking Shake Table Motion in Configuration of Free Rocking, FP Isolator Type B with 0.12 Nominal Friction in Kobe 50% Motion

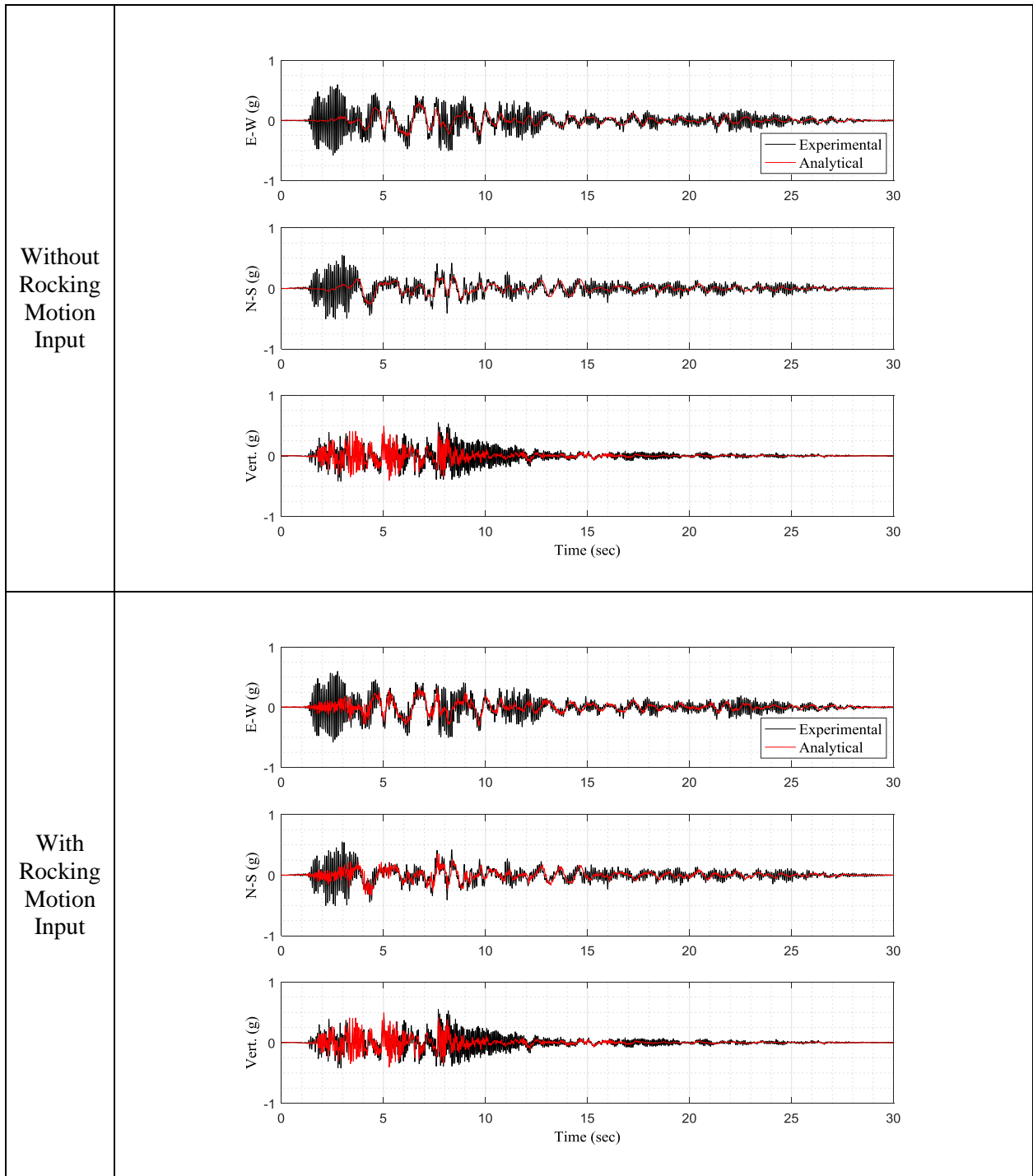


Figure 5-57 Comparison of Experimental and Analytical Results of Acceleration Histories at Bushing Top with and without Consideration of Rocking Shake Table Motion in Configuration of Free Rocking, FP Isolator Type B with 0.12 Nominal Friction in Jensen 100% Motion

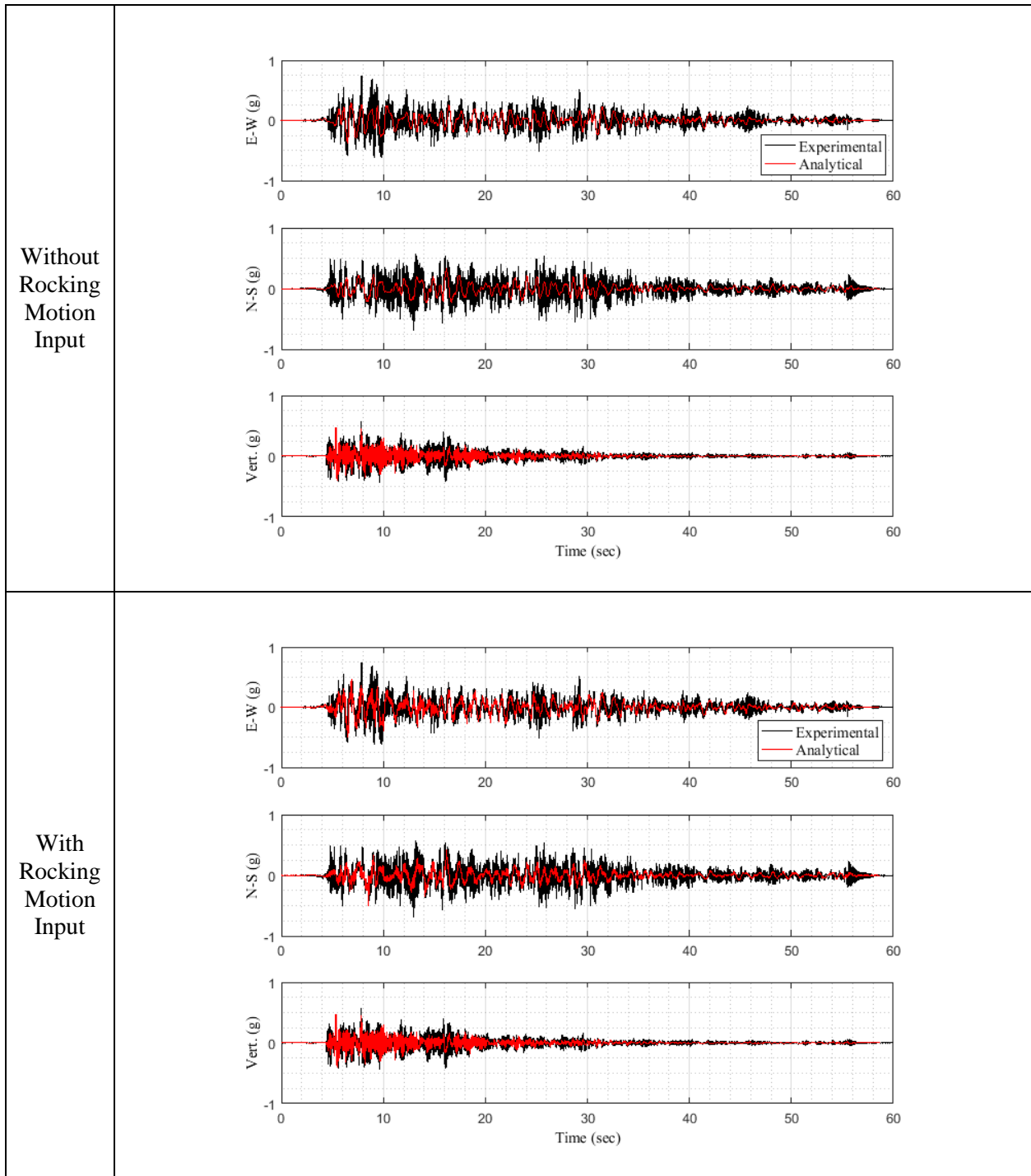


Figure 5-58 Comparison of Experimental and Analytical Results of Acceleration Histories at Bushing Top with and without Consideration of Rocking Shake Table Motion in Configuration of Limited Rocking, FP Isolator Type B with 0.12 Nominal Friction in El Centro 250% Motion

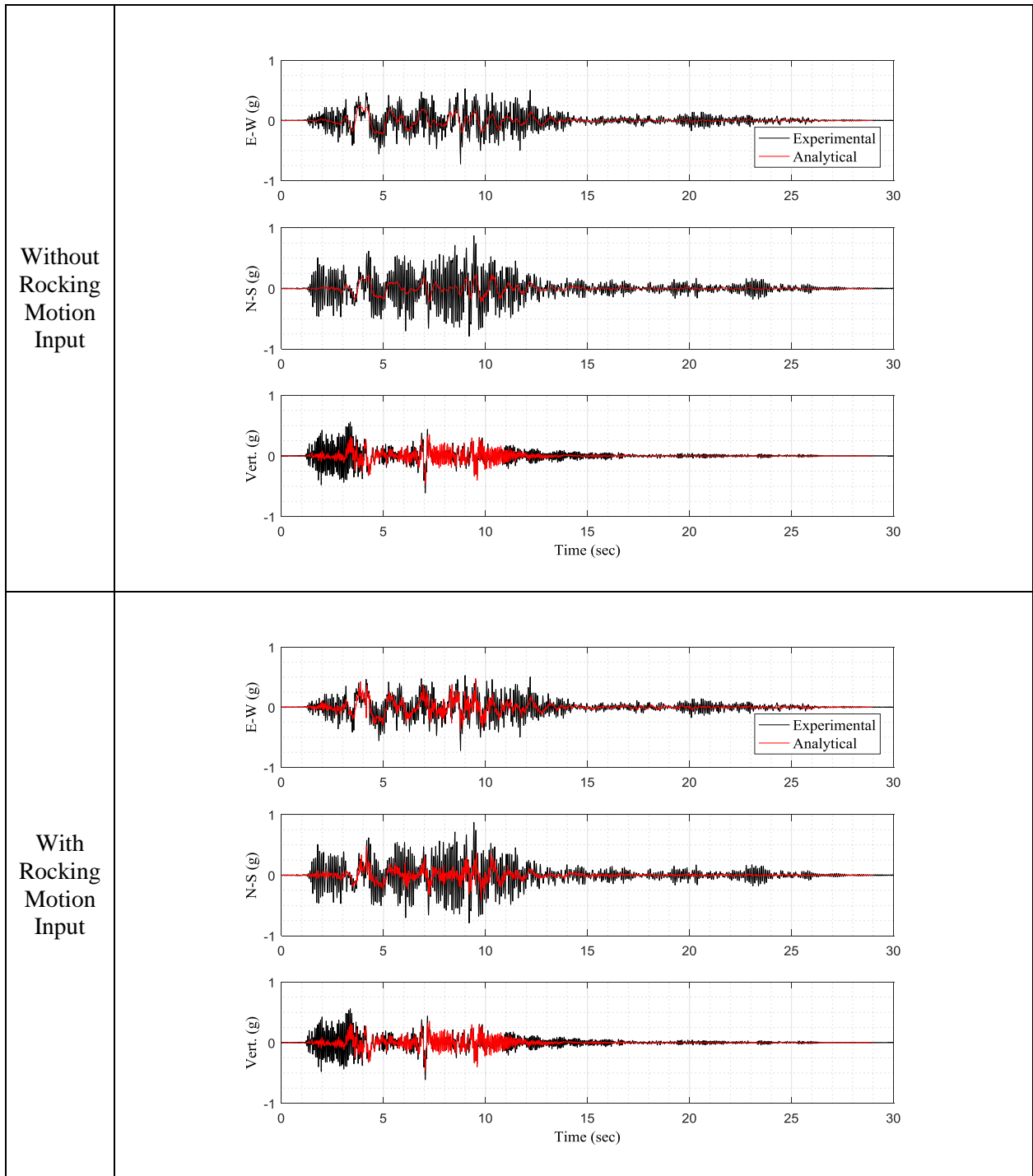


Figure 5-59 Comparison of Experimental and Analytical Results of Acceleration Histories at Bushing Top with and without Consideration of Rocking Shake Table Motion in Configuration of Limited Rocking, FP Isolator Type B with 0.12 Nominal Friction in Pacoima 75% Motion

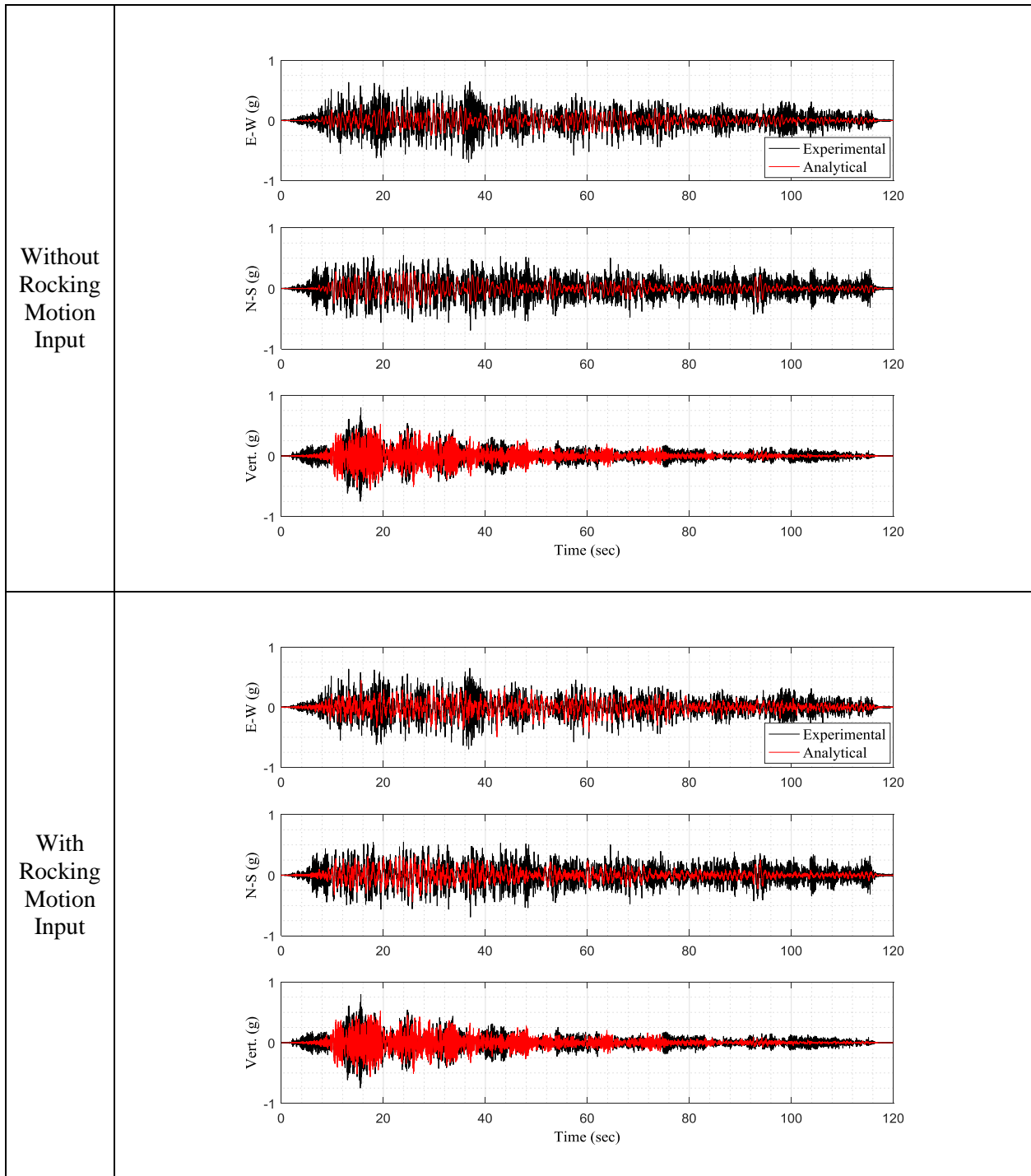


Figure 5-60 Comparison of Experimental and Analytical Results of Acceleration Histories at Bushing Top with and without Consideration of Rocking Shake Table Motion in Configuration of Limited Rocking, FP Isolator Type B with 0.12 Nominal Friction in Chile 100% Motion

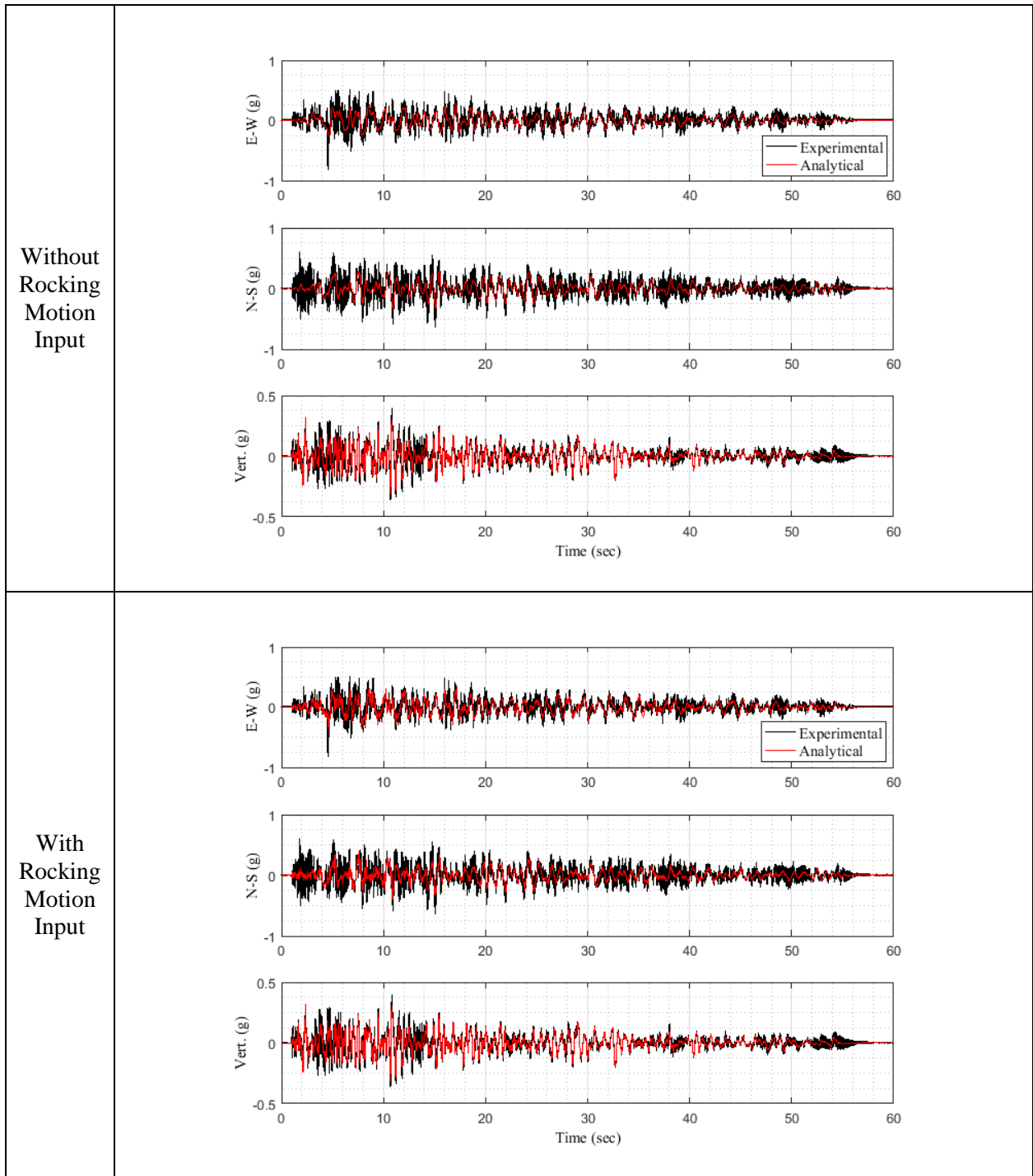


Figure 5-61 Comparison of Experimental and Analytical Results of Acceleration Histories at Bushing Top with and without Consideration of Rocking Shake Table Motion in Configuration of Limited Rocking, FP Isolator Type B with 0.12 Nominal Friction in Taft 400% Motion

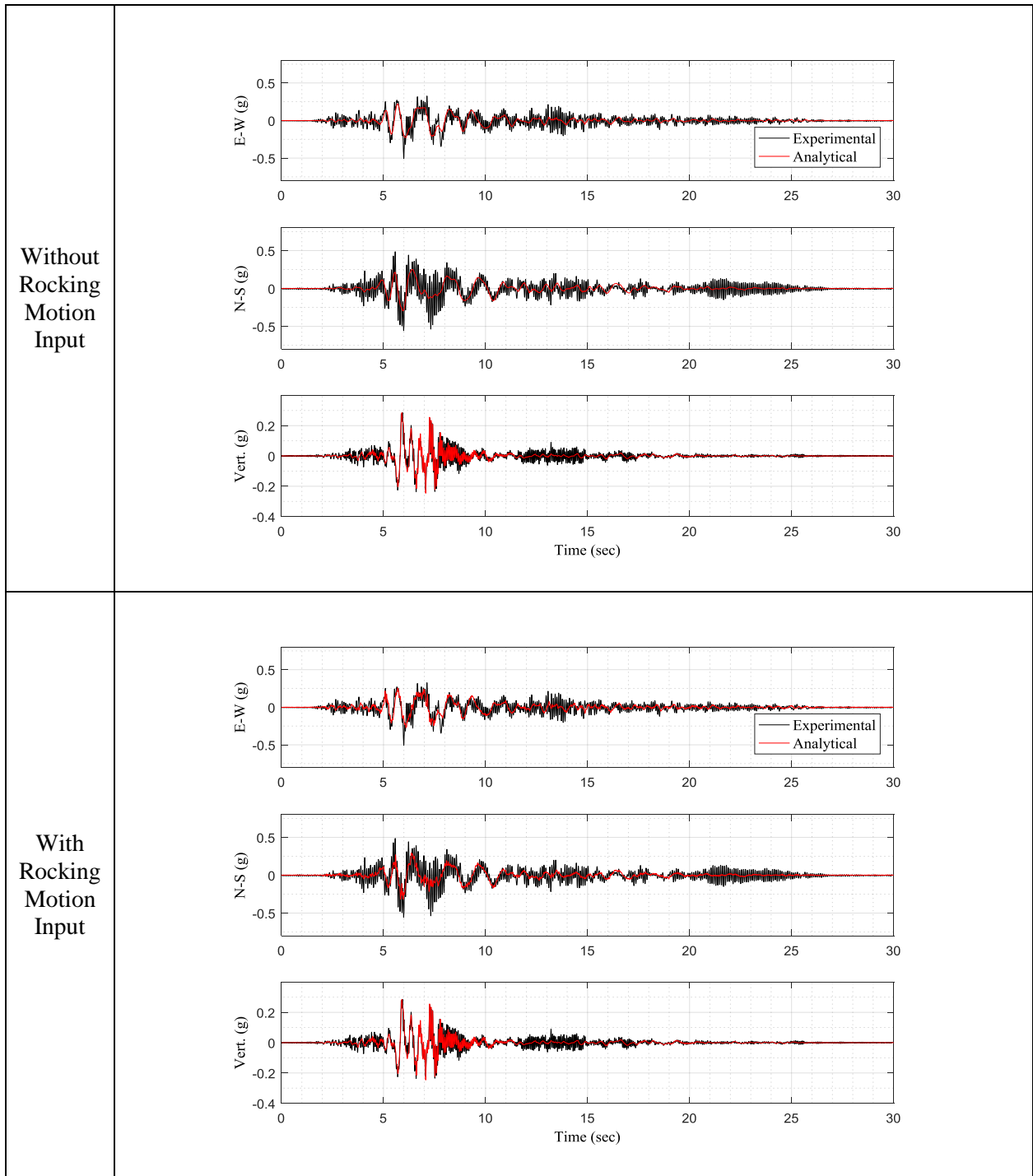


Figure 5-62 Comparison of Experimental and Analytical Results of Acceleration Histories at Bushing Top with and without Consideration of Rocking Shake Table Motion in Configuration of Limited Rocking, FP Isolator Type B with 0.12 Nominal Friction in Kobe 65% Motion

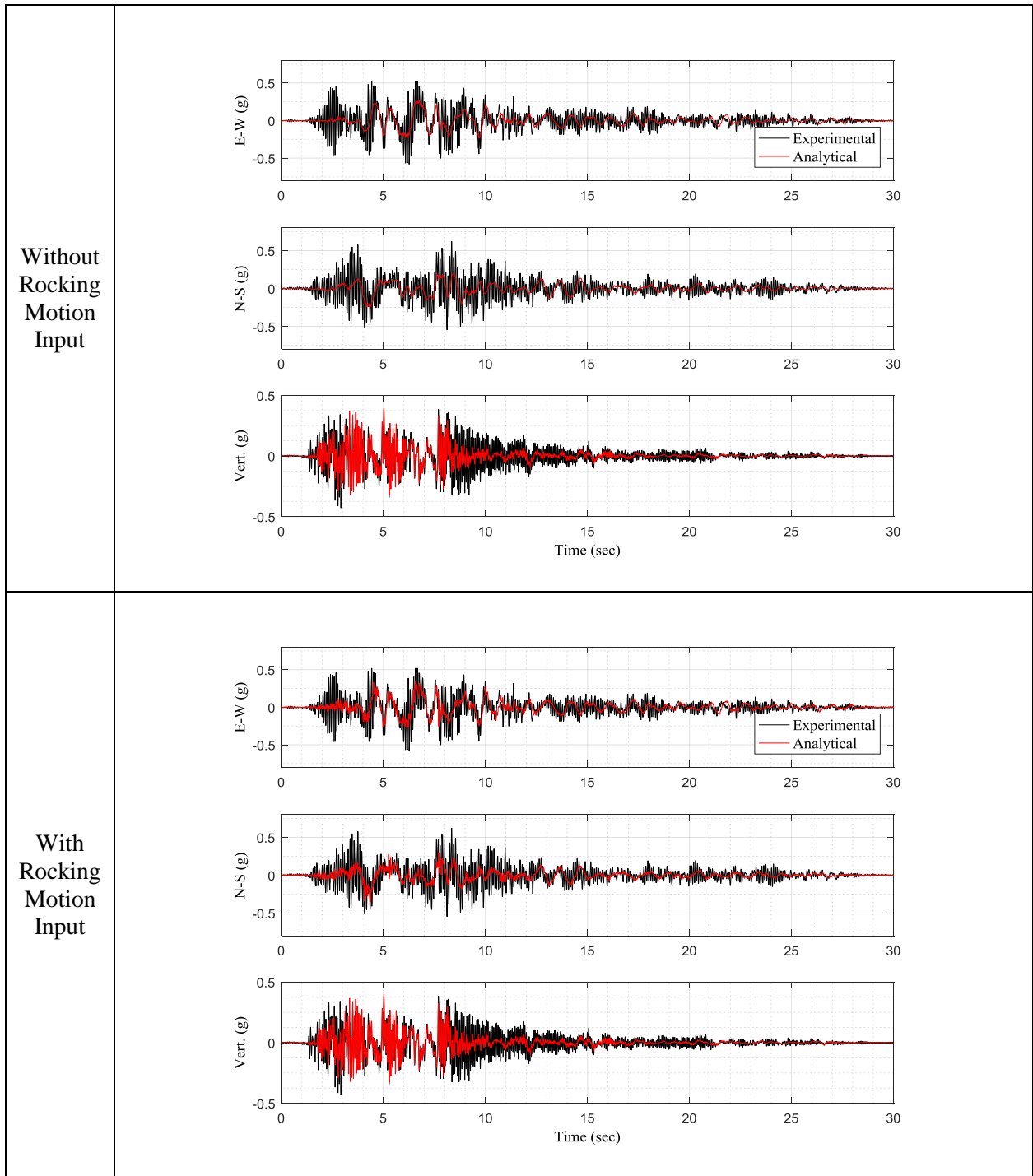


Figure 5-63 Comparison of Experimental and Analytical Results of Acceleration Histories at Bushing Top with and without Consideration of Rocking Shake Table Motion in Configuration of Limited Rocking, FP Isolator Type B with 0.12 Nominal Friction in Jensen 85% Motion

5.5 Effect of Friction in the Spring-Damper Units

All analytical results presented in Section 5.4 were based on the model of Figure 5-1 in which the spring-damper units were modelled by a linear elastic and linear viscous representation using the measured values of stiffness and damping constant. The results of testing of the units (see Section 3.4) indicated the existence of friction, which was measured to be on the average 0.65kip per unit. However, identification tests of the entire model on the shake table produced transfer functions that could be exactly predicted by analytical models without friction, thus indicating the absence of friction. It was theorized in Section 3 that the measured friction force was the result of some significant lateral loading of the spring-damper units during component testing.

The lateral force transferred by the FP isolators to the spring-damper unit below varied depending on the friction and value of displacement. Considering a lateral displacement of 5inch or less in the isolator type B with 0.12 nominal friction (this is the recorded response, see response parameters in Table 4-5), the lateral force for the configuration that is free to rock ($W=68.1\text{kip}$ is about $0.19W=12.9\text{kip}$ or less). This corresponds to 3.23kip per support. The ratio of the friction force of 0.65kip to the lateral force of 3.23kip per support is 0.20. This would have been the coefficient of friction at the sliding interface of the telescopic tube system of the spring-damper units (see Figure 3-6). In the case of the FP isolator of type A with nominal friction of 0.07 (peak displacement in the tests was 7inch or less, see Table 4-5, and lateral force equal to 2.85kip or less per support), the friction coefficient in the spring-damper unit telescopic system would have been $0.65/2.85=0.23$. Accordingly, analysis with a constant friction force of 0.65kip per support corresponds to the use of a friction coefficient in the spring-damper telescopic unit of the order of 0.20 or more. This is large.

Analyses were performed with the model of Figure 5-64, which is identical to the model of Figure 5-1 but with added friction force of 0.65kip at each support. Results are presented in Figures 5-65 to 5-100 in which experimental results are compared to analytical results with and without the effect of friction in the spring-damper units. In all analyses the rocking motion of the shake table was not included. Results are compared for the response spectra at the frame top NE corner, acceleration histories at the frame top NE corner, and the isolator horizontal and vertical displacements. The comparison demonstrates that the inclusion of the friction force in the

spring-damper units does not improve the accuracy of the analytical prediction. It actually results in under-prediction of the vertical isolator displacements. We conclude that friction in the spring-damper units during shake table testing was smaller than what was measured in the component testing of Section 3 and it did not have any important effect on the response.

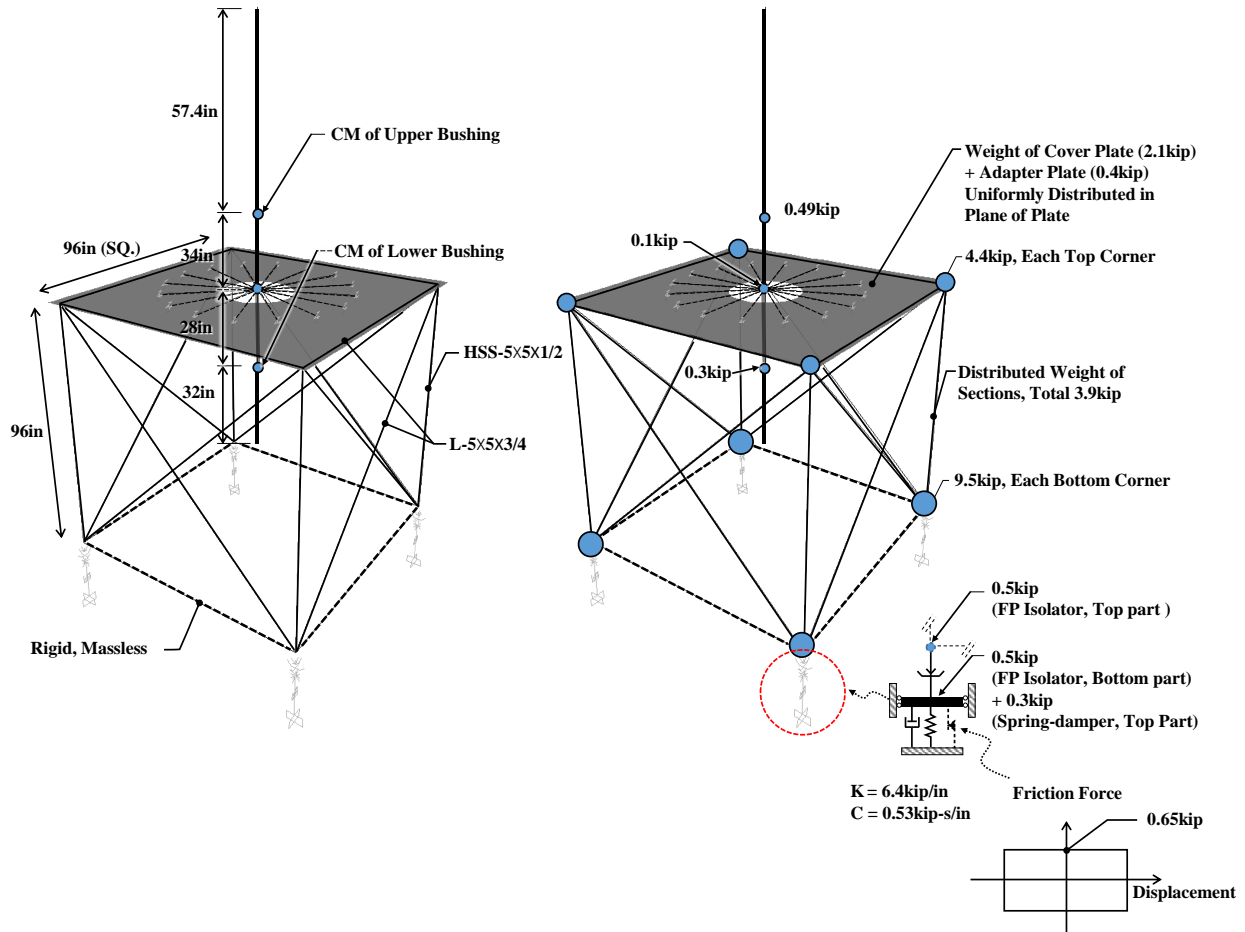


Figure 5-64 Analytical Model of Tested Model in Configuration of Free Rocking with Spring-Damper Unit Friction Included

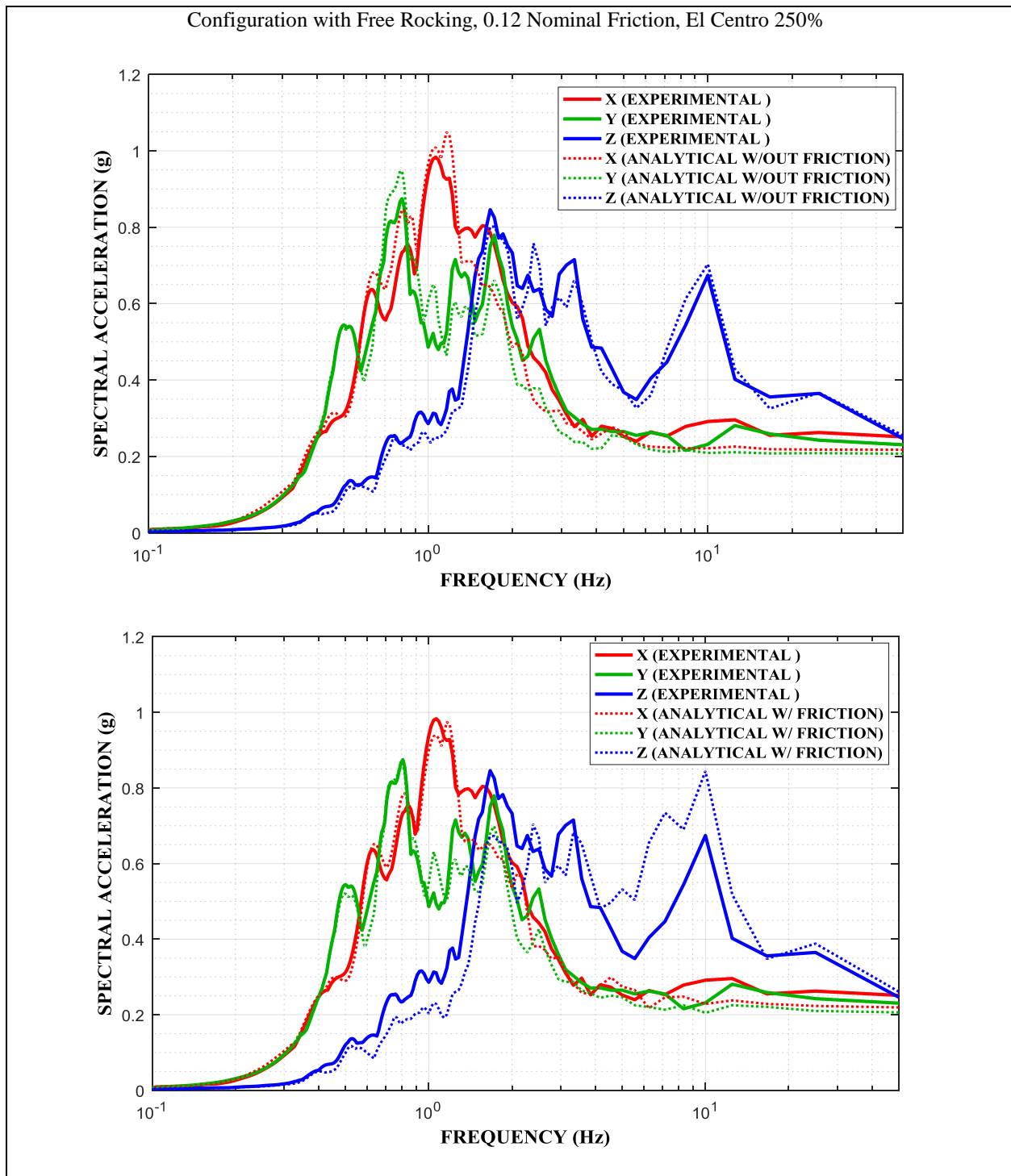


Figure 5-65 Comparison of Experimental and Analytical 5%-damped Response Spectra at Frame NE Top Corner With and Without Due Consideration for Friction Forces in Spring-damper Units in Configuration of Free Rocking, FP Isolator Type B with 0.12 Nominal Friction in El Centro 250% Motion

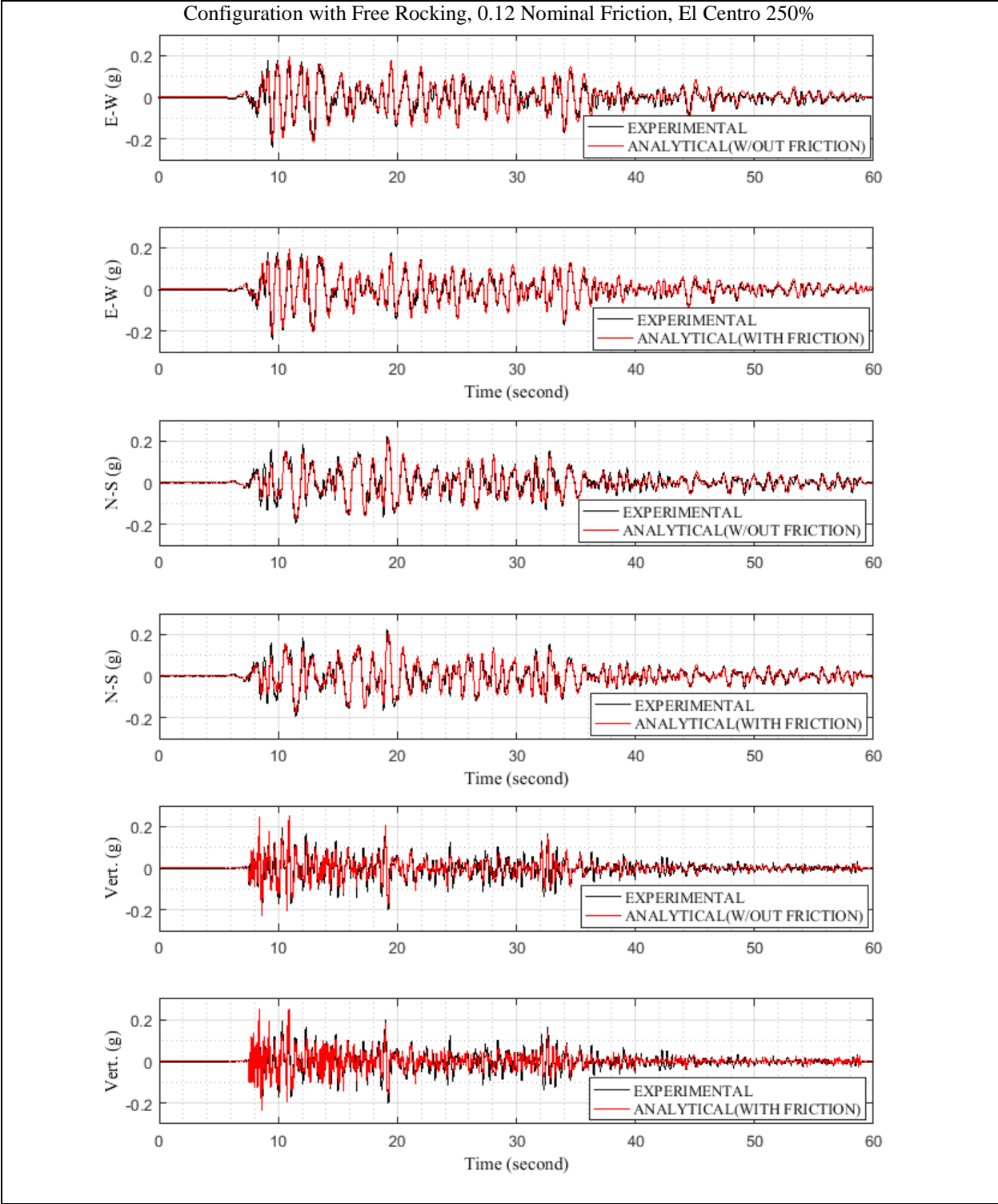


Figure 5-66 Comparison of Experimental and Analytical Acceleration Histories at Frame NE Top Corner With and Without Due Consideration for Friction Forces in Spring-damper Units in Configuration of Free Rocking, FP Isolator Type B with 0.12 Nominal Friction in El Centro 250% Motion

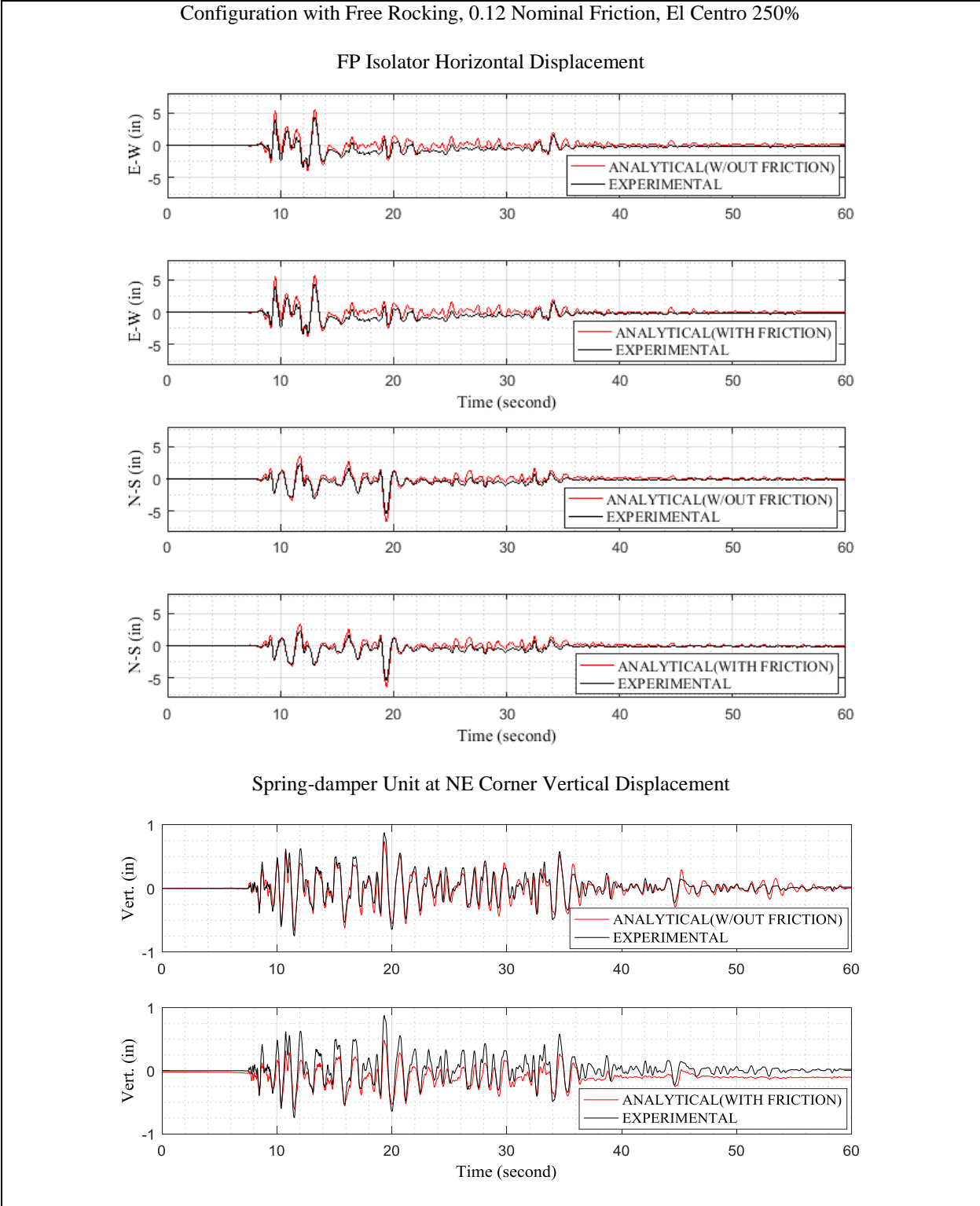


Figure 5-67 Comparison of Experimental and Analytical Isolator Displacement Histories With and Without Due Consideration for Friction Forces in Spring-damper Units in Configuration of Free Rocking, FP Isolator Type B with 0.12 Nominal Friction in El Centro 250% Motion

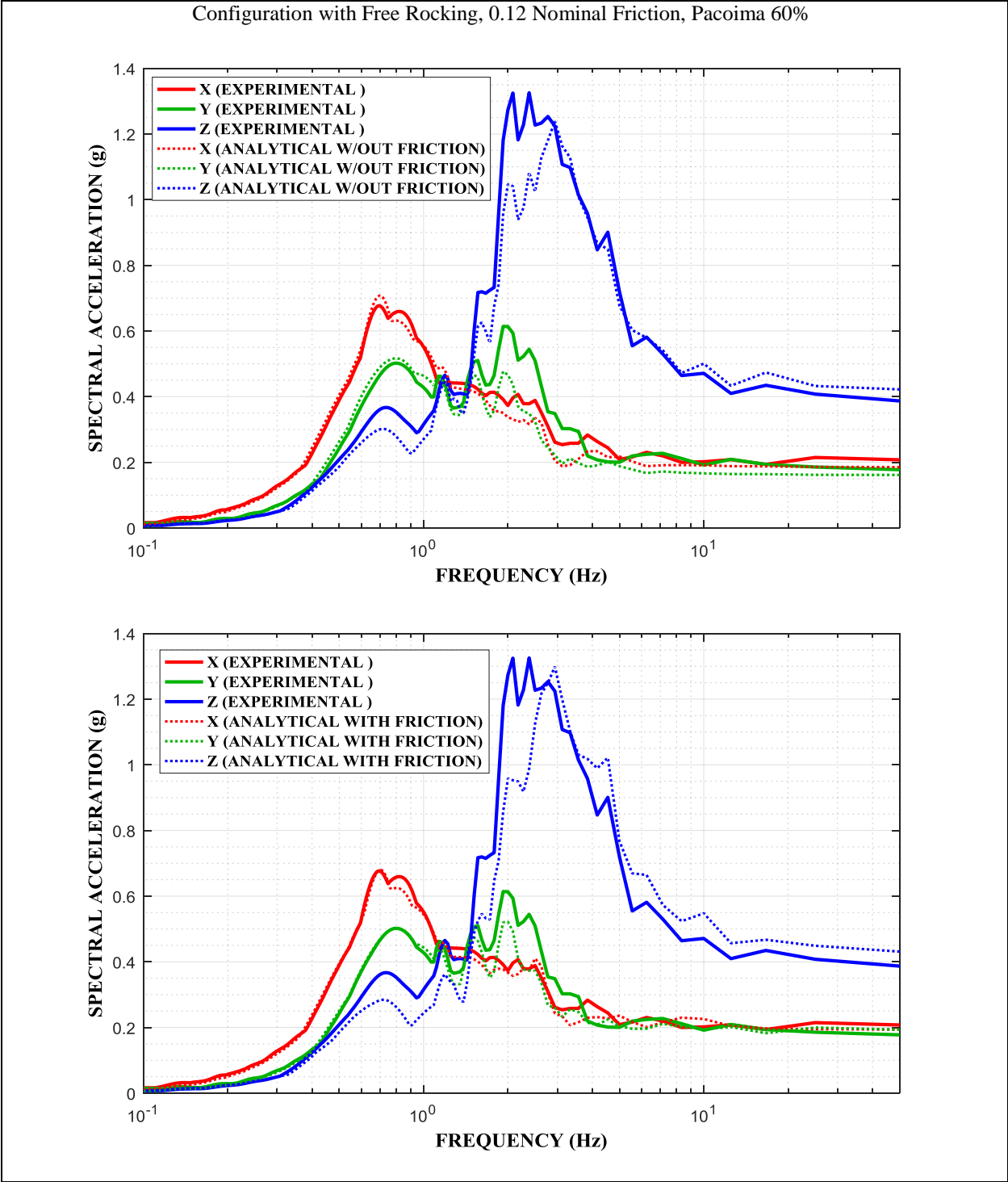


Figure 5-68 Comparison of Experimental and Analytical 5%-damped Response Spectra at Frame NE Top Corner With and Without Due Consideration for Friction Forces in Spring-damper Units in Configuration of Free Rocking, FP Isolator Type B with 0.12 Nominal Friction in Pacoima 60% Motion

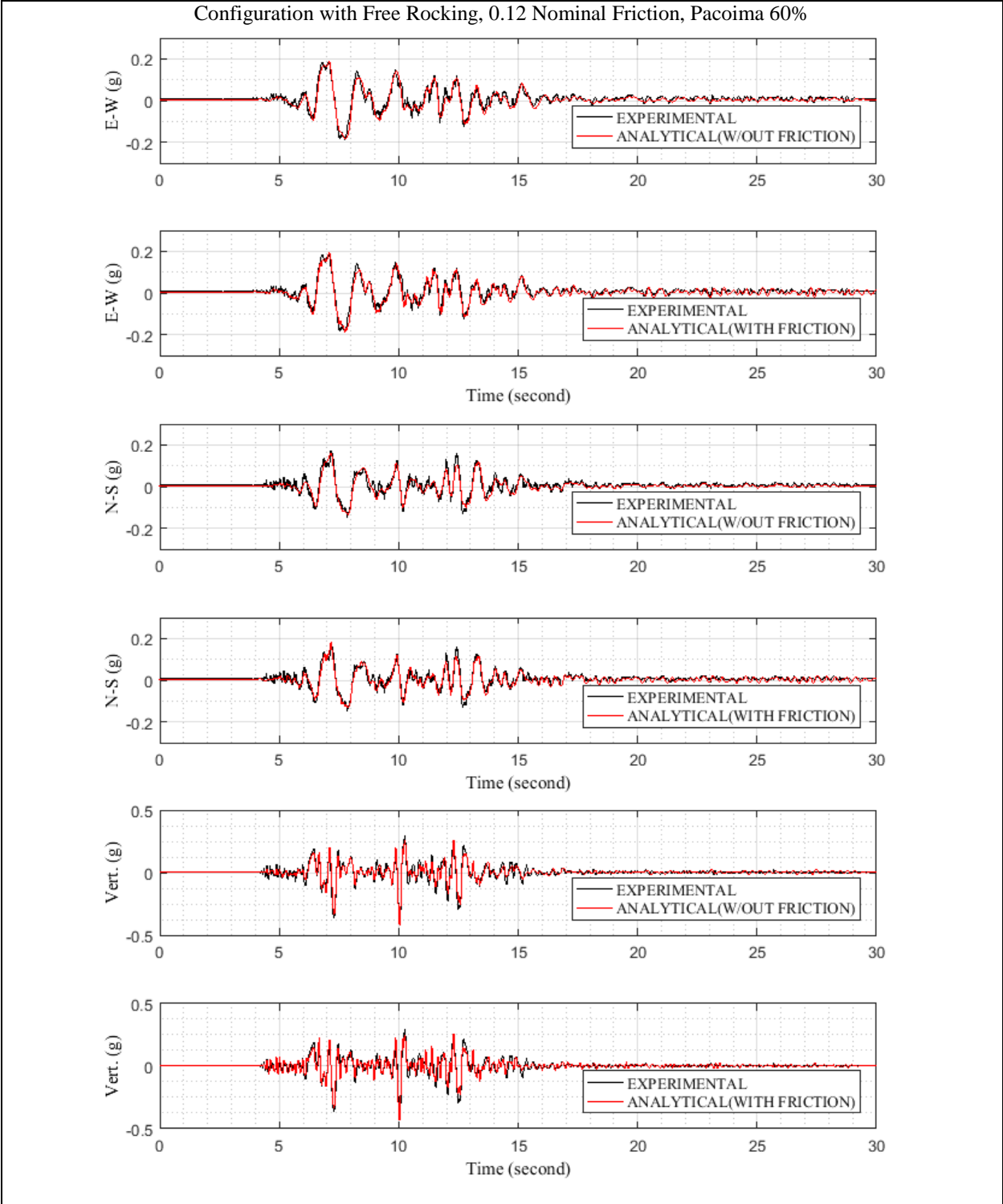


Figure 5-69 Comparison of Experimental and Analytical Acceleration Histories at Frame NE Top Corner With and Without Due Consideration for Friction Forces in Spring-damper Units in Configuration of Free Rocking, FP Isolator Type B with 0.12 Nominal Friction in Pacoima 60% Motion

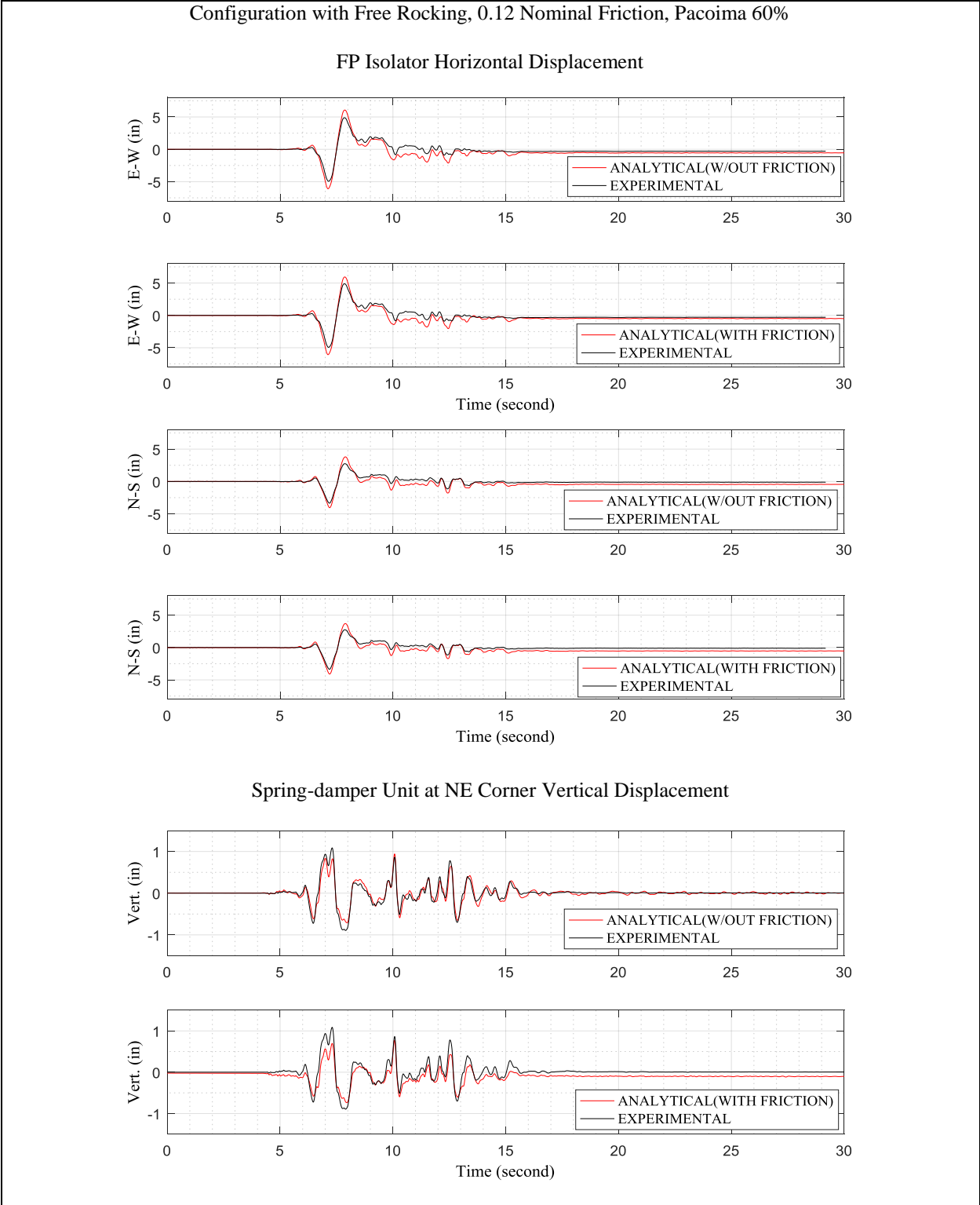


Figure 5-70 Comparison of Experimental and Analytical Isolator Displacement Histories With and Without Due Consideration for Friction Forces in Spring-damper Units in Configuration of Free Rocking, FP Isolator Type B with 0.12 Nominal Friction in Pacoima 60% Motion

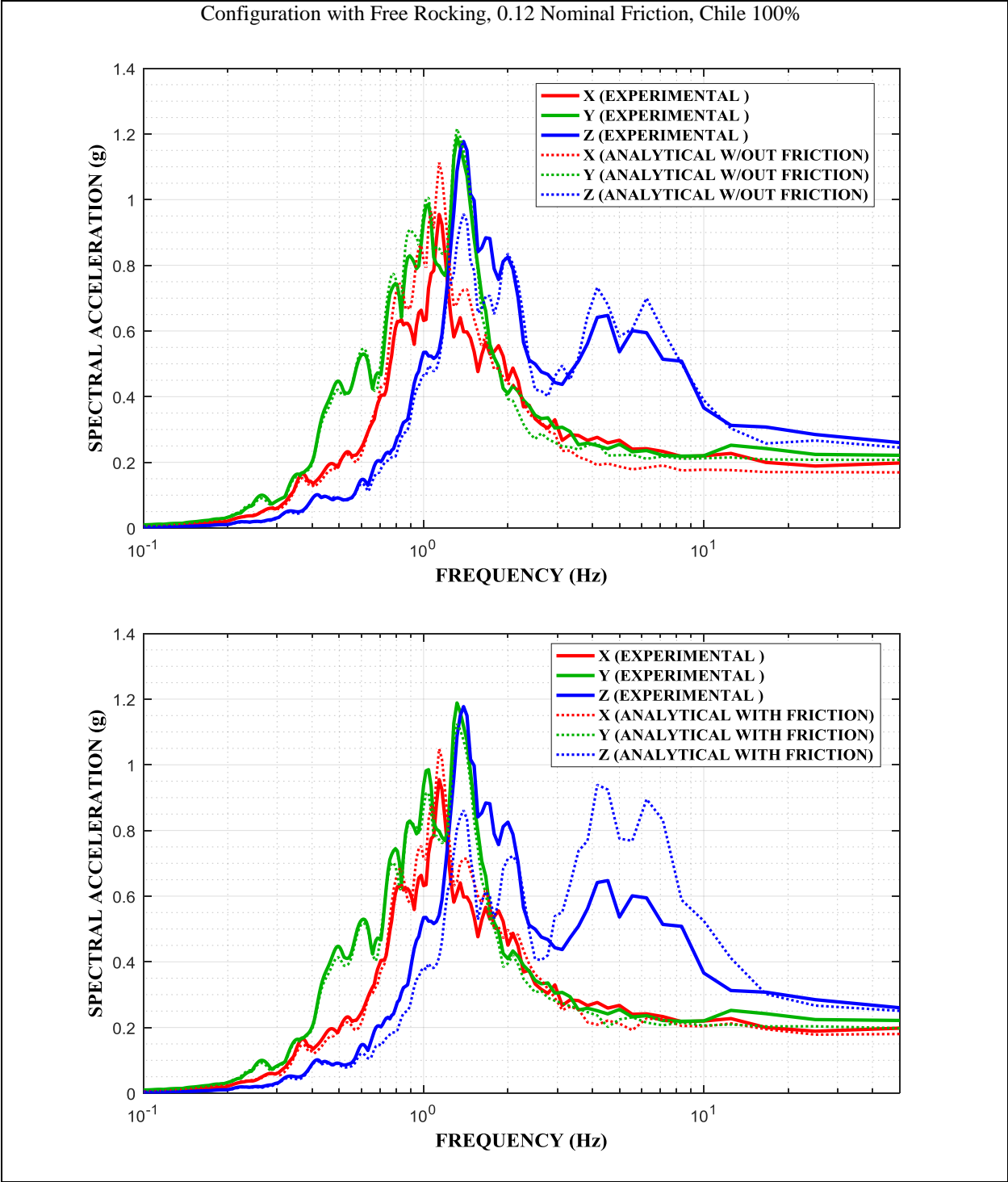


Figure 5-71 Comparison of Experimental and Analytical 5%-damped Response Spectra at Frame NE Top Corner With and Without Due Consideration for Friction Forces in Spring-damper Units in Configuration of Free Rocking, FP Isolator Type B with 0.12 Nominal Friction in Chile 100% Motion

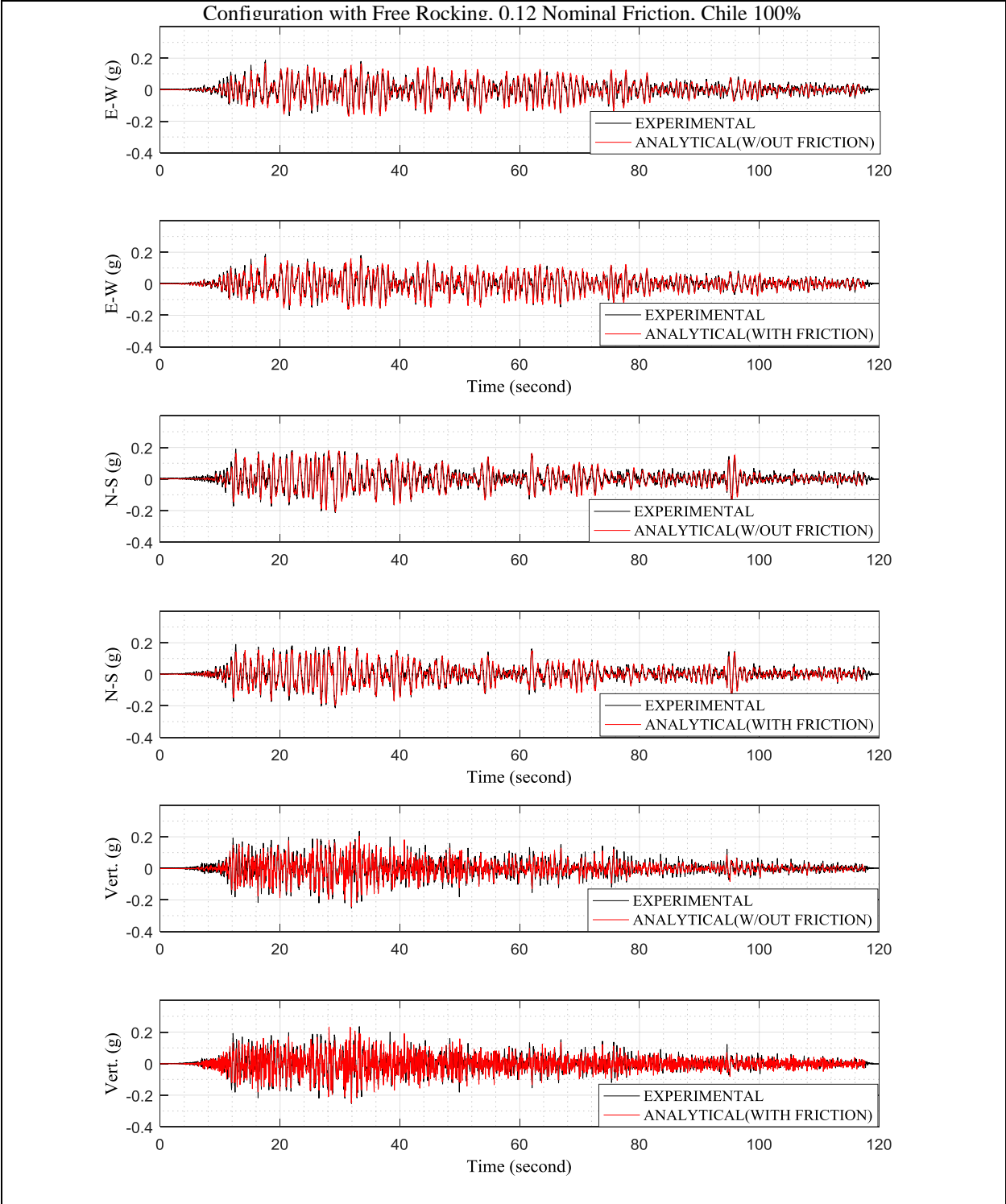


Figure 5-72 Comparison of Experimental and Analytical Acceleration Histories at Frame NE Top Corner With and Without Due Consideration for Friction Forces in Spring-damper Units in Configuration of Free Rocking, FP Isolator Type B with 0.12 Nominal Friction in Chile 100% Motion

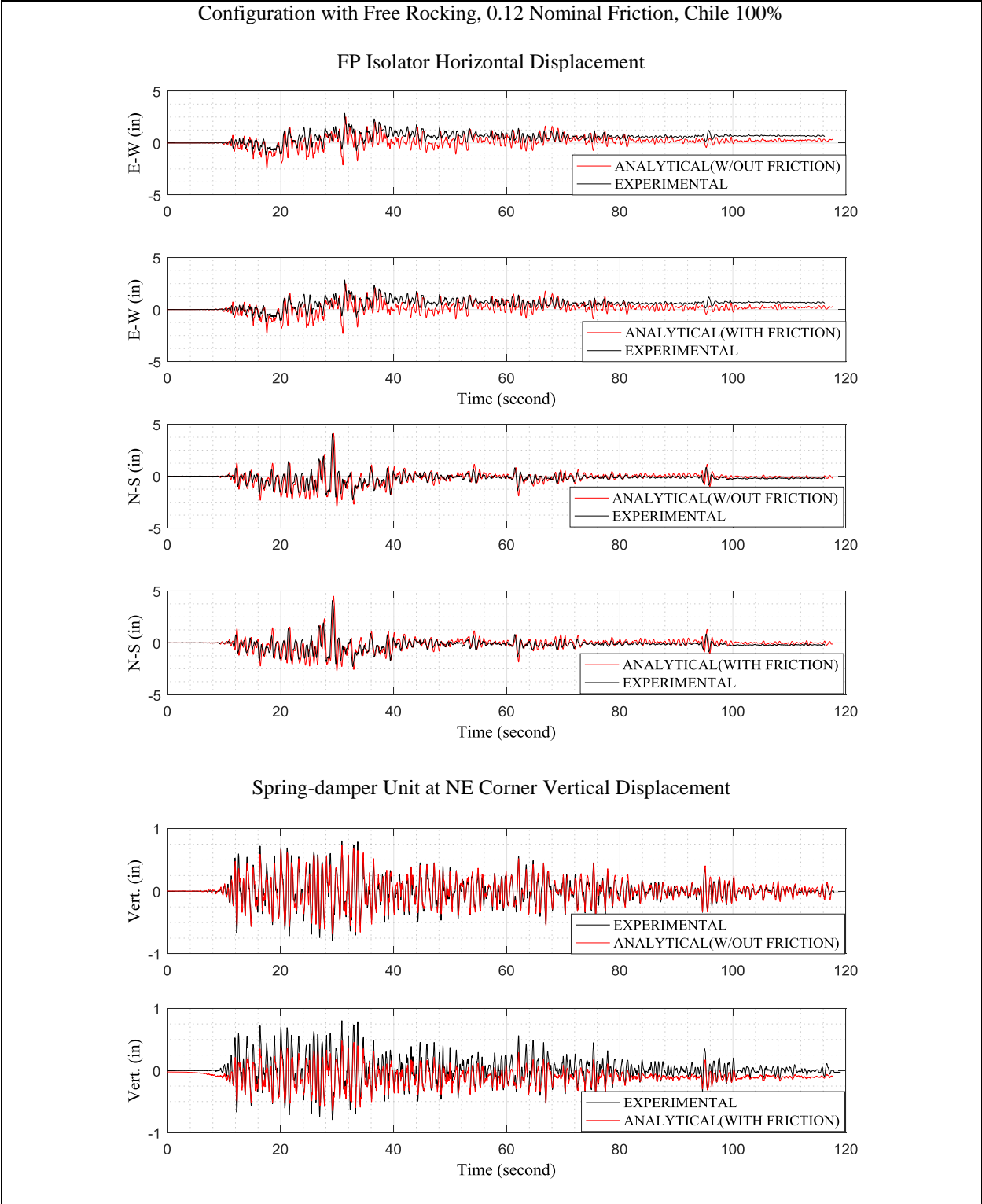


Figure 5-73 Comparison of Experimental and Analytical Isolator Displacement Histories With and Without Due Consideration for Friction Forces in Spring-damper Units in Configuration of Free Rocking, FP Isolator Type B with 0.12 Nominal Friction in Chile 100% Motion

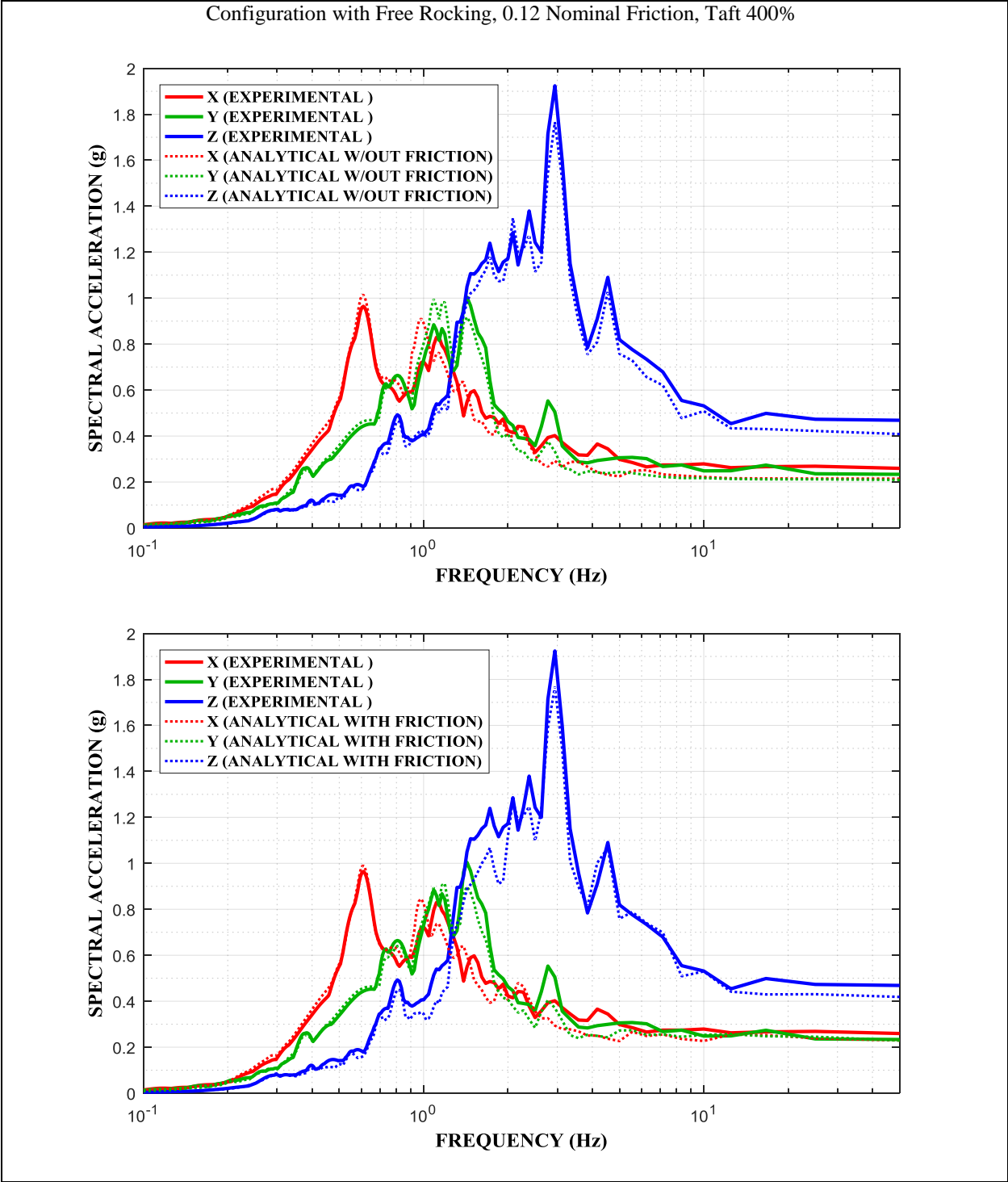


Figure 5-74 Comparison of Experimental and Analytical 5%-damped Response Spectra at Frame NE Top Corner With and Without Due Consideration for Friction Forces in Spring-damper Units in Configuration of Free Rocking, FP Isolator Type B with 0.12 Nominal Friction in Taft 400% Motion

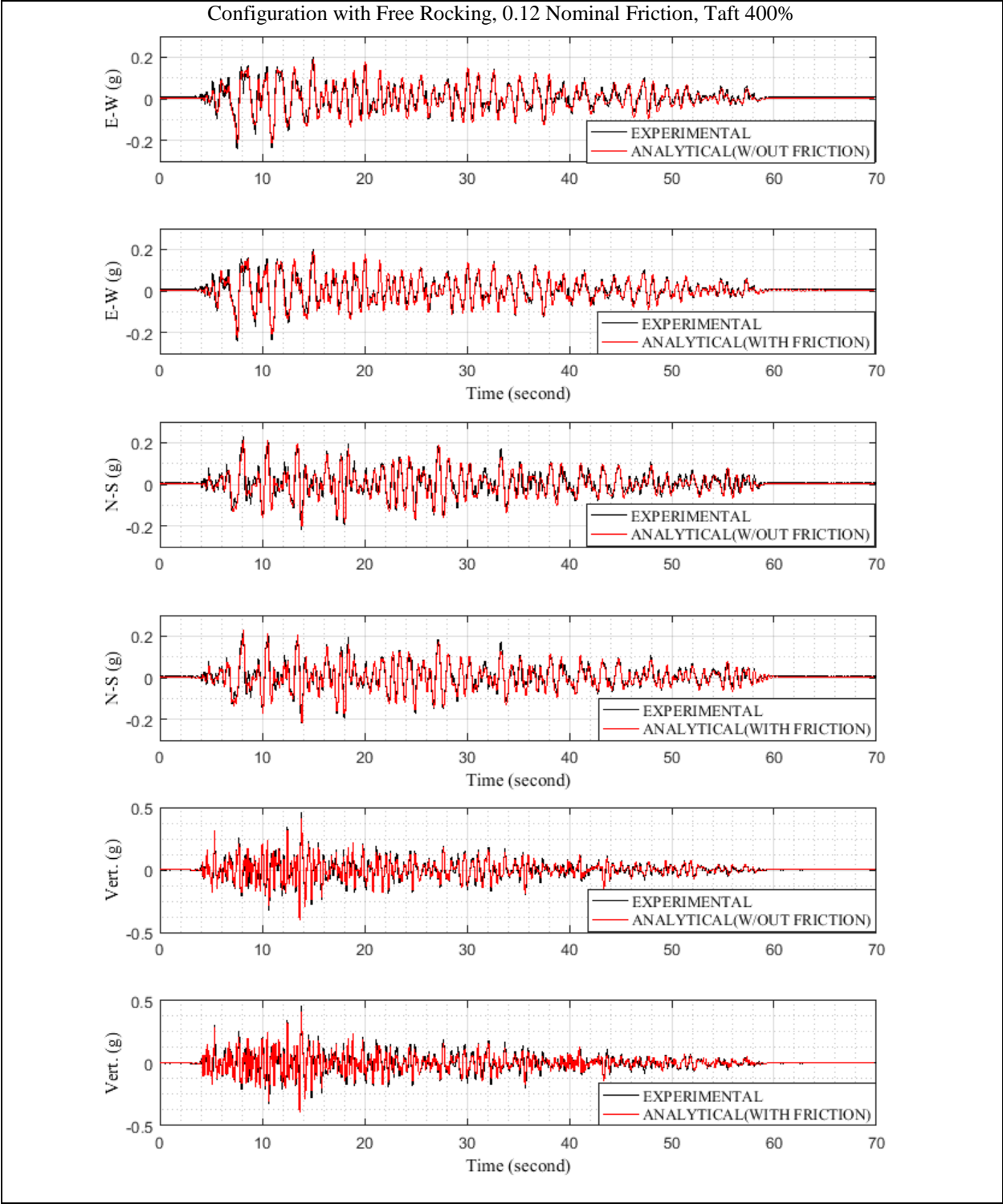


Figure 5-75 Comparison of Experimental and Analytical Acceleration Histories at Frame NE Top Corner With and Without Due Consideration for Friction Forces in Spring-damper Units in Configuration of Free Rocking, FP Isolator Type B with 0.12 Nominal Friction in Taft 400% Motion

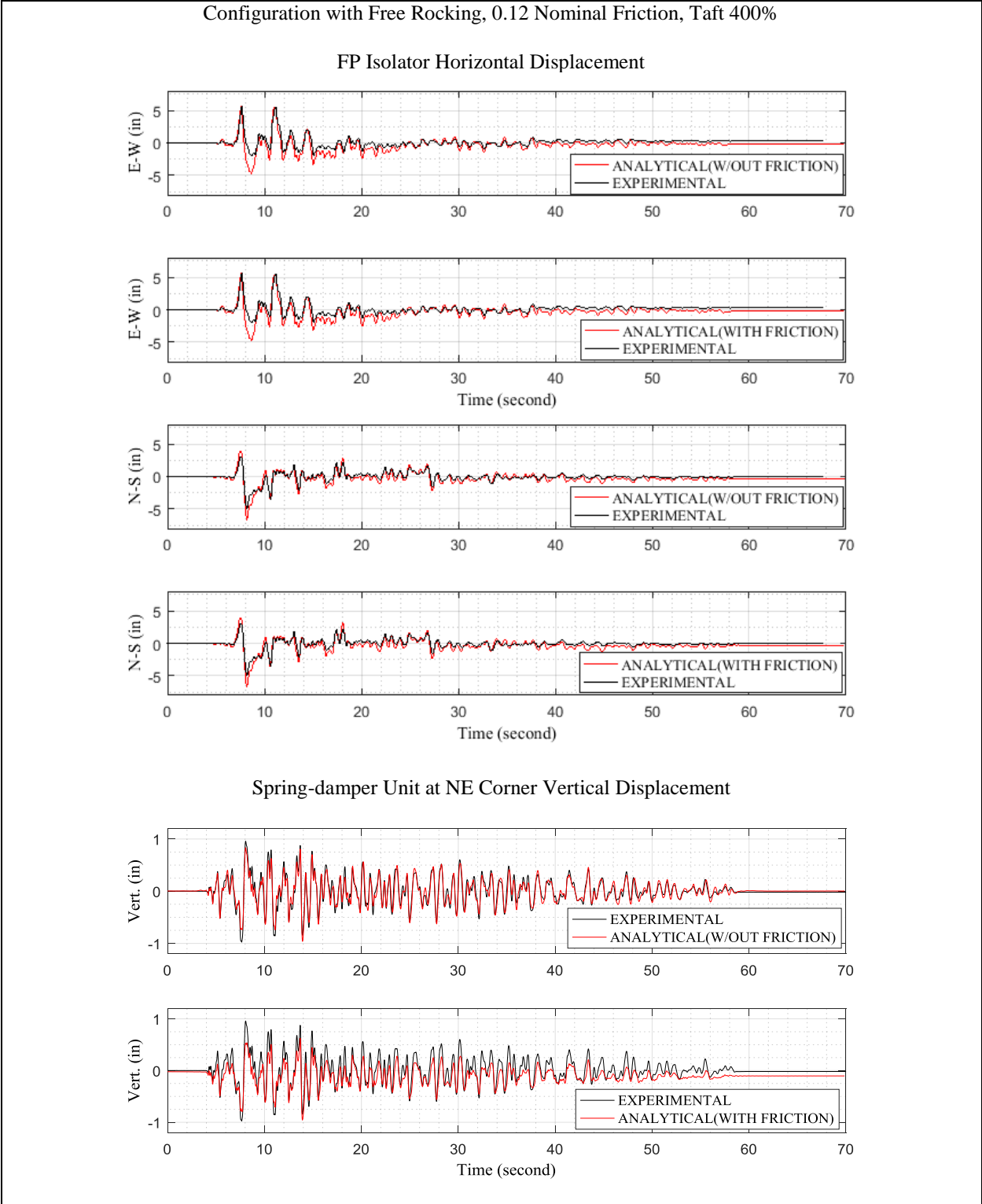


Figure 5-76 Comparison of Experimental and Analytical Isolator Displacement Histories With and Without Due Consideration for Friction Forces in Spring-damper Units in Configuration of Free Rocking, FP Isolator Type B with 0.12 Nominal Friction in Taft 400% Motion

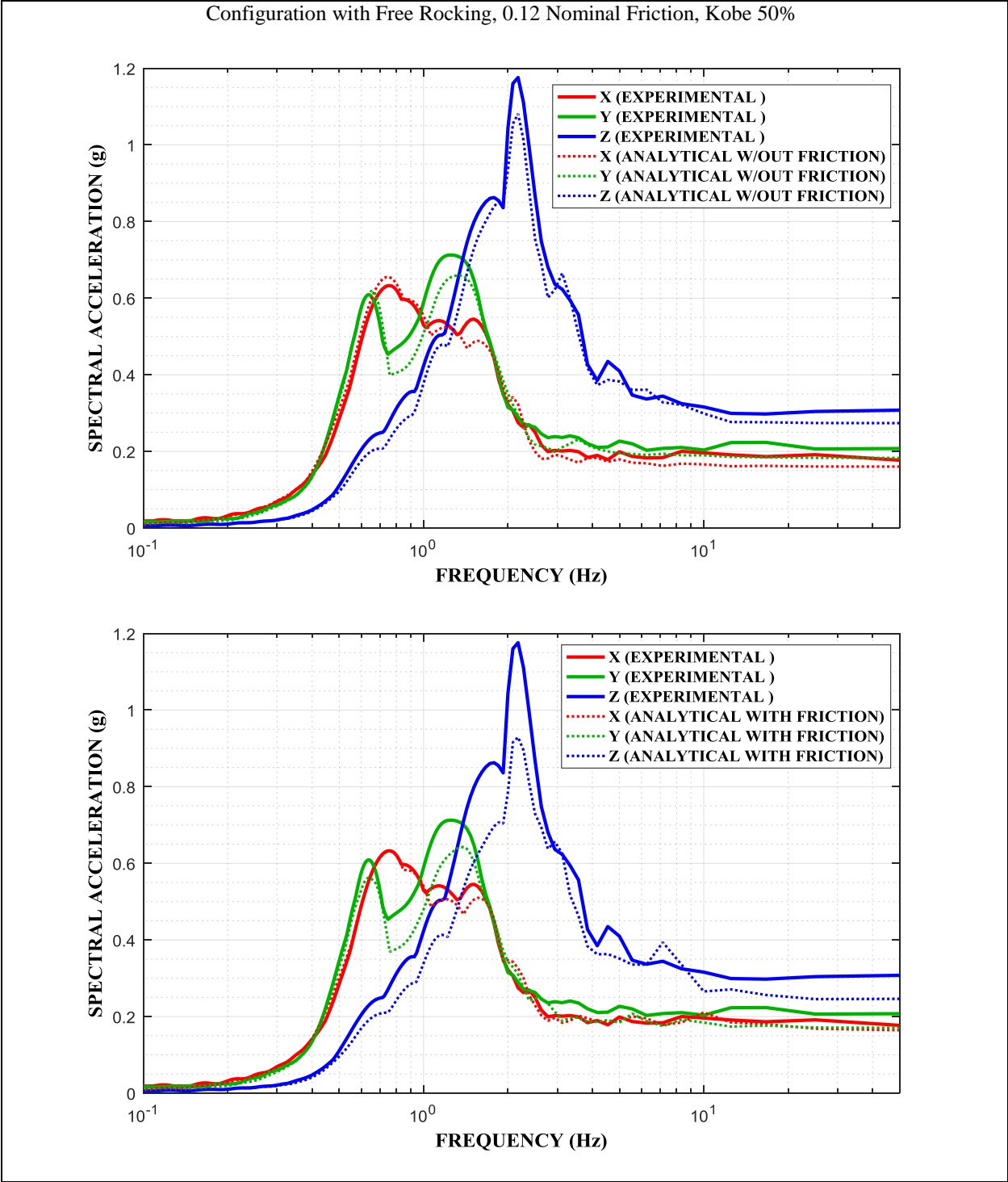


Figure 5-77 Comparison of Experimental and Analytical 5%-damped Response Spectra at Frame NE Top Corner With and Without Due Consideration for Friction Forces in Spring-damper Units in Configuration of Free Rocking, FP Isolator Type B with 0.12 Nominal Friction in Kobe 50% Motion

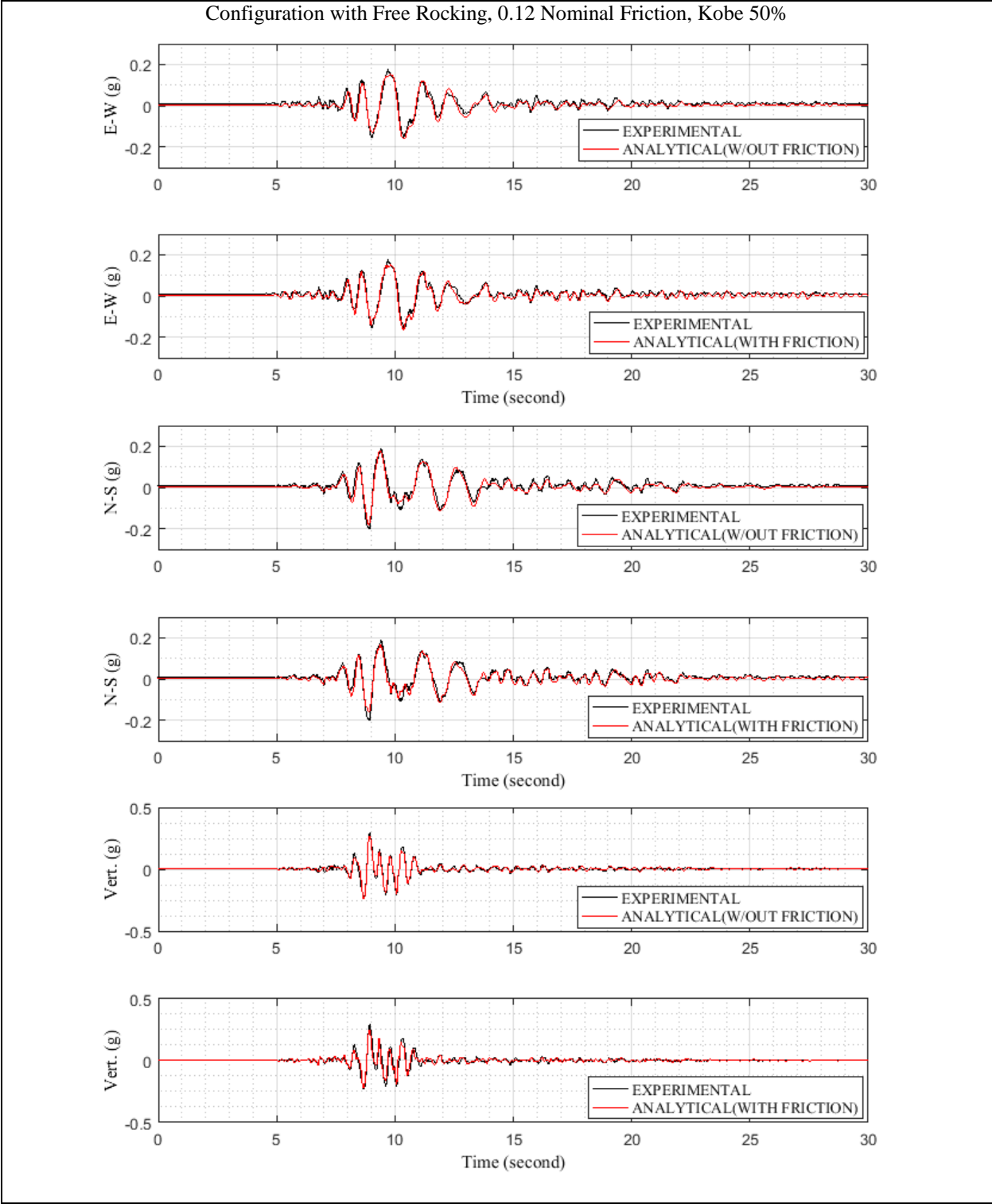


Figure 5-78 Comparison of Experimental and Analytical Acceleration Histories at Frame NE Top Corner With and Without Due Consideration for Friction Forces in Spring-damper Units in Configuration of Free Rocking, FP Isolator Type B with 0.12 Nominal Friction in Kobe 50% Motion

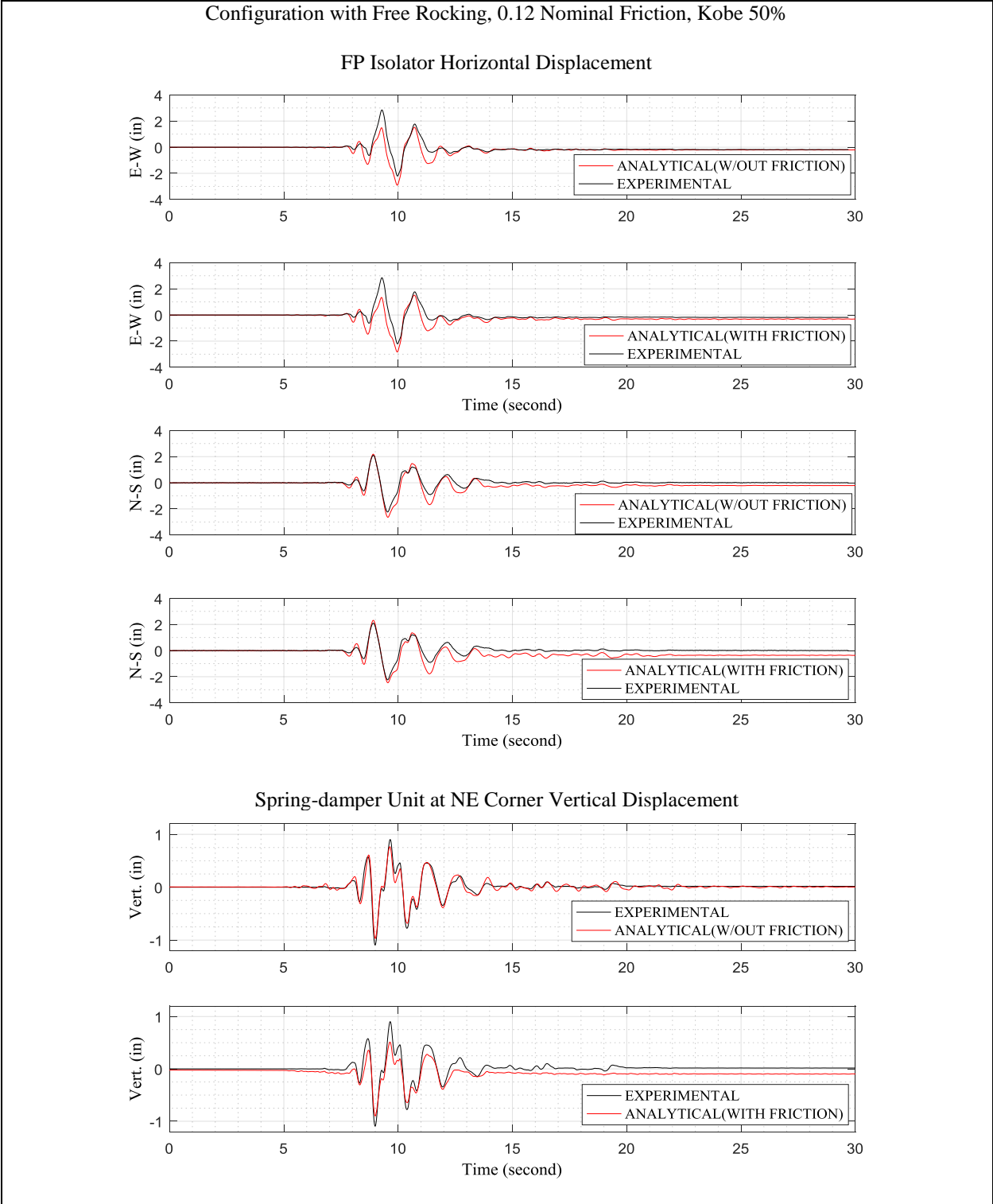


Figure 5-79 Comparison of Experimental and Analytical Isolator Displacement Histories With and Without Due Consideration for Friction Forces in Spring-damper Units in Configuration of Free Rocking, FP Isolator Type B with 0.12 Nominal Friction in Kobe 50% Motion

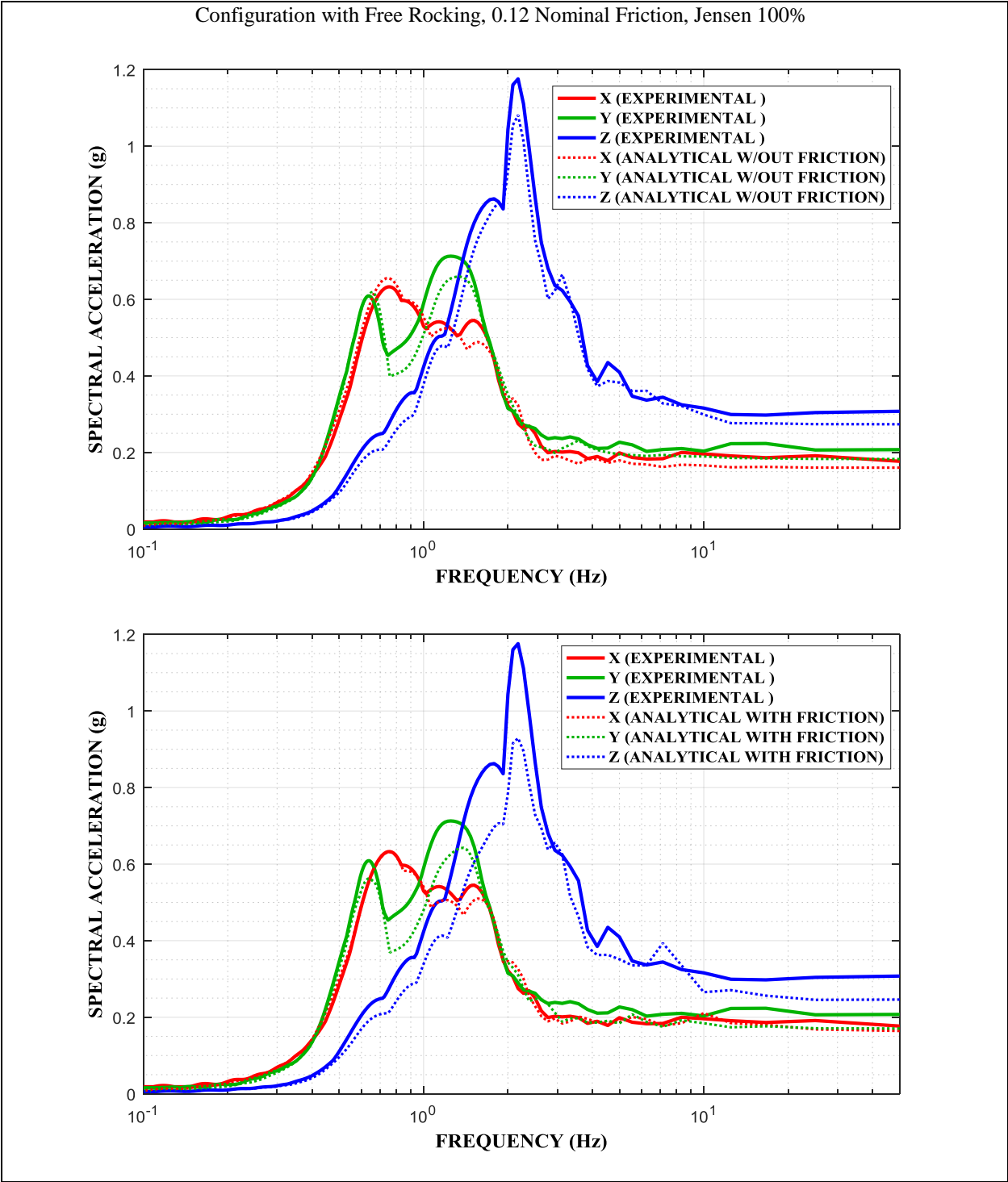


Figure 5-80 Comparison of Experimental and Analytical 5%-damped Response Spectra at Frame NE Top Corner With and Without Due Consideration for Friction Forces in Spring-damper Units in Configuration of Free Rocking, FP Isolator Type B with 0.12 Nominal Friction in Jensen 100% Motion

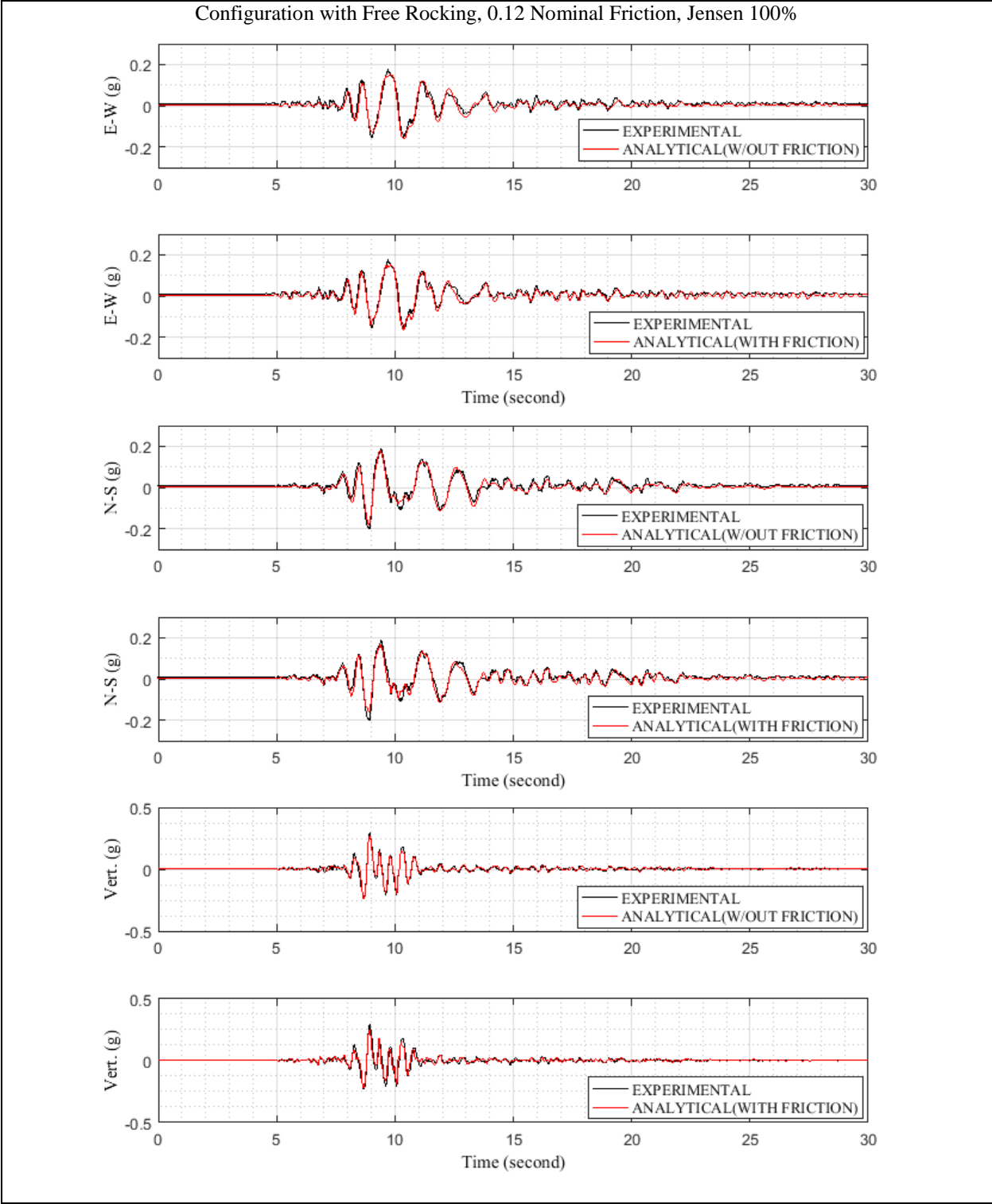


Figure 5-81 Comparison of Experimental and Analytical Acceleration Histories at Frame NE Top Corner With and Without Due Consideration for Friction Forces in Spring-damper Units in Configuration of Free Rocking, FP Isolator Type B with 0.12 Nominal Friction in Jensen 100% Motion

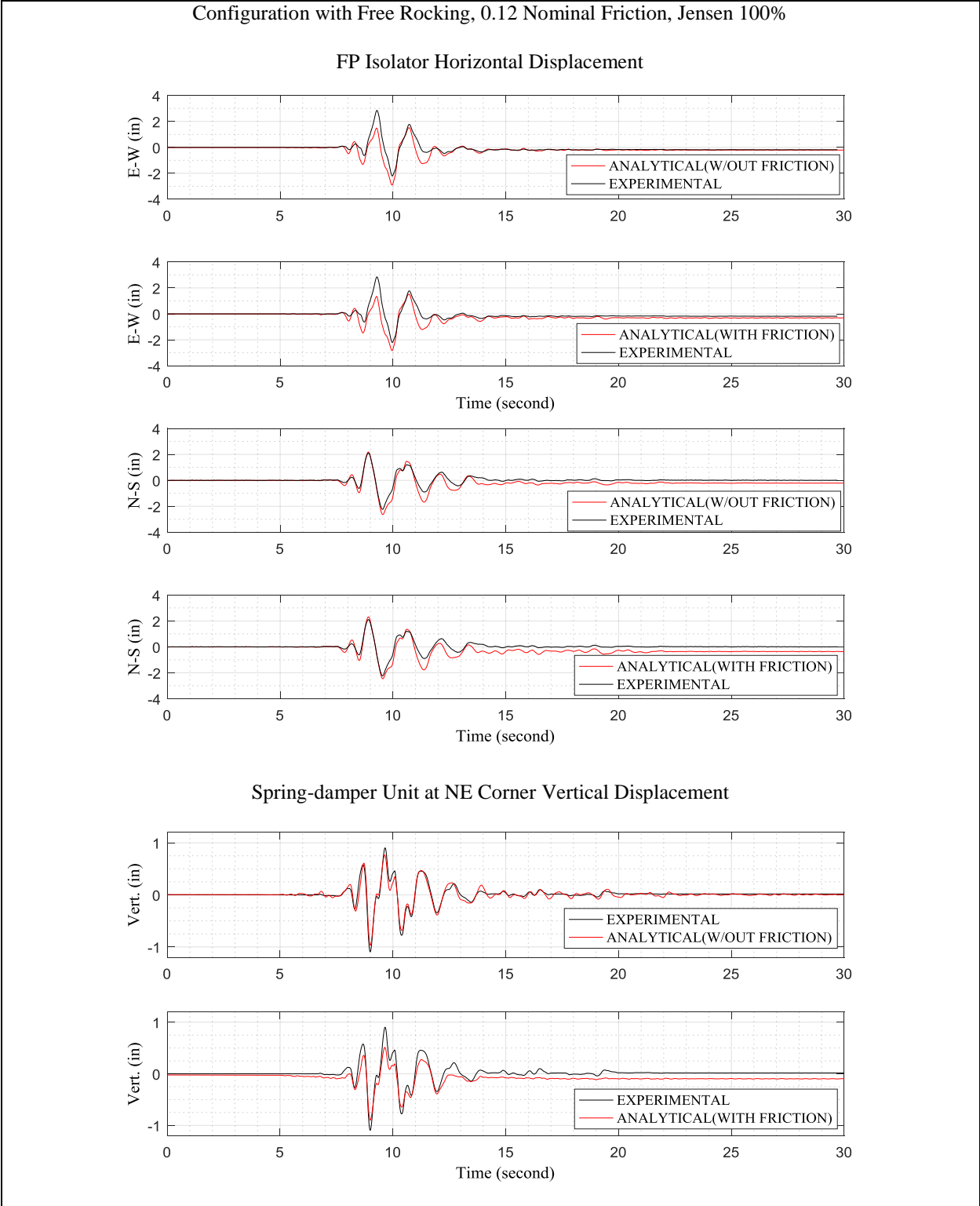


Figure 5-82 Comparison of Experimental and Analytical Isolator Displacement Histories With and Without Due Consideration for Friction Forces in Spring-damper Units in Configuration of Free Rocking, FP Isolator Type B with 0.12 Nominal Friction in Jensen 100% Motion

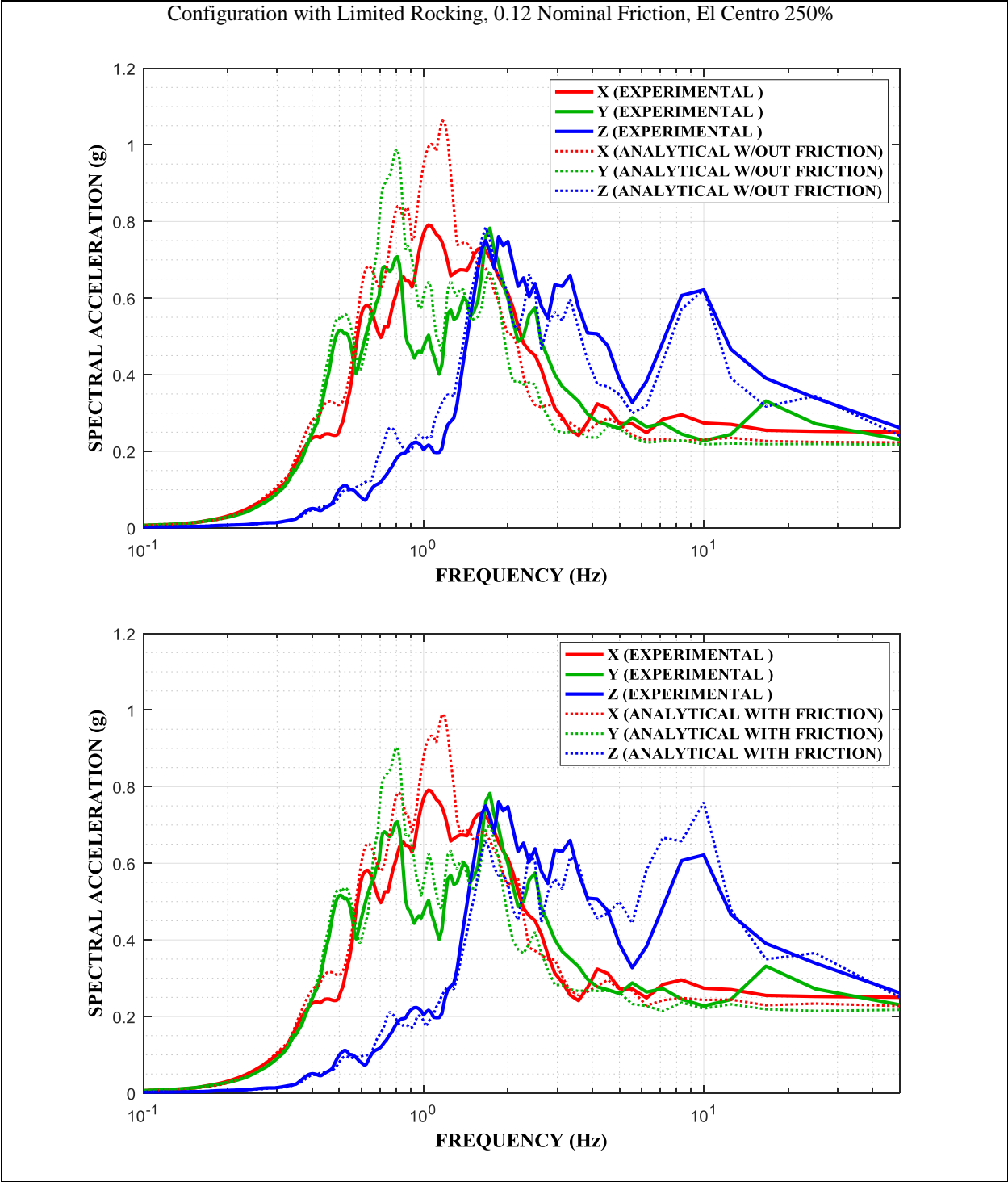


Figure 5-83 Comparison of Experimental and Analytical 5%-damped Response Spectra at Frame NE Top Corner With and Without Due Consideration for Friction Forces in Spring-damper Units in Configuration of Limited Rocking, FP Isolator Type B with 0.12 Nominal Friction in El Centro 250% Motion

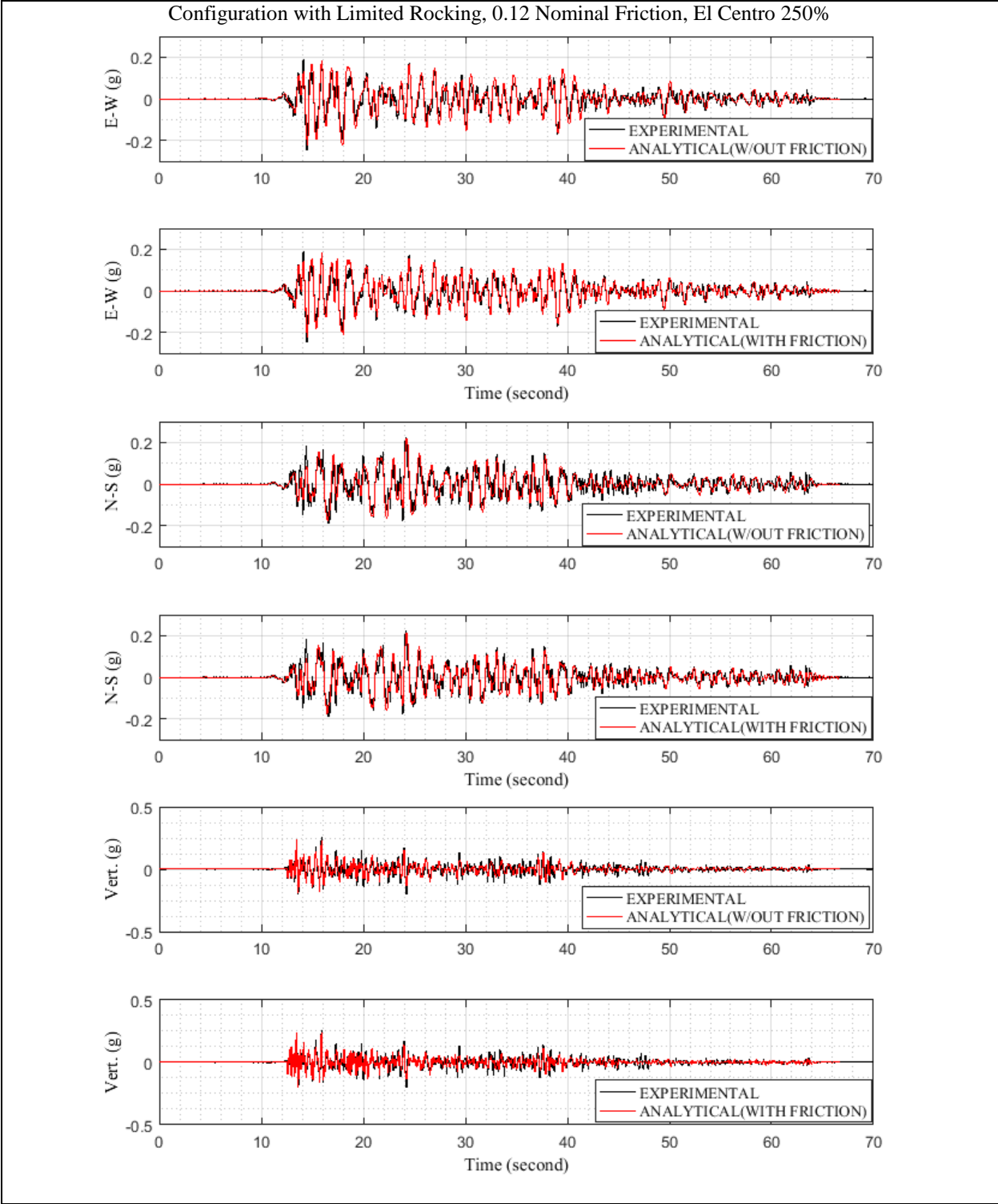


Figure 5-84 Comparison of Experimental and Analytical Acceleration Histories at Frame NE Top Corner With and Without Due Consideration for Friction Forces in Spring-damper Units in Configuration of Limited Rocking, FP Isolator Type B with 0.12 Nominal Friction in El Centro 250% Motion

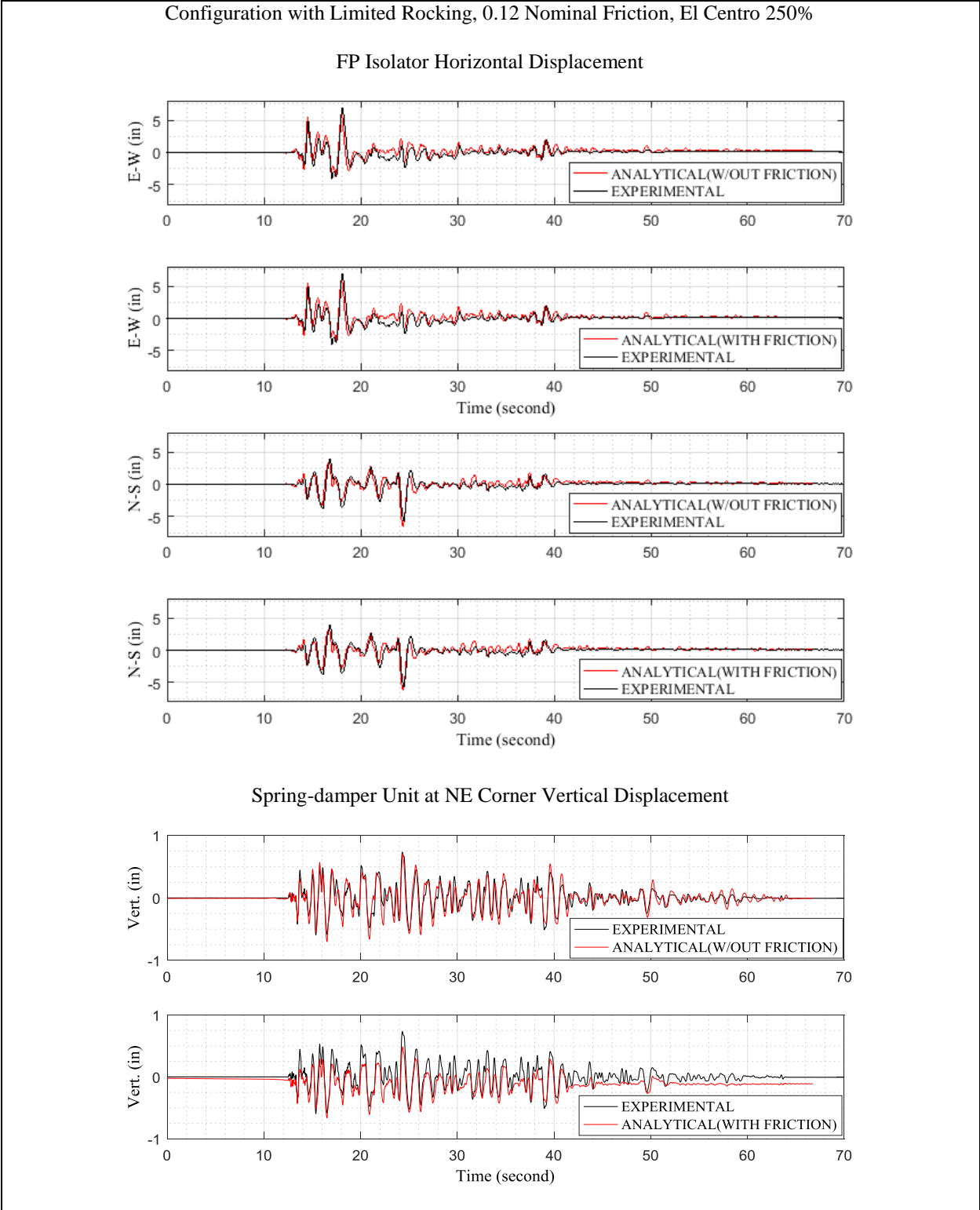


Figure 5-85 Comparison of Experimental and Analytical Isolator Displacement Histories With and Without Due Consideration for Friction Forces in Spring-damper Units in Configuration of Limited Rocking, FP Isolator Type B with 0.12 Nominal Friction in El Centro 250% Motion

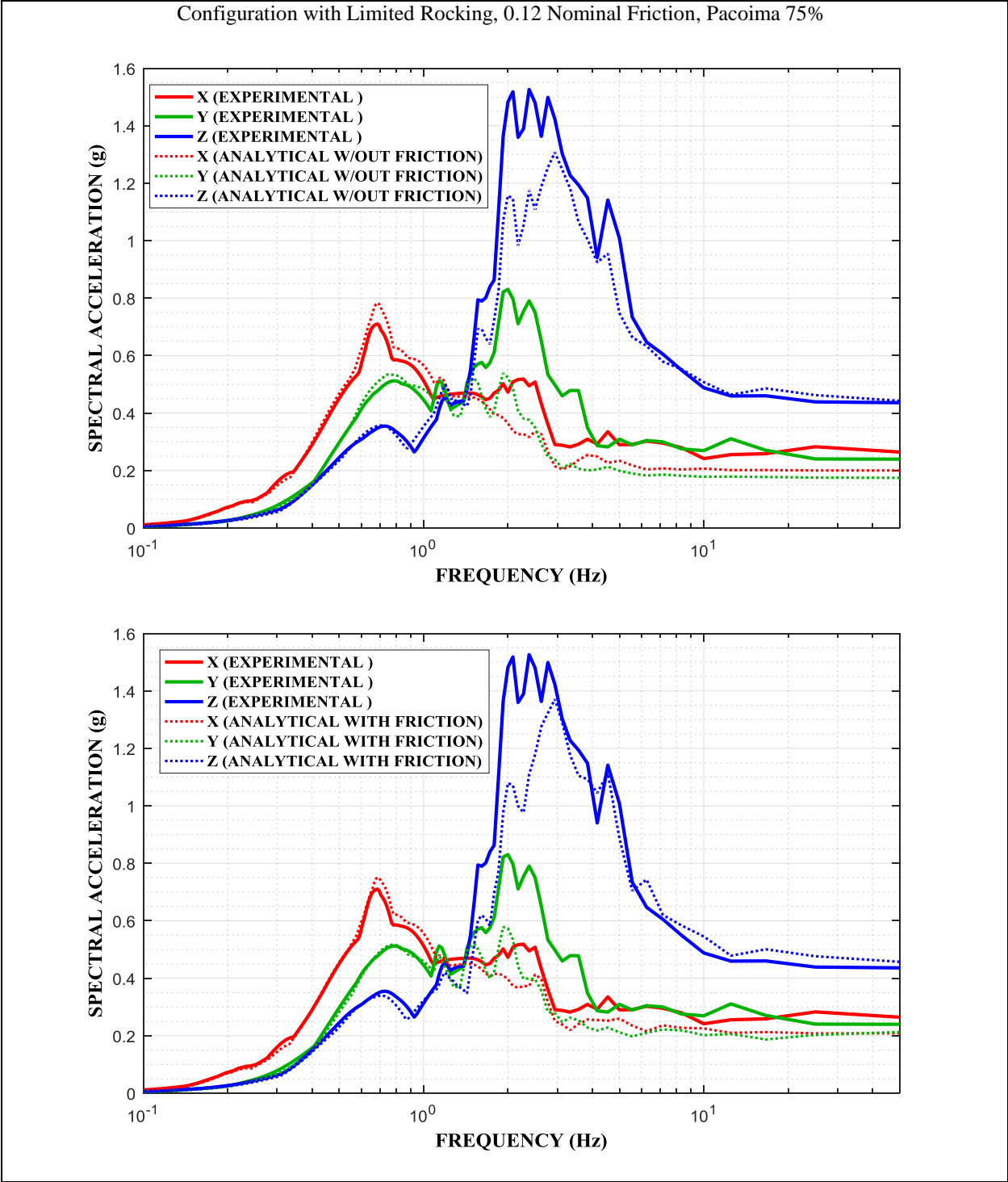


Figure 5-86 Comparison of Experimental and Analytical 5%-damped Response Spectra at Frame NE Top Corner With and Without Due Consideration for Friction Forces in Spring-damper Units in Configuration of Limited Rocking, FP Isolator Type B with 0.12 Nominal Friction in Pacoima 75% Motion

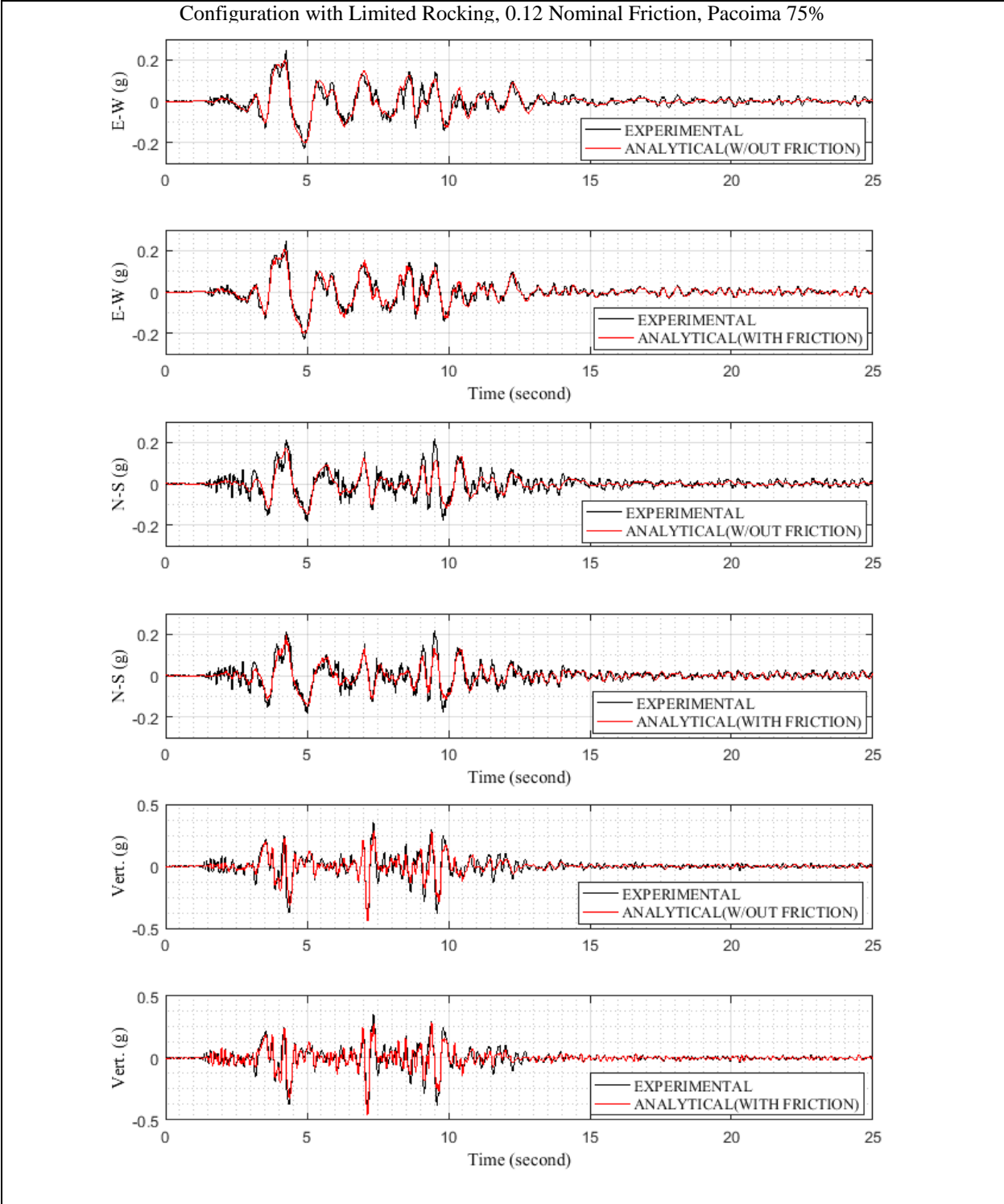


Figure 5-87 Comparison of Experimental and Analytical Acceleration Histories at Frame NE Top Corner With and Without Due Consideration for Friction Forces in Spring-damper Units in Configuration of Limited Rocking, FP Isolator Type B with 0.12 Nominal Friction in Pacoima 75% Motion

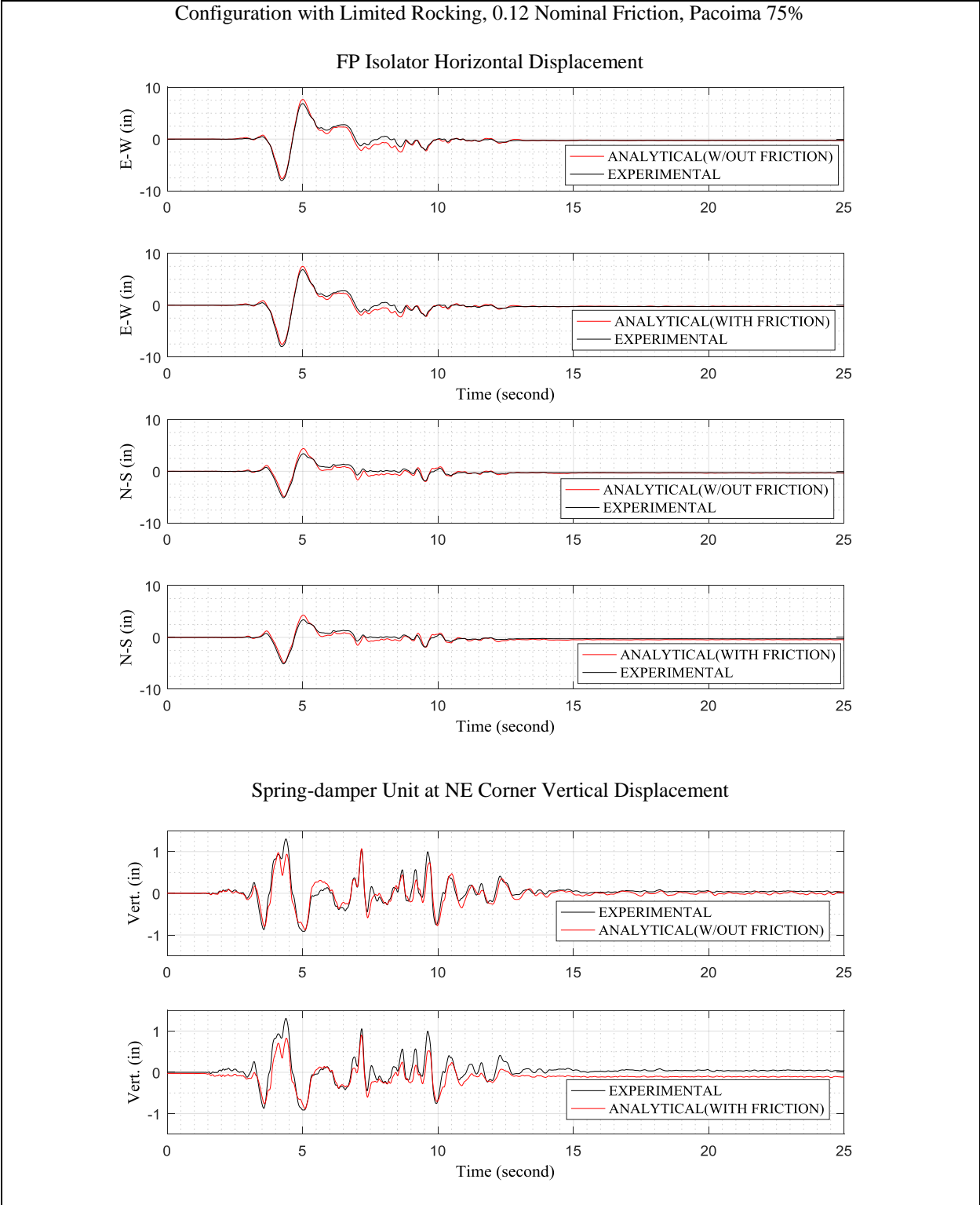


Figure 5-88 Comparison of Experimental and Analytical Isolator Displacement Histories With and Without Due Consideration for Friction Forces in Spring-damper Units in Configuration of Limited Rocking, FP Isolator Type B with 0.12 Nominal Friction in Pacoima 75% Motion

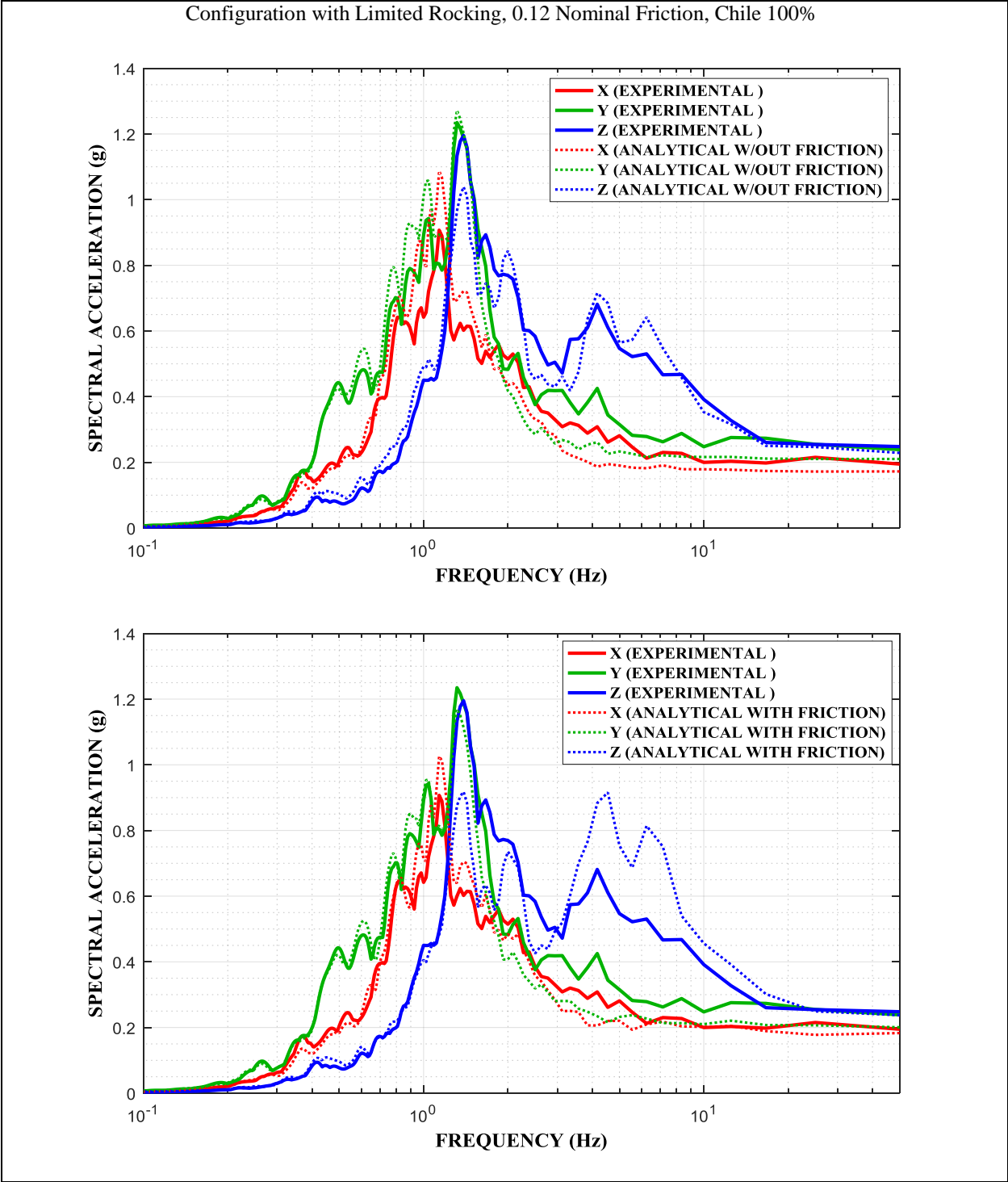


Figure 5-89 Comparison of Experimental and Analytical 5%-damped Response Spectra at Frame NE Top Corner With and Without Due Consideration for Friction Forces in Spring-damper Units in Configuration of Limited Rocking, FP Isolator Type B with 0.12 Nominal Friction in Chile 100% Motion

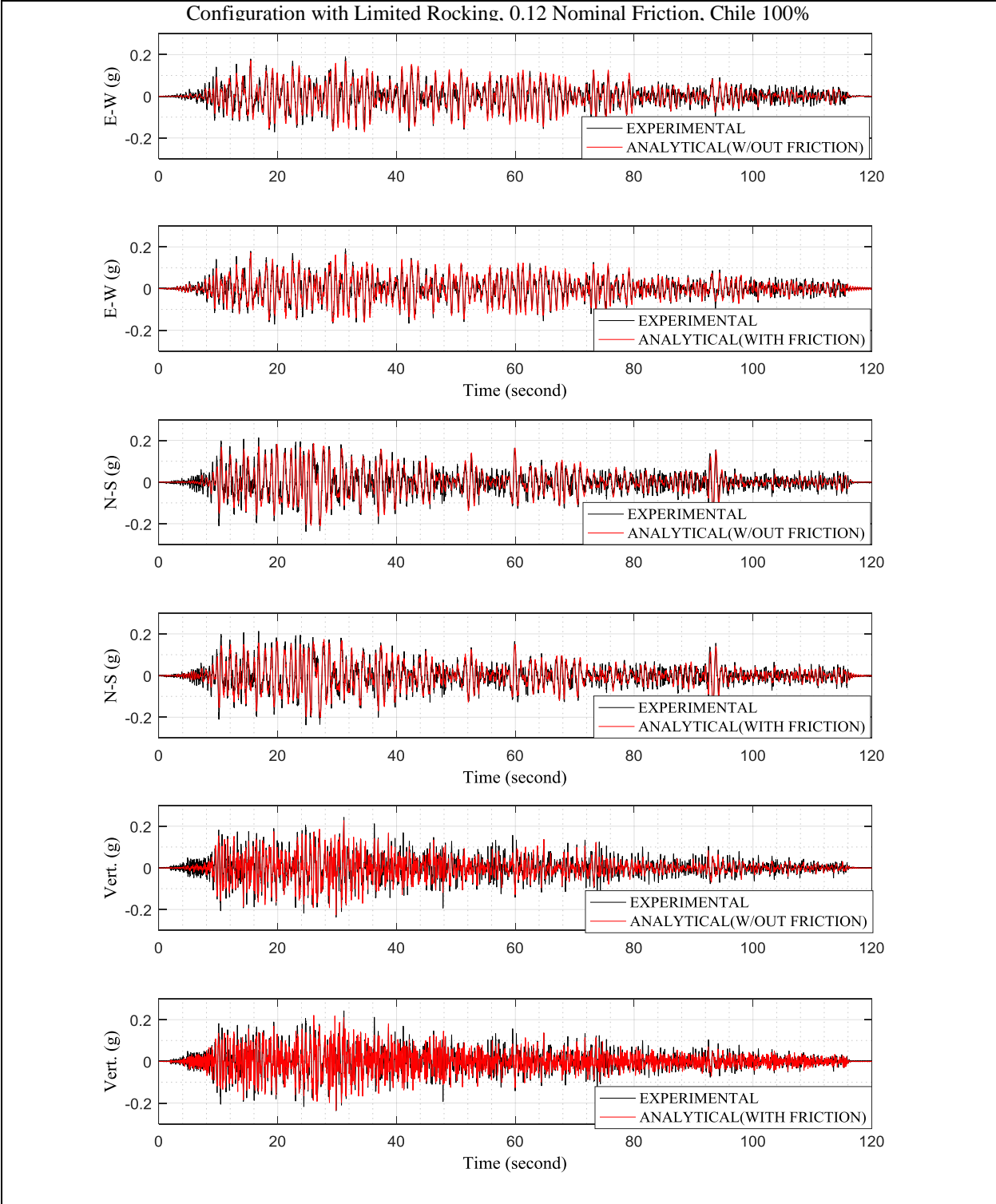


Figure 5-90 Comparison of Experimental and Analytical Acceleration Histories at Frame NE Top Corner With and Without Due Consideration for Friction Forces in Spring-damper Units in Configuration of Limited Rocking, FP Isolator Type B with 0.12 Nominal Friction in Chile 100% Motion

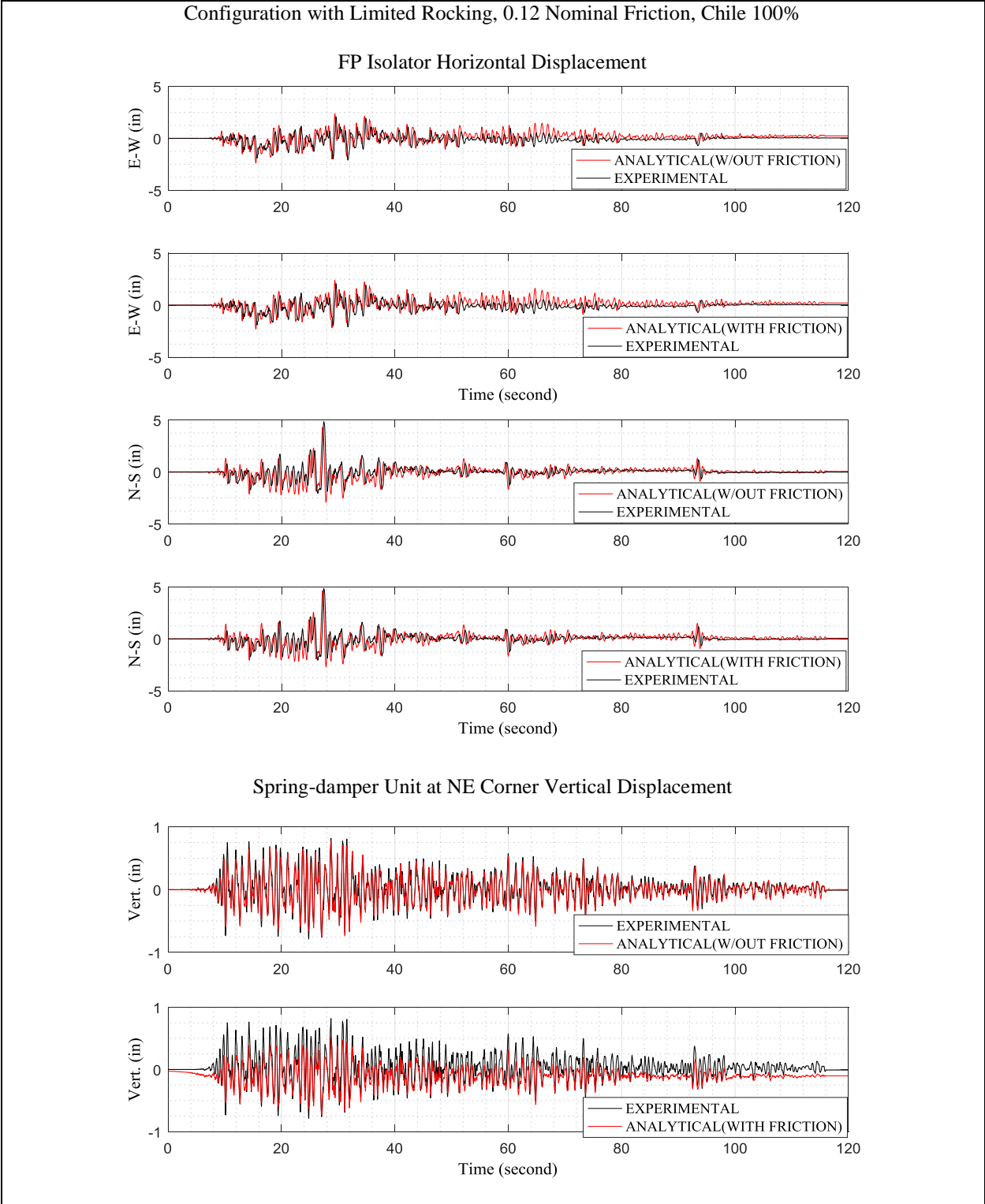


Figure 5-91 Comparison of Experimental and Analytical Isolator Displacement Histories With and Without Due Consideration for Friction Forces in Spring-damper Units in Configuration of Limited Rocking, FP Isolator Type B with 0.12 Nominal Friction in Chile 100% Motion

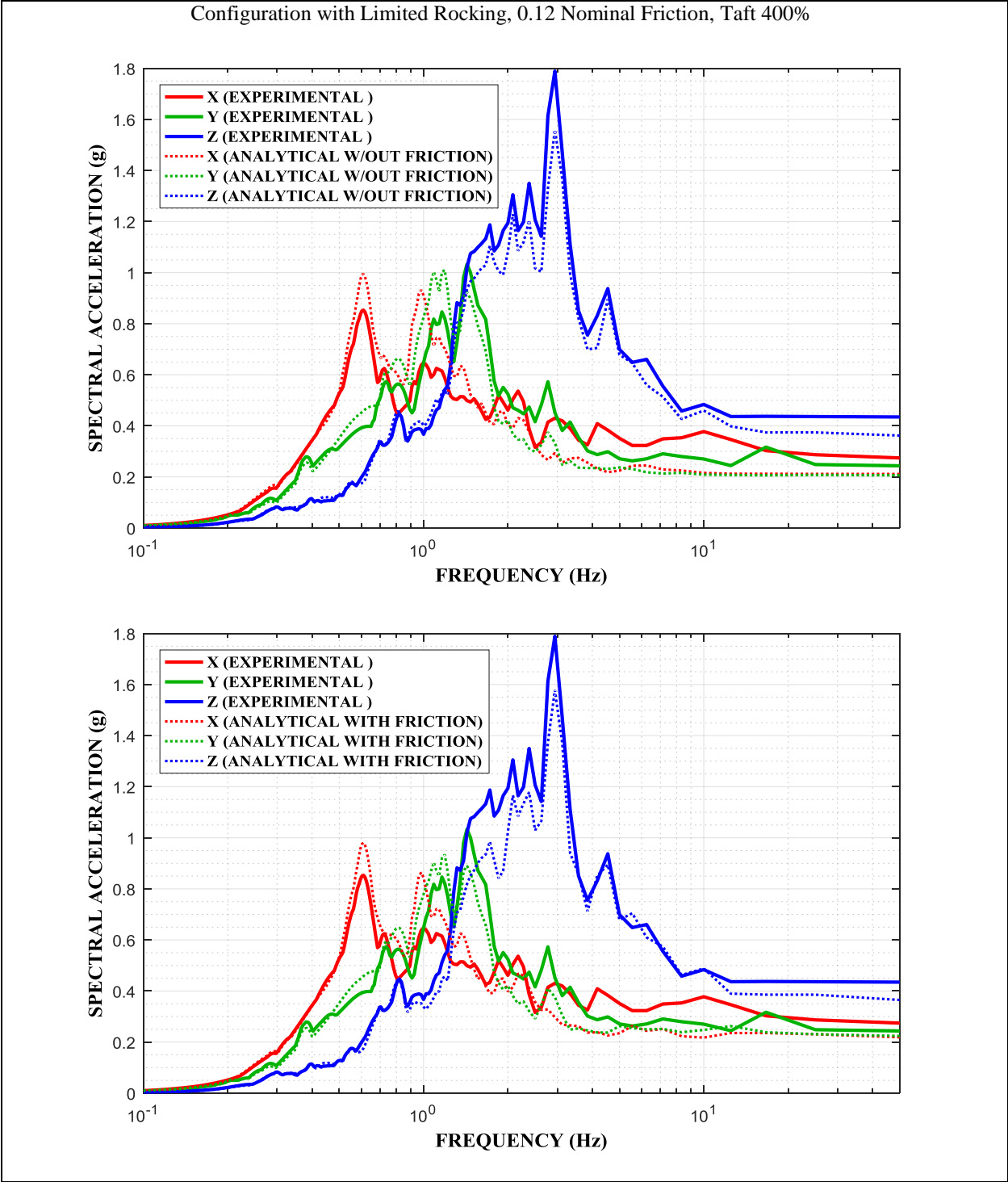


Figure 5-92 Comparison of Experimental and Analytical 5%-damped Response Spectra at Frame NE Top Corner With and Without Due Consideration for Friction Forces in Spring-damper Units in Configuration of Limited Rocking, FP Isolator Type B with 0.12 Nominal Friction in Taft 400% Motion

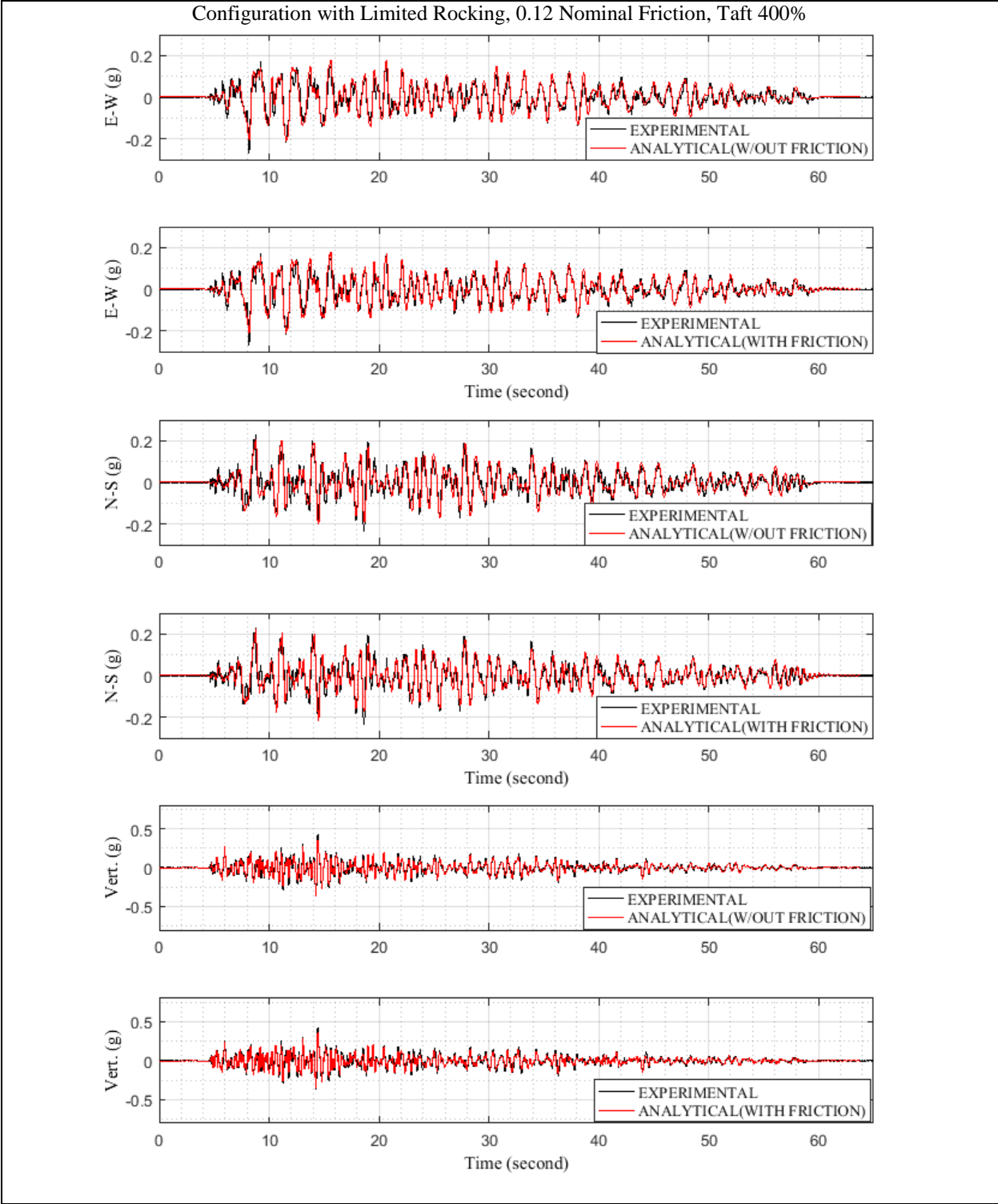


Figure 5-93 Comparison of Experimental and Analytical Acceleration Histories at Frame NE Top Corner With and Without Due Consideration for Friction Forces in Spring-damper Units in Configuration of Limited Rocking, FP Isolator Type B with 0.12 Nominal Friction in Taft 400% Motion

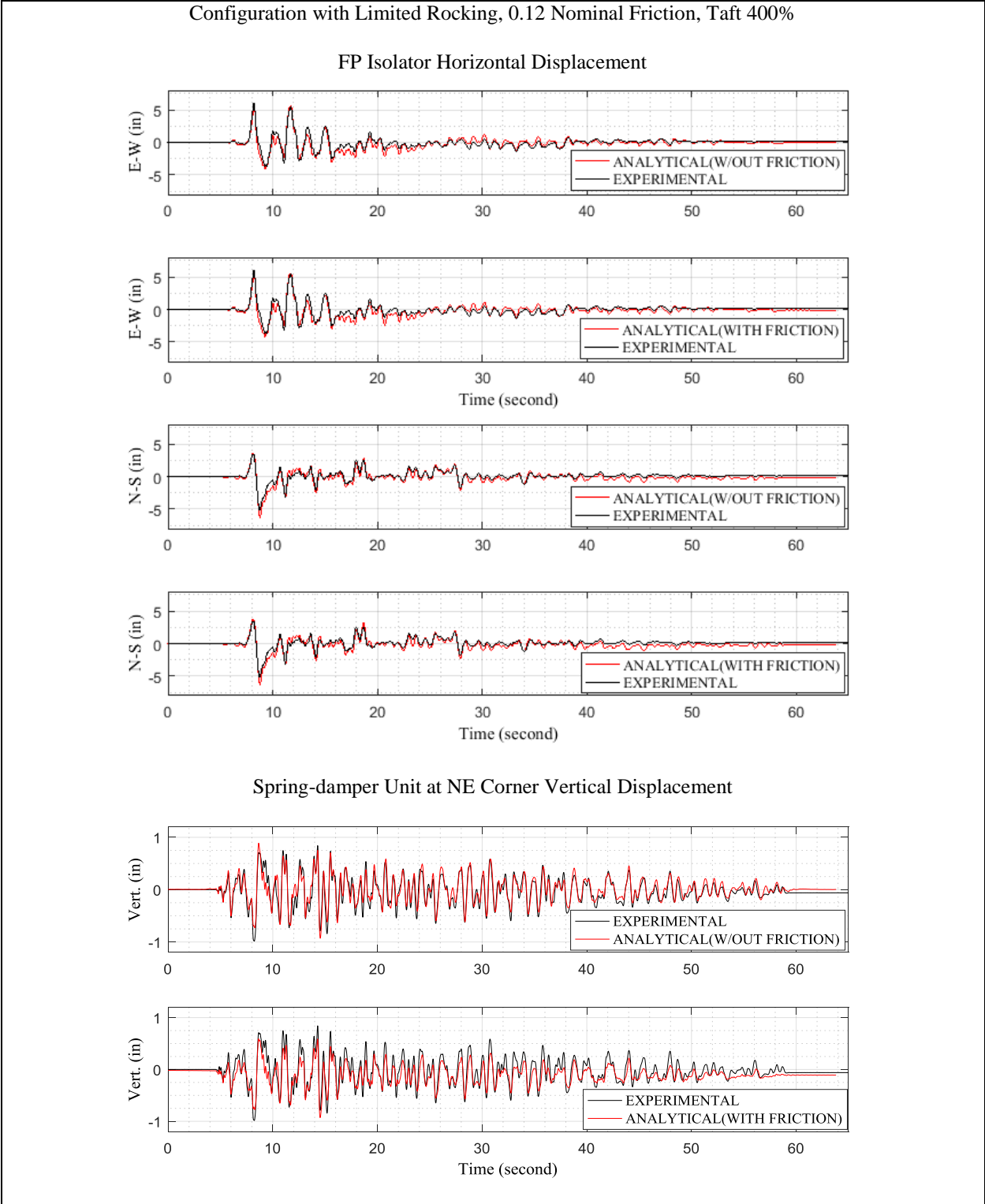


Figure 5-94 Comparison of Experimental and Analytical Isolator Displacement Histories With and Without Due Consideration for Friction Forces in Spring-damper Units in Configuration of Limited Rocking, FP Isolator Type B with 0.12 Nominal Friction in Taft 400% Motion

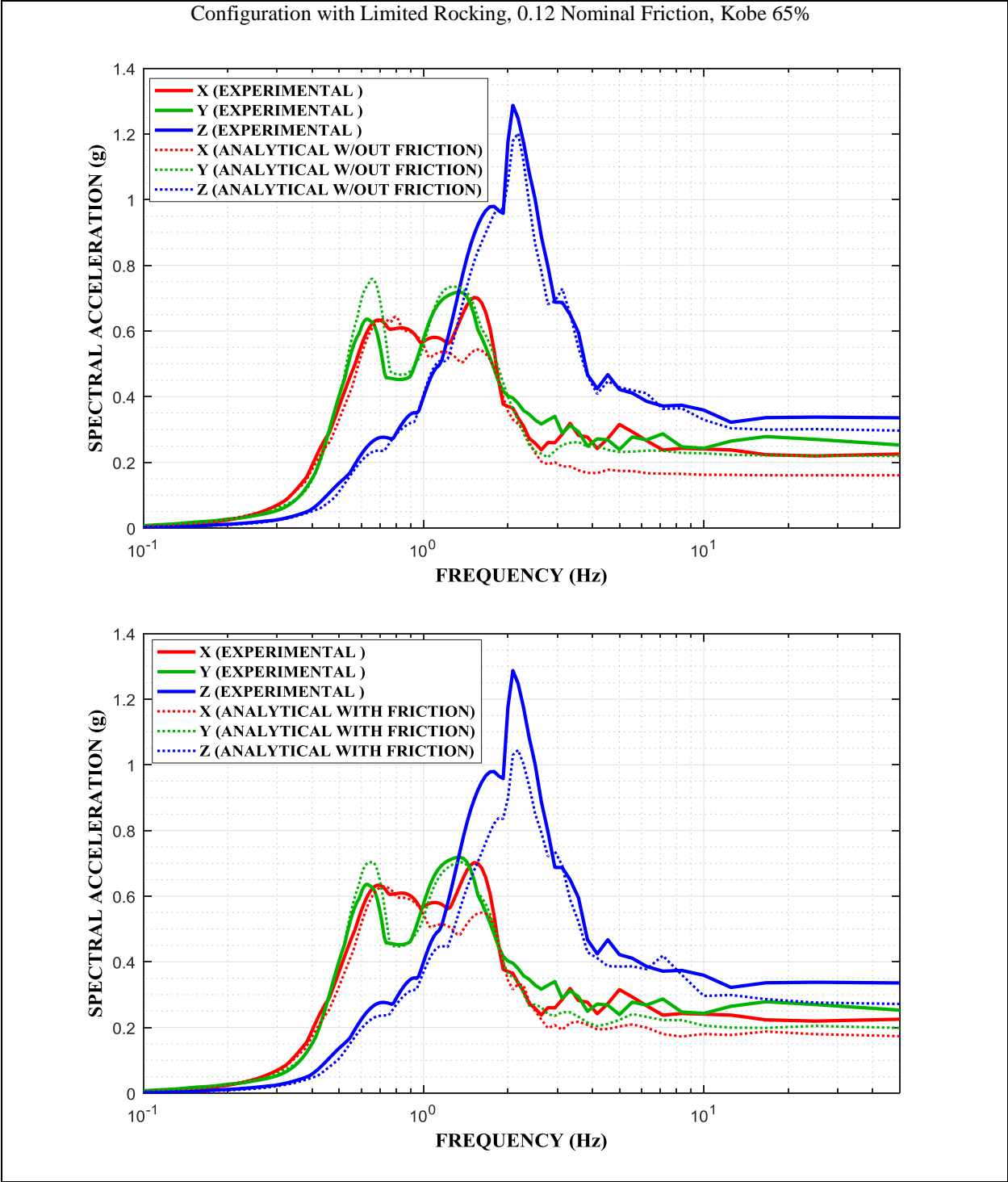


Figure 5-95 Comparison of Experimental and Analytical 5%-damped Response Spectra at Frame NE Top Corner With and Without Due Consideration for Friction Forces in Spring-damper Units in Configuration of Limited Rocking, FP Isolator Type B with 0.12 Nominal Friction in Kobe 65% Motion

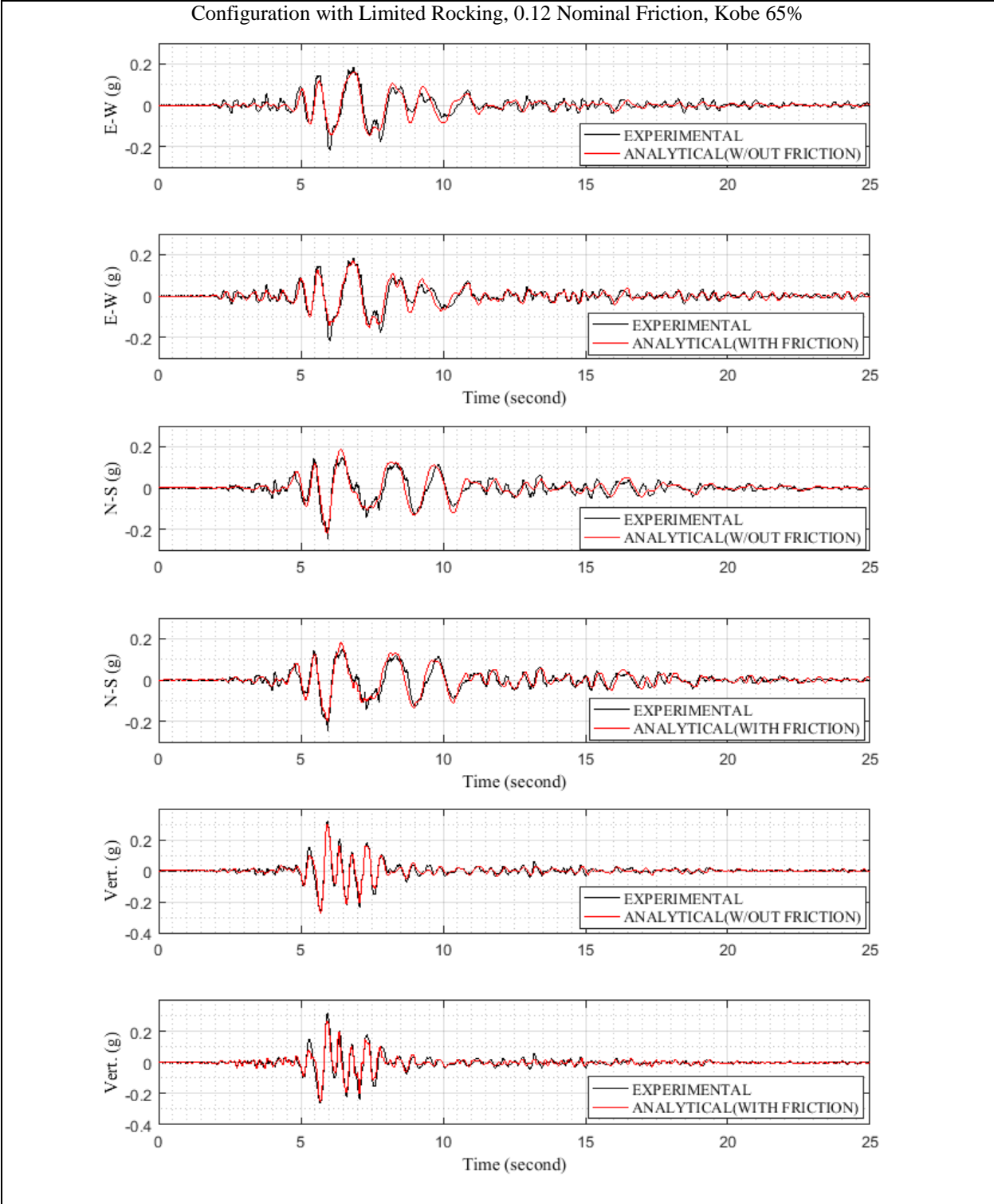


Figure 5-96 Comparison of Experimental and Analytical Acceleration Histories at Frame NE Top Corner With and Without Due Consideration for Friction Forces in Spring-damper Units in Configuration of Limited Rocking, FP Isolator Type B with 0.12 Nominal Friction in Kobe 65% Motion

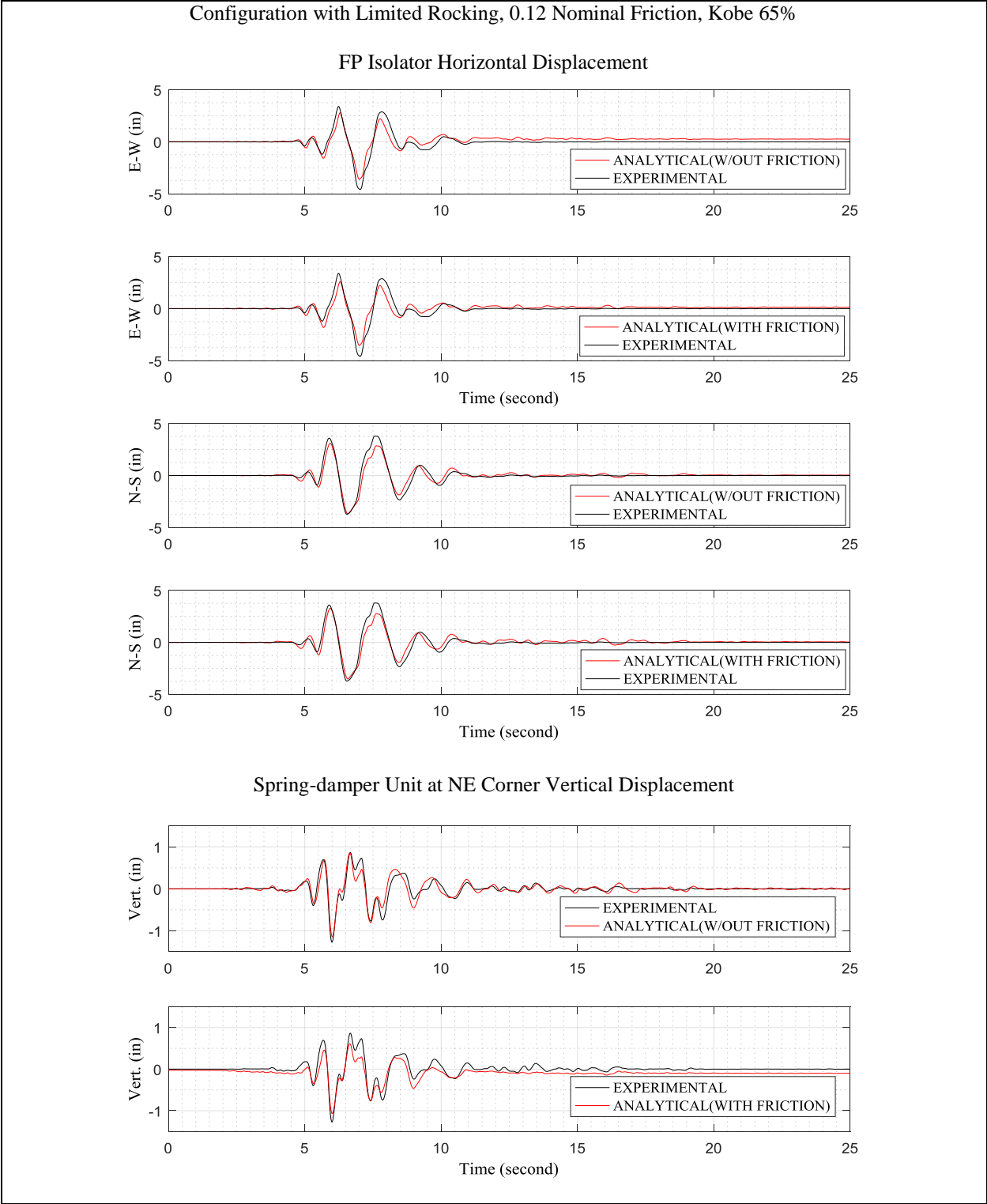


Figure 5-97 Comparison of Experimental and Analytical Isolator Displacement Histories With and Without Due Consideration for Friction Forces in Spring-damper Units in Configuration of Limited Rocking, FP Isolator Type B with 0.12 Nominal Friction in Kobe 65% Motion

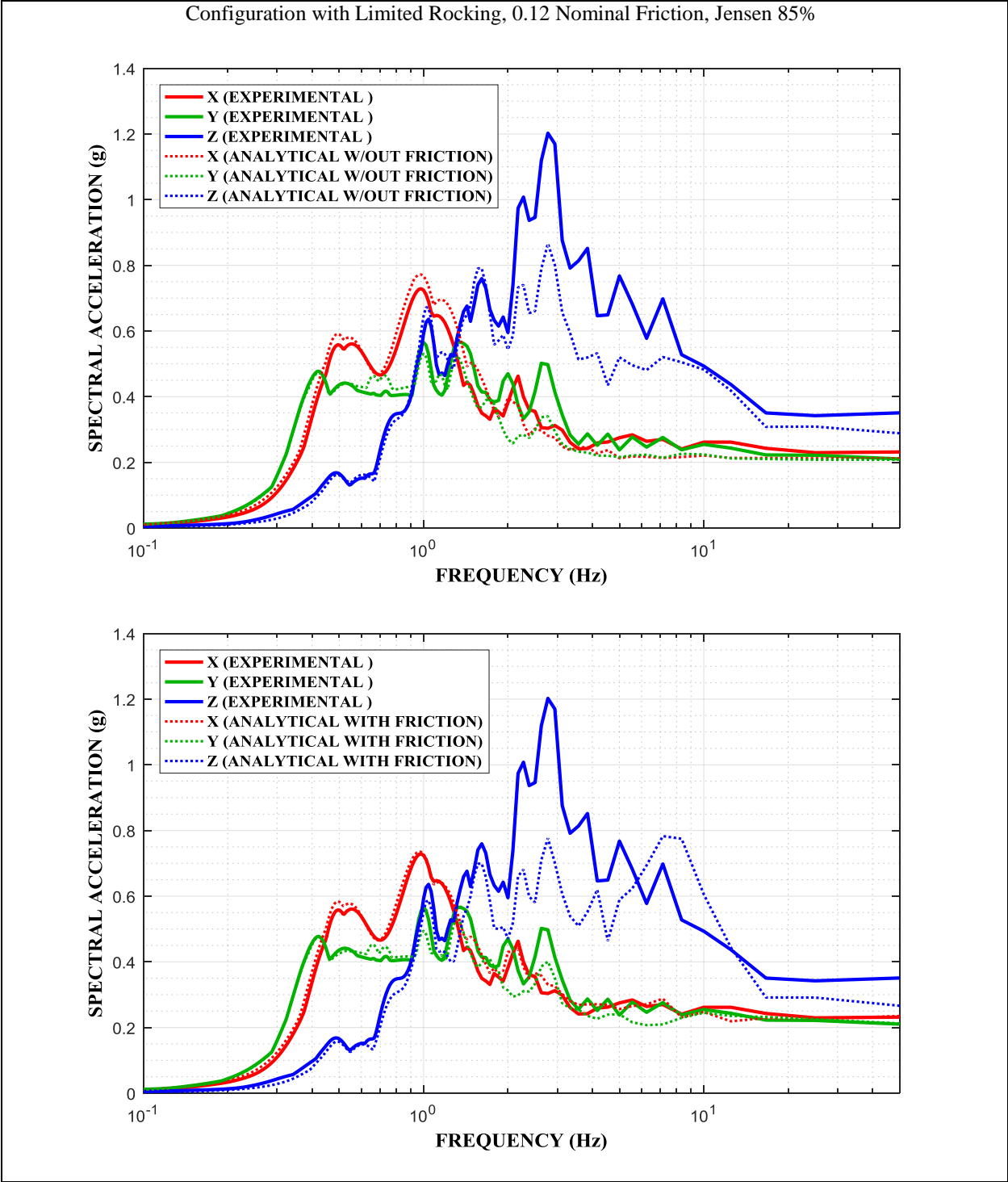


Figure 5-98 Comparison of Experimental and Analytical 5%-damped Response Spectra at Frame NE Top Corner With and Without Due Consideration for Friction Forces in Spring-damper Units in Configuration of Limited Rocking, FP Isolator Type B with 0.12 Nominal Friction in Jensen 85% Motion

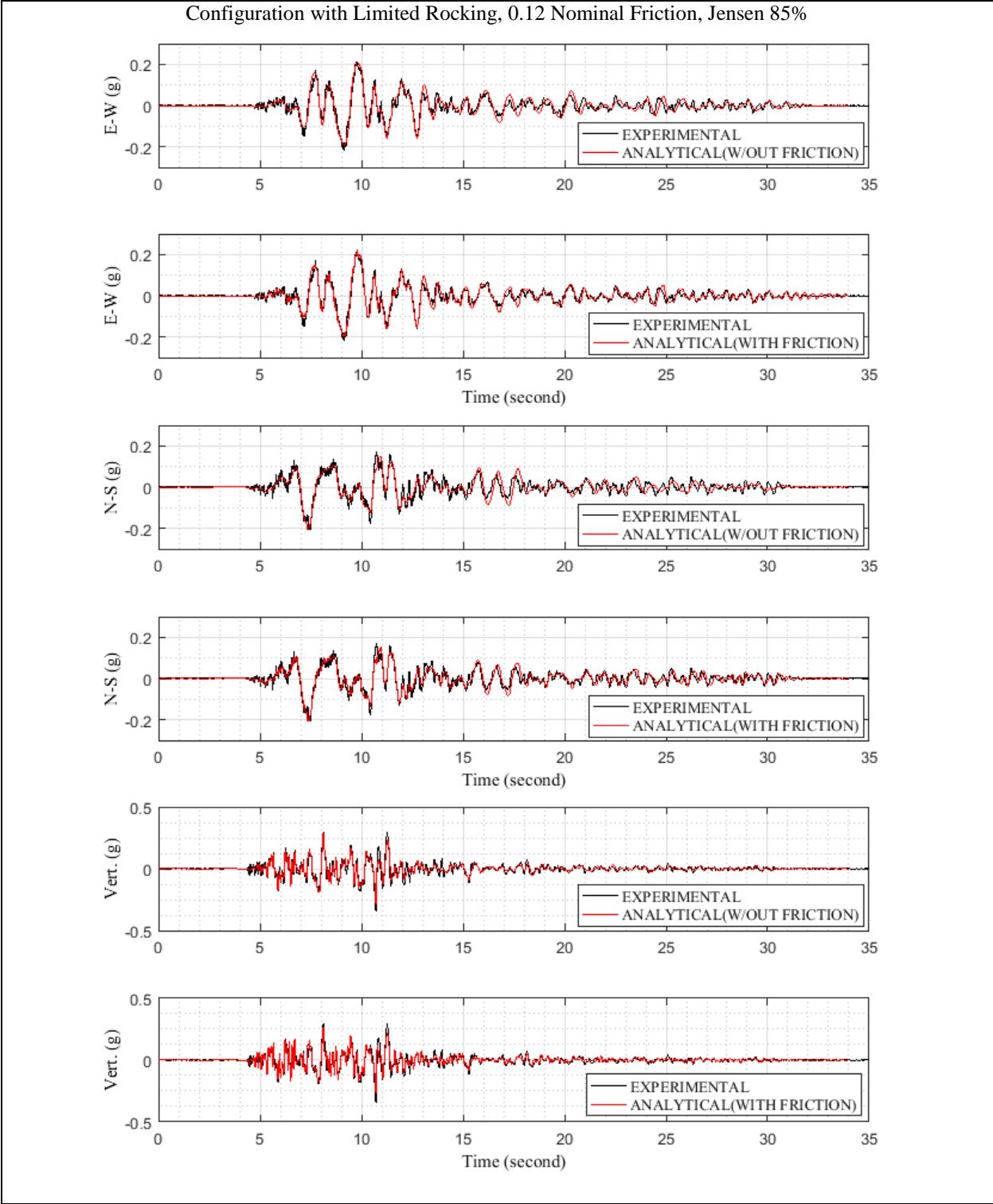


Figure 5-99 Comparison of Experimental and Analytical Acceleration Histories at Frame NE Top Corner With and Without Due Consideration for Friction Forces in Spring-damper Units in Configuration of Limited Rocking, FP Isolator Type B with 0.12 Nominal Friction in Jensen 85% Motion

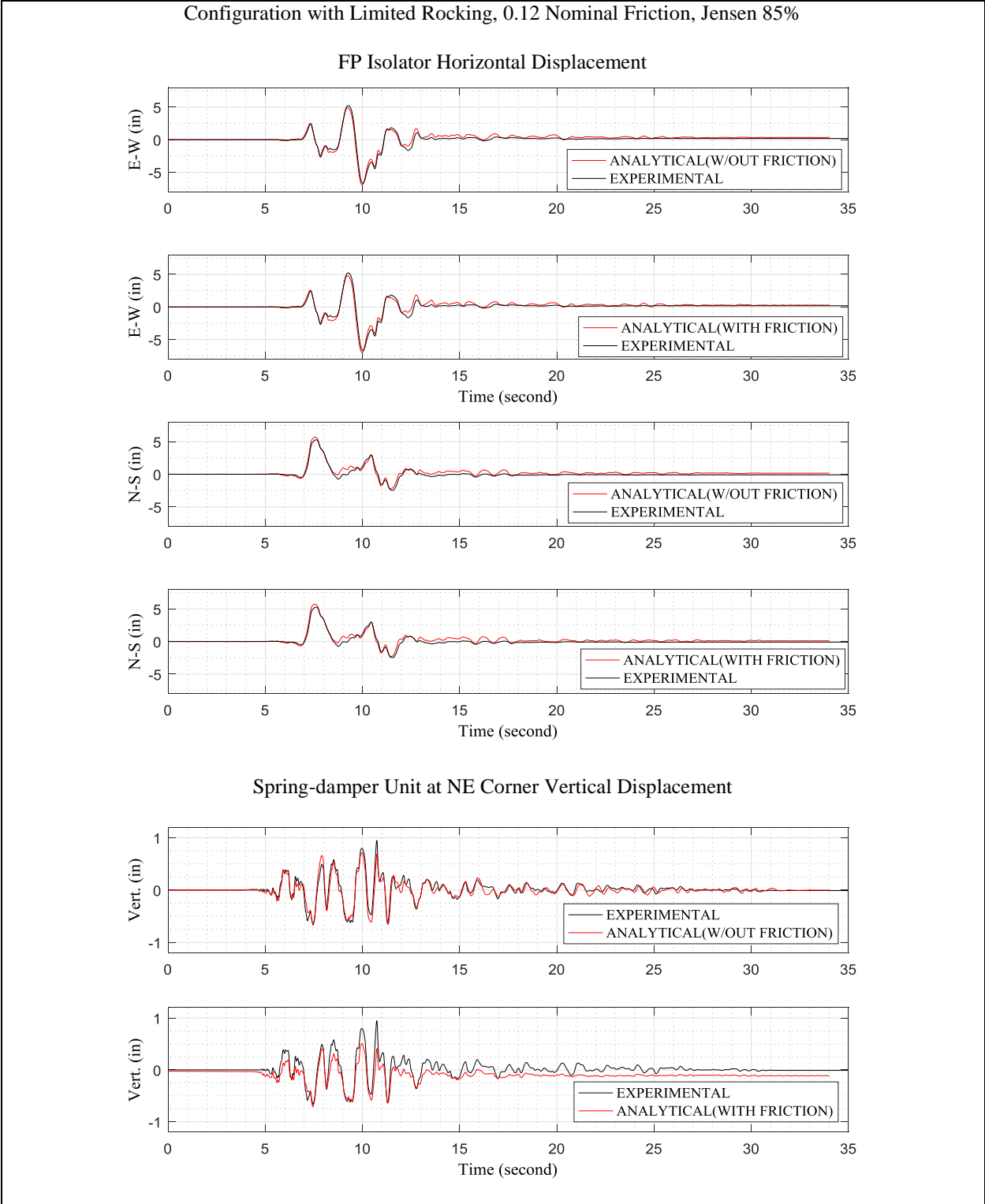


Figure 5-100 Comparison of Experimental and Analytical Isolator Displacement Histories With and Without Due Consideration for Friction Forces in Spring-damper Units in Configuration of Limited Rocking, FP Isolator Type B with 0.12 Nominal Friction in Jensen 85% Motion

5.6 Summary

It has been demonstrated in this section that it is possible to predict the response of the tested model of a transformer supported by a combined horizontal and vertical seismic isolation system in tri-axial seismic excitation with sufficient accuracy. Specifically, the acceleration histories on the main body of the model and their response spectra and the isolator's horizontal and vertical displacements could be predicted with sufficient accuracy. However, the acceleration histories of the top of the flexibly-installed bushing of the model were significantly under-estimated. It was determined that rocking motion of the shake table contributed to the motion of the bushing top in the horizontal direction and its inclusion in the analysis improved the accuracy of the prediction. However, the main contributor to the underestimation of the acceleration at the top of the bushing was that the actual damping in the bushing was less than the value used in the analytical model.

On the basis of the results of the analysis and comparisons to experimental results, and on the basis of observations in identification tests of the tested model, it was concluded that the spring-damper units of the isolation system did not exhibit large enough friction to affect the response. Particularly, the inclusion of friction in the model of the devices resulted in under-prediction of the vertical motion of the isolators and some deterioration in the accuracy of the analytical prediction of other response quantities by comparison to a model without friction.

SECTION 6

EXAMPLES OF ANALYSIS AND DESIGN

6.1 Introduction

Example designs are presented with the intention of providing guidance in the application of seismic isolation to electrical transformers rather than presenting one detailed design. A typical transformer and a site of moderate seismicity (in terms of qualification of the equipment) were selected and a detailed analysis study was conducted. Then additional assumptions were made on the seismic hazard for the design and additional summary results were obtained. Specifically:

- a) The site of the transformer was selected to be in Eugene, Oregon in an area with a peak ground acceleration of 0.34g (per ASCE 7-2010, $S_s=0.85g$, $PGA=S_s/2.5=0.34g$) for which the equipment qualification level per IEEE (2005) is moderate. The seismic hazard for the site and triplets of ground motions for the site were developed and used for the analysis and design.
- b) A second hypothetical site was then assumed in which the PGA exceeds 0.5g so that the equipment qualification level per IEEE (2005) is high. The site-specific response spectrum and ground motions representing it were assumed to be those of the site at Eugene, Oregon multiplied by factor of 1.5.
- c) A typical transformer was selected for the example. It is the one shown in Figure 2-1 which is isolated with a horizontal isolation system only in a location different than that the site of the example. The transformer features three bushings of which the as-installed dynamic characteristics are unknown but assumed in consistency with values in Table 2-1. The assessment of performance of the developed seismic isolation design includes calculations of the accelerations at the center of mass of the bushings. Accordingly, a more detailed model of the bushings (particularly the location of their center of mass with respect to the isolation system) was developed. Based on the fragility analysis results for electrical transformers reported in Kitayama et al (2016), seismic isolation for the considered location in Eugene, Oregon provides significant benefits summarized as follows. For a

transformer of similar configuration as the one of Figure 2-1, the probability of failure in 50 years of lifetime is about (a) 3.84% when non-isolated, (b) 0.60% when isolated with a two-dimensional isolation system, and (c) 0.33% (allowed to freely rock) to 0.39% (rocking restrained) when isolated by a three-dimensional isolation system (Kitayama et al, 2016, Table 9-10, 1g bushing acceleration limit at its center of mass, location 7). These results indicate that three-dimensional seismic isolation does not offer a significant advantage and just two-dimensional isolation is sufficient for this case. This is verified in the study of this section. (The results on the probability of failure quoted above were based on a model in which failure was dominated by the acceleration at the center of mass of the bushings, which was assumed to be located lower than as assumed in the design presented in this section. Accordingly, we expect the probability of failure for the transformer considered in the study of this section when allowed to freely rock to be higher than in the study of Kitayama et al, 2016).

- d) The transformer with the designed two-dimensional and three-dimensional isolation systems is then transported to the hypothetical location of higher seismicity as described in item b above and re-analyzed. The benefits of three-dimensional isolation become then clearer.

6.2 Seismic Hazard Analysis for the Site and Selection and Scaling of Motions for Dynamic Analysis

The site for the example transformer is near Eugene, Oregon and has latitude of [REDACTED] and longitude of [REDACTED] (coordinates are not shown in the publicly available report). The site class is characterized as C with a shear wave velocity $V_{s30}=535\text{m/sec}$. A seismic hazard analysis for this site and selection and scaling of motions for response history analysis was performed by Mazzoni and Bozorgnia (2017). The main results of this study are presented in this report.

The target spectrum was defined as the Uniform Hazard Spectrum (UHS) with a return period of 2475 years (2% probability of being exceeded in 50 years). The UHS was obtained by interpolating the seismic hazard curves at the selected annual frequency of exceedance (inverse of return period in years) using the data (in text form) of the 2008 USGS Hazard-Curve Application

(the data were validated by comparison to data obtained using the NEHRP 2015 Uniform Hazard Tool-<https://earthquake.usgs.gov/designmaps/beta/us/>). Figure 6-1 presents the 5%-damped target spectrum (UHS). For comparison the figure also presents the spectrum of maximum considered earthquake (MCE_R) obtained on the basis of the procedures in ASCE 7-2010 (<https://earthquake.usgs.gov/designmaps/us/application.php>) and in NEHRP 2015 (<https://earthquake.usgs.gov/designmaps/beta/us/>). The parameters of the MCE_R spectra in Figure 6-1 are presented in Table 6-1. The comparison in the figure demonstrates that the uniform hazard spectrum with 2475 year return period is consistent with the maximum earthquake design-map values. Note that the MCE_R spectra in Figure 6-1 are maximum direction spectra while the uniform hazard spectrum values represent the “average” of two horizontal components (RotD50).

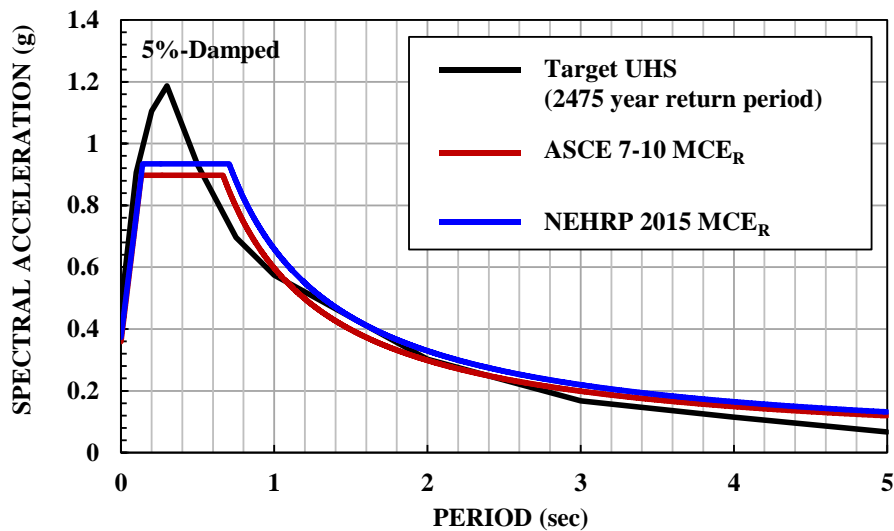


Figure 6-1 Target UHS Spectrum (2475 year return period) and MCE_R Spectra for Site

Table 6-1 Spectral Parameters for Site

Parameter	ASCE 7-10 (2009 NEHRP)	NEHRP 2015
S_s	0.846g	0.779g
S_1	0.439g	0.439g
F_a	1.062	1.2
F_v	1.361	1.5
$S_{MS} (=F_a \times S_s)$	0.898g	0.934g
$S_{M1} (=F_v \times S_1)$	0.597g	0.659g
$S_{DS} (=2/3 \times S_{MS})$	0.599g	0.623g
$S_{D1} (=2/3 \times S_{M1})$	0.398g	0.439g

De-aggregation of hazard was used to determine a range of magnitude and distance for the selection of ground motions (the 2015 USGS Unified Hazard Tool was used- <https://earthquake.usgs.gov/hazards/interactive/index.php>). The analysis determined that appropriate records are of magnitude above 8 and of rRup distance (closest distance to rupture plane) between 40 and 120km. Of the subduction zones across the world, only the regions of Japan and South America have records with large magnitude to meet the requirements of the de-aggregation study.

Table 6-2 presents eleven records that were selected for scaling in order to represent the target spectrum for the site. All satisfy the magnitude and distance criteria obtained in the de-aggregation study. The 11 selected records were then scaled by a single factor (applied to both horizontal and vertical components of the seed motions) such that the average of the horizontal spectrum RotD50 resultant of the suite closely matched the target spectrum by minimizing the mean square error in the period range of 0.1 to 5 seconds. The scale factors are presented in Table 6-2.

Figure 6-2 presents the 5%-damped horizontal resultant spectra of the 11 scaled motions, their average spectrum and the target spectrum. Figure 6-3 presents the 5%-damped vertical spectra of the 11 scaled motions and their average spectrum.

Table 6-2 Characteristics of Selected Motions and Scale Factors

Designation	Earthquake	Recording Station	Moment Magnitude	rRup (km)	Peak Ground Motion (g)		Scale Factor
					H1	H2	
Valparaiso	2010 Chile	Valparaiso Almendral	8.8	101.15	H1	0.22	2.61
					H2	0.27	
					V	0.15	
Talca	1985 Chile	Talca	8.16	92.79	H1	0.17	3.97
					H2	0.17	
					V	0.07	
Hualane	1985 Chile	Hualane	8.16	47.71	H1	0.14	4.16
					H2	0.17	
					V	0.09	
Chile	2015 Chile	GO04	8.3	73.11	H1	0.24	2.01
					H2	0.34	
					V	0.16	
Hokkaido	1994 Hokkaido	47420	8.32	130.22	H1	0.33	1.77
					H2	0.38	
					V	0.19	
Hanasaki	1994 Hokkaido	Hanasaki-f	8.32	131.83	H1	0.36	1.55
					H2	0.37	
					V	0.27	
Peru	2001 Peru	MOQ1	8.2	77.19	H1	0.30	2.16
					H2	0.22	
					V	0.17	
Tohoku-A	2011 Tohoku	41207	9.13	89.33	H1	0.22	2.08
					H2	0.22	
					V	0.11	
Tohoku-B	2011 Tohoku	47256	9.13	108.59	H1	0.14	3.07
					H2	0.18	
					V	0.10	
Nukabira	2003 Tokachi-oki	Nukabira	8.2	100.53	H1	0.13	3.94
					H2	0.11	
					V	0.10	
Tokachi-Oki	2003 Tokachi-Oki	42111	8.2	117.72	H1	0.34	1.97
					H2	0.29	
					V	0.14	

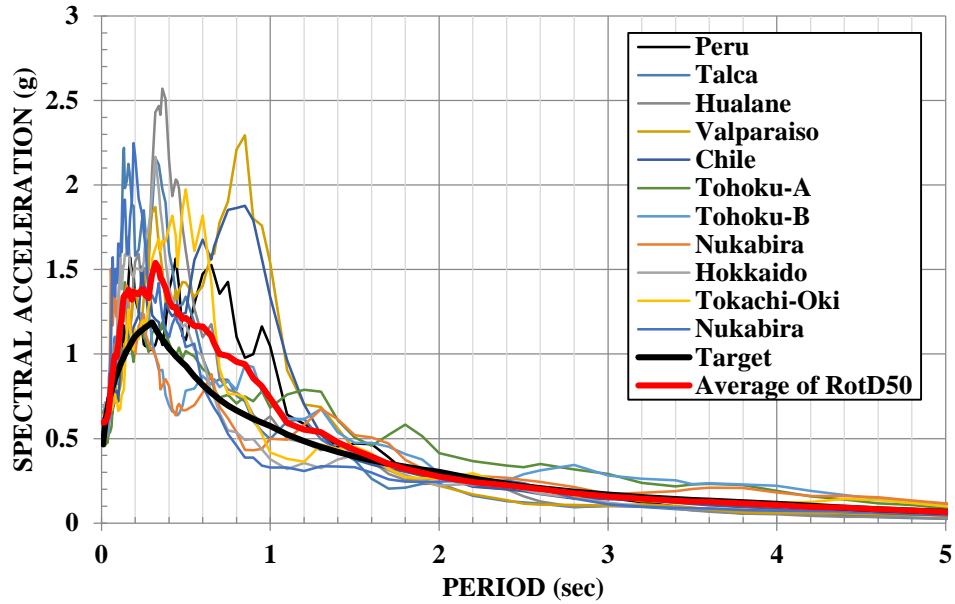


Figure 6-2 5%-damped Horizontal Resultant Spectra (RotD50) of 11 Scaled Motions and Average and Target Spectra

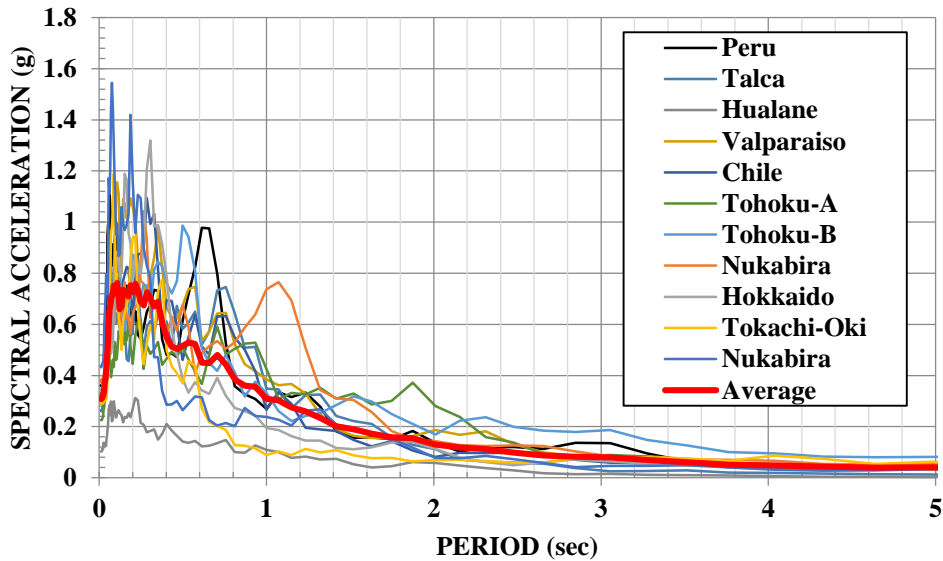


Figure 6-3 5%-damped Vertical Spectra of 11 Scaled Motions and Average Spectrum

6.3 Description of Transformer and its Isolation System

Figure 6-4 shows sections of the transformer that reveal its overall dimensions. The transformer weighs 380kip with its center of mass located 81inch above its base at the centerline in the

transverse direction and off by 4inch from the centerline in the longitudinal direction. This is the transformer shown in Figure 2-1 and with important dimensions shown in the sections of Figure 2-6. The weight distribution and the as-installed frequencies of the three bushings are not known. However based on their dimensions and comparison to the properties of known bushings in Table 2-1, the center of mass of each bushing was assumed to be located at distance of 44inch above the bushing turret and its weight to be 0.8kip lumped at the center of mass and another 0.7kip lumped at the connection to the turret. The as-installed frequencies were assumed to be 8Hz in the transverse direction and 10Hz in the longitudinal direction. These values are within the range of the properties of the bushings in Table 2-1. Also the 8Hz frequency is the largest frequency in the peak spectral acceleration range of the horizontal response spectrum for the site and the 10Hz frequency is centered in the peak spectral acceleration range of the vertical spectrum for the site (Figures 6-2 and 6-3). That is, the selected frequencies for the bushing should produce conservative results for the bushing accelerations. Per IEEE (2005), damping in the bushings was assumed to be 0.02 of critical.

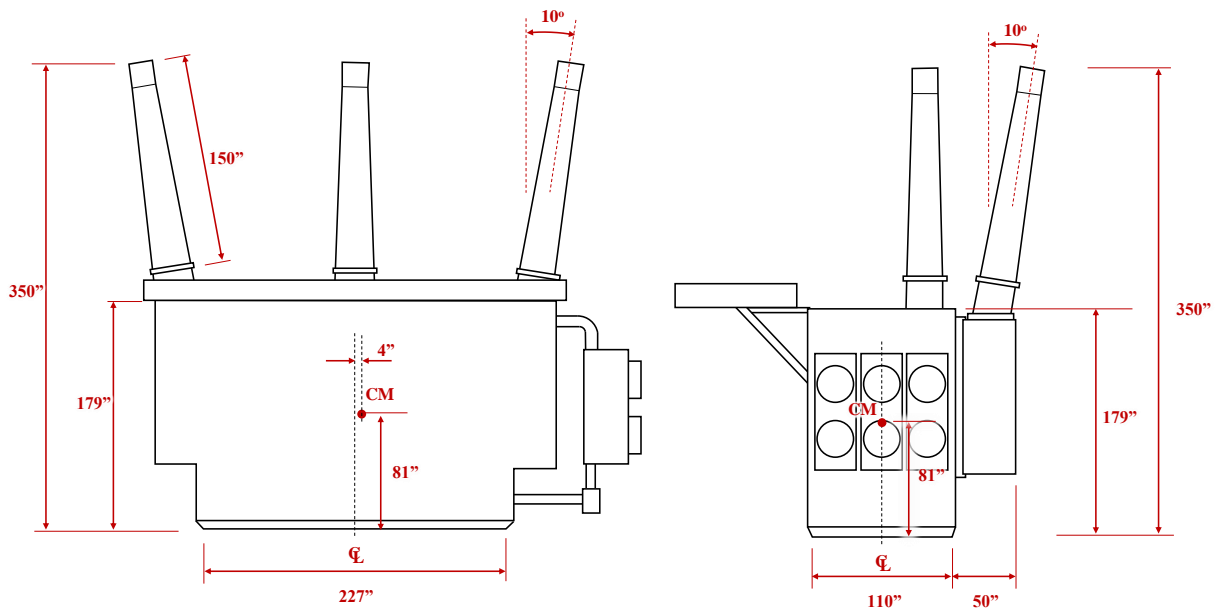


Figure 6-4 Longitudinal and Transverse Sections of Example Transformer

The isolation system for the transformer is based on the tested configuration that allows for free rocking. Figure 6-5 shows sections of the isolated transformer, Figure 6-6 shows a three-

dimensional schematic of the foundation and Figure 6-7 shows sections of the foundation, all in the case of the isolation system with allowance for free rocking. The foundation is envisioned to be embedded in the ground so that only the FP isolators project above the top of the ground. Access to the isolation system is provided at locations along one dimension (longest although for the presented design the foundation is square) and on both sides. The isolators are shown installed on pedestals. There is sufficient height in the isolation pit for people to enter for inspecting the isolators and for maintenance if needed. Note that the presented schematics represent one possible configuration out of many for the foundation.

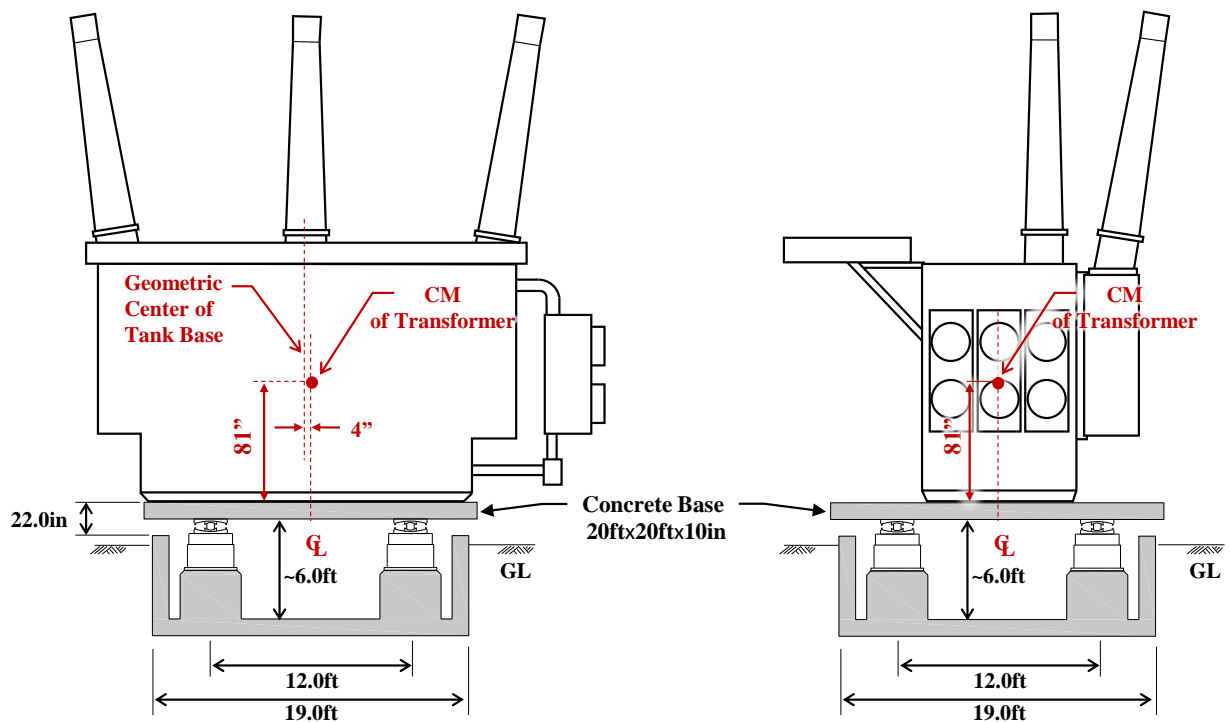


Figure 6-5 Longitudinal and Transverse Direction Sections of Seismically Isolated Transformer with Free Rocking

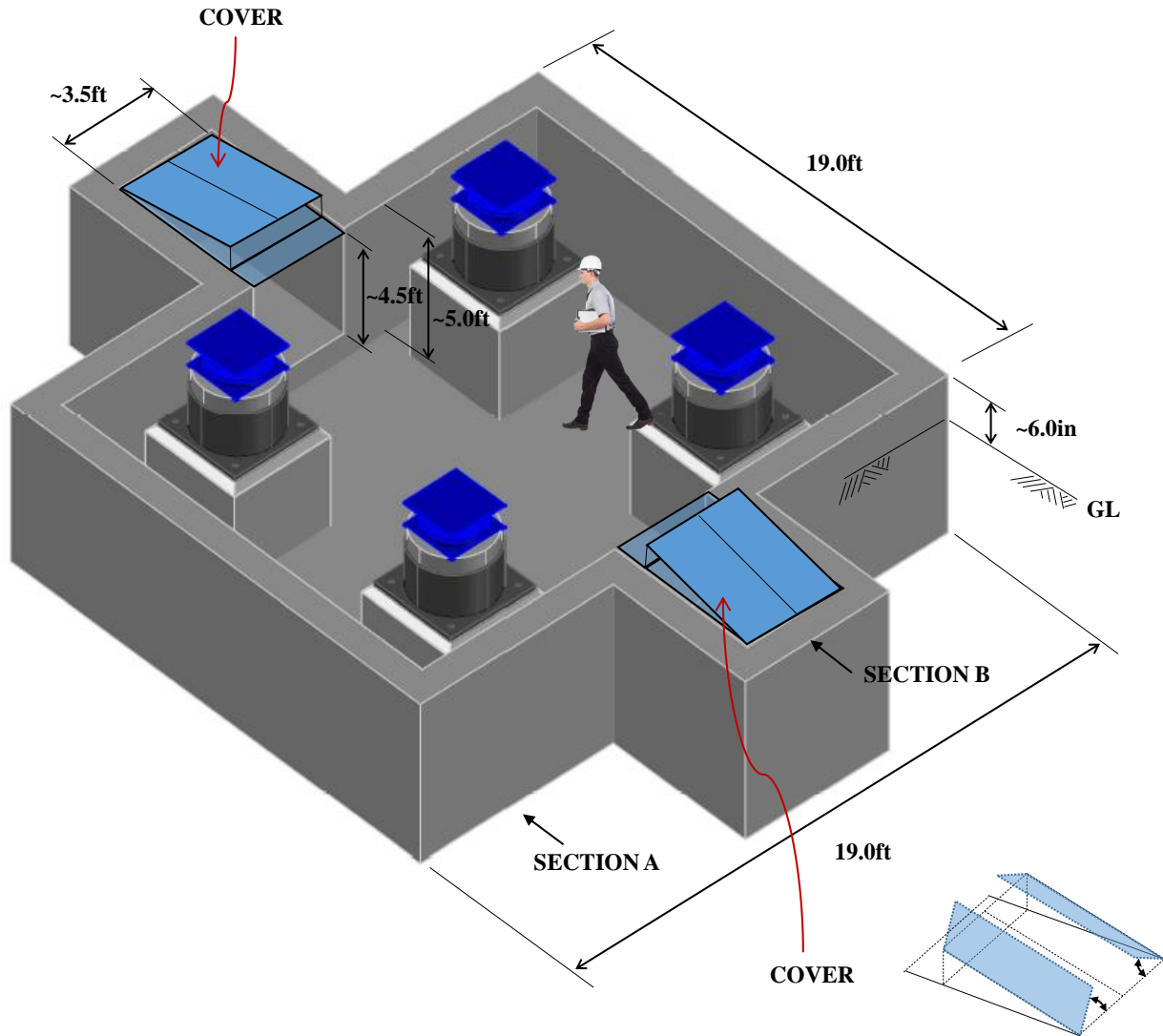


Figure 6-6 Three-dimensional Schematic of Foundation

The transformer is supported by a concrete base, which in turn is supported by the isolators. The base is shown to have plan dimensions larger than the foundation by 6inch on each side so that water flowing down the base does not collect in the foundation pit. The concrete base has dimensions of 20feet by 20feet by 10inch so that it is larger than the plan dimensions of the transformer (18.9feet by 9.2feet). It weighs 50kip so that the total weight on the FP isolators sliding interface is 430kip (380kip plus 50kip base) and the total weight supported by the vertical spring-damper system is about 434kip (430kip plus weight of FP isolator bottom part plus weight of top part of spring-damper units). The transformer is placed on top of the base so that its center

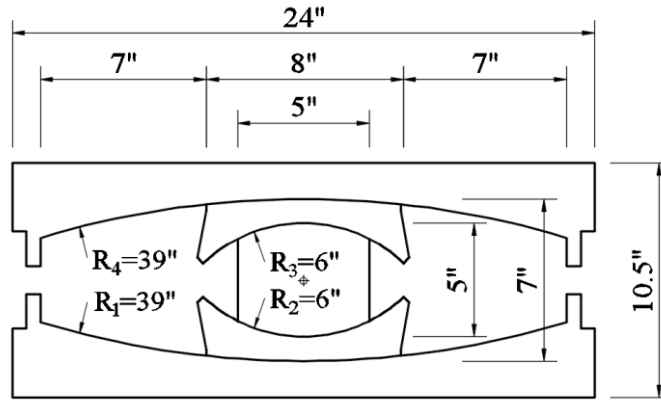


Figure 6-9 Section of Triple Friction Pendulum Isolator

The properties of the triple FP isolators are listed in Table 6-3. The frictional properties are identical to those listed in Appendix B for a set of four tested bearings at load of 104.5kip (which is essentially the same as the 107.5kip calculated for the bearings of this example). Figure 6-10 presents force-displacement loops of the isolator in the lower and upper bound friction conditions and for a displacement equal to their displacement capacity of 14.8inch. Note that the FP isolator has a displacement capacity of 13.0inch at initiation of stiffening in the lower bound friction condition. It will be shown in the dynamic analysis that the average displacement in the considered 2475-year return period earthquake is about half of the displacement capacity at initiation of stiffening.

Table 6-3 Properties of Triple FP Isolator Assumed in Analysis

Property	Value
$\mu_1=\mu_4$ (lower/upper bound)	0.11/0.15
$\mu_2=\mu_3$ (lower/upper bound)	0.08/0.09
$R_{1eff}=R_{4eff}$ (inch)	35.5
$R_{2eff}=R_{3eff}$ (inch)	3.5
$d_1^*=d_4^*$ (inch)	6.4
$d_2^*=d_3^*$ (inch)	1.0
Displacement capacity (inch)	14.8

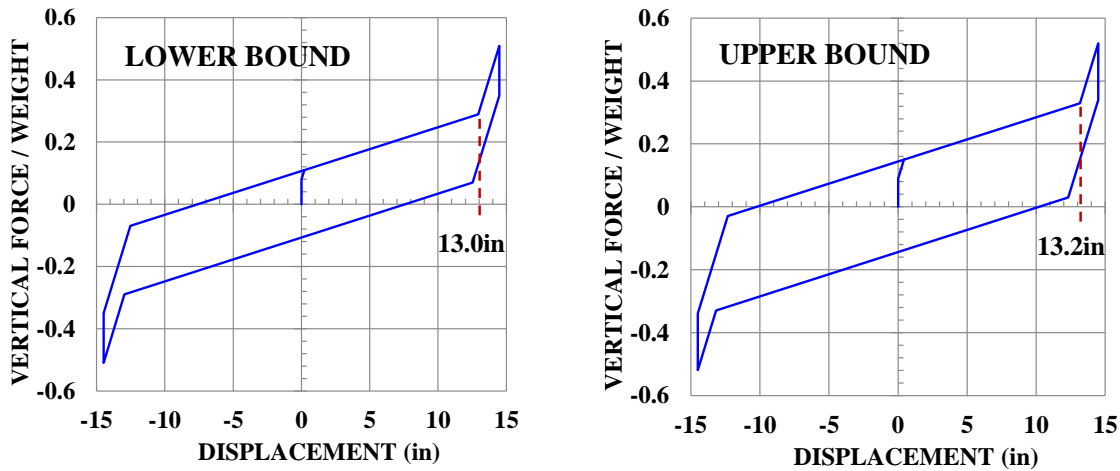


Figure 6-10 Force-displacement Relations of Triple FP isolators

The spring-damper units were designed (courtesy of Taylor Devices, North Tonawanda, NY) to provide a vertical frequency of 2.5Hz and a corresponding damping ratio of 0.90 when carrying a load of 108.5kip for the system that is free to rock (the frequency and damping ratio reduce when the second heavy base to limit rocking is added). The higher frequency and damping ratio were selected to limit rocking based on results of parametric studies. Figure 6-11 shows a schematic of the spring-damper unit. Table 6-4 presents the design parameters for the spring-damper units based on the results of dynamic analysis using the scaled motions in Table 6-2. Motions of 100% and 150% seismic intensity were considered per Section 6.1 for the two three-dimensional isolation systems. The design parameters for the spring-damper units apply for the system that is free to rock for both cases of seismic intensity.

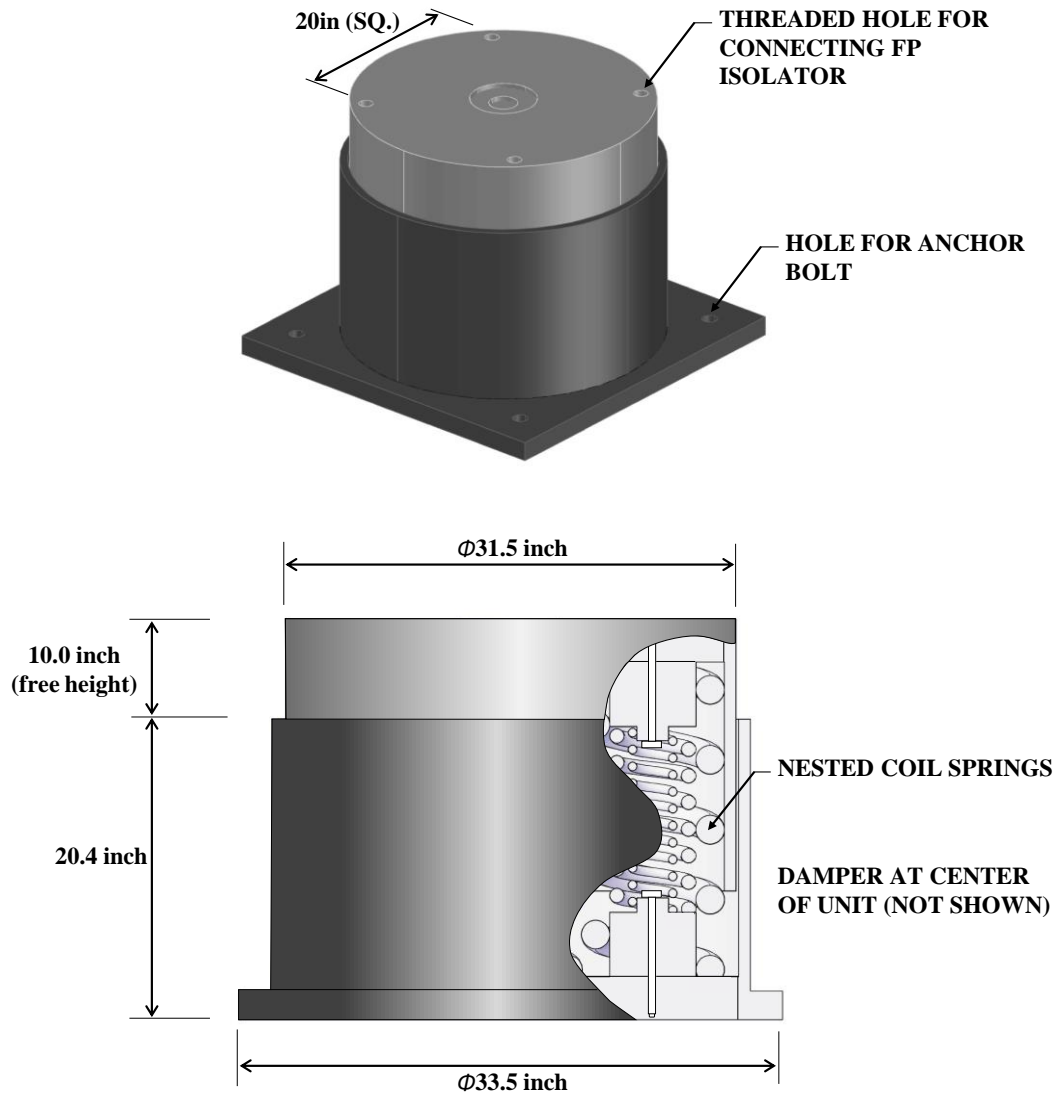


Figure 6-11 Schematic of Vertical Spring-Damper Unit

Table 6-4 Response and Design Parameters for Spring-Damper Units (two values apply for earthquake motions scaled by factors of 100% and 150%)

System	Free To Rock	Restrained Rocking	Design (Free to Rock)
Static load (kip)	108.5	123.5	108.5
Static deflection (inch)	1.5	1.8	1.5
Vertical frequency (Hz)	2.5	2.34	2.5
Vertical damping ratio	0.90	0.85	0.90
Stiffness per unit (kip/in)	70.3	70.3	70.3
Damping constant per unit (linear viscous damping) (kip-sec/in)	8.1	8.1	8.1
Dynamic deflection (inch)	±0.8/1.0	±0.3/0.5	±1.0
Design total deflection (inch)	2.3/2.5	2.1/2.3	3.0
Peak axial force per unit (kip)	192/217	161/181	220
Peak damping force per unit (kip)	54/60	39/59	60
Peak lateral force per unit (to be resisted by unit) (kip)	65	65	65
Peak overturning moment per unit (to be resisted by unit) (kip-inch)	1600	1400	1600

6.4 Model for Dynamic Analysis

Figure 6-12 shows a three-dimensional view of the model used in response history analysis of the system that is free to rock. The model was developed in SAP2000 (Computers and Structures, 2016). Dynamic analysis of the isolated transformer was conducted using the 11 scaled triplets of scaled ground motions. In the analysis, components H1 were applied in the transverse direction and components H2 were applied in the longitudinal direction. No additional analyses were conducted with the motions rotated as the transformer isolation system was symmetric in plan and the model of the transformer was essentially the same in the two orthogonal directions. (The small eccentricity in one direction was ignored in the analysis model. The bushing inclinations slightly differed in the two directions but it was deemed insignificant). The average peak values of response quantities in the 11 analyses were used in design.

To describe the dynamic characteristics of the seismically isolated transformer, Table 6-5 presents the frequencies obtained in eigenvalue analysis in program SAP2000. In the eigenvalue analysis the FP isolators were represented by their actual stiffness in the absence of friction and when sliding occurs on the two main surface (stiffness equal to $W/2R_{eff1}$). Table 6-4 also presents results on frequencies, mode shapes and damping ratio obtained by a simpler analytical model as described below.

Two-dimensional representations of the isolated transformer in the longitudinal-vertical and transverse-vertical planes are presented in Figure 6-13. The assumed mass distribution is shown in Figure 6-14. Based on this distribution of mass, the location of the center of mass of the isolated transformer (see Figure 6-12) was determined at a height $d_{CM}=85.8$ inch above the level of the FP isolator pivot points. The mass moments of inertia about the center of mass were calculated to be 2541kip-s-in^2 about the transverse axis and 5826kip-s-in^2 about the longitudinal axis. The weight used in calculating I_{CM} was the one supported by the FP isolators (430kip). The properties of the isolators are those of Table 6-4 except that the individual isolator values were doubled for the two-dimensional representation. For the FP isolators, the effective stiffness value is $K_{eff}=W/2R_{eff1}=107.5/(2 \times 35.5)=1.51\text{kip/in}$ and the effective damping constant was assigned a value zero (friction neglected).

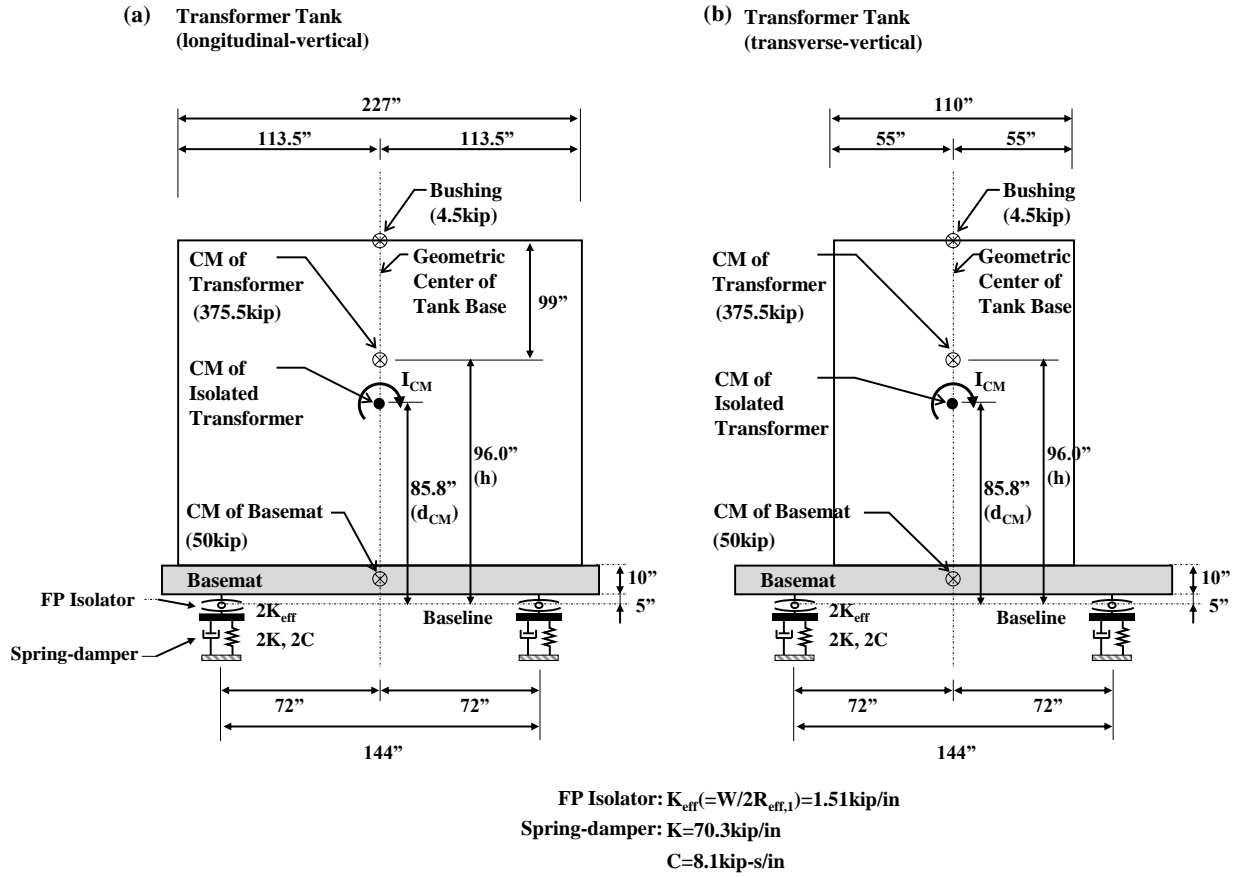


Figure 6-13 Two-dimensional Representations of Isolated Transformer (Free to Rock) in (a) Longitudinal/vertical Plane and (b) Transverse/vertical Plane

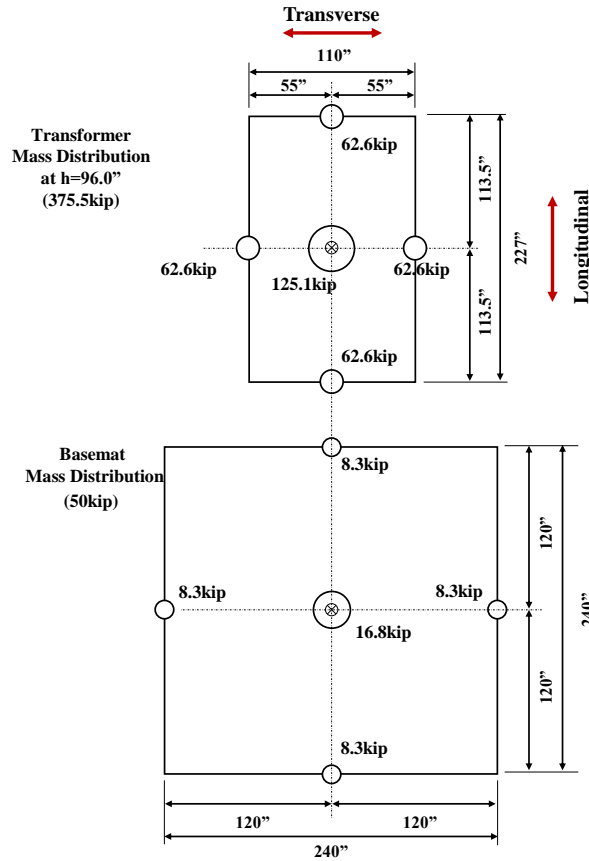


Figure 6-14 Distribution of Mass in Simplified Model of Isolated Transformer (Free to Rock)

Table 6-5 Frequencies, Damping Ratio and Mode Shapes of the Example Transformer with Isolation System that is Free to Rock

Model	Plane	Longitudinal-Vertical			Transverse-Vertical			
	Mode	1	2	3	1	2	3	
Computational in SAP2000	Frequency (Hz)	0.37	2.50	2.48	0.37	2.50	3.66	
Simplified Analytical Model	Frequency (Hz)	0.37	2.50	2.54	0.37	2.50	3.85 ¹	
	Damping Ratio	0	0.90	0.88	0	0.90	1.23	
	Undamped Mode Shape	u	1	0	1	1	0	1
		v	0	1	0	0	1	0
θh		0.04	0	-51.44	0.04	0	-119.34	

1: Frequency does not have physical significance as there is no oscillatory motion

6.5 Results of Dynamic Analysis

Tables 6-6 to 6-11 and Figures 6-15 to 6-18 present results of the dynamic analysis which consist of (a) maximum FP isolator resultant horizontal displacement, (b) maximum horizontal resultant and vertical accelerations at the CM of the transformer, (c) maximum horizontal resultant and vertical accelerations at the CM of the bushing, (d) spring-damper system peak vertical displacement, velocity and force, (e) maximum horizontal resultant and vertical displacements of the top of the bushing, and (f) 5%-damped response spectra of acceleration at the CM of the transformer in the transverse, longitudinal and vertical directions. Each response quantity reported for the bushing is the maximum among the three bushings.

Results for individual motions and the average are presented for the isolator horizontal and vertical displacements, velocities and forces, and the transformer CM and the bushing CM peak values of acceleration. Only the average spectra of the accelerations at the CM of the transformer are presented.

Results are presented for (a) the two-dimensional isolation system consisting of just the FP isolators (2D), (b) the three-dimensional isolation system (3D) allowed to rock and (c) the 3D isolation system with restrained rocking. Two levels of intensity of the seismic excitation are considered (100% and 150%).

The results in Tables 6-6 to 6-11 and Figures 6-15 to 6-18 demonstrate the following:

- 1) All three systems (2D, 3D free to rock and 3D with restrained rocking) have about the same FP isolator displacement demands, of which the average in the 11 motions is within the displacement capacity of the isolators prior to initiation of stiffening.
- 2) There is a benefit, although moderate, in reducing the vertical acceleration at the CM of the transformer offered by the two 3D systems. For example, in the 150% intensity motion for the upper bound friction conditions the peak vertical accelerations are 0.49g for the 2D, and 0.41 or 0.40g for the two 3D systems (Table 6-8). More benefits are seen in the response spectra of the acceleration histories at the CM of the transformer in Figures 6-15 to 6-18 where spectral values for a range of frequencies of interest (5 to 25Hz) are about half in the 3D systems than in the 2D system.

- 3) All three systems provide effective isolation in the horizontal direction. All systems result in substantial reduction of accelerations at the CM of the transformer by comparison to a non-isolated transformer (as seen in comparisons of the ground spectra to the isolated transformer spectra of Figures 6-15 to 6-18). The reduction in acceleration is essentially the same for the three systems with some small additional reduction offered by the two 3D systems.
- 4) The benefits offered by the three systems are more interesting to observe in the peak values of acceleration at the CM of the bushing in Table 6-8. Concentrating on the case of 150% intensity motion and lower bound friction, the 2D system has a peak vertical acceleration of 2.01g against the 1.14g and 0.93g values in the 3D free to rock and the 3D with restrained rocking systems, respectively. The reduction in vertical acceleration to about half is important. For the 3D system that is free to rock, this reduction comes at the expense of some rocking motion that is amplified both in the vertical (by some 20% by comparison to the 2D system and the 3D system with restrained rocking) and in the horizontal direction due to the large distance of the CM to the pivot point (by about 25%).
- 5) Given the complexity of the 3D system with restrained rocking, it appears that the 3D system that is free to rock is a viable option for use in a location of a higher seismic intensity than that of the site at Eugene, OR (herein the higher seismic intensity location is represented by motions magnified by factor of 150%). It provides effective vertical and horizontal isolation although the horizontal accelerations at the CM of the bushing are magnified by a moderate amount. It is the penalty to pay for a significant reduction in the vertical acceleration.
- 6) The same conclusion as that of item 5 above may be arrived at for a transformer at the Eugene, OR location. However, in this case the vertical accelerations at the CM of the bushing in the 2D system may be acceptable so that use of the two-dimensional isolation system appears to be the appropriate choice for this site. This is consistent with the results of the transformer fragility analysis in Kitayama et al (2016) for this site where it was concluded that a 3D seismic isolation system does not offer any significant advantage in

terms of the probability of failure in its lifetime over that of a comparable 2D seismic isolation system.

Following the presented discussion of the results of the dynamic analysis it is appropriate to comment on the effect of the stiffness of the additional base used in the 3D isolation system with restrained rocking. Figure 6-19 presents the peak values of acceleration at the CM of the transformer as function of the moment of inertia of the cross section of the second base (the area was also varied accordingly) in motion Valparaiso (see Table 6-2) with intensity of 100%. A moment of inertia of about 17000in^4 is needed to effectively restrain rocking, although a value of about 8500in^4 would suffice. This illustrates the difficulty in restraining rocking in slender systems.

Table 6-6 FP Isolator Peak Resultant Horizontal Displacement (in inch)

Isolator Friction	Lower Bound					
Seismic Intensity	100%			150%		
Isolation System/ Earthquake	2D	3D Free to Rock	3D Restrained Rocking	2D	3D Free to Rock	3D Restrained Rocking
Valparaiso	7.94	7.69	8.13	11.54	11.51	11.94
Talca	4.74	4.65	4.79	9.54	9.27	9.59
Hualane	3.29	3.46	3.30	6.65	6.54	6.59
Chile	7.96	7.80	8.16	12.74	12.61	13.09
Hokkaido	3.72	3.43	3.82	8.19	8.09	8.50
Hanasaki	2.00	2.06	2.02	4.94	4.83	4.91
Peru	5.77	5.77	5.73	10.17	9.92	10.09
Tohoku-A	6.82	6.62	6.81	15.58	14.98	15.59
Tohoku-B	7.07	6.82	7.07	17.52	17.62	17.57
Nukabira	4.22	4.17	4.21	9.90	9.81	9.98
Tokachi-Oki	6.58	6.40	6.58	13.24	13.02	13.23
Average	5.46	5.35	5.51	10.91	10.75	11.01
Isolator Friction	Upper Bound					
Seismic Intensity	100%			150%		
Isolation System/ Earthquake	2D	3D Free to Rock	3D Restrained Rocking	2D	3D Free to Rock	3D Restrained Rocking
Valparaiso	8.06	7.73	8.31	11.71	11.51	12.19
Talca	3.65	3.71	3.71	8.05	7.80	8.13
Hualane	3.40	3.48	3.47	5.33	5.44	5.43
Chile	7.45	7.36	7.69	12.03	11.90	12.42
Hokkaido	3.11	2.68	2.99	6.20	6.01	6.54
Hanasaki	1.91	1.75	1.85	3.56	3.49	3.55
Peru	5.26	5.14	5.16	9.38	9.00	9.25
Tohoku-A	4.55	4.42	4.51	12.15	11.71	12.12
Tohoku-B	4.62	4.26	4.50	12.41	12.11	12.43
Nukabira	3.35	3.77	3.39	7.45	7.67	7.48
Tokachi-Oki	5.15	4.89	5.15	10.91	10.65	10.89
Average	4.59	4.47	4.61	9.02	8.85	9.13

Table 6-7 Transformer Peak Accelerations at CM of Transformer (in g)

Isolator Friction	Lower Bound											
Seismic Intensity	100%						150%					
Isolation System	2D		3D Free to Rock		3D Restrained Rocking		2D		3D Free to Rock		3D Restrained Rocking	
Direction/ Earthquake	Res. Hor.	Vert.	Res. Hor.	Vert.	Res. Hor.	Vert.	Res. Hor.	Vert.	Res. Hor.	Vert.	Res. Hor.	Vert.
Valparaiso	0.29	0.43	0.22	0.37	0.23	0.35	0.30	0.58	0.28	0.55	0.29	0.53
Talca	0.20	0.31	0.18	0.25	0.18	0.25	0.26	0.42	0.24	0.37	0.25	0.37
Hualane	0.23	0.47	0.15	0.29	0.16	0.28	0.23	0.63	0.22	0.43	0.22	0.42
Chile	0.26	0.32	0.26	0.28	0.27	0.28	0.37	0.48	0.38	0.42	0.39	0.42
Hokkaido	0.19	0.31	0.18	0.28	0.19	0.27	0.28	0.49	0.28	0.41	0.28	0.41
Hanasaki	0.17	0.41	0.15	0.28	0.15	0.26	0.26	0.61	0.20	0.42	0.20	0.39
Peru	0.19	0.35	0.18	0.27	0.18	0.27	0.27	0.53	0.23	0.41	0.24	0.40
Tohoku-A	0.22	0.21	0.21	0.18	0.21	0.18	0.36	0.32	0.35	0.27	0.35	0.27
Tohoku-B	0.20	0.30	0.20	0.29	0.20	0.28	0.37	0.46	0.37	0.44	0.36	0.42
Nukabira	0.18	0.37	0.18	0.31	0.17	0.31	0.26	0.56	0.25	0.47	0.26	0.46
Tokachi-Oki	0.19	0.28	0.19	0.24	0.19	0.23	0.29	0.42	0.27	0.36	0.28	0.34
Average	0.21	0.34	0.19	0.27	0.19	0.26	0.29	0.49	0.27	0.41	0.28	0.40
Isolator Friction	Upper Bound											
Seismic Intensity	100%						150%					
Isolation System	2D		3D Free to Rock		3D Restrained Rocking		2D		3D Free to Rock		3D Restrained Rocking	
Direction/ Earthquake	Res. Hor.	Vert.	Res. Hor.	Vert.	Res. Hor.	Vert.	Res. Hor.	Vert.	Res. Hor.	Vert.	Res. Hor.	Vert.
Valparaiso	0.30	0.43	0.26	0.37	0.27	0.35	0.34	0.58	0.33	0.55	0.33	0.53
Talca	0.24	0.31	0.20	0.25	0.20	0.25	0.29	0.42	0.27	0.37	0.27	0.37
Hualane	0.23	0.48	0.19	0.29	0.19	0.28	0.25	0.63	0.24	0.43	0.24	0.42
Chile	0.30	0.32	0.30	0.28	0.31	0.28	0.41	0.48	0.42	0.42	0.43	0.42
Hokkaido	0.23	0.31	0.19	0.28	0.21	0.27	0.31	0.49	0.29	0.41	0.30	0.41
Hanasaki	0.20	0.41	0.20	0.28	0.20	0.26	0.27	0.61	0.23	0.42	0.23	0.39
Peru	0.24	0.35	0.22	0.27	0.23	0.27	0.30	0.53	0.26	0.41	0.27	0.40
Tohoku-A	0.20	0.21	0.20	0.18	0.19	0.18	0.35	0.32	0.34	0.27	0.34	0.27
Tohoku-B	0.23	0.30	0.22	0.29	0.23	0.28	0.33	0.46	0.32	0.44	0.32	0.43
Nukabira	0.20	0.37	0.20	0.31	0.20	0.31	0.28	0.56	0.27	0.47	0.28	0.46
Tokachi-Oki	0.22	0.28	0.20	0.24	0.20	0.23	0.30	0.42	0.28	0.35	0.29	0.34
Average	0.23	0.34	0.21	0.27	0.22	0.26	0.31	0.49	0.29	0.41	0.29	0.40

Table 6-8 Bushing Peak Accelerations at CM of Bushing (in g)

Isolator Friction	Lower Bound											
Seismic Intensity	100%						150%					
Isolation System	2D		3D Free to Rock		3D Restrained Rocking		2D		3D Free to Rock		3D Restrained Rocking	
Direction/ Earthquake	Res. Hor.	Vert.	Res. Hor.	Vert.	Res. Hor.	Vert.	Res. Hor.	Vert.	Res. Hor.	Vert.	Res. Hor.	Vert.
Valparaiso	0.50	2.14	0.69	1.15	0.56	0.88	0.91	3.18	0.93	1.57	0.71	1.31
Talca	0.53	1.19	1.05	0.84	0.77	0.54	0.76	1.66	1.27	1.01	0.90	0.73
Hualane	0.55	1.29	0.88	0.86	0.68	0.61	0.79	2.06	1.05	1.22	0.74	0.94
Chile	0.46	1.00	0.69	0.76	0.48	0.58	0.81	1.79	0.77	1.15	0.64	0.88
Hokkaido	0.56	1.75	0.97	0.84	0.86	0.71	0.84	2.34	1.03	1.25	0.82	1.00
Hanasaki	0.59	1.49	0.95	0.84	0.86	0.67	0.87	2.07	1.13	1.07	1.08	0.93
Peru	0.45	1.41	0.76	0.95	0.59	0.67	0.74	1.95	1.01	1.27	0.65	0.96
Tohoku-A	0.44	0.71	0.95	0.55	0.67	0.39	0.72	1.09	1.11	0.76	0.82	0.62
Tohoku-B	0.50	1.44	0.99	0.89	0.74	0.66	1.23	2.14	0.95	1.31	0.99	1.04
Nukabira	0.45	1.41	1.00	0.76	0.64	0.63	0.79	1.89	1.02	0.98	0.73	0.87
Tokachi-Oki	0.53	1.28	0.71	0.74	0.57	0.64	0.66	1.97	0.78	1.02	0.69	0.97
Average	0.50	1.37	0.87	0.83	0.67	0.63	0.82	2.01	1.00	1.14	0.79	0.93
Isolator Friction	Upper Bound											
Seismic Intensity	100%						150%					
Isolation System	2D		3D Free to Rock		3D Restrained Rocking		2D		3D Free to Rock		3D Restrained Rocking	
Direction/ Earthquake	Res. Hor.	Vert.	Res. Hor.	Vert.	Res. Hor.	Vert.	Res. Hor.	Vert.	Res. Hor.	Vert.	Res. Hor.	Vert.
Valparaiso	0.70	2.11	0.82	1.15	0.57	0.92	1.02	3.18	0.97	1.73	0.68	1.29
Talca	0.72	1.11	1.28	0.90	0.84	0.56	0.78	1.65	1.51	1.13	0.91	0.78
Hualane	0.70	1.37	0.87	0.91	0.71	0.65	0.92	2.06	1.03	1.22	0.84	0.93
Chile	0.60	1.18	0.77	0.72	0.56	0.60	0.78	1.75	0.96	0.98	0.68	0.82
Hokkaido	0.65	1.54	1.04	0.85	0.93	0.73	0.95	2.35	1.17	1.25	1.06	1.07
Hanasaki	0.81	1.39	1.18	0.98	0.97	0.76	1.03	2.09	1.32	1.11	1.11	0.96
Peru	0.70	1.30	1.01	1.08	0.84	0.70	0.77	1.96	0.98	1.32	0.74	0.96
Tohoku-A	0.58	0.73	0.76	0.61	0.74	0.41	0.70	1.09	1.16	0.81	0.89	0.59
Tohoku-B	0.83	1.41	1.26	0.96	0.97	0.67	1.24	2.17	1.07	1.38	1.05	1.07
Nukabira	0.77	1.26	1.50	0.83	0.98	0.61	0.66	1.90	1.20	1.14	0.79	0.91
Tokachi-Oki	0.67	1.31	0.88	0.77	0.68	0.64	0.74	1.96	0.93	1.13	0.74	0.97
Average	0.70	1.33	1.03	0.88	0.79	0.65	0.87	2.01	1.11	1.19	0.86	0.94

Table 6-9 Spring-damper System Peak Vertical Displacement, Velocity and Force for Lower Bound Friction

Isolator Friction/ Intensity	Lower Bound/100%									
Isolation System	3D Free to Rock					3D Restrained Rocking				
Parameter/ Earthquake	Dynamic Displ. (in)	Velocity (in/s)	Spring Force (kip)	Damper Force (kip)	Total Force (kip)	Dynamic Displ. (in)	Velocity (in/s)	Spring Force (kip)	Damper Force (kip)	Total Force (kip)
Valparaiso	0.54	5.29	146.9	42.9	160.7	0.30	4.84	143.0	39.2	161.1
Talca	0.51	5.19	145.2	42.1	156.8	0.28	3.00	141.6	24.3	154.5
Hualane	0.45	5.26	140.7	42.6	161.0	0.27	3.26	141.1	26.4	156.7
Chile	0.73	5.82	160.7	47.2	184.6	0.25	3.73	139.3	30.2	155.5
Hokkaido	0.52	5.72	144.8	46.3	164.4	0.20	3.73	136.0	30.2	154.1
Hanasaki	0.34	4.75	132.5	38.5	158.2	0.18	4.00	134.4	32.4	150.2
Peru	0.52	4.75	145.4	38.5	160.8	0.28	3.67	141.4	29.7	155.8
Tohoku-A	0.51	3.78	145.2	30.6	152.7	0.21	2.30	136.7	18.6	143.6
Tohoku-B	0.44	5.18	139.5	42.0	157.8	0.22	3.79	137.7	30.7	154.5
Nukabira	0.52	5.12	145.9	41.5	156.0	0.30	3.44	143.3	27.9	151.9
Tokachi-Oki	0.42	5.23	138.0	42.4	155.7	0.14	3.30	132.0	26.7	141.7
Average	0.50	5.10	144.0	41.3	160.7	0.23	3.54	138.7	28.7	152.6
Isolator Friction/ Intensity	Lower Bound/150%									
Isolation System	3D Free to Rock					3D Restrained Rocking				
Parameter/ Earthquake	Dynamic Displ. (in)	Velocity (in/s)	Spring Force (kip)	Damper Force (kip)	Total Force (kip)	Dynamic Displ. (in)	Velocity (in/s)	Spring Force (kip)	Damper Force (kip)	Total Force (kip)
Valparaiso	0.68	6.85	156.7	55.4	179.5	0.44	7.26	153.2	58.8	180.7
Talca	0.62	6.64	152.5	53.8	173.5	0.41	4.56	151.2	36.9	168.2
Hualane	0.58	6.70	149.9	54.3	179.8	0.40	4.85	150.5	39.3	174.0
Chile	1.02	7.40	181.1	59.9	217.7	0.37	5.54	147.9	44.9	172.3
Hokkaido	0.76	7.29	161.7	59.0	189.5	0.30	5.49	142.9	44.5	169.0
Hanasaki	0.53	6.57	146.3	53.2	178.2	0.26	6.00	140.3	48.6	163.7
Peru	0.65	6.29	154.6	50.9	179.7	0.41	5.51	150.9	44.6	172.6
Tohoku-A	0.83	4.96	167.7	40.2	179.3	0.31	3.44	143.8	27.9	155.1
Tohoku-B	0.79	7.16	164.1	58.0	177.7	0.33	5.56	145.2	45.1	171.1
Nukabira	0.77	6.48	163.6	52.4	180.2	0.45	5.20	153.9	42.1	166.9
Tokachi-Oki	0.66	6.78	154.6	54.9	172.5	0.21	4.96	136.8	40.1	151.6
Average	0.71	6.64	159.3	53.8	182.5	0.35	5.30	146.9	42.9	167.7

Table 6-10 Spring-damper System Peak Vertical Displacement, Velocity and Force for Upper Bound Friction

Isolator Friction/ Intensity	Upper Bound/100%									
Isolation System	3D Free to Rock					3D Restrained Rocking				
Parameter/ Earthquake	Dynamic Displ. (in)	Velocity (in/s)	Spring Force (kip)	Damper Force (kip)	Total Force (kip)	Dynamic Displ. (in)	Velocity (in/s)	Spring Force (kip)	Damper Force (kip)	Total Force (kip)
Valparaiso	0.68	6.17	156.6	50.0	171.9	0.30	4.85	143.1	39.3	160.7
Talca	0.59	5.78	150.9	46.8	162.5	0.28	3.00	141.6	24.3	156.0
Hualane	0.49	5.67	143.2	46.0	163.7	0.27	3.22	141.2	26.1	156.9
Chile	0.82	6.71	166.5	54.4	192.0	0.25	3.93	139.4	31.8	155.6
Hokkaido	0.53	5.70	145.4	46.2	165.8	0.20	3.70	136.1	30.0	153.9
Hanasaki	0.38	4.88	135.6	39.5	163.7	0.18	4.02	134.4	32.6	151.3
Peru	0.57	5.41	149.5	43.9	165.8	0.28	3.67	141.5	29.7	155.8
Tohoku-A	0.54	4.27	146.2	34.6	158.2	0.21	2.30	136.8	18.6	143.7
Tohoku-B	0.51	5.15	144.6	41.7	160.3	0.22	3.83	137.6	31.0	154.4
Nukabira	0.59	5.50	150.3	44.6	161.6	0.30	3.58	143.3	29.0	152.2
Tokachi-Oki	0.43	5.59	138.9	45.3	158.8	0.14	3.32	132.2	26.9	142.2
Average	0.55	5.53	147.9	44.8	165.8	0.23	3.58	138.8	29.0	152.9
Isolator Friction/ Intensity	Upper Bound/150%									
Isolation System	3D Free to Rock					3D Restrained Rocking				
Parameter/ Earthquake	Dynamic Displ. (in)	Velocity (in/s)	Spring Force (kip)	Damper Force (kip)	Total Force (kip)	Dynamic Displ. (in)	Velocity (in/s)	Spring Force (kip)	Damper Force (kip)	Total Force (kip)
Valparaiso	0.75	7.20	161.7	58.3	184.0	0.45	7.28	153.4	58.9	180.0
Talca	0.74	7.47	161.1	60.5	179.5	0.42	4.46	151.3	36.1	170.5
Hualane	0.66	7.56	155.7	61.2	186.1	0.41	4.88	150.6	39.5	174.5
Chile	1.11	8.42	187.3	68.2	225.7	0.37	5.58	148.0	45.2	172.4
Hokkaido	0.79	7.95	163.8	64.4	193.4	0.30	5.55	142.8	45.0	169.7
Hanasaki	0.52	7.24	145.0	58.6	184.3	0.26	5.99	140.5	48.5	163.5
Peru	0.76	6.71	162.6	54.4	185.1	0.41	5.51	151.0	44.6	172.6
Tohoku-A	0.81	5.39	166.4	43.6	178.1	0.31	3.45	143.9	27.9	154.5
Tohoku-B	0.69	7.43	156.7	60.2	179.4	0.33	5.64	145.4	45.7	171.7
Nukabira	0.79	7.15	164.5	57.9	185.5	0.45	5.27	153.9	42.7	167.0
Tokachi-Oki	0.64	7.54	153.3	61.1	177.2	0.21	4.94	136.9	40.0	151.6
Average	0.75	7.27	161.6	58.9	187.1	0.35	5.32	147.0	43.1	168.0

Table 6-11 Bushing Top Peak Displacements (in inch)

Isolator Friction	Lower Bound											
Seismic Intensity	100%						150%					
Isolation System	2D		3D Free to Rock		3D Restrained Rocking		2D		3D Free to Rock		3D Restrained Rocking	
Direction/ Earthquake	Res. Hor.	Vert.	Res. Hor.	Vert.	Res. Hor.	Vert.	Res. Hor.	Vert.	Res. Hor.	Vert.	Res. Hor.	Vert.
Valparaiso	8.08	0.36	9.36	2.30	8.35	2.19	11.68	0.46	13.56	2.44	12.13	2.36
Talca	4.92	0.26	6.09	2.21	5.00	2.18	9.69	0.29	11.15	2.53	9.77	2.34
Hualane	3.44	0.27	4.40	2.22	3.51	2.18	6.70	0.34	8.30	2.37	6.75	2.35
Chile	8.17	0.22	9.74	2.44	8.41	2.13	13.07	0.30	15.19	2.82	13.41	2.26
Hokkaido	3.94	0.31	4.93	2.36	4.05	2.13	8.33	0.35	10.14	2.73	8.70	2.21
Hanasaki	2.14	0.27	3.17	2.16	2.27	2.08	5.22	0.36	6.17	2.40	5.27	2.19
Peru	5.86	0.28	7.15	2.29	5.87	2.16	10.32	0.32	11.69	2.46	10.26	2.32
Tohoku-A	6.98	0.20	8.36	2.21	7.00	2.10	15.79	0.24	17.74	2.50	15.83	2.21
Tohoku-B	7.20	0.28	8.46	2.28	7.49	2.15	17.73	0.33	20.57	2.59	18.02	2.30
Nukabira	4.35	0.27	5.43	2.36	4.34	2.21	10.11	0.32	11.62	2.65	10.22	2.39
Tokachi-Oki	6.71	0.28	7.92	2.25	6.84	2.06	13.39	0.32	15.21	2.63	13.39	2.14
Average	5.61	0.27	6.81	2.27	5.73	2.14	11.09	0.32	12.84	2.55	11.25	2.27
Isolator Friction	Upper Bound											
Seismic Intensity	100%						150%					
Isolation System	2D		3D Free to Rock		3D Restrained Rocking		2D		3D Free to Rock		3D Restrained Rocking	
Direction/ Earthquake	Res. Hor.	Vert.	Res. Hor.	Vert.	Res. Hor.	Vert.	Res. Hor.	Vert.	Res. Hor.	Vert.	Res. Hor.	Vert.
Valparaiso	8.24	0.34	9.77	2.49	8.56	2.19	11.89	0.46	13.88	2.54	12.42	2.36
Talca	3.79	0.23	5.05	2.33	3.88	2.19	8.19	0.28	9.91	2.46	8.37	2.34
Hualane	3.56	0.27	4.62	2.30	3.60	2.17	5.48	0.35	6.72	2.48	5.60	2.34
Chile	7.69	0.24	9.59	2.52	7.94	2.14	12.34	0.29	14.80	2.85	12.74	2.27
Hokkaido	3.21	0.27	4.07	2.36	3.13	2.14	6.39	0.35	8.23	2.76	6.79	2.26
Hanasaki	2.04	0.27	3.06	2.30	2.12	2.09	3.73	0.36	4.93	2.36	3.76	2.19
Peru	5.45	0.26	6.78	2.37	5.34	2.18	9.58	0.32	10.95	2.56	9.44	2.31
Tohoku-A	4.65	0.20	5.89	2.31	4.66	2.11	12.36	0.24	14.38	2.48	12.37	2.22
Tohoku-B	5.05	0.27	5.92	2.40	4.99	2.17	12.84	0.34	14.68	2.61	12.97	2.31
Nukabira	3.54	0.25	5.40	2.47	3.61	2.24	7.58	0.32	9.59	2.72	7.65	2.39
Tokachi-Oki	5.39	0.27	6.28	2.22	5.49	2.04	11.01	0.32	12.90	2.57	11.12	2.15
Average	4.78	0.26	6.03	2.36	4.84	2.15	9.21	0.33	10.99	2.58	9.38	2.28

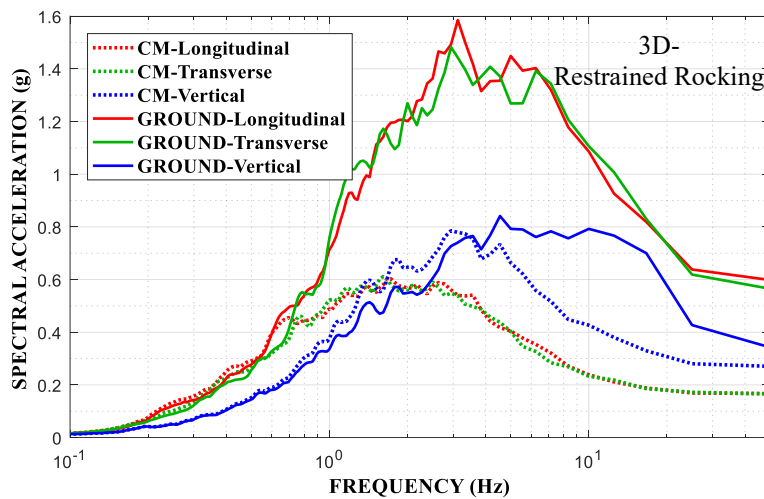
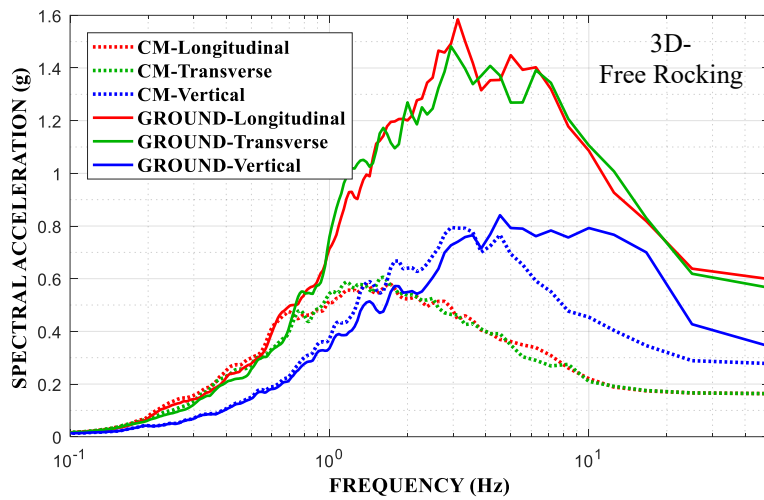
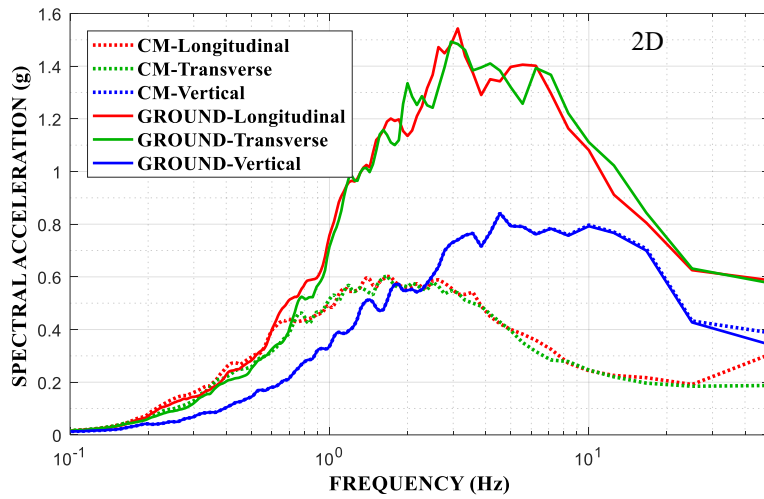


Figure 6-15 5%-Damped Response Spectra of Acceleration at CM of Transformer for Lower Bound Friction in 100% Intensity Motion

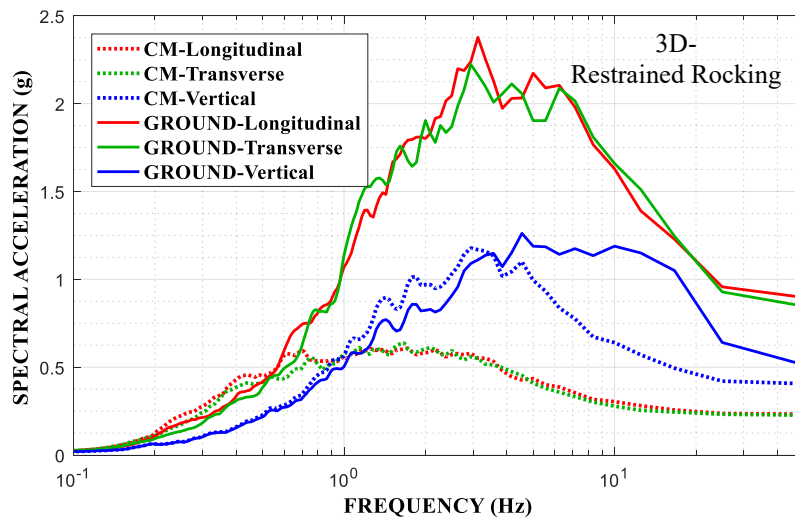
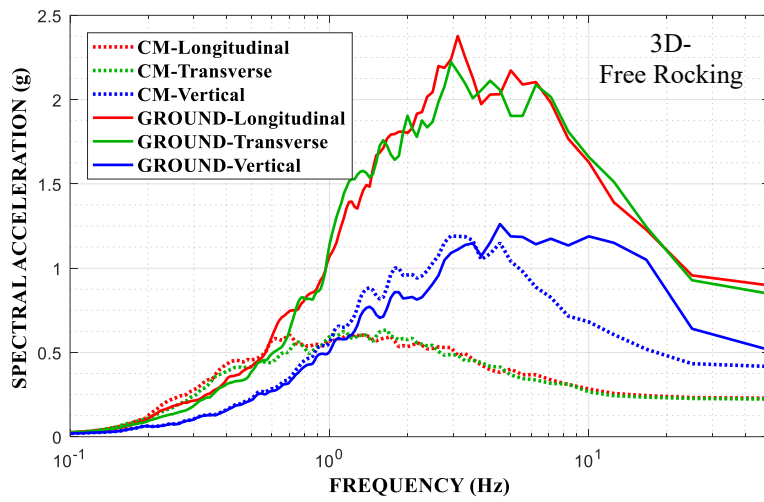
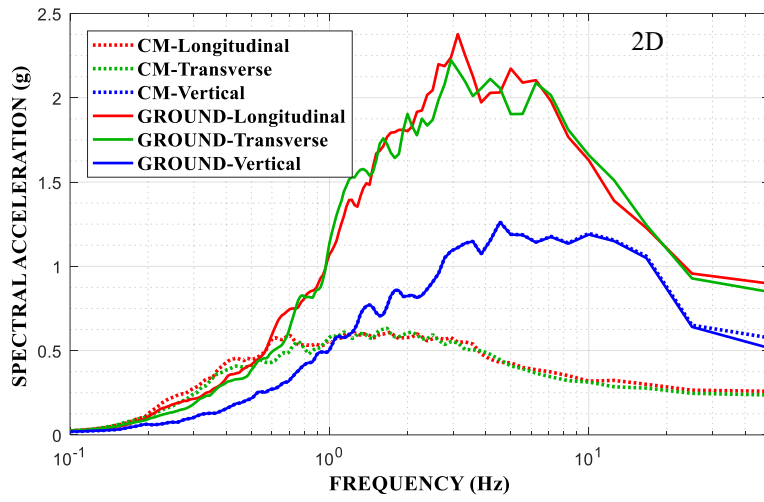


Figure 6-16 5%-Damped Response Spectra of Acceleration at CM of Transformer for Lower Bound Friction in 150% Intensity Motion

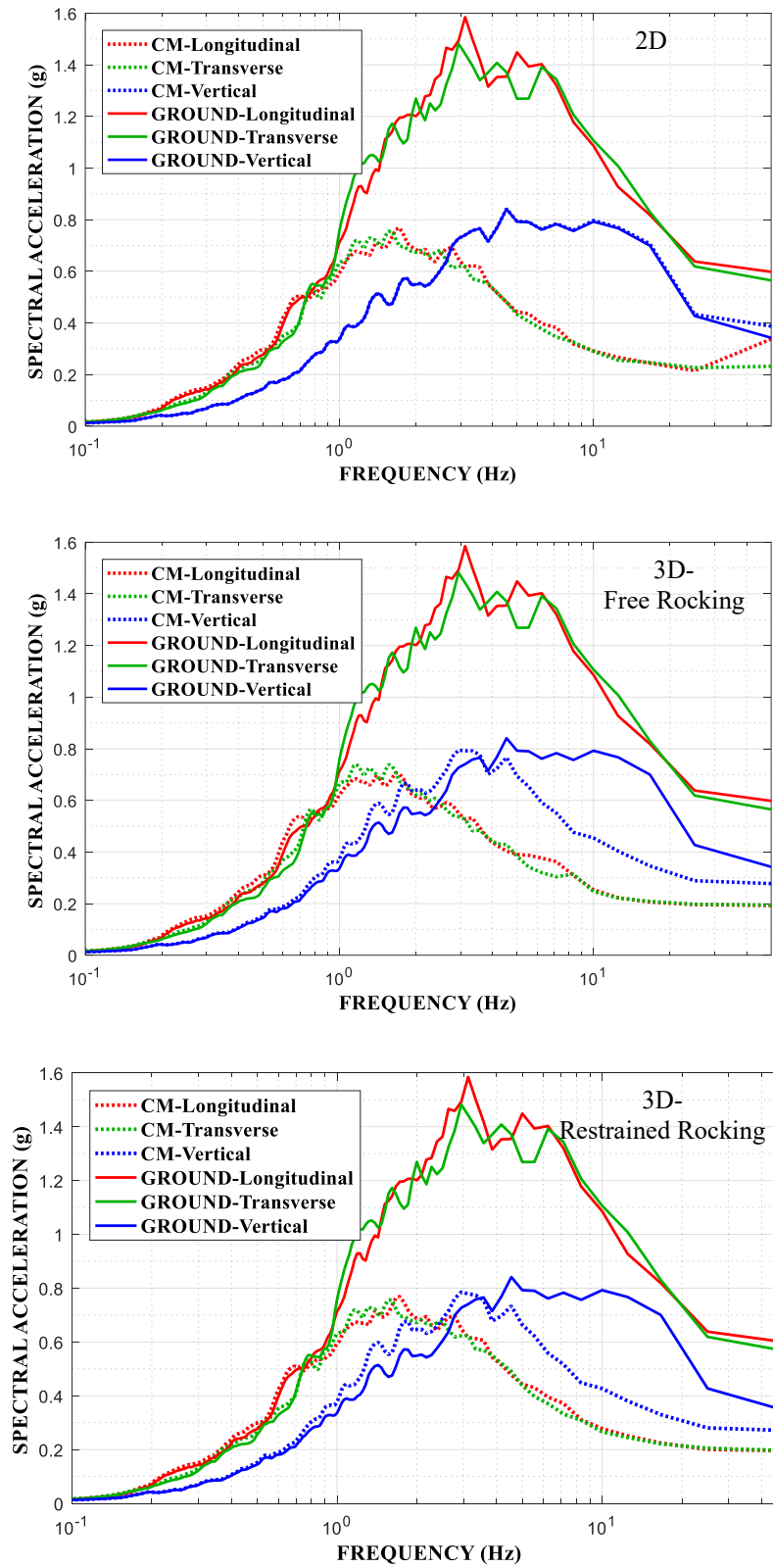


Figure 6-17 5%-Damped Response Spectra of Acceleration at CM of Transformer for Upper Bound Friction in 100% Intensity Motion

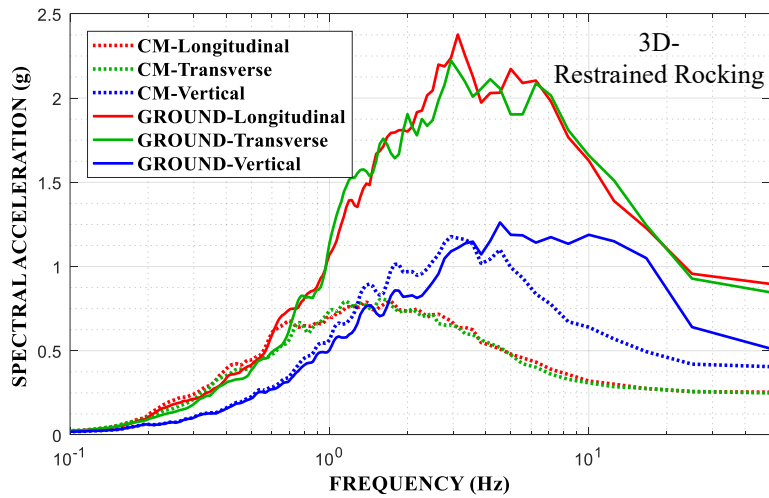
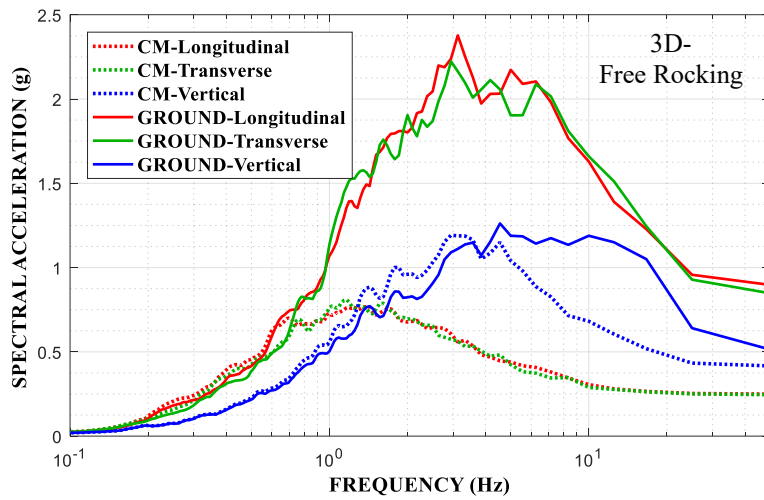
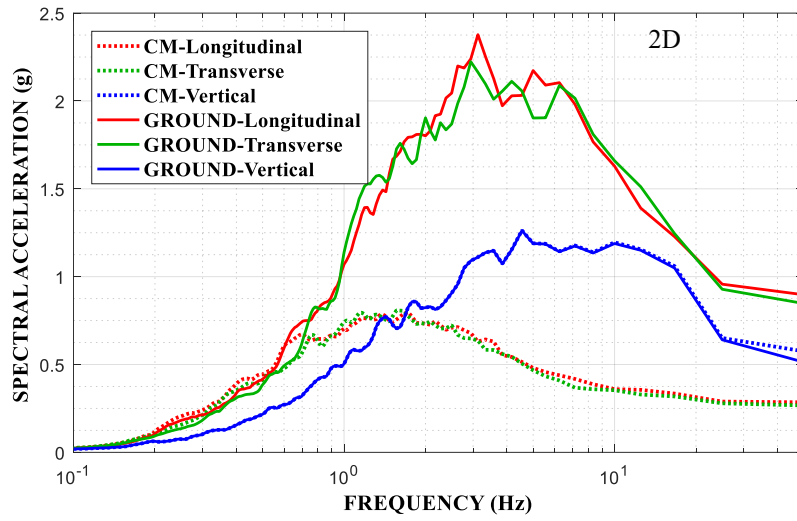


Figure 6-18 5%-Damped Response Spectra of Acceleration at CM of Transformer for Upper Bound Friction in 150% Intensity Motion

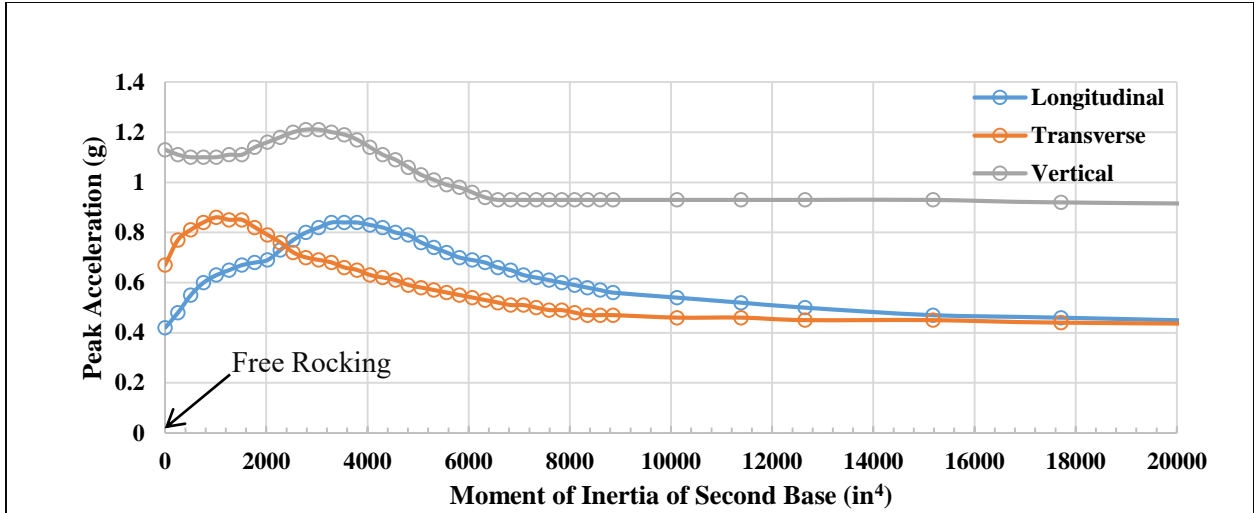


Figure 6-19 Peak Acceleration at CM of Bushing in 3D Isolation System with Restrained Rocking in Motion Valparaiso (100%) as Function of Base Moment of Inertia

“This Page Intentionally Left Blank”

SECTION 7

SUMMARY AND CONCLUSIONS

This report described a research effort for the development and testing of a three-dimensional (3D) seismic isolation system suitable for electrical transformers, the development and validation of analytical models for the prediction of the dynamic response of transformers equipped with the system and the presentation of examples of analysis and design of the isolation system of a sample transformer.

The report started with a comprehensive review of past efforts to develop 3D seismic isolation systems. These included (a) elastomeric bearings with low vertical stiffness, (b) systems consisting of helical springs and dampers and (c) complex 3D isolation systems of Japanese origin utilizing air springs, accumulators, piping, valves, leveling systems and active components. It was concluded that (a) purely elastomeric isolation systems cannot provide effective vertical isolation due to their high vertical stiffness and problems with creep and low capacity to carry vertical load under large lateral deformation, (b) helical spring and damper systems generally have all frequencies larger than about 1.5Hz to be able to provide effective isolation in all directions, (c) the 3D isolation systems developed in Japan, while effective, are exceptionally complex, require continued maintenance, are likely unreliable and are costly. They are unacceptable for use in the seismic isolation of electrical transformers where reliability, minimum maintenance, compactness and reasonable costs are required.

The report then proceeded to analytically investigate the performance of two alternate 3D seismic isolation systems: (a) one consisting of helical springs and viscous dampers that allow for motions in all directions, and (b) one consisting of triple FP isolators for providing horizontal isolation, which are supported by a vertically driven spring-damper system for providing vertical isolation. The study determined that a system consisting of helical springs and viscous dampers is limited in performance by the fact that its fundamental frequency is high and typically larger than about 1.5Hz. This results in large acceleration responses in the horizontal directions which may be further magnified due to rocking of the isolated structure. The system consisting of Triple FP isolators and their vertically-driven spring-damper supports provide for a very

effective horizontal isolation with a limited vertical isolation effect. The latter is due to the fact that the isolation system is vertically stiff in order to meet the serviceability criteria (limited static deflection). In essence, the system functions in the vertical direction like a highly damped system rather than as an isolation system. The study then determined the design parameters for the vertical spring-damper system for use in the shake table testing. The selected system had a vertical frequency of 2.0Hz and a corresponding damping ratio of 0.50. The conducted studies also determined that a higher damping ratio could provide additional benefits which include limiting rotation of the isolation system and increasing the insensitivity of the system to the details of the vertical ground motion.

A model of an electrical transformer, including a flexibly-installed bushing, was built for shake table testing. The model weighed at 68.1kip when configured with allowance for free rocking and weighed at 72.4kip when a second basemat was added to limit rocking. Three different types of triple FP isolators were used in the testing. They were characterized by their nominal friction (force at zero displacement divided by the vertical load) which was 0.07, 0.12 and 0.20. The value desired for actual applications is 0.12. The Triple FP isolators and the spring-damper units were tested and their properties were determined for use in the dynamic analysis of the tested model.

The model was tested on the shake table using three-component seismic excitation as recorded in historic earthquakes without any scaling in time. That is, the time scale factor was unity. Results were acquired in terms of isolator displacement demands, accelerations below and above the isolators, displacements of the bushing and rotations of the entire model. The recorded acceleration histories were used to construct response spectra at various locations below and above the isolators. These spectra demonstrated a marked isolation effect in the two horizontal directions and a limited isolation effect in the vertical direction. The latter was expected as the vertical system acted as a damping rather than as an isolation system.

The testing was conducted with two configurations of the model: one that freely allowed for rocking of the model and one that restricted the freedom to rock. The latter configuration proved complex in its construction and did not achieve the desired effect as the connection of the added

base to the isolators proved to have undesired flexibility. The test results revealed that increases in friction of the FP isolators result in the expected reduction in FP isolator displacements and an increase in horizontal accelerations at the frame top, bushing base and bushing top. Performance was best when the nominal friction was 0.12 when the isolator horizontal and vertical displacement demands were manageable and within the capacities of the system and accelerations were within acceptable bounds.

Analytical models of the tested electrical transformer model were developed in program SAP2000. Comparisons of the results of the dynamic analysis to the test data demonstrated that it is possible to predict the response of the tested model in tri-axial seismic excitation with sufficient accuracy. Specifically, the acceleration histories on the main body of the model and their response spectra and the isolator's horizontal and vertical displacements could be predicted with sufficient accuracy. However, the acceleration histories of the top of the flexibly-installed bushing of the model were significantly under-estimated. It was determined that rocking motion of the shake table contributed to the motion of the bushing top in the horizontal direction and its inclusion in the analysis improved the accuracy of the prediction. However, the main contributor to the underestimation of the acceleration at the top of the bushing was that the actual damping in the bushing was less than the value used in the analytical model.

A design example was developed for a location in Eugene, Oregon, for which the equipment qualification level per IEEE (2005) is moderate. A seismic hazard analysis for the site was conducted by the University of California, Berkeley that resulted in site-specific response spectra for a return period of 2475 years and in triplets of 11 compatible ground motion acceleration histories for use in the analysis and design. Analysis was also conducted for the same system for a hypothetical location for which the equipment qualification level per IEEE (2005) is high by using the same spectra and motions after multiplication by a factor of 1.5.

The presented isolation system design was configured for a high equipment qualification level. Details were presented that offer an option for designers to consider in an actual implementation. The isolation hardware dimensions are appropriate for the considered equipment locations and details of the installation include provisions for access to the equipment for inspection and replacement, protection from the elements and embedment for limiting the height above ground.

The detailed isolation system was of the configuration that allows for free rocking as it is the easiest to implement. An alternate configuration with a second massive basemat to effectively restrict rocking was also presented.

Results were presented for (a) the two-dimensional isolation system consisting of just the FP isolators (2D), (b) the three-dimensional isolation system (3D) allowed to rock, (c) the 3D isolation system with restrained rocking and (d) the non-isolated transformer. Two levels of intensity of the seismic excitation were considered (100% and 150%).

The results of the analysis and design examples demonstrated the following:

- 1) All three systems (2D, 3D free to rock and 3D with restrained rocking) have about the same FP isolator displacement demands which were within the displacement capacity of the isolators prior to initiation of stiffening.
- 2) All three systems provided effective isolation in the horizontal direction. All systems resulted in substantial reduction of accelerations at the CM of the transformer by comparison to a non-isolated transformer.
- 3) The benefits offered by the three isolation systems are best described by the calculated vertical accelerations at the center of mass of the bushings. Concentrating on the case of 150% intensity motion and lower bound friction, the following obtained results are informative: the 2D system has a peak vertical acceleration of 2.01g whereas values of 1.14g and 0.93g were obtained in the 3D free to rock and the 3D with restrained rocking systems, respectively. The reduction in vertical acceleration to about half is important. For the 3D system that is free to rock, this reduction comes at the expense of some rocking motion that is amplified both in the vertical (by some 20% by comparison to the 2D system and the 3D system with restrained rocking) and in the horizontal direction due to the large distance of the CM to the pivot point (by about 25%).
- 4) Given the complexity of the 3D system with restrained rocking, it appears that the 3D system that is free to rock is a viable option for use in a location of a higher seismic intensity than that of the site at Eugene, OR (herein the higher seismic intensity location

is represented by motions magnified by a factor of 150%). It provides effective vertical and horizontal isolation although the horizontal accelerations at the CM of the bushing are magnified by a moderate amount. It is the penalty to pay for a significant reduction in the vertical acceleration.

- 5) For the location in Eugene, Oregon, the vertical accelerations at the CM of the bushing in the 2D system appeared acceptable so that use of the two-dimensional isolation system appears to be the appropriate choice for this site. This is consistent with the results of the transformer fragility analysis in Kitayama et al (2016) for this site where it was concluded that a 3D seismic isolation system does not offer any significant advantage in terms of the probability of failure in its lifetime over that of a comparable 2D seismic isolation system.

While the developed system, testing, analysis and the presented examples concentrated on applications of electrical transformers, the developed system and results are readily applicable to building applications.

“This Page Intentionally Left Blank”

SECTION 8

REFERENCES

Aiken ID, Kelly JM, Tajirian FF (1989). "Mechanics of Low Shape Factor Elastomeric Seismic Isolation Bearings." Report No. UCB/EERC-89/13, Earthquake Engineering Research Center, University of California Berkeley, Berkeley, CA.

Computers and Structures, I. (2015). SAP2000: Static and Dynamic Finite Element Analysis of Structures (Version 17.2.0). Berkeley, CA: Computers and Structures.

Constantinou MC, Mokha A, Reinhorn A. (1990). "Teflon Bearings in Base Isolation. II: Modeling", J. Structural Engineering, ASCE, 116(2), 455-474.

DIN 2089 (1984). "Helical Springs made from Round Wire or Rod. Calculation and Design of Compression Springs in German." Deutsches Institut für Normung e. V, Germany.

Fenz DM, Constantinou MC (2008). "Spherical Sliding Isolation Bearings with Adaptive Behavior: Theory." Earthquake Engineering and Structural Dynamics 37, 163-183, DOI: 10.1002/eqe.751

Gilani AS, Whittaker AS, Fenves GL (2001). "Seismic Evaluation and Retrofit of 230-kV Porcelain Transformer Bushings." Earthquake spectra 17, 597-616.

IEEE (2005). IEEE Recommended Practice for Seismic Design of Substations: IEEE Standard 693, IEEE Power Engineering Society, Institute of Electrical and Electronics Engineers, Inc. NY.

Inoue K, Fushimi M, Moro S, Morishita M, Kitamura S, Fujita T (2004). "Development of Three-Dimensional Seismic Isolation System for Next Generation Nuclear Power Plant." 13th World Conference on Earthquake Engineering, Vancouver, Canada.

Harris CM, Piersol AG, (2002). "Shock and Vibration Handbook." McGraw-Hill, New York.

Kageyama M, Iba T, Umeki K, Somaki T, Moro S (2003). "Development of Three-Dimensional Base Isolation System with Cable Reinforcing Air Spring." 17th Structural Mechanics in Reactor Technology (SMiRT 17), Paper # K09-2, Prague, Czech Republic.

Kageyama M, Iba T, Umeki K, Somaki T, Hino Y, Moro S, Ikutama S (2004). "Study on Three-Dimensional Seismic Isolation System for Next Generation Nuclear Power Plant: Independent Cable Reinforced Rolling-Seal Air Spring." 13th World Conference on Earthquake Engineering, Vancouver, Canada.

Kashiwazaki A, Shimada T, Fujiwaka T, Moro S (2003). "Study on 3-Dimensional Base Isolation System Applying to New Type Power Plant Reactor (Hydraulic 3-Dimensional Base Isolation System: No.1)." 17th Structural Mechanics in Reactor Technology (SMiRT 17), Paper # K09-2, Prague, Czech Republic.

Kelly JM (1988). "Base Isolation in Japan." Report No. UCB/EERC-88/20, Earthquake Engineering Research Center, University of California Berkeley, Berkeley, CA.

Kitayama S, Constantinou MC, Lee D (2016). "Procedures and Results of Assessment of Seismic Performance of Seismically Isolated Electrical Transformers with Due Consideration for Vertical Isolation and Vertical Ground Motion Effects." Technical Report MCEER-16-0010, Multidisciplinary Center for Earthquake Engineering Research, University at Buffalo, Buffalo, NY.

Makris N, Constantinou MC (1992). "Spring-Viscous Damper Systems for Combined Seismic and Vibration Isolation." *Earthquake Engineering and Structural Dynamics*, Vol. 21, 649-664.

Makris N, Deoskar HS (1996). "Prediction of Observed Response of Base-Isolated Structure," *Journal of Structural Engineering*, Vol. 122, 485-493.

Mazzoni, S. and Bozorgnia, Y. (2017). "Eugene BPA Site Hazard and Ground Motions", Confidential report prepared for BPA, University of California, Berkeley, June 16, 2017.

McVitty WJ, Constantinou MC (2015). "Property Modification Factors for Seismic Isolators: Design Guidance for Buildings." Technical Report MCEER-15-0005, Multidisciplinary Center for Earthquake Engineering Research, University at Buffalo, Buffalo, NY.

Mori S, Suhara I, Saruta M, Okada K, Tomizawa T, Tsuyuki Y, Fujita T (2012). "Simulation Analysis of Free Vibration Test in a Building "Chisuikan" using Three-Dimensional Seismic Base Isolation System." 15th World Conference on Earthquake Engineering, Lisbon, Portugal.

Oikonomou K, Constantinou MC, Reinhorn AM, Kempner Jr. L (2016). "Seismic Isolation of High Voltage Electrical Power Transformers." Technical Report MCEER-16-0010, Multidisciplinary Center for Earthquake Engineering Research, University at Buffalo, Buffalo, NY.

Okamura S, Kamishima Y, Negishi K, Sakamoto Y, Kitamura S, Kotake S. (2011). "Seismic Isolation Design for JSFR." *Journal of Nuclear Science and Technology*, 48(4), 688-692.

Sarlis AS and Constantinou MC (2010). "Modeling Triple Friction Pendulum Isolators in SAP2000." document distributed to the engineering community together with example files, University at Buffalo, June.

Sarlis AS and Constantinou MC (2013). "Model of Triple Friction Pendulum Bearing for General Geometric and Frictional Parameters and for Uplift Conditions." Technical Report MCEER-13-0010, Multidisciplinary Center for Earthquake Engineering Research, University at Buffalo, Buffalo, NY.

Sarlis AA, Pasala DTR, Constantinou MC, Reinhorn AM, Nagarajaiah S (2013). "Negative Stiffness Device for Seismic Protection of Structures." *J. Struct. Eng.*, 139(7), 1124-1133.

Staudacher E, Habacher C, Siegenthaler R (1970). *Erdbebensicherung in Baum*, Neue Zurcher Zeitung, Technikbeilage." Zurich, Switzerland.

Suhara J, Tamura T, Ohta K, Okada Y, Moro S (2003). “Research on 3-D Base Isolation System Applied to New Power Reactor 3-D Seismic Isolation Device with Rolling Seal Type Air Spring: Part1.” 17th Structural Mechanics in Reactor Technology (SMiRT 17), Paper # K09-4, Prague, Czech Republic.

Suhara J, Matsumoto R, Oguri S, Okada Y, Inoue K, Takahashi K (2005). “Research on 3-D Base Isolation System Applied to New Power Reactor 3-D Seismic Isolation Device with Rolling Seal Type Air Spring: Part2.” 18th Structural Mechanics in Reactor Technology (SMiRT 18), Paper # K09-4, Beijing, China.

Suhara J, Matsumoto R, Torita H, Tsuyuki Y, Kamei T, Takahashi O, Kunimatsu Y, Aida H, Fujita T (2008). “Construction of Civil Building Using Three Dimensional Seismic Isolation System (Part 2, Tests for Three Dimensional Seismic Isolation System).” 14th World Conference on Earthquake Engineering, Beijing, China.

Takahashi K, Inoue K, Kato A, Morishita M, Fujita T (2005). “A Development of Three-Dimensional Seismic Isolation for Advanced Reactor Systems in Japan-Part 2.” 18th Structural Mechanics in Reactor Technology (SMiRT 18), Paper # K10-2, Beijing, China.

Takahashi O, Aida H, Suhara J, Matsumoto R, Tsuyuki Y, Fujita T (2008). “Construction of Civil Building Using Three Dimensional Seismic Isolation System (Part 1, Design of Building Using Three Dimensional Seismic Isolation System).” 14th World Conference on Earthquake Engineering, Beijing, China.

Tajirian FF, Kelly JM, Aiken ID, Veljovich W (1990). “Elastomeric Bearings for Three-Dimensional Seismic Isolation, in Proceedings.” ASME PVP Conference, Nashville, Tennessee.

Tomizawa T, Takahashi O, Aida H, Suhara J, Okada K, Tsuyuki Y, Suzuki T, Fujita T (2011). “Earthquake Observation Record in a Building named Chisuikan.” 2011 Council on Tall Buildings and Urban Habitat, Seoul, Korea.

Tsutsumi H, Yamada H, Mori K, Ebisawa K, Shibata K (2000). “Characteristics and Dynamic Response of 3-D Component Base Isolation System Using Ball Bearings and Air Springs.” JAERI-Tech 2000-086 in Japanese, Japan Atomic Energy Research Institute, Japan.

Tsutsumi H, Yamada H, Ebisawa K, Shibata K, Fujimoto S (2001). “Shaking Table Test and Dynamic Response Analysis of 3-D Component Base Isolation System Using Multi-Layer Rubber Bearings and Coil Springs.” JAERI-Tech 2001-033 in Japanese, Japan Atomic Energy Research Institute, Japan.

Wahl A (1949). “Mechanical Springs. Penton Publishing Company.” Cleveland, Ohio.

“This Page Intentionally Left Blank”

APPENDIX A
**EIGENVALUE ANALYSIS OF TRANSFORMER WITH 3D SPRING-
DAMPER ISOLATION SYSTEM**

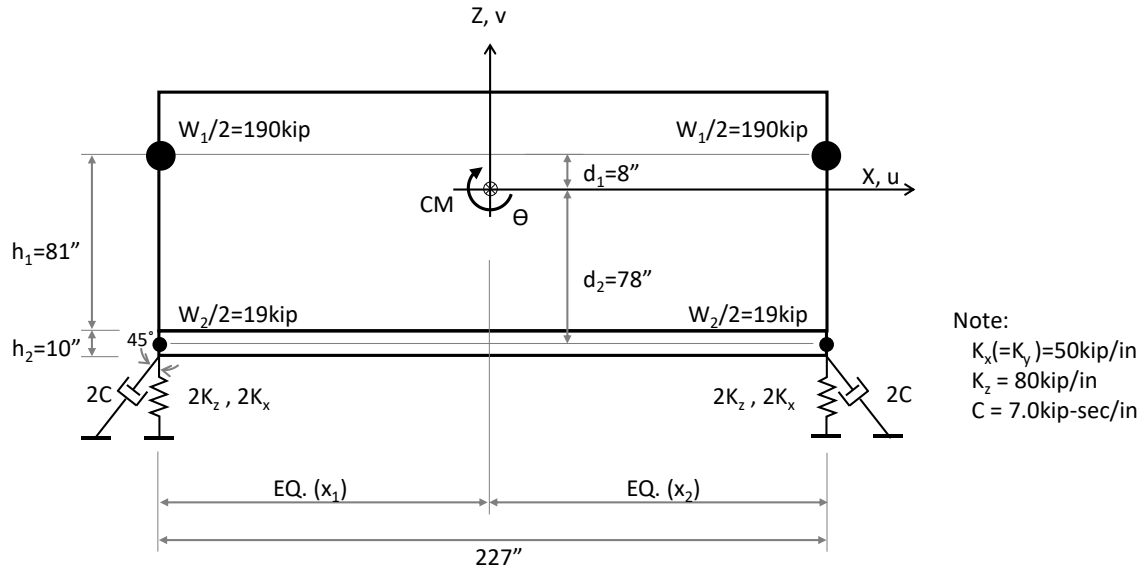
A-1 Complex Eigenvalue Analysis of Two-Dimensional Representation of Isolated Transformer

Figure A-1 presents two-dimensional representations of the transformer with the 3D spring-damper isolation system (see Figure 2-7 for complete model representation) in the longitudinal (1-2) and transverse (3-4) directions. The mass of the transformer ($m_1=380\text{kip/g}$) was represented by two lumped masses at a height of 81inch above the concrete basemat. A small eccentricity of 4inch between the center of mass and the geometric center in the longitudinal direction (see Figure 2-6) was neglected. The basemat has 10inch thickness and its mass ($m_2=38\text{kip/g}$) is lumped in two parts as shown in Figure A-1. Note that the mass distribution shown in Figure A-1 is that of case 1 in Table 2-2, which is the only case presented in the appendix. Given the two-dimensional representation of the isolated transformer, the stiffness and damping parameters at each corner are doubled to represent two supports.

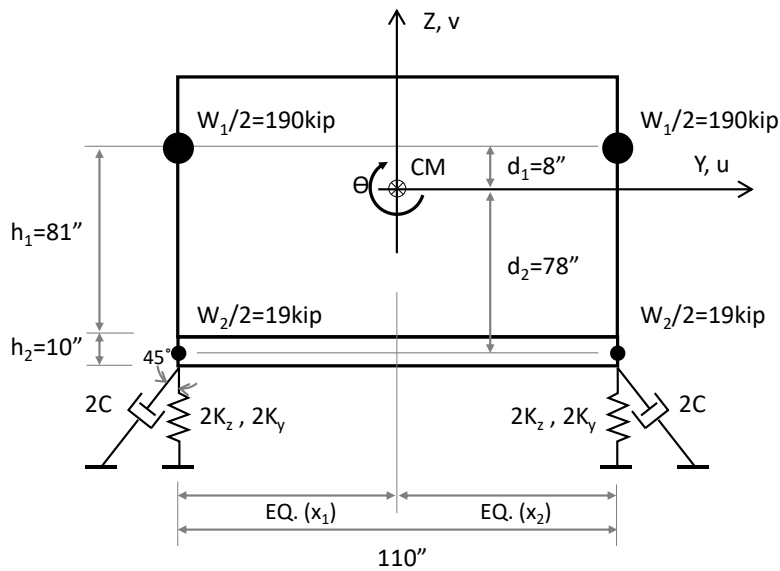
The center of mass of the isolated transformer is shown in Figure A-1 to be located 8 inches below the top masses. The distances of the masses from the center of mass are denoted as d_1 and d_2 , as shown in Figure A-1. The mass moment of inertia of the system about the horizontal axis at the center of mass (I_{CM}) is given by

$$I_{CM,1-2 \text{ (or } 3-4)} = I_{CM,X \text{ (or } Y)} + I_{CM,Z} = m_1 d_1^2 + m_2 d_2^2 + (m_1/2 + m_2/2)(x_1^2 + x_2^2) \quad (\text{A-1})$$

Note that m_1 and m_2 are masses associated with weights W_1 and W_2 , respectively, and x_1 and x_2 are distances as shown in Figure A-1.



(a) Longitudinal (1-2)-Vertical



(b) Transverse (3-4)-Vertical

FIGURE A-1 Two-dimensional Representation of Spring-Damper Isolated Transformer in (a) Longitudinal (1-2)-Vertical Plane and (b) Transverse (3-4)-Vertical Plane

The dampers are inclined at an angle ϕ ($=54.7$ degrees) with respect to three orthogonal directions (x , y , and z) as shown in Figure A-2. The damping constants in the horizontal directions (C_x and C_y) and the vertical direction (C_z) for each support are given by:

$$C_x = C_y = C_z = C \cos^2 \phi \quad (A-2)$$

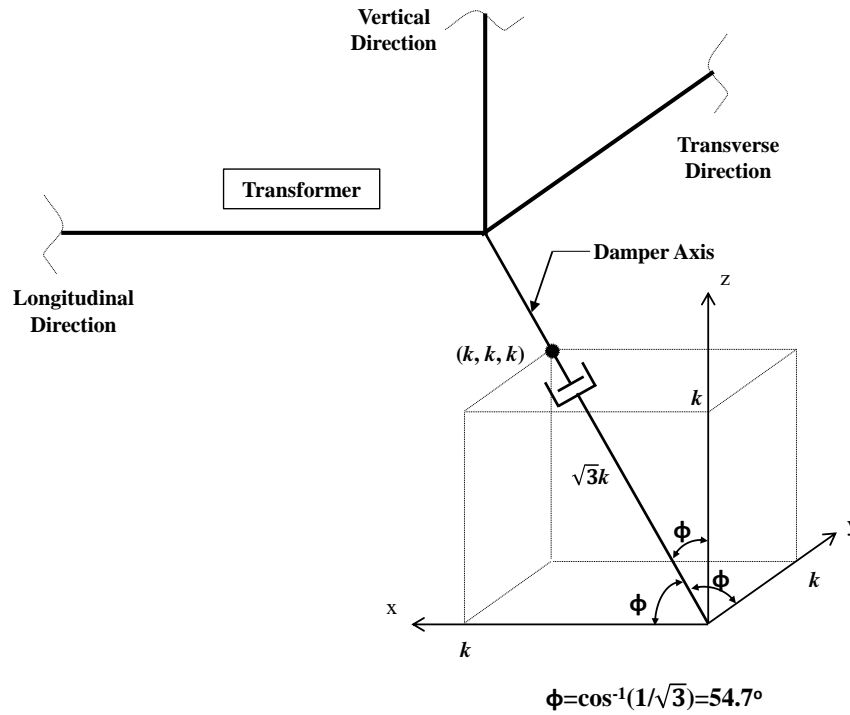


FIGURE A-2 Damper Installation Angles

The equations of motion for free vibration and for degrees of freedom being the horizontal displacement u , the vertical displacement v , and the angle of rotation about the center of mass θ are:

$$\begin{bmatrix} m & 0 & 0 \\ 0 & m & 0 \\ 0 & 0 & I_{CM} \end{bmatrix} \begin{pmatrix} \ddot{u} \\ \ddot{v} \\ \ddot{\theta} \end{pmatrix} + \begin{bmatrix} 4C_x & 0 & -4C_x d_2 \\ 0 & 4C_z & 2C_z(x_1 - x_2) \\ -4C_x d_2 & 2C_z(x_1 - x_2) & 4C_x d_2^2 + 2C_z(x_1^2 + x_2^2) \end{bmatrix} \begin{pmatrix} \dot{u} \\ \dot{v} \\ \dot{\theta} \end{pmatrix} + \begin{bmatrix} 4K_x & 0 & -4K_x d_2 \\ 0 & 4K_z & 2K_z(x_1 - x_2) \\ -4K_x d_2 & 2K_z(x_1 - x_2) & 4K_x d_2^2 + 2K_z(x_1^2 + x_2^2) \end{bmatrix} \begin{pmatrix} u \\ v \\ \theta \end{pmatrix} = \begin{pmatrix} 0 \\ 0 \\ 0 \end{pmatrix} \quad (A-3)$$

The eigenvalue problem of Equations (A-3) has been solved for parameters: $C=7.0\text{kip-s/in}$, $C_x=C_y=C_z=2.33\text{kip-s/in}$, $K_x=K_y=80\text{kip/in}$, and $K_z=50\text{kip/in}$. Solution of the complex eigenvalue problem resulted in the values of frequencies and damping ratios in Table A-1. Solution of the eigenvalue problem of the undamped equations of motion resulted in the mode shapes presented in Table A-1. Table A-1 also includes values of the frequencies calculated in program SAP2000 (in parenthesis) for a three-dimensional representation of the transformer with mass uniformly distributed at the basemat level and at the height of 86inch above the basemat centerline (81inch

above the basemat top). Details of the SAP2000 model and results are presented in Section A-2. The modal quantity θh is the horizontal displacement at some point at distance of 86inch (see Section 2) from the center of mass due to rotation.

It should be noted that the simple two-dimensional representation of Equations A-3 predicts well the first two frequencies (as compared to the results of the presumably more accurate three-dimensional model in program SAP2000) but not the third. Actually, analysis using a two-dimensional representation based on the mass distribution of case 2 in Table 2-2 resulted in the third mode frequency close to that of the analysis in SAP2000. The reason is that the case 2 distribution of mass in Table 2-2 better approximates the uniform mass distribution assumed in the SAP2000 model. However, it should be noted that the exact mass distribution (that affects the mass moment of inertia and thus the third mode of vibration which has a dominant rocking component) is not known and is likely somewhere in-between cases 1 and 2 in Table 2-2.

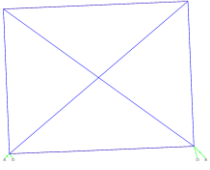
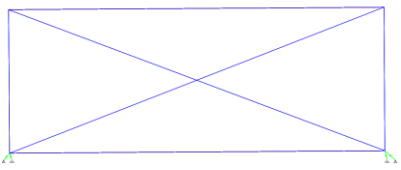
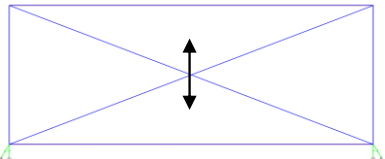
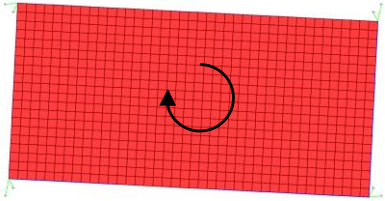
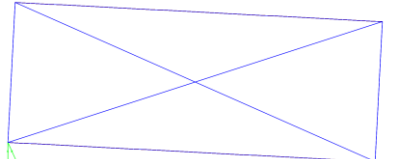
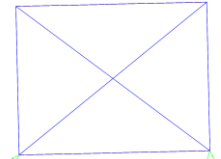
TABLE A-1 Results of Eigenvalue Analysis of Isolated Transformer with Spring-Damper System in Mass Distribution Case 1 (values in parenthesis are frequencies calculated in program SAP2000-see Section A-2)

Representation		Longitudinal (1-2) - Vertical			Transverse (3-4) - Vertical			
Mass Moment of Inertia (kip-in-sec ²)		14612			3938			
Mode		1	2	3	1	2	3	
Spring-Damper System	Frequency (Hz)	1.76 (1.85)	2.74 (2.74)	3.29 (5.07)	1.31 (1.38)	2.74 (2.74)	4.13 (5.71)	
	Damping Ratio	0.21	0.25	0.39	0.14	0.25	0.54	
	Mode Shape	u	1	0	1	1	0	1
		v	0	1	0	0	1	0
		θh	0.38	0	-1.45	0.70	0	-2.91

A-2 Eigenvalue Analysis of Three-Dimensional Representation of Isolated Transformer in Program SAP2000

The model used in the analysis is the one used for response history analysis and shown in Figure 2-7, however with the three bushings removed and the mass uniformly distributed at the basemat level and at the height of 86inch. Table A-2 presents the results of the eigenvalue analysis in terms of frequencies and images of mode shapes. Another analysis with the model shown in Figure 2-7 (masses lumped at the corners) and with the three bushings removed resulted in frequencies identical to those obtained by the two-dimensional model of Figure A-1 and presented in Table A-1.

TABLE A-2 Frequencies and Images of Mode Shapes Obtained in Program SAP2000 for 3D Uniform Mass Model of Transformer with Spring-Damper Isolation System

Mode 1	Mode 2
 <p>f = 1.38 Hz Translation (3-4 direction) + Some Rocking</p>	 <p>f = 1.85 Hz Translation (1-2 direction) + Some Rocking</p>
Mode 3	Mode 4
 <p>f = 2.74 Hz Vertical Translation</p>	 <p>f = 3.64 Hz Torsion</p>
Mode 5	Mode 6
 <p>f = 5.07 Hz Rocking (1-2 direction)</p>	 <p>f = 5.71 Hz Translation (3-4 direction)</p>

“This Page Intentionally Left Blank”

APPENDIX B

PROPERTIES OF TRIPLE FRICTION PENDULUM ISOLATORS USED IN ANALYSIS OF SECTION 2

Figure B-1 presents a section of the Triple FP isolator used in the analysis of Section 2. The properties of this isolator are presented in Table B-1 and its force-displacement loops, calculated based on the theory of Fenz and Constantinou (2008), are presented in Figure B-2 for the upper and lower bound frictional properties. The bounds of frictional properties were obtained on the basis of the following considerations (McVitty and Constantinou, 2015) and test data on the production bearings for the Vancouver, WA transformer:

1) Average friction coefficient of tested production bearings

$$\mu_2 = \mu_3 = 0.08 \text{ (3rd cycle) and } 0.08 \text{ (1st cycle)}$$

$$\mu_1 = \mu_4 = 0.11 \text{ (3rd cycle) and } 0.13 \text{ (1st cycle)}$$

2) Lower bound friction coefficient values are the third cycle values without any adjustment for uncertainty (λ_{spec}) as the data are based on all production bearings. That is,

$$\mu_2 = \mu_3 = 0.08$$

$$\mu_1 = \mu_4 = 0.11$$

3) Upper bound friction coefficient values are the first cycle values without any adjustment for uncertainty (λ_{spec}) as the data are based on all production bearings and multiplied by the aging/contamination factor of 1.1 (without application of the property adjustment factor). There were no adjustments for low temperature as those are dependent on the geographic location. That is,

$$\mu_2 = \mu_3 = 0.08 \times 1.1 = 0.088 \text{ and rounded to } 0.09$$

$$\mu_1 = \mu_4 = 0.13 \times 1.1 = 0.143 \text{ and rounded to } 0.15$$

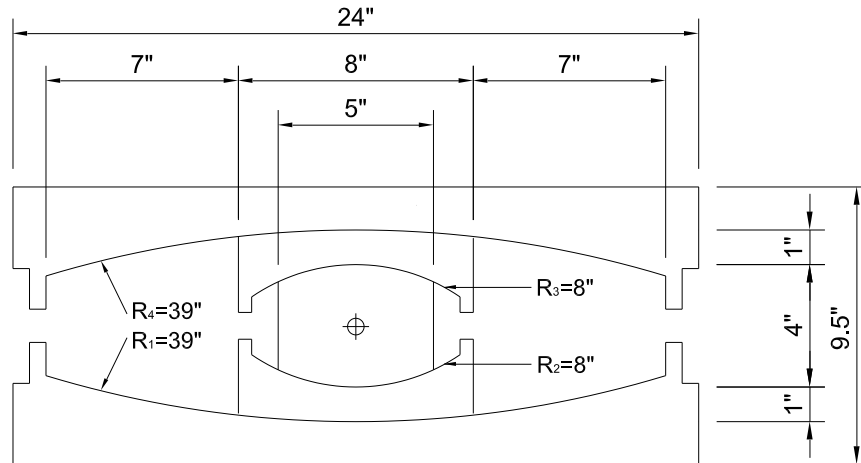


FIGURE B-1 Section of Triple FP Isolator

TABLE B-1 Properties of Triple FP Isolator (for vertical load of 104.5kip, corresponding to transformer weight of 418kip including basemat)

Property	Value
$R_1=R_4$ (inch)	39.0
$R_2=R_3$ (inch)	8.0
$d_1=d_4$ (inch)	7.0
$d_2=d_3$ (inch)	1.0
$h_1=h_4$ (inch)	3.0
$h_2=h_3$ (inch)	2.0
$\mu_1=\mu_4$ (lower/upper bound)	0.11 / 0.15
$\mu_2=\mu_3$ (lower/upper bound)	0.08 / 0.09
$R_{1\text{eff}}=R_{4\text{eff}}$ ($=R_1-h_1$) (inch)	36.0
$R_{2\text{eff}}=R_{3\text{eff}}$ ($=R_2-h_2$) (inch)	6.0
$d_1^*=d_4^*=d_1R_{1\text{eff}}/R_1$ (inch)	6.46
$d_2^*=d_3^*=d_2R_{2\text{eff}}/R_2$ (inch)	0.75

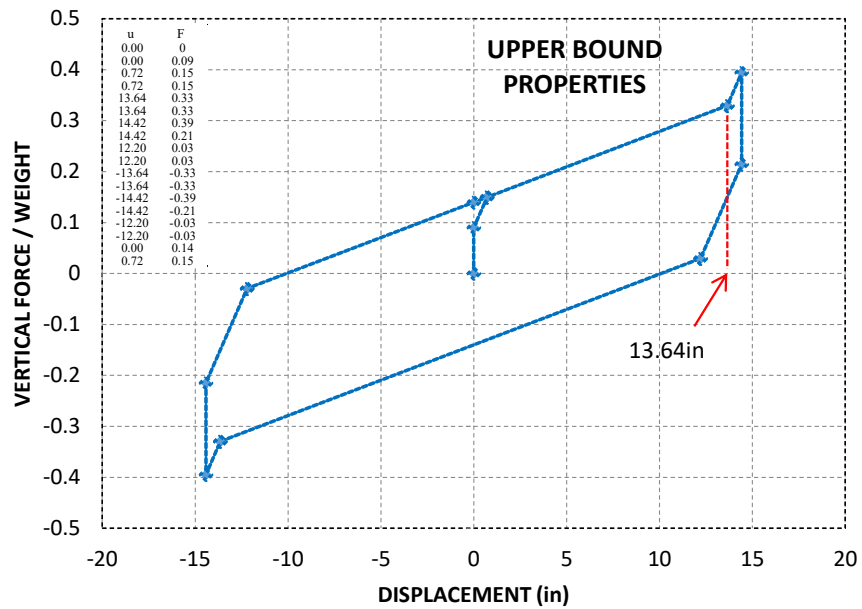
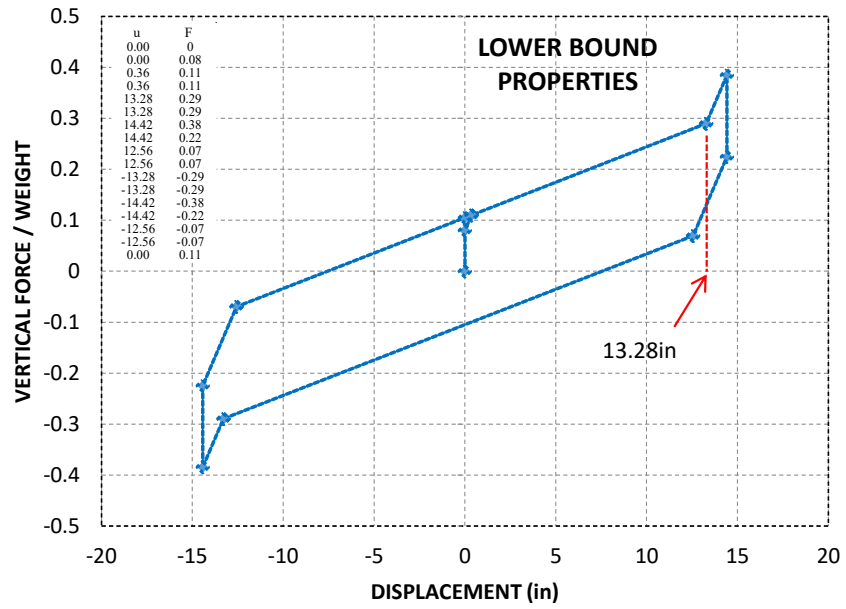


FIGURE B-2 Force-Displacement Loops of Triple FP Isolator for Lower and Upper Friction Conditions

For the analysis in program SAP2000, the triple FP isolators were modelled using the parallel model of Sarlis and Constantinou (2011). Table B-2 presents the parameters of the model.

TABLE B-2 Parameters of Parallel Model of Triple FP Isolator in Program SAP2000

Elements	FP1	FP2
Element Height (in)	9.5	9.5
Element Weight (kip)	0.25	0.25
Shear deformation location (in) (distance from top joint of FP element)	4.25	4.25
Supported Weight (kip)	52.3	52.3
Vertical stiffness ¹⁾ (kip/in)	14,985	14,985
(Elastic) Stiffness ²⁾ (kip/in)	Upper Bound: 205.0 Lower Bound: 161.9	7.3
Yield displacement (inch)	Upper Bound: 0.0220 Lower Bound: 0.0245	-
Radius (inch)	0	36
Friction coefficient FAST	Upper Bound: 0.18 Lower Bound: 0.16	Upper Bound: 0.12 Lower Bound: 0.06
Friction coefficient SLOW	Upper Bound: 0.09 Lower Bound: 0.08	Upper Bound: 0.06 Lower Bound: 0.03
Effective stiffness ³⁾ (kip/in)	0	1.5
Rate parameter (sec/in)	1.27	1.27
Rotational moment of inertia (kip-in-sec ²)	0.006	0.006
Rotational / torsional stiffness (R1,R2,R3)	0	0
For calculations of vertical stiffness (1), elastic stiffness (2) and effective stiffness (3) , see below		

The vertical stiffness, the elastic stiffness and the effective stiffness values in Table B-2 were calculated as follows:

1) Vertical stiffness

$$(\pi 2.5^2)(14500)/9.5 = 29969 \text{kip/in}$$

The stiffness of each of the two elements comprising the isolator model was assigned a value equal to half of the value, that is, 14985kip/in.

2) Elastic Stiffness

$$\bar{K}_{1,upper} = \frac{\mu_{2,upper}W}{2\bar{Y}_1} - \frac{W}{2R_{eff2}} = \frac{0.09 \times 104.5}{2 \times 0.0220} - \frac{104.5}{2 \times 6} = 205.0kip/in$$

$$\bar{K}_{1,lower} = \frac{\mu_{2,upper}W}{2\bar{Y}_1} - \frac{W}{2R_{eff2}} = \frac{0.08 \times 104.5}{2 \times 0.0245} - \frac{104.5}{2 \times 6} = 161.9kip/in$$

Note that per recommendations in Sarlis and Constantinou (2011), \bar{Y}_1 was determined such that the elastic stiffness of parallel model is same as that of series model. The relationship is $\bar{Y}_1 = \left(1 + \frac{2\mu_2}{\mu_1}\right)Y$ for the case of $\mu_2 = \mu_3$ and $\mu_1 = \mu_4$. In the analysis, the yield displacement, Y , was assumed as 0.01inch.

$$\bar{K}_2 = \frac{W}{2R_{eff2}} = \frac{104.5}{2 \times 6} = 8.7kip/in$$

The value used in program SAP2000 was

$$\bar{K}_{2,SAP} = \frac{W}{2R_{eff2}} - \frac{W}{2R_{eff1}} = 8.7 - \frac{104.5}{2 \times 36} = 7.3kip/in$$

3) Effective stiffness

$$\bar{K}_1 = 0$$

$$\bar{K}_2 = \frac{W}{2R_{eff1}} = \frac{104.5}{2 \times 36} = 1.45kip/in$$

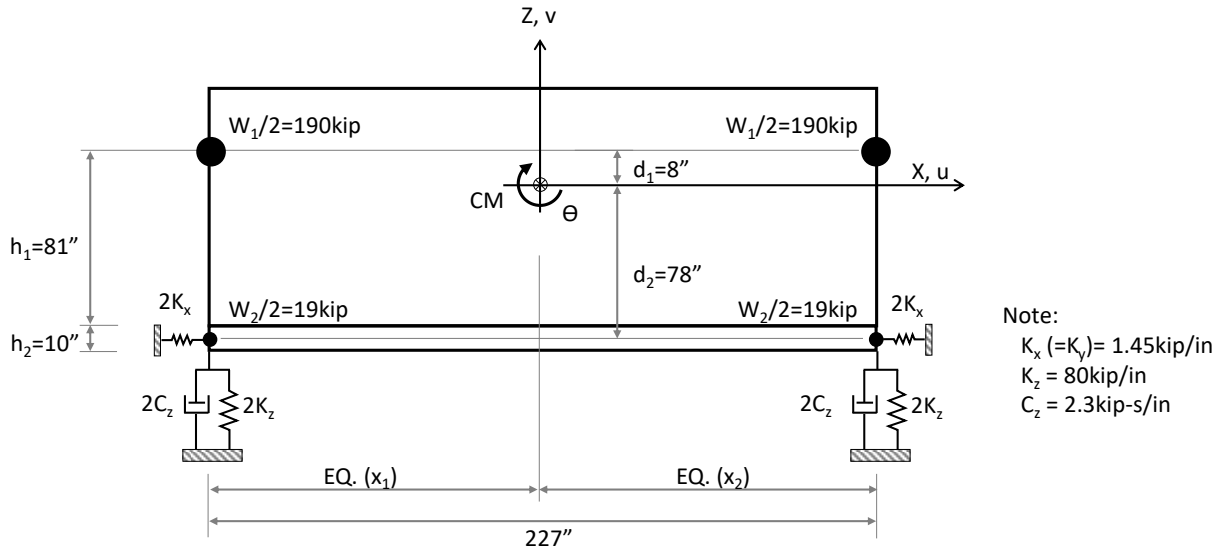
“This Page Intentionally Left Blank”

APPENDIX C

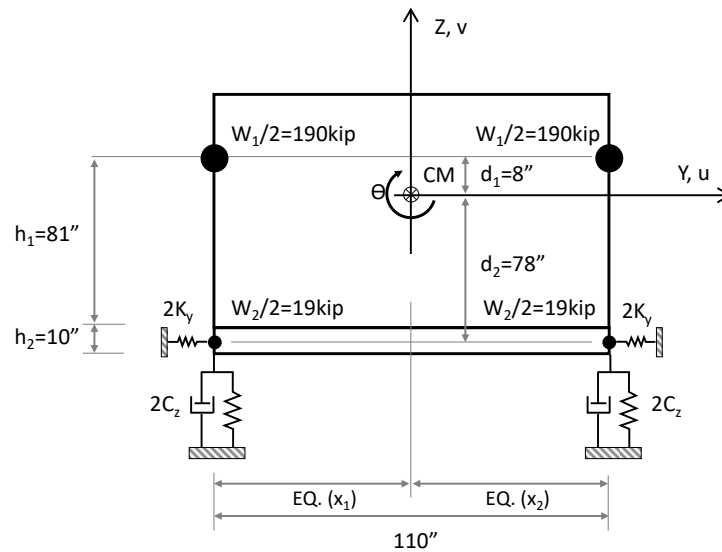
EIGENVALUE ANALYSIS FOR TRANSFORMER WITH TRIPLE FP- SPRING-DAMPER SYSTEM

Figure C-1 presents two-dimensional representations of the transformer with the 3D triple FP and spring-damper isolation system (see Figure 2-10 for complete model representation) in the longitudinal (1-2) and transverse (3-4) directions. The mass of the transformer ($m_1=380\text{kip/g}$) was represented by two lumped masses at a height of 81inch above the concrete basemat. A small eccentricity of 4inch between the center of mass and the geometric center in the longitudinal direction (see Figure 2-6) was neglected. The basemat has a 10inch thickness and its mass ($m_2=38\text{kip/g}$) is lumped into two components as shown in Figure C-1. Note the mass distribution shown in Figure C-1 is that of case 1 in Table 2-2, which is the only case presented in this appendix. Given the two-dimensional representation of the isolated transformer, the stiffness and damping parameters at each corner are doubled to represent two supports.

In the eigenvalue analysis, the triple FP isolators are represented in the horizontal directions by springs of stiffness K_x or K_y that is equal to the post-elastic stiffness of the isolators calculated in Appendix B (the stiffness in the absence of friction).



(a)



(b)

FIGURE C-1 Two-dimensional Representation of Triple FP and Spring-Damper Isolated Transformer in (a) Longitudinal (1-2) and (b) Transverse (3-4) Directions

The equations of motion of the system are given by Equations (A-3) with K_x , K_y , K_z and C_z having the values shown in Figure C-1 and with $C_x=C_y=0$. Table C-1 presents the results of the complex eigenvalue analysis on the frequencies and damping ratio. The mode shapes presented was calculated using the undamped equations of motion. Again quantity $h=86$ inch (see Appendix A).

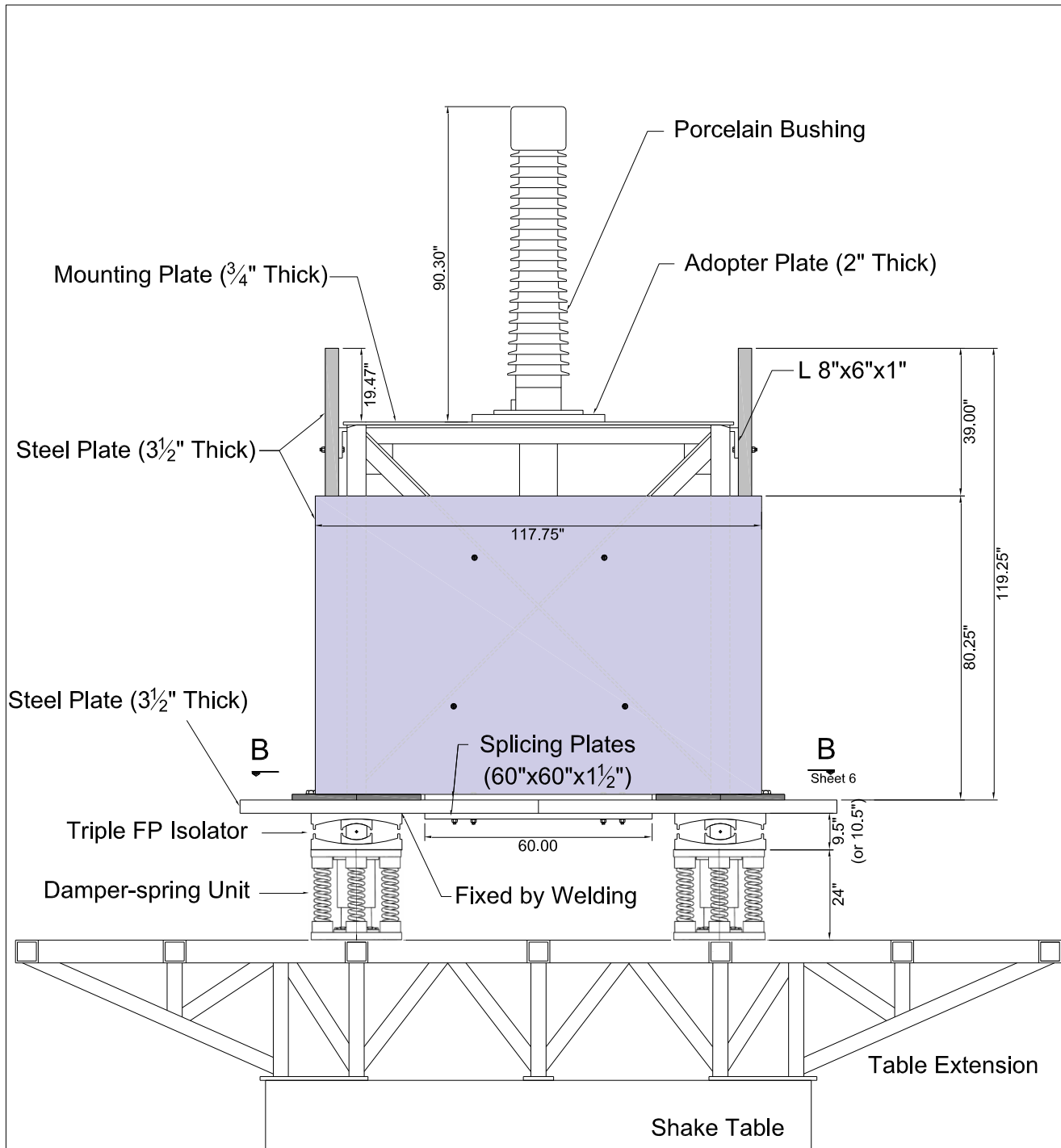
TABLE C-1 Results of Eigenvalue Analysis of Isolated Transformer with Triple FP and Spring-Damper System in Mass Distribution Case 1

Representation		Longitudinal (1-2) - Vertical			Transverse (3-4) - Vertical			
Mass Moment of Inertia (kip-in-sec ²)		14,612			3,938			
Mode		1st Mode	2nd Mode	3rd Mode	1st Mode	2nd Mode	3rd Mode	
FP-Spring-Damper System	Frequency (Hz)	0.37	2.68	2.74	0.36	2.54	2.74	
	Damping Ratio	0	0.24	0.25	0	0.22	0.25	
	Mode Shape	<i>u</i>	1	1	0	1	0	0
		<i>v</i>	0	0	1	0	1	1
<i>θh</i>		0.009	-57.46	0	0.043	-51.37	0	

The results show that the leading mode is a nearly pure horizontal motion mode at the frequency of the pendulum motion of the isolator ($\sqrt{g/2R_{eff1}}/2\pi=0.37\text{Hz}$). The corresponding damping ratio is shown as zero since a zero effective damping was assumed in the analysis. The third mode is the vertical mode and the second mode is nearly a pure rocking mode. The frequency of the rocking mode is significantly affected by the assumed distribution of mass.

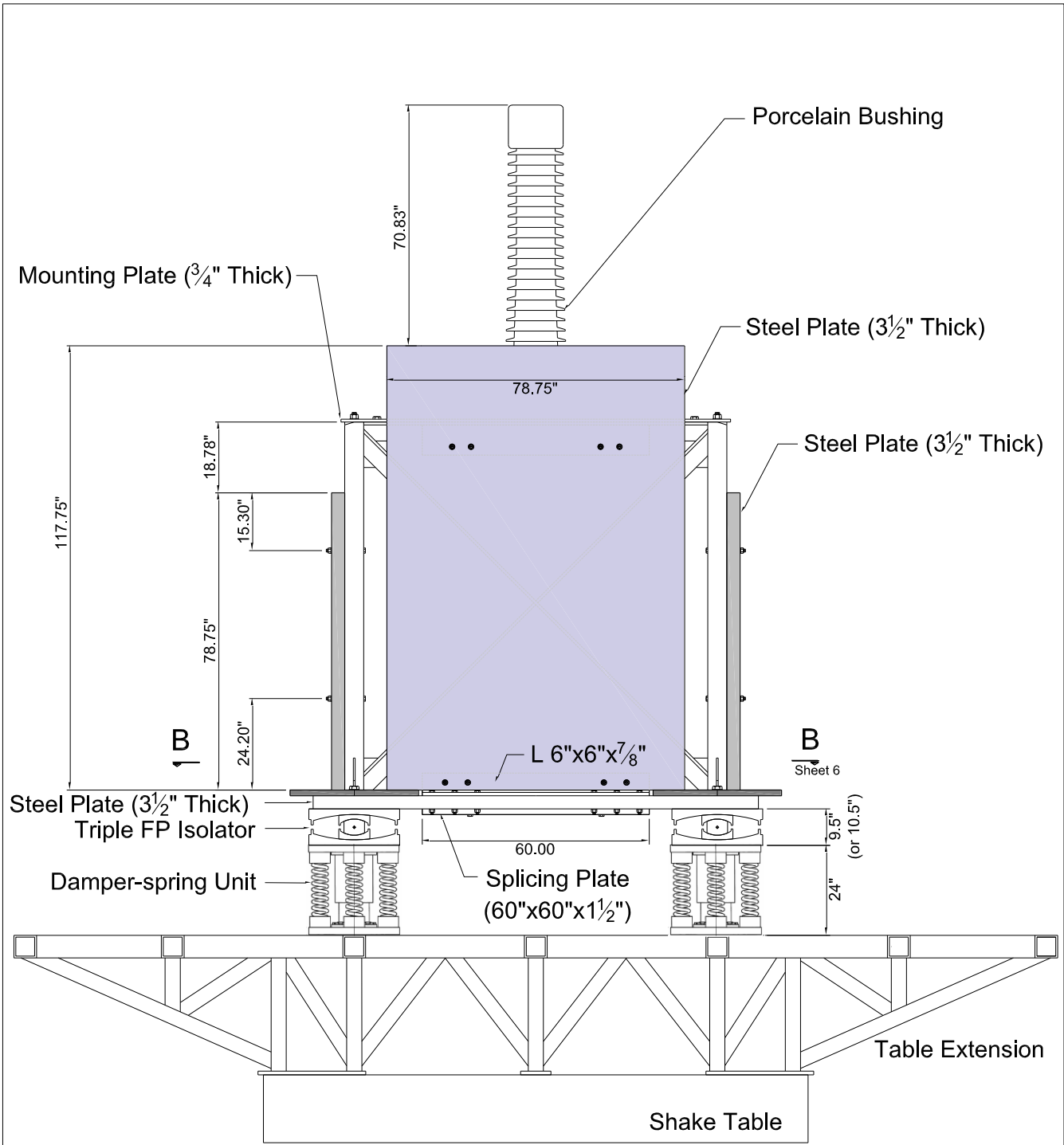
“This Page Intentionally Left Blank”

APPENDIX D
DRAWINGS OF TEST MODEL



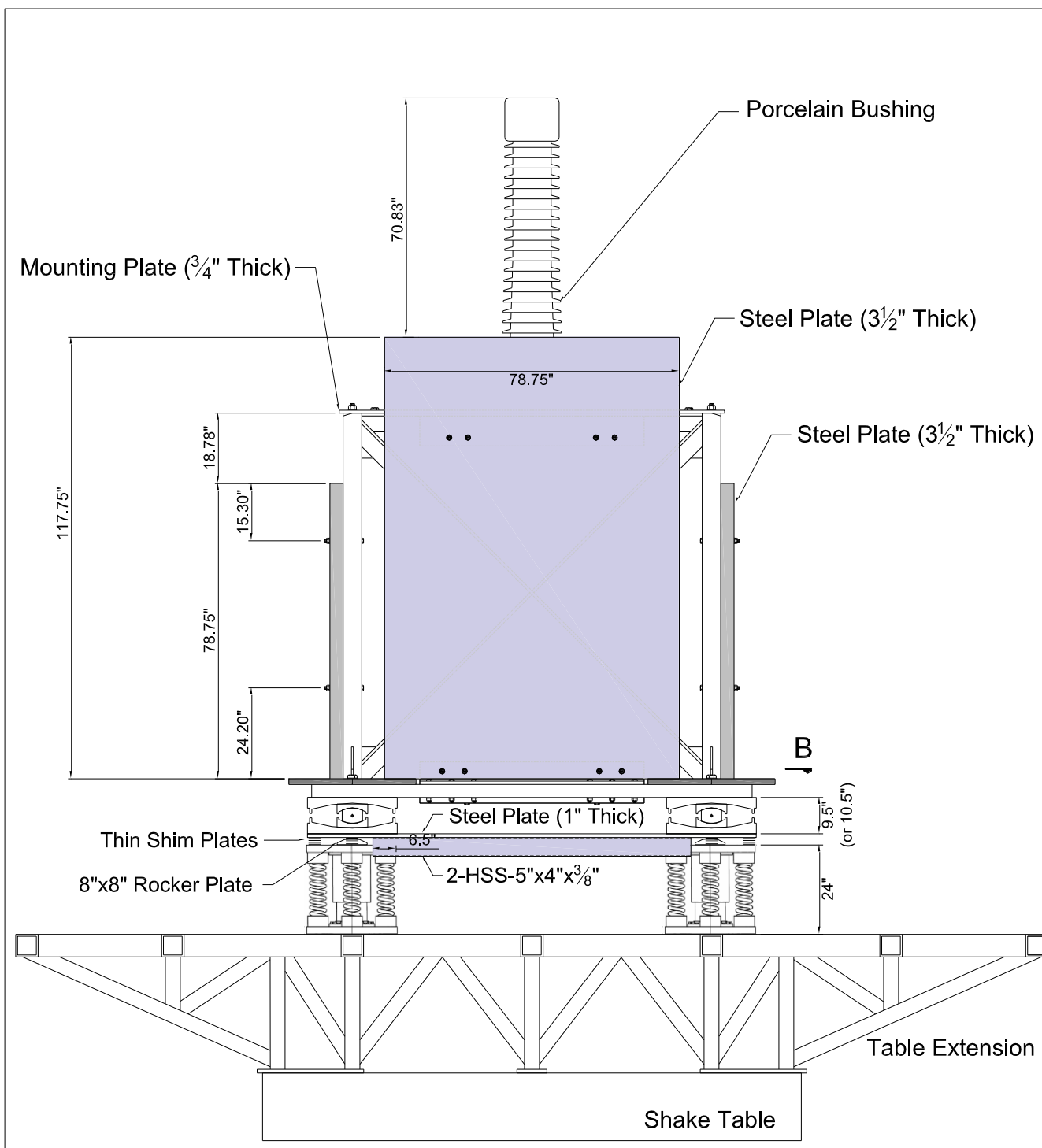
SOUTH ELEVATION

Revision	University at Buffalo, the State University of New York Dept. of Civil, Structural and Environmental Engineering		
	TEST SETUP FOR SEISMIC ISOLATION OF TRANSFORMER (FREE ROCKING)		
	South Elevation View	Sheet 02	Date January 8, 2016



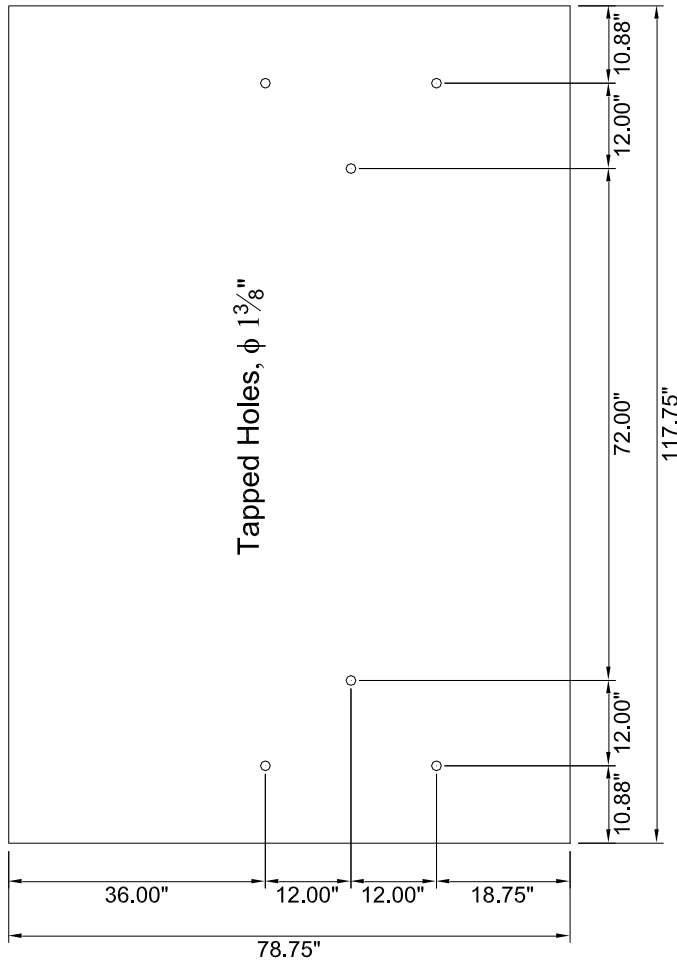
WEST ELEVATION

Revision	University at Buffalo, the State University of New York Dept. of Civil, Structural and Environmental Engineering		
	TEST SETUP FOR SEISMIC ISOLATION OF TRANSFORMER (FREE ROCKING)		
	West Elevation View	Sheet 03	Date January 8, 2016

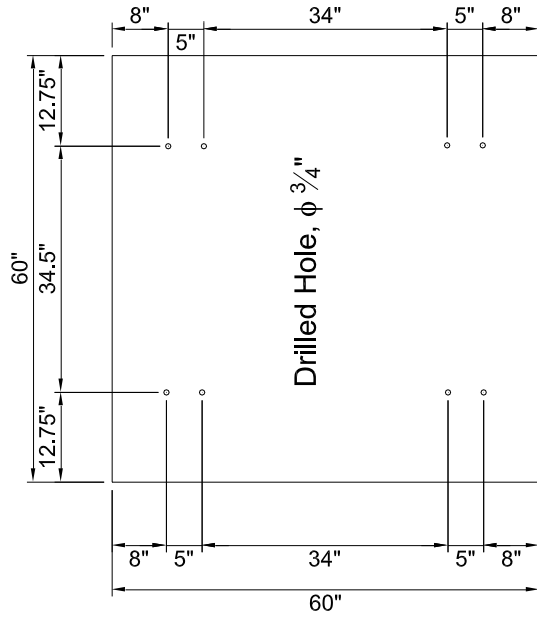


WEST ELEVATION

Revision	University at Buffalo, the State University of New York Dept. of Civil, Structural and Environmental Engineering		
	TEST SETUP FOR SEISMIC ISOLATION OF TRANSFORMER (LIMITED ROCKING)		
	West Elevation View	Sheet 04	Date January 8, 2016

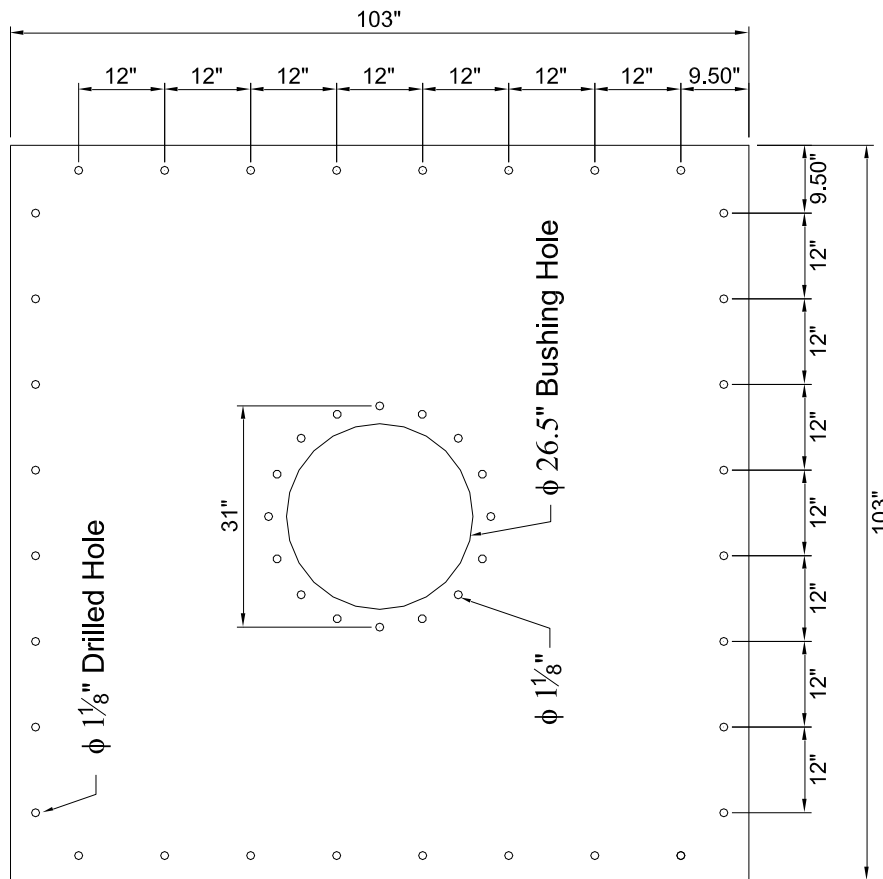


PL-117.75" x 78.75" x 3 1/2"
 (BASE-MAT, VERTICAL/HORIZONTAL PLATE)

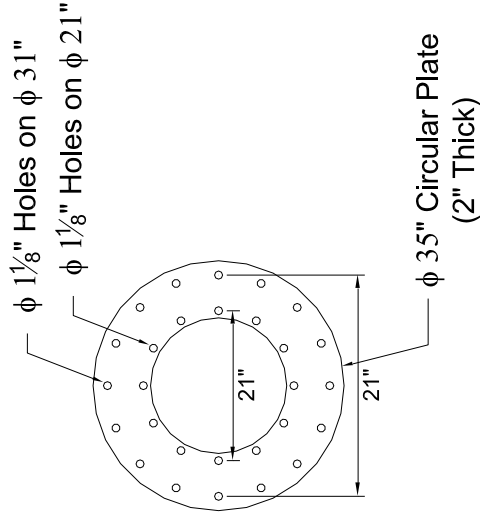


PL-60" x 60" x 1 1/2"
 (SP LICING PLATE)

Revision	University at Buffalo, the State University of New York Dept. of Civil, Structural and Environmental Engineering		
	TEST SETUP FOR SEISMIC ISOLATION OF TRANSFORMER		
	Tapped and Drilled Holes on Base Plates	Sheet 08	Date January 8, 2016

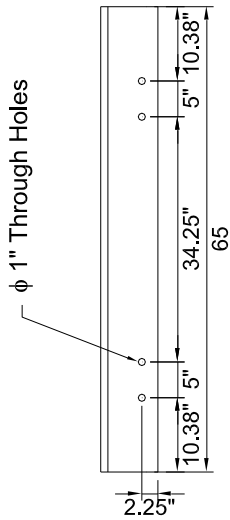


MOUNT PLATE



ADAPTOR PLATE

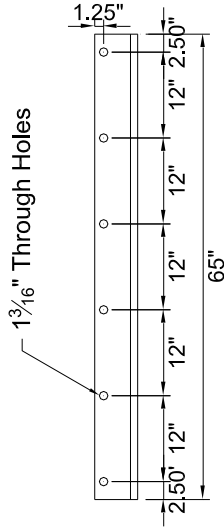
Revision	University at Buffalo, the State University of New York Dept. of Civil, Structural and Environmental Engineering		
	TEST SETUP FOR SEISMIC ISOLATION OF TRANSFORMER		
	Mount Plate, Bushing Flange and Adaptor Plate	Sheet 09	Date January 8, 2016



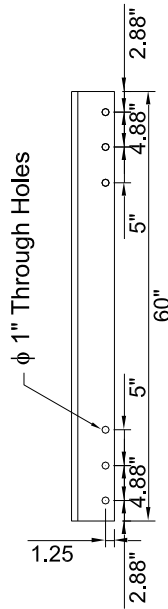
Top View

2-L 8"x6"x1"

(Plate Connection to Frame at East and West Top)



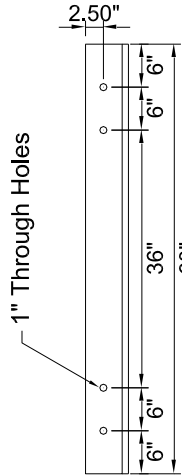
Side View



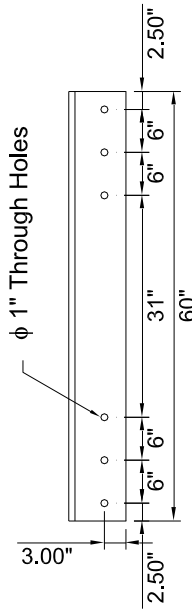
Top View

1-L 6"x6"x7/8"

(Plate Connection to Base Plate at East Bottom)



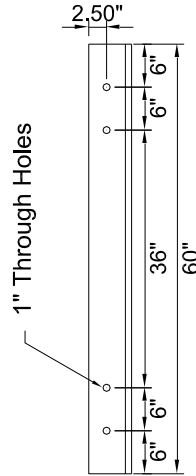
Side View



Top View

1-L 8"x6"x7/8"

(Plate Connection to Base Plate at West Bottom)



Side View

Revision	University at Buffalo, the State University of New York Dept. of Civil, Structural and Environmental Engineering	
	TEST SETUP FOR SEISMIC ISOLATION OF TRANSFORMER	
	Steel Members, Bolts, Nuts and Washers	Date January 8, 2016
	Sheet 10	

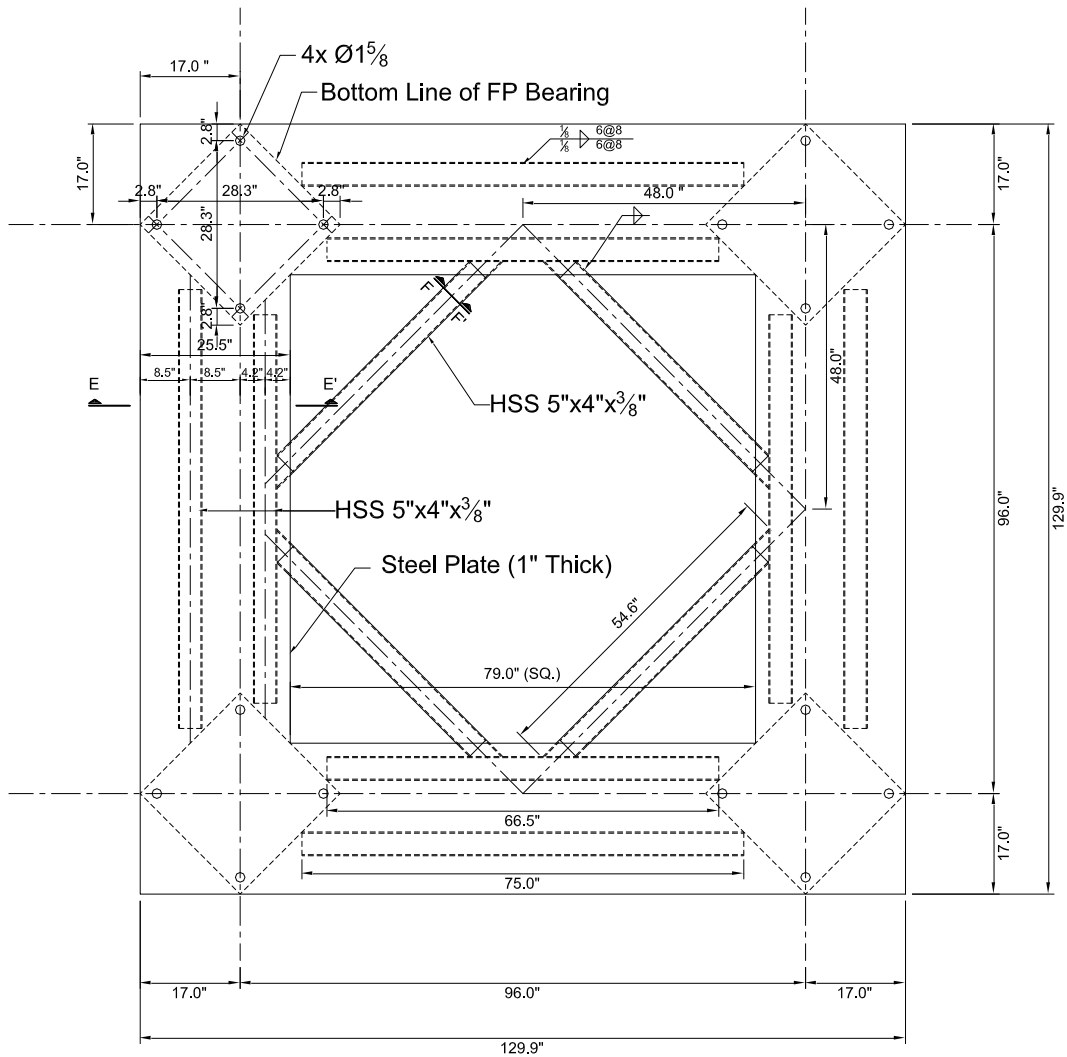
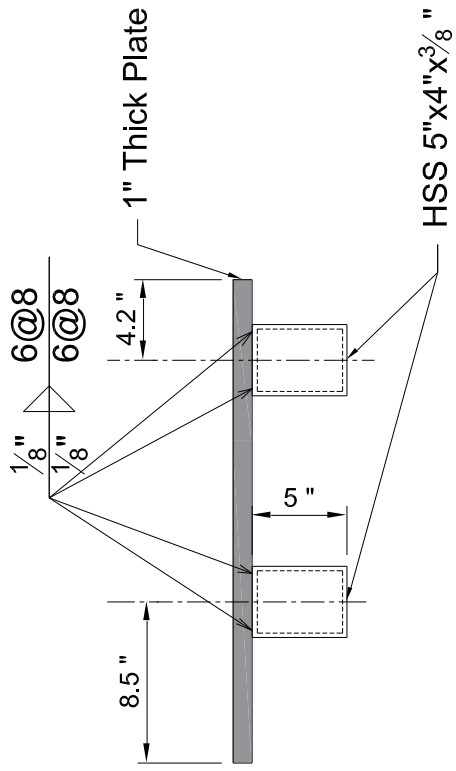


PLATE 1" THK. W/ STIFFENERS

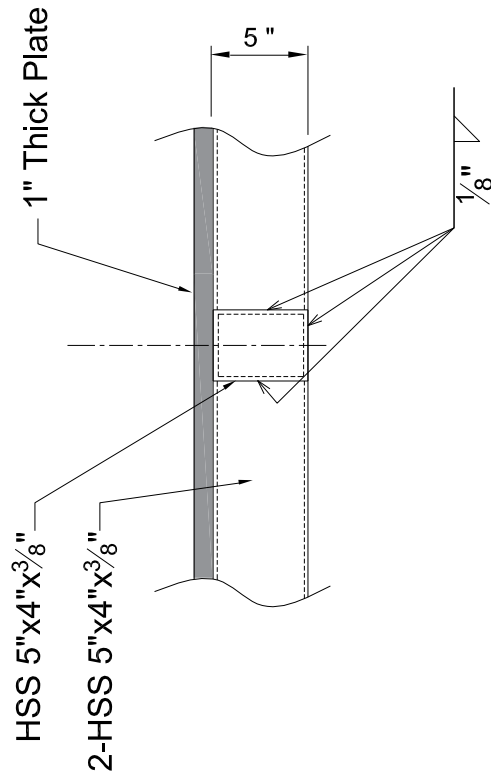
MEMBER SCHEDULE

Revision	University at Buffalo, the State University of New York Dept. of Civil, Structural and Environmental Engineering		
	TEST SETUP FOR SEISMIC ISOLATION OF TRANSFORMER		
	Rocking Limiting Base	Sheet 11	Date APRIL 9, 2016

1" Thk. Plate (Qty. = 1)	HSS-4"x3"x3/16" (Qty. = 4 per each)	HSS-4"x3"x3/16" (Qty. = 4)



SECTION A



SECTION B

Revision	University at Buffalo, the State University of New York Dept. of Civil, Structural and Environmental Engineering		
	TEST SETUP FOR SEISMIC ISOLATION OF TRANSFORMER		
	Rocking Limiting Base Section	Sheet 12	Date APRIL 9, 2016

“This Page Intentionally Left Blank”

APPENDIX E

TEST DATA FOR SPRING-DAMPER UNITS AND TRIPLE FRICTION PENDULUM ISOLATORS

Each of Figures E-1 to E-3 presents the recorded histories of displacement and the force-displacement loops of the four spring-damper units in tests at peak velocity of 0.03in/sec, 3.14in/sec, and 6.28in/sec, respectively. The test procedure was described in Section 3-4.

Figures E-4 to E-9 present the normalized (lateral force divided by instantaneous vertical load) of the tested triple FP isolators. Figures E-4 to E-7 presents the loops of the four isolators of type A and nominal friction of 0.20. Each of the figures presents four graphs of loops, each at a different peak velocity: 0.2, 3.5, 6.9 and 10.4in/sec.

Figures E-8 and E-9 present the recorded normalized force-displacement loops of isolator No. 2 of type B and nominal friction of 0.12 and isolator No. 2 of type B of nominal friction of 0.07. Only one isolator of these two types was tested.

The figures also include analytical force-displacement loops predicted by the model of Fenz and Constantinou (2008) using a constant friction model with the values shown in each graph. More details on the modeling and additional results were presented in Section 3-5.

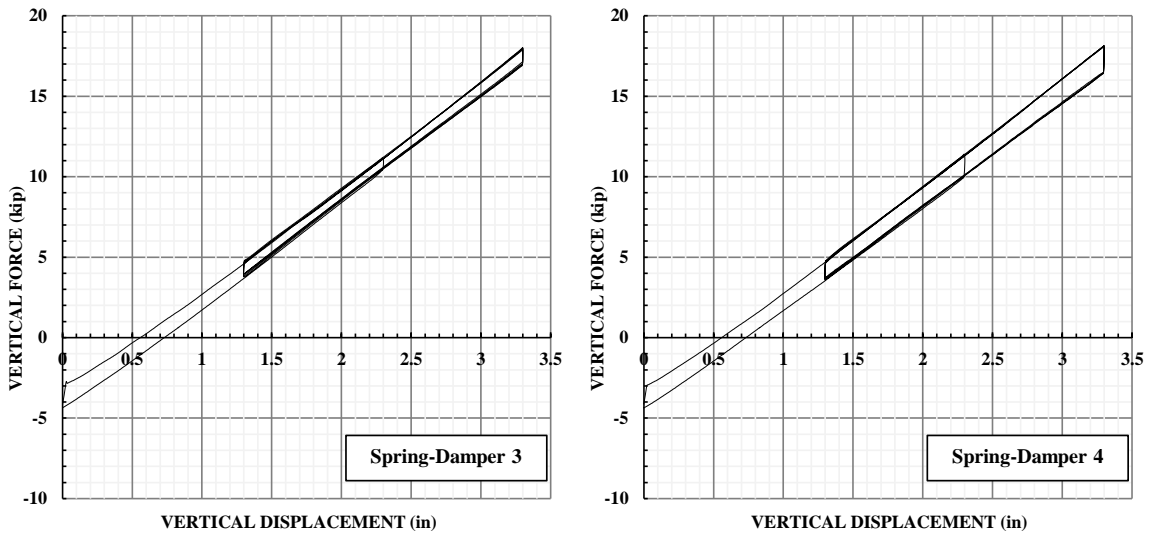
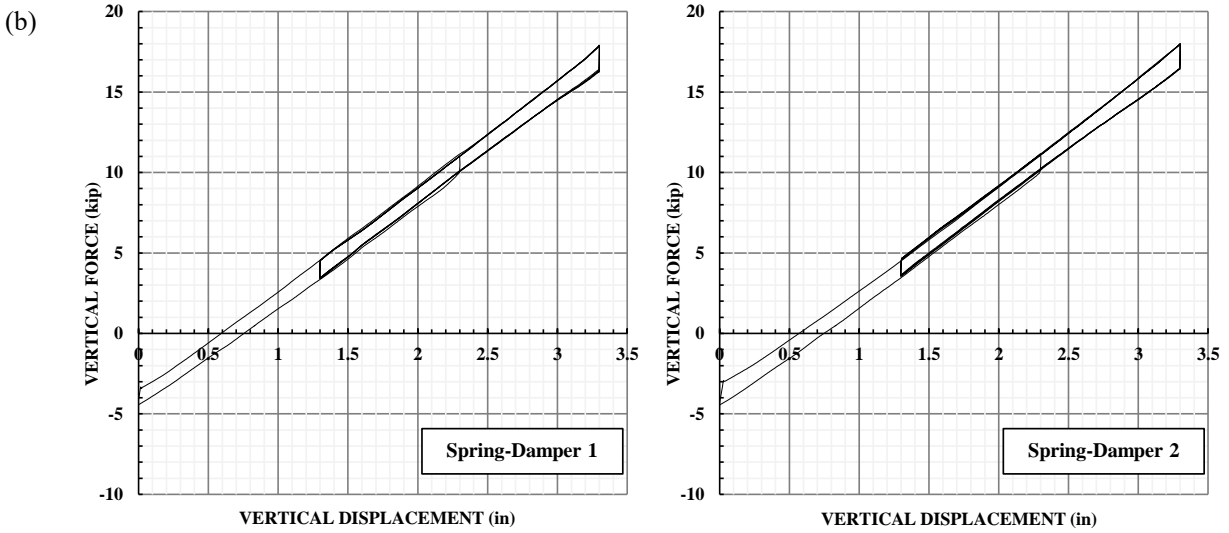
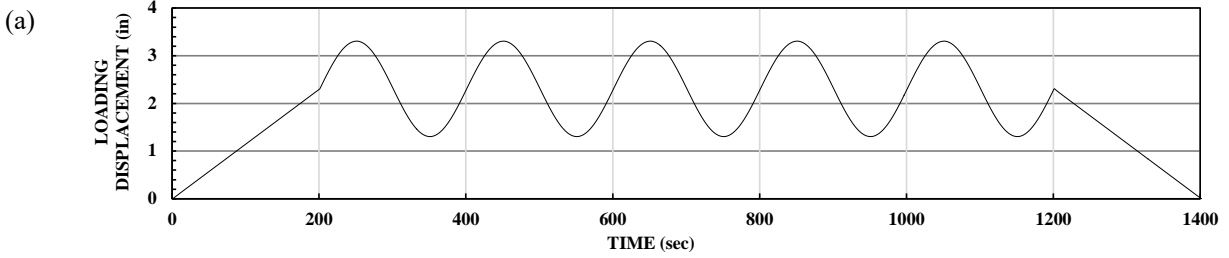


FIGURE E-1 (a) Displacement History and (b) Force-Displacement Loops of Spring-Damper Units in Test at Peak Velocity of 0.03in/sec (frequency of 0.005Hz)

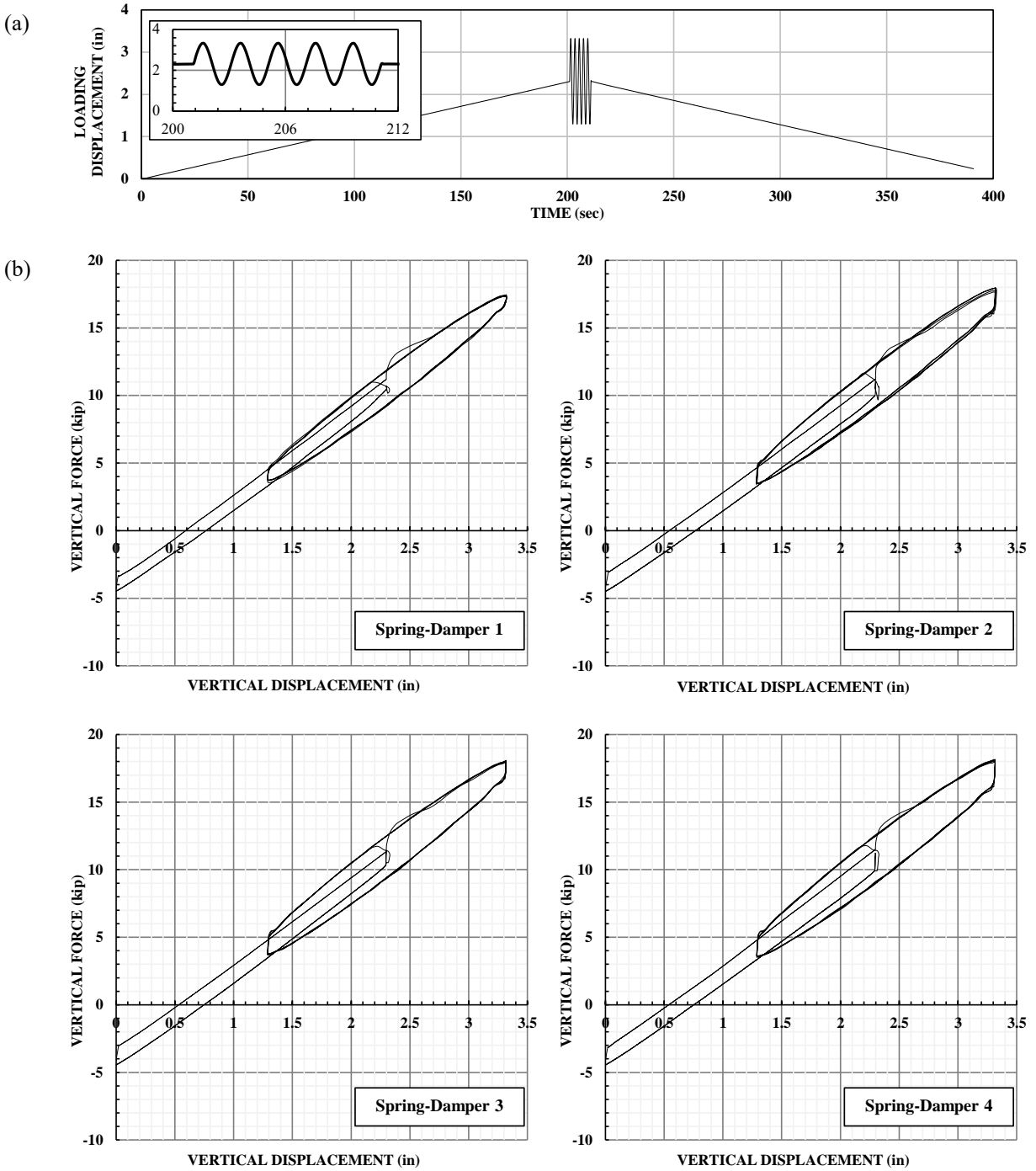


FIGURE E-2 (a) Displacement History and (b) Force-Displacement Loops of Spring-Damper Units in Test at Peak Velocity of 3.14in/sec (frequency of 0.5Hz)

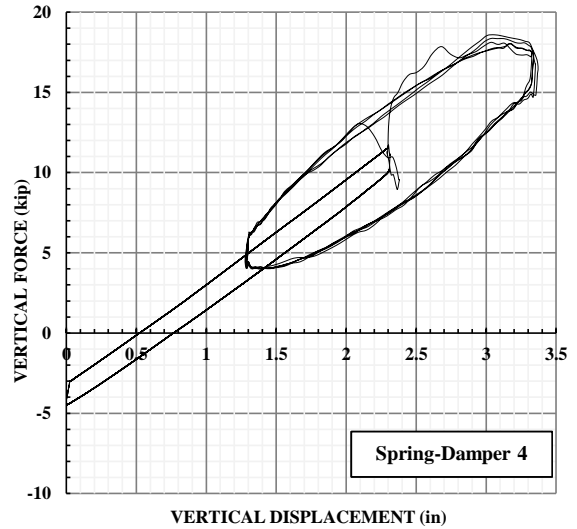
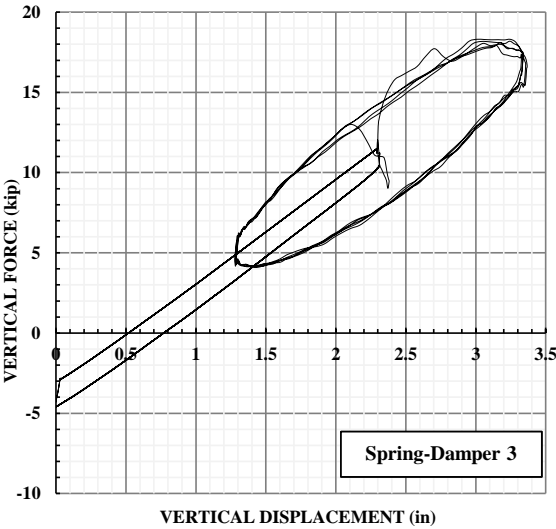
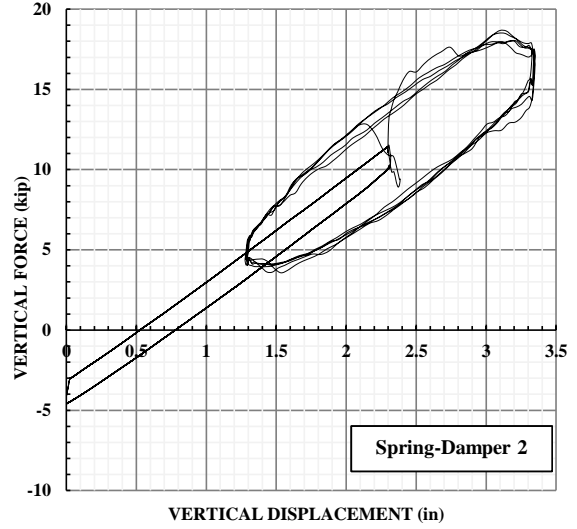
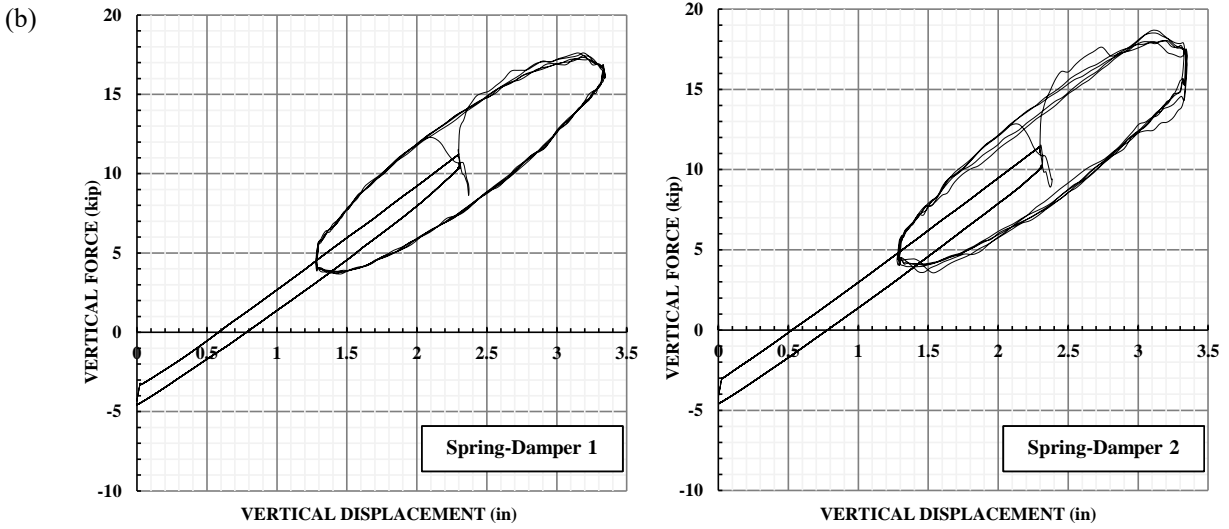
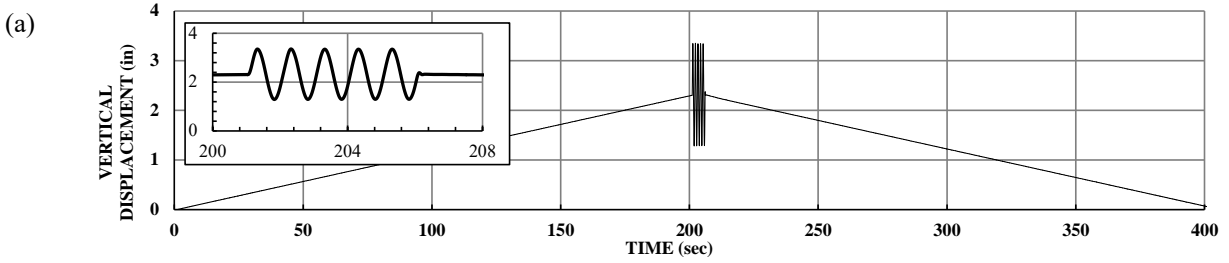


FIGURE E-3 (a) Displacement History and (b) Force-Displacement Loops of Spring-Damper Units in Test at Peak Velocity of 6.28in/sec (frequency of 1.0Hz)

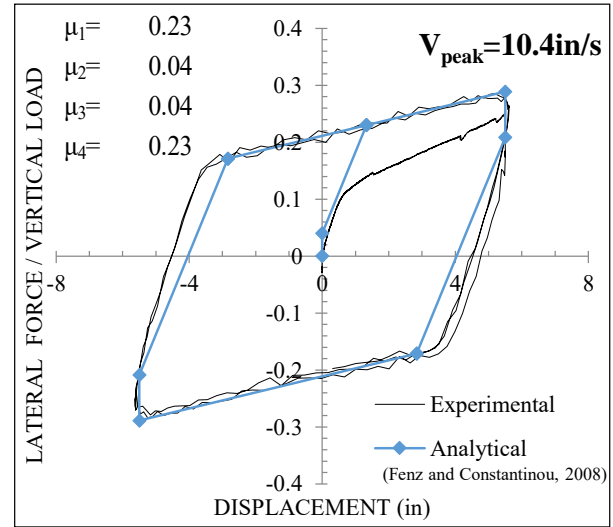
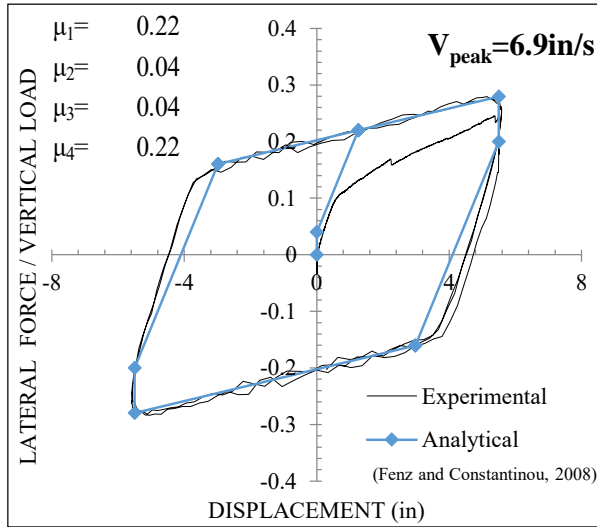
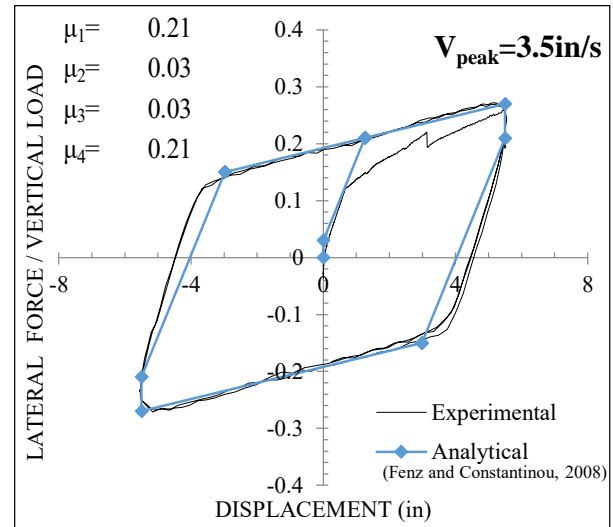
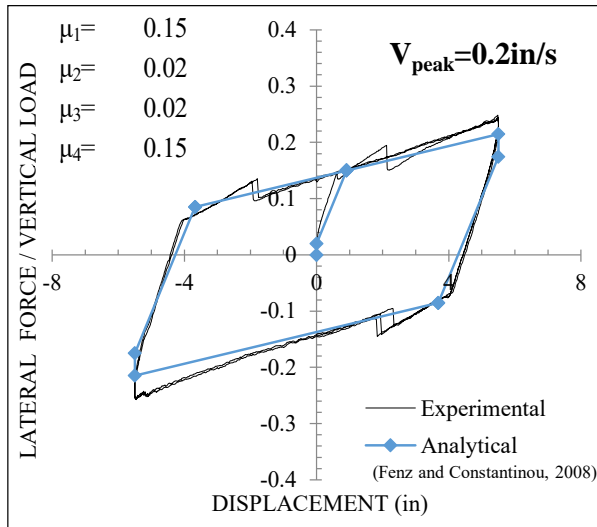


FIGURE E-4 Experimental and Analytical Normalized Force-Displacement Loops of Triple FP Isolator No.1 of Type A without Lubrication (nominal friction 0.20)

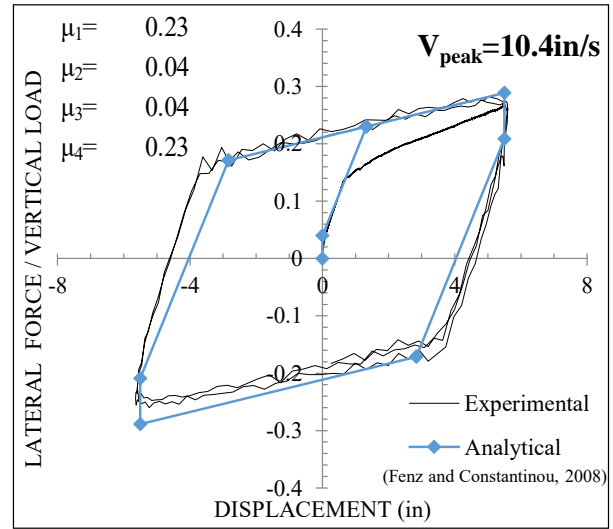
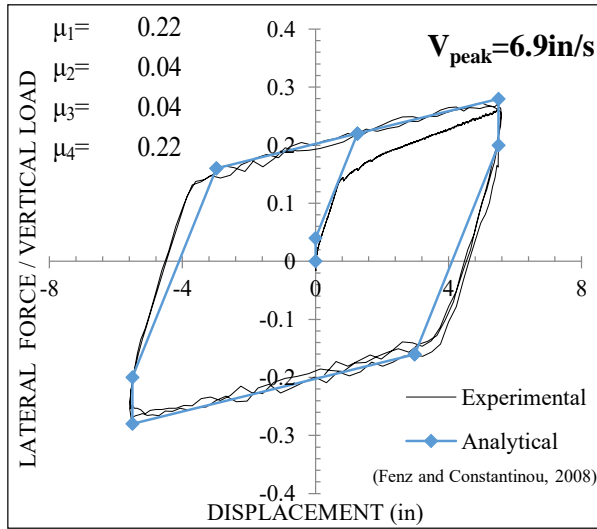
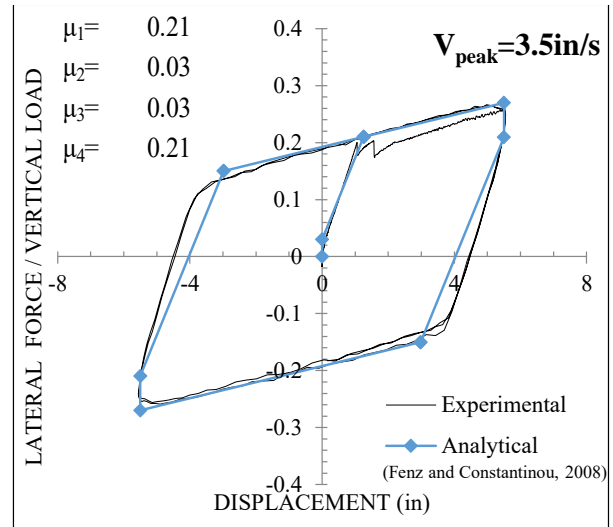
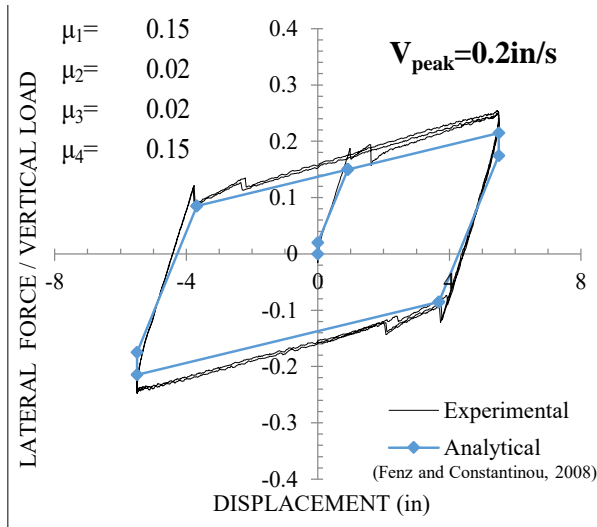


FIGURE E-5 Experimental and Analytical Normalized Force-Displacement Loops of Triple FP Isolator No.2 of Type A without Lubrication (nominal friction 0.20)

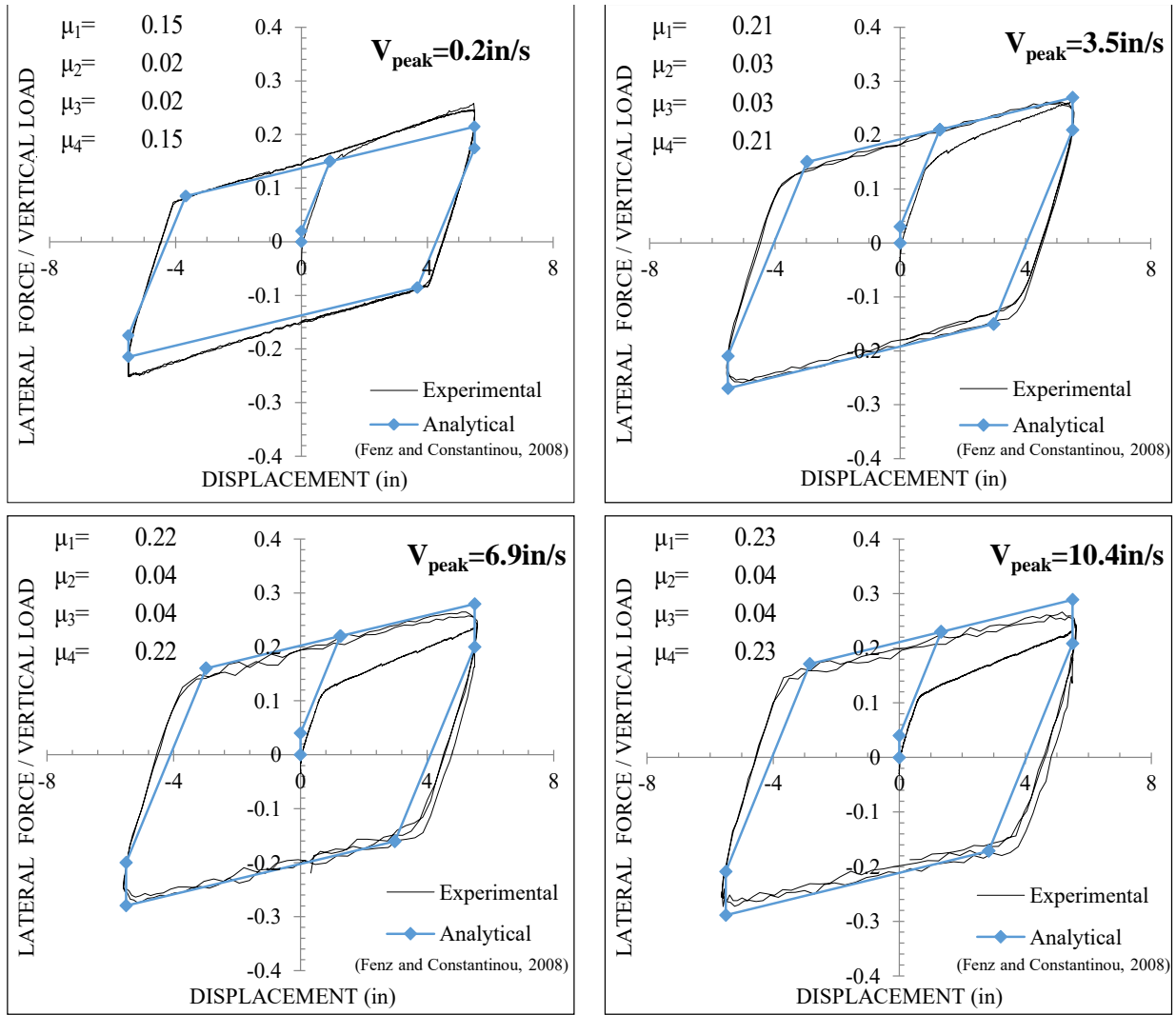


FIGURE E-6 Experimental and Analytical Normalized Force-Displacement Loops of Triple FP Isolator No.3 of Type A without Lubrication (nominal friction 0.20)

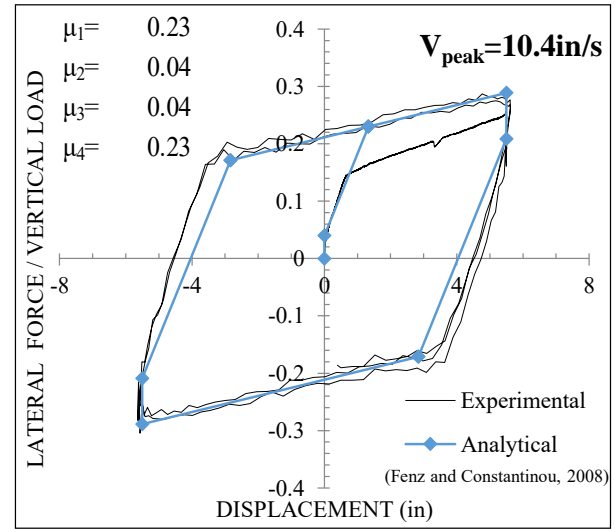
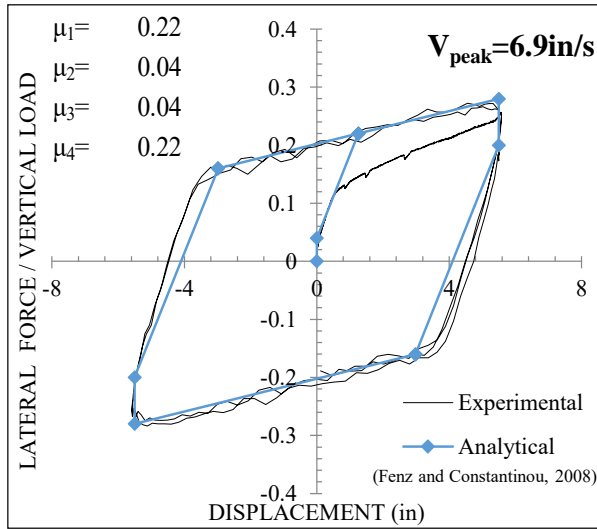
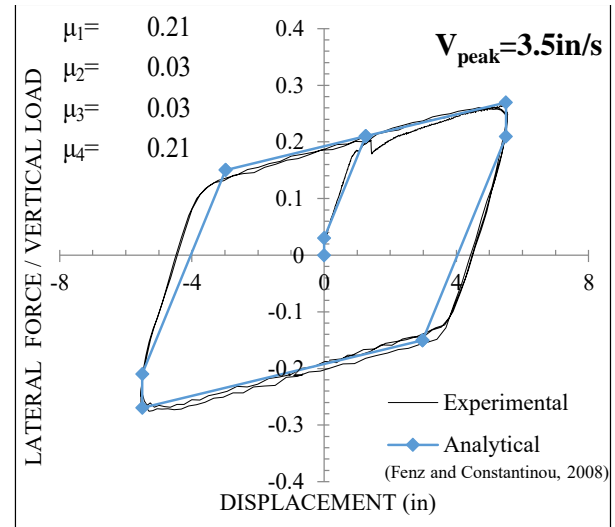
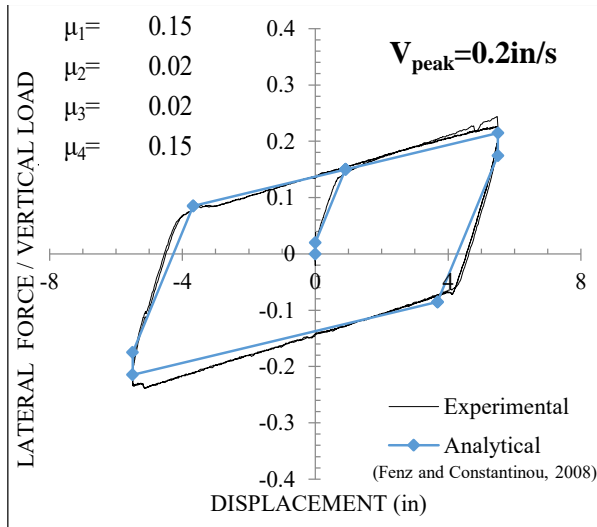


FIGURE E-7 Experimental and Analytical Normalized Force-Displacement Loops of Triple FP Isolator No.4 of Type A without Lubrication (nominal friction 0.20)

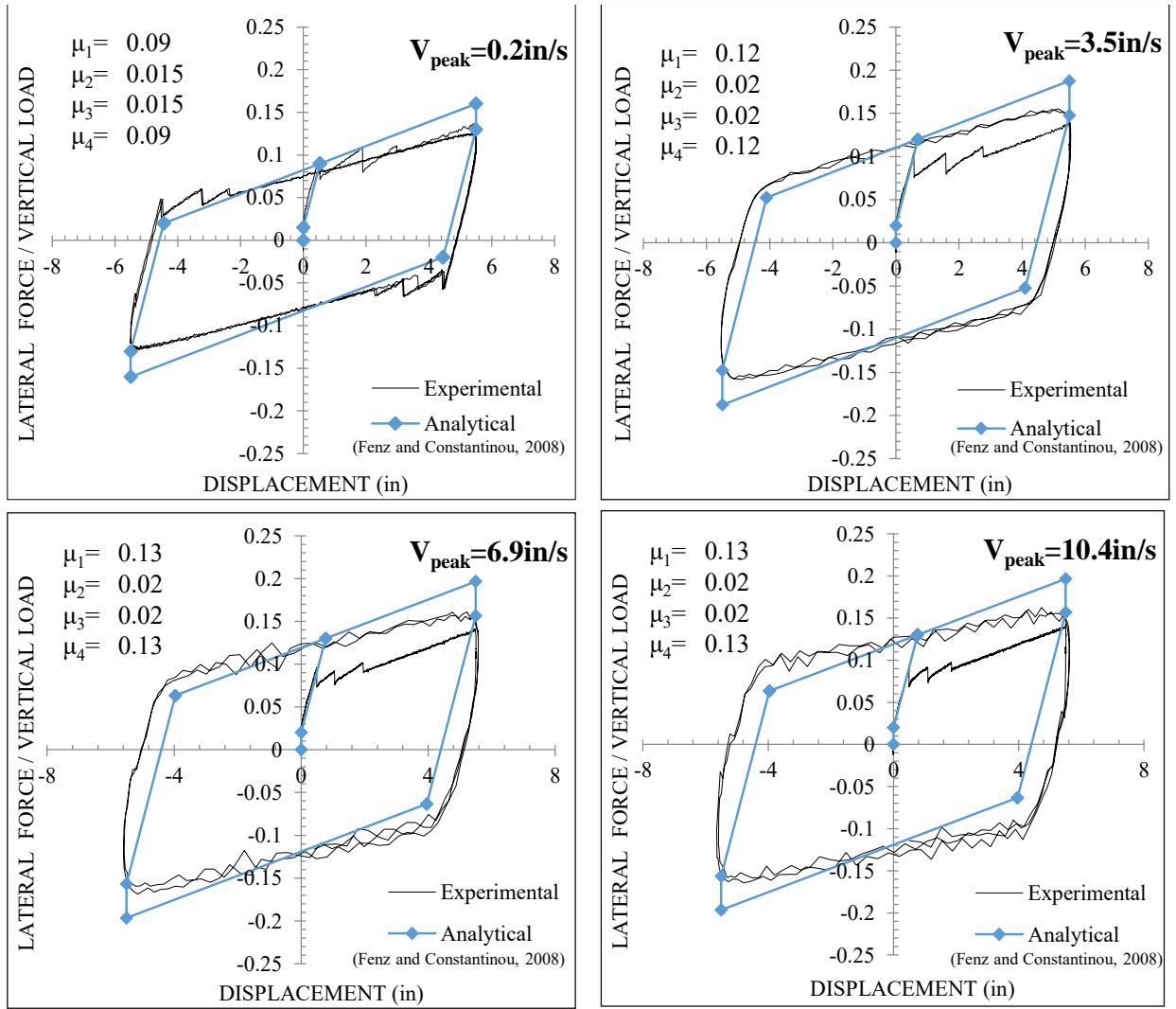


Figure E-8 Experimental and Analytical Normalized Force-Displacement Loops of Triple FP Isolator No. 2 of Type B (nominal friction 0.12)

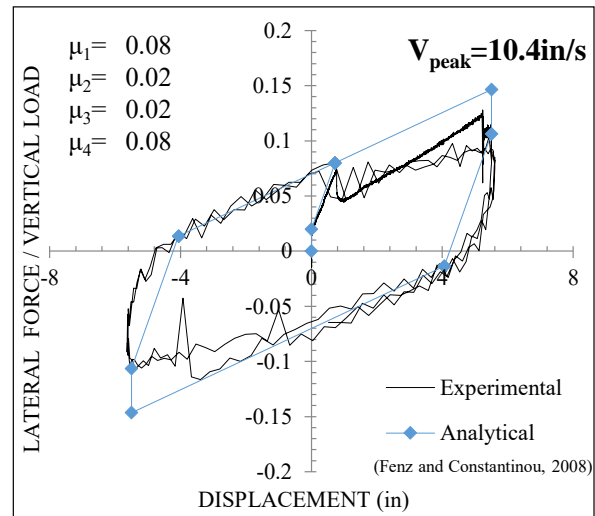
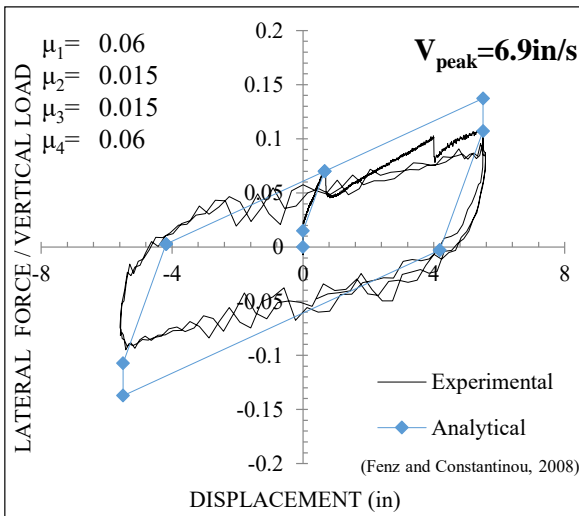
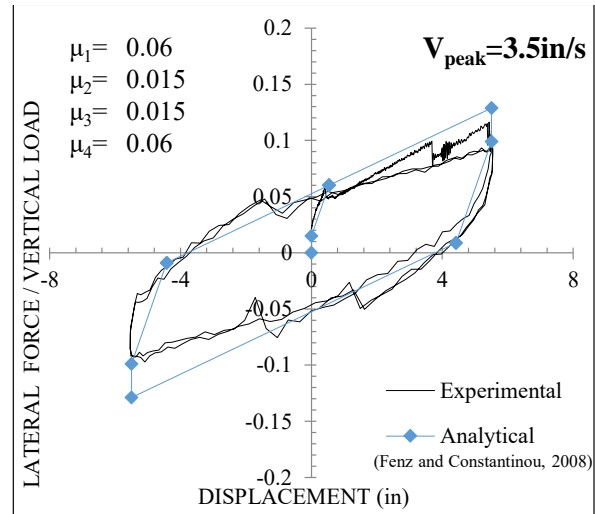
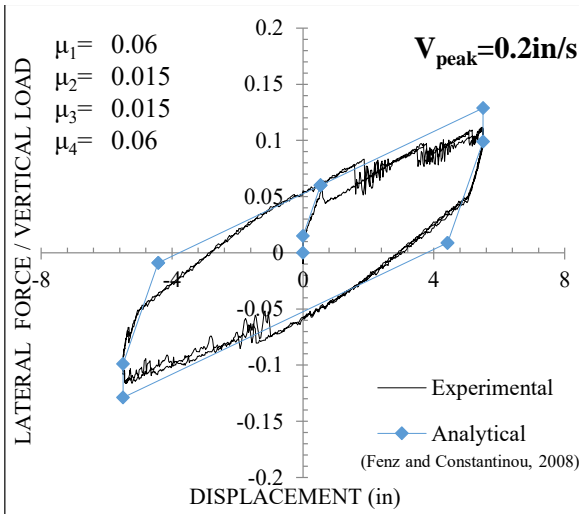


Figure E-9 Experimental and Analytical Normalized Force-Displacement Loops of Triple FP Isolator No. 2 of Type A with Lubrication (nominal friction 0.07)

MCEER Technical Reports

MCEER publishes technical reports on a variety of subjects written by authors funded through MCEER. These reports can be downloaded from the MCEER website at <http://www.buffalo.edu/mceer>. They can also be requested through NTIS, P.O. Box 1425, Springfield, Virginia 22151. NTIS accession numbers are shown in parenthesis, if available.

- NCEER-87-0001 "First-Year Program in Research, Education and Technology Transfer," 3/5/87, (PB88-134275, A04, MF-A01).
- NCEER-87-0002 "Experimental Evaluation of Instantaneous Optimal Algorithms for Structural Control," by R.C. Lin, T.T. Soong and A.M. Reinhorn, 4/20/87, (PB88-134341, A04, MF-A01).
- NCEER-87-0003 "Experimentation Using the Earthquake Simulation Facilities at University at Buffalo," by A.M. Reinhorn and R.L. Ketter, not available.
- NCEER-87-0004 "The System Characteristics and Performance of a Shaking Table," by J.S. Hwang, K.C. Chang and G.C. Lee, 6/1/87, (PB88-134259, A03, MF-A01). This report is available only through NTIS (see address given above).
- NCEER-87-0005 "A Finite Element Formulation for Nonlinear Viscoplastic Material Using a Q Model," by O. Gyebi and G. Dasgupta, 11/2/87, (PB88-213764, A08, MF-A01).
- NCEER-87-0006 "Symbolic Manipulation Program (SMP) - Algebraic Codes for Two and Three Dimensional Finite Element Formulations," by X. Lee and G. Dasgupta, 11/9/87, (PB88-218522, A05, MF-A01).
- NCEER-87-0007 "Instantaneous Optimal Control Laws for Tall Buildings Under Seismic Excitations," by J.N. Yang, A. Akbarpour and P. Ghaemmaghami, 6/10/87, (PB88-134333, A06, MF-A01). This report is only available through NTIS (see address given above).
- NCEER-87-0008 "IDARC: Inelastic Damage Analysis of Reinforced Concrete Frame - Shear-Wall Structures," by Y.J. Park, A.M. Reinhorn and S.K. Kunnath, 7/20/87, (PB88-134325, A09, MF-A01). This report is only available through NTIS (see address given above).
- NCEER-87-0009 "Liquefaction Potential for New York State: A Preliminary Report on Sites in Manhattan and Buffalo," by M. Budhu, V. Vijayakumar, R.F. Giese and L. Baumgras, 8/31/87, (PB88-163704, A03, MF-A01). This report is available only through NTIS (see address given above).
- NCEER-87-0010 "Vertical and Torsional Vibration of Foundations in Inhomogeneous Media," by A.S. Veletsos and K.W. Dotson, 6/1/87, (PB88-134291, A03, MF-A01). This report is only available through NTIS (see address given above).
- NCEER-87-0011 "Seismic Probabilistic Risk Assessment and Seismic Margins Studies for Nuclear Power Plants," by Howard H.M. Hwang, 6/15/87, (PB88-134267, A03, MF-A01). This report is only available through NTIS (see address given above).
- NCEER-87-0012 "Parametric Studies of Frequency Response of Secondary Systems Under Ground-Acceleration Excitations," by Y. Yong and Y.K. Lin, 6/10/87, (PB88-134309, A03, MF-A01). This report is only available through NTIS (see address given above).
- NCEER-87-0013 "Frequency Response of Secondary Systems Under Seismic Excitation," by J.A. HoLung, J. Cai and Y.K. Lin, 7/31/87, (PB88-134317, A05, MF-A01). This report is only available through NTIS (see address given above).
- NCEER-87-0014 "Modelling Earthquake Ground Motions in Seismically Active Regions Using Parametric Time Series Methods," by G.W. Ellis and A.S. Cakmak, 8/25/87, (PB88-134283, A08, MF-A01). This report is only available through NTIS (see address given above).
- NCEER-87-0015 "Detection and Assessment of Seismic Structural Damage," by E. DiPasquale and A.S. Cakmak, 8/25/87, (PB88-163712, A05, MF-A01). This report is only available through NTIS (see address given above).

- NCEER-87-0016 "Pipeline Experiment at Parkfield, California," by J. Isenberg and E. Richardson, 9/15/87, (PB88-163720, A03, MF-A01). This report is available only through NTIS (see address given above).
- NCEER-87-0017 "Digital Simulation of Seismic Ground Motion," by M. Shinozuka, G. Deodatis and T. Harada, 8/31/87, (PB88-155197, A04, MF-A01). This report is available only through NTIS (see address given above).
- NCEER-87-0018 "Practical Considerations for Structural Control: System Uncertainty, System Time Delay and Truncation of Small Control Forces," J.N. Yang and A. Akbarpour, 8/10/87, (PB88-163738, A08, MF-A01). This report is only available through NTIS (see address given above).
- NCEER-87-0019 "Modal Analysis of Nonclassically Damped Structural Systems Using Canonical Transformation," by J.N. Yang, S. Sarkani and F.X. Long, 9/27/87, (PB88-187851, A04, MF-A01).
- NCEER-87-0020 "A Nonstationary Solution in Random Vibration Theory," by J.R. Red-Horse and P.D. Spanos, 11/3/87, (PB88-163746, A03, MF-A01).
- NCEER-87-0021 "Horizontal Impedances for Radially Inhomogeneous Viscoelastic Soil Layers," by A.S. Veletsos and K.W. Dotson, 10/15/87, (PB88-150859, A04, MF-A01).
- NCEER-87-0022 "Seismic Damage Assessment of Reinforced Concrete Members," by Y.S. Chung, C. Meyer and M. Shinozuka, 10/9/87, (PB88-150867, A05, MF-A01). This report is available only through NTIS (see address given above).
- NCEER-87-0023 "Active Structural Control in Civil Engineering," by T.T. Soong, 11/11/87, (PB88-187778, A03, MF-A01).
- NCEER-87-0024 "Vertical and Torsional Impedances for Radially Inhomogeneous Viscoelastic Soil Layers," by K.W. Dotson and A.S. Veletsos, 12/87, (PB88-187786, A03, MF-A01).
- NCEER-87-0025 "Proceedings from the Symposium on Seismic Hazards, Ground Motions, Soil-Liquefaction and Engineering Practice in Eastern North America," October 20-22, 1987, edited by K.H. Jacob, 12/87, (PB88-188115, A23, MF-A01). This report is available only through NTIS (see address given above).
- NCEER-87-0026 "Report on the Whittier-Narrows, California, Earthquake of October 1, 1987," by J. Pantelic and A. Reinhorn, 11/87, (PB88-187752, A03, MF-A01). This report is available only through NTIS (see address given above).
- NCEER-87-0027 "Design of a Modular Program for Transient Nonlinear Analysis of Large 3-D Building Structures," by S. Srivastav and J.F. Abel, 12/30/87, (PB88-187950, A05, MF-A01). This report is only available through NTIS (see address given above).
- NCEER-87-0028 "Second-Year Program in Research, Education and Technology Transfer," 3/8/88, (PB88-219480, A04, MF-A01).
- NCEER-88-0001 "Workshop on Seismic Computer Analysis and Design of Buildings With Interactive Graphics," by W. McGuire, J.F. Abel and C.H. Conley, 1/18/88, (PB88-187760, A03, MF-A01). This report is only available through NTIS (see address given above).
- NCEER-88-0002 "Optimal Control of Nonlinear Flexible Structures," by J.N. Yang, F.X. Long and D. Wong, 1/22/88, (PB88-213772, A06, MF-A01).
- NCEER-88-0003 "Substructuring Techniques in the Time Domain for Primary-Secondary Structural Systems," by G.D. Manolis and G. Juhn, 2/10/88, (PB88-213780, A04, MF-A01).
- NCEER-88-0004 "Iterative Seismic Analysis of Primary-Secondary Systems," by A. Singhal, L.D. Lutes and P.D. Spanos, 2/23/88, (PB88-213798, A04, MF-A01).
- NCEER-88-0005 "Stochastic Finite Element Expansion for Random Media," by P.D. Spanos and R. Ghanem, 3/14/88, (PB88-213806, A03, MF-A01).
- NCEER-88-0006 "Combining Structural Optimization and Structural Control," by F.Y. Cheng and C.P. Pantelides, 1/10/88, (PB88-213814, A05, MF-A01).

- NCEER-88-0007 "Seismic Performance Assessment of Code-Designed Structures," by H.H-M. Hwang, J-W. Jaw and H-J. Shau, 3/20/88, (PB88-219423, A04, MF-A01). This report is only available through NTIS (see address given above).
- NCEER-88-0008 "Reliability Analysis of Code-Designed Structures Under Natural Hazards," by H.H-M. Hwang, H. Ushiba and M. Shinozuka, 2/29/88, (PB88-229471, A07, MF-A01). This report is only available through NTIS (see address given above).
- NCEER-88-0009 "Seismic Fragility Analysis of Shear Wall Structures," by J-W Jaw and H.H-M. Hwang, 4/30/88, (PB89-102867, A04, MF-A01).
- NCEER-88-0010 "Base Isolation of a Multi-Story Building Under a Harmonic Ground Motion - A Comparison of Performances of Various Systems," by F-G Fan, G. Ahmadi and I.G. Tadjbakhsh, 5/18/88, (PB89-122238, A06, MF-A01). This report is only available through NTIS (see address given above).
- NCEER-88-0011 "Seismic Floor Response Spectra for a Combined System by Green's Functions," by F.M. Lavelle, L.A. Bergman and P.D. Spanos, 5/1/88, (PB89-102875, A03, MF-A01).
- NCEER-88-0012 "A New Solution Technique for Randomly Excited Hysteretic Structures," by G.Q. Cai and Y.K. Lin, 5/16/88, (PB89-102883, A03, MF-A01).
- NCEER-88-0013 "A Study of Radiation Damping and Soil-Structure Interaction Effects in the Centrifuge," by K. Weissman, supervised by J.H. Prevost, 5/24/88, (PB89-144703, A06, MF-A01).
- NCEER-88-0014 "Parameter Identification and Implementation of a Kinematic Plasticity Model for Frictional Soils," by J.H. Prevost and D.V. Griffiths, not available.
- NCEER-88-0015 "Two- and Three- Dimensional Dynamic Finite Element Analyses of the Long Valley Dam," by D.V. Griffiths and J.H. Prevost, 6/17/88, (PB89-144711, A04, MF-A01).
- NCEER-88-0016 "Damage Assessment of Reinforced Concrete Structures in Eastern United States," by A.M. Reinhorn, M.J. Seidel, S.K. Kunnath and Y.J. Park, 6/15/88, (PB89-122220, A04, MF-A01). This report is only available through NTIS (see address given above).
- NCEER-88-0017 "Dynamic Compliance of Vertically Loaded Strip Foundations in Multilayered Viscoelastic Soils," by S. Ahmad and A.S.M. Israil, 6/17/88, (PB89-102891, A04, MF-A01).
- NCEER-88-0018 "An Experimental Study of Seismic Structural Response With Added Viscoelastic Dampers," by R.C. Lin, Z. Liang, T.T. Soong and R.H. Zhang, 6/30/88, (PB89-122212, A05, MF-A01). This report is available only through NTIS (see address given above).
- NCEER-88-0019 "Experimental Investigation of Primary - Secondary System Interaction," by G.D. Manolis, G. Juhn and A.M. Reinhorn, 5/27/88, (PB89-122204, A04, MF-A01).
- NCEER-88-0020 "A Response Spectrum Approach For Analysis of Nonclassically Damped Structures," by J.N. Yang, S. Sarkani and F.X. Long, 4/22/88, (PB89-102909, A04, MF-A01).
- NCEER-88-0021 "Seismic Interaction of Structures and Soils: Stochastic Approach," by A.S. Veletsos and A.M. Prasad, 7/21/88, (PB89-122196, A04, MF-A01). This report is only available through NTIS (see address given above).
- NCEER-88-0022 "Identification of the Serviceability Limit State and Detection of Seismic Structural Damage," by E. DiPasquale and A.S. Cakmak, 6/15/88, (PB89-122188, A05, MF-A01). This report is available only through NTIS (see address given above).
- NCEER-88-0023 "Multi-Hazard Risk Analysis: Case of a Simple Offshore Structure," by B.K. Bhartia and E.H. Vanmarcke, 7/21/88, (PB89-145213, A05, MF-A01).

- NCEER-88-0024 "Automated Seismic Design of Reinforced Concrete Buildings," by Y.S. Chung, C. Meyer and M. Shinozuka, 7/5/88, (PB89-122170, A06, MF-A01). This report is available only through NTIS (see address given above).
- NCEER-88-0025 "Experimental Study of Active Control of MDOF Structures Under Seismic Excitations," by L.L. Chung, R.C. Lin, T.T. Soong and A.M. Reinhorn, 7/10/88, (PB89-122600, A04, MF-A01).
- NCEER-88-0026 "Earthquake Simulation Tests of a Low-Rise Metal Structure," by J.S. Hwang, K.C. Chang, G.C. Lee and R.L. Ketter, 8/1/88, (PB89-102917, A04, MF-A01).
- NCEER-88-0027 "Systems Study of Urban Response and Reconstruction Due to Catastrophic Earthquakes," by F. Kozin and H.K. Zhou, 9/22/88, (PB90-162348, A04, MF-A01).
- NCEER-88-0028 "Seismic Fragility Analysis of Plane Frame Structures," by H.H-M. Hwang and Y.K. Low, 7/31/88, (PB89-131445, A06, MF-A01).
- NCEER-88-0029 "Response Analysis of Stochastic Structures," by A. Kardara, C. Bucher and M. Shinozuka, 9/22/88, (PB89-174429, A04, MF-A01).
- NCEER-88-0030 "Nonnormal Accelerations Due to Yielding in a Primary Structure," by D.C.K. Chen and L.D. Lutes, 9/19/88, (PB89-131437, A04, MF-A01).
- NCEER-88-0031 "Design Approaches for Soil-Structure Interaction," by A.S. Veletsos, A.M. Prasad and Y. Tang, 12/30/88, (PB89-174437, A03, MF-A01). This report is available only through NTIS (see address given above).
- NCEER-88-0032 "A Re-evaluation of Design Spectra for Seismic Damage Control," by C.J. Turkstra and A.G. Tallin, 11/7/88, (PB89-145221, A05, MF-A01).
- NCEER-88-0033 "The Behavior and Design of Noncontact Lap Splices Subjected to Repeated Inelastic Tensile Loading," by V.E. Sagan, P. Gergely and R.N. White, 12/8/88, (PB89-163737, A08, MF-A01).
- NCEER-88-0034 "Seismic Response of Pile Foundations," by S.M. Mamoon, P.K. Banerjee and S. Ahmad, 11/1/88, (PB89-145239, A04, MF-A01).
- NCEER-88-0035 "Modeling of R/C Building Structures With Flexible Floor Diaphragms (IDARC2)," by A.M. Reinhorn, S.K. Kunnath and N. Panahshahi, 9/7/88, (PB89-207153, A07, MF-A01).
- NCEER-88-0036 "Solution of the Dam-Reservoir Interaction Problem Using a Combination of FEM, BEM with Particular Integrals, Modal Analysis, and Substructuring," by C-S. Tsai, G.C. Lee and R.L. Ketter, 12/31/88, (PB89-207146, A04, MF-A01).
- NCEER-88-0037 "Optimal Placement of Actuators for Structural Control," by F.Y. Cheng and C.P. Pantelides, 8/15/88, (PB89-162846, A05, MF-A01).
- NCEER-88-0038 "Teflon Bearings in Aseismic Base Isolation: Experimental Studies and Mathematical Modeling," by A. Mokha, M.C. Constantinou and A.M. Reinhorn, 12/5/88, (PB89-218457, A10, MF-A01). This report is available only through NTIS (see address given above).
- NCEER-88-0039 "Seismic Behavior of Flat Slab High-Rise Buildings in the New York City Area," by P. Weidlinger and M. Ettouney, 10/15/88, (PB90-145681, A04, MF-A01).
- NCEER-88-0040 "Evaluation of the Earthquake Resistance of Existing Buildings in New York City," by P. Weidlinger and M. Ettouney, 10/15/88, not available.
- NCEER-88-0041 "Small-Scale Modeling Techniques for Reinforced Concrete Structures Subjected to Seismic Loads," by W. Kim, A. El-Attar and R.N. White, 11/22/88, (PB89-189625, A05, MF-A01).
- NCEER-88-0042 "Modeling Strong Ground Motion from Multiple Event Earthquakes," by G.W. Ellis and A.S. Cakmak, 10/15/88, (PB89-174445, A03, MF-A01).

- NCEER-88-0043 "Nonstationary Models of Seismic Ground Acceleration," by M. Grigoriu, S.E. Ruiz and E. Rosenblueth, 7/15/88, (PB89-189617, A04, MF-A01).
- NCEER-88-0044 "SARCF User's Guide: Seismic Analysis of Reinforced Concrete Frames," by Y.S. Chung, C. Meyer and M. Shinozuka, 11/9/88, (PB89-174452, A08, MF-A01).
- NCEER-88-0045 "First Expert Panel Meeting on Disaster Research and Planning," edited by J. Pantelic and J. Stoyke, 9/15/88, (PB89-174460, A05, MF-A01).
- NCEER-88-0046 "Preliminary Studies of the Effect of Degrading Infill Walls on the Nonlinear Seismic Response of Steel Frames," by C.Z. Chrysostomou, P. Gergely and J.F. Abel, 12/19/88, (PB89-208383, A05, MF-A01).
- NCEER-88-0047 "Reinforced Concrete Frame Component Testing Facility - Design, Construction, Instrumentation and Operation," by S.P. Pessiki, C. Conley, T. Bond, P. Gergely and R.N. White, 12/16/88, (PB89-174478, A04, MF-A01).
- NCEER-89-0001 "Effects of Protective Cushion and Soil Compliancy on the Response of Equipment Within a Seismically Excited Building," by J.A. HoLung, 2/16/89, (PB89-207179, A04, MF-A01).
- NCEER-89-0002 "Statistical Evaluation of Response Modification Factors for Reinforced Concrete Structures," by H.H-M. Hwang and J-W. Jaw, 2/17/89, (PB89-207187, A05, MF-A01).
- NCEER-89-0003 "Hysteretic Columns Under Random Excitation," by G-Q. Cai and Y.K. Lin, 1/9/89, (PB89-196513, A03, MF-A01).
- NCEER-89-0004 "Experimental Study of 'Elephant Foot Bulge' Instability of Thin-Walled Metal Tanks," by Z-H. Jia and R.L. Ketter, 2/22/89, (PB89-207195, A03, MF-A01).
- NCEER-89-0005 "Experiment on Performance of Buried Pipelines Across San Andreas Fault," by J. Isenberg, E. Richardson and T.D. O'Rourke, 3/10/89, (PB89-218440, A04, MF-A01). This report is available only through NTIS (see address given above).
- NCEER-89-0006 "A Knowledge-Based Approach to Structural Design of Earthquake-Resistant Buildings," by M. Subramani, P. Gergely, C.H. Conley, J.F. Abel and A.H. Zaghaw, 1/15/89, (PB89-218465, A06, MF-A01).
- NCEER-89-0007 "Liquefaction Hazards and Their Effects on Buried Pipelines," by T.D. O'Rourke and P.A. Lane, 2/1/89, (PB89-218481, A09, MF-A01).
- NCEER-89-0008 "Fundamentals of System Identification in Structural Dynamics," by H. Imai, C-B. Yun, O. Maruyama and M. Shinozuka, 1/26/89, (PB89-207211, A04, MF-A01).
- NCEER-89-0009 "Effects of the 1985 Michoacan Earthquake on Water Systems and Other Buried Lifelines in Mexico," by A.G. Ayala and M.J. O'Rourke, 3/8/89, (PB89-207229, A06, MF-A01).
- NCEER-89-R010 "NCEER Bibliography of Earthquake Education Materials," by K.E.K. Ross, Second Revision, 9/1/89, (PB90-125352, A05, MF-A01). This report is replaced by NCEER-92-0018.
- NCEER-89-0011 "Inelastic Three-Dimensional Response Analysis of Reinforced Concrete Building Structures (IDARC-3D), Part I - Modeling," by S.K. Kunnath and A.M. Reinhorn, 4/17/89, (PB90-114612, A07, MF-A01). This report is available only through NTIS (see address given above).
- NCEER-89-0012 "Recommended Modifications to ATC-14," by C.D. Poland and J.O. Malley, 4/12/89, (PB90-108648, A15, MF-A01).
- NCEER-89-0013 "Repair and Strengthening of Beam-to-Column Connections Subjected to Earthquake Loading," by M. Corazao and A.J. Durrani, 2/28/89, (PB90-109885, A06, MF-A01).
- NCEER-89-0014 "Program EXKAL2 for Identification of Structural Dynamic Systems," by O. Maruyama, C-B. Yun, M. Hoshiya and M. Shinozuka, 5/19/89, (PB90-109877, A09, MF-A01).

- NCEER-89-0015 "Response of Frames With Bolted Semi-Rigid Connections, Part I - Experimental Study and Analytical Predictions," by P.J. DiCorso, A.M. Reinhorn, J.R. Dickerson, J.B. Radzimirski and W.L. Harper, 6/1/89, not available.
- NCEER-89-0016 "ARMA Monte Carlo Simulation in Probabilistic Structural Analysis," by P.D. Spanos and M.P. Mignolet, 7/10/89, (PB90-109893, A03, MF-A01).
- NCEER-89-P017 "Preliminary Proceedings from the Conference on Disaster Preparedness - The Place of Earthquake Education in Our Schools," Edited by K.E.K. Ross, 6/23/89, (PB90-108606, A03, MF-A01).
- NCEER-89-0017 "Proceedings from the Conference on Disaster Preparedness - The Place of Earthquake Education in Our Schools," Edited by K.E.K. Ross, 12/31/89, (PB90-207895, A012, MF-A02). This report is available only through NTIS (see address given above).
- NCEER-89-0018 "Multidimensional Models of Hysteretic Material Behavior for Vibration Analysis of Shape Memory Energy Absorbing Devices, by E.J. Graesser and F.A. Cozzarelli, 6/7/89, (PB90-164146, A04, MF-A01).
- NCEER-89-0019 "Nonlinear Dynamic Analysis of Three-Dimensional Base Isolated Structures (3D-BASIS)," by S. Nagarajaiah, A.M. Reinhorn and M.C. Constantinou, 8/3/89, (PB90-161936, A06, MF-A01). This report has been replaced by NCEER-93-0011.
- NCEER-89-0020 "Structural Control Considering Time-Rate of Control Forces and Control Rate Constraints," by F.Y. Cheng and C.P. Pantelides, 8/3/89, (PB90-120445, A04, MF-A01).
- NCEER-89-0021 "Subsurface Conditions of Memphis and Shelby County," by K.W. Ng, T-S. Chang and H-H.M. Hwang, 7/26/89, (PB90-120437, A03, MF-A01).
- NCEER-89-0022 "Seismic Wave Propagation Effects on Straight Jointed Buried Pipelines," by K. Elhmadi and M.J. O'Rourke, 8/24/89, (PB90-162322, A10, MF-A02).
- NCEER-89-0023 "Workshop on Serviceability Analysis of Water Delivery Systems," edited by M. Grigoriu, 3/6/89, (PB90-127424, A03, MF-A01).
- NCEER-89-0024 "Shaking Table Study of a 1/5 Scale Steel Frame Composed of Tapered Members," by K.C. Chang, J.S. Hwang and G.C. Lee, 9/18/89, (PB90-160169, A04, MF-A01).
- NCEER-89-0025 "DYNA1D: A Computer Program for Nonlinear Seismic Site Response Analysis - Technical Documentation," by Jean H. Prevost, 9/14/89, (PB90-161944, A07, MF-A01). This report is available only through NTIS (see address given above).
- NCEER-89-0026 "1:4 Scale Model Studies of Active Tendon Systems and Active Mass Dampers for Aseismic Protection," by A.M. Reinhorn, T.T. Soong, R.C. Lin, Y.P. Yang, Y. Fukao, H. Abe and M. Nakai, 9/15/89, (PB90-173246, A10, MF-A02). This report is available only through NTIS (see address given above).
- NCEER-89-0027 "Scattering of Waves by Inclusions in a Nonhomogeneous Elastic Half Space Solved by Boundary Element Methods," by P.K. Hadley, A. Askar and A.S. Cakmak, 6/15/89, (PB90-145699, A07, MF-A01).
- NCEER-89-0028 "Statistical Evaluation of Deflection Amplification Factors for Reinforced Concrete Structures," by H.H.M. Hwang, J-W. Jaw and A.L. Ch'ng, 8/31/89, (PB90-164633, A05, MF-A01).
- NCEER-89-0029 "Bedrock Accelerations in Memphis Area Due to Large New Madrid Earthquakes," by H.H.M. Hwang, C.H.S. Chen and G. Yu, 11/7/89, (PB90-162330, A04, MF-A01).
- NCEER-89-0030 "Seismic Behavior and Response Sensitivity of Secondary Structural Systems," by Y.Q. Chen and T.T. Soong, 10/23/89, (PB90-164658, A08, MF-A01).
- NCEER-89-0031 "Random Vibration and Reliability Analysis of Primary-Secondary Structural Systems," by Y. Ibrahim, M. Grigoriu and T.T. Soong, 11/10/89, (PB90-161951, A04, MF-A01).

- NCEER-89-0032 "Proceedings from the Second U.S. - Japan Workshop on Liquefaction, Large Ground Deformation and Their Effects on Lifelines, September 26-29, 1989," Edited by T.D. O'Rourke and M. Hamada, 12/1/89, (PB90-209388, A22, MF-A03).
- NCEER-89-0033 "Deterministic Model for Seismic Damage Evaluation of Reinforced Concrete Structures," by J.M. Bracci, A.M. Reinhorn, J.B. Mander and S.K. Kunnath, 9/27/89, (PB91-108803, A06, MF-A01).
- NCEER-89-0034 "On the Relation Between Local and Global Damage Indices," by E. DiPasquale and A.S. Cakmak, 8/15/89, (PB90-173865, A05, MF-A01).
- NCEER-89-0035 "Cyclic Undrained Behavior of Nonplastic and Low Plasticity Silts," by A.J. Walker and H.E. Stewart, 7/26/89, (PB90-183518, A10, MF-A01).
- NCEER-89-0036 "Liquefaction Potential of Surficial Deposits in the City of Buffalo, New York," by M. Budhu, R. Giese and L. Baumgrass, 1/17/89, (PB90-208455, A04, MF-A01).
- NCEER-89-0037 "A Deterministic Assessment of Effects of Ground Motion Incoherence," by A.S. Veletsos and Y. Tang, 7/15/89, (PB90-164294, A03, MF-A01).
- NCEER-89-0038 "Workshop on Ground Motion Parameters for Seismic Hazard Mapping," July 17-18, 1989, edited by R.V. Whitman, 12/1/89, (PB90-173923, A04, MF-A01).
- NCEER-89-0039 "Seismic Effects on Elevated Transit Lines of the New York City Transit Authority," by C.J. Costantino, C.A. Miller and E. Heymsfield, 12/26/89, (PB90-207887, A06, MF-A01).
- NCEER-89-0040 "Centrifugal Modeling of Dynamic Soil-Structure Interaction," by K. Weissman, Supervised by J.H. Prevost, 5/10/89, (PB90-207879, A07, MF-A01).
- NCEER-89-0041 "Linearized Identification of Buildings With Cores for Seismic Vulnerability Assessment," by I-K. Ho and A.E. Aktan, 11/1/89, (PB90-251943, A07, MF-A01).
- NCEER-90-0001 "Geotechnical and Lifeline Aspects of the October 17, 1989 Loma Prieta Earthquake in San Francisco," by T.D. O'Rourke, H.E. Stewart, F.T. Blackburn and T.S. Dickerman, 1/90, (PB90-208596, A05, MF-A01).
- NCEER-90-0002 "Nonnormal Secondary Response Due to Yielding in a Primary Structure," by D.C.K. Chen and L.D. Lutes, 2/28/90, (PB90-251976, A07, MF-A01).
- NCEER-90-0003 "Earthquake Education Materials for Grades K-12," by K.E.K. Ross, 4/16/90, (PB91-251984, A05, MF-A05). This report has been replaced by NCEER-92-0018.
- NCEER-90-0004 "Catalog of Strong Motion Stations in Eastern North America," by R.W. Busby, 4/3/90, (PB90-251984, A05, MF-A01).
- NCEER-90-0005 "NCEER Strong-Motion Data Base: A User Manual for the GeoBase Release (Version 1.0 for the Sun3)," by P. Friberg and K. Jacob, 3/31/90 (PB90-258062, A04, MF-A01).
- NCEER-90-0006 "Seismic Hazard Along a Crude Oil Pipeline in the Event of an 1811-1812 Type New Madrid Earthquake," by H.H.M. Hwang and C-H.S. Chen, 4/16/90, (PB90-258054, A04, MF-A01).
- NCEER-90-0007 "Site-Specific Response Spectra for Memphis Sheahan Pumping Station," by H.H.M. Hwang and C.S. Lee, 5/15/90, (PB91-108811, A05, MF-A01).
- NCEER-90-0008 "Pilot Study on Seismic Vulnerability of Crude Oil Transmission Systems," by T. Ariman, R. Dobry, M. Grigoriu, F. Kozin, M. O'Rourke, T. O'Rourke and M. Shinozuka, 5/25/90, (PB91-108837, A06, MF-A01).
- NCEER-90-0009 "A Program to Generate Site Dependent Time Histories: EQGEN," by G.W. Ellis, M. Srinivasan and A.S. Cakmak, 1/30/90, (PB91-108829, A04, MF-A01).
- NCEER-90-0010 "Active Isolation for Seismic Protection of Operating Rooms," by M.E. Talbott, Supervised by M. Shinozuka, 6/8/9, (PB91-110205, A05, MF-A01).

- NCEER-90-0011 "Program LINEARID for Identification of Linear Structural Dynamic Systems," by C-B. Yun and M. Shinozuka, 6/25/90, (PB91-110312, A08, MF-A01).
- NCEER-90-0012 "Two-Dimensional Two-Phase Elasto-Plastic Seismic Response of Earth Dams," by A.N. Yiagos, Supervised by J.H. Prevost, 6/20/90, (PB91-110197, A13, MF-A02).
- NCEER-90-0013 "Secondary Systems in Base-Isolated Structures: Experimental Investigation, Stochastic Response and Stochastic Sensitivity," by G.D. Manolis, G. Juhn, M.C. Constantinou and A.M. Reinhorn, 7/1/90, (PB91-110320, A08, MF-A01).
- NCEER-90-0014 "Seismic Behavior of Lightly-Reinforced Concrete Column and Beam-Column Joint Details," by S.P. Pessiki, C.H. Conley, P. Gergely and R.N. White, 8/22/90, (PB91-108795, A11, MF-A02).
- NCEER-90-0015 "Two Hybrid Control Systems for Building Structures Under Strong Earthquakes," by J.N. Yang and A. Daniellians, 6/29/90, (PB91-125393, A04, MF-A01).
- NCEER-90-0016 "Instantaneous Optimal Control with Acceleration and Velocity Feedback," by J.N. Yang and Z. Li, 6/29/90, (PB91-125401, A03, MF-A01).
- NCEER-90-0017 "Reconnaissance Report on the Northern Iran Earthquake of June 21, 1990," by M. Mehrain, 10/4/90, (PB91-125377, A03, MF-A01).
- NCEER-90-0018 "Evaluation of Liquefaction Potential in Memphis and Shelby County," by T.S. Chang, P.S. Tang, C.S. Lee and H. Hwang, 8/10/90, (PB91-125427, A09, MF-A01).
- NCEER-90-0019 "Experimental and Analytical Study of a Combined Sliding Disc Bearing and Helical Steel Spring Isolation System," by M.C. Constantinou, A.S. Mokha and A.M. Reinhorn, 10/4/90, (PB91-125385, A06, MF-A01). This report is available only through NTIS (see address given above).
- NCEER-90-0020 "Experimental Study and Analytical Prediction of Earthquake Response of a Sliding Isolation System with a Spherical Surface," by A.S. Mokha, M.C. Constantinou and A.M. Reinhorn, 10/11/90, (PB91-125419, A05, MF-A01).
- NCEER-90-0021 "Dynamic Interaction Factors for Floating Pile Groups," by G. Gazetas, K. Fan, A. Kaynia and E. Kausel, 9/10/90, (PB91-170381, A05, MF-A01).
- NCEER-90-0022 "Evaluation of Seismic Damage Indices for Reinforced Concrete Structures," by S. Rodriguez-Gomez and A.S. Cakmak, 9/30/90, PB91-171322, A06, MF-A01).
- NCEER-90-0023 "Study of Site Response at a Selected Memphis Site," by H. Desai, S. Ahmad, E.S. Gazetas and M.R. Oh, 10/11/90, (PB91-196857, A03, MF-A01).
- NCEER-90-0024 "A User's Guide to Strongmo: Version 1.0 of NCEER's Strong-Motion Data Access Tool for PCs and Terminals," by P.A. Friberg and C.A.T. Susch, 11/15/90, (PB91-171272, A03, MF-A01).
- NCEER-90-0025 "A Three-Dimensional Analytical Study of Spatial Variability of Seismic Ground Motions," by L-L. Hong and A.H.-S. Ang, 10/30/90, (PB91-170399, A09, MF-A01).
- NCEER-90-0026 "MUMOID User's Guide - A Program for the Identification of Modal Parameters," by S. Rodriguez-Gomez and E. DiPasquale, 9/30/90, (PB91-171298, A04, MF-A01).
- NCEER-90-0027 "SARCF-II User's Guide - Seismic Analysis of Reinforced Concrete Frames," by S. Rodriguez-Gomez, Y.S. Chung and C. Meyer, 9/30/90, (PB91-171280, A05, MF-A01).
- NCEER-90-0028 "Viscous Dampers: Testing, Modeling and Application in Vibration and Seismic Isolation," by N. Makris and M.C. Constantinou, 12/20/90 (PB91-190561, A06, MF-A01).
- NCEER-90-0029 "Soil Effects on Earthquake Ground Motions in the Memphis Area," by H. Hwang, C.S. Lee, K.W. Ng and T.S. Chang, 8/2/90, (PB91-190751, A05, MF-A01).

- NCEER-91-0001 "Proceedings from the Third Japan-U.S. Workshop on Earthquake Resistant Design of Lifeline Facilities and Countermeasures for Soil Liquefaction, December 17-19, 1990," edited by T.D. O'Rourke and M. Hamada, 2/1/91, (PB91-179259, A99, MF-A04).
- NCEER-91-0002 "Physical Space Solutions of Non-Proportionally Damped Systems," by M. Tong, Z. Liang and G.C. Lee, 1/15/91, (PB91-179242, A04, MF-A01).
- NCEER-91-0003 "Seismic Response of Single Piles and Pile Groups," by K. Fan and G. Gazetas, 1/10/91, (PB92-174994, A04, MF-A01).
- NCEER-91-0004 "Damping of Structures: Part 1 - Theory of Complex Damping," by Z. Liang and G. Lee, 10/10/91, (PB92-197235, A12, MF-A03).
- NCEER-91-0005 "3D-BASIS - Nonlinear Dynamic Analysis of Three Dimensional Base Isolated Structures: Part II," by S. Nagarajaiah, A.M. Reinhorn and M.C. Constantinou, 2/28/91, (PB91-190553, A07, MF-A01). This report has been replaced by NCEER-93-0011.
- NCEER-91-0006 "A Multidimensional Hysteretic Model for Plasticity Deforming Metals in Energy Absorbing Devices," by E.J. Graesser and F.A. Cozzarelli, 4/9/91, (PB92-108364, A04, MF-A01).
- NCEER-91-0007 "A Framework for Customizable Knowledge-Based Expert Systems with an Application to a KBES for Evaluating the Seismic Resistance of Existing Buildings," by E.G. Ibarra-Anaya and S.J. Fennes, 4/9/91, (PB91-210930, A08, MF-A01).
- NCEER-91-0008 "Nonlinear Analysis of Steel Frames with Semi-Rigid Connections Using the Capacity Spectrum Method," by G.G. Deierlein, S-H. Hsieh, Y-J. Shen and J.F. Abel, 7/2/91, (PB92-113828, A05, MF-A01).
- NCEER-91-0009 "Earthquake Education Materials for Grades K-12," by K.E.K. Ross, 4/30/91, (PB91-212142, A06, MF-A01). This report has been replaced by NCEER-92-0018.
- NCEER-91-0010 "Phase Wave Velocities and Displacement Phase Differences in a Harmonically Oscillating Pile," by N. Makris and G. Gazetas, 7/8/91, (PB92-108356, A04, MF-A01).
- NCEER-91-0011 "Dynamic Characteristics of a Full-Size Five-Story Steel Structure and a 2/5 Scale Model," by K.C. Chang, G.C. Yao, G.C. Lee, D.S. Hao and Y.C. Yeh, 7/2/91, (PB93-116648, A06, MF-A02).
- NCEER-91-0012 "Seismic Response of a 2/5 Scale Steel Structure with Added Viscoelastic Dampers," by K.C. Chang, T.T. Soong, S-T. Oh and M.L. Lai, 5/17/91, (PB92-110816, A05, MF-A01).
- NCEER-91-0013 "Earthquake Response of Retaining Walls; Full-Scale Testing and Computational Modeling," by S. Alampalli and A-W.M. Elgamal, 6/20/91, not available.
- NCEER-91-0014 "3D-BASIS-M: Nonlinear Dynamic Analysis of Multiple Building Base Isolated Structures," by P.C. Tsopelas, S. Nagarajaiah, M.C. Constantinou and A.M. Reinhorn, 5/28/91, (PB92-113885, A09, MF-A02).
- NCEER-91-0015 "Evaluation of SEAOC Design Requirements for Sliding Isolated Structures," by D. Theodossiou and M.C. Constantinou, 6/10/91, (PB92-114602, A11, MF-A03).
- NCEER-91-0016 "Closed-Loop Modal Testing of a 27-Story Reinforced Concrete Flat Plate-Core Building," by H.R. Somaprasad, T. Toksoy, H. Yoshiyuki and A.E. Aktan, 7/15/91, (PB92-129980, A07, MF-A02).
- NCEER-91-0017 "Shake Table Test of a 1/6 Scale Two-Story Lightly Reinforced Concrete Building," by A.G. El-Attar, R.N. White and P. Gergely, 2/28/91, (PB92-222447, A06, MF-A02).
- NCEER-91-0018 "Shake Table Test of a 1/8 Scale Three-Story Lightly Reinforced Concrete Building," by A.G. El-Attar, R.N. White and P. Gergely, 2/28/91, (PB93-116630, A08, MF-A02).
- NCEER-91-0019 "Transfer Functions for Rigid Rectangular Foundations," by A.S. Veletsos, A.M. Prasad and W.H. Wu, 7/31/91, not available.

- NCEER-91-0020 "Hybrid Control of Seismic-Excited Nonlinear and Inelastic Structural Systems," by J.N. Yang, Z. Li and A. Daniellians, 8/1/91, (PB92-143171, A06, MF-A02).
- NCEER-91-0021 "The NCEER-91 Earthquake Catalog: Improved Intensity-Based Magnitudes and Recurrence Relations for U.S. Earthquakes East of New Madrid," by L. Seeber and J.G. Armbruster, 8/28/91, (PB92-176742, A06, MF-A02).
- NCEER-91-0022 "Proceedings from the Implementation of Earthquake Planning and Education in Schools: The Need for Change - The Roles of the Changemakers," by K.E.K. Ross and F. Winslow, 7/23/91, (PB92-129998, A12, MF-A03).
- NCEER-91-0023 "A Study of Reliability-Based Criteria for Seismic Design of Reinforced Concrete Frame Buildings," by H.H.M. Hwang and H-M. Hsu, 8/10/91, (PB92-140235, A09, MF-A02).
- NCEER-91-0024 "Experimental Verification of a Number of Structural System Identification Algorithms," by R.G. Ghanem, H. Gavin and M. Shinozuka, 9/18/91, (PB92-176577, A18, MF-A04).
- NCEER-91-0025 "Probabilistic Evaluation of Liquefaction Potential," by H.H.M. Hwang and C.S. Lee," 11/25/91, (PB92-143429, A05, MF-A01).
- NCEER-91-0026 "Instantaneous Optimal Control for Linear, Nonlinear and Hysteretic Structures - Stable Controllers," by J.N. Yang and Z. Li, 11/15/91, (PB92-163807, A04, MF-A01).
- NCEER-91-0027 "Experimental and Theoretical Study of a Sliding Isolation System for Bridges," by M.C. Constantinou, A. Kartoum, A.M. Reinhorn and P. Bradford, 11/15/91, (PB92-176973, A10, MF-A03).
- NCEER-92-0001 "Case Studies of Liquefaction and Lifeline Performance During Past Earthquakes, Volume 1: Japanese Case Studies," Edited by M. Hamada and T. O'Rourke, 2/17/92, (PB92-197243, A18, MF-A04).
- NCEER-92-0002 "Case Studies of Liquefaction and Lifeline Performance During Past Earthquakes, Volume 2: United States Case Studies," Edited by T. O'Rourke and M. Hamada, 2/17/92, (PB92-197250, A20, MF-A04).
- NCEER-92-0003 "Issues in Earthquake Education," Edited by K. Ross, 2/3/92, (PB92-222389, A07, MF-A02).
- NCEER-92-0004 "Proceedings from the First U.S. - Japan Workshop on Earthquake Protective Systems for Bridges," Edited by I.G. Buckle, 2/4/92, (PB94-142239, A99, MF-A06).
- NCEER-92-0005 "Seismic Ground Motion from a Haskell-Type Source in a Multiple-Layered Half-Space," A.P. Theoharis, G. Deodatis and M. Shinozuka, 1/2/92, not available.
- NCEER-92-0006 "Proceedings from the Site Effects Workshop," Edited by R. Whitman, 2/29/92, (PB92-197201, A04, MF-A01).
- NCEER-92-0007 "Engineering Evaluation of Permanent Ground Deformations Due to Seismically-Induced Liquefaction," by M.H. Baziar, R. Dobry and A-W.M. Elgamal, 3/24/92, (PB92-222421, A13, MF-A03).
- NCEER-92-0008 "A Procedure for the Seismic Evaluation of Buildings in the Central and Eastern United States," by C.D. Poland and J.O. Malley, 4/2/92, (PB92-222439, A20, MF-A04).
- NCEER-92-0009 "Experimental and Analytical Study of a Hybrid Isolation System Using Friction Controllable Sliding Bearings," by M.Q. Feng, S. Fujii and M. Shinozuka, 5/15/92, (PB93-150282, A06, MF-A02).
- NCEER-92-0010 "Seismic Resistance of Slab-Column Connections in Existing Non-Ductile Flat-Plate Buildings," by A.J. Durrani and Y. Du, 5/18/92, (PB93-116812, A06, MF-A02).
- NCEER-92-0011 "The Hysteretic and Dynamic Behavior of Brick Masonry Walls Upgraded by Ferrocement Coatings Under Cyclic Loading and Strong Simulated Ground Motion," by H. Lee and S.P. Prawel, 5/11/92, not available.
- NCEER-92-0012 "Study of Wire Rope Systems for Seismic Protection of Equipment in Buildings," by G.F. Demetriades, M.C. Constantinou and A.M. Reinhorn, 5/20/92, (PB93-116655, A08, MF-A02).

- NCEER-92-0013 "Shape Memory Structural Dampers: Material Properties, Design and Seismic Testing," by P.R. Witting and F.A. Cozzarelli, 5/26/92, (PB93-116663, A05, MF-A01).
- NCEER-92-0014 "Longitudinal Permanent Ground Deformation Effects on Buried Continuous Pipelines," by M.J. O'Rourke, and C. Nordberg, 6/15/92, (PB93-116671, A08, MF-A02).
- NCEER-92-0015 "A Simulation Method for Stationary Gaussian Random Functions Based on the Sampling Theorem," by M. Grigoriu and S. Balopoulou, 6/11/92, (PB93-127496, A05, MF-A01).
- NCEER-92-0016 "Gravity-Load-Designed Reinforced Concrete Buildings: Seismic Evaluation of Existing Construction and Detailing Strategies for Improved Seismic Resistance," by G.W. Hoffmann, S.K. Kunnath, A.M. Reinhorn and J.B. Mander, 7/15/92, (PB94-142007, A08, MF-A02).
- NCEER-92-0017 "Observations on Water System and Pipeline Performance in the Limón Area of Costa Rica Due to the April 22, 1991 Earthquake," by M. O'Rourke and D. Ballantyne, 6/30/92, (PB93-126811, A06, MF-A02).
- NCEER-92-0018 "Fourth Edition of Earthquake Education Materials for Grades K-12," Edited by K.E.K. Ross, 8/10/92, (PB93-114023, A07, MF-A02).
- NCEER-92-0019 "Proceedings from the Fourth Japan-U.S. Workshop on Earthquake Resistant Design of Lifeline Facilities and Countermeasures for Soil Liquefaction," Edited by M. Hamada and T.D. O'Rourke, 8/12/92, (PB93-163939, A99, MF-E11).
- NCEER-92-0020 "Active Bracing System: A Full Scale Implementation of Active Control," by A.M. Reinhorn, T.T. Soong, R.C. Lin, M.A. Riley, Y.P. Wang, S. Aizawa and M. Higashino, 8/14/92, (PB93-127512, A06, MF-A02).
- NCEER-92-0021 "Empirical Analysis of Horizontal Ground Displacement Generated by Liquefaction-Induced Lateral Spreads," by S.F. Bartlett and T.L. Youd, 8/17/92, (PB93-188241, A06, MF-A02).
- NCEER-92-0022 "IDARC Version 3.0: Inelastic Damage Analysis of Reinforced Concrete Structures," by S.K. Kunnath, A.M. Reinhorn and R.F. Lobo, 8/31/92, (PB93-227502, A07, MF-A02).
- NCEER-92-0023 "A Semi-Empirical Analysis of Strong-Motion Peaks in Terms of Seismic Source, Propagation Path and Local Site Conditions, by M. Kamiyama, M.J. O'Rourke and R. Flores-Berrones, 9/9/92, (PB93-150266, A08, MF-A02).
- NCEER-92-0024 "Seismic Behavior of Reinforced Concrete Frame Structures with Nonductile Details, Part I: Summary of Experimental Findings of Full Scale Beam-Column Joint Tests," by A. Beres, R.N. White and P. Gergely, 9/30/92, (PB93-227783, A05, MF-A01).
- NCEER-92-0025 "Experimental Results of Repaired and Retrofitted Beam-Column Joint Tests in Lightly Reinforced Concrete Frame Buildings," by A. Beres, S. El-Borgi, R.N. White and P. Gergely, 10/29/92, (PB93-227791, A05, MF-A01).
- NCEER-92-0026 "A Generalization of Optimal Control Theory: Linear and Nonlinear Structures," by J.N. Yang, Z. Li and S. Vongchavalitkul, 11/2/92, (PB93-188621, A05, MF-A01).
- NCEER-92-0027 "Seismic Resistance of Reinforced Concrete Frame Structures Designed Only for Gravity Loads: Part I - Design and Properties of a One-Third Scale Model Structure," by J.M. Bracci, A.M. Reinhorn and J.B. Mander, 12/1/92, (PB94-104502, A08, MF-A02).
- NCEER-92-0028 "Seismic Resistance of Reinforced Concrete Frame Structures Designed Only for Gravity Loads: Part II - Experimental Performance of Subassemblages," by L.E. Aycaardi, J.B. Mander and A.M. Reinhorn, 12/1/92, (PB94-104510, A08, MF-A02).
- NCEER-92-0029 "Seismic Resistance of Reinforced Concrete Frame Structures Designed Only for Gravity Loads: Part III - Experimental Performance and Analytical Study of a Structural Model," by J.M. Bracci, A.M. Reinhorn and J.B. Mander, 12/1/92, (PB93-227528, A09, MF-A01).

- NCEER-92-0030 "Evaluation of Seismic Retrofit of Reinforced Concrete Frame Structures: Part I - Experimental Performance of Retrofitted Subassemblages," by D. Choudhuri, J.B. Mander and A.M. Reinhorn, 12/8/92, (PB93-198307, A07, MF-A02).
- NCEER-92-0031 "Evaluation of Seismic Retrofit of Reinforced Concrete Frame Structures: Part II - Experimental Performance and Analytical Study of a Retrofitted Structural Model," by J.M. Bracci, A.M. Reinhorn and J.B. Mander, 12/8/92, (PB93-198315, A09, MF-A03).
- NCEER-92-0032 "Experimental and Analytical Investigation of Seismic Response of Structures with Supplemental Fluid Viscous Dampers," by M.C. Constantinou and M.D. Symans, 12/21/92, (PB93-191435, A10, MF-A03). This report is available only through NTIS (see address given above).
- NCEER-92-0033 "Reconnaissance Report on the Cairo, Egypt Earthquake of October 12, 1992," by M. Khater, 12/23/92, (PB93-188621, A03, MF-A01).
- NCEER-92-0034 "Low-Level Dynamic Characteristics of Four Tall Flat-Plate Buildings in New York City," by H. Gavin, S. Yuan, J. Grossman, E. Pekelis and K. Jacob, 12/28/92, (PB93-188217, A07, MF-A02).
- NCEER-93-0001 "An Experimental Study on the Seismic Performance of Brick-Infilled Steel Frames With and Without Retrofit," by J.B. Mander, B. Nair, K. Wojtkowski and J. Ma, 1/29/93, (PB93-227510, A07, MF-A02).
- NCEER-93-0002 "Social Accounting for Disaster Preparedness and Recovery Planning," by S. Cole, E. Pantoja and V. Razak, 2/22/93, (PB94-142114, A12, MF-A03).
- NCEER-93-0003 "Assessment of 1991 NEHRP Provisions for Nonstructural Components and Recommended Revisions," by T.T. Soong, G. Chen, Z. Wu, R-H. Zhang and M. Grigoriu, 3/1/93, (PB93-188639, A06, MF-A02).
- NCEER-93-0004 "Evaluation of Static and Response Spectrum Analysis Procedures of SEAOC/UBC for Seismic Isolated Structures," by C.W. Winters and M.C. Constantinou, 3/23/93, (PB93-198299, A10, MF-A03).
- NCEER-93-0005 "Earthquakes in the Northeast - Are We Ignoring the Hazard? A Workshop on Earthquake Science and Safety for Educators," edited by K.E.K. Ross, 4/2/93, (PB94-103066, A09, MF-A02).
- NCEER-93-0006 "Inelastic Response of Reinforced Concrete Structures with Viscoelastic Braces," by R.F. Lobo, J.M. Bracci, K.L. Shen, A.M. Reinhorn and T.T. Soong, 4/5/93, (PB93-227486, A05, MF-A02).
- NCEER-93-0007 "Seismic Testing of Installation Methods for Computers and Data Processing Equipment," by K. Kosar, T.T. Soong, K.L. Shen, J.A. HoLung and Y.K. Lin, 4/12/93, (PB93-198299, A07, MF-A02).
- NCEER-93-0008 "Retrofit of Reinforced Concrete Frames Using Added Dampers," by A. Reinhorn, M. Constantinou and C. Li, not available.
- NCEER-93-0009 "Seismic Behavior and Design Guidelines for Steel Frame Structures with Added Viscoelastic Dampers," by K.C. Chang, M.L. Lai, T.T. Soong, D.S. Hao and Y.C. Yeh, 5/1/93, (PB94-141959, A07, MF-A02).
- NCEER-93-0010 "Seismic Performance of Shear-Critical Reinforced Concrete Bridge Piers," by J.B. Mander, S.M. Waheed, M.T.A. Chaudhary and S.S. Chen, 5/12/93, (PB93-227494, A08, MF-A02).
- NCEER-93-0011 "3D-BASIS-TABS: Computer Program for Nonlinear Dynamic Analysis of Three Dimensional Base Isolated Structures," by S. Nagarajaiah, C. Li, A.M. Reinhorn and M.C. Constantinou, 8/2/93, (PB94-141819, A09, MF-A02).
- NCEER-93-0012 "Effects of Hydrocarbon Spills from an Oil Pipeline Break on Ground Water," by O.J. Helweg and H.H.M. Hwang, 8/3/93, (PB94-141942, A06, MF-A02).
- NCEER-93-0013 "Simplified Procedures for Seismic Design of Nonstructural Components and Assessment of Current Code Provisions," by M.P. Singh, L.E. Suarez, E.E. Matheu and G.O. Maldonado, 8/4/93, (PB94-141827, A09, MF-A02).
- NCEER-93-0014 "An Energy Approach to Seismic Analysis and Design of Secondary Systems," by G. Chen and T.T. Soong, 8/6/93, (PB94-142767, A11, MF-A03).

- NCEER-93-0015 "Proceedings from School Sites: Becoming Prepared for Earthquakes - Commemorating the Third Anniversary of the Loma Prieta Earthquake," Edited by F.E. Winslow and K.E.K. Ross, 8/16/93, (PB94-154275, A16, MF-A02).
- NCEER-93-0016 "Reconnaissance Report of Damage to Historic Monuments in Cairo, Egypt Following the October 12, 1992 Dahshur Earthquake," by D. Sykora, D. Look, G. Croci, E. Karaesmen and E. Karaesmen, 8/19/93, (PB94-142221, A08, MF-A02).
- NCEER-93-0017 "The Island of Guam Earthquake of August 8, 1993," by S.W. Swan and S.K. Harris, 9/30/93, (PB94-141843, A04, MF-A01).
- NCEER-93-0018 "Engineering Aspects of the October 12, 1992 Egyptian Earthquake," by A.W. Elgamal, M. Amer, K. Adalier and A. Abul-Fadl, 10/7/93, (PB94-141983, A05, MF-A01).
- NCEER-93-0019 "Development of an Earthquake Motion Simulator and its Application in Dynamic Centrifuge Testing," by I. Krstelj, Supervised by J.H. Prevost, 10/23/93, (PB94-181773, A-10, MF-A03).
- NCEER-93-0020 "NCEER-Taisei Corporation Research Program on Sliding Seismic Isolation Systems for Bridges: Experimental and Analytical Study of a Friction Pendulum System (FPS)," by M.C. Constantinou, P. Tsopelas, Y-S. Kim and S. Okamoto, 11/1/93, (PB94-142775, A08, MF-A02).
- NCEER-93-0021 "Finite Element Modeling of Elastomeric Seismic Isolation Bearings," by L.J. Billings, Supervised by R. Shepherd, 11/8/93, not available.
- NCEER-93-0022 "Seismic Vulnerability of Equipment in Critical Facilities: Life-Safety and Operational Consequences," by K. Porter, G.S. Johnson, M.M. Zadeh, C. Scawthorn and S. Eder, 11/24/93, (PB94-181765, A16, MF-A03).
- NCEER-93-0023 "Hokkaido Nansei-oki, Japan Earthquake of July 12, 1993, by P.I. Yanev and C.R. Scawthorn, 12/23/93, (PB94-181500, A07, MF-A01).
- NCEER-94-0001 "An Evaluation of Seismic Serviceability of Water Supply Networks with Application to the San Francisco Auxiliary Water Supply System," by I. Markov, Supervised by M. Grigoriu and T. O'Rourke, 1/21/94, (PB94-204013, A07, MF-A02).
- NCEER-94-0002 "NCEER-Taisei Corporation Research Program on Sliding Seismic Isolation Systems for Bridges: Experimental and Analytical Study of Systems Consisting of Sliding Bearings, Rubber Restoring Force Devices and Fluid Dampers," Volumes I and II, by P. Tsopelas, S. Okamoto, M.C. Constantinou, D. Ozaki and S. Fujii, 2/4/94, (PB94-181740, A09, MF-A02 and PB94-181757, A12, MF-A03).
- NCEER-94-0003 "A Markov Model for Local and Global Damage Indices in Seismic Analysis," by S. Rahman and M. Grigoriu, 2/18/94, (PB94-206000, A12, MF-A03).
- NCEER-94-0004 "Proceedings from the NCEER Workshop on Seismic Response of Masonry Infills," edited by D.P. Abrams, 3/1/94, (PB94-180783, A07, MF-A02).
- NCEER-94-0005 "The Northridge, California Earthquake of January 17, 1994: General Reconnaissance Report," edited by J.D. Goltz, 3/11/94, (PB94-193943, A10, MF-A03).
- NCEER-94-0006 "Seismic Energy Based Fatigue Damage Analysis of Bridge Columns: Part I - Evaluation of Seismic Capacity," by G.A. Chang and J.B. Mander, 3/14/94, (PB94-219185, A11, MF-A03).
- NCEER-94-0007 "Seismic Isolation of Multi-Story Frame Structures Using Spherical Sliding Isolation Systems," by T.M. Al-Hussaini, V.A. Zayas and M.C. Constantinou, 3/17/94, (PB94-193745, A09, MF-A02).
- NCEER-94-0008 "The Northridge, California Earthquake of January 17, 1994: Performance of Highway Bridges," edited by I.G. Buckle, 3/24/94, (PB94-193851, A06, MF-A02).
- NCEER-94-0009 "Proceedings of the Third U.S.-Japan Workshop on Earthquake Protective Systems for Bridges," edited by I.G. Buckle and I. Friedland, 3/31/94, (PB94-195815, A99, MF-A06).

- NCEER-94-0010 "3D-BASIS-ME: Computer Program for Nonlinear Dynamic Analysis of Seismically Isolated Single and Multiple Structures and Liquid Storage Tanks," by P.C. Tsopelas, M.C. Constantinou and A.M. Reinhorn, 4/12/94, (PB94-204922, A09, MF-A02).
- NCEER-94-0011 "The Northridge, California Earthquake of January 17, 1994: Performance of Gas Transmission Pipelines," by T.D. O'Rourke and M.C. Palmer, 5/16/94, (PB94-204989, A05, MF-A01).
- NCEER-94-0012 "Feasibility Study of Replacement Procedures and Earthquake Performance Related to Gas Transmission Pipelines," by T.D. O'Rourke and M.C. Palmer, 5/25/94, (PB94-206638, A09, MF-A02).
- NCEER-94-0013 "Seismic Energy Based Fatigue Damage Analysis of Bridge Columns: Part II - Evaluation of Seismic Demand," by G.A. Chang and J.B. Mander, 6/1/94, (PB95-18106, A08, MF-A02).
- NCEER-94-0014 "NCEER-Taisei Corporation Research Program on Sliding Seismic Isolation Systems for Bridges: Experimental and Analytical Study of a System Consisting of Sliding Bearings and Fluid Restoring Force/Damping Devices," by P. Tsopelas and M.C. Constantinou, 6/13/94, (PB94-219144, A10, MF-A03).
- NCEER-94-0015 "Generation of Hazard-Consistent Fragility Curves for Seismic Loss Estimation Studies," by H. Hwang and J-R. Huo, 6/14/94, (PB95-181996, A09, MF-A02).
- NCEER-94-0016 "Seismic Study of Building Frames with Added Energy-Absorbing Devices," by W.S. Pong, C.S. Tsai and G.C. Lee, 6/20/94, (PB94-219136, A10, A03).
- NCEER-94-0017 "Sliding Mode Control for Seismic-Excited Linear and Nonlinear Civil Engineering Structures," by J. Yang, J. Wu, A. Agrawal and Z. Li, 6/21/94, (PB95-138483, A06, MF-A02).
- NCEER-94-0018 "3D-BASIS-TABS Version 2.0: Computer Program for Nonlinear Dynamic Analysis of Three Dimensional Base Isolated Structures," by A.M. Reinhorn, S. Nagarajaiah, M.C. Constantinou, P. Tsopelas and R. Li, 6/22/94, (PB95-182176, A08, MF-A02).
- NCEER-94-0019 "Proceedings of the International Workshop on Civil Infrastructure Systems: Application of Intelligent Systems and Advanced Materials on Bridge Systems," Edited by G.C. Lee and K.C. Chang, 7/18/94, (PB95-252474, A20, MF-A04).
- NCEER-94-0020 "Study of Seismic Isolation Systems for Computer Floors," by V. Lambrou and M.C. Constantinou, 7/19/94, (PB95-138533, A10, MF-A03).
- NCEER-94-0021 "Proceedings of the U.S.-Italian Workshop on Guidelines for Seismic Evaluation and Rehabilitation of Unreinforced Masonry Buildings," Edited by D.P. Abrams and G.M. Calvi, 7/20/94, (PB95-138749, A13, MF-A03).
- NCEER-94-0022 "NCEER-Taisei Corporation Research Program on Sliding Seismic Isolation Systems for Bridges: Experimental and Analytical Study of a System Consisting of Lubricated PTFE Sliding Bearings and Mild Steel Dampers," by P. Tsopelas and M.C. Constantinou, 7/22/94, (PB95-182184, A08, MF-A02).
- NCEER-94-0023 "Development of Reliability-Based Design Criteria for Buildings Under Seismic Load," by Y.K. Wen, H. Hwang and M. Shinozuka, 8/1/94, (PB95-211934, A08, MF-A02).
- NCEER-94-0024 "Experimental Verification of Acceleration Feedback Control Strategies for an Active Tendon System," by S.J. Dyke, B.F. Spencer, Jr., P. Quast, M.K. Sain, D.C. Kaspari, Jr. and T.T. Soong, 8/29/94, (PB95-212320, A05, MF-A01).
- NCEER-94-0025 "Seismic Retrofitting Manual for Highway Bridges," Edited by I.G. Buckle and I.F. Friedland, published by the Federal Highway Administration (PB95-212676, A15, MF-A03).
- NCEER-94-0026 "Proceedings from the Fifth U.S.-Japan Workshop on Earthquake Resistant Design of Lifeline Facilities and Countermeasures Against Soil Liquefaction," Edited by T.D. O'Rourke and M. Hamada, 11/7/94, (PB95-220802, A99, MF-E08).

- NCEER-95-0001 “Experimental and Analytical Investigation of Seismic Retrofit of Structures with Supplemental Damping: Part 1 - Fluid Viscous Damping Devices,” by A.M. Reinhorn, C. Li and M.C. Constantinou, 1/3/95, (PB95-266599, A09, MF-A02).
- NCEER-95-0002 “Experimental and Analytical Study of Low-Cycle Fatigue Behavior of Semi-Rigid Top-And-Seat Angle Connections,” by G. Pekcan, J.B. Mander and S.S. Chen, 1/5/95, (PB95-220042, A07, MF-A02).
- NCEER-95-0003 “NCEER-ATC Joint Study on Fragility of Buildings,” by T. Anagnos, C. Rojahn and A.S. Kiremidjian, 1/20/95, (PB95-220026, A06, MF-A02).
- NCEER-95-0004 “Nonlinear Control Algorithms for Peak Response Reduction,” by Z. Wu, T.T. Soong, V. Gattulli and R.C. Lin, 2/16/95, (PB95-220349, A05, MF-A01).
- NCEER-95-0005 “Pipeline Replacement Feasibility Study: A Methodology for Minimizing Seismic and Corrosion Risks to Underground Natural Gas Pipelines,” by R.T. Eguchi, H.A. Seligson and D.G. Honegger, 3/2/95, (PB95-252326, A06, MF-A02).
- NCEER-95-0006 “Evaluation of Seismic Performance of an 11-Story Frame Building During the 1994 Northridge Earthquake,” by F. Naeim, R. DiSulio, K. Benuska, A. Reinhorn and C. Li, not available.
- NCEER-95-0007 “Prioritization of Bridges for Seismic Retrofitting,” by N. Basöz and A.S. Kiremidjian, 4/24/95, (PB95-252300, A08, MF-A02).
- NCEER-95-0008 “Method for Developing Motion Damage Relationships for Reinforced Concrete Frames,” by A. Singhal and A.S. Kiremidjian, 5/11/95, (PB95-266607, A06, MF-A02).
- NCEER-95-0009 “Experimental and Analytical Investigation of Seismic Retrofit of Structures with Supplemental Damping: Part II - Friction Devices,” by C. Li and A.M. Reinhorn, 7/6/95, (PB96-128087, A11, MF-A03).
- NCEER-95-0010 “Experimental Performance and Analytical Study of a Non-Ductile Reinforced Concrete Frame Structure Retrofitted with Elastomeric Spring Dampers,” by G. Pekcan, J.B. Mander and S.S. Chen, 7/14/95, (PB96-137161, A08, MF-A02).
- NCEER-95-0011 “Development and Experimental Study of Semi-Active Fluid Damping Devices for Seismic Protection of Structures,” by M.D. Symans and M.C. Constantinou, 8/3/95, (PB96-136940, A23, MF-A04).
- NCEER-95-0012 “Real-Time Structural Parameter Modification (RSPM): Development of Innervated Structures,” by Z. Liang, M. Tong and G.C. Lee, 4/11/95, (PB96-137153, A06, MF-A01).
- NCEER-95-0013 “Experimental and Analytical Investigation of Seismic Retrofit of Structures with Supplemental Damping: Part III - Viscous Damping Walls,” by A.M. Reinhorn and C. Li, 10/1/95, (PB96-176409, A11, MF-A03).
- NCEER-95-0014 “Seismic Fragility Analysis of Equipment and Structures in a Memphis Electric Substation,” by J-R. Huo and H.H.M. Hwang, 8/10/95, (PB96-128087, A09, MF-A02).
- NCEER-95-0015 “The Hanshin-Awaji Earthquake of January 17, 1995: Performance of Lifelines,” Edited by M. Shinozuka, 11/3/95, (PB96-176383, A15, MF-A03).
- NCEER-95-0016 “Highway Culvert Performance During Earthquakes,” by T.L. Youd and C.J. Beckman, available as NCEER-96-0015.
- NCEER-95-0017 “The Hanshin-Awaji Earthquake of January 17, 1995: Performance of Highway Bridges,” Edited by I.G. Buckle, 12/1/95, not available.
- NCEER-95-0018 “Modeling of Masonry Infill Panels for Structural Analysis,” by A.M. Reinhorn, A. Madan, R.E. Valles, Y. Reichmann and J.B. Mander, 12/8/95, (PB97-110886, MF-A01, A06).
- NCEER-95-0019 “Optimal Polynomial Control for Linear and Nonlinear Structures,” by A.K. Agrawal and J.N. Yang, 12/11/95, (PB96-168737, A07, MF-A02).

- NCEER-95-0020 "Retrofit of Non-Ductile Reinforced Concrete Frames Using Friction Dampers," by R.S. Rao, P. Gergely and R.N. White, 12/22/95, (PB97-133508, A10, MF-A02).
- NCEER-95-0021 "Parametric Results for Seismic Response of Pile-Supported Bridge Bents," by G. Mylonakis, A. Nikolaou and G. Gazetas, 12/22/95, (PB97-100242, A12, MF-A03).
- NCEER-95-0022 "Kinematic Bending Moments in Seismically Stressed Piles," by A. Nikolaou, G. Mylonakis and G. Gazetas, 12/23/95, (PB97-113914, MF-A03, A13).
- NCEER-96-0001 "Dynamic Response of Unreinforced Masonry Buildings with Flexible Diaphragms," by A.C. Costley and D.P. Abrams, 10/10/96, (PB97-133573, MF-A03, A15).
- NCEER-96-0002 "State of the Art Review: Foundations and Retaining Structures," by I. Po Lam, not available.
- NCEER-96-0003 "Ductility of Rectangular Reinforced Concrete Bridge Columns with Moderate Confinement," by N. Wehbe, M. Saiidi, D. Sanders and B. Douglas, 11/7/96, (PB97-133557, A06, MF-A02).
- NCEER-96-0004 "Proceedings of the Long-Span Bridge Seismic Research Workshop," edited by I.G. Buckle and I.M. Friedland, not available.
- NCEER-96-0005 "Establish Representative Pier Types for Comprehensive Study: Eastern United States," by J. Kulicki and Z. Prucz, 5/28/96, (PB98-119217, A07, MF-A02).
- NCEER-96-0006 "Establish Representative Pier Types for Comprehensive Study: Western United States," by R. Imbsen, R.A. Schamber and T.A. Osterkamp, 5/28/96, (PB98-118607, A07, MF-A02).
- NCEER-96-0007 "Nonlinear Control Techniques for Dynamical Systems with Uncertain Parameters," by R.G. Ghanem and M.I. Bujakov, 5/27/96, (PB97-100259, A17, MF-A03).
- NCEER-96-0008 "Seismic Evaluation of a 30-Year Old Non-Ductile Highway Bridge Pier and Its Retrofit," by J.B. Mander, B. Mahmoodzadegan, S. Bhadra and S.S. Chen, 5/31/96, (PB97-110902, MF-A03, A10).
- NCEER-96-0009 "Seismic Performance of a Model Reinforced Concrete Bridge Pier Before and After Retrofit," by J.B. Mander, J.H. Kim and C.A. Ligozio, 5/31/96, (PB97-110910, MF-A02, A10).
- NCEER-96-0010 "IDARC2D Version 4.0: A Computer Program for the Inelastic Damage Analysis of Buildings," by R.E. Valles, A.M. Reinhorn, S.K. Kunnath, C. Li and A. Madan, 6/3/96, (PB97-100234, A17, MF-A03).
- NCEER-96-0011 "Estimation of the Economic Impact of Multiple Lifeline Disruption: Memphis Light, Gas and Water Division Case Study," by S.E. Chang, H.A. Seligson and R.T. Eguchi, 8/16/96, (PB97-133490, A11, MF-A03).
- NCEER-96-0012 "Proceedings from the Sixth Japan-U.S. Workshop on Earthquake Resistant Design of Lifeline Facilities and Countermeasures Against Soil Liquefaction, Edited by M. Hamada and T. O'Rourke, 9/11/96, (PB97-133581, A99, MF-A06).
- NCEER-96-0013 "Chemical Hazards, Mitigation and Preparedness in Areas of High Seismic Risk: A Methodology for Estimating the Risk of Post-Earthquake Hazardous Materials Release," by H.A. Seligson, R.T. Eguchi, K.J. Tierney and K. Richmond, 11/7/96, (PB97-133565, MF-A02, A08).
- NCEER-96-0014 "Response of Steel Bridge Bearings to Reversed Cyclic Loading," by J.B. Mander, D-K. Kim, S.S. Chen and G.J. Premus, 11/13/96, (PB97-140735, A12, MF-A03).
- NCEER-96-0015 "Highway Culvert Performance During Past Earthquakes," by T.L. Youd and C.J. Beckman, 11/25/96, (PB97-133532, A06, MF-A01).
- NCEER-97-0001 "Evaluation, Prevention and Mitigation of Pounding Effects in Building Structures," by R.E. Valles and A.M. Reinhorn, 2/20/97, (PB97-159552, A14, MF-A03).
- NCEER-97-0002 "Seismic Design Criteria for Bridges and Other Highway Structures," by C. Rojahn, R. Mayes, D.G. Anderson, J. Clark, J.H. Hom, R.V. Nutt and M.J. O'Rourke, 4/30/97, (PB97-194658, A06, MF-A03).

- NCEER-97-0003 "Proceedings of the U.S.-Italian Workshop on Seismic Evaluation and Retrofit," Edited by D.P. Abrams and G.M. Calvi, 3/19/97, (PB97-194666, A13, MF-A03).
- NCEER-97-0004 "Investigation of Seismic Response of Buildings with Linear and Nonlinear Fluid Viscous Dampers," by A.A. Seleemah and M.C. Constantinou, 5/21/97, (PB98-109002, A15, MF-A03).
- NCEER-97-0005 "Proceedings of the Workshop on Earthquake Engineering Frontiers in Transportation Facilities," edited by G.C. Lee and I.M. Friedland, 8/29/97, (PB98-128911, A25, MR-A04).
- NCEER-97-0006 "Cumulative Seismic Damage of Reinforced Concrete Bridge Piers," by S.K. Kunnath, A. El-Bahy, A. Taylor and W. Stone, 9/2/97, (PB98-108814, A11, MF-A03).
- NCEER-97-0007 "Structural Details to Accommodate Seismic Movements of Highway Bridges and Retaining Walls," by R.A. Imbsen, R.A. Schamber, E. Thorkildsen, A. Kartoum, B.T. Martin, T.N. Rosser and J.M. Kulicki, 9/3/97, (PB98-108996, A09, MF-A02).
- NCEER-97-0008 "A Method for Earthquake Motion-Damage Relationships with Application to Reinforced Concrete Frames," by A. Singhal and A.S. Kiremidjian, 9/10/97, (PB98-108988, A13, MF-A03).
- NCEER-97-0009 "Seismic Analysis and Design of Bridge Abutments Considering Sliding and Rotation," by K. Fishman and R. Richards, Jr., 9/15/97, (PB98-108897, A06, MF-A02).
- NCEER-97-0010 "Proceedings of the FHWA/NCEER Workshop on the National Representation of Seismic Ground Motion for New and Existing Highway Facilities," edited by I.M. Friedland, M.S. Power and R.L. Mayes, 9/22/97, (PB98-128903, A21, MF-A04).
- NCEER-97-0011 "Seismic Analysis for Design or Retrofit of Gravity Bridge Abutments," by K.L. Fishman, R. Richards, Jr. and R.C. Divito, 10/2/97, (PB98-128937, A08, MF-A02).
- NCEER-97-0012 "Evaluation of Simplified Methods of Analysis for Yielding Structures," by P. Tsopelas, M.C. Constantinou, C.A. Kircher and A.S. Whittaker, 10/31/97, (PB98-128929, A10, MF-A03).
- NCEER-97-0013 "Seismic Design of Bridge Columns Based on Control and Repairability of Damage," by C-T. Cheng and J.B. Mander, 12/8/97, (PB98-144249, A11, MF-A03).
- NCEER-97-0014 "Seismic Resistance of Bridge Piers Based on Damage Avoidance Design," by J.B. Mander and C-T. Cheng, 12/10/97, (PB98-144223, A09, MF-A02).
- NCEER-97-0015 "Seismic Response of Nominally Symmetric Systems with Strength Uncertainty," by S. Balopoulou and M. Grigoriu, 12/23/97, (PB98-153422, A11, MF-A03).
- NCEER-97-0016 "Evaluation of Seismic Retrofit Methods for Reinforced Concrete Bridge Columns," by T.J. Wipf, F.W. Klaiber and F.M. Russo, 12/28/97, (PB98-144215, A12, MF-A03).
- NCEER-97-0017 "Seismic Fragility of Existing Conventional Reinforced Concrete Highway Bridges," by C.L. Mullen and A.S. Cakmak, 12/30/97, (PB98-153406, A08, MF-A02).
- NCEER-97-0018 "Loss Assessment of Memphis Buildings," edited by D.P. Abrams and M. Shinozuka, 12/31/97, (PB98-144231, A13, MF-A03).
- NCEER-97-0019 "Seismic Evaluation of Frames with Infill Walls Using Quasi-static Experiments," by K.M. Mosalam, R.N. White and P. Gergely, 12/31/97, (PB98-153455, A07, MF-A02).
- NCEER-97-0020 "Seismic Evaluation of Frames with Infill Walls Using Pseudo-dynamic Experiments," by K.M. Mosalam, R.N. White and P. Gergely, 12/31/97, (PB98-153430, A07, MF-A02).
- NCEER-97-0021 "Computational Strategies for Frames with Infill Walls: Discrete and Smeared Crack Analyses and Seismic Fragility," by K.M. Mosalam, R.N. White and P. Gergely, 12/31/97, (PB98-153414, A10, MF-A02).

- NCEER-97-0022 "Proceedings of the NCEER Workshop on Evaluation of Liquefaction Resistance of Soils," edited by T.L. Youd and I.M. Idriss, 12/31/97, (PB98-155617, A15, MF-A03).
- MCEER-98-0001 "Extraction of Nonlinear Hysteretic Properties of Seismically Isolated Bridges from Quick-Release Field Tests," by Q. Chen, B.M. Douglas, E.M. Maragakis and I.G. Buckle, 5/26/98, (PB99-118838, A06, MF-A01).
- MCEER-98-0002 "Methodologies for Evaluating the Importance of Highway Bridges," by A. Thomas, S. Eshenaur and J. Kulicki, 5/29/98, (PB99-118846, A10, MF-A02).
- MCEER-98-0003 "Capacity Design of Bridge Piers and the Analysis of Overstrength," by J.B. Mander, A. Dutta and P. Goel, 6/1/98, (PB99-118853, A09, MF-A02).
- MCEER-98-0004 "Evaluation of Bridge Damage Data from the Loma Prieta and Northridge, California Earthquakes," by N. Basoz and A. Kiremidjian, 6/2/98, (PB99-118861, A15, MF-A03).
- MCEER-98-0005 "Screening Guide for Rapid Assessment of Liquefaction Hazard at Highway Bridge Sites," by T. L. Youd, 6/16/98, (PB99-118879, A06, not available on microfiche).
- MCEER-98-0006 "Structural Steel and Steel/Concrete Interface Details for Bridges," by P. Ritchie, N. Kauh and J. Kulicki, 7/13/98, (PB99-118945, A06, MF-A01).
- MCEER-98-0007 "Capacity Design and Fatigue Analysis of Confined Concrete Columns," by A. Dutta and J.B. Mander, 7/14/98, (PB99-118960, A14, MF-A03).
- MCEER-98-0008 "Proceedings of the Workshop on Performance Criteria for Telecommunication Services Under Earthquake Conditions," edited by A.J. Schiff, 7/15/98, (PB99-118952, A08, MF-A02).
- MCEER-98-0009 "Fatigue Analysis of Unconfined Concrete Columns," by J.B. Mander, A. Dutta and J.H. Kim, 9/12/98, (PB99-123655, A10, MF-A02).
- MCEER-98-0010 "Centrifuge Modeling of Cyclic Lateral Response of Pile-Cap Systems and Seat-Type Abutments in Dry Sands," by A.D. Gadre and R. Dobry, 10/2/98, (PB99-123606, A13, MF-A03).
- MCEER-98-0011 "IDARC-BRIDGE: A Computational Platform for Seismic Damage Assessment of Bridge Structures," by A.M. Reinhorn, V. Simeonov, G. Mylonakis and Y. Reichman, 10/2/98, (PB99-162919, A15, MF-A03).
- MCEER-98-0012 "Experimental Investigation of the Dynamic Response of Two Bridges Before and After Retrofitting with Elastomeric Bearings," by D.A. Wendichansky, S.S. Chen and J.B. Mander, 10/2/98, (PB99-162927, A15, MF-A03).
- MCEER-98-0013 "Design Procedures for Hinge Restrainers and Hinge Sear Width for Multiple-Frame Bridges," by R. Des Roches and G.L. Fenves, 11/3/98, (PB99-140477, A13, MF-A03).
- MCEER-98-0014 "Response Modification Factors for Seismically Isolated Bridges," by M.C. Constantinou and J.K. Quarshie, 11/3/98, (PB99-140485, A14, MF-A03).
- MCEER-98-0015 "Proceedings of the U.S.-Italy Workshop on Seismic Protective Systems for Bridges," edited by I.M. Friedland and M.C. Constantinou, 11/3/98, (PB2000-101711, A22, MF-A04).
- MCEER-98-0016 "Appropriate Seismic Reliability for Critical Equipment Systems: Recommendations Based on Regional Analysis of Financial and Life Loss," by K. Porter, C. Scawthorn, C. Taylor and N. Blais, 11/10/98, (PB99-157265, A08, MF-A02).
- MCEER-98-0017 "Proceedings of the U.S. Japan Joint Seminar on Civil Infrastructure Systems Research," edited by M. Shinozuka and A. Rose, 11/12/98, (PB99-156713, A16, MF-A03).
- MCEER-98-0018 "Modeling of Pile Footings and Drilled Shafts for Seismic Design," by I. PoLam, M. Kapuskar and D. Chaudhuri, 12/21/98, (PB99-157257, A09, MF-A02).

- MCEER-99-0001 "Seismic Evaluation of a Masonry Infilled Reinforced Concrete Frame by Pseudodynamic Testing," by S.G. Buonopane and R.N. White, 2/16/99, (PB99-162851, A09, MF-A02).
- MCEER-99-0002 "Response History Analysis of Structures with Seismic Isolation and Energy Dissipation Systems: Verification Examples for Program SAP2000," by J. Scheller and M.C. Constantinou, 2/22/99, (PB99-162869, A08, MF-A02).
- MCEER-99-0003 "Experimental Study on the Seismic Design and Retrofit of Bridge Columns Including Axial Load Effects," by A. Dutta, T. Kokorina and J.B. Mander, 2/22/99, (PB99-162877, A09, MF-A02).
- MCEER-99-0004 "Experimental Study of Bridge Elastomeric and Other Isolation and Energy Dissipation Systems with Emphasis on Uplift Prevention and High Velocity Near-source Seismic Excitation," by A. Kasalanati and M. C. Constantinou, 2/26/99, (PB99-162885, A12, MF-A03).
- MCEER-99-0005 "Truss Modeling of Reinforced Concrete Shear-flexure Behavior," by J.H. Kim and J.B. Mander, 3/8/99, (PB99-163693, A12, MF-A03).
- MCEER-99-0006 "Experimental Investigation and Computational Modeling of Seismic Response of a 1:4 Scale Model Steel Structure with a Load Balancing Supplemental Damping System," by G. Pekcan, J.B. Mander and S.S. Chen, 4/2/99, (PB99-162893, A11, MF-A03).
- MCEER-99-0007 "Effect of Vertical Ground Motions on the Structural Response of Highway Bridges," by M.R. Button, C.J. Cronin and R.L. Mayes, 4/10/99, (PB2000-101411, A10, MF-A03).
- MCEER-99-0008 "Seismic Reliability Assessment of Critical Facilities: A Handbook, Supporting Documentation, and Model Code Provisions," by G.S. Johnson, R.E. Sheppard, M.D. Quilici, S.J. Eder and C.R. Scawthorn, 4/12/99, (PB2000-101701, A18, MF-A04).
- MCEER-99-0009 "Impact Assessment of Selected MCEER Highway Project Research on the Seismic Design of Highway Structures," by C. Rojahn, R. Mayes, D.G. Anderson, J.H. Clark, D'Appolonia Engineering, S. Gloyd and R.V. Nutt, 4/14/99, (PB99-162901, A10, MF-A02).
- MCEER-99-0010 "Site Factors and Site Categories in Seismic Codes," by R. Dobry, R. Ramos and M.S. Power, 7/19/99, (PB2000-101705, A08, MF-A02).
- MCEER-99-0011 "Restrainer Design Procedures for Multi-Span Simply-Supported Bridges," by M.J. Randall, M. Saiidi, E. Maragakis and T. Isakovic, 7/20/99, (PB2000-101702, A10, MF-A02).
- MCEER-99-0012 "Property Modification Factors for Seismic Isolation Bearings," by M.C. Constantinou, P. Tsopelas, A. Kasalanati and E. Wolff, 7/20/99, (PB2000-103387, A11, MF-A03).
- MCEER-99-0013 "Critical Seismic Issues for Existing Steel Bridges," by P. Ritchie, N. Kauh and J. Kulicki, 7/20/99, (PB2000-101697, A09, MF-A02).
- MCEER-99-0014 "Nonstructural Damage Database," by A. Kao, T.T. Soong and A. Vender, 7/24/99, (PB2000-101407, A06, MF-A01).
- MCEER-99-0015 "Guide to Remedial Measures for Liquefaction Mitigation at Existing Highway Bridge Sites," by H.G. Cooke and J. K. Mitchell, 7/26/99, (PB2000-101703, A11, MF-A03).
- MCEER-99-0016 "Proceedings of the MCEER Workshop on Ground Motion Methodologies for the Eastern United States," edited by N. Abrahamson and A. Becker, 8/11/99, (PB2000-103385, A07, MF-A02).
- MCEER-99-0017 "Quindío, Colombia Earthquake of January 25, 1999: Reconnaissance Report," by A.P. Asfura and P.J. Flores, 10/4/99, (PB2000-106893, A06, MF-A01).
- MCEER-99-0018 "Hysteretic Models for Cyclic Behavior of Deteriorating Inelastic Structures," by M.V. Sivaselvan and A.M. Reinhorn, 11/5/99, (PB2000-103386, A08, MF-A02).

- MCEER-99-0019 "Proceedings of the 7th U.S.- Japan Workshop on Earthquake Resistant Design of Lifeline Facilities and Countermeasures Against Soil Liquefaction," edited by T.D. O'Rourke, J.P. Bardet and M. Hamada, 11/19/99, (PB2000-103354, A99, MF-A06).
- MCEER-99-0020 "Development of Measurement Capability for Micro-Vibration Evaluations with Application to Chip Fabrication Facilities," by G.C. Lee, Z. Liang, J.W. Song, J.D. Shen and W.C. Liu, 12/1/99, (PB2000-105993, A08, MF-A02).
- MCEER-99-0021 "Design and Retrofit Methodology for Building Structures with Supplemental Energy Dissipating Systems," by G. Pekcan, J.B. Mander and S.S. Chen, 12/31/99, (PB2000-105994, A11, MF-A03).
- MCEER-00-0001 "The Marmara, Turkey Earthquake of August 17, 1999: Reconnaissance Report," edited by C. Scawthorn; with major contributions by M. Bruneau, R. Eguchi, T. Holzer, G. Johnson, J. Mander, J. Mitchell, W. Mitchell, A. Papageorgiou, C. Scaethorn, and G. Webb, 3/23/00, (PB2000-106200, A11, MF-A03).
- MCEER-00-0002 "Proceedings of the MCEER Workshop for Seismic Hazard Mitigation of Health Care Facilities," edited by G.C. Lee, M. Ettouney, M. Grigoriu, J. Hauer and J. Nigg, 3/29/00, (PB2000-106892, A08, MF-A02).
- MCEER-00-0003 "The Chi-Chi, Taiwan Earthquake of September 21, 1999: Reconnaissance Report," edited by G.C. Lee and C.H. Loh, with major contributions by G.C. Lee, M. Bruneau, I.G. Buckle, S.E. Chang, P.J. Flores, T.D. O'Rourke, M. Shinozuka, T.T. Soong, C-H. Loh, K-C. Chang, Z-J. Chen, J-S. Hwang, M-L. Lin, G-Y. Liu, K-C. Tsai, G.C. Yao and C-L. Yen, 4/30/00, (PB2001-100980, A10, MF-A02).
- MCEER-00-0004 "Seismic Retrofit of End-Sway Frames of Steel Deck-Truss Bridges with a Supplemental Tendon System: Experimental and Analytical Investigation," by G. Pekcan, J.B. Mander and S.S. Chen, 7/1/00, (PB2001-100982, A10, MF-A02).
- MCEER-00-0005 "Sliding Fragility of Unrestrained Equipment in Critical Facilities," by W.H. Chong and T.T. Soong, 7/5/00, (PB2001-100983, A08, MF-A02).
- MCEER-00-0006 "Seismic Response of Reinforced Concrete Bridge Pier Walls in the Weak Direction," by N. Abo-Shadi, M. Saiidi and D. Sanders, 7/17/00, (PB2001-100981, A17, MF-A03).
- MCEER-00-0007 "Low-Cycle Fatigue Behavior of Longitudinal Reinforcement in Reinforced Concrete Bridge Columns," by J. Brown and S.K. Kunnath, 7/23/00, (PB2001-104392, A08, MF-A02).
- MCEER-00-0008 "Soil Structure Interaction of Bridges for Seismic Analysis," I. PoLam and H. Law, 9/25/00, (PB2001-105397, A08, MF-A02).
- MCEER-00-0009 "Proceedings of the First MCEER Workshop on Mitigation of Earthquake Disaster by Advanced Technologies (MEDAT-1), edited by M. Shinozuka, D.J. Inman and T.D. O'Rourke, 11/10/00, (PB2001-105399, A14, MF-A03).
- MCEER-00-0010 "Development and Evaluation of Simplified Procedures for Analysis and Design of Buildings with Passive Energy Dissipation Systems, Revision 01," by O.M. Ramirez, M.C. Constantinou, C.A. Kircher, A.S. Whittaker, M.W. Johnson, J.D. Gomez and C. Chrysostomou, 11/16/01, (PB2001-105523, A23, MF-A04).
- MCEER-00-0011 "Dynamic Soil-Foundation-Structure Interaction Analyses of Large Caissons," by C-Y. Chang, C-M. Mok, Z-L. Wang, R. Settgast, F. Waggoner, M.A. Ketchum, H.M. Gonnermann and C-C. Chin, 12/30/00, (PB2001-104373, A07, MF-A02).
- MCEER-00-0012 "Experimental Evaluation of Seismic Performance of Bridge Restrainers," by A.G. Vlassis, E.M. Maragakis and M. Saiid Saiidi, 12/30/00, (PB2001-104354, A09, MF-A02).
- MCEER-00-0013 "Effect of Spatial Variation of Ground Motion on Highway Structures," by M. Shinozuka, V. Saxena and G. Deodatis, 12/31/00, (PB2001-108755, A13, MF-A03).
- MCEER-00-0014 "A Risk-Based Methodology for Assessing the Seismic Performance of Highway Systems," by S.D. Werner, C.E. Taylor, J.E. Moore, II, J.S. Walton and S. Cho, 12/31/00, (PB2001-108756, A14, MF-A03).

- MCEER-01-0001 “Experimental Investigation of P-Delta Effects to Collapse During Earthquakes,” by D. Vian and M. Bruneau, 6/25/01, (PB2002-100534, A17, MF-A03).
- MCEER-01-0002 “Proceedings of the Second MCEER Workshop on Mitigation of Earthquake Disaster by Advanced Technologies (MEDAT-2),” edited by M. Bruneau and D.J. Inman, 7/23/01, (PB2002-100434, A16, MF-A03).
- MCEER-01-0003 “Sensitivity Analysis of Dynamic Systems Subjected to Seismic Loads,” by C. Roth and M. Grigoriu, 9/18/01, (PB2003-100884, A12, MF-A03).
- MCEER-01-0004 “Overcoming Obstacles to Implementing Earthquake Hazard Mitigation Policies: Stage 1 Report,” by D.J. Alesch and W.J. Petak, 12/17/01, (PB2002-107949, A07, MF-A02).
- MCEER-01-0005 “Updating Real-Time Earthquake Loss Estimates: Methods, Problems and Insights,” by C.E. Taylor, S.E. Chang and R.T. Eguchi, 12/17/01, (PB2002-107948, A05, MF-A01).
- MCEER-01-0006 “Experimental Investigation and Retrofit of Steel Pile Foundations and Pile Bents Under Cyclic Lateral Loadings,” by A. Shama, J. Mander, B. Blabac and S. Chen, 12/31/01, (PB2002-107950, A13, MF-A03).
- MCEER-02-0001 “Assessment of Performance of Bolu Viaduct in the 1999 Duzce Earthquake in Turkey” by P.C. Roussis, M.C. Constantinou, M. Erdik, E. Durukal and M. Dicleli, 5/8/02, (PB2003-100883, A08, MF-A02).
- MCEER-02-0002 “Seismic Behavior of Rail Counterweight Systems of Elevators in Buildings,” by M.P. Singh, Rildova and L.E. Suarez, 5/27/02. (PB2003-100882, A11, MF-A03).
- MCEER-02-0003 “Development of Analysis and Design Procedures for Spread Footings,” by G. Mylonakis, G. Gazetas, S. Nikolaou and A. Chauncey, 10/02/02, (PB2004-101636, A13, MF-A03, CD-A13).
- MCEER-02-0004 “Bare-Earth Algorithms for Use with SAR and LIDAR Digital Elevation Models,” by C.K. Huyck, R.T. Eguchi and B. Houshmand, 10/16/02, (PB2004-101637, A07, CD-A07).
- MCEER-02-0005 “Review of Energy Dissipation of Compression Members in Concentrically Braced Frames,” by K.Lee and M. Bruneau, 10/18/02, (PB2004-101638, A10, CD-A10).
- MCEER-03-0001 “Experimental Investigation of Light-Gauge Steel Plate Shear Walls for the Seismic Retrofit of Buildings” by J. Berman and M. Bruneau, 5/2/03, (PB2004-101622, A10, MF-A03, CD-A10).
- MCEER-03-0002 “Statistical Analysis of Fragility Curves,” by M. Shinozuka, M.Q. Feng, H. Kim, T. Uzawa and T. Ueda, 6/16/03, (PB2004-101849, A09, CD-A09).
- MCEER-03-0003 “Proceedings of the Eighth U.S.-Japan Workshop on Earthquake Resistant Design of Lifeline Facilities and Countermeasures Against Liquefaction,” edited by M. Hamada, J.P. Bardet and T.D. O’Rourke, 6/30/03, (PB2004-104386, A99, CD-A99).
- MCEER-03-0004 “Proceedings of the PRC-US Workshop on Seismic Analysis and Design of Special Bridges,” edited by L.C. Fan and G.C. Lee, 7/15/03, (PB2004-104387, A14, CD-A14).
- MCEER-03-0005 “Urban Disaster Recovery: A Framework and Simulation Model,” by S.B. Miles and S.E. Chang, 7/25/03, (PB2004-104388, A07, CD-A07).
- MCEER-03-0006 “Behavior of Underground Piping Joints Due to Static and Dynamic Loading,” by R.D. Meis, M. Maragakis and R. Siddharthan, 11/17/03, (PB2005-102194, A13, MF-A03, CD-A00).
- MCEER-04-0001 “Experimental Study of Seismic Isolation Systems with Emphasis on Secondary System Response and Verification of Accuracy of Dynamic Response History Analysis Methods,” by E. Wolff and M. Constantinou, 1/16/04 (PB2005-102195, A99, MF-E08, CD-A00).
- MCEER-04-0002 “Tension, Compression and Cyclic Testing of Engineered Cementitious Composite Materials,” by K. Kesner and S.L. Billington, 3/1/04, (PB2005-102196, A08, CD-A08).

- MCEER-04-0003 "Cyclic Testing of Braces Laterally Restrained by Steel Studs to Enhance Performance During Earthquakes," by O.C. Celik, J.W. Berman and M. Bruneau, 3/16/04, (PB2005-102197, A13, MF-A03, CD-A00).
- MCEER-04-0004 "Methodologies for Post Earthquake Building Damage Detection Using SAR and Optical Remote Sensing: Application to the August 17, 1999 Marmara, Turkey Earthquake," by C.K. Huyck, B.J. Adams, S. Cho, R.T. Eguchi, B. Mansouri and B. Houshmand, 6/15/04, (PB2005-104888, A10, CD-A00).
- MCEER-04-0005 "Nonlinear Structural Analysis Towards Collapse Simulation: A Dynamical Systems Approach," by M.V. Sivaselvan and A.M. Reinhorn, 6/16/04, (PB2005-104889, A11, MF-A03, CD-A00).
- MCEER-04-0006 "Proceedings of the Second PRC-US Workshop on Seismic Analysis and Design of Special Bridges," edited by G.C. Lee and L.C. Fan, 6/25/04, (PB2005-104890, A16, CD-A00).
- MCEER-04-0007 "Seismic Vulnerability Evaluation of Axially Loaded Steel Built-up Laced Members," by K. Lee and M. Bruneau, 6/30/04, (PB2005-104891, A16, CD-A00).
- MCEER-04-0008 "Evaluation of Accuracy of Simplified Methods of Analysis and Design of Buildings with Damping Systems for Near-Fault and for Soft-Soil Seismic Motions," by E.A. Pavlou and M.C. Constantinou, 8/16/04, (PB2005-104892, A08, MF-A02, CD-A00).
- MCEER-04-0009 "Assessment of Geotechnical Issues in Acute Care Facilities in California," by M. Lew, T.D. O'Rourke, R. Dobry and M. Koch, 9/15/04, (PB2005-104893, A08, CD-A00).
- MCEER-04-0010 "Scissor-Jack-Damper Energy Dissipation System," by A.N. Sigaher-Boyle and M.C. Constantinou, 12/1/04 (PB2005-108221).
- MCEER-04-0011 "Seismic Retrofit of Bridge Steel Truss Piers Using a Controlled Rocking Approach," by M. Pollino and M. Bruneau, 12/20/04 (PB2006-105795).
- MCEER-05-0001 "Experimental and Analytical Studies of Structures Seismically Isolated with an Uplift-Restraint Isolation System," by P.C. Roussis and M.C. Constantinou, 1/10/05 (PB2005-108222).
- MCEER-05-0002 "A Versatile Experimentation Model for Study of Structures Near Collapse Applied to Seismic Evaluation of Irregular Structures," by D. Kusumastuti, A.M. Reinhorn and A. Rutenberg, 3/31/05 (PB2006-101523).
- MCEER-05-0003 "Proceedings of the Third PRC-US Workshop on Seismic Analysis and Design of Special Bridges," edited by L.C. Fan and G.C. Lee, 4/20/05, (PB2006-105796).
- MCEER-05-0004 "Approaches for the Seismic Retrofit of Braced Steel Bridge Piers and Proof-of-Concept Testing of an Eccentrically Braced Frame with Tubular Link," by J.W. Berman and M. Bruneau, 4/21/05 (PB2006-101524).
- MCEER-05-0005 "Simulation of Strong Ground Motions for Seismic Fragility Evaluation of Nonstructural Components in Hospitals," by A. Wanitkorkul and A. Filiatrault, 5/26/05 (PB2006-500027).
- MCEER-05-0006 "Seismic Safety in California Hospitals: Assessing an Attempt to Accelerate the Replacement or Seismic Retrofit of Older Hospital Facilities," by D.J. Alesch, L.A. Arendt and W.J. Petak, 6/6/05 (PB2006-105794).
- MCEER-05-0007 "Development of Seismic Strengthening and Retrofit Strategies for Critical Facilities Using Engineered Cementitious Composite Materials," by K. Kesner and S.L. Billington, 8/29/05 (PB2006-111701).
- MCEER-05-0008 "Experimental and Analytical Studies of Base Isolation Systems for Seismic Protection of Power Transformers," by N. Murota, M.Q. Feng and G-Y. Liu, 9/30/05 (PB2006-111702).
- MCEER-05-0009 "3D-BASIS-ME-MB: Computer Program for Nonlinear Dynamic Analysis of Seismically Isolated Structures," by P.C. Tsopelas, P.C. Roussis, M.C. Constantinou, R. Buchanan and A.M. Reinhorn, 10/3/05 (PB2006-111703).
- MCEER-05-0010 "Steel Plate Shear Walls for Seismic Design and Retrofit of Building Structures," by D. Vian and M. Bruneau, 12/15/05 (PB2006-111704).

- MCEER-05-0011 "The Performance-Based Design Paradigm," by M.J. Astrella and A. Whittaker, 12/15/05 (PB2006-111705).
- MCEER-06-0001 "Seismic Fragility of Suspended Ceiling Systems," H. Badillo-Almaraz, A.S. Whittaker, A.M. Reinhorn and G.P. Cimellaro, 2/4/06 (PB2006-111706).
- MCEER-06-0002 "Multi-Dimensional Fragility of Structures," by G.P. Cimellaro, A.M. Reinhorn and M. Bruneau, 3/1/06 (PB2007-106974, A09, MF-A02, CD A00).
- MCEER-06-0003 "Built-Up Shear Links as Energy Dissipators for Seismic Protection of Bridges," by P. Dusicka, A.M. Itani and I.G. Buckle, 3/15/06 (PB2006-111708).
- MCEER-06-0004 "Analytical Investigation of the Structural Fuse Concept," by R.E. Vargas and M. Bruneau, 3/16/06 (PB2006-111709).
- MCEER-06-0005 "Experimental Investigation of the Structural Fuse Concept," by R.E. Vargas and M. Bruneau, 3/17/06 (PB2006-111710).
- MCEER-06-0006 "Further Development of Tubular Eccentrically Braced Frame Links for the Seismic Retrofit of Braced Steel Truss Bridge Piers," by J.W. Berman and M. Bruneau, 3/27/06 (PB2007-105147).
- MCEER-06-0007 "REDARS Validation Report," by S. Cho, C.K. Huyck, S. Ghosh and R.T. Eguchi, 8/8/06 (PB2007-106983).
- MCEER-06-0008 "Review of Current NDE Technologies for Post-Earthquake Assessment of Retrofitted Bridge Columns," by J.W. Song, Z. Liang and G.C. Lee, 8/21/06 (PB2007-106984).
- MCEER-06-0009 "Liquefaction Remediation in Silty Soils Using Dynamic Compaction and Stone Columns," by S. Thevanayagam, G.R. Martin, R. Nashed, T. Shenthan, T. Kanagalingam and N. Ecemis, 8/28/06 (PB2007-106985).
- MCEER-06-0010 "Conceptual Design and Experimental Investigation of Polymer Matrix Composite Infill Panels for Seismic Retrofitting," by W. Jung, M. Chiewanichakorn and A.J. Aref, 9/21/06 (PB2007-106986).
- MCEER-06-0011 "A Study of the Coupled Horizontal-Vertical Behavior of Elastomeric and Lead-Rubber Seismic Isolation Bearings," by G.P. Warn and A.S. Whittaker, 9/22/06 (PB2007-108679).
- MCEER-06-0012 "Proceedings of the Fourth PRC-US Workshop on Seismic Analysis and Design of Special Bridges: Advancing Bridge Technologies in Research, Design, Construction and Preservation," Edited by L.C. Fan, G.C. Lee and L. Ziang, 10/12/06 (PB2007-109042).
- MCEER-06-0013 "Cyclic Response and Low Cycle Fatigue Characteristics of Plate Steels," by P. Dusicka, A.M. Itani and I.G. Buckle, 11/1/06 (PB2007-106987).
- MCEER-06-0014 "Proceedings of the Second US-Taiwan Bridge Engineering Workshop," edited by W.P. Yen, J. Shen, J-Y. Chen and M. Wang, 11/15/06 (PB2008-500041).
- MCEER-06-0015 "User Manual and Technical Documentation for the REDARSTM Import Wizard," by S. Cho, S. Ghosh, C.K. Huyck and S.D. Werner, 11/30/06 (PB2007-114766).
- MCEER-06-0016 "Hazard Mitigation Strategy and Monitoring Technologies for Urban and Infrastructure Public Buildings: Proceedings of the China-US Workshops," edited by X.Y. Zhou, A.L. Zhang, G.C. Lee and M. Tong, 12/12/06 (PB2008-500018).
- MCEER-07-0001 "Static and Kinetic Coefficients of Friction for Rigid Blocks," by C. Kafali, S. Fathali, M. Grigoriu and A.S. Whittaker, 3/20/07 (PB2007-114767).
- MCEER-07-0002 "Hazard Mitigation Investment Decision Making: Organizational Response to Legislative Mandate," by L.A. Arendt, D.J. Alesch and W.J. Petak, 4/9/07 (PB2007-114768).
- MCEER-07-0003 "Seismic Behavior of Bidirectional-Resistant Ductile End Diaphragms with Unbonded Braces in Straight or Skewed Steel Bridges," by O. Celik and M. Bruneau, 4/11/07 (PB2008-105141).

- MCEER-07-0004 “Modeling Pile Behavior in Large Pile Groups Under Lateral Loading,” by A.M. Dodds and G.R. Martin, 4/16/07(PB2008-105142).
- MCEER-07-0005 “Experimental Investigation of Blast Performance of Seismically Resistant Concrete-Filled Steel Tube Bridge Piers,” by S. Fujikura, M. Bruneau and D. Lopez-Garcia, 4/20/07 (PB2008-105143).
- MCEER-07-0006 “Seismic Analysis of Conventional and Isolated Liquefied Natural Gas Tanks Using Mechanical Analogs,” by I.P. Christovasilis and A.S. Whittaker, 5/1/07, not available.
- MCEER-07-0007 “Experimental Seismic Performance Evaluation of Isolation/Restraint Systems for Mechanical Equipment – Part 1: Heavy Equipment Study,” by S. Fathali and A. Filiatrault, 6/6/07 (PB2008-105144).
- MCEER-07-0008 “Seismic Vulnerability of Timber Bridges and Timber Substructures,” by A.A. Sharma, J.B. Mander, I.M. Friedland and D.R. Allicock, 6/7/07 (PB2008-105145).
- MCEER-07-0009 “Experimental and Analytical Study of the XY-Friction Pendulum (XY-FP) Bearing for Bridge Applications,” by C.C. Marin-Artieda, A.S. Whittaker and M.C. Constantinou, 6/7/07 (PB2008-105191).
- MCEER-07-0010 “Proceedings of the PRC-US Earthquake Engineering Forum for Young Researchers,” Edited by G.C. Lee and X.Z. Qi, 6/8/07 (PB2008-500058).
- MCEER-07-0011 “Design Recommendations for Perforated Steel Plate Shear Walls,” by R. Purba and M. Bruneau, 6/18/07, (PB2008-105192).
- MCEER-07-0012 “Performance of Seismic Isolation Hardware Under Service and Seismic Loading,” by M.C. Constantinou, A.S. Whittaker, Y. Kalpakidis, D.M. Fenz and G.P. Warn, 8/27/07, (PB2008-105193).
- MCEER-07-0013 “Experimental Evaluation of the Seismic Performance of Hospital Piping Subassemblies,” by E.R. Goodwin, E. Maragakis and A.M. Itani, 9/4/07, (PB2008-105194).
- MCEER-07-0014 “A Simulation Model of Urban Disaster Recovery and Resilience: Implementation for the 1994 Northridge Earthquake,” by S. Miles and S.E. Chang, 9/7/07, (PB2008-106426).
- MCEER-07-0015 “Statistical and Mechanistic Fragility Analysis of Concrete Bridges,” by M. Shinozuka, S. Banerjee and S-H. Kim, 9/10/07, (PB2008-106427).
- MCEER-07-0016 “Three-Dimensional Modeling of Inelastic Buckling in Frame Structures,” by M. Schachter and AM. Reinhorn, 9/13/07, (PB2008-108125).
- MCEER-07-0017 “Modeling of Seismic Wave Scattering on Pile Groups and Caissons,” by I. Po Lam, H. Law and C.T. Yang, 9/17/07 (PB2008-108150).
- MCEER-07-0018 “Bridge Foundations: Modeling Large Pile Groups and Caissons for Seismic Design,” by I. Po Lam, H. Law and G.R. Martin (Coordinating Author), 12/1/07 (PB2008-111190).
- MCEER-07-0019 “Principles and Performance of Roller Seismic Isolation Bearings for Highway Bridges,” by G.C. Lee, Y.C. Ou, Z. Liang, T.C. Niu and J. Song, 12/10/07 (PB2009-110466).
- MCEER-07-0020 “Centrifuge Modeling of Permeability and Pinning Reinforcement Effects on Pile Response to Lateral Spreading,” by L.L Gonzalez-Lagos, T. Abdoun and R. Dobry, 12/10/07 (PB2008-111191).
- MCEER-07-0021 “Damage to the Highway System from the Pisco, Perú Earthquake of August 15, 2007,” by J.S. O’Connor, L. Mesa and M. Nykamp, 12/10/07, (PB2008-108126).
- MCEER-07-0022 “Experimental Seismic Performance Evaluation of Isolation/Restraint Systems for Mechanical Equipment – Part 2: Light Equipment Study,” by S. Fathali and A. Filiatrault, 12/13/07 (PB2008-111192).
- MCEER-07-0023 “Fragility Considerations in Highway Bridge Design,” by M. Shinozuka, S. Banerjee and S.H. Kim, 12/14/07 (PB2008-111193).

- MCEER-07-0024 "Performance Estimates for Seismically Isolated Bridges," by G.P. Warn and A.S. Whittaker, 12/30/07 (PB2008-112230).
- MCEER-08-0001 "Seismic Performance of Steel Girder Bridge Superstructures with Conventional Cross Frames," by L.P. Carden, A.M. Itani and I.G. Buckle, 1/7/08, (PB2008-112231).
- MCEER-08-0002 "Seismic Performance of Steel Girder Bridge Superstructures with Ductile End Cross Frames with Seismic Isolators," by L.P. Carden, A.M. Itani and I.G. Buckle, 1/7/08 (PB2008-112232).
- MCEER-08-0003 "Analytical and Experimental Investigation of a Controlled Rocking Approach for Seismic Protection of Bridge Steel Truss Piers," by M. Pollino and M. Bruneau, 1/21/08 (PB2008-112233).
- MCEER-08-0004 "Linking Lifeline Infrastructure Performance and Community Disaster Resilience: Models and Multi-Stakeholder Processes," by S.E. Chang, C. Pasion, K. Tatebe and R. Ahmad, 3/3/08 (PB2008-112234).
- MCEER-08-0005 "Modal Analysis of Generally Damped Linear Structures Subjected to Seismic Excitations," by J. Song, Y-L. Chu, Z. Liang and G.C. Lee, 3/4/08 (PB2009-102311).
- MCEER-08-0006 "System Performance Under Multi-Hazard Environments," by C. Kafali and M. Grigoriu, 3/4/08 (PB2008-112235).
- MCEER-08-0007 "Mechanical Behavior of Multi-Spherical Sliding Bearings," by D.M. Fenz and M.C. Constantinou, 3/6/08 (PB2008-112236).
- MCEER-08-0008 "Post-Earthquake Restoration of the Los Angeles Water Supply System," by T.H.P. Tabucchi and R.A. Davidson, 3/7/08 (PB2008-112237).
- MCEER-08-0009 "Fragility Analysis of Water Supply Systems," by A. Jacobson and M. Grigoriu, 3/10/08 (PB2009-105545).
- MCEER-08-0010 "Experimental Investigation of Full-Scale Two-Story Steel Plate Shear Walls with Reduced Beam Section Connections," by B. Qu, M. Bruneau, C-H. Lin and K-C. Tsai, 3/17/08 (PB2009-106368).
- MCEER-08-0011 "Seismic Evaluation and Rehabilitation of Critical Components of Electrical Power Systems," S. Ersoy, B. Feizi, A. Ashrafi and M. Ala Saadeghvaziri, 3/17/08 (PB2009-105546).
- MCEER-08-0012 "Seismic Behavior and Design of Boundary Frame Members of Steel Plate Shear Walls," by B. Qu and M. Bruneau, 4/26/08 . (PB2009-106744).
- MCEER-08-0013 "Development and Appraisal of a Numerical Cyclic Loading Protocol for Quantifying Building System Performance," by A. Filiatrault, A. Wanitkorkul and M. Constantinou, 4/27/08 (PB2009-107906).
- MCEER-08-0014 "Structural and Nonstructural Earthquake Design: The Challenge of Integrating Specialty Areas in Designing Complex, Critical Facilities," by W.J. Petak and D.J. Alesch, 4/30/08 (PB2009-107907).
- MCEER-08-0015 "Seismic Performance Evaluation of Water Systems," by Y. Wang and T.D. O'Rourke, 5/5/08 (PB2009-107908).
- MCEER-08-0016 "Seismic Response Modeling of Water Supply Systems," by P. Shi and T.D. O'Rourke, 5/5/08 (PB2009-107910).
- MCEER-08-0017 "Numerical and Experimental Studies of Self-Centering Post-Tensioned Steel Frames," by D. Wang and A. Filiatrault, 5/12/08 (PB2009-110479).
- MCEER-08-0018 "Development, Implementation and Verification of Dynamic Analysis Models for Multi-Spherical Sliding Bearings," by D.M. Fenz and M.C. Constantinou, 8/15/08 (PB2009-107911).
- MCEER-08-0019 "Performance Assessment of Conventional and Base Isolated Nuclear Power Plants for Earthquake Blast Loadings," by Y.N. Huang, A.S. Whittaker and N. Luco, 10/28/08 (PB2009-107912).

- MCEER-08-0020 “Remote Sensing for Resilient Multi-Hazard Disaster Response – Volume I: Introduction to Damage Assessment Methodologies,” by B.J. Adams and R.T. Eguchi, 11/17/08 (PB2010-102695).
- MCEER-08-0021 “Remote Sensing for Resilient Multi-Hazard Disaster Response – Volume II: Counting the Number of Collapsed Buildings Using an Object-Oriented Analysis: Case Study of the 2003 Bam Earthquake,” by L. Gusella, C.K. Huyck and B.J. Adams, 11/17/08 (PB2010-100925).
- MCEER-08-0022 “Remote Sensing for Resilient Multi-Hazard Disaster Response – Volume III: Multi-Sensor Image Fusion Techniques for Robust Neighborhood-Scale Urban Damage Assessment,” by B.J. Adams and A. McMillan, 11/17/08 (PB2010-100926).
- MCEER-08-0023 “Remote Sensing for Resilient Multi-Hazard Disaster Response – Volume IV: A Study of Multi-Temporal and Multi-Resolution SAR Imagery for Post-Katrina Flood Monitoring in New Orleans,” by A. McMillan, J.G. Morley, B.J. Adams and S. Chesworth, 11/17/08 (PB2010-100927).
- MCEER-08-0024 “Remote Sensing for Resilient Multi-Hazard Disaster Response – Volume V: Integration of Remote Sensing Imagery and VIEWS™ Field Data for Post-Hurricane Charley Building Damage Assessment,” by J.A. Womble, K. Mehta and B.J. Adams, 11/17/08 (PB2009-115532).
- MCEER-08-0025 “Building Inventory Compilation for Disaster Management: Application of Remote Sensing and Statistical Modeling,” by P. Sarabandi, A.S. Kiremidjian, R.T. Eguchi and B. J. Adams, 11/20/08 (PB2009-110484).
- MCEER-08-0026 “New Experimental Capabilities and Loading Protocols for Seismic Qualification and Fragility Assessment of Nonstructural Systems,” by R. Retamales, G. Mosqueda, A. Filiatrault and A. Reinhorn, 11/24/08 (PB2009-110485).
- MCEER-08-0027 “Effects of Heating and Load History on the Behavior of Lead-Rubber Bearings,” by I.V. Kalpakidis and M.C. Constantinou, 12/1/08 (PB2009-115533).
- MCEER-08-0028 “Experimental and Analytical Investigation of Blast Performance of Seismically Resistant Bridge Piers,” by S.Fujikura and M. Bruneau, 12/8/08 (PB2009-115534).
- MCEER-08-0029 “Evolutionary Methodology for Aseismic Decision Support,” by Y. Hu and G. Dargush, 12/15/08.
- MCEER-08-0030 “Development of a Steel Plate Shear Wall Bridge Pier System Conceived from a Multi-Hazard Perspective,” by D. Keller and M. Bruneau, 12/19/08 (PB2010-102696).
- MCEER-09-0001 “Modal Analysis of Arbitrarily Damped Three-Dimensional Linear Structures Subjected to Seismic Excitations,” by Y.L. Chu, J. Song and G.C. Lee, 1/31/09 (PB2010-100922).
- MCEER-09-0002 “Air-Blast Effects on Structural Shapes,” by G. Ballantyne, A.S. Whittaker, A.J. Aref and G.F. Dargush, 2/2/09 (PB2010-102697).
- MCEER-09-0003 “Water Supply Performance During Earthquakes and Extreme Events,” by A.L. Bonneau and T.D. O’Rourke, 2/16/09 (PB2010-100923).
- MCEER-09-0004 “Generalized Linear (Mixed) Models of Post-Earthquake Ignitions,” by R.A. Davidson, 7/20/09 (PB2010-102698).
- MCEER-09-0005 “Seismic Testing of a Full-Scale Two-Story Light-Frame Wood Building: NEESWood Benchmark Test,” by I.P. Christovasilis, A. Filiatrault and A. Wanitkorkul, 7/22/09 (PB2012-102401).
- MCEER-09-0006 “IDARC2D Version 7.0: A Program for the Inelastic Damage Analysis of Structures,” by A.M. Reinhorn, H. Roh, M. Sivaselvan, S.K. Kunnath, R.E. Valles, A. Madan, C. Li, R. Lobo and Y.J. Park, 7/28/09 (PB2010-103199).
- MCEER-09-0007 “Enhancements to Hospital Resiliency: Improving Emergency Planning for and Response to Hurricanes,” by D.B. Hess and L.A. Arendt, 7/30/09 (PB2010-100924).

- MCEER-09-0008 “Assessment of Base-Isolated Nuclear Structures for Design and Beyond-Design Basis Earthquake Shaking,” by Y.N. Huang, A.S. Whittaker, R.P. Kennedy and R.L. Mayes, 8/20/09 (PB2010-102699).
- MCEER-09-0009 “Quantification of Disaster Resilience of Health Care Facilities,” by G.P. Cimellaro, C. Fumo, A.M. Reinhorn and M. Bruneau, 9/14/09 (PB2010-105384).
- MCEER-09-0010 “Performance-Based Assessment and Design of Squat Reinforced Concrete Shear Walls,” by C.K. Gulec and A.S. Whittaker, 9/15/09 (PB2010-102700).
- MCEER-09-0011 “Proceedings of the Fourth US-Taiwan Bridge Engineering Workshop,” edited by W.P. Yen, J.J. Shen, T.M. Lee and R.B. Zheng, 10/27/09 (PB2010-500009).
- MCEER-09-0012 “Proceedings of the Special International Workshop on Seismic Connection Details for Segmental Bridge Construction,” edited by W. Phillip Yen and George C. Lee, 12/21/09 (PB2012-102402).
- MCEER-10-0001 “Direct Displacement Procedure for Performance-Based Seismic Design of Multistory Woodframe Structures,” by W. Pang and D. Rosowsky, 4/26/10 (PB2012-102403).
- MCEER-10-0002 “Simplified Direct Displacement Design of Six-Story NEESWood Capstone Building and Pre-Test Seismic Performance Assessment,” by W. Pang, D. Rosowsky, J. van de Lindt and S. Pei, 5/28/10 (PB2012-102404).
- MCEER-10-0003 “Integration of Seismic Protection Systems in Performance-Based Seismic Design of Woodframed Structures,” by J.K. Shinde and M.D. Symans, 6/18/10 (PB2012-102405).
- MCEER-10-0004 “Modeling and Seismic Evaluation of Nonstructural Components: Testing Frame for Experimental Evaluation of Suspended Ceiling Systems,” by A.M. Reinhorn, K.P. Ryu and G. Maddaloni, 6/30/10 (PB2012-102406).
- MCEER-10-0005 “Analytical Development and Experimental Validation of a Structural-Fuse Bridge Pier Concept,” by S. El-Bahey and M. Bruneau, 10/1/10 (PB2012-102407).
- MCEER-10-0006 “A Framework for Defining and Measuring Resilience at the Community Scale: The PEOPLES Resilience Framework,” by C.S. Renschler, A.E. Frazier, L.A. Arendt, G.P. Cimellaro, A.M. Reinhorn and M. Bruneau, 10/8/10 (PB2012-102408).
- MCEER-10-0007 “Impact of Horizontal Boundary Elements Design on Seismic Behavior of Steel Plate Shear Walls,” by R. Purba and M. Bruneau, 11/14/10 (PB2012-102409).
- MCEER-10-0008 “Seismic Testing of a Full-Scale Mid-Rise Building: The NEESWood Capstone Test,” by S. Pei, J.W. van de Lindt, S.E. Pryor, H. Shimizu, H. Isoda and D.R. Rammer, 12/1/10 (PB2012-102410).
- MCEER-10-0009 “Modeling the Effects of Detonations of High Explosives to Inform Blast-Resistant Design,” by P. Sherkar, A.S. Whittaker and A.J. Aref, 12/1/10 (PB2012-102411).
- MCEER-10-0010 “L’Aquila Earthquake of April 6, 2009 in Italy: Rebuilding a Resilient City to Withstand Multiple Hazards,” by G.P. Cimellaro, I.P. Christovasilis, A.M. Reinhorn, A. De Stefano and T. Kirova, 12/29/10.
- MCEER-11-0001 “Numerical and Experimental Investigation of the Seismic Response of Light-Frame Wood Structures,” by I.P. Christovasilis and A. Filiatrault, 8/8/11 (PB2012-102412).
- MCEER-11-0002 “Seismic Design and Analysis of a Precast Segmental Concrete Bridge Model,” by M. Anagnostopoulou, A. Filiatrault and A. Aref, 9/15/11.
- MCEER-11-0003 “Proceedings of the Workshop on Improving Earthquake Response of Substation Equipment,” Edited by A.M. Reinhorn, 9/19/11 (PB2012-102413).
- MCEER-11-0004 “LRFD-Based Analysis and Design Procedures for Bridge Bearings and Seismic Isolators,” by M.C. Constantinou, I. Kalpakidis, A. Filiatrault and R.A. Ecker Lay, 9/26/11.

- MCEER-11-0005 “Experimental Seismic Evaluation, Model Parameterization, and Effects of Cold-Formed Steel-Framed Gypsum Partition Walls on the Seismic Performance of an Essential Facility,” by R. Davies, R. Retamales, G. Mosqueda and A. Filiatrault, 10/12/11.
- MCEER-11-0006 “Modeling and Seismic Performance Evaluation of High Voltage Transformers and Bushings,” by A.M. Reinhorn, K. Oikonomou, H. Roh, A. Schiff and L. Kempner, Jr., 10/3/11.
- MCEER-11-0007 “Extreme Load Combinations: A Survey of State Bridge Engineers,” by G.C. Lee, Z. Liang, J.J. Shen and J.S. O’Connor, 10/14/11.
- MCEER-12-0001 “Simplified Analysis Procedures in Support of Performance Based Seismic Design,” by Y.N. Huang and A.S. Whittaker.
- MCEER-12-0002 “Seismic Protection of Electrical Transformer Bushing Systems by Stiffening Techniques,” by M. Koliou, A. Filiatrault, A.M. Reinhorn and N. Oliveto, 6/1/12.
- MCEER-12-0003 “Post-Earthquake Bridge Inspection Guidelines,” by J.S. O’Connor and S. Alampalli, 6/8/12.
- MCEER-12-0004 “Integrated Design Methodology for Isolated Floor Systems in Single-Degree-of-Freedom Structural Fuse Systems,” by S. Cui, M. Bruneau and M.C. Constantinou, 6/13/12.
- MCEER-12-0005 “Characterizing the Rotational Components of Earthquake Ground Motion,” by D. Basu, A.S. Whittaker and M.C. Constantinou, 6/15/12.
- MCEER-12-0006 “Bayesian Fragility for Nonstructural Systems,” by C.H. Lee and M.D. Grigoriu, 9/12/12.
- MCEER-12-0007 “A Numerical Model for Capturing the In-Plane Seismic Response of Interior Metal Stud Partition Walls,” by R.L. Wood and T.C. Hutchinson, 9/12/12.
- MCEER-12-0008 “Assessment of Floor Accelerations in Yielding Buildings,” by J.D. Wieser, G. Pekcan, A.E. Zaghi, A.M. Itani and E. Maragakis, 10/5/12.
- MCEER-13-0001 “Experimental Seismic Study of Pressurized Fire Sprinkler Piping Systems,” by Y. Tian, A. Filiatrault and G. Mosqueda, 4/8/13.
- MCEER-13-0002 “Enhancing Resource Coordination for Multi-Modal Evacuation Planning,” by D.B. Hess, B.W. Conley and C.M. Farrell, 2/8/13.
- MCEER-13-0003 “Seismic Response of Base Isolated Buildings Considering Pounding to Moat Walls,” by A. Masroor and G. Mosqueda, 2/26/13.
- MCEER-13-0004 “Seismic Response Control of Structures Using a Novel Adaptive Passive Negative Stiffness Device,” by D.T.R. Pasala, A.A. Sarlis, S. Nagarajaiah, A.M. Reinhorn, M.C. Constantinou and D.P. Taylor, 6/10/13.
- MCEER-13-0005 “Negative Stiffness Device for Seismic Protection of Structures,” by A.A. Sarlis, D.T.R. Pasala, M.C. Constantinou, A.M. Reinhorn, S. Nagarajaiah and D.P. Taylor, 6/12/13.
- MCEER-13-0006 “Emilia Earthquake of May 20, 2012 in Northern Italy: Rebuilding a Resilient Community to Withstand Multiple Hazards,” by G.P. Cimellaro, M. Chiriatti, A.M. Reinhorn and L. Tirca, June 30, 2013.
- MCEER-13-0007 “Precast Concrete Segmental Components and Systems for Accelerated Bridge Construction in Seismic Regions,” by A.J. Aref, G.C. Lee, Y.C. Ou and P. Sideris, with contributions from K.C. Chang, S. Chen, A. Filiatrault and Y. Zhou, June 13, 2013.
- MCEER-13-0008 “A Study of U.S. Bridge Failures (1980-2012),” by G.C. Lee, S.B. Mohan, C. Huang and B.N. Fard, June 15, 2013.
- MCEER-13-0009 “Development of a Database Framework for Modeling Damaged Bridges,” by G.C. Lee, J.C. Qi and C. Huang, June 16, 2013.

- MCEER-13-0010 “Model of Triple Friction Pendulum Bearing for General Geometric and Frictional Parameters and for Uplift Conditions,” by A.A. Sarlis and M.C. Constantinou, July 1, 2013.
- MCEER-13-0011 “Shake Table Testing of Triple Friction Pendulum Isolators under Extreme Conditions,” by A.A. Sarlis, M.C. Constantinou and A.M. Reinhorn, July 2, 2013.
- MCEER-13-0012 “Theoretical Framework for the Development of MH-LRFD,” by G.C. Lee (coordinating author), H.A. Capers, Jr., C. Huang, J.M. Kulicki, Z. Liang, T. Murphy, J.J.D. Shen, M. Shinozuka and P.W.H. Yen, July 31, 2013.
- MCEER-13-0013 “Seismic Protection of Highway Bridges with Negative Stiffness Devices,” by N.K.A. Attary, M.D. Symans, S. Nagarajaiah, A.M. Reinhorn, M.C. Constantinou, A.A. Sarlis, D.T.R. Pasala, and D.P. Taylor, September 3, 2014.
- MCEER-14-0001 “Simplified Seismic Collapse Capacity-Based Evaluation and Design of Frame Buildings with and without Supplemental Damping Systems,” by M. Hamidia, A. Filiatrault, and A. Aref, May 19, 2014.
- MCEER-14-0002 “Comprehensive Analytical Seismic Fragility of Fire Sprinkler Piping Systems,” by Siavash Soroushian, Emmanuel “Manos” Maragakis, Arash E. Zaghi, Alicia Echevarria, Yuan Tian and Andre Filiatrault, August 26, 2014.
- MCEER-14-0003 “Hybrid Simulation of the Seismic Response of a Steel Moment Frame Building Structure through Collapse,” by M. Del Carpio Ramos, G. Mosqueda and D.G. Lignos, October 30, 2014.
- MCEER-14-0004 “Blast and Seismic Resistant Concrete-Filled Double Skin Tubes and Modified Steel Jacketed Bridge Columns,” by P.P. Fouche and M. Bruneau, June 30, 2015.
- MCEER-14-0005 “Seismic Performance of Steel Plate Shear Walls Considering Various Design Approaches,” by R. Purba and M. Bruneau, October 31, 2014.
- MCEER-14-0006 “Air-Blast Effects on Civil Structures,” by Jinwon Shin, Andrew S. Whittaker, Amjad J. Aref and David Cormie, October 30, 2014.
- MCEER-14-0007 “Seismic Performance Evaluation of Precast Girders with Field-Cast Ultra High Performance Concrete (UHPC) Connections,” by G.C. Lee, C. Huang, J. Song, and J. S. O’Connor, July 31, 2014.
- MCEER-14-0008 “Post-Earthquake Fire Resistance of Ductile Concrete-Filled Double-Skin Tube Columns,” by Reza Imani, Gilberto Mosqueda and Michel Bruneau, December 1, 2014.
- MCEER-14-0009 “Cyclic Inelastic Behavior of Concrete Filled Sandwich Panel Walls Subjected to In-Plane Flexure,” by Y. Alzeni and M. Bruneau, December 19, 2014.
- MCEER-14-0010 “Analytical and Experimental Investigation of Self-Centering Steel Plate Shear Walls,” by D.M. Dowden and M. Bruneau, December 19, 2014.
- MCEER-15-0001 “Seismic Analysis of Multi-story Unreinforced Masonry Buildings with Flexible Diaphragms,” by J. Aleman, G. Mosqueda and A.S. Whittaker, June 12, 2015.
- MCEER-15-0002 “Site Response, Soil-Structure Interaction and Structure-Soil-Structure Interaction for Performance Assessment of Buildings and Nuclear Structures,” by C. Bolisetti and A.S. Whittaker, June 15, 2015.
- MCEER-15-0003 “Stress Wave Attenuation in Solids for Mitigating Impulsive Loadings,” by R. Rafiee-Dehkharghani, A.J. Aref and G. Dargush, August 15, 2015.
- MCEER-15-0004 “Computational, Analytical, and Experimental Modeling of Masonry Structures,” by K.M. Dolatshahi and A.J. Aref, November 16, 2015.
- MCEER-15-0005 “Property Modification Factors for Seismic Isolators: Design Guidance for Buildings,” by W.J. McVitty and M.C. Constantinou, June 30, 2015.

- MCEER-15-0006 “Seismic Isolation of Nuclear Power Plants using Sliding Bearings,” by Manish Kumar, Andrew S. Whittaker and Michael C. Constantinou, December 27, 2015.
- MCEER-15-0007 “Quintuple Friction Pendulum Isolator Behavior, Modeling and Validation,” by Donghun Lee and Michael C. Constantinou, December 28, 2015.
- MCEER-15-0008 “Seismic Isolation of Nuclear Power Plants using Elastomeric Bearings,” by Manish Kumar, Andrew S. Whittaker and Michael C. Constantinou, December 29, 2015.
- MCEER-16-0001 “Experimental, Numerical and Analytical Studies on the Seismic Response of Steel-Plate Concrete (SC) Composite Shear Walls,” by Siamak Epackachi and Andrew S. Whittaker, June 15, 2016.
- MCEER-16-0002 “Seismic Demand in Columns of Steel Frames,” by Lisa Shrestha and Michel Bruneau, June 17, 2016.
- MCEER-16-0003 “Development and Evaluation of Procedures for Analysis and Design of Buildings with Fluidic Self-Centering Systems” by Shoma Kitayama and Michael C. Constantinou, July 21, 2016.
- MCEER-16-0004 “Real Time Control of Shake Tables for Nonlinear Hysteretic Systems,” by Ki Pung Ryu and Andrei M. Reinhorn, October 22, 2016.
- MCEER-16-0006 “Seismic Isolation of High Voltage Electrical Power Transformers,” by Kostis Oikonomou, Michael C. Constantinou, Andrei M. Reinhorn and Leon Kemper, Jr., November 2, 2016.
- MCEER-16-0007 “Open Space Damping System Theory and Experimental Validation,” by Erkan Polat and Michael C. Constantinou, December 13, 2016.
- MCEER-16-0008 “Seismic Response of Low Aspect Ratio Reinforced Concrete Walls for Buildings and Safety-Related Nuclear Applications,” by Bismarck N. Luna and Andrew S. Whittaker.
- MCEER-16-0009 “Buckling Restrained Braces Applications for Superstructure and Substructure Protection in Bridges,” by Xiaone Wei and Michel Bruneau, December 28, 2016.
- MCEER-16-0010 “Procedures and Results of Assessment of Seismic Performance of Seismically Isolated Electrical Transformers with Due Consideration for Vertical Isolation and Vertical Ground Motion Effects,” by Shoma Kitayama, Michael C. Constantinou and Donghun Lee, December 31, 2016.
- MCEER-17-0001 “Diagonal Tension Field Inclination Angle in Steel Plate Shear Walls,” by Yushan Fu, Fangbo Wang and Michel Bruneau, February 10, 2017.
- MCEER-17-0002 “Behavior of Steel Plate Shear Walls Subjected to Long Duration Earthquakes,” by Ramla Qureshi and Michel Bruneau, September 1, 2017.
- MCEER-17-0003 “Response of Steel-plate Concrete (SC) Wall Piers to Combined In-plane and Out-of-plane Seismic Loadings,” by Brian Terranova, Andrew S. Whittaker, Siamak Epackachi and Nebojsa Orbovic, July 17, 2017.
- MCEER-17-0004 “Design of Reinforced Concrete Panels for Wind-borne Missile Impact,” by Brian Terranova, Andrew S. Whittaker and Len Schwer, July 18, 2017.
- MCEER-17-0005 “A Simple Strategy for Dynamic Substructuring and its Application to Soil-Foundation-Structure Interaction,” by Aikaterini Stefanaki and Mettupalayam V. Sivaselvan, December 15, 2017.
- MCEER-17-0006 “Dynamics of Cable Structures: Modeling and Applications,” by Nicholas D. Oliveto and Mettupalayam V. Sivaselvan, December 1, 2017.
- MCEER-17-0007 “Development and Validation of a Combined Horizontal-Vertical Seismic Isolation System for High-Voltage-Power Transformers,” by Donghun Lee and Michael C. Constantinou, November 3, 2017.



EARTHQUAKE ENGINEERING TO EXTREME EVENTS

University at Buffalo, The State University of New York

133A Ketter Hall ■ Buffalo, New York 14260-4300

Phone: (716) 645-3391 ■ Fax: (716) 645-3399

Email: mceer@buffalo.edu ■ Web: <http://mceer.buffalo.edu>



University at Buffalo The State University of New York

ISSN 1520-295X